Australian Government
Geoscience Australia

Geological Framework of the Continental Margin in the region of the Australian Antarctic Territory

H.M.J Stagg, J.B. Colwell, N.G. Direen, P.E. O'Brien, B.J. Brown, G. Bernardel, I. Borissova, L. Carson, & D.B. Close

Record
2004/25

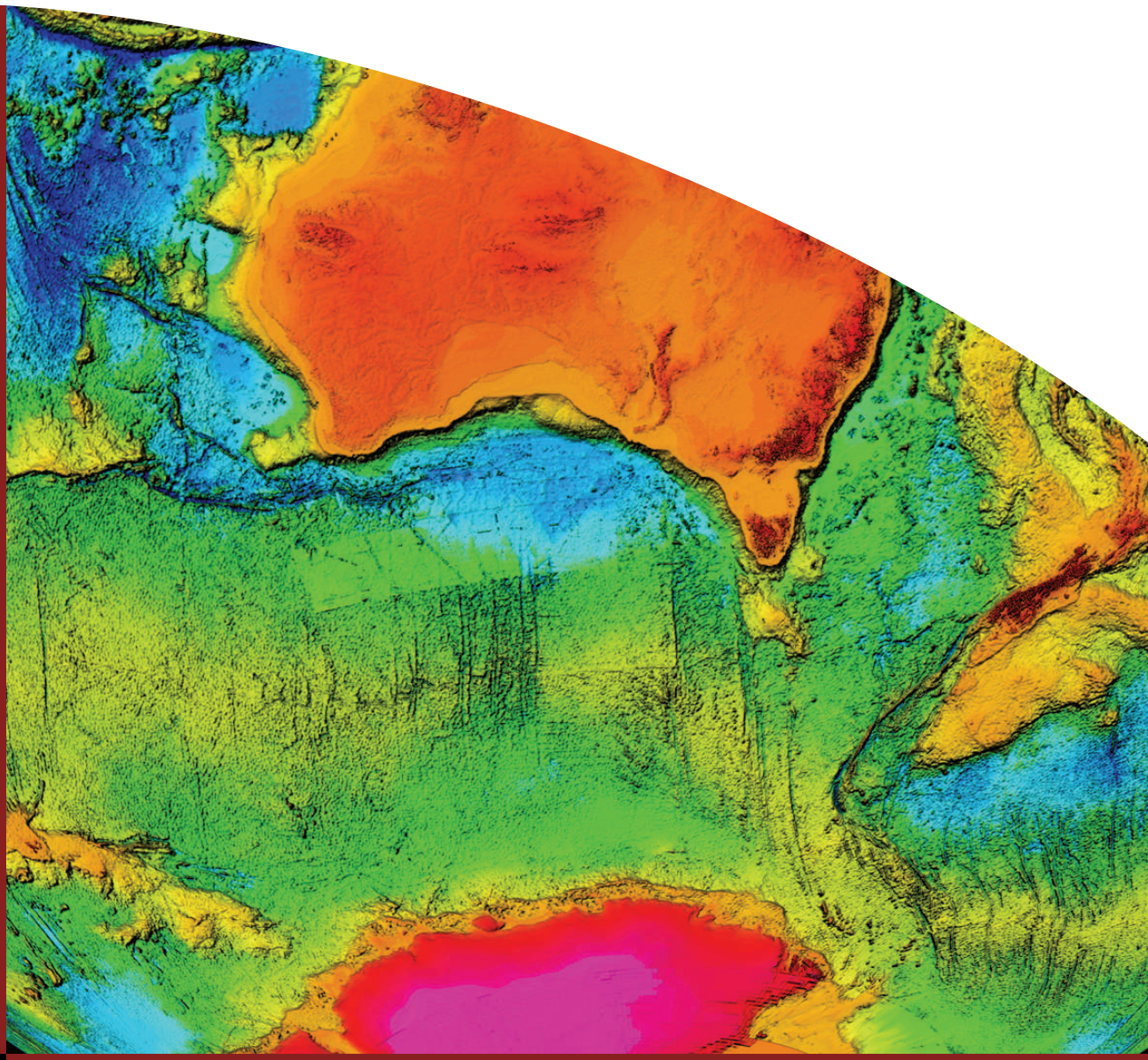

GEOSCIENCE AUSTRALIA
DEPARTMENT OF INDUSTRY, TOURISM & RESOURCES

Geoscience Australia Record 2004/25

GEOLOGICAL FRAMEWORK OF THE CONTINENTAL MARGIN IN THE REGION OF THE AUSTRALIAN ANTARCTIC TERRITORY

H.M.J Stagg, J.B. Colwell, N.G. Direen[1], P.E. O'Brien, B.J. Brown[2], G. Bernardel, I. Borissova, L. Carson, & D.B. Close[3]

Petroleum & Marine Division, Geoscience Australia
GPO Box 378, Canberra, ACT 2601

CANBERRA, 2004

[1] Continental Evolution Research Group, University of Adelaide
[2] School of Geosciences, The University of Sydney
[3] Department of Earth Sciences, University of Oxford

Department of Industry, Tourism & Resources

Minister for Industry, Tourism & Resources: The Hon. Ian Macfarlane, MP
Parliamentary Secretary: The Hon. Warren Entsch, MP
Secretary: Mark Patterson

Geoscience Australia

Chief Executive Officer: Neil Williams

ISSN: **1448-2177**
ISBN: **1 920871 20 9**

GeoCat No. 61823

Bibliographic reference: Stagg, H.M.J., Colwell, J.B., Direen, N.G., O'Brien, P.E., Brown, B.J., Bernardel, G., Borissova, I., Carson, L. & Close, D.B., 2005. Geological framework of the continental margin in the region of the Australian Antarctic Territory. *Geoscience Australia Record* 2004/25.

CONTENTS

Tables

Figures

63. Detailed seismic section line GA-228/10, eastern end of the Princess Elizabeth Trough and southeast of Kerguelen Plateau, showing seaward-dipping reflector sequences (*sdrs*). Full line shown in Plate 13.

64. Detailed seismic section line GA-229/23, northwest of Bruce Rise, showing the deep trough that marks the boundary between ?oceanic crustal types *peo6* and *peo7*. Full line shown in Plate 13.

65. Detailed seismic section line GA-229/23, northwest of Bruce Rise, showing the complex faulting and structural fabric of the *peo6* crust immediately south of the deep trough shown in the previous figure. Full line shown in Plate 13.

66. Potential field model for composite line GA-228/12 + GA-229/22 + GA-229/23, offshore Queen Mary Land. South on the left. Model bodies are identified in full in Appendix 7.

67. Detailed seismic section line GA-228/13, on Bruce Rise, showing faulted continental basement and the typical Bruce Rise sedimentary section. The basal blue erosional unconformity above the graben on the left of the section is probably of Valanginian age. Red arrows point to a bottom-simulating reflector (BSR). Full line shown in Plate 14.

68. Detailed seismic section line GA-228/14, northern flank of Bruce Rise, showing the large-offset basement faults that characterise this margin of Bruce Rise and the narrow COT zone. COB is interpreted continent–ocean boundary. The crustal type *qmu3* is probably oceanic; however, there is the possibility that it is of continental origin. Full line shown in Plate 14.

69. Detailed seismic section line GA-229/19, eastern flank of Bruce Rise, showing the steep Vincennes Fracture Zone. The deeply-subsided crustal type *qmu8* is probably continental or transitional. Full line shown in Plate 14.

70. Detailed seismic section line GA-229/21, northwest flank of Bruce Rise, showing the typical form of the western half of Bruce Rise. Full line shown in Plate 14.

71. Detailed seismic section line GA-229/21, north of Bruce Rise, showing the complex boundary between the undifferentiated crustal types *qmu1* and *qmu2*. Full line shown in Plate 14.

72. Detailed seismic section line GA-228/13, north of Bruce Rise showing the boundary between the undifferentiated crustal type *qmu2* and the fast-spreading Eocene crust of the Australian–Antarctic Basin (*aabo*). Full line shown in Plate 14.

73. Detailed seismic section line GA-229/21, northwest flank of Bruce Rise, showing the showing the thicker post-rift sedimentary section on the western half of Bruce Rise and a strong bottom-simulating reflector (BSR; shown by red arrows). Full line shown in Plate 14.

74. Satellite gravity pre-Early Eocene reconstruction of the Naturaliste Plateau – Bruce Rise region (after Borissova, 2002). Continental blocks are shown by yellow hachuring and possible continental blocks are shown by hachuring. Diamantina Zone is outlined by the thick red line. NP – Naturaliste Plateau; BrR – Bruce Rise; DZ – Diamantina Zone; GTr – Gonneville Triangle; BR –

profile shows the interpreted peridotite ridge, faulted Moho, transparent lower crust and thick, faulted Cretaceous sedimentary section.

87. Detailed seismic section, line GA-228/24, offshore Wilkes Land, outboard of the interpreted peridotite ridge. This section is interpreted to be a basin containing highly faulted and rotated sedimentary rocks of pre-Turonian age overlying either very thin crystalline continental crust or altered mantle. Full line shown in Plate 17.

88. Detailed seismic section, line GA-228/24, offshore Wilkes Land, immediately outboard of the interpreted peridotite ridge. This an enlargement of the left-hand end of the section shown in Figure 87. Full line shown in Plate 17.

89. Detailed seismic section, line GA-228/23, central Wilkes Land, showing the characteristic appearance of oceanic crustal type *wlo1*. Full line shown in Plate 16.

90. Detailed seismic section, line GA-229/08, central Wilkes Land, showing the characteristic appearance of oceanic crustal type *wlo2*. Full line shown in Plate 16.

91. Potential field model for line GA-228/28, eastern Wilkes Land. COB is the location of the interpreted continent–ocean boundary. South on the left. Model bodies are identified in full in Appendix 7.

92. Potential field model for line GA-228/29, eastern Wilkes Land. COB is the location of the interpreted continent–ocean boundary. South on the left. Model bodies are identified in full in Appendix 7.

93. Potential field model for line GA-229/06, offshore Terre Adélie (after Colwell et al., in press). COB is the location of the interpreted continent–ocean boundary. The Adélie Rift Block extends from SP 2200–5500. South on the left. Model bodies are identified in full in Appendix 7.

94. Detailed seismic section, line GA-229/06, offshore Terre Adélie, showing the thick sedimentary section near the crest of the Adélie Rift Block. *tur* – Turonian; *maas* – Maastrichtian; *eoc* - Eocene Full line shown in Plate 18.

95. Detailed seismic section, line GA-229/06, offshore Terre Adélie, showing the thick, folded and faulted sedimentary section outboard of the crest of the Adélie Rift Block. Note the pinch-and-swell structures in the lower crust that have strongly influenced the structuring of the overlying sedimentary section. *maas* – Maastrichtian; *eoc* - Eocene Full line shown in Plate 18.

96. Detailed seismic section, line GA-229/06, offshore Terre Adélie, showing the thick, folded and faulted sedimentary section outboard of the crest of the Adélie Rift Block. *maas* – Maastrichtian; *eoc* - Eocene Full line shown in Plate 18.

97. Detailed seismic section, line GA-228/32, off George V Land, showing the nature of oceanic crust *gvo1*.

98. Detailed seismic section, line GA-229/02, off George V Land, showing the more-highly-faulted nature of oceanic crust type *gvo2* in comparison to type *gvo1*. The deep slot between the two crustal types corresponds to the western part of the Tasman Fracture Zone (Plate 21).

Plates

EXECUTIVE SUMMARY

In the austral summers of 2000/01 and 2001/02, the Australian Antarctic and Southern Ocean Profiling Project (AASOPP) acquired a major new deep-water geophysical data set along the margin of East Antarctica from western Enderby Land to George V Land (38-160° E). This data set provides valuable insights into the geology of this part of the Antarctic margin. The data set comprises more than 20 000 km of high-quality deep-seismic reflection, gravity and magnetic data, and 97 refraction/wide-angle reflection sonobuoy stations on lines that extend from the mid to lower continental slope out to oceanic crust, at an average along-margin separation of 90 km. The average line length is approximately 320 km. In addition, 3437 km of fair to moderate quality, 4-fold, high-speed seismic data were recorded mainly over the mid to upper continental slope.

The interpretation of these data can best be considered in terms of three discrete sectors that are defined on the basis of their breakup histories — the Greater India–Antarctica, Greater India–Antarctica–Australia and Australia–Antarctica sectors.

Greater India–Antarctica sector (38–84°E)

This part of the Antarctic continental margin formed during the breakup of the eastern margin of Greater India and East Antarctica, which culminated with the onset of seafloor spreading in the Valanginian. The geology of the margin and the adjacent oceanic crust is divided into distinct east and west sectors by a crustal boundary at approximately 58°E. Across this boundary, the continent–ocean boundary (COB), defined as the inboard edge of unequivocal oceanic crust, steps outboard from west to east by about 100 km.

Structuring in the sector west of 58°E is largely controlled by the mixed rift–transform setting. The edge of the onshore Archaean–Proterozoic Napier Complex is downfaulted oceanwards near the shelf edge by at least 6 km and these rocks are interpreted to underlie a rift basin beneath the continental slope. The thickness of rift and pre-rift rocks cannot be accurately determined with the available data, but they appear to be relatively thin. The margin is overlain by a blanket of post-rift sedimentary rocks that are up to 6 km thick beneath the lower continental slope.

The COB in this sector is interpreted from the seismic reflection data and potential field modelling to be marked by a basement depression at 8–8.5 s two-way time, approximately 170 km oceanwards of the shelf-edge bounding fault system. Oceanic crust in this sector is highly variable in character, from rugged with a relief of more than 1 km over distances of 10-20 km, to rugose with low-amplitude relief superimposed on a long-wavelength undulating basement.

The sector east of 58°E formed in a normal rifted margin setting, with complexities in the east from the underlying structure of the N–S trending Palaeozoic Lambert Graben. The Napier Complex is downfaulted to depths of 8–10 km beneath the upper continental slope, and the margin rift basin is more than 300 km wide. As in the western sector, the rift-stage rocks are probably relatively thin. This part of the margin is blanketed by post-rift sediments that are up to about 8 km thick.

The interpreted COB in the eastern sector is the most prominent boundary in deep water, and typically coincides with a prominent oceanwards step-up in the basement

level of up to 1 km. As in the west, the interpretation of this boundary is supported by potential field modelling. The oceanic crust adjacent to the COB in this sector has a highly distinctive character, commonly with 1) a smooth upper surface underlain by short, seaward-dipping flows; 2) a transparent upper crustal layer; 3) a lower crust dominated by dipping high-amplitude reflections that probably reflect intruded or altered shears; 4) a strong reflection Moho, confirmed by refraction modelling; and 5) prominent landward-dipping upper mantle reflections on several adjacent lines. A similar style of oceanic crust is also found in contemporaneous ocean basins that developed between Greater India and Australia–Antarctica west of Bruce Rise on the Antarctic margin, and along the Cuvier margin of northwest Australia.

Greater India–Antarctica–Australia sector (84–105°E)

This sector of the Antarctic continental margin was formed by the overprinting of the Early Cretaceous separation of Greater India from Antarctica–Australia by the Late Cretaceous breakup of Australia and Antarctica. Margin structuring is often complex, particularly in deep water, and it can be difficult to discriminate between primary and overprinted structures.

Because of the extensive permanent ice cover in this area, there is no seismic coverage of the continental shelf and only very sparse lines on the upper continental slope. As there are also no seabed samples from the shelf and uppermost slope we have no direct knowledge of the geology of this area. However, as with the sectors to the east and west, it is likely that the shelf edge is underlain by a major fault system with crystalline basement being down-faulted oceanwards to depths of several kilometres.

The continental slope is dominated by the mid-slope plateau of the Bruce Rise. Seismic coverage of this structure is limited, except on the plateau margins which are crossed by Japanese lines and Survey GA-228 and GA-229 lines. The Japanese have also recovered three dredge samples from the eastern margin of the Bruce Rise that contained granite, schist and sandstone; however, these rocks have been interpreted as being ice-rafted.

Seismic data show that the Bruce Rise is very similar to the conjugate feature on the Australian margin, the Naturaliste Plateau, being underlain by shallow acoustic basement, with faulted pockets of interpreted Jurassic–Cretaceous sediments. Both plateaus are covered with a veneer of ?Cainozoic sediments a few hundred metres thick. The eastern and northern margins of the Bruce Rise are sharply defined: the extremely steep, northwest-trending eastern margin is underpinned by the Vincennes Fracture Zone, while the E–W trending northern margin is down-faulted by at least 3 km across several major, high-angle faults. The western margin of the Bruce Rise is poorly-defined, with no seismic lines extending landward of the lower slope.

The deep ocean basin adjacent to the Bruce Rise (the Shackleton Basin) is highly variable in structure and seismic character and its origins are enigmatic. Between the western flank of the Bruce Rise and the eastern end of Princess Elizabeth Trough, the crust appears to be oceanic. Potential field modelling, the identification of Early Cretaceous seafloor spreading magnetic anomalies and similarities of seismic character with oceanic crust in the Enderby Basin, suggest that this crust was generated during the separation of Greater India from Australia–Antarctica. In contrast, the basement between the northern flank of the Bruce Rise and the fast-

spreading crust of the Australian–Antarctic Basin to the north has seismic characteristics suggesting that, despite the presence of interpreted seafloor spreading magnetic anomalies, there may be fragments of continental crust that have been left stranded in an overall setting of oceanic crust. Alternatively, these fragments may comprise oceanic crust that has subsequently been faulted during the period of very slow spreading between Australia and Antarctica in the Late Cretaceous. A small, triangular-outline crustal fragment east of the Vincennes Fracture Zone is also enigmatic. Satellite gravity data suggest that it was also formed during the separation of Greater India from Antarctica–Australia.

Australia–Antarctica sector (105–160°E)

West of 140°E, the margin in this sector was formed by mainly orthogonal rifting between Antarctica and Australia; these rift structures are largely oriented parallel to the margin. East of 140°E, margin formation was strongly influenced by the largely strike-slip separation of Antarctica from southeast Australia and the South Tasman Rise.

As with other sectors of the AAT continental margin, the shelf edge and upper slope are probably underlain by a major basin-bounding fault system, beyond which the crystalline basement underlying much of the shelf and immediate hinterland are down-faulted oceanwards by several kilometres. Beyond this fault zone, the slope is underlain by the depocentre of a major rift basin that extends for at least 1500 km along the margin offshore from Wilkes Land and Terre Adélie. Beneath this depocentre, the crust thins oceanwards through extensive faulting of the rift and pre-rift sedimentary section and by dominantly ductile deformation of the crystalline crust. The maximum thickness of sedimentary rocks in the rift basin is at least 7 km. Seismic correlations with the conjugate Australian margin suggest that the major sedimentary unconformities can be dated as being of base Turonian, late Maastrichtian and early Middle Eocene age.

Outboard of the depocentre, a 90 to 180 km-wide continent-ocean transition zone is interpreted to consist primarily of continental crust with magmatic components that can account for the lineated magnetic anomalies that have been interpreted in this zone. The thick sedimentary section in the COT zone is floored by dense lower crustal or mantle rocks indicating massive (>10 km) thinning of the lower and middle crust in this zone.

The boundary between the inner depocentre of the margin rift basin and the COT is commonly marked by a basement ridge which potential field modelling indicates is probably composed of altered/serpentinised peridotite. This ridge is similar in form and interpreted composition to a basement ridge located in a similar structural position at the inboard edge of the COT on the conjugate margin of the Great Australian Bight. Both ridges are probably the product of mantle up-welling and partial melting focussed at the point of maximum change/necking of crustal thickness.

Integrated deep-seismic and potential field interpretations and dredged rock samples of continental origin off Terre Adélie indicate very strongly that the boundary between unequivocal oceanic crust and largely continental crust of the continent–ocean transition lies in very deep water, and well seaward of earlier interpretations. The continent–ocean boundary is considered to be well-constrained from 124–131°E and unequivocal from 131–140°E, but more debatable in the sector from 110–124°E.

INTRODUCTION

The 1982 United Nations Convention on the Law of the Sea (UNCLOS) defines a nation's legal seabed and subsoil jurisdiction as extending throughout its Continental Shelf[1]. Where the continental margin of a nation extends beyond 200 nautical miles (the nation's Exclusive Economic Zone, or EEZ), the outer limit of the 'legal' Continental Shelf is defined by a series of rules contained within Article 76 of UNCLOS (UNCLOS, 1983). These rules require definition of the foot of the continental slope, knowledge of sediment thickness and good bathymetric information defining the 2500 m bathymetric contour. Where the Continental Shelf extends beyond 200 nautical miles (M), its location must be defined at an interval of no more than 60 M. Therefore, in those areas of 'extended Continental Shelf' a comprehensive seismic and bathymetric database, together with a detailed understanding of the continental margin geology, is essential to optimising the extent of the Continental Shelf.

On December 2, 1999, the Ministers for Foreign Affairs & Trade and Environment & Heritage announced that Australia would carry out the necessary work to place Australia in a position to be able to prepare a submission delineating the extended Continental Shelf off the Australian Antarctic Territory (AAT). Such a submission would have to be made to the UN Commission on the Limits of the Continental Shelf (CLCS) by November 16 2004.

Under the Cabinet Decision, funding was provided for the then Australian Geological Survey Organisation (now Geoscience Australia), the then Australian Surveying and Land Information Group (AUSLIG; now National Mapping Division of Geoscience Australia) and the Australian Antarctic Division to carry out the necessary data acquisition and processing and to undertake the interpretation of the data. In early 2000, management of the project (the Australian Antarctic and Southern Ocean Profiling Project, AASOPP) was taken over by the Department of Finance and Administration who handled this task until the completion of all the major acquisition in late 2003.

Marine geophysical surveys were conducted for the Australian government by an industry contractor, Fugro Geoteam AS, from January–April, 2001, and January–April, 2002. These surveys (Geoscience Australia surveys GA-227, GA-228 and GA-229) acquired more than 20 000 km of deep-seismic, magnetic and gravity data and more than 3400 km of high-speed seismic data along the margin of East Antarctica from approximately 38°E to 160°E (Fig. 1). This report provides a summary of the interpretation of these data.

[1] The legal Continental Shelf, defined by a complex series of rules or formulae, is quite distinct from the geomorphic continental shelf as understood by a marine scientist. The legal Continental Shelf includes the geomorphic continental shelf, the continental slope, marginal plateaus and sometimes the continental rise and the inboard edge of the deep ocean floor.

BACKGROUND

BACKGROUND TO THIS REPORT

This report is the compilation of an interpretation that was carried out both inside and outside Geoscience Australia in the period 2001–2004. While the interpretation was coordinated by Geoscience Australia, the responsibilities for the scientific content of the component sections is as follows:

Seismic reflection – Geoscience Australia

Seismic refraction – Geoscience Australia

Synthesis of geological samples – Geoscience Australia

Potential field modelling – N.G. Direen (University of Adelaide) with input from Geoscience Australia

Plate kinematics – B.J. Brown (University of Sydney) with input from Geoscience Australia.

PREVIOUS DATA

While the interpretation contained in this report is based primarily on data acquired by Australia under the Australian Antarctic and Southern Ocean Profiling Project (AASOPP), a range of other surveys and data sources were also integrated into the study. The following section comprises a brief summary of the most important of these data sets.

Bathymetry

Although bathymetric data are routinely recorded on most research surveys off Antarctica, the distribution of ship tracks is extremely irregular, and tends to be concentrated in relatively ice-free areas and on the approaches to Antarctic bases.

The main source of gridded bathymetric data for this report is the 2 arc-minute predicted bathymetry of Smith et al. (1997; Plates 1 & 2), derived principally from the satellite altimeter gravity data set. The accuracy of these data is dependent both on the accuracy of the original altimeter data and on the algorithm used to predict the bathymetry. These data are an invaluable aid to understanding the regional morphology, given the sparseness and irregularity of conventional survey data.

Digital contour strings are available from the General Bathymetric Chart of the Oceans (GEBCO; Jones et al., 1997) at a 500 m contour interval. These data are valuable for portraying the gross bathymetry of the Antarctic margin and have been used in the basemaps for this report (Plates 3–7).

Geological samples

Geological samples from the Antarctic continental margin are scarce, particularly so in the case of samples that are of value for the interpretation of seismic data. In brief, the available samples include:

Deep Sea Drilling Program (DSDP) and Ocean Drilling Program (ODP) sites in Prydz Bay Enderby Basin, the Australian-Antarctic Basin and the continental slope east of Bruce Rise.

Core samples from the Mac. Robertson Shelf and the continental shelf off George V Land.

Dredge samples from the eastern flank of Bruce Rise and from seamounts in deep water off Terre Adélie.

Details of the relevant samples are given in the separate interpretation chapters, while a listing of all the samples is included as Appendix 2.

Seismic reflection

Since early 1982, a number of multichannel seismic (MCS) surveys have been acquired off East Antarctica, in the area covered by this report. The locations of these surveys are shown in Plates 3–7 and acquisition details are included in Appendix 3. These surveys include:

GA Survey 33 (Australia; Stagg, 1985): Approximately 5000 km of 3- and 6-fold data of fair to moderate quality were recorded by Geoscience Australia (then BMR) in 1982 on a regular grid of lines in Prydz Bay, on the Mac. Robertson Shelf and on the adjacent upper continental slope.

TH82 (Japan; Sato et al., 1984): 820 km of 6-fold data of fair quality were recorded by the Japan National Oil Corporation in 1982/83 along 3 lines off Terre Adélie. One line provides a tie to DSDP Site 269.

ATC82 (France; Wannesson et al., 1985): 3190 km of 24-fold data of moderate to good quality were recorded by the Institut Français du Pétrole in 1982 along a set of lines off Terre Adélie and western George Land. One line is tied to DSDP Site 269.

TH83 (Japan; Tsumuraya et al., 1985): 3700 km of 6-fold data of fair to moderate quality were recorded by the Japan National Oil Corporation in 1983/84 along lines between western Wilkes Land and Terre Adélie. The data set comprises several widely-spaced dip lines tied by a 1400 km-long margin strike line.

L184AN (USA; Eittreim & Smith, 1987): 1800 km of 24-fold data of moderate to good quality were recorded along lines off eastern Wilkes Land, Terre Adélie and western George V Land. The data set comprises 14 dip, strike and margin-oblique lines.

TH84 (Japan; Mizukoshi et al., 1986): 2350 km of 6-fold data of fair to moderate quality were recorded by the Japan National Oil Corporation in 1984/85. The widely-spaced grid of lines are mainly located offshore from Prydz Bay, although two lines extend on to the outer continental shelf of Prydz Bay.

TH89 (Japan; Nakao, 1990): 1836 km of 6-fold data of fair to moderate quality were recorded by the Japan National Oil Corporation in 1989/90. The data set comprises a small grid of mainly E-W oriented lines in Prydz Bay, a single long line from Prydz Bay to the southern Kerguelen Plateau, and a short line from the Enderby Basin to the southern Kerguelen Plateau.

TH94 (Japan; Ishihara et al., 1996): 2377 km of 12-fold data of moderate quality were recorded by the Japan National Oil Corporation in 1994/95. A widely-spaced set of six dip lines was recorded between the eastern flank of Bruce Rise and central Wilkes Land. These lines were tied with a single margin strike line and a further two short lines were recorded over the flank of Bruce Rise.

TH95 (Japan; Tanahashi et al., 1997): 1978 km of 21- and 24-fold data of moderate to good quality were recorded in the Victoria Land Basin of the Ross Sea and off Terre Adélie. Four of these lines were recorded off Terre Adélie.

TH98 (Japan; Murakami et al., 2000): 2490 km of 30-fold data of moderate to high quality were recorded by the Japan National Oil Corporation in 1998/99. The data set comprises a number of dip lines and two margin strike lines in the Princess Elizabeth Trough, Shackleton Basin (new name in this report), and on the northern and western flanks of Bruce Rise.

TH99 (Japan; Joshima et al., 2001): 2195 km of 30- and 60-fold data of good quality were recorded by the Japan National Oil Corporation in 1999/2000. The data set comprises seven dip lines and one margin strike line mainly to the northwest of Prydz Bay. A single line was shot into central Prydz Bay.

Russian surveys: A large number of surveys have been carried out by the Soviet Antarctic Expeditions (SAE) and the Russian Antarctic Expeditions (RAE) since the mid-1980s. Some of the later surveys were carried out collaboratively with Norway. These surveys used a number of different platforms and recording configurations and the data range from fair quality for the oldest surveys to moderate for the more recent surveys. The surveys concentrated on the Antarctic margin from eastern Dronning Maud Land to Princess Elizabeth Trough. Reports of these surveys are very limited.

GA Survey 217 (Italy & Australia; Brancolini & Harris, 2000): 1827 km of 12-fold data of moderate quality were acquired jointly by the Italian and Australian National Antarctic Research Programs. The data were recorded along a detailed network of lines on the continental shelf and upper slope off western George V Land.

Velocity information

While a large number of sonobuoy stations were recorded prior to Surveys GA-228 & GA-229 on the margin of the AAT, velocity solutions are not always available, and the quality of many of the solutions that are available is uncertain. In some cases, solutions are only available graphically in published papers (e.g. Sato et al., 1984). The locations of sonobuoy stations and summaries of the velocity solutions are included in Appendix 4.

The sonobuoy data sets include:

Japan: The Japan National Oil Corporation (JNOC) has routinely deployed sonobuoys on its multiple surveys off the AAT. These surveys have included TH82 off Adélie Land (Sato et al., 1984; 3 stations, with results); TH83 off Wilkes Land (Tsumuraya et al., 1985; 19 stations, results not published); TH84 in and offshore from Prydz Bay (Mizukoshi et al., 1986; 10 stations, with results); TH89 in and offshore from Prydz Bay (Nakao, 1990; 10 stations, results not published); TH94 offshore from Budd Coast (Ishihara et al., 1996; results published for 4 OBS stations); TH98 offshore from Queen Mary Land (Murakami et al., 2000; results published for 2

OBS stations). No refraction stations were recorded for survey TH99, offshore from Prydz Bay (Joshima et al., 2001).

United States: The US Geological Survey (USGS) recorded 30 sonobuoy stations during the survey L1-84-AN off Wilkes Land in 1984. The results from these stations (head-waves and wide-angle reflections) are reported in Childs & Stagg (1987).

Russia: The Soviet Antarctic Expeditions (SAE) have recorded a number of sonobuoy stations in Prydz Bay and the adjacent deep ocean basins. However, details of these stations are not available, other than a small-scale map contained in Leitchenkov et al. (1990) which shows about 18 stations, and velocities included in a potential field model discussed in Gandyukhin et al. (2002).

Potential field

Potential field data (gravity and/or magnetic data) have been recorded on many Antarctic geophysical surveys since the early 1980s. In addition, satellite gravity coverage of offshore Antarctic is also available. The distribution and availability of these datasets is discussed elsewhere in this report by B.J. Brown.

NEW DATA: AUSTRALIAN ANTARCTIC & SOUTHERN OCEAN PROFILING PROJECT

Under the Australian Antarctic and Southern Ocean Profiling Project (AASOPP), data were acquired on three contract surveys offshore from the Australian Antarctic Territory, as follows:

Survey GA-227: 3437 km of 4-fold data of fair to moderate quality were recorded for the Australian government by Fugro Geoteam AS in early 2001. The data were recorded along dip lines mainly on the upper continental slope between eastern Dronning Maud Land and George V Land.

Survey GA-228 & GA-229: 10612 km (Survey GA-228) and 9607 km (Survey GA-229) of 36-fold data of very high quality were recorded for the Australian government by Fugro Geoteam AS in early 2001 and early 2002. The data were recorded along dip lines across the continental slope and deep ocean basins between eastern Dronning Maud Land and George V Land. The inboard ends of many of the lines tie in to the Survey GA-227 lines.

During Surveys GA-228 and GA-229, a total of 120 sonobuoys were deployed for the recording of refraction and wide-angle reflection data. Sonobuoys were recorded coincidentally with the reflection seismic data using the airgun array as the source. None of the sonobuoy profiles was reversed. Of the sonobuoys deployed, 97 recorded wide-angle reflections and/or refraction events that could be analysed for velocities. Of these stations, 80 provided 'basement' velocities in the range 5.0-7.5 $km.s^{-1}$, and 33 provided velocities of $\geq$7.6 $km.s^{-1}$. Appendix 5 lists the velocity solutions for all these sonobuoys. The locations of the sonobuoys are shown on maps in Plates 3–7 and on the reflection seismic profiles in Plates 10–19.

MORPHOLOGY OF THE AAT MARGIN

INTRODUCTION

The morphology of the margin of the region of the AAT is shown as three-dimensional images in Plates 1 and 2 and Figures 2–4, and as contours in Plates 3–7.

The development of the margin of the AAT has been dominated for the past ~35 million years by glacial processes that have produced a morphology very different to 'normal' passive continental margins. The morphologic shelf and slope are particularly affected by ice loading on the continent, and by erosion and depositional processes arising from the interaction of the outlet ice streams and the Circum-Antarctic Current.

Anderson (1991) noted that the shelf is characterised by:

- an average depth of 500 m, approximately eight times the world average;
- rugged topography;
- highly variable and commonly broad width; and
- a typical profile that deepens towards the continent, in contrast to continental shelves in more temperate regions.

The nearshore margin of the shelf off Antarctica is often more than 600 m deep, and occasionally attains depths of more than 1000 m in narrow troughs near the coast. The shelf break typically lies at depths of 300-400 m.

Whereas much of the southern Australian margin has been generally starved of sediments since breakup, and hence has a physiography reflecting pre-breakup tectonics, the AAT margin is markedly different. Off the AAT, there has been a very large thickness of sediments deposited, much of it during the Cainozoic, and the effect has been to blanket most of the rift structures beneath up to 6 km of marine deposits. A consequence of this depositional environment is that seabed gradients are typically lower than on most other continental margins. Most of the post-breakup sedimentary section is continuous from the continental shelf out to the deep ocean basin.

The AAT continental margin rarely exhibits the classic form of a continental margin. Kennett (1982) states that the slope gradient on a non-glaciated margin averages about 4^{o} and is greater than 1:40 (~1.4°); in contrast, the continental rise is marked by a gentle seaward gradient of 1:100 to 1:700 (~0.57–0.1°). However, the margin of the AAT typically shows a steep upper slope with gradients of 1° to >6°, and a lower slope with gradients of <0.4° to about 1°. The slope is frequently incised by canyons and its lowest part is commonly modified by sediment drifts and channels. The lower slope is typically wide (up to several hundred kilometres).

The approximate 5500 km length of the AAT margin can be divided into segments that have characteristic morphologies. The remainder of this section will briefly describe the morphology of each sector.

ENDERBY LAND (38–58°E)

Controlling factors: Breakup between Greater India and Antarctica; post-breakup sediment drifts and canyons.

Description: The margin off Enderby and Kemp Lands is characterised by a narrow continental shelf (30–70 km) and a continental slope that is dominated by spur and canyon topography for 150–250 km oceanwards from the shelf edge. The upper slope, in particular, is characterised by closely-spaced, small-scale spurs and canyons. Down-slope, these features coalesce into broad (70–90 km width) spurs and canyons with up to 1000 m of relief that merge with the northwest-deepening Enderby Basin at more than 4500 m depth.

Gradients on the continental slope are highly variable, due to the local topography. The upper slope has an average gradient of about 1.5–2°. At approximately 3000 m depth, the gradient decreases to generally less than 1°, although local gradients can be more than 10° on the walls of canyons.

OFFSHORE PRYDZ BAY (58–80°E)

Controlling factors: Breakup between Greater India and Antarctica; sediment discharge from Prydz Bay.

Description: The shelf in this sector is highly variable in width, ranging from <100 km on the Mac.Robertson Shelf in the west, to more than 280 km in central Prydz Bay, and about 180 km east of Prydz Bay. Prydz Bay is the outlet for the Lambert Glacier, the largest ice stream in East Antarctica; sediments derived from the Lambert Glacier are the major controlling factor for the margin morphology. The Mac.Robertson Shelf is notable for the inshore Nielsen Basin, which descends to more than 1300 m depth.

West and east of Prydz Bay, the upper continental slope is steep, with gradients typically more than 5° down to about 3000 m depth. The surface of the upper slope is extensively incised by small-scale canyons. Below the upper slope, the margin is dominated by large-scale fans and troughs (Wild Drift; Wild Canyon; Prydz Channel trough mouth fan). These features extend for more than 250 km from the upper slope and are characterised by their broad, low relief. Bathymetric profiles from the shelf edge to the eastern Enderby Basin typically approximate the form of a catenary with no significant breaks in gradient.

PRINCESS ELIZABETH TROUGH (80–87°E)

Controlling factors: Breakup between Greater India and Antarctica; proximity of southern Kerguelen Plateau.

Description: The morphology of this part of the continental margin is quite simple. The shelf is broad, with a width of 100–200 km, and is partially permanently covered by the West Ice Shelf. The upper slope is steep, with gradients of as much as 10–20°. At 2000–2500 m depth this breaks to a lower slope with gradients of 1–2° down to about 3000–3500 m. Below this, the seabed slopes more gently down to the axis of the Princess Elizabeth Trough at about 3800 m, northwards of which it shallows towards the southern Kerguelen Plateau.

WILHELM II – QUEEN MARY LANDS (87–108^{O}E)

Controlling factors: Interaction of breakup between Greater India and Antarctica, and between Australia and Antarctica.

Description: This is one of the morphologically complex parts of the margin of the AAT. The shelf is highly variable in width, ranging from ~100–150 km wide to the east and west of Bruce Rise, to about 250 km wide in the centre of the sector, inboard of Bruce Rise. Approximately 30% of the shelf in the central sector is covered by the permanent ice of the Shackleton Ice Shelf.

West of the Bruce Rise, the shelf edge is strongly linear with an ENE–WSW trend, probably reflecting the earlier Greater India-Antarctica breakup phase. Canyon development on the upper slope is muted in this area. The gradient of the upper slope is about 7° down to about 2000 m depth. Below this depth, there are consistent gradient segments of about 1–1.5° and 0.6° and less. There is some canyon development on the lower slope.

East of the Bruce Rise, the shelf edge generally trends ESE-WNW, being more affected by Australia-Antarctica breakup. Canyon development on the upper slope is widespread and gradients are far more variable than to the west. While the overall gradient of the slope is low, generally less than 1°, local gradients can also be more than 10°. Despite the low gradients, the area is strongly incised by canyons down to depths of 3500–4000 m.

This segment of the margin is dominated by the Bruce Rise, the only significant marginal plateau off the AAT. It comprises two distinct parts, separated by a northwest-trending canyon (Bruce Canyon) that incises more than 1000 m into the seabed and debouches on to the lower slope at more than 3500 m depth. The eastern half of the Bruce Rise is the shallower, at less than 1500 m depth. It is bounded by the upper slope to the south, the aforementioned canyon to the west, an E-W trending rugged lower slope with average gradients of 3–4° to the north, and the NW-SE trending Vincennes Fracture Zone (Tikku & Cande, 1999) to the east. The western half of the Bruce Rise is deeper than the eastern half, at slightly less than 2000 m, and its flanks are less well-defined.

North of the Bruce Rise, the deep ocean basin lies at depths close to 4500 m. It is notable that the bathymetry does not reflect the major spreading history and basement depth change at the northern ends of several lines that is strongly reflected in the satellite gravity.

WILKES LAND – TERRE ADÉLIE (108–140°E)

Controlling factors: Breakup of Australia and Antarctica; post-breakup sediment drifts and canyons.

Description: The generally E-W striking Wilkes Land and Terre Adélie margins formed during the normal rifting of Australia and Antarctica and have a relatively consistent morphology along their 1400 km length. The shelf is broad (100–200 km width) and contains some characteristic inner shelf basins with depths greater than 1000 m (cf. Mac.Robertson Shelf above).

As with much of the AAT margin, there is an upper slope with gradients of 2–4° that extends down to about 2000 m. There is then a distinct gradient change to a lower

slope down to ~3500 m depth with gradients between 0.7–1.4°. Beyond this lower slope province, gradients are variable between 0.2–0.6°. The slope in this sector is extensively incised by canyons or valleys that extend from the shelf edge out to the edge of the abyssal plain at about 4000 m depth.

GEORGE V LAND (140–160°E)

Controlling factors: Breakup of Australia and Antarctica; strike-slip tectonics.

Description: The morphology of the George V Land sector is strongly influenced by the strike-slip motion between East Antarctica and southeast Australia, prior to clearance of the plates in the Oligocene. The shelf is highly variable in width, ranging from about 120 km in the west of the sector, to almost 300 km at about 150°E. Much of this shelf is semi-permanently covered by ice, and little is known of its morphology.

The morphology of the slope is similarly variable. In the west of the sector, where the plate tectonic setting is more rift-derived than strike-slip, the upper slope has gradients that average 3° but are locally from 10–20°. At 2000–3000 m depth, the gradient abruptly decreases to less than 1°, with this gradient being fairly consistent down to the deep ocean basin at about 3500 m depth. The slope in this sector is extensively incised by canyons that generally trend oblique to the slope.

In the easternmost part of this sector, where the major fracture zones between western Tasmania and Antarctica converge with the Antarctic margin, the slope has a quite simple morphology. The upper slope is steep (5–20°) and extends down to 2000–2500 m depth. Beyond this province, gradients are low (~0.5°) and depths increase gradually to about 3000 m. The deep ocean basin here shows strong NW-SE trending relief, reflecting both the fracture zone traces and the thin sediment cover.

ONSHORE GEOLOGY

The metamorphic rocks of Enderby Land consist of the Archaean Napier Complex (granulite facies) bounded to the south by the Proterozoic Rayner Complex, a lower grade reworking of the Napier Complex. No unmetamorphosed sedimentary rocks have been found from the area.

In the Mac.Robertson Land-Prydz Bay area, most of the onshore rock exposures occur along the coast and inland in the Prince Charles Mountains chain, which extends south of Prydz Bay for at least 600 km. Most exposures consist of Precambrian metamorphics, metasediments, and intrusives. The only known onshore outcrops of Phanerozoic sedimentary rocks are coal-bearing Permian continental strata in the Beaver Lake area, more than 200 km south-southwest of Prydz Bay (Mond, 1972).

The Prince Charles Mountains are exposed along the flanks of, and in, a regional ice-surface depression caused by ice drainage through the Lambert Glacier. Gravity surveys (Wellman & Tingey, 1976) and deep seismic soundings (Kurinin & Grikurov, 1982; Fedorov et al., 1982) showed that a major graben structure underlies the Lambert Glacier and Amery Ice Shelf and extends inland for almost 700 km. Soviet aeromagnetic data offshore suggest that the Lambert Graben continues into Prydz Bay, and this is confirmed by marine seismic surveys (e.g. Stagg, 1985).

In the area of Princess Elizabeth-Wilhelm II Lands, the only known coastal outcrops are of Precambrian granulite facies metamorphic rocks and Cainozoic volcanics.

In Queen Mary Land, the coastal outcrops again consist of Precambrian granulite facies and charnockite bodies. No sedimentary rocks have been reported from the coastal strip, but Cambrian sandstones are abundant in moraines and crop out inland.

Along the coastline of Wilkes Land, rare onshore outcrops consist of Precambrian granulite facies and charnockite bodies. Coastal outcrops in Terre Adélie and western George V Land contain more unmetamorphosed sedimentary rocks than are usually found in East Antarctica. In addition to the Precambrian granulite facies and charnockite bodies, common to much of the East Antarctic Shield, Beacon Group sediments (blue and purple shale, sandstone, and argillaceous sandstone; Mawson, 1942) overlain by ?Jurassic dolerite have been found in the cliffs of Horn Bluff (approximately 150°E). Davey (1985) suggested that sediments of Beacon Group age (Permian – Jurassic) may also be present deep under the margin.

Steed (1980, 1983) and Steed & Drewry (1982) have interpreted a major sub-ice basin beneath the eastern AAT (Wilkes Basin), from radio echo-sounding data. Steed (1983) concluded that the basin is sedimentary in origin and developed by tensional growth and subsidence similar to the development of the North Sea Basin.

Beacon Group sediments are found in the west of George V Land at Horn Bluff, while Upper Precambrian metasediments and older Precambrian medium- to high-grade metasediments and metavolcanics are found in the east. The Horn Bluff dolerites are an important potential geological tie to Australia.

PLATE KINEMATICS

B.J. Brown

INTRODUCTION

The East Antarctic continental margin between 30°E and 160°E is a key to reconstructing the breakup and separation history of India, Australia and Antarctica. To date, this history has been poorly understood because of the limited and widely spaced data coverage. However, marine surveys conducted by a number of countries since the early 1990s have vastly improved shiptrack data coverage across the East Antarctic margin. Data agreements developed in association with this project have provided a unique opportunity to compile virtually all the available marine potential field data between longitudes 30°E and 160°E. In particular, the improved coverage of magnetic anomaly data has allowed the application of gridding techniques to augment more conventional profile-based identification of magnetic anomaly lineations. This has allowed the development of models for the timing and orientation of breakup and seafloor spreading, thereby documenting the separation of India and Australia from Antarctica.

A series of maps are presented here that show:

- satellite gravity images of the study area (from McAdoo & Laxon, 1997; Figs 5, 8, 13, 18, 23 & 28);
- the shiptrack coverage of marine geophysical data (Figs 9, 10, 14, 15, 19, 20, 24, 25, 29 & 30);
- the newly collated magnetic anomaly data shown as profiles superimposed on the satellite gravity (Figs 11, 16, 21, 26 & 31), as selected stacked profiles (Figs 33 & 34) and the resulting gridded magnetic anomaly maps (Figs 12, 17, 22, 27 & 32) ; and
- refined Mesozoic plate reconstructions derived from an interpretation of the early seafloor spreading history between East Antarctica, India and Australia (Figs 35 & 36).

In addition, the satellite gravity data and gridded magnetic anomaly data are shown for the entire margin in Plate 8.

BACKGROUND

The fragmentation of Gondwana and changes in global plate motions provide a general framework for the breakup and dispersal of the Australian, Antarctic and Indian continents. From the Early Jurassic to mid-Cretaceous, East and West Gondwanaland broke apart as Africa, Madagascar and India separated from Antarctica, and South America split from Africa. Early seafloor spreading developed at about 155 Ma (early Late Jurassic) between Africa and Dronning Maud Land in Antarctica. The separation of Greater India from Western Australia commenced in the Argo Abyssal Plain also during the Jurassic (~155 Ma), and propagated southwards, via the Gascoyne Abyssal Plain and Cuvier Basin, to the Perth Basin in the mid-Cretaceous (~136 Ma). The timing of seafloor spreading between Antarctica and India has not been as well-constrained due to sparse data. The uncertainty in

magnetic anomaly identification in the Bay of Bengal on the conjugate Indian margin and sparse data coverage in the Enderby Basin off the Antarctic margin has led to two alternative models for Cretaceous plate reconstructions for the Indian Ocean. These models assume either Mesozoic M-sequence (120 Ma and older) crust exists in the Enderby and Bengal Basins, or that mainly Cretaceous Quiet Zone (~118–83.5 Ma) crust developed between India and Antarctica (e.g. Royer & Coffin, 1992; cf. Powell et al., 1988).

Continental breakup and seafloor spreading propagated anti-clockwise around Australia through time (Veevers, 2000). Slow seafloor spreading began between Australia and Antarctica in the Late Cretaceous, with the precise timing of onset still being debated (~83 Ma, according to Sayers et al., 2001). Seafloor spreading in the south Tasman Sea, between eastern Australia and Lord Howe Rise and New Zealand, began in the late Cretaceous (~83 Ma) and propagated northwards to the Coral Sea in the Tertiary, where spreading stopped at about 52 Ma (Gaina et al., 1998). The Late Cretaceous (~61 Ma) marked the end of the first phase of Indian Ocean spreading in a probable NW-SE direction, and the onset of a second phase of spreading on a N–S azimuth (Veevers, 2000). At about 43 Ma (Middle Eocene), a major change in motion of the Pacific Plate is documented by the bend in the Hawaii-Emperor seamount chain. At the same time, rapid seafloor spreading commenced in the Australian-Antarctic Basin (AAB) as Australia continued to move northwards from Antarctica (Cande & Mutter, 1982), with the final clearance of the Australian and Antarctic Plates southwest of the South Tasman Rise taking place by the Early Oligocene (~33.5 Ma; Exon et al., 2002). This resulted in the establishment of open marine conditions and the subsequent development of the Circum-Antarctic Current in the Southern Ocean in the Miocene.

Seafloor spreading and plate reconstruction models between Australia and Antarctica have been presented by König & Talwani (1977), Talwani et al. (1979), Cande & Mutter (1982), Mutter & Cande (1983), Mutter et al. (1985), Veevers (1986, 1988), Veevers et al. (1990), Royer & Rollet (1997) and Tikku & Cande (1999, 2000). Tikku & Cande (1999) have produced the most recent plate tectonic model of continental breakup and separation between Australia and Antarctica. They reappraised the older magnetic anomalies using magnetic data from the conjugate Australian and Antarctic margins, and new Japanese magnetic data from the Wilkes Land margin of Antarctica combined with satellite-derived free air gravity data to determine the earliest seafloor spreading magnetic anomalies. Seafloor spreading magnetic anomalies younger than chron 20 (~43 Ma) can be identified with confidence, but synthetic magnetic anomaly profiles based on the global geo-magnetic reversal time scale (Cande & Kent, 1995) do not provide an unequivocal fit to the observed magnetic anomaly sequence between chron 20 (~43 Ma) and chron 34 (~83 Ma). The stage rotation pole and plate reconstruction model from this interpretation (Tikku & Cande, 1999, 2000) indicates rift propagation from east to west, contradicting the sedimentary record that shows progressive marine inundation from west to east (e.g. Totterdell et al., 2000). The model also indicates slow to very slow initial spreading rates, possibly with a spreading hiatus, or deformation of early oceanic crust. These results led to the suggestion that magnetic anomalies older than chron 31 (~68 Ma) may not be representative of sea-floor spreading alone (Tikku & Cande, 1999).

MARINE POTENTIAL FIELD DATA IN THE REGION OF THE AAT

Figures 10, 15, 20, 25 and 30 show the magnetic data coverage that is now available from the recent compilation. For this study, virtually all the potential field data collected in the offshore region from 55–70°S and 30–160°E has been integrated. The maps presented are divided into five geographic sectors along the margin:

- Sector One (30–60°E) and Sector Two (60–90°E) cover the area conjugate to the east coast of India, and are referred to here collectively as the 'Greater India–Antarctica segment' (~30–90°E; GI–A segment) lying offshore from Enderby, Kemp, Mac.Robertson, Princess Elizabeth and Wilhelm II Lands.
- Sector Three (85–115°E) covers the area where India and Australia were formerly joined to Antarctica at a triple junction, in the region offshore from Princess Elizabeth, Wilhelm II and Queen Mary Lands, and is referred to here as the 'Greater India–Australia–Antarctica segment' (GI–A–A segment)..
- Sector Four (100–140°E) and Sector Five (130–160°E) cover the area conjugate to the Australian margin, which is referred to here as the 'Australia–Antarctica segment' (~100–160°E; A–A segment) lying offshore from Wilkes Land, Terre Adélie, and George V and Oates Lands.

The digital age grid of the ocean floor (Müller et al., 1997; Figs 6 & 7) shows the large area of seafloor of unknown age in most of the GI–A segment; in comparison, the age of seafloor in the GI–A segment has previously been dated as Late Cretaceous (see Tikku & Cande, 1999, and references therein). The paucity of data in the GI–A segment has produced uncertainty in models of the breakup of East Antarctica and India, and Mesozoic plate reconstructions of Gondwana in general. The data compilation presented here is an important opportunity to constrain the properties of the seafloor in the largely unknown region of the GI–A segment.

GREATER INDIA–ANTARCTICA SEGMENT

The GI–A segment includes the Enderby Basin, southern Crozet Basin, Princess Elizabeth Trough and the southern Kerguelen Plateau. The Enderby Basin is bounded to the south by the Antarctic margin, to the northeast by the Kerguelen Plateau, to the west by the Astrid Ridge and Astrid Fracture Zone, and to the northwest by the Crozet Basin. Princess Elizabeth Trough, east of the Enderby Basin, is a narrow bathymetric trough separating the southernmost Kerguelen Plateau from the Antarctic margin and is probably underlain by oceanic crust. The Enderby Basin is up to 4500–5000 metres deep adjacent to the Kerguelen Plateau, and up to 5000–5500 metres deep further west on the Enderby Abyssal Plain. The sediment thickness in the basin is generally 1–2 km, but it increases markedly towards the continental margin, masking the bathymetric and gravimetric expressions of fracture zones. This sediment masking effect is particularly pronounced offshore from Prydz Bay, where the seismic data presented in this report show the total sediment thickness to be ~3s TWT (ca. 5–6km) at the COB.

Recent Japanese, Russian and Australian survey data have significantly improved data coverage in parts of the GI–A segment. While the magnetic anomaly data coverage in the western Enderby Basin (~30–65°E) is still sparse north of 62°S, there is

reasonable coverage in the eastern Enderby Basin (~65–75°E). In the Enderby Basin, Princess Elizabeth Trough and southern Labuan Basin, magnetic anomalies trend approximately ENE; this indicates seafloor spreading occurred on a NNW azimuth, which is consistent with the contemporaneous spreading between India and Australia in the Perth Abyssal Plain.

GI–A segment – Sector 1

The area from 30–60°E extends from the Gunnerus Ridge, along the Kron Prinz Olav Coast (mainly Proterozoic Rayner Complex) to east of the Enderby Land Promontory (Archaean Napier Complex). There are no ODP/DSDP drill sites offshore this area.

Gravity field

There is a strong gravity edge effect at the continental shelf break (Fig. 8). This anomaly has a strong linear northeast trend that is offset to the southeast at a gravity high at about 47–48°E. At 52°E, the trend of the edge effect anomaly changes abruptly to east-southeast and the negative limb of the anomaly becomes more subdued.

Gravity anomalies on the upper continental slope strongly reflect the canyon and spur topography, suggesting that these sedimentary and erosional features are largely uncompensated. There is no obvious gravity expression of the underlying crustal structure.

Gravity trends in the Enderby Basin are very subdued, except to the north-northeast of the Gunnerus Ridge where there is a number of closely spaced lineations that trend slightly east of north.

The Enderby Basin is separated from the Crozet Basin to the northwest by the intense gravity expression of the NE-trending Kerguelen Fracture Zone. The trend of this fracture zone suggests that it is related to the younger spreading phase between Australia–Broken Ridge and Antarctica–Kerguelen. Some north-trending gravity anomalies appear to splay off the Kerguelen Fracture Zone into the Enderby Basin (see also Rotstein et al., 2001).

Magnetic field

While the Russian and Australian magnetic anomaly data (Figs 11 & 12) have added enough data to allow the interpretation of seafloor spreading anomalies, the coverage north of about 61°S is still very sparse.

The magnetic anomalies trend approximately ENE but they have low continuity and amplitude compared to the anomalies to the east in Sector 2 (cf. Figs 12 & 17). There are several factors that may account for this. Comparison of the oceanic basement topography from seismic reflection profiles (eg cf. line GA-229/35 in Sector 1 and line GA-228/07 in Sector 2) shows that basement topography in Sector 1 is very rugged while the basement topography in Sector 2 is generally very smooth. Given the location of the profiles, and the inferred separation azimuth of India and Antarctica, this area may be strongly affected by oceanic transforms; these would account for the rugged basement and would also suggest that the ENE trend of the anomalies is an aliasing effect caused by the wide line separation. The low continuity of the anomalies may also be partly due to the different survey methods used in acquiring the data – the Australian surveys used a conventional single-sensor

magnetometer, whereas the recent Russian surveys used a differential magnetometer with the data being processed to reduce the temporal effects.

Near the base of the upper continental slope, a magnetic trough is prominent on lines that extend this far south (e.g. GA-229/35, GA-229/38, GA-228/01); this anomaly approximately correlates with a trough in the gravity and bathymetry data and with a prominent basement depression in the seismic reflection data. To the south, the continental shelf is characterized by a high-amplitude magnetic anomaly observed in the gridded data (Fig. 12), which approximately follows the Prince Olav and Enderby Land promontory coastline, as far as the Edward VIII Gulf.

GI–A segment – Sector 2

Sector 2 (60–90°E) extends from the Mac.Robertson Land Coast (mainly Rayner Complex) to the Princess Elizabeth Land (Rauer Group Terrane) Coast. The inboard part of the margin includes Prydz Bay, the discharge point for the Lambert Glacier.

This sector is dominated by the Large Igneous Province (LIP) of the Kerguelen Plateau, which incorporates the Elan Bank micro-continent (Fig. 13). While the sector has been quite well sampled by the Ocean Drilling Program (ODP), none of the sites is located on oceanic crust, and hence are of no value in dating seafloor spreading magnetic anomalies.

Gravity field

The shelf break edge effect is a high-amplitude, lineated gravity anomaly. Offshore from the western half of Prydz Bay (69–74°E), the negative limb of this anomaly is interrupted by a prominent gravity high. While this anomaly approximately correlates with the Prydz Channel Fan (O'Brien & Leitchenkov, 1997), the amplitude of the anomaly suggests that it is due to an underlying crustal feature, perhaps a non-magnetic intrusion. However, reflection seismic data in this area (e.g. Stagg, 1985) do not show evidence for any such feature, at least in the shallow section.

Gravity anomalies in the eastern Enderby Basin are very subdued and primarily reflect the broad sedimentary fans and troughs that emanate from Prydz Bay. There is little evidence of any fracture zones or of the continent-ocean boundary, probably because of the extremely thick sediments. The only exception to this bland signature is south of Elan Bank, where some strong gravity lineaments appear to be sub-parallel to the Kerguelen Fracture Zone and the spreading azimuth of the Australian-Antarctic Basin, rather than to the interpreted spreading azimuth of the Enderby Basin.

North of the Enderby Basin, the gravity field is dominated by the positive anomalies of the Kerguelen province. Within this province, strong lineated anomalies reflect the development of pronounced graben (e.g. the 77° Graben of Houtz et al., 1977). The southwestern margin of the Kerguelen province is not sharply defined, indicating that the basement of the Kerguelen Plateau merges into the oceanic basement of the Enderby Basin. In contrast, a strong edge effect anomaly on the southern margin of Elan Bank indicates a sharp contact, perhaps reflecting the boundary between the interpreted continental fragment of Elan Bank and the oceanic crust of the Enderby Basin. The northeastern part of this province is marked by NW-trending anomalies in the Labuan Basin that reflect the ridges and troughs in this area, and the sharp

boundary of the Labuan Basin with the fast-spreading oceanic crust of the Australian–Antarctic Basin.

Magnetic field

Magnetic data coverage has improved with the new magnetic anomaly database (Fig. 15). A series of north-south survey lines from Japanese surveys TH98 and TH99 traverse an area from the continental slope to far out on the abyssal plain south of the Elan Bank micro-continent. This data set extends data coverage far enough north to cover a larger section of oceanic crust in the Enderby Basin, although most surveys are still concentrated on the Antarctic flank of the Enderby Basin. The density of magnetic anomaly data between Prydz Bay and Elan Bank is sufficient to allow the use of gridding (Fig. 17). The magnetic anomalies exhibit strong parallel and sub-parallel lineations, with an unequivocal ENE trend. The strong lineations of the eastern Enderby Basin are terminated eastwards at about 75°E, north of central Prydz Bay. East of 75°E and in the Princess Elizabeth Trough, magnetic anomalies are of high amplitude and the anomaly character is indistinguishable from that of the southern Kerguelen Plateau.

The southern limit of identified seafloor spreading anomalies is marked by a prominent high-amplitude magnetic anomaly, flanked to the south by a negative anomaly. This anomaly is arcuate in map view and trends approximately E-W, somewhat oblique to the seafloor spreading lineations (Fig. 17). This anomaly (referred to as the 'Mac.Robertson Coast Anomaly', or MCA; Brown et al., 2003), coincides with a oceanwards step-up in basement that is observed in both the Japanese and Australian reflection seismic data (Joshima et al. 2001, Stagg et al., in press; interpretation of this report), and is interpreted to mark a major crustal boundary, probably the continent-ocean boundary.

GREATER INDIA–AUSTRALIA–ANTARCTICA SEGMENT

GI–A–A segment – Sector 3

Sector Three extends from 85–115°E and incorporates the southeast Kerguelen Plateau, Shackleton Basin (first named in this report; equates with the southern Labuan Basin in Borissova et al., 2002) and Bruce Rise. This region overlaps both the GI–A and A–A segments and includes a complex zone of oceanic crust (the Shackleton Basin) that was formed adjacent to the triple junction where Antarctica, Greater India and Australia were once joined.

Gravity field

The continental margin in this sector is probably the most complex of the Australian Antarctic Territory and this is reflected in the satellite gravity field (Fig. 18). The shelf-break edge-effect anomaly is distinctly different in character to elsewhere along the margin. The positive limb of the anomaly is of high amplitude; however, the negative limb west of Bruce Rise is low-amplitude compared to adjacent areas. Somewhat unexpectedly, the gravity expression of Bruce Rise is also indistinct; in contrast, the conjugate Naturaliste Plateau off southwest Australia has a very strong gravity signature (e.g. Borissova, 2002, fig. 3).

The margins of Bruce Rise are delineated by sharp, parallel, linear anomalies with E–W and NW–SE trends. The most prominent of these anomalies is that from the NW-trending Vincennes Fracture Zone, interpreted by Tikku & Cande (1999) to be a continuation of the Perth Fracture Zone on the conjugate margin. The E–W trending anomaly is probably an edge effect from the steep northern scarp of Bruce Rise and appears to also coincide with the continent-ocean boundary determined from reflection seismic data.

North of Bruce Rise, the gravity field of the eastern Shackleton Basin is generally negative and there is little evidence of the presence of fracture zones, other than the Vincennes Fracture Zone. The gravity data suggest that a small fragment of Shackleton Basin crust is located in a triangular-shaped compartment immediately east of the Vincennes Fracture Zone. Magnetic and seismic data indicate that this crust is most likely of oceanic origin. The boundary between the Shackleton Basin and the oceanic crust of the Australian–Antarctic Basin to the north is marked by a prominent, sinuous gravity anomaly that becomes collinear with the Williams Ridge anomaly to the northwest.

Magnetic field

The magnetic data coverage (Figs 19 & 20) has been greatly improved by the addition of the Japanese and Australian surveys which include a series of north-south profiles that are at a high angle to the spreading systems of both the South West Indian Ridge (SWIR) and the South East Indian Ridge (SEIR); previously there were few tracklines with a suitable orientation. The magnetic anomaly profiles and the gridded data clearly show the different trends of the Mesozoic (ENE-trending) and Cainozoic (WNW-trending) spreading systems (Figs 21 & 22).

The crust abutting the Antarctic margin is characterised by a truncated sequence of ENE-trending Mesozoic anomalies interpreted to range in age from M9y to M4y, and was most likely produced during India–Antarctica spreading contemporaneous with the development of the Enderby Basin. This crust is terminated northwards by the boundary with the younger crust of the Australian-Antarctic Basin with its highly linear WNW-trending magnetic anomalies, and to the east by the Vincennes Fracture Zone (Fig. 18). The distinctive, sinuous, WNW-trending gravity lineament that marks the boundary between India–Antarctica (Shackleton Basin) and Australia–Antarctica (AAB) oceanic crust does not show a corresponding linear magnetic anomaly, despite the juxtaposition of crust of very different ages at very different depths. However, the magnetic fabric and trends of the Shackleton Basin and the AAB do show distinctly different characters.

AUSTRALIA–ANTARCTICA SEGMENT

The A–A segment comprises the margins of Wilkes Land (~100–136°E), Terre Adélie (~136–142°E), George V Land (~142–152°E) and Oates Land (~152–160°E). It is bounded to the west by Bruce Rise and the Vincennes Fracture Zone and to the east by the major fracture zone systems that were generated by the strike-slip separation of Tasmania and Antarctica. The Wilkes Land and Terre Adélie rifted margin is characterised by a broad zone of highly-extended continental crust that predates the formation of oceanic crust (see seismic interpretation of this report). There is strong symmetry with the conjugate Australian margin, reflected in the correlations between

profiles of magnetic anomaly, free-air gravity and bathymetric data (König & Talwani, 1977). In contrast to the Wilkes-Adélie margin, the structures and morphology of the George V-Oates Land margin are strongly influenced by the strike-slip motion between Tasmania and Antarctica.

The A–A segment has been more widely surveyed than the GI–A segment and there are numerous publications available, particularly on the separation of Australia and Antarctica and the spreading history of the Southern Ocean. Between Bruce Rise and eastern Wilkes Land, the prime sources of data, prior to this study, were the Japanese TH82, TH83 and TH94 surveys (Sato et al., 1984; Tsumuraya et al., 1985; Ishihara et al., 1996). Between eastern Wilkes Land and George V Land, surveys have been carried out by Japan (TH95; Tanahashi et al., 1997), France (ATC82; Wannesson et al., 1985) and the USA (L184AN; Eittreim & Smith, 1987). However, the far eastern end of the sector (Oates Land) is almost totally unsurveyed, due to persistent heavy ice cover.

A–A segment – Sector Four

Sector Four (100–140°E) encompasses the Wilkes Land and Terre Adélie margin and is conjugate to the southern margin of Australia from the Bremer Basin in the southwest to the eastern end of the Bight Basin.

Gravity field

The gravity signature of the margin of Wilkes Land and Terre Adélie (Fig. 23) is in marked contrast to that of the Enderby Basin in the GI–A segment, pointing to fundamental geological differences. The gravity field of the Wilkes-Adélie margin is dominated by long-wavelength, margin-parallel (and sub-parallel) anomalies and probably mainly reflects rift-related structures. In contrast, the gravity field of the Enderby Basin reflects the present-day morphology and hence the post-rift sediment distribution. It is not clear why the gravity expression of rift-related structures is suppressed in the GI–A segment, whereas the gravity expression of the post-rift sediment distribution is suppressed in the A–A segment.

The shelf-break edge-effect anomaly is characterised by a narrow, high-amplitude positive anomaly. A flanking negative anomaly is either largely absent or is masked by the very broad, strong negative anomaly that characterises the deep-water part of the margin. The positive anomaly is disrupted at several locations along the shelf edge, most markedly by a 90 km-wide, ?NW-trending negative anomaly at about 109–112°E. The only rocks known from this general locality are of Proterozoic age (Tingey, 1991) and there is no obvious explanation for this anomaly. We speculate that there may be a NW-trending graben beneath the continental shelf in this area, perhaps analogous to the Lambert Graben and Prydz Bay Basin.

As noted above, the deep-water continental margin is characterised by a broad, E-W trending, negative gravity field. Within this gravity province, which includes highly-extended continental crust, the continent-ocean transition and slow-spreading oceanic crust, there are several positive and negative anomalies that have along-margin extent of hundreds of kilometres. The significance of these anomalies will be discussed in the section of this report dealing with the seismic interpretation and potential field modelling. To the north, the change from slow- to fast-spreading oceanic crust is not

reflected in the gravity field. The gravity signature of the fast-spreading crust is generally bland, although there are some fracture zones evident (e.g. at 111–114°E).

Magnetic field

As noted above, the Japanese surveys first added enough data to make a magnetic anomaly interpretation, and the AASOPP profiles have further improved data coverage (Figs 24 & 25). These data also support the presence of magnetic anomaly lineations for the sequence (34y to 20o) outlined in Tikku & Cande (1999). However, the magnetic anomaly lineations may not be the product of seafloor spreading processes alone. The data also support observations in studies by König & Talwani (1977), Talwani et al. (1979), and Tikku & Cande (1999) who noted the presence of several conjugate margin-parallel features, such as the magnetic trough (MT), the magnetic quiet zone (MQZ), and the quiet zone boundary magnetic anomaly (QZB). The distance from the QZB to the interpreted anomaly 34y is approximately constant off both the Australian and Antarctic margins.

The magnetic anomalies and gridded magnetic anomaly lineations (Figs 26 & 27) off the Wilkes Land margin reflect the change in spreading rate between Australia and Antarctica from early slow spreading (with broad, poorly defined lineations) to fast spreading (with well-defined, parallel lineations) at about Cainozoic anomaly 20 (~43 Ma, Middle Eocene). North of approximately 60°S the lineations show a generally E-W trend and are characteristic symmetric, fast-spreading seafloor magnetic anomalies.

The area from approximately 127–134°E shows a slight change in trend to ENE in the magnetic anomaly lineations. This change in orientation may be significant in interpreting along-margin segmentation and breakup geometry. The approximately symmetric Magnetic Quiet Zone (MQZ), observed along the central Great Australian Bight and Wilkes Land margins appears to be truncated eastwards at about 128°E; the magnetic trough (MT) appears to shift closer to the shelf-break in this zone, and then disappear to the east. This may be related to the increased density of the major fracture zone between Australia and Antarctica, which begins east of the Spencer Fracture Zone, and the change from a normally rifted to a strike-slip regime.

A–A segment – Sector 5

Sector Five extends from 130–160°E along the Terre Adélie, George V Land and Oates Land margins. It overlaps with Sector Four to the west in order to show the transition from normally rifted to strike-slip margins.

Gravity field

In this sector the gravity field is dominated by the transition from the normally rifted continental margin of Wilkes land and Terre Adélie to the strike-slip margin that formed as a result of the separation of Tasmania and the South Tasman Rise from East Antarctica (Fig. 28). East of 136°E, the positive limb of the shelf-break anomaly is strongly suppressed, except for two strong anomalies at 149–151°E and 154–158°E. These latter anomalies are probably due to the juxtaposition of continental and oceanic crust at the base of a very steep continental slope formed by the Tasman Fracture Zone.

From 135–150°E, the gravity field of the deep-water margin reflects the eastwards transition from normal rifting to a strike slip margin, with the development of crustal fragments with a general triangular outline (e.g. at 61–63°E, 136–142°E). The deep-seismic data (see later section) provide excellent imaging of some of these crustal fragments.

Magnetic field

The AASOPP data have improved north-south track coverage to the north on the abyssal plain (Figs 29 & 30). However, data coverage in most of this region is poor for magnetic anomaly identification (Fig. 31); the gaps in the gridded magnetic anomaly map (Fig. 32) further illustrate this. There is a lack of distinct magnetic anomaly lineations closer to the margin outer rise; this is partly due to the data coverage, which includes widely spaced E-W oriented tracks that are of little value in anomaly identification.

SEAFLOOR SPREADING AND PLATE RECONSTRUCTION MODEL

A key unknown in the Mesozoic global plate circuit is the timing and orientation of the breakup between East Antarctica and India. The lack of understanding of the role of India in the dispersal of Gondwana stems from a previous lack of marine magnetic and seismic reflection data to constrain the Mesozoic breakup and seafloor spreading history between India/Madagascar/Sri Lanka and East Antarctica.

GI–A segment

A Mesozoic magnetic anomaly sequence has been identified from at least M9o (~130.2 Ma) to M2y (~124.0 Ma) in the Enderby Basin (Fig. 33). The distance between the last anomaly sequence pick (M9o, 130.2 Ma) and the interpreted continent-ocean boundary implies that the oldest oceanic crust may be of about anomaly M10 age (~130.2-130.8 Ma). The inferred onset of seafloor spreading in the Enderby Basin is similar in age to that in the Perth Basin, which is dated at about M10 time.

The M2, M3 and M4 magnetic anomalies are prominent in the observed magnetic anomaly sequence and form a basis for interpretation of the early spreading system. The M2 (~124.0 Ma) and M4 (~127.6 Ma) anomalies are high-amplitude positive anomalies, separated by M3 which is characterised by a large negative anomaly, which represents a reversal period of two million years duration (124.7–126.7 Ma) in the geomagnetic timescale (Gradstein *et al.* 1994). Parts of the M9 to M2 sequence have been identified from magnetic anomaly data in the GI–A segment, but determination of the extent of the partial to full sequence identification will require the acquisition of additional magnetic data.

In the eastern Enderby Basin, the magnetic anomaly identifications extend further to the north. In this area, an anomaly sequence from M2 to M9 can be identified symmetrically about an inferred extinct spreading ridge. The symmetry of the gridded magnetic anomalies (Fig. 17) provides additional evidence that there is a mirror image sequence. The broad amplitude and distance of the magnetic anomaly profiles between the identified M2 lineations suggests an extinct ridge at about 61ºS. This ridge may be younger than M2, as spreading is likely to have slowed before it

stopped, but there is no clear signal from such a spreading rate change. It is likely that spreading in this compartment ceased at about M0 time (~120 Ma) as the spreading ridge jumped towards the Kerguelen Plume, during the early formation of Kerguelen Plateau. Comparison of the widths of the M9y to M2o sequences indicates that the spreading was slightly asymmetric, with half-spreading rates of approximately 3.5 $cm.a^{-1}$ on the southern limb of the system and 4.8 $cm.a^{-1}$ in the north.

In the Shackleton Basin, west and north of Bruce Rise, anomalies M9y to M6y and M6y to M4y have been identified in two spreading compartments, separated by an inferred transform. The trend of these anomalies indicates that the Shackleton Basin crust was formed as part of the India and Australia-Antarctica spreading episode. The computed half-spreading rates for this very narrow sequence are 4.6 $cm.a^{-1}$ (M9y to M6y) and 7 $cm.a^{-1}$ (M6y to M4y).

A–A segment

The central part of the Wilkes Land margin is the clearest area for observing the correlation between magnetic anomaly lineations, from approximately 115°E to 127°E there is a large approximately E-W trending magnetic anomaly feature (Fig. 34); this corresponds to the Quiet Zone Boundary (QZB) anomaly and anomaly 34y of Tikku & Cande (1999).

It is possible to follow the magnetic anomaly trough between 34y (~83 Ma) and 33o (~79 Ma) quite well with an E-W lineation. This part of the sequence exhibits the largest peak-trough amplitude and it has a quite regular width; it is consistently followed by a peak between 33o (~79 Ma) and 32y (~71 Ma). The next part of the sequence to the north, between 32y and 20o, is less regular, with variable width and character along strike. However, the 31o (~68.7 Ma) to 27y (~60.9 Ma) sequence forms a reasonably prominent positive anomaly feature when correlating the magnetic anomalies along strike. The proposed sequence for anomalies 34y (~83 Ma) to 20o (~43.7 Ma) extends for approximately 330 km of crust in a north-south direction and represents a period of about 40 million years, if the crust was formed by oceanic spreading. The along-axis variations in the 34y to 20o sequence are partly a result of data coverage, sediment thickness, but in particular the complication of very slow seafloor spreading rates and other breakup processes.

SUMMARY

The model derived from the data compilation and interpretation presented here indicates that the breakup of India and Antarctica was roughly contemporaneous with the breakup of India and Australia (Perth Basin), at about 130 Ma, with breakup propagating southwestwards. Spreading rates vary between the different spreading compartments from the Perth Basin to the Enderby Basin; these variations may be partly due to the early influence of the Kerguelen Plume and also to large-scale plate motions. Opening of the central Australian-Antarctic margin segment was very slow from the onset of seafloor formation (~83 Ma, according to Sayers et al., 2001) for a period of approximately 40 million years until the start of fast seafloor spreading in the Eocene (~43 Ma; Figs 35 & 36).

Overall, the revised plate reconstruction leads to a tighter, pre-rift reconstruction between India, Australia, and Antarctica. Rotations derived from the magnetic anomaly picks have been consistent in the fit of India, Madagascar and Antarctica from M9 to M2 in the Enderby Basin. In Mesozoic plate reconstructions for the Indian and Southern Ocean the identification of magnetic anomalies in the Somali Basin and the revised fit of Madagascar to the east of Gunnerus Ridge (cf. Marks & Tikku, 2001) require a new pre-rift fit of Australia and India relative to Antarctica further to the east. This shift subsequently leads to less overlap between Australia, Tasmania, the South Tasman Rise (STR) and Antarctica. The reconstruction model also implies that left-lateral strike-slip motion occurred through the Otway Basin and STR. As a consequence of constraining the motion between Kerguelen Plateau (KP) and Broken Ridge (BR) as a right-lateral strike slip boundary, there is a small degree of transpressional motion between the STR (fixed to Antarctica) and Tasmania during this period.

INTERPRETATION METHODOLOGY

Seismic reflection

The prime dataset underpinning the interpretation in this report is the more than 20 000 km of deep-seismic data recorded on Surveys GA-228 and GA-229. These data were interpreted on hard copy and interactively on workstations. This interpretation was then used to constrain the geometries of the refraction/wide-angle reflection modelling and the potential field modelling.

It is evident from the shot-point location maps that opportunities for tying seismic sequences between lines were limited, except at the inboard ends of some lines. Therefore, the prime means of tying reflectors and sequences between lines was the correlation of seismic characters. This was of limited value in the generally very thick post-rift sedimentary section, except in the case of characteristic unconformities and sequences of regional extent, but is considered to be reliable in the interpretation of the main crustal features. Because of these limitations, and also because of the geological detail evident in the post-rift sedimentary section, the interpretation of this report will concentrate on the crustal structure of the margin and the distribution of mega-sequences, and leave the detailed sedimentary interpretation for future reports.

Given the extremely long along-margin distance covered by this study (~5500 km) and the generally sparse coverage of good-quality, pre-AASOPP seismic data, it is not unexpected that there is no published interpretation of the regionally important seismic reflectors. Some published interpretations have proposed seismic horizon nomenclatures specific to the area studied (e.g. Stagg, 1985; Eittreim & Smith, 1987; De Santis et al., 2003; and the multiple Japanese surveys between 1982 and 1999) while Brancolini et al. (1995) integrated the available interpretations in the Ross Sea, based on German, French, US, Italian, Russian and Japanese data. However, the majority of these interpretations have concentrated on the post-rift sedimentary section, mainly because of the limited seismic penetration achieved on many surveys and the very large thickness of post-rift sediments.

The high quality and deep penetration of the data available to this study make it possible to interpret the reflectors that have margin-wide significance, particularly in the rift and pre-rift section and to discriminate between the different basement types. The main characteristics of the principal regional crustal seismic reflectors in continental, transitional and oceanic crust are as follows:

Horizon *cont* (Fig. 37): top of pre-rift continental crust. This faulted horizon is identified on the inboard ends of some lines. Due to the generally thick overlying sedimentary section and the interfering effect of seabed multiples on the inboard ends of most lines, little can be said about the seismic character of this crust or the geometries of the faulting. While the top of acoustic basement can be unequivocally identified on some lines as a discrete reflector, most notably on Bruce Rise north of Queen Mary Land (e.g. line GA-228/13, Plate 14), in other places it is identified only as a change in character from stratified to non-stratified section.

Horizon *cot* (Fig. 38): top of main crustal layer in the continent-ocean transition (COT) zone. This horizon is a composite surface that has been interpreted generically along the margin of the AAT. The underlying rocks are probably any (or a mixture)

of continental basement (crystalline or indurated sediments), volcanics or unroofed peridotites. Beneath the continental margin west of the Kerguelen Plateau, this horizon is further subdivided into horizons *ecot1* and *ecot2*, according to the degree of faulting interpreted.

Horizon *moho* (Fig. 39): reflection Moho beneath transitional or oceanic crust. The character of this reflector varies considerably, from strong and with high continuity to low and poor continuity. This reflector is generally located at 9.5–10.5 s TWT and can be observed beneath oceanic crust or the COT, but not beneath extended continental crust.

Refraction & wide-angle reflection

During Surveys GA-228 and GA-229, a total of 120 sonobuoys were deployed for the determination of velocities in the sedimentary section and crystalline crust from wide-angle reflections and headwaves. Of the sonobuoys, 97 recorded wide-angle reflections and/or refraction events that could be analysed for velocities. Of these stations, 80 provided 'basement' velocities in the range 5.0–7.5 km.s^{-1}, and 33 provided velocities of ≥7.6 km.s^{-1}.

All successful sonobuoys were subsequently modelled using the SIGMA ray-tracing software developed by the Geological Survey of Canada (Seismic Image Software, 1995). The modelling process is shown as a flow-chart in Figure 40, and can be summarised as follows.

Interpretation of sonobuoy record: All sonobuoys were redisplayed from the field tapes using the Disco/Focus software. Each record was then examined for prominent wide-angle reflections and for headwaves and those events were digitised using the Petroseis™ seismic mapping software. It should be noted that, while the headwaves are produced by velocity discontinuities, the wide-angle reflections were selected on the basis of their continuity and ease of interpretation. That is, while the wide-angle reflections provide an interval velocity above the reflector that is interpreted, they do not necessarily correlate with a velocity discontinuity. Consequently, in the subsequent modelling, headwaves were given priority over wide-angle reflections. The direct arrival from the sonobuoy was used to compute the apparent shot-point interval; typically, this was from 47–52 m, compared with the true shot-point interval of 50 m.

After digitising and editing, the sonobuoy picks were exported as ascii files.

Interpretation of stacked or migrated section: The reflection seismic section that corresponded to the interval recorded by the sonobuoy was interpreted and digitised into Petroseis. The time section was then depth converted using approximate interval velocities that were based on a combination of stacking velocities and velocities previously derived from other sonobuoys. While these velocities were only approximations, they were only required to give a starting model, with all boundaries and velocities subsequently being varied in SIGMA.

After depth conversion, the depth data for all horizons were exported as ascii files.

Reformat sonobuoy pick and starting model files: Both the sonobuoy pick file and the starting model file were run through scripts and reformatted to be read directly into SIGMA.

Modelling in SIGMA: The sonobuoy pick and starting model files were input into SIGMA, together with other starting parameters necessary to correctly correlate the two files. Modelling started at the seabed, and progressed down through the section as each interval was successfully modelled. As noted above, headwaves were given priority over wide-angle reflections in the modelling. Where boundaries that produced a headwave in the sonobuoy had not been interpreted in the starting model, these boundaries were inserted into the model.

Potential field modelling

The interpretation adopted here was designed to quantitatively validate preliminary time-based interpretations of structurally significant seismic sections against coincident potential field data, with the objective of elucidating the tectonic framework of the margin. This was done by integrating migrated depth-converted seismic reflection images and their interpretations, with density data derived from numeric conversion of seismic refraction and stacking velocities. The gravity and magnetic fields of these petrophysically-attributed geometric models were then concurrently forward-modelled in 3 dimensions, by giving the sections limited strike extents. Limited information on magnetic physical properties has been derived from analysis of dredge samples at analogue sites in the Southern Ocean; however, the magnetic properties remain the least constrained part of the validation process.

The crooked line acquisition geometry of the seismic reflection surveys has been accommodated by modelling the data in three dimensions, rather than by projecting onto a common datum. Models have been continued out of the plane of the section for distances up to 125 km in both directions, where regional strike allows. Because the geological information is limited out of the plane, this approach is equivalent to '2.5D' methods that calculate the potential field anomalies in 2D assuming 'infinite' strike lengths.

Gravity and magnetic forward models were constructed for a total of 13 lines from western Enderby Land to Terre Adélie

Modelling

The workflow for the potential field modelling is described in more detail in Appendix 7.

Initial density estimates were derived by conversion of both seismic refraction velocities from sonobuoys acquired on the lines, and stacking velocities derived from the seismic processing sequence. These velocities were converted using the equation of Ludwig et al. (1971). This equation is in the form

$$\rho_{app} = -0.6997 + 2.23 \times V_p - 0.598 \times V_p^2 + 0.07036 \times V_p^3 - 0.0028311 \times V_p^4$$

where:

ρ_{app} is the apparent density; and

v_p is the P-wave refraction or stacking velocity in km s^{-1} of the interval for which a density is required.

This method is designed only to produce a set of starting parameters for the initial forward model, as the densities may be later varied during modelling and inversion.

Methods

Two-way time seismic data were converted to depth using smoothed stacking velocities in DISCO-Focus. A range of megasequences was then interpreted from these data and images of the profiles exported from Geoquest. The data were imported into ModelVision Pro v4.0 as 8-bit per pixel bitmaps and stretched using the SOL and EOL geodetic coordinates, projected into SUTM rectangular Cartesian coordinates. The base of the section was set at 20 km below sea level, with the top of section being 0m (msl).

Gravity data were 1967 GRS Free Air Anomalies at msl in milligals. These data had been smoothed using a 3-minute RC filter on averaged one second data. The data have been meter, drift, tide and Eotvos corrected, and then further low-pass filtered to reduce high frequency signals / noise. The estimated final RMS noise envelope of the data is 5 –10 $\mu m.s^{-2}$.

Three-component total magnetic intensity data supplied were residual after removal of the IGRF (2001.3 / 2002.3 epochs). These data have been filtered and smoothed using a three point de-spiking and interpolation process, but have not been diurnally corrected. Thus, as well as remanent and induced magnetisations, the data will also include a time-variant component. High frequency sferics noise is apparent on some of the lines modelled.

General Modelling Assumptions

Background density contrast of model 2.67 x 10^3 $kg.m^{-3}$

Body responses are modelled in their correct x, y, and z locations, not projected into a plane. The solutions are 3D analytic for polyhedra, based on the algorithms of Coggon (1976) and Lee (1980).

Calculations do not account for sphericity of the earth over the distances of the baselines. Induced errors due to this assumption, based on comparison of similar 2.5 and spherical 3D models by Takin & Talwani (1966), are of the order of 30 $\mu m.s^{-2}$ and are not expected to exceed 50 $\mu m.s^{-2}$. Given the noise envelope of ~10 $\mu m.s^{-2}$, and the dynamic range of the data (typically ~550 $\mu m.s^{-2}$), this is not considered significant.

INTERPRETATION: GREATER INDIA–ANTARCTICA SECTOR

INTRODUCTION

The sector from western Enderby Land to the western end of the Princess Elizabeth Trough is one of the better-surveyed parts of the East Antarctic margin. Since the early 1980s, Australian, Russian and Japanese seismic surveys have been carried out from the continental shelf to the oceanic crust of the Enderby Basin. Russian surveys have also acquired a large quantity of refraction data throughout the Enderby Basin. However, the number of published interpretations from this sector is quite limited, with only Stagg et al. (in press), from which much of the interpretation in this section is taken, providing an interpretation at the regional scale.

In addition to the seismic surveying, three drilling legs of the Ocean Drilling Program have been undertaken on the southern Kerguelen Plateau, in the Enderby Basin and in Prydz Bay. Legs 119 (Barron, Larsen et al., 1989) and 120 (Schlich, Wise et al., 1989) were designed as a latitudinal traverse from the Kerguelen Archipelago to Prydz Bay, Antarctica, while Leg 183 (Coffin, Frey, Wallace et al., 2000) was designed to investigate the timing of Kerguelen Plateau magmatism and the mineralogy of the basement in order to better understand the composition and origin of the lithosphere. The samples recovered on these drilling legs are of limited value to this study. The only other useful sample data comes from cores taken on the continental shelf off Mac. Robertson Land (Truswell et al., 1999; Quilty et al., 1999). While these samples are not tied directly to the seismic profiles used in this study, they are valuable in that they provide confirmation of the presence of Jurassic and Cretaceous sediments on this part of the East Antarctic margin.

GEOLOGY

This section will focus only on geological samples that are tied by the Survey GA-227–229 geophysical data, and those other samples that have direct relevance to the interpretation of the deep continental margin.

Ocean Drilling Program

ODP Site 1165

Ocean Drilling Program (ODP) Site 1165 is situated on the deep margin offshore from Prydz Bay (O'Brien, Cooper, Richter et al., 2001) and is tied by line GA-228/07, Japanese line TH99-26-1 and the Russian line 33006. The site targeted mixed sediment-drift and channel–levee sediments of the central Wilkins Drift, an elongate sediment body formed by the interaction of sediment supplied from the shelf and westward flowing currents on the lower continental slope. The site is at 3537 m water depth and was selected to provide a record of sedimentation that extends back to the onset of contour current influenced deposition. The main objective was to obtain a proximal record of Antarctic glacial and interglacial periods, for comparison with sites around Antarctica and with Northern Hemisphere ice sheets. As the sedimentary section at Site 1165 is more than 3 s TWT (*ca.* 4–5 km) thick (Fig. 41), it is evident that a large part of this section is therefore not sampled.

The sedimentary section at Site 1165 consists of three lithostratigraphic units:

Unit I

The uppermost unit (0–63.8 m below sea floor [bsf]) consists of brown diatom clay with minor diatom-bearing clay with lonestones. This unit is predominantly hemipelagic sediment.

Unit II

The underlying unit (63.8–307.8 m bsf) is composed of interbedded structureless greenish-grey diatom clay and dark grey diatom–bearing clay. The uppermost and lower part of this unit contain dispersed sand grains, granules, and lonestones. This unit is a mixture of hemipelagic sediment and contourite deposits.

Unit III

The lowermost unit (307.8–999.1 m bsf) consists of interbedded dark, thinly bedded, planar laminated claystones and thin beds of greenish grey bioturbated claystone with rare dispersed sand grains, granules, and lonestones. This unit is almost entirely contourites.

The majority of the sedimentary column consists of fine-grained terrigenous material, largely in the clay-sized range, with various admixtures of silt-sized materials, and of biogenic opal in the upper half of the sediment column. Foraminifera are a significant component (>1%) only in the topmost 11 m bsf. Components in the silt-size range are mainly quartz, but also plagioclase, biotite, amphibole, and other heavy minerals. XRD analysis shows that the sediment is primarily composed of quartz, calcite, plagioclase, K-feldspar, and a mixture of clay minerals as well as minor hornblende and pyrite. The number of ice-rafted clasts decreases downhole and isolated lonestones become rare below 500 mbsf.

An excellent record of siliceous microfossils is present in Hole 1165B, allowing the application of the Neogene high-latitude zonal schemes for both diatoms and radiolarians (O'Brien, Cooper, Richter et al., 2001). Twenty-one diatom and 12 radiolarian biostratigraphic datums were identified to approximately 600 m bsf, where dissolution became extensive. Below this level, age assignments are inferred from occasional calcareous nannofossil occurrences. Nannofossils are generally rare and sporadic at Site 1165 with only a few discrete intervals of higher abundance and moderate to good preservation of assemblages that have low diversity, like previously found in this region. Nannofossils yield Pleistocene to lowermost Miocene ages. Benthic foraminifera are more common than planktonic ones, which are rare. Foraminfers indicate several intervals of redeposited material.

A magnetostratigraphy was determined for Holes 1165B and 1165C, for the intervals 0–94 m bsf and 362–999 m bsf. Magnetostratigraphic and biostatigraphic ages, when combined, yield an age-depth model that shows relatively rapid sedimentation in the Early Miocene (~120 m/m.y.), slower sedimentation in the Middle to Late Miocene (~50 m/m.y.), and slow sedimentation from the Late Miocene to present (~15 m/m.y.). The bottom of Hole 1165C (999.1 m) is ~21.8 Ma.

Handwerger et al. (2001) produced a synthetic seismogram to tie the site to the short line shot by the *JOIDES Resolution* before the well was spudded. They used the

impedance log and the wavelet from the watergun used on that line. They were able to identify the major seismic reflectors intersected in the hole. They are:

1. A regional reflector at ~5.25 s that corresponds to the Unit II – Unit III boundary at 308 m bsf.
2. A reflector package at 5.56 s that represents the diagenetic opal A/CT transition at about 610 m bsf. This transition can be seen in reduced porosity and increased bulk density and resistivity in the hole. Siliceous microfossils are not preserved below this horizon.
3. A reflector at ~5.9 s that was the original target horizon for the site. This reflector is at 907 m bsf and was thought to mark the transition from predominantly turbidite sedimentation to predominantly contourite drift sedimentation at the Oligocene-Miocene boundary (Kuvaas & Leitchenkov, 1992). The cores show very similar silty claystone above and below the transition indicating continued contourite deposition, however XRD and smear slides show increased silt content below the horizon. Higher densities and velocities shown by log and core measurements produced the reflection. Lower porosities caused higher resistivity readings.

ODP Site 740

ODP Site 740 was drilled in the southeast part of Prydz Bay and was not tied by the lines interpreted in this report. Site 740 reached a total depth of 1043.5 m and penetrated 225.5 m of rocks (Barron, Larsen et al., 1989). Although the sedimentary section is incomplete, due to poor core recovery, it can be divided into three lithological units, as follows (Barron, Larsen et al., 1989):

Unit I
The uppermost unit (0–23.2 m bsf) is a soft diatomaceous ooze of late Pliocene to Holocene age.

Unit II
The underlying unit (23.2–56.6 m bsf) is drilling breccia composed of gneiss clasts and acid/intermediate rocks. This unit is of Pliocene to Holocene age.

Unit III
The lowermost unit (56.6–225.5 m bsf) is a greenish grey and red sandstone alternating with siltstone and claystone. The age of this unit is unknown as palaeontological data are lacking. However, this continental red bed unit was suggested to be of Permian to Mesozoic age by Stagg (1985), an interpretation that was also proposed by Cooper et al. (1991).

ODP Site 740 is significant to this study in that it provides definitive *in situ* samples of the rocks that are likely to underlie the continental margin at depth further offshore.

Dredges and cores

Gravity coring and dredging by Australian Antarctic Research Expedition surveys (GA surveys 901, 149 and 186; O'Brien et al., 1993, 1995; Harris et al., 1997) on the Mac. Robertson Shelf have produced evidence of Cainozoic and Mesozoic outcrops on the sea floor (Fig. 42). Truswell et al. (1999) described the Mesozoic

palynomorphs and the setting of the sediments that produced them and Quilty et al. (1999) described the Cainozoic material recovered from the area.

Truswell et al. (1999) found that the Nielsen Basin, an inner shelf topographic deep on the Mac.Robertson Shelf, contained the erosional remnant of a half graben down-faulted within Precambrian charnockite by a seaward-dipping normal fault (Fig. 43). The outer shelf is underlain by seaward-dipping sediments that onlap Precambrian basement. The core cutter samples from gravity cores from the inner- to mid-shelf contain assemblages of palynomorphs of Jurassic to Cretaceous ages. These assemblages are unmixed with other assemblages, except for Pleistocene diatoms, which led Truswell et al. (1999) to conclude that the sediments were re-deposited very close to their outcrop. The ages range from Toarcian–Bajocian to Valanginian–Aptian. The location of the cores on the shelf suggest the stratigraphic relationships shown in Figure 43 (Truswell et al., 1999, their figure 8). The absence of recycled Mesozoic marine fossils on the inner shelf suggests that the source sediments are non-marine.

Core cutter samples and a benthic sled from the outer part of the Mac. Robertson Shelf also recovered Cainozoic fossils, mostly mixed with Pleistocene diatoms (Quilty et al., 1999). The exception is the sled sample that recovered sandy siltstone fragments containing Eocene dinocysts. Some samples contain a mixture of Cainozoic, Mesozoic and Permian palynomorphs, indicating recycling, but others contain unmixed assemblages of Cainozoic foraminifera and palynomorphs. Cainozoic ages range from Late Paleocene to Mid Eocene, except for one sample that contains a Late Miocene form. Some cores also contain recycled prisms of the Cretaceous bivalve *Inoceramus* (Quilty et al., 1999) indicating Cretaceous marine sediments as a source.

The distribution of Mesozoic and Palaeogene sediments on the Mac.Robertson Shelf suggests the following geological history (Truswell et al., 1999; O'Brien, Cooper, Richter et al., 2001):

1. Deposition of sediments in an intracratonic sag or early rift basin during the Toarcian to Bajocian.
2. Extension and normal faulting from the Callovian to at least the Aptian.
3. Continental shelf sedimentation through the Palaeocene to the Late Eocene, possible continuing until the Middle Miocene.
4. Erosion of the shelf by grounded ice since the Middle Miocene.

Sample	Latitude	Longitude	Age and fossils
GA 149/GC03	67° 29.9'S	064° 59.8'E	Valanginian–Aptian palynomorphs
GA 149/GC05	67°24.21'S	065°55.82'E	Tithonian–Valanginian palynomorphs
GA 149/GC06	67°17'S	066°01.3'E	Callovian–Bajocian palynomorphs
GA 149/GC39	67°09.4'S	065°45.1'E	Toarcian–Bajocian palynomorphs
GA 149/GC40	67°09.4'S	065°45.1'E	Toarcian–Bajocian palynomorphs
GA 901/SL2 (KROCK) (epibenthic sled)	66°53.95'S	063°09.3'E	Eocene palynomorphs
GA 149/GC07	66°50.7'S	064°55.2'E	Late Miocene
GA 149/GC09	67°05.2'S	65°19.3'E	Paleocene, E–M Eocene palyn. Eocene foraminifera
GA 149/GC10	67°05.1'S	65°27.9'E	Paleocene–Eocene foraminifers, palynomorphs
GA 149/GC13	67°05.3'S	65°59.0'E	Paleocene–M. Eocene palyn.
GA 149/GC21	66°33.1'S	72°17.6'E	Miocene? Foram. Cretaceous–Paleocene palyn.
GA 149/GC45	67°00'S	063°05.0'E	M–L Eocene palyn, L. Paleocene foram.
GA 149/GC46	66°54.3'S	063°06.0'E	Eocene foram, M. Eocene palyn., *Inoceramous* prisms
GA 149/GC47	66°49.0'S	063°14.0'E	M. Eocene palyn., *Inoceramous* prisms
GA 186/GC33	66°44.9'S	063°18.2'E	M–L. Eocene foram., *Inoceramous* prisms

Table 1: Cores and dredges containing Mesozoic and Cainozoic fossil material (Truswell et al., 1999; Quilty et al., 1999).

GEOPHYSICAL INTERPRETATION

The following interpretation is largely taken from Stagg et al. (in press), with the permission of Springer Science & Business Media B.V., publishers of *Marine Geophysical Researches*.

Crustal Structure from Seismic Data

Continental rift crust

As with most Antarctic margin seismic surveys, the new data only provide limited coverage of the continental shelf due to widespread ice coverage. Other than beneath Prydz Bay, the seismic data on the continental shelf suggest that pre-rift basement generally lies at shallow depths and has only a thin syn- and post-rift sedimentary cover. ODP Site 740 in southeast Prydz Bay penetrated non-fossiliferous continental

red beds (Turner, 1991) that have been interpreted to be of Permian to Mesozoic age (Stagg, 1985; Cooper et al., 1991). Harrowfield et al. (in press) consider the Antarctic shelf in this region to be primarily a Permian feature that, as with the Australian shelf (Chen et al., 2002), underwent little modification during Indo-Antarctic rifting and breakup. However, as noted above, Truswell et al. (1999) and O'Brien, Cooper, Richter et al. (2001) have inferred the presence of Jurassic–Cretaceous half graben beneath the inner part of the shelf to the west of Prydz Bay.

Profiles offshore from western Enderby Land (e.g. line GA-229/35, Plate 10) and Mac. Robertson Land (Stagg et al., in press) show that acoustic basement is down-faulted beneath the upper continental slope to depths of 7–8 s TWT (*ca* 8–10 km) across several major faults. While this basement may be of crystalline origin, discontinuous reflectors near the top of fault blocks (e.g. Fig. 37) suggest that basement also contains pre-rift (e.g. Palaeozoic to Early Mesozoic) sedimentary rocks, as at ODP Site 740. As the GA-228/229 and TH99 seismic data consistently show the presence of a very thick syn- and post-rift sedimentary section beneath the continental slope along this margin, the shelf edge and upper slope is interpreted to generally coincide with a major basement fault zone and the landward limit of a major margin-parallel sedimentary basin (Fig. 44; Plate 21). Russian seismic profiles in the area have been similarly interpreted (e.g. Gandyukhin et al., 2002). Golynsky et al. (1996, 2002) also interpreted a high-amplitude magnetic anomaly west of 50°E (the 'Antarctic Continental Margin Magnetic Anomaly'), at approximately the same location as the shelf–slope basement fault zone shown in Figure 44, and noted that '*(I)t represents one of the longest continuous tectonic features of Antarctica and presumably marks a continental crustal discontinuity formed during Gondwana breakup*' (Golynsky et al., 2002). The northern limb of this anomaly is seen on the inboard end of line GA-229/35 (Plate 9), which is one of the few survey GA-228/229 lines that extends as far south as the upper slope. The seismic data for this line (Plate 10) clearly show that acoustic basement is down-faulted northwards across several major faults at the same location.

Structuring beneath the outer edge of Prydz Bay is complicated by the presence of the NE-SW trending Prydz Bay Basin (Fig. 44), interpreted by Stagg (1985) to be a failed rift at a triple or four-armed junction that contains at least 5 km of Permian and younger sedimentary rocks deposited on the underlying, N–S trending, Palaeozoic–Mesozoic Lambert Graben. Fedorov et al. (1982) suggested that the Lambert Graben could be correlated with the Mahanadi Graben on the northeast coast of India; this correlation was also used by Stagg (1985). However, recent work by Harrowfield et al. (in press) interprets across-rift alignment of the Lambert Graben with the Godavari Valley, some 650 km southwest of the Mahanadi Graben. However, none of these correlations takes account of the known presence of continental fragments of unknown areal extent that now underpin parts of the Kerguelen Plateau.

The Cretaceous and Cainozoic section beneath the outer shelf and continental slope shown in Stagg et al. (in press, fig. 5b) has been dated through a direct tie to ODP Site 742 and via other seismic lines to ODP Site 741. Beneath this sedimentary section, acoustic basement is interpreted at a depth of about 2.5 s TWT (*ca* 3.5 km) approximately 60 km landwards of the shelf break. Beneath the continental slope, a minimum of 8 km of sedimentary rocks is observed, indicating that basement is

downfaulted by at least 6 km. However, the strong and ubiquitous seabed multiples beneath the shelf and upper slope preclude direct seismic imaging of the faulting.

Beyond the shelf–slope fault zone, there is a zone of deeply-subsided and probably rifted crust (Fig. 45) that varies in width from approximately 300 km, offshore from Prydz Bay and eastern Enderby Land, to 150–200 km off central and western Enderby Land. Basement in this area is not well-defined in the reflection data, probably due to two main factors. Firstly, the seismic signal is degraded by the very large thickness of sedimentary section overlying basement beneath the margin, which ranges from 6 km to more than 8 km thick. Secondly, while the Enderby–Mac. Robertson Land margin is classified as 'non-volcanic' on the basis of the absence of seaward-dipping reflector sequences (SDRS), it is still likely that there are igneous rocks within and overlying basement. These rocks have probably blurred the seismic imaging of any basement fault blocks. The timing of volcanic emplacement is unclear; it might be of pre-breakup age or it could be related to the mantle plume which generated large parts of the Kerguelen Plateau.

Seven sonobuoys in this crustal zone recorded refracted arrivals from the main crustal layer, mainly offshore from Mac. Robertson Land (Table 3). The interpreted velocities range from 5.7–6.3 km.s^{-1} (average 6.1 km.s^{-1}), which is consistent with the presence of continental crust. No higher velocities were recorded at these sites, probably due to the large thickness of overburden, the size of the seismic source used (60 litres) and the limited recording range of the sonobuoys (generally less than 35 km). While Russian surveys have recorded many refraction stations in this region, reporting of the results is limited. Gandyukhin at el. (2002) reported basement velocities of 5.9–6.3 km.s^{-1} from this deeply-subsided crust; they also showed velocities of 6.0–6.2 km.s^{-1} in the crustal section that they model from seismic and gravity data (Fig. 46). Largely on the basis of the distribution of crustal velocities, they further interpreted the transition from continental to oceanic crust to be located at approximately 64^{o}S offshore from Mac. Robertson Land.

Lineated magnetic anomalies that could be identified as the product of seafloor spreading have not been interpreted from this zone of crust. Brown et al. (2003) and Brown (this report) note that the southern limit of identified seafloor spreading magnetic anomalies is marked by an approximately E–W trending, prominent, high-amplitude magnetic anomaly (their 'MacRobertson Coast Anomaly', or MCA) flanked to the south by a magnetic anomaly low. This anomaly often has the form of a simple dipole in profile (e.g. line GA-229/34, Plate 9). The location of this anomaly correlates closely with the change in basement seismic character and the basement step that is shown by an arrow in Figure 47.

After integrating the seismic reflection character, crustal velocities and the distribution of lineated magnetic anomalies, we are therefore confident in interpreting this zone of rifted crust as being primarily of continental origin. This interpretation is discussed further in this chapter in the section detailing the potential field modelling.

Oceanic crust

Oceanward of the belt of deeply-subsided, probable continental crust, the basement is interpreted as unequivocally oceanic on the basis of its reflection seismic character and velocity structure. This crust is particularly notable for a range of distinctive seismic reflection characters, and the consistency of those characters over broad areas,

suggesting that the crust is divided into a number of discrete spreading compartments. There is also some correlation of the broad crustal types with variations in the crustal velocity profile. The characteristics of the identified crustal types are listed in Table 2 and all the types are illustrated in Plates 10–12 and Figures 47–51. Along the margin, oceanic crust can be split into three discrete zones: from 58–76°E; from 52–58°E; and west of 52°E.

The eastern sector from 58–76°E contains the most distinctive Enderby Basin oceanic crustal type, *ebo 2* ('ebo' for 'Enderby Basin oceanic'), characterised by:

- A generally smooth, high-amplitude reflection from the basement surface (horizon *ebo 2*; Fig. 47).
- Short, north-dipping reflectors, probably indicating lava flows, in the uppermost few hundred metres of basement (Fig. 47).
- A layer of seismically transparent crust, approximately 0.6 s TWT (*ca* 1.5 km) thick, underlying the upper crustal flows (Fig. 47). There are hints of sub-horizontal reflections in the lower part of this zone (e.g. Fig. 48, at about 8.5 s TWT).
- Highly-reflective lower crust, averaging 1.5 s TWT (*ca* 5 km) thickness, with both north- and south-dipping planar reflectors (Figs 47–49). The apparent dip of these reflectors averages 30°, and the dip and distribution of individual reflectors is very regular.
- Oceanic layer 3 refraction velocities from sonobuoys averaging 6.7 $km.s^{-1}$ (range from 6.5–7.0 $km.s^{-1}$).
- A very strong sub-horizontal reflection at about 10 s TWT. This reflector has very high continuity in some places (e.g. Figs 47 & 48) but can also be discontinuous (e.g. Fig. 49). Sonobuoy solutions from several lines show velocities greater than 8 $km.s^{-1}$ at about this depth, supporting the reflection being from Moho. In some areas, the dipping reflectors in the overlying crust sole out on to the Moho (Fig. 48), but elsewhere they appear to disrupt Moho and continue into the upper mantle (Fig. 49). There is also some long-wavelength relief on the Moho; for example, in Figure 50 it shallows from 10 s to 9.5 s TWT (*ca* 1.6 km) over a distance of about 25 km, before deepening again northwards.

The *ebo 2* crust is approximately rectangular in outline, extending for about 900 km along the margin, from the eastern side of Prydz Bay west to central Enderby Land, and for 150–200 km orthogonal to the margin (Fig. 44). The eastern boundary is indistinct, possibly due to thermal and volcanic overprinting from the Kerguelen plume (Coffin, Frey, Wallace et al., 2000). In contrast, the western boundary at approximately 58°E is relatively sharply defined (albeit by data along widely separated lines), probably by a fracture zone.

A further distinctive characteristic of this sector is the presence of strong high-continuity dipping reflections in the upper mantle (e.g. at 10–11 s TWT in Figs 49 & 50). These reflections are observed on four adjacent lines for approximately 300 km along-strike on the margin. These reflections are only observed beneath *ebo 2* crust, which suggests that they are perhaps related to the spreading processes that account

for this very unusual crust. In each example, the reflection dips at 20–30^{o} towards the continent and can be traced to at least 8 km depth below Moho. In the east, this reflection appears to bifurcate from the reflection Moho, while to the west (e.g. Fig. 49), it appears to be continuous with strong reflections in the lower oceanic crust. The amplitude of this reflection is comparable to the amplitude of the strongest Moho reflections. At present, we see no obvious explanation for these mantle reflections, and their high-amplitude is particularly difficult to explain, as it would require large velocity contrasts in the upper mantle.

To the north, the distinctive *ebo 2* crust merges with the less distinctive *ebo 1* crust (Fig. 50). On the basis of the limited seismic data available, *ebo 1* crust appears to characterise much of the eastern Enderby Basin, between Mac. Robertson Land and Elan Bank of the Kerguelen Plateau to the north. In comparison to the *ebo 2* crust, the *ebo 1* crust is largely devoid of internal reflections, although there are low-continuity, low-amplitude reflections that appear to be continuous with reflection Moho in the *ebo 2* sector (Fig. 50). The upper surface of the crust shallows by about 1 km in the transition from *ebo 2* to *ebo 1* and the total crustal thickness increases by about 1.5 km. Taken together, these character and thickness variations indicate a significant change in spreading parameters (spreading rate and magma volume) at this time. Only two sonobuoy stations were recorded on the *ebo 1* crust; neither of these indicates a significant change from the velocity profile in the *ebo 2* crust.

The narrow sector from 52–58^{o}E (offshore central Enderby Land) is characterised by a fragment of much deeper oceanic crust (*ebo 3*; Fig. 51). The upper surface of basement is at 8–8.7 s TWT depth, approximately 0.5 s (*ca.* 0.8 km) deeper than the crust immediately to the east. The basement surface is dominated by short, landward-dipping volcanic flows with distinct scarps on their oceanward flanks. The anomalous basement depth suggests that this crust may be a remnant of an older phase of seafloor spreading. The depth is very close to that recorded for the Late Jurassic crust of the Argo Abyssal Plain off northwestern Australia (e.g. see figure 4 in AGSO North West Shelf Study Group, 1994), and we speculate that this may also be the approximate age of the *ebo3* crust.

In the sector west of about 52^{o}E (western Enderby Land), the character of oceanic crust becomes much more varied (types *ebo 4* to *ebo 10*; Table 2). The wide line spacing does not permit accurate spatial delineation of these crustal types, but their variability may be a function of the inferred mixed rift/transform setting of this part of the margin that is implied by the orientation of crustal elements summarised in Figure 44. The general characteristics of these crustal types include:

- An upper surface that varies from rough (e.g. *ebo 7* and *ebo 8* in line GA-229/35, Plate 10) to extremely rugged (relief of up to 1 km; e.g. *ebo 5*, in GA-229/35, Plate 10) at a range of wavelengths from a few kilometres to 20 km.
- Long wavelength undulations in the basement surface (*ca* 100 km; e.g. *ebo 7* and *ebo 8*; GA-229/35, Plate 10).
- Generally reflection-free internal crustal character (GA-229/35 & GA-228/01, Plate 10). While there is sometimes a slightly increased level of reflectivity in the lower crust, there are few coherent reflections.

- No distinct reflection Moho.

There appears to be a significant difference in the velocities in the deep crust or uppermost mantle between the eastern and western sectors. Whereas mantle velocities in the east are uniformly high (average 8.4 km.s^{-1} from six stations), there are no unequivocal mantle velocities of >7.9 km.s^{-1} in the western sector. Although one sonobuoy in this sector gave a velocity of 7.95 km.s^{-1}, this came from a depth of about 10.5 km; as basement lies at about 7 km depth, this is probably too shallow to be coming from Moho. Four other sonobuoy stations provided velocities of 7.6–7.8 km.s^{-1} at depths that give overlying crustal thicknesses of approximately 4 km. Again, these velocities are unlikely to derive from Moho, unless there has been extensive alteration of the lower oceanic crust, or else closely-spaced transforms have produced crust that is generally thinner than average. Alternatively, the low western sector velocities could be due to all the sonobuoys being shot down-dip with respect to the 7.6–7.8 km.s^{-1} refractor (no reflections at this depth were observed to constrain the models).

Potential field modelling

A total of five lines have been modelled to a consistent level of detail. These lines are located off western Enderby Land (lines GA-229/35 & GA-228/01; Figs 52 & 53), Mac. Robertson Land (line GA-228/06; Fig. 54), and the western side of Prydz Bay (lines GA-229/30 & GA-229/31; Figs 55 & 56). While the description here concentrates on the interpretation of two of these lines – GA-229/35 and GA-229/30; Figs 52 & 55), all models show a strong structural consistency along the margin, and the lines described here are representative. Full details of the parameters used in each model are included in Appendix 7.

The gravity profile for line GA-229/35 (Fig. 52) displays a second-order (polynomial) regional field, that increases from ~0 μm.s^{-2} at the southern end of the line to ~250 μm.s^{-2} at about shot-point (SP) 4500, then decreases to ~ 200 μm.s^{-2} at the northern end of the line. Three major gravity highs are superimposed on the regional trend. These have amplitudes of up to 200 μm.s^{-2} peak-to-peak (ptp), and are located between SP 1000-3500, over clearly imaged continental crust. A major negative excursion of ~ –420 μm.s^{-2} ptp, occurs near the southern end of the line.

The base level of the gravity field in line GA-229/30 (Fig. 55) is approximately 50 μm.s^{-2}. The regional field is a second-order polynomial field that decreases from ~70 μm.s^{-2} in the south to ~-45 μm.s^{-2} at about SP 6000, then increases to ~140 μm.s^{-2} at the northern end of the line. Superimposed on this field are three significant anomalies: a ~–70 μm.s^{-2} asymmetric anomaly from SP 7300–5700 over interpreted rifted continental crust; a 130 μm.s^{-2} ptp symmetric anomaly from SP 5700–3000 in the continent-ocean transition zone; and a 125 μm.s^{-2} ptp asymmetric anomaly from SP 3000–1000 over seismically-defined oceanic crust.

High-frequency atmospheric noise is apparent in the magnetic profiles (e.g. SP 2500–4000, GA-229/35; SP 6500–5000, and the abrupt ~80 nT offset at about SP 3500 in GA-299/30 are probably storm-related.).

The parameters of the inducing magnetic field used in modelling were calculated using the geodetic coordinates of the midpoint of the line. The computed values for

GA-229/35 were B = 41800 nT; I = -63°; D = -50°; and for GA-229/30 B = 51 400 nT; I = -69.7°; D = -68.5°. The general north-south orientation of the lines and the line length of more than 400 km mean that there are significant departures from these values at the ends of the lines. Experimenting with the field values derived for the start and end of line locations (67.001°S, 45.4403°E; and 62.9021°S, 40.8479°E for GA-229/35; 62.2818°S 72.1501°E to 66.1321°S 72.2354°E, for GA-229/30) showed a maximum 1800 nT difference in the inducing field strength, a 1° change in the inclination, and 3° change in the declination compared to the field values used in modelling. Further trials of the impact of changing these variables during modelling showed that these result in a maximum 0.2 change in the RMS error compared to the RMS error of the models with the mid-point parameters. Consequently, the difference in inducing field strength across the lines is not considered significant. The IGRF-corrected magnetic field in both lines shows a base level of ~ 0 nT, indicating adequate modelling of the geocentric axial dipole field in this region.

On line GA-299/35, superimposed on this regional baseline are a series of ~120 km spatial wavelength anomalies, with superimposed high frequency noise from the southern end of the line to about SP 3500. These anomalies have amplitudes of 200–600 nT ptp and are interpreted to be derived from continental crust, based on the seismic interpretation. North of about SP 4000, the residual field shows pronounced high-amplitude, variable-wavelength anomalies. These anomalies have half-wavelengths of ~30–60 km, and amplitudes of 30–260 nT ptp. High-frequency noise (average 20 nT ptp), which may be either instrumental noise or atmospheric transient signals, is superimposed on these anomalies; these high-frequency signals were not modelled.

On line GA-229/30, the regional field is augmented by a series of ~80 km spatial wavelength anomalies with superimposed high frequency noise from the southern end of the line to SP 4500, associated with seismically-defined continental crust. The average amplitude of these anomalies is 75 nT ptp. Seaward of SP 4500, the magnetic character changes markedly, with pronounced high-amplitude, variable-wavelength anomalies being associated with seismically-defined oceanic crust. These anomalies have half-wavelengths from ~25 to ~40 km, and amplitudes of 40 nT to 200 nT ptp. They also display high-frequency superimposed noise (average 20 nT ptp).

Line GA-229/35 (western Enderby Land)

Model bodies A to E (Fig. 52) correspond to the post-rift sedimentary section. The densities of these bodies range from 1.89–2.45 x 10^3 kg.m^{-3}, and all bodies are non-magnetised.

The major density change (from 2.45 to 2.8 x 10^3 kg.m^{-3}) takes place at the transition from rift/pre-rift to post-rift sediments interpreted at the base of bodies E1 and E2. This corresponds to a change in seismic character from high-amplitude, high-continuity, laminar reflections in the shallow section, to more discontinuous reflections at depth that are offset by interpreted seaward-dipping normal faults. The base of bodies F1 and F2 is relatively unconstrained, with no corresponding seismic reflection boundary with the underlying bodies. F1 and F2 (and the equivalent thickness of the top of body H) thus may represent the fault-disrupted top of basement.

The high-velocity, pre-rift basement forms two distinct packages resolvable in the potential field analysis. Bodies G1 and G2 are dense (2.8 x 10^3 kg.m^{-3}), normally-magnetised units which produce significant high-amplitude, long-wavelength magnetic anomalies. The seismic character is diffuse with steeply-dipping reflectors. G1 and G2 are interpreted as ?Archaean-Proterozoic metamorphic basement rocks, such as schists or gneisses, that have high velocities, densities and significant anisotropy. Non-magnetic, continuous, steeply-dipping reflectors in the seismic data are interpreted as major ductile shear zones, consistent with this interpretation. G1 and G2 are therefore likely to be equivalent to the exposed rocks of the Eastern Ghats of peninsular India.

Bodies G1 and G2 are separated by body H, a thick, broad wedge of reversely-magnetised rocks, of similar metamorphic basement density. This body is required to fit the long wavelength (120 km) high-amplitude (300 nT) low in the magnetic signal. Such a large feature can either be explained by a shallow tabular magnetised source (e.g. sill complex) for which there is no velocity or seismic reflection evidence, or by a deep-seated basement feature. We have chosen the latter to model this anomaly. This body may be a Palaeozoic or Proterozoic infra-rift basin, equivalents of which may be exposed on the conjugate east Indian coast and hinterland (e.g. Cuddapah Basin). If this interpretation is correct, the basin may trend at a high angle to the present rifted margin, and the seismic transect is likely to image it obliquely. In conjunction with its antiquity, this geometric effect may account for the general lack of seismic reflectivity from this body, and also means that the modelled architecture of the basin and its underlying basement may not be representative of the overall structure of this crustal element, especially towards the landward end of the line.

Metamorphic basement overlies a high density body (3.4 x 10^3 kg.m^{-3}) at 10–40 km depth, interpreted as continental lithospheric mantle.

The oceanic crystalline crust interpreted from the reflection seismic data has been modelled using a variable three-layer structure. As no internal crustal layering is discernible in the reflection seismic data, the layers that are used as the basis for the potential field model are derived from the velocities listed in Table 3. The upper layer (body I) is bounded at its top by a rugose basement surface that shallows to the north. All blocks in this layer are modelled with the same density (2.55 x 10^3 kg.m^{-3}), but the magnetic susceptibilities vary from 0.005–0.05 SI, and the Konigsberger Ratios vary from 0.5-2.

Underlying the normal and reversely magnetised blocks is a single high-density layer (body J; 2.75 x 10^3 kg.m^{-3}) with negligible magnetisation, interpreted as relatively unaltered dolerite dyke swarms and/or layered gabbro (oceanic layer 2B/3). This is, in turn, underlain by a uniformly denser layer (body K; 2.85 x 10^3 kg.m^{-3}) of non-magnetised peridotites (oceanic layer 3).

A notable feature of the boundary between the rifted and attenuated continental crust and distinctive oceanic crust in this model is the generally low-amplitude (~200 μm.s^{-2} ptp) gravity response, and the broad wavelength (~80 km), negative magnetic anomaly. In this case, the subdued magnetic signature is due to an edge effect where non-magnetic supracrustal rocks are in contact with magnetised, negative polarity seafloor crust. Both crustal columns have approximately the same overall bulk average density, leading to little gravity discrimination of the transition between

the crustal types. This situation highlights the degree of complexity that is potentially involved in the transition from continental to oceanic crust, and consequently the interpretation of the magnetic or gravity data without reference to the seismic data can produce an erroneous estimate of the position of this transition on the margin, due to complex edge effects.

Line GA-229/30 (offshore Prydz Bay)

Model bodies A to G represent the rift and post-rift sedimentary section (Fig. 55). The densities of these bodies range from 1.82–2.49 x 10^3 kg.m^{-3}, and bodies A to F are non-magnetised. The transition from rift/pre-rift to post-rift sediments is located at the boundary between bodies F and G. The total thickness of sediments is almost 9 km, most of which is of post-rift origin. Body G is distinguished by an apparent reversed magnetisation, interpreted to be due to interbedded mafic volcanic detritus or lavas.

Normal faults controlling the deposition of body G cut down into basement that has a noisy, diffuse seismic character. This basement (body H) has been modelled with a significantly higher density than the sedimentary section (2.9 x 10^3 kg.m^{-3}) and with minor normal magnetisation (k = 0.008 SI, normal polarity). Basement is interpreted to be metamorphic rocks of the continental shield. Onshore to the west of Prydz Bay, there is an exposed gneissic basement (Napier Complex) of mixed marbles, calc-silicates, mafic orthoamphibolites, and garnet-bearing gneisses (Tingey, 1991), which would produce a response consistent with the properties of body H.

The distinctive, higher-amplitude, longer-wavelength magnetic anomalies associated with this crust have been modelled with discrete highly-magnetised bodies (bodies I1 to I6). These may represent syn-rift mafic intrusions (e.g. dykes, plugs), compartments of syn-rift volcanics, or alternatively, magnetic amphibolites within metamorphic basement. These bodies have high densities (2.90 x 10^3 kg.m^{-3}), equal to that of the surrounding basement, but these densities are non-diagnostic of any of the proposed sources. The significant magnetisations attributed to these bodies are all apparently reversed, perhaps indicating a temporal link to the reversed signature of the syn-rift layered sedimentary package (body G), although this is not conclusive evidence of their origin.

The oceanic crust interpreted from the reflection seismic data in this sector has also been modelled using a variable three-layer structure. The upper layer (body J) is bounded at its top by a rugose basement surface with occasionally rugged topography that shallows northwards with an average gradient of about 0.6^o. Normally and reversely magnetised blocks in this layer have highly variable densities, from 2.45-2.8 x 10^3 kg.m^{-3} (average 2.58 x 10^3 kg.m^{-3}), perhaps indicative of variable hydrothermal alteration and submarine weathering. The modelled magnetic susceptibilities are also quite variable, ranging from 0.006–0.06 SI, with Konigsberger Ratios of 1–2.

The crust underlying the upper layer is modelled with a dense, (ρ = 2.85 x 10^3 kg.m^{-3}) non-magnetised layer (body K; ρ = 2.85 x 10^3 kg.m^3; k = 0 SI). Sonobuoy stations give refraction velocities from the near the top of this body that indicate it is probably oceanic layer 3. Beneath this is a layer of variable density and magnetisation (body L), interpreted as faulted and altered oceanic peridotites of oceanic layer 3. Four main blocks are modelled in this lower layer, with the boundary between L3 and L4

corresponding to the boundary between the seismically-defined *ebo 2* and *ebo 1* crust. Whereas three of the four blocks have high densities (average 2.90 x 10^3 kg.m^{-3}) and are non-magnetised, the outermost block of the *ebo 2* crust has a significantly lower density (L3: ρ 2.75 x 10^3 kg.m^{-3}) and an unusually high component of normal magnetisation (k = 0.05 SI; Q = 1.5). These variations in properties and in seismic character, and the significant variations in properties of the shallow basaltic layer, are interpreted to reflect the widespread influence of hydrothermal alteration (spilitisation) of the basalts, and widespread serpentinisation of the peridotites around active faults through the oceanic crust (e.g. Minshull et al., 1998). If this is the case, hydrothermal fluids either from above or below may have been mobilised through the crust, altering reactive olivine to serpentine and magnetite, and simultaneously reducing the density and increasing the magnetic susceptibility.

The bulk mantle under this transect has a higher density than on line GA-229/35 off western Enderby Land. This higher than normal density (ρ = 3.4 x 10^3 kg.m^{-3}), confirmed by seismic refraction sonobuoy modelling (Table 3), may be indicative of metasomatism or igneous underplating of the mantle during the Palaeozoic formation of the Lambert Graben. The Moho under oceanic crust appears in places as a broken, high amplitude reflector with up to 2 km of relief, indicative of tectonic complexity. This appears to be localised under the lowest density panel of the oceanic crust described above (body L3), perhaps indicating either through-going lithospheric-scale shear zones or soft-linked (i.e. viscously decoupled or non-throughgoing) shear systems, with linked fluid transfer pathways.

The boundary between attenuated continental crust and oceanic crust on this profile is within a zone of long-wavelength, high amplitude (~200 μm.s^{-2} ptp) gravity signature, and negative (~–50 nT), moderate wavelength (~30 km) magnetic anomaly. No single anomaly marks the inferred contact between the two types of crust. In this case, the broad negative magnetic signature is due to reversely magnetised intrusions within the continental metamorphic basement adjacent to more weakly remanently magnetised, negative polarity seafloor crust, with little discrimination between the two on magnetic grounds. This situation, different to GA-229/35 above, but similar in other respects, again highlights the degree of complexity that is involved in areas of continent–ocean transition, and the importance of deep-seismic reflection data, as well as refraction and potential field data, in locating this transition and defining its structure.

Synthesis of potential field modelling

Both transects modelled for this report show a relatively uncomplicated transition from rifted continental to oceanic crust. The post-rift sections are strikingly similar in stratal geometry, seismic character and potential field character. These strata wedge out to an approximately constant thickness of ~1.5 km, overlying a rough oceanic basement, with interpreted M-series magnetic anomalies (Brown et al., 2003). This crust appears to have formed during several discrete episodes of generation, with differing seismic reflection, velocity and density characteristics. This crust is readily distinguishable from the more uniform seismic reflection and velocity characteristics of the Archaean shield metamorphic basement that underlies the continental margin further inboard. The transition from thinned continental to oceanic crust in this sector thus reflects a significant sharp character change in the seismic reflection and velocity data, particularly off Mac. Robertson and western Enderby Lands, which is replicated

by a distinct boundary in the potential field models. However, the transition is not always clearly defined in the magnetic signal, due to the presence of remanently magnetised intrusions within the adjacent continental crust. These intrusions can produce obscuring, longer wavelength magnetic anomalies.

The potential field modelling also indicates distinct differences between the oceanic crust of the western and eastern sectors. The crust off western Enderby Land (Fig. 52) is slightly thinner and it shows less variation in thickness and in magnetic properties below the basalt layer than the crust off Mac. Robertson Land (Fig. 55). In both profiles, the continental and oceanic crusts have behaved as a semi-rigid plate that has been depressed landwards by the thick (4-9 km) post-rift sediment loading.

Post-rift Sedimentary Section

The sedimentary section on the margin of Mac. Robertson and Enderby Lands is extremely thick, particularly offshore from Prydz Bay. Sediment thicknesses computed from seismic processing stacking velocity analyses and potential field modelling (see above) indicate that the sedimentary section below the continental slope oceanward of Prydz Bay is at least 8 km thick. Most of the section that is visible in seismic data is of post-margin breakup age (i.e. Late Cretaceous and Cainozoic); these sediments are underlain by an unknown thickness of rift and pre-rift sediments that cannot be reliably distinguished in seismic data because of the thick overburden (Stagg et al., in press, fig. 5b). The post-rift section thins gradually oceanwards, but it is still more than 2 km thick at more than 500 km from the shelf edge. Offshore from Enderby Land in the west, the post-rift sediments are generally thinner than off Prydz Bay, but there is still more than 8 km of this section in some inboard locations.

The post-rift sedimentary section can be divided into four distinct provinces. From east to west, these are: offshore from eastern Prydz Bay (75–80^{o}E); offshore from western Prydz Bay to eastern Mac. Robertson Land (65–75^{o}E); offshore from western Mac. Robertson Land, Kemp Land and eastern Enderby Land (50–65^{o}E); and offshore from western Enderby Land 38–50^{o}E.

The eastern Prydz Bay sector is characterised by a prograding shelf edge and upper slope of Cainozoic sediments that passes seawards into a sedimentary section at least 4 s TWT thick (Stagg et al., in press, fig. 5b). The prograding wedge is composed largely of diamicts deposited by slumping of subglacial debris delivered to the shelf edge by an expanded Lambert Glacier (Barron, Larsen et al., 1989). The sediments beneath the slope show moderate reflector continuity and variable amplitude. The upper part of the section contains extensive canyons, channels and levee deposits, indicating a predominance of transport and deposition by down-slope currents (e.g. line GA-229/30, Plate 12).

The western Prydz Bay province has a very thick slope section (e.g. lines GA-228/07 and GA-229/30, Plate 12; Kuvaas & Leitchenkov, 1992). The basal 1–2 s TWT of the sedimentary section displays similar moderately-continuous reflectors as to the east, but the upper 2–3 s TWT comprises large sediment mounds with high-continuity reflectors, areas of mud waves and stacked channel-levee complexes with abundant evidence of vertical accretion. The largest mounds trend north-northwest and are separated by the broad canyons. Small-displacement faults are widespread,

suggesting out-of-section slumping into the canyons. Kuvaas & Leitchenkov (1992) interpreted the mounds as mixed contourite-turbidite drifts formed by contour current reworking of sediment delivered to the lower slope by turbidity currents, mostly emanating from Prydz Bay. ODP Site 1165 was drilled to 999.1 m below sea floor on a sediment drift northwest of Prydz Bay (Fig. 41; O'Brien, Cooper, Richter et al., 2001; Cooper & O'Brien, 2004). It encountered Early Miocene contourites that passed upwards into contourites, hemipelagic muds and oozes with evidence for rapidly reducing current activity and sedimentation rates through the Late Miocene and Plio-Pleistocene. Plio-Pleistocene deposition was concentrated on the upper slope where the Lambert Glacier built a trough mouth fan that downlaps on to the major Miocene drifts (Passchier et al., 2003; O'Brien et al., 2004).

In the western Mac. Robertson to eastern Enderby Land sector, the upper 1–2 s TWT of sediment includes mounds that show some characteristics of contourite drifts but which are cut by numerous canyons and gullies (Stagg et al., in press, fig. 5a; line GA-228/06, Plate 11). These sediments do not exhibit the channel-levee deposits that are dominant to the east, but generally appear to be deposits that are presently being dissected by down-slope currents. However, some canyon-fill deposits are also present (e.g. southern end of line GA-228/06, near the intersection with TH99-27; Stagg et al., in press, fig. 5a). More distal regions show moderate-continuity reflectors and small channels suggesting distal submarine fan deposition (e.g. Stagg et al., in press, fig. 5a; line TH99-06). The deeper sedimentary section is generally similar in character to areas to the east, with moderate-continuity reflectors that onlap oceanic crust seaward.

The western Enderby Land sector is characterised by a thick sedimentary section (>6 km) in which the thickest sediments appear to be older than those offshore from Prydz Bay. These sediments are thickest beneath the landward end of the lines and thin rapidly seaward, pinching out against oceanic crust (e.g. lines GA-229/35 & GA-228/01, Plate 10). The sequence is heavily dissected by channels that range in scale from large canyons to small tributary gullies. Probable Cainozoic contourite sediments onlap the upper surface of this sediment pile. This ?Cainozoic section is characterised by high-continuity, parallel reflectors with some mudwaves. In places there is a well-developed moat at the inboard edge of this deposit indicating contourite sedimentation (Faugère et al., 1999). Farther outboard on the margin, channel and levee deposits are visible at the seabed indicating distal submarine fan sedimentation is currently taking place.

DISCUSSION

Figure 44 summarises the tectonic elements of the continental margin of Enderby Land, the adjacent deep-ocean basins and the southern Kerguelen Plateau. This map is a synthesis of the interpretation presented here with previously published information on the structure and age of the Enderby Basin (Brown et al., 2003; Rotstein et al., 2001), and the structure of the Kerguelen Plateau (Borissova et al., 2002). The tectonic features are broadly similar to those mapped by Gandyukhin et al. (2002).

The inboard part of the margin is dominated by the shallow crystalline basement of the Napier Complex. In the east, the north–south trending Palaeozoic–Mesozoic Lambert Graben is overlain by the approximately NE–SW trending Mesozoic–

Cainozoic Prydz Bay Basin. As the Lambert Graben is a major feature of the onshore crust, it is likely that it also continues offshore beneath the marginal rift. However, with the extremely thick post-rift overburden and the orientation of the available seismic lines, it is not discernible offshore. The northern flank of the Napier Complex is generally delineated by a major fault zone that underlies the outer shelf and upper continental slope, beyond which basement deepens by at least 6–8 km.

As shown in Figure 44, the deep-water part of the continental margin and the adjacent oceanic crust are divided into western and eastern sectors by the N–S offset in the boundary between interpreted continental and unequivocal oceanic crust and the E–W change in the character of oceanic crust at about 58°E.

Western sector

In the western sector (west of 58°E), the continental margin is underlain by a band of rifted and thinned crust north of the shelf-slope fault zone. This band is relatively narrow (100–200 km), due to the influence of the mixed rift–transform nature of this part of the margin. The maximum sediment thickness here is 6–8 km, with most of these sediments being of post-rift age. The name 'Rayner Basin' (after Rayner Glacier, in western Enderby Land) is proposed by Stagg et al. (in press) for the major depocentre on this part of the margin.

The character of the oceanic crust in the western sector, with its highly variable basement surface, is likely to be a function of its location in a mixed rift–transform zone, as indicated by the irregular distribution of the identified magnetic anomalies and the fracture zone interpretation of Rotstein et al. (2001; Fig. 44). The panel of over-deepened crust (*ebo 3*) is more difficult to explain. As suggested above, its anomalous depth suggests that it is a remnant of an older episode of seafloor spreading.

The oceanic crustal velocity structure of the western sector is distinctive, particularly in the deep crust below 'normal' layer 3. The highest velocities recorded here range from 7.6–7.95 km.s^{-1}, which could be considered representative of 'slow' mantle. However, the modelled depth for these refractions is in the range 9.5–12.3 km, which results in a thickness of about 4 km for the overlying crust (Table 3). This is considerably less than the extreme minimum thickness of 5.0 km for normal oceanic crust noted by White et al. (1992), but is near to their average of 4.87 km for oceanic crust adjacent to non-volcanic rifted margins (i.e. slow-spreading crust with a spreading rate <2.0 cm.a^{-1}) and 3.97 km for fracture zone crust. This indicates that either the >7.6 km.s^{-1} velocity is not from mantle, or that the crust is anomalously thin. While the computed spreading rate for the eastern part of the Enderby Basin does not qualify as slow-spreading crust by this definition (except immediately prior to the cessation of spreading), the separation of the magnetic spreading anomalies (Fig. 44) indicates that the spreading rate to the west is distinctly lower, and perhaps close to the 2.0 cm.a^{-1} referred to above; however, as this area in general does not represent slow-spreading crust, this explanation for the velocity profile is not considered likely. The existence of fracture zones to account for the apparently thinned crust is also a possibility off western Enderby Land; however, this requires that all the sonobuoys that recorded velocities >7.6 km.s^{-1} were deployed close to or on fracture zones, and/or that the fracture zones in this region are very closely spaced, producing a broad zone of anomalous oceanic crust. A third, and preferred

explanation is that the >7.6 km.s^{-1} velocities derive from lower crust that has been strongly altered by the intrusion of mantle rocks. This possibility is consistent with the reflection seismic character of this crust, which shows a slightly higher reflectivity than the overlying crust with some discontinuous reflectors, but no distinct reflection Moho, as is found to the east.

Eastern sector

In the eastern sector, the rift beneath the continental margin is considerably broader (ca. 300 km) than to the west, and the maximum sediment thickness is at least 8 km, with the sediments again predominantly of post-rift age. The greater thickness of sediment here reflects the discharge of sediment from the Lambert Glacier and Prydz Bay. We propose the name 'Mawson Basin' (after Mawson Station) for the major E-W trending depocentre on this part of the margin (Fig. 44).

The seismic character of oceanic crust in this sector is highly distinctive. In particular, the *ebo 2* oceanic crust has strong similarities with the oceanic crust along the Cuvier margin (Sayers et al., 2002) and in the southeast Argo Abyssal Plain (Stagg & Symonds, 1995), off northwest Australia. Oceanic crust with a similar reflection character is also observed in the Shackleton Basin between Bruce Rise and the southern Kerguelen Plateau. While the Argo crust is interpreted to have formed in the Late Jurassic (Mihut & Müller, 1998), spreading along the Cuvier margin commenced prior to anomaly M10 time (Valanginian; Larson et al., 1979), at the same time that spreading is interpreted to have commenced in the Enderby Basin (Brown et al., 2003; Gaina et al., 2003), and almost certainly contemporaneous with the crust in the Shackleton Basin. The half-spreading rates in the Cuvier and Enderby Basins are also comparable — 3.3 cm.a^{-1} in the Cuvier Basin (Larson et al., 1979) and about 3.4 cm.a^{-1} in the Enderby Basin based on the anomalies shown in Figure 44. The strong seismic character similarity between Cuvier and Enderby oceanic crust is consistent with this spreading history.

The high-quality seismic images used in this study clearly show three sub-horizontal layers in the *ebo2* crust (Fig. 47; these may be related to the classical sub-divisions of oceanic crust as summarised, for example, by Kennett (1982). The uppermost 0.2–0.3 s TWT of basement is characterised by short, seaward dipping reflectors; these are likely to be the pillow basalts and sheet lava flows of Layer 2A. This layer is underlain by a layer that is largely transparent to seismic energy but which also contains faint sub-horizontal reflections, and a layer of highly reflective crust. The sonobuoys recorded in this sector show that the boundary between the transparent and reflective crustal layers approximately coincides with the onset of Layer 3 velocities. It is therefore possible that the transparent layer corresponds to the sheeted dykes of Layer 2B, while the highly reflective crust corresponds to the gabbros of Layer 3. The faint reflectors within the interpreted Layer 2B possibly reflect hydrothermal alteration fronts within the sheeted dyke complex caused by the infusion of seawater early in the spreading history when the overlying sediment cover was thin. The combined thickness of 7 km for the dipping flows/transparent layer and the underlying reflective crust is very close to the world-wide thickness range of 7.1 +/– 0.8 km reported by White et al. (1992).

The highly reflective lower crustal layer within *ebo 2* crust is characterised by:

- high-amplitude reflections that dip consistently both landwards and oceanwards at about 30°;
- low-amplitude reflections that are antithetic to the high-amplitude reflections, giving the strong impression of fault-bounded tilt-blocks in the lower crust;
- a reflection Moho at the base of the crust that varies from moderate-amplitude and low-continuity to high-amplitude and high-continuity. The overlying dipping reflections sometimes appear to correlate with offsets in the reflection Moho (e.g. Fig. 49). Elsewhere, they sole out onto a reflection Moho that is a continuous, high-amplitude reflection (e.g. Fig. 48).

The presence of structured reflections and high reflectivity zones within basement in oceanic crust has been reported in a number of papers (e.g. White et al., 1990; Morris et al., 1993; Mutter & Karson, 1992). Mutter & Karson (1992) concluded that the reflectivity of oceanic crust could be categorised in two ways. Firstly, in oceanic crust generated at 'slow' spreading rates (less than about 35 $mm.a^{-1}$), they saw no obvious reflection Moho, while the main part of the crust exhibited a wide variety of reflecting horizons. Secondly, in crust generated at spreading rates greater than 50 $mm.a^{-1}$, they typically found a strong reflection Moho, while the main part of the crust was essentially transparent to seismic energy. From these observations, Mutter & Karson (1992) developed a model in which continuous magma injection was the dominating process in fast-spreading crust, whereas in slow-spreading crust, mechanical extension played the critical role.

As the spreading rate for the Enderby Basin oceanic crust is at the upper end of Mutter & Karson's (1992) slow spreading classification, it might be expected that this crust would show evidence of strong reflectivity while any reflections from Moho would be subdued or absent. However, the *ebo 2* crust shows both pronounced lower crustal reflectivity and a strong Moho reflection with very high continuity (e.g. Fig. 48). We also note that the reflection character in the *ebo 2* crust is distinctly different to that reported by Mutter & Karson, and it is therefore unlikely that their model can be applied here.

A further feature of the *ebo 2*-type crust is that it appears to have been emplaced over a relatively short period of about 4 My at three widely-separated locations on the axis of breakup between India and Australia–Antarctica — in the Enderby Basin; northwest of Bruce Rise some 1000 km to the east (see relevant section later in this report; and along the Cuvier margin off northwest Australia (Sayers et al., 2002), 1500 km farther to the north. If the crust of the southeast Argo Abyssal Plain (Stagg & Symonds, 1995) is also included in this type, then there is a further example of this crust (albeit from an older spreading episode) 1500 km to the northeast of the Cuvier margin. While there is no obvious explanation for the highly distinctive *ebo 2*-type crust, we note that in each case the crust has been emplaced adjacent to an area where large volumes of volcanics (including seaward-dipping reflector sequences, or SDRS) were generated at around the time of margin breakup.

The high-amplitude, landward-dipping mantle reflections observed on several lines are also difficult to explain. The reflections are observed on four adjacent lines over a distance of more than 250 km along strike on the margin. The strike of these reflections, which can be traced for about 8 km into the mantle, is sub-parallel to the continental margin and the boundary between *ebo 2* and *ebo 1* crust, implying that

they probably represent a primary geological structure formed coincidentally with spreading. These reflections are not observed in the other sectors (Bruce Rise and Cuvier margin) of this style of crust, but this might be due to the data quality in those areas. Reston (1993) reported widespread upper mantle reflections from offshore Britain (e.g. the Flannan mantle reflection) and concluded that most of these reflections were some form of extensional shear zone in the mantle. However, unlike the Cuvier-Enderby crust, the mantle reflections reported by Reston (1993) were located beneath continental crust. We are unaware of such reflections being reported from beneath oceanic crust.

Continent–ocean boundary

In this report, we use the term *continent–ocean boundary* to refer to the inboard edge of unequivocal oceanic crust. Landward of the COB, the *continent–ocean transition* (COT) refers to the region on the margin that lies between the outboard edge of highly-attenuated continental crust and the COB. While the COT is predominantly of continental origin, it may also include magmatic components that have derived from the nearby emplacement of oceanic crust and possibly also areas of incipient oceanic crust.

As outlined in Stagg et al. (in press), it is possible to discriminate oceanic crust from extended continental crust on the margins of Enderby and Mac. Robertson Lands on the basis of crustal velocities, reflection seismic character and the presence or absence of lineated magnetic anomalies. This discrimination is pronounced in the east, off Mac. Robertson and eastern Enderby Lands, but is considerably less clear further west, with the change occurring at the major offset in oceanic crustal types at approximately 58^{o}E (Fig. 44).

In the east, the COB is interpreted at the inboard edge of the highly-distinctive type *ebo* 2 oceanic crust. On most lines over an along-margin distance of 800 km (e.g. see lines in Plate 12), this boundary correlates with a distinctive oceanwards step-up in basement level (from about 8 s to 7.5 s TWT, equivalent to a step of 500-1000 m over a distance of less than 5 km). Gandyukhin et al. (2002; Fig. 46) reported a similar basement step at the COB, while Joshima et al. (2001) and Brown et al. (2003) noted the presence of the prominent, high-amplitude Mac. Robertson Coast Anomaly in magnetic profiles at the same location.

Figure 47 shows the reflection seismic detail at the interpreted COB in this sector. On the left of the profile, the interpreted continent-ocean transition crust is characterised by broken reflections of variable amplitude that are probably due to a mixture of extensive small-scale fracturing of basement and widespread intrusion of oceanic magma as dykes and sills. On the right of the profile, the distinctive layered structure of the *ebo 2* crust, with its underlying Moho reflection provides a marked contrast. The boundary between the two crustal types is a complex structure with a width of about 15 km. At depth, the boundary is interpreted to be at the point where the strong reflection Moho disappears landwards. This also coincides with the landwards termination of the *ebo 2* lower oceanic crust, with its characteristic dipping reflectors. In the shallow crust, the boundary is located at the base of the basement step (arrow in Fig. 47), where it appears that seismically transparent volcanic flows have flowed landwards over the more reflective transitional crust.

West of the boundary in oceanic crustal types at 58°E, the COB is much less distinctive, and our interpretation of its location is based largely on the oceanwards change in seismic reflection character (e.g. Fig. 57). The interpreted continental and/or transitional crust on the left of this profile is characterised by a basement surface that appears to be downfaulted oceanwards towards a basement depression. In contrast, the interpreted oceanic crust on the right of the profile (type *ebo 8*) is essentially unbroken by faulting and the crust is almost transparent to seismic energy down to approximately 9 s TWT. On most lines in this sector (e.g. lines GA-228/01 and GA-229/35, Plate 10), the change in seismic character from ?continental to oceanic crust appears to coincide with the zone of the deepest basement along the profile. Gandyukhin et al. (2002) also noted that the COB in the western sector is poorly expressed in seismic reflection data. On the basis of limited refraction data, they located their COB either at about the same geographic location as shown here (Fig. 44), or even further seaward.

SUMMARY

1. The shelf edge and upper slope are underlain by a major basin-bounding fault system, beyond which the crystalline basement underlying much of the shelf and immediate hinterland are down-faulted oceanwards by at least 6 km. The continental margin is underlain by a rift basin system that ranges from about 100 km wide off western Enderby Land to more than 300 km wide off eastern Enderby and Mac. Robertson Lands. The thickness of rift-phase sediments in this basin is uncertain, due to the loss of seismic energy in the very thick post-rift sedimentary section.

2. The sedimentary section appears to be primarily of post-rift age. This section is at least 8 km thick north of Prydz Bay and at least 6 km thick off western Enderby Land. The section thins gradually oceanwards, but is still greater than 2 km thick more than 500 km from the shelf edge. The post-rift sedimentary section can be divided into four distinct geographic provinces offshore from: eastern Prydz Bay; western Prydz Bay; west Mac. Robertson to east Enderby Land; and west Enderby Land. The division of these provinces is on the basis of the thickness of sediments present and the processes that controlled their deposition.

3. The margin is divided into distinct western and eastern sectors by a strong, north-south crustal boundary at about 58°E. Structuring in the western sector appears to be strongly influenced by the mixed rift-transform setting. In contrast, the eastern sector was formed in a normal rifted margin setting, albeit with complexities caused by the major N–S trending crustal-scale Lambert Graben and the overlying Prydz Bay Basin.

4. As with the marginal rift basins, the continent-ocean boundary (COB), defined here as the inboard edge of unequivocal oceanic crust, shows a marked change in character across the crustal boundary at 58°E. In the western sector, the location of the COB is defined mainly on the basis of a change in the reflection seismic character, supplemented by potential field modelling; here, its location appears to coincide with the zone of deepest basement on the margin. However, in the eastern sector, the COB is a prominent and sharp boundary in the reflection seismic data which correlates with a marked change in the crustal velocity profile as shown by the interpretation of sonobuoy records. Potential field modelling

confirms this interpretation. As noted by previous workers (Gandyukhin et al., 2002), this boundary often correlates with an oceanward step-up in the basement level of up to 1 km.

5. The character of oceanic crust is also highly distinctive, again with a major west-to-east character change at 58°E. In the western sector, the basement surface is of variable character, from rugged with a relief of more than 1 km over distances of 10-20 km, to rugose with low-amplitude relief on long-wavelength undulations. The crustal velocity structure is unusual, with velocities of 7.6–7.95 km.s^{-1} being recorded at several stations at a depth that gives a thickness of overlying crust of only 4 km. It is possible that these velocities are from mantle, in which case the thin crust may be due to the presence of fracture zones. Alternatively, the velocities may be coming from a lower crust that has been heavily altered by the intrusion of mantle rocks. Oceanic crust in the eastern sector has a more typical oceanic velocity structure and is particularly characterised by its internal reflection fabric, which comprises: a smooth upper surface underlain by short, seaward-dipping reflectors; a transparent upper crustal layer, probably correlating with a sheeted dyke complex; a lower crust dominated by dipping high-amplitude reflections that probably reflect intruded or altered shears; a strong reflection Moho, confirmed by refraction modelling; and prominent landward-dipping upper mantle reflections on several adjacent lines. Current models for reflective oceanic crust cannot be readily applied to this crust.

6. Potential field modelling indicates that the gross margin structure is relatively simple, and that both the continental and oceanic crusts have behaved as a semi-rigid plate that has been depressed landwards by the thick post-rift sediment loading.

Name	*Depth of basement top (s)*	*Basement surface*	*Internal reflections & character*	*Reflection Moho*	*Comments*
ebo 1	7.3 – 8.8	rough (0.2 s relief) to rugged (0.6 s)	Reflection-free.	Weak; appears continuous with Moho beneath ebo2.	Merges with *ebo2*, but crust is thicker and upper surface is shallower.
ebo 2, 2a	7.6 – 8.0	smooth strong reflector; some minor roughness	Short seaward-dipping flows; transparent upper crust; highly-reflective shears in lower crust	Strong and continuous. Relief up to 0.7 s at wavelength of 30-50 km.	Strong similarity with oceanic crust beneath Cuvier and southernmost Argo Abyssal Plains. Mantle shears; prominent step (~0.5 km) at COB.
ebo 3	8.0 – 8.7	rough (0.2 s) to rugged (0.6 s)	Reflection-free.	Faint Moho at 9.8-10.0 s on some lines.	Upper surface appears to comprise short, south-dipping flows with seaward scarps, possibly faulted.
ebo 4	5.6 – 7.6	extremely rugged; up to 2 s relief	Reflection-free.	Not observed.	Possible fracture zone. Observed at northern end of only one line.
ebo 5/6	7.1 – 8.5	rough (0.1–0.2 s) to rugged (0.6 s)	Slightly higher reflectivity in lower crust.	Not observed.	Rugged crust in interpreted rift-transform sector west of Enderby Land.
ebo 7	7.5 – 7.8	rough (<0.1 s); long wavelength relief	Some minor reflectors	Not observed.	Small areal distribution in interpreted rift-transform sector west of Enderby Land.
ebo 8	7.7 – 8.4	smooth to rough (<0.2 s); long wavelength relief	Reflection-free.	Not observed.	Small areal distribution in interpreted rift-transform sector west of Enderby Land. Similar to *ebo 7*, except deeper.

Name	*Depth of basement top (s)*	*Basement surface*	*Internal reflections & character*	*Reflection Moho*	*Comments*
ebo 9, ebo 10	7.7 – 7.8	smooth to rough (0.1–0.2 s)	Mainly reflection-free; crustal reflector at ~9.2 s on one line	No.	Small areal distribution in interpreted rift-transform sector west of Enderby Land.

Table 2: Seismic reflection characteristics of different types of oceanic crust in the Enderby Basin. All time-depths are seconds two-way time (TWT). 'Rough' refers to short-wavelength, generally low-amplitude basement topography , whereas 'rugged' refers to longer-wavelength topography generally with high-amplitudes.

Sono #	*Line*	*Lat*	*Long*	*WD*	*Vel*	*Depth*	*Vel*	*Depth*	*Vel*	*Depth*	*Correlation with reflection interpretation*
228/SB02	228/06	-65.39	65.25	2.7	6.1	9.7					Continental or transitional crust.
228/SB05	228/08	-62.20	70.55	4.1	5.4	6.2	*6.8*	*8.3*			Oceanic (ebo 1).
229/SB50	229/27	-64.08	79.65	3.7	5.2	~6.1	*6.2*	*9.4*			Probable oceanic.
229/SB52	229/28	-63.55	77.07	3.8	5.4	6.7	*6.8*	*8.7*	*8.3*	*13.5*	Oceanic (?ebo 1).
229/SB53	229/28	-64.45	77.07	3.7	6.1	8.2	*7.4*	*12.2*			Oceanic (?ebo 2).
229/SB54	229/28	-65.03	77.13	3.6	*5.1*	*9.8*					Transitional crust.
229/SB55	229/28	-65.58	77.23	3.2	(5.0)	~7.8	*5.7*	*9.7*			Transitional crust.
229/SB56	229/29	-65.55	75.65	3.4	(5.2)	~8.6	*6.0*	*12.4*			Continental or transitional crust.
229/SB58	229/30	-62.40	72.15	4.1	(5.0)	6.6	*6.3*	*7.9*			Oceanic (ebo 1).
229/SB59	229/30	-63.17	72.15	4.1	(5.0)	7.6	*6.5*	*8.0*	8.4	14.2	Oceanic (ebo 2).
229/SB60	229/30	-64.18	72.15	3.6	4.8	~8.0	*6.5*	*10.2*			?Oceanic (?ebo 2a).
229/SB61	229/30	-65.02	72.15	3.3	(5.0)	~10.2	*5.6*	*11.7*			Continental or transitional crust.
229/SB62	229/31	-65.83	72.20	2.7	*5.1*	*8.0*					Continental or transitional crust.
229/SB63	229/31	-64.83	70.05	3.3	*5.0*	*8.1*	*5.3*	*9.8*	*6.1*	*11.4*	Continental or transitional crust.
229/SB64	229/31	-64.03	68.83	3.5	*6.0*	*8.8*	*6.9*	*9.8*	8.5	14.7	Oceanic crust, adjacent to continent-ocean boundary.
229/SB65	229/31	-62.72	68.85	4.3	(5.0)	7.1	*6.6*	*8.5*	8.4	13.6	Oceanic (ebo 2).
229/SB67	229/32	-62.23	65.45	4.5	(5.0)	6.8	*6.3*	*7.2*			Oceanic (ebo 1).

Sono #	*Line*	*Lat*	*Long*	*WD*	*Vel*	*Depth*	*Vel*	*Depth*	*Vel*	*Depth*	*Correlation with reflection interpretation*
229/SB68	229/32	-63.60	65.45	4.2	(5.0)	7.3	*7.0*	*9.0*	8.0	~15.1	Oceanic (ebo 2).
229/SB69	229/32	-64.57	65.30	4.0	(5.3)	~9.2	*6.2*	*10.1*			Continental or transitional crust.
229/SB71	229/33	-63.97	62.68	4.0	*6.2*	*8.7*	*7.7*	*10.9*			Straddles continent-ocean boundary. 7.7 $km.s^{-1}$ appears too shallow for mantle.
229/SB72	229/33	-63.00	62.03	4.5	4.9	7.2	*6.5*	*7.5*	8.5	13.1	Oceanic (ebo 2).
229/SB73	229/34	-63.58	60.47	4.4	(5.0)	~6.8	*6.4*	*7.9*			Oceanic (ebo 1 / ebo 2).
229/SB74	229/35	-66.63	44.95	2.3	(4.8)	~7.6	*5.5*	*11.2*			Continental.
229/SB77	229/35	-63.65	41.50	4.8	(5.0)	~6.2	*6.2*	*6.4*			Oceanic (ebo 5).
229/SB79	229/36	-64.50	40.37	4.8	(5.0)	~7.2	*6.7*	*7.6*			Oceanic (ebo 8).
229/SB80	229/37	-64.50	45.58	4.1	5.4	~7.5	*6.6*	*7.7*	7.8	11.4	Oceanic (ebo 10). 7.84 $km.s^{-1}$ may be too shallow for mantle.
229/SB81	229/37	-62.97	44.98	4.8	(5.0)	6.5	*6.2*	*7.0*	7.7	10.6	Oceanic (ebo 5). 7.65 $km.s^{-1}$ too shallow for mantle.
229/SB82	229/38	-63.07	43.18	5.0	6.3	~6.7	*6.9*	*8.2*			Oceanic (ebo 5).
229/SB84	229/38	-64.07	43.73	4.5	*6.9*	*7.0*	*8.0*	*10.5*			Oceanic (ebo 6). 7.95 $km.s^{-1}$ too shallow for mantle.
229/SB85	229/39	-64.30	49.23	3.9	(5.2)	~8.5	6.3	9.1	*7.6*	*12.3*	Continental or transitional crust. 7.6 $km.s^{-1}$ may be too shallow for mantle.

Sono #	*Line*	*Lat*	*Long*	*WD*	*Vel*	*Depth*	*Vel*	*Depth*	*Vel*	*Depth*	*Correlation with reflection interpretation*
229/SB89	229/41	-63.22	53.37	4.9	*6.3*	*7.6*	*7.7*	*10.3*			Oceanic (ebo 3). 7.7 km.s^{-1} too shallow for mantle.
229/SB90	229/41	-62.78	54.67	5.1	5.7	7.1	*7.6*	*9.5*			Oceanic (ebo 3). 7.6 km.s^{-1} too shallow for mantle.

Table 3: Sonobuoy locations and solutions for Surveys GA-228 and GA-229 in the Greater India–Antarctica sector; only basement and deeper velocities are shown. Depths are km below sea level; velocities are km.s^{-1}. Velocities in parentheses are assumed. Depths preceded by a tilde ('~') are approximate, usually because of short-wavelength relief on an interface. Velocity/depth pairs in italics are solutions for interfaces that are not observed in the reflection seismic data and are therefore unconstrained with regard to dip.

INTERPRETATION: GREATER INDIA–ANTARCTICA–AUSTRALIA SECTOR

INTRODUCTION

The sector from the eastern end of the Princess Elizabeth Trough to western Wilkes Land (Plate 21) is probably the most complex part of the margin of the AAT. This complexity is due to its proximity to the triple junction in the spreading systems between Greater India, Antarctica and Australia (GI–A–A), combined with the complications introduced by the proximity of the geologically-complex and volcanically-dominated Kerguelen Plateau. To compound these geological complexities, this area is also one of the more difficult parts of the AAT margin on which to acquire reflection seismic data, due mainly to the large volume of ice that derives from the Shackleton Ice Shelf, which dominates the continental shelf.

The distribution of survey tracks in Plate 5 clearly reflects the restrictions on acquiring seismic data in this area. Prior to the AASOPP surveys, the only multichannel seismic data that have been acquired were on the Japanese TH94 survey (Ishihara et al., 1996) on the eastern flank of Bruce Rise and off western Wilkes Land, and the TH98 survey (Murakami et al., 2000) between central Bruce Rise and the eastern end of the Princess Elizabeth Trough. Since the AASOPP surveys, Russia has completed two seasons of surveying between Princess Elizabeth Trough and the area to the east of the Bruce Rise (Leitchenkov, pers. comm.). These lines, which include data across the main part of the Bruce Rise, were not available for inspection for this study.

Sample data are similarly scarce. DSDP Site 268 was drilled to the east of the Bruce Rise, and penetrated 474.5 m of mid-Oligocene and younger sediments. The only other samples recovered that may be of direct value to the interpretation of the seismic data were three dredge hauls from the eastern flank of Bruce Rise that recovered sandstone, siltstone and mudstone, with basement rocks comprising granite and schist (Ishihara et al., 1996). Nothing has been published on these samples beyond the basic lithologies.

Reconstructions based on satellite gravity show that the Bruce Rise was formerly conjugate to the Naturaliste Plateau area off southwestern Australia prior to continental separation (e.g. Borissova, 2002). Some geological data are available from the Naturaliste Plateau and its margins and these will be reviewed here as they are relevant to the interpretation of the Bruce Rise.

GEOLOGY

This section will focus only on geological samples that have direct relevance to the interpretation of the Survey GA-227–229 geophysical data from the deep continental margin.

Deep Sea Drilling Project

Deep Sea Drilling Project (DSDP) Site 268 is located on the lower continental slope, east of Bruce Rise, at a water depth of about 3500 meters. This site is tied by lines GA-228/16 (Fig. 58) and GA-227/1502, and by the Japanese lines TH83-10 and

TH94-19. The sedimentary section at this site is *ca.* 2.6 s TWT thick (~3.5 km), but only 474.5 m were penetrated.

The sequence penetrated was divided into three main units according to lithological characteristics, especially the presence/absence of nanno ooze and ice-rafted pebbles and granules (Hayes, Frakes et al., 1975). These units were:

> *Unit 1* — ~160 m of Pliocene to Quaternary of ooze, clay, silty clay, silt and sand with variable preservation of diatoms; some ice-rafted granules and coarse sands; some cores also recovered granite, gneiss and gabbro lithologies, which are assumed to be from ice-rafted boulders.
>
> *Unit 2* — ~68 m of Early Miocene clay, silty clay and nanno ooze.
>
> *Unit 3* — ~256.5 m of mid-Oligocene or older to Early Miocene silty clays and porcellanous cherts.

Details of the lithologies and physical properties are contained in O'Brien et al. (2002).

Dredges and cores

The only reported seabed samples from this area that contained consolidated rocks come from the southern end of the Vincennes Fracture Zone on the eastern flank of Bruce Rise (Table 5). The rocks were dredged on the TH94 survey (Ishihara et al., 1996) and include sandstone, siltstone, mudstone, granite and schist. Ishihara et al. (1996) noted that "unconsolidated sediments included in the samples do not have enough fossils for the micropaleontological study". T. Ishihara (pers. comm., 2004) suggests that the granites, schists and quartzose sandstones included in the samples are glacier-derived, and that no *in-situ* basement rocks were recovered.

Site	***Latitude***	***Longitude***	***Water depth (m)***	***Description***
D1502	-63.4523 -63.4470	102.6933 102.6833	2446 – 2495	Semi-consolidated siltstone, granite, schist
D1503	-63.6961 -63.6911	102.7233 102.6950	2744 – 2834	Semi-consolidated siltstone, granite, schist
D1504	-63.7911 -63.8017	103.0083 103.0433	2896 – 2668	Semi-consolidated mudstone, granite, schist, quartzose sandstone

Table 5: Summary of dredge samples recovered from the Bruce Rise on survey TH94 (Ishihara et al., 1996).

Conjugate margin samples

In view of the limited rock samples available from the Bruce Rise sector, it is necessary to examine samples from the Naturaliste Plateau region of the conjugate Australian margin for additional information. While also limited in number, these samples provide valuable background on what rocks might be present on the Antarctic margin. The summary descriptions below are derived from Borissova (2002).

Deep Sea Drilling Project (DSDP) Sites 258 and 264 were drilled on the eastern and southern parts of the Naturaliste Plateau (Fig. 59), respectively, and recovered a succession of Cretaceous to Miocene sedimentary rocks (Davies, Luyendyk et al., 1974; Hayes, Frakes et al., 1975; Figs 60 & 61). While neither site reached basement, volcaniclastic conglomerates of Cenomanian or older age were recovered at Site 264 a short distance above acoustic basement (Ford, 1975).

The first sample of the plateau basement was dredged by the *Eltanin* (ELT55-12) from the northern margin of the plateau (Heezen & Tharp, 1973; Fig. 59). Plagioclase-rich rocks from this dredge were originally interpreted as continental. However, a more detailed petrographic analysis (Coleman et al., 1982; Storey et al., 1992) showed that these rock clasts are in fact altered tholeiitic basalts similar to the Bunbury Tholeiitic Suite (132–122 Ma) on the Australian mainland.

Four plagioclase-rich *Eltanin* dredge rocks (ELT55-12) and a cobble from volcaniclastic conglomerate at DSDP Site 264 were analysed by Mahoney et al. (1995), who confirmed their mostly basaltic composition. However, they also noted that the Naturaliste Plateau samples are chemically and isotopically different from typical hotspot basalts and their composition suggests contamination of the magmas by continental crust.

A continental origin for the Naturaliste Plateau is supported by a dredge sample recovered by the *Marion Dufresne* in 1998 on the faulted southern flank of the plateau (MD110-DR11; Royer & Beslier, 1998; Fig. 59). Analysis of the recovered material showed the presence of high-grade gneisses similar in composition to those of the Australian craton (Beslier et al., 2001). It is now apparent that the Naturaliste Plateau, as with other Indian Ocean plateaus such as the Wallaby Plateau and Kerguelen Plateau, is at least partly cored by continental rocks, as originally proposed by Petkovic (1975). Recent potential-field modelling is consistent with basement of the plateau being largely of granitic and/or gneissic composition (Direen, 2004).

GEOPHYSICAL INTERPRETATION

As noted previously, this area comprises the most geologically complex part of the margin of the AAT, reflecting continental extension, breakup and seafloor spreading firstly between Greater India and Australia–Antarctica and, secondly, between Australia and Antarctica. Despite these complexities, this part of the margin can be considered in two quite distinct sectors for the purpose of interpretation, as shown in the map of tectonic elements (Fig. 62), *viz*:

- From the eastern end of the Princess Elizabeth Trough to approximately 95°E, partially coincident with the western flank of the Bruce Rise. This sector will be referred to as the *Shackleton sector*, after the deep-water Shackleton Basin (named in this report), which dominates this sector.

- From approximately 95°E to east of the Vincennes Fracture Zone (approximately 95–105°E). This sector will be referred to as the *Bruce sector*, after the Bruce Rise, which is the dominant morphological and geological feature of this sector.

The interpretation here is illustrated by reference to the map of the interpreted tectonic elements (Fig. 62), a number of detailed seismic sections, and the plates containing small-scale interpretations of all the relevant seismic profiles.

Shackleton Sector

Continental Crust

In this sector, the only seismic data that have been recorded as far south as continental crust are some lines recorded on the Japanese TH98 survey (Murakami et al. (2000). These lines appear to have imaged the outermost edge of extended continental crust and the continent–ocean boundary. In the absence of seismic data extending further inboard, we speculate that, as with other areas of the Antarctic continental margin, the continental slope correlates with the zone of maximum crustal thinning and the continental shelf is probably mainly underlain by shallow crystalline basement.

Oceanic Crust

The sector between the eastern end of Princess Elizabeth Trough and the western flank of Bruce Rise encompasses much of the area that was referred to as the 'southern Labuan Basin' by Borissova et al. (2002), who noted:

> *The Labuan Basin is located along the eastern margin of the Kerguelen Plateau and contains 2.5–4 km of sedimentary rocks above rugged faulted basement. In the north it is separated from the Australian–Antarctic Basin by Williams Ridge. The eastern boundary is delineated by a deep (9 s TWT) basement trough containing up to 5 km of sedimentary rocks, which separates it from the oceanic crust of the Australian-Antarctic Basin.*

Analysis of seismic data shows that there are significant differences in basement character between the eastern, western and southern parts of the Labuan Basin. Borissova et al. (2002) also noted:

> *The western part of the basin is 130–150 km wide and is extensively faulted. The dominant fault-style is extensional, with planar normal faults typically dipping to the SW and resulting in a series of tilted fault blocks. ... The eastern Labuan Basin is about 120 km wide and is characterised by large NNW-trending basement highs. The appearance of these blocks is different from the faulted blocks of the western part of the basin. They are usually larger and dome-shaped. Analysis of magnetic anomalies over these basement blocks shows that most of them do not have a magnetic signature typical of intrusions. One of these blocks in the northern part of the basin was dredged in 1991 (Montigny et al., 1993) and yielded one and a half ton of metamorphic and granitic rocks interpreted as ice rafted debris. However, if these rocks are representative of Labuan Basin basement, rather than being ice-rafted, then the absence of a magnetic signature is readily explained.*

This area is underlain by basement that has markedly different seismic character to the eastern and western Labuan Basins. It is therefore misleading to continue with the

name ‘southern Labuan Basin’, as it implies a genetic relationship with the basin to the northwest. To avoid this implied relationship, we introduce the name *Shackleton Basin* (after the Shackleton Ice Shelf; basin location in Plate 21 and Fig. 62) in lieu of the southern Labuan Basin. The crustal types in this area have been given the prefix *peo* and their characteristics are noted in Table 6.

Within the Shackleton Basin, basement types can be grouped into a number of provinces, as described below. Because of the widely-spaced seismic lines, the boundaries between these provinces are generally ill-defined and not all can be shown in Figure 62.

SDRS province

Immediately to the southeast of the Kerguelen Plateau, well-defined seaward-dipping reflector sequences (SDRS) are observed on several lines (GA-228/10, GA-228/11, GA-229/24, Plate 13; Fig. 63). These SDRS are thick (~2+ s; *ca.* 5 km), with individual reflector packages being up to ~20 km in length. While there is an apparent correlation between the SDRS and the excessive volcanism that produced much of the Kerguelen Plateau, the temporal and spatial relationships are not easily determined. In particular, the following observations should be explained:

- The SDRS are detached from the continental margin and are surrounded by probable oceanic crust (shown as ‘Shackleton Basin oceanic crust – shallow’ in Fig. 62).
- The SDRS thicken away from the Antarctic continent but towards the Kerguelen Plateau.
- The upper surface of the SDRS gradually shallows towards the Kerguelen Plateau.
- The long individual flow lengths suggest subaerial or marginal marine extrusion.

These observations indicate that the SDRS were emplaced during the formation of the Antarctic margin, but prior to the major episode of volcanism on the Kerguelen Plateau. They may have become detached from the Antarctic margin by a spreading ridge jump. The shallowing of the basement surface away from Antarctica and towards the Kerguelen Plateau suggests that volcanism on the plateau was accompanied by substantial thermal uplift.

Southern/central oceanic province

Much of the southern and central part of the Shackleton Basin is floored by basement that appears characteristically oceanic (types *peo1* to *peo5*; e.g. line GA-228/11, Plate 13). This province is shown as ‘Shackleton Basin oceanic crust – deep’ in Figure 62. The basement surface is generally rough and highly reflective. While the upper crust is devoid of coherent reflections, there is frequently a distinct increase in reflectivity at about 8 s. Brown (this report) has interpreted magnetic spreading anomalies M9y and M4y (Hauterivian to Barremian) in this area.

Central crustal step

On two NW–SE oriented profiles (GA-229/24, GA-229/25; Plate 13), there is an abrupt change in basement level, with basement shallowing from east to west by

approximately 0.8 s (*ca*. 1 km). This step is shown as the boundary between the shallow (~7 s) and deep (~8 s) Shackleton Basin oceanic crust in Figure 62. The basement surface at the step (basement type *peo8*) is rugged and suggestive of volcanism. While only observed on two lines, the step is distinctive. The trend of this step is slightly east of north, approximately orthogonal to the margin, and we therefore speculate that it is the expression of a transform fault.

Two sonobuoy stations (229/SB48 and 229/SB49) at this step produced mantle velocities of 8.4 km.s^{-1} (shot east to west) and 7.6 km.s^{-1} (shot west to east), with unusually shallow Moho depths of slightly greater than 10 km. A shallow Moho depth would not be unexpected at a fracture zone. As the sonobuoys were shot in opposite directions, it is possible that the different velocities could be due to dip on Moho, which was unconstrained by the reflection data. If the Moho dip was the same at both stations, then the true mantle velocity would be 8.0 km.s^{-1}.

Eastern reflective crustal province

Within the area shown as deep Shackleton Basin oceanic crust in Figure 62, we observe a basement type that is highly distinctive. This type (*peo5*; e.g. line GA-229/22, Plate 13) is characterised by:

- generally smooth basement surface, with indications of short, seaward-dipping flows in the shallow basement;
- seismically transparent upper crust;
- highly reflective lower crust, with dipping reflectors;
- reflection Moho with high continuity.

This crustal type is also observed in the Enderby Basin (Stagg et al., in press) and in the Cuvier Basin (Sayers et al., 2002), areas where the crust was generated during the early stages of separation of Greater India from Australia–Antarctica.

A single sonobuoy station in this sector (229/SB44) gave a 'typical' oceanic profile, with a layer 3 velocity of 6.8 km.s^{-1}, Moho (velocity 8.5 km.s^{-1}) at a depth of 13.4 km and a total layer 2 & 3 thickness of about 5 km.

Northern faulted province

To the north of the Shackleton Basin, basement is characteristically rugged and faulted appearance (basement type *peo6*) and contains a deep and narrow basement trough between basement types *peo6* and *peo7* (Fig. 64). This trough continues for about 800 km along the northeast flank of the Labuan Basin, where it is correlates with a strong, negative gravity anomaly. It is likely that this crust is part of the eastern Labuan Basin of Borissova et al. (2002), and it is shown as such in Figure 62. Basement type *peo6*, south of the trough, is characterised by a highly reflective fabric that is strongly indicative of extensional faulting (Fig. 65).

Three sonobuoy stations were recorded in this sector (229/SB45–47). While the mantle velocities varied considerably (7.7–8.3 km.s^{-1}), all were reasonably constrained by the reflection data and can be considered representative. The Moho depths were in a narrow range (13.4–13.9 km), and the velocity profiles were consistent with an oceanic origin.

A single potential field model has been constructed for the India-Australia-Antarctica sector, this being a composite of lines GA-228/12, GA-229/22 and GA-229/23 (Plate 5; Fig. 66; model parameters in Appendix 7). This model was designed to test the composition of the crust northwest of Bruce Rise and demonstrates that the crust is likely to be oceanic in origin.

Bruce Sector

Continental Crust

Because of the prevailing ice conditions, the only continental crust to have been imaged anywhere in this region is that which underlies the margins of the Bruce Rise. These limited data, combined with the pre-breakup reconstruction of Bruce Rise against the Naturaliste Plateau on the margin southwest of Australia, suggest that the geology of these two features is broadly similar. The Naturaliste Plateau has been the subject of several studies since the mid-1970s (e.g. Petkovic, 1975; Ford, 1975; Jongsma & Petkovic, 1977; Coleman et al., 1982); Borissova (2002) summarises these studies and provides an interpretation of the most recent data available.

Morphologically and geologically, Bruce Rise is divided into eastern and western sectors (eBR and wBR in Fig. 62), separated by an interpreted north-northwest trending strike-slip fault zone that underlies the Bruce Canyon at about 98–99^{o}E.

Where imaged by seismic data, the outer margin of the east Bruce Rise is underlain by acoustic basement at a shallow depth below the seabed (Fig. 67; Plate 14, lines GA-228/13 & GA-228/14). On the higher-standing parts of the Bruce Rise, the basement is often planated (e.g. line GA-228/14). Some layering is evident at depths of up to 1 s below the basement surface, suggesting that this basement comprises old (?Palaeozoic) sediments and metasediments. Basement faulting is high-angle, indicating that there was minimal upper crustal extension during rifting. Fault trends cannot be determined with the widely-spaced seismic lines, however, on the northern margin, they appear to be sub-parallel to the plateau margin. Basement beneath the lower slope is downfaulted into the deep ocean basin across several major faults that have a combined throw of 4-5 s (*ca.* 6–7 km; Fig. 68). As with faults further inboard on Bruce Rise, these are high-angle faults.

The inboard part of the Bruce Rise is only imaged by a single seismic line (TH94-21; Ishihara et al., 1996), located near the eastern flank of the Bruce Rise and oblique to the margin. This line shows the presence of approximately 2 s (*ca.* 3 km) of south-dipping rift section with an overlying, flat, erosional unconformity and about 0.5 s (*ca.* 0.5 km) of flat-lying, post-rift sediments. Further examination of this line in the SCAR Seismic Data Library System (SCAR, 1992) shows that the thick sedimentary section continues as far south as the upper slope.

The eastern flank of the Bruce Rise is underpinned by the NNW-trending, high-angle (seabed slopes >20^{o}) Vincennes Fracture Zone (Tikku & Cande, 1999). This fracture zone, and its counterpart on the conjugate margin, the Leeuwin Fracture Zone (the Perth Fracture Zone of Tikku & Cande, 1999), are major constraints on the early extension azimuth between Australia and Antarctica. Across the Vincennes Fracture Zone, basement is downfaulted to the northeast by ~6 s (*ca.* 6+ km; Fig. 69). Adjacent to the Vincennes Fracture Zone, the interpreted sedimentary section extends to 9–9.5 s depth, indicating that the crystalline crust is extremely thin beneath the

fracture zone. As with the northern margin of Bruce Rise, the eastern margin appears to have been uplifted during rifting, with the rift sediments thickening westwards, away from the plateau margin (Ishihara et al., 1996, fig. 15).

Pockets of syn-rift sediments have been deposited within basement half graben on the Bruce Rise (Fig. 67), but these sediments are rarely more than 0.5 s (*ca.* 0.5–1 km) thick adjacent to the outer margin. Seismic character correlations with the Naturaliste Plateau and the known breakup history suggest that these sediments are likely to be of ?Late Jurassic to Early Cretaceous age, with the erosional unconformity at the top of the synrift section being Valanginian–Hauterivian. The sediments are likely to have been deposited in a continental to shallow marine environment. Post-rift sediments form a blanket that is less than 1 s (ca. 1 km) thick on the outer part of the plateau but which thickens southwards (see example sections in Ishihara et al., 1996).

The deeper western sector of Bruce Rise is only imaged by line GA-229/21 (Plate 14) and the Japanese profiles TH98-27 and TH98-26 (Murakami et al., 2000). Line GA-229/21 shows a package of reflectors that thicken seawards against a faulted basement high beneath the lower slope (Fig. 70). This reflective package attains a maximum thickness of 2 s (*ca.* 3–4 km) adjacent to the basement high.

Continent–ocean transition (COT)

The Bruce sector is characterised by a rapid change from distinctive continental crust to crust beneath the deep ocean basin that is more oceanic in character. This is in strong contrast to both the Greater India–Antarctica and Australia–Antarctica sectors, where transitional crust is interpreted to underlie a broad band beneath the continental margin. Transitional crust (horizon *cot*) has been identified on several profiles (GA-228/13, GA-228/14, GA-229/21; Plate 14; Fig. 68). However, on each of these profiles, it is possible that this crust actually consists only of deeply-subsided continental fragments.

The situation on the conjugate Australian margin is markedly different (Borissova et al., 2003a, b). There, the Diamantina Zone, south of the Naturaliste Plateau is interpreted as a continent-ocean transitional zone, and sampling indicates that the southernmost part is comprised of peridotite ridges. Therefore, the breakup of the Naturaliste Plateau and the Bruce Rise appears to have been highly asymmetric with most of the extended continental or transitional crust being attached to the Australian margin.

A further possibility is that there is a zone of transitional crust that is entirely detached from the Antarctic margin and now located immediately to the south of the fast-spreading crust of the Australian–Antarctic Basin. This possibility is examined in more detail later in this chapter.

Oceanic and undifferentiated crust

As with the sector to the west, the basement in this sector is divided into a number of different types. The characteristics of these crustal types (prefixes *qmu* and *qmo*) are listed in Table 7 and several are illustrated in Figures 68, 69, 71 & 72. The Bruce Rise sector can be further divided into western and eastern provinces on the basis of the gross basement character.

Western province

The western province (approximately 95–100°E) is characterised by two distinct basement types — *qmu1* (inboard) and *qmu2* (outboard; Figs 71 & 72). These are shown as '*Shackleton Basin ?oceanic – no internal fabric*' and '*... – complex internal fabric*' in Figure 62. While both basement types have a moderately rugged upper surface, the relief on the upper surface of *qmu2* is generally greater and has a longer wavelength. The crustal boundary between *qmu1* and *qmu2* is sharply defined by an undulating, north-dipping, high-amplitude reflection (Fig. 71). Both basement types exhibit some minor reflectivity in the upper crust, and there are indications of a reflection Moho beneath *qmu1*. The outboard edge of *qmu2* is marked by the major basement step to the fast-spreading crust of the Australian-Antarctic Basin (type *aabo*; profiles GA-228/13, GA-229/21, Plate 14; Fig. 72). The abrupt nature of this basement step suggests that the basement change is the result of a spreading ridge jump, rather than just a change in spreading rate.

Two sonobuoy stations were recorded in this sector, both on profile GA-229/20. 229/SB37, on *qmu1* crust, had a velocity of 7.1 $km.s^{-1}$ for the main crustal layer. 229/SB38, straddling the boundary between *qmu2* and *aabo* crust, provided no basement velocities, but did give a mantle velocity of 8.2 $km.s^{-1}$ at a depth of 12.9 km. Both of these sonobuoy stations give solutions that are consistent with (although not definitive of) oceanic crust.

Eastern province

The eastern province (lines GA-228/14 to GA-229/17; Plates 14 & 15) contains a wide variety of crustal types (*qmu3* to *qmu11*; *qmo1* and *qmo2*) in a tectonically complex area. The characteristics of the crustal types range from typically oceanic (*qmu6*, *qmu7*, *qmu9*, *qmu10*, *qmu11*, *qmo1*, *qmo2*), with a rugged basement surface and minimal crustal reflectivity, to 'undifferentiated', with a basement surface that appears to be extensively faulted and containing variable degrees of upper crustal reflectivity and which may be either continental or oceanic in origin.

Lines GA-228/14 and GA-229/19 (Plate 14) straddle the Vincennes Fracture Zone (VFZ) and show a particularly wide range of basement styles. The inboard half of line GA-228/14, west of the VFZ, is dominated by deep basement (~8 s) that is strongly faulted. In contrast, basement beneath the outboard half of the line is far more volcanic in appearance, with very high relief (up to 2.5 s, ~2.5 km on basement type *qmu7*). Basement beneath line GA-229/19, mainly east of the VFZ, is similarly volcanic in appearance with moderately rugged relief. It is likely that the rugged volcanic basement is due to extrusion along the VFZ. At the northern end of this line, basement shallows rapidly, probably correlating with the boundary to the fast-spreading Eocene oceanic crust of the Australian–Antarctic Basin.

Three sonobuoy stations (229/SB33–35) on line GA-229/19 provided basement velocities of 5.9–6.2 $km.s^{-1}$. While such velocities are normally reached in the deeper part of oceanic layer 2 (e.g. White et al., 1992), they rarely produce refractions on oceanic crust because they occur within a velocity gradient zone rather than at a velocity step. Rather, such velocities are more typically associated with continental crust. However, an interpretation of continental crust in this area would be in conflict with the observed reflection seismic character. Two of the stations also provided

mantle velocities of 8.0 and 8.5 km.s^{-1} with Moho depths of 12.7 and 11.2 km, consistent with an interpretation of oceanic crust.

Further east (lines GA-228/15–229/18 and GA-229/17; Plates 14 & 15), two basement types are identified (*qmo1* and *qmo2*). Basement on both these lines is extremely rugged, with relief of up to 2 s (*ca*. 3.5 km). There is little internal reflectivity, and we are confident in interpreting it as oceanic crust.

Two sonobuoy stations recorded basement or deeper velocities from this area (229/SB31–32). The basement velocities of 6.3–7.1 km.s^{-1} are consistent with the interpretation of oceanic crust. Station 229/SB31 also recorded a velocity of 8.0 km.s^{-1}; however, the depth of approximately 9 km to this refractor is likely to be too shallow for Moho and it is considered to be dubious.

A notable feature of the eastern part of this province is the presence of a segment of deep, faulted crust containing apparent sedimentary section down to approximately 9 s depth (Plate 14; line GA-228/15, SP 1300–1800). This crust is surrounded by the interpreted oceanic crustal types *qmo1* and *qmo2,* yet does not appear to be obviously oceanic. We speculate that it is s small fragment of continental crust that became detached from the margin during the complex breakup that characterises this part of the Antarctic margin.

Post-rift Sedimentary Section

Bruce Rise

The basement of the outer flank of the Bruce Rise is down-faulted oceanwards across a series of high-angle, stepped faults. The post-rift sediments on each basement step form mounds characterised by continuous, moderate- to high-amplitude reflectors that thicken towards the mound crests and which exhibit bidirectional downlap at the base of each mound. The seaward boundary of the Bruce Rise is a steep, faulted, rugged basement surface with only minor sediment accumulations in small half grabens in places (e.g. line GA-228/14; Plate 14).

The sediments on top of western Bruce Rise have a well-developed Bottom Simulating Reflector (BSR; Fig. 73). It comprises a zone parallel to the sea floor of high amplitude portions of reflectors that dip relative to this zone. The BSR does not exactly parallel all modern sea floor features, such as submarine canyons, suggesting that it is a relict feature rather than the product of modern pressure-temperature conditions.

Shackleton Basin

North and northeast of the Bruce Rise, the sedimentary section is relatively thin compared to most of the East Antarctic margin, being about 2 km thick. Internal reflectors are continuous and quite high-amplitude with some of the characteristics of contourites (Faugères et al., 1999). In particular, line GA-228/14 (Plate 14) shows well-developed moat and ridge topography with reflectors thickening towards the crest of the ridge. Precursors of the modern mound can be seen to have ‘climbed’ the unconformity at the base of the well stratified interval. This geometry is classified as a ‘separated drift’ by Faugères et al. (1999). Similarly, line GA-227/1401 (Plate 14) displays a mound separated from the steep eastern flank of Bruce Rise by a trough with a rough, eroded base. This topography resembles the contourite mounds on the

western Antarctic Peninsula margin described by Rebessco et al. (1997). Other lines (e.g. line GA-229/19; Plate 14) show deep-sea sediments abutting the same scarp.

The northwest flank of the Bruce Rise is also down-faulted oceanwards (e.g. line GA-229/21; Plate 14). However, fault throws are smaller than to the east and the basement scarp is buried beneath the onlapping and oceanwards-thickening post-rift sediments. The sea floor is undulating and erosional in places. Reflectors are moderately continuous and wavy, suggesting some small-scale erosion and channelling. Further seaward of the Bruce Rise, the sea floor becomes smoother, apart from low-relief channels and levees, and the subsurface reflectors exhibit higher continuity. The seismic facies and sea floor topography on the western side of Bruce Rise indicate deposition in submarine fans fed by canyons that originate on Bruce Rise and the adjacent continental slope.

DSDP Site 268, drilled to the east of Bruce Rise (Hayes, Frakes et al., 1975) penetrated 160 m of diatom ooze, silts and clays and beds of normally graded fine sand of Pliocene to Quaternary age (Unit I; Hayes, Frakes et al., 1975). Piper & Brisco (1975) interpreted the sand beds as turbidites. Line GA-228/16 shows that Unit I overlies an erosion surface that forms a large channel. This erosion surface is cut into Early Miocene to Early Oligocene sediments that are dominated by muds with thin silt laminae and which probably formed as contourites (Piper & Brisco, 1975). This stratigraphy suggests a history of contourite deposition from the Oligocene to the Miocene followed by canyon cutting and submarine channel and fan deposition through the Pliocene and Quaternary.

DISCUSSION

Figure 62 summarises the tectonic elements of the Antarctic continental margin from the eastern end of the Princess Elizabeth Trough to western Wilkes Land. This map, the first of its type produced from this part of the Antarctic margin, clearly reflects the complexities of the region. These complexities stem from a combination of its proximity to a triple junction that was produced by two breakup and spreading episodes of different styles, ages and azimuths that are overprinted by an intervening period of intense hotspot activity.

The Continental shelf is probably dominated by shallow crystalline basement. As with the Antarctic margin to the west and to the east, it is possible that this area also contains some rift basins. However, unlike those areas, there are no seismic data or rock samples from the shelf that could show the presence or otherwise of such basins.

The upper continental slope is interpreted to mark the onset of rapid, oceanward crustal thinning. The continental margin is divided into three structurally-distinct sectors: the narrow western sector from the Princess Elizabeth Trough to western Bruce Rise; the central sector, dominated by the approximately rectilinear, mid-slope plateau, Bruce Rise; and the eastern sector in which the continental margin appears to rapidly broaden eastwards towards Wilkes Land.

The conjugate setting of the Naturaliste Plateau and the Bruce Rise is obvious, particularly in satellite gravity images from the Southern Ocean (e.g. Borissova, 2002; Fig. 74). Similarities in the structure of the Naturaliste Plateau and the Bruce Rise interpreted from seismic data are also very pronounced (Figs 67, 75 & 76). These similarities include:

- shallow seismic basement;
- development of small half graben within the basement, bounded by high-angle faults and containing a syn-rift section up to about 1 s in thickness;
- development of a strong erosional unconformity (Valanginian–Hauterivian on the Naturaliste Plateau) at the top of the syn-rift section;
- relatively thin post-rift sedimentary section.
- development of a thick sedimentary basin inboard of the shallow basement and outboard of the continental shelf (Mentelle Basin inboard of the Naturaliste Plateau; un-named basin seen in seismic data in Ishihara et al., 1996).

Given these similarities, and the reconstruction of Naturaliste Plateau and the Bruce Rise shown by Borissova (2002; Fig. 74), it is reasonable to extrapolate the stratigraphy of the Naturaliste Plateau to the Bruce Rise, at least until the onset of fast spreading in the Eocene, at which time the plateaus were probably no more than about 500 km apart. This stratigraphy and the associated tectonic events identified on the Naturaliste Plateau are shown in Figure 77.

The margin complexities are most marked in the deep ocean basins that lie between the continental margin and the fast-spreading Eocene and younger oceanic crust of the Australian-Antarctic Basin. Broadly, the structural styles of these basins reflect the continental margin sectors referred to above.

The western sector (Princess Elizabeth sector) probably formed contemporaneously with the Enderby, Perth and Cuvier Basins and therefore would be underlain by Early Cretaceous oceanic crust that was generated at 'normal' spreading rates. Correlation of the crustal ages between the basins is supported by the presence of oceanic crust with distinctive lower crustal reflectivity and reflection Moho on lines in the Enderby and Cuvier Basins and on lines west of the Bruce Rise.

Prior to breakup, the rift between Greater India and Australia–Antarctica extended for approximately 6000 km from the Argo Abyssal Plain in the northeast to the western Enderby Basin in the west. The margins developed along this rift vary from a classical volcanic margin northwest of Australia (outer Exmouth Plateau and Wallaby Plateau), to a predominantly non-volcanic margin in the Enderby Basin (interpretation of Stagg et al., in press). The GI–A–A triple junction sector lies between these two end-member types and probably contains both volcanic and non-volcanic components. Of particular note here are the thick and areally extensive SDRS, diagnostic of a volcanic rifted margin, that have developed between the southern Kerguelen Plateau and the Bruce Rise. While these SDRS are located adjacent to the southeast Kerguelen Plateau, which also contains identified SDRS, they thicken away from the Antarctic margin and towards the Kerguelen Plateau. This suggests that the SDRS may have formed within the Antarctic margin, prior to their development on the Kerguelen Plateau, and have subsequently been detached from the margin by a spreading ridge jump. The presence of the SDRS means that the interpretation of a short segment of seafloor spreading magnetic lineation (dated as M4y in Fig. 62; Brown, this report) from the same area is unlikely to be correct.

The crust in the western sector, which is interpreted to be wholly oceanic, is sub-divided into a shallow western and a deep eastern and southern sector by a major N–S trending basement step of about 1 km relief. Presumably, the northwards- and westwards-shallowing corresponds to a major change in the age of the oceanic crust. The abruptness of the step implies that it is the result of juxtaposition of crust of considerably different ages — either at an oceanic transform, across which there is a considerable amount of offset, or due to a spreading ridge jump.

In the central sector (Bruce–Vincennes sector), the crust is likely to be largely oceanic as indicated by both the seismic reflection data and velocity information. Borissova et al. (2003a, b) have interpreted breakup between the Naturaliste Plateau and the Bruce Rise to have been highly asymmetric, with most of the continent–ocean transition crust remaining attached to the Australian margin, south of the Naturaliste Plateau. However, in some parts of this sector on the Antarctic margin, the reflection and velocity data indicate the presence of some crust with continental affinities. Therefore, we suggest that this sector probably comprises mainly oceanic crust with some stranded fragments of either continental or transitional crust. Brown (this report; Fig. 62) interprets magnetic anomalies M9y and M4y (Hauterivian–Barremian) in the panel of crust (shown as 'Shackleton Basin ?oceanic crust – no internal fabric' in Fig. 62). If this identification is correct, then it appears that oceanic crust of the GI-AA spreading episode may have penetrated eastwards from the triple junction between Australia and Antarctica leading to a minor degree of separation between those continents prior to final A-A breakup.

It is also possible that the crust shown as 'Shackleton Basin ?oceanic crust – complex internal fabric' in Figure 62 may be transitional crust that, prior to breakup between the Bruce Rise and Naturaliste Plateau, was a counterpart to the crust shown as 'inner COT' by Borissova (2002; Fig. 75). Alternative origins for this panel of crust are:

- Early Cretaceous GI–AA oceanic crust that was extended and rifted during pre-breakup extension between Australia and Antarctica; or
- Late Cretaceous, mechanically-extended oceanic crust contemporaneous with the oceanic crust first emplaced between Australia and Antarctica.

The sector immediately to the east of the Vincennes Fracture Zone is probably the most complex part of the region. The crustal character and velocity structure are highly varied and there are indications of fragments of thick sedimentary section that are caught up in an overall oceanic crust setting. Further definition of this sector will require more detailed seismic profiling than was available to this study.

SUMMARY

1. Bruce Rise, which is conjugate to the Naturaliste Plateau on the Australian margin, is a mid-slope plateau embedded in the Antarctic continental margin. Such plateaus are a very rare feature on the continental margin of East Antarctica. The Bruce Rise appears to largely consist of shallow basement of likely Precambrian or Palaeozoic age. This basement has been subjected to some faulting and minor extension which has led to the deposition of probable Cretaceous rocks in small half-graben. The post-rift sedimentary cover is probably rarely more than 1 km thick and contains a prominent bottom-simulating reflector.

2. The eastern margin of Bruce Rise is formed by the northwest-trending, high-angle Vincennes Fracture Zone, that probably reflects the early extension azimuth between Australia and Antarctica. The northern margin is underpinned by high-angle, large-throw basement faults. The western margin is less clearly defined, but there may be a northwest-trending strike-slip fault underlying the Bruce Canyon that separates the eastern, shallower part of Bruce Rise from the deeper western part.
3. Unlike other parts of the margin of the AAT, a continent-ocean transition zone is not particularly distinctive and the transition from continental to oceanic crust appears to be abrupt, particularly adjacent to Bruce Rise.
4. The deep ocean basins are complexly structured, probably reflecting the proximity to a major triple junction, at least two episodes of extension and spreading, and the proximity of the Kerguelen hot spot. In broad terms, three different crustal types can be recognised: Princess Elizabeth Trough to west of Bruce Rise; north of Bruce Rise; and east of Bruce Rise. While integrated seismic interpretation and potential field modelling supports the first of these crustal types as being oceanic, there is some doubt about the nature of the crust north of Bruce Rise. In this area, it is possible that the bulk of the crust is of oceanic origin, but it possibly has rifted fragments of continental crust included in it. Alternatively, the apparently rifted fragments of crust may be due to re-rifting of Early Cretaceous oceanic crust during the early (slow) spreading between Australia and Antarctica in the Late Cretaceous.
5. Comparisons with the Australian margin suggest that there are strong similarities between Bruce Rise and the Naturaliste Plateau. However, the deep-water part of the margins are highly asymmetric and it appears that final breakup took place close to the Antarctic margin, leaving a band of highly-extended continental-affinity crust and upper mantle attached to the Australian margin where it is now preserved as the Diamantina Zone.

Name	*Depth of basement top (s)*	*Basement surface*	*Internal reflections & character*	*Reflection Moho*	*Comments*
peo 1	7.0–7.3	Rough and rugged, up to 0.5 s relief.	Some reflectors below ~8 s; upper crust largely reflection-free	Not observed.	Consistent low seaward gradient.
peo 2	7.3–7.6	Rough, up to 0.1 s relief.	Some reflectors below ~9 s; upper crust largely reflection-free	Not observed.	Consistent low seaward gradient.
peo 3	7.6–8.0	Smooth to slightly rough	Some reflectors below ~8.5 s; upper crust largely reflection-free	Low amplitude; moderate continuity; up to 0.5 s relief.	Consistent low landward gradient.
peo 4	6.3–8.3	Rough, up to 0.25 s relief	Some reflectivity in shallow crust; possibly faulted.	Not observed.	Consistent low seaward gradient.
peo 5	7.6–8.6	Generally smooth; faulted in one area	Somewhat transparent in shallow crust and distinctly reflective in deeper crust.	Moderate amplitude and continuity.	Similar to *ebo 2*, but not as distinctive as that type. Sub-Moho strongly reflective on GA-229/23, including landward-dipping reflections similar to *ebo 2*.
peo 6	7.6–9.3	Rugged where faulted; smooth elsewhere.	Highly reflective; dipping reflectors indicating strongly faulted.	Low amplitude; moderate continuity.	Eastern Labuan basin crust. Highly distinctive and does not appear to be 'normal' oceanic.

Name	*Depth of basement top (s)*	*Basement surface*	*Internal reflections & character*	*Reflection Moho*	*Comments*
peo 7	7.0–9.3	Extremely rugged, up to 2.5 s relief	Dipping reflectors in shallow crust; possibly faulted.	Not observed.	Highly distinctive; could be fast-spreading crust of Australian–Antarctic Basin (equivalent to *aabo* crust).
peo 8	6.6–7.3	Rough and rugged	Minimal internal reflectivity.	Not observed.	Minor crust at inboard flank of *peo 9* crust.
peo 9	6.6–7.0	Generally smooth	somewhat transparent in shallow crust and distinctly reflective in deeper crust	Moderate amplitude and continuity.	Similar to *peo 5* and *ebo 2*, but not as distinctive as those types.
sdrs	5.5–7.6	Smooth, with high-relief areas (?buildups)	SDRS down to ~8–9 s.	Faint & discontinuous on GA-228/11 only	Classic SDRS sequences down to 8-9 s (*ca.* 5-6 km thick); some intra-SDRS buildups.

Table 6: Seismic reflection characteristics of different types of crust in the Shackleton Basin, west of Bruce Rise. All time-depths are seconds two-way time (TWT). 'Rough' refers to short-wavelength, generally low-amplitude basement topography , whereas 'rugged' refers to longer-wavelength topography generally with high-amplitudes.

Name	*Depth of basement top (s)*	*Basement surface*	*Internal reflections & character*	*Reflection Moho*	*Comments*
qmu 1	7.0–8.3	Moderately rugged; up to 0.6 s relief.	Minor reflectivity in upper crust	Occasional low-amplitude and continuity.	Indications of some faulting in upper crust.
qmu 2	7.0–8.1	Rugged; relief up to 1 s.	Reflective in uppermost 1 s of basement.	Not observed.	Reflectivity in upper crust may be flows and extensional faulting.
qmu 3	7.3–8.3	Moderately rugged; relief up to 0.7 s.	Some mid- and deep-crustal reflectivity.	Occasional low-amplitude and continuity.	Seaward-facing scarps and crustal reflectivity indicate faulting.
qmu 4	7.6–8.0	Moderately rugged; relief up to 0.5 s.	Minimal internal reflectivity.	Occasional low-amplitude and continuity.	Seaward-facing scarps either faults or flow edges. Similar to *qmu 3*, although slightly less relief and shorter wavelength basement faulting/scarps.
qmu 5	7.5–8.8	Rugged, relief >0.7 s	Some upper-crustal reflectivity	Not observed.	Seaward-facing scarps and upper-crustal reflectivity indicate faulting.
qmu 6	7.3–8.3	Rugged, irregular basement, relief up to 1 s.	Minimal internal reflectivity.	Occasional low-amplitude and continuity.	Appears to be a rugged volcanic surface; irregular relief not indicative of any faulting.
qmu 7	4.8–7.5	Generally low relief, except for large volcanic peaks with relief >2 s.	Upper- and mid-crustal reflectivity, mainly seaward-dipping.	Not observed.	Basement peaks may be fracture zones. Upper crustal reflectivity could be faulting, but this does not offset basement surface.

Name	*Depth of basement top (s)*	*Basement surface*	*Internal reflections & character*	*Reflection Moho*	*Comments*
qmu 8	7.0–9.6	Steeply-dipping faulted surface	Coherent reflectivity beneath basement surface.	Not observed.	Basement adjacent to Vincennes Fracture Zone; probably continental/transitional.
qmu 9	7.0–7.8	Rugged, mounded basement, relief up to 0.9 s.	Minimal internal reflectivity.	Not observed.	Probable volcanic basement.
qmu 10	6.6–7.3	Moderately rugged; relief up to 0.7 s.	No internal reflectivity.	Not observed.	Probable volcanic basement.
qmu 11	6.3–7.6	Moderately rugged; relief up to 0.5 s.	Some upper-crustal reflectivity.	Not observed.	Probable volcanic basement. Some suggestions of upper-crustal faulting.
qmo 1	4.9–7.6	Extremely rugged; relief up to 2 s.	No discernible reflectivity.	Not observed.	Volcanic basement.
qmo 2	6.0–7.8	Extremely rugged; relief up to 1.8 s.	Occasional upper-crustal reflectivity.	Not observed.	Volcanic basement.
aabo	6.0–8.0	Rugged; relief up to 1 s, except at inboard edge where it is ~1.6 s.	Some shallow crustal reflectivity.	Not observed.	Fast-spreading crust of Australian-Antarctic Basin.

Table 7: Seismic reflection characteristics of different types of crust in the Shackleton Basin, north and east of the Bruce Rise. All time-depths are seconds two-way time (TWT). 'Rough' refers to short-wavelength, generally low-amplitude basement topography , whereas 'rugged' refers to longer-wavelength topography generally with high-amplitudes.

Sono #	*Line*	*WD*	*Vel*	*Depth*	*Vel*	*Depth*	*Vel*	*Depth*	*Comments*
229/SB31	229/17	4.36	6.3	~6.2	8.0	~9.0			*qmo2*; 6.3 km.s^{-1} approximates top of rugged basement. 8.0 km.s^{-1} is very shallow for Moho.
229/SB32	229/18	4.42	6.8	7.5	7.1	9.5			*qmo2*
229/SB33	229/19	4.45	5.9	8.5	8.5	11.2			*qmu11*
229/SB34	229/19	4.55	6.2	7.3	8.0	12.7			*qmu10*
229/SB35	229/19	4.48	5.9	~6.6					*qmu9*; 5.9 km.s^{-1} is near top of rugged basement.
229/SB37	229/20	4.1	(5.1)	~7.3	7.1	8.5			*qmu1*
229/SB38	229/20	4.53	(5.0)	~6.5	(6.7)	~7.8	8.2	12.9	Boundary between *qmu2* and *aabo*.
229/SB39	229/21	4.6	4.9	~6.8	6.3	~8.6			*qmu2*, near boundary with *aabo*; 4.9 km.s^{-1} is at top basement.
229/SB40	229/21	4.24	6.6	~9.2					Boundary between *qmu1* and *qmu2*.
229/SB41	229/21	3.93	6.5	~7.0					*qmu1*; 6.5 km.s^{-1} is near top basement.
229/SB42	229/21	3.7	(5.0)	~5.5	6.4	6.8			Boundary between continental and transitional crust; basement is complex and faulted.
229/SB43	229/22	3.88	5.7	8.4					*peo4*; 5.7 km.s^{-1} is near top basement.
229/SB44	229/22	4.25	5.0	7.3	6.8	8.7	8.5	13.4	*peo5*; 5.0 km.s^{-1} is near top basement; 8.5 km.s^{-1} correlates with reflection Moho.
229/SB45	229/22	4.52	5.5	~6.8	7.1	8.6	7.7	13.9	*peo6*; 5.5 km.s^{-1} is within basement; 7.7 km.s^{-1} correlates with reflection Moho.

Sono #	*Line*	*WD*	*Vel*	*Depth*	*Vel*	*Depth*	*Vel*	*Depth*	*Correlation with reflection interpretation*
229/SB46	229/23	4.37	(4.9)	~7.2	(6.7)	8.8	7.9	13.4	Boundary between *peo6* and *peo7*; 7.9 km.s^{-1} has approximate correlation with dipping reflection Moho.
229/SB47	229/23	4.4	6.7	8.9	8.3	13.5			*peo5*; 8.3 km.s^{-1} slightly deeper than reflection Moho.
229/SB48	229/24	4.2	5.5	~6.7	6.5	~6.8	8.4	10.2	Boundary between *peo8* and *peo9*; Moho reflection at ~10 s.
229/SB49	229/25	4.04	6.5	~6.8	7.6	10.8			Boundary between *peo2* and *peo8*; 6.5 km.s^{-1} is near top basement.

Table 8: Sonobuoy locations and solutions for Surveys GA-228 and GA-229 in the Greater India–Antarctica–Australia sector; only basement and deeper velocities are shown. Depths are km below sea level; velocities are km.s^{-1}. Velocities in parentheses are assumed. Depths preceded by a tilde ('~') are approximate, usually because of short-wavelength relief on an interface.

INTERPRETATION: AUSTRALIA–ANTARCTICA SECTOR

INTRODUCTION

The sector from western Wilkes Land to George V Land (~105–160°E) was formed during the separation of Australia and East Antarctica, culminating with the onset of seafloor spreading in the Late Cretaceous. Geologically, the margin can be divided into two broad zones: one from western Wilkes Land to Terre Adélie, which formed predominantly in an orthogonal extensional setting involving the margins of western-central southern Australia and East Antarctica; and the other off George V Land, which formed in an overall oblique-slip to strike-slip setting involving the margins of the Otway Basin/western Tasmania/South Tasman Rise and Antarctica east of about 140°E. Incidentally, the Wilkes-Adélie segment is one of the better-surveyed (although survey lines are still generally widely-spaced) and studied parts of the East Antarctic margin, while the George V Land segment is one of the more poorly-known due to the extensive semi-permanent ice cover that, in most seasons, severely restricts the area in which marine seismic operations can be undertaken.

Prior to surveys GA-227–229, the best-surveyed part of this sector was offshore eastern Wilkes Land to George V Land where work has been carried out by France (Wannesson et al., 1985), the USA (Eittreim & Smith, 1987) and Japan (Sato et al., 1984; Tsumuraya et al., 1985; Ishihara et al., 1996; Tanahashi et al., 1997). However, west of this area, only Japan has undertaken any surveying, and this was only on widely-spaced lines.

On the basis of the single, moderate-quality French multichannel seismic line acquired off Terre Adélie in 1982, Wannesson et al. (1985) interpreted a thick sedimentary basin beneath the outer shelf and slope and noted the presence of a structurally high zone in deep water (corresponding to the 'Adélie Rift Block' of Colwell et al., *in press*). They referred to this zone as being an 'anomalous oceanic zone', apparently on the basis that previous workers (e.g. Cande & Mutter, 1982) had identified seafloor spreading magnetic anomalies in this area (see Discussion section of this chapter).

Eittreim & Smith (1987) reported the interpretation of the multichannel seismic data set acquired by the USGS L1-84-AN survey which took place in 1984 offshore eastern Wilkes Land, Terre Adélie and western George V Land from approximately 130–146°E. This data set extends from the shelf edge to the inner edge of the deep-ocean basin, overlapping with the inner ends of GA-228 and GA-229 survey lines. Beneath the continental slope, they identified rift-onset (K2) and breakup (K1) unconformities in a broad, margin-parallel sedimentary basin. They also identified a deep-water marginal rift basin, about 40 km in width, adjacent to the inboard edge of elevated basement that they interpreted as oceanic crust. In the vicinity of their continent-ocean boundary, they identified three volcanic sequences, interpreted as flood basalts above thinned continental crust (sequence V1), stratoid or Icelandic basalts of earliest oceanic crust (V2) and normal oceanic crust (V3). Consistent with the interpretation of Wannesson et al. (1985), they identified a persistent reflection Moho beneath the outer part of the rift basin and the oldest oceanic crust and interpreted the COB well inboard on the margin.

Tanahashi et al. (1987, 1997) interpreted two long lines acquired on the Japanese TH82 and TH95 surveys. Their interpretation shows marked differences with those of both Wannesson et al. (1985) and Eittreim & Smith (1987), as the TH82 and TH95 data sets extend more than 350 km seaward of the L1-84-AN data into deep water of the Australian–Antarctic Basin. Tanahashi et al. (1997) noted the presence of a 'marginal high' (equivalent to the 'Adélie Rift Block'), and reported continental rocks (including granite, gneiss, slate and diorite) dredged from seamounts that are outboard of the 'marginal high' (see Geology section below). Yuasa et al. (1997) also reported *in situ* peridotite blocks dredged from the same area that were interpreted as having 'fertile subcontinental characteristics', inferring that oceanic crust was not being actively produced in this area at the time and that continental crust remained. Based on this seismic and geological evidence, Tanahashi et al. (1997) interpreted a COB at 61.5–62.3°S off Terre Adélie, a location that is approximately 300 km seaward of the location interpreted by Eittreim & Smith (1987).

Other sample data are sparse in the region. The Deep Sea Drilling Project (DSDP) drilled one hole in the area, DSDP Site 269 (Plate 7), which reached a total depth below sea floor of 958 m. The oldest sediments recovered were of at least Middle Oligocene age (Hayes, Frakes et al., 1975). One Cretaceous core (DF 79-38-PC) has been recovered from the inner continental shelf off George V Land; details of these samples are given below.

GEOLOGY

This section focuses on the geological samples that have direct relevance to the interpretation of the Survey GA-227–229 geophysical data from the deep continental margin.

Deep Sea Drilling Project

Deep Sea Drilling Project (DSDP) Site 269 is located near the southern edge of the south Indian Abyssal Plain (Australian–Antarctic Basin) at a water depth of 4285 m (Plate 7), and reached a total depth of 958 m below sea floor in Middle Oligocene or older sediments (Hayes, Frakes et al., 1975). The total sediment thickness is estimated to be about 1400 m based on seismic data. The hole is tied by the Japanese seismic line TH82-02SMG and the French line ATC82-101, but is not tied directly by Surveys GA-227–229.

The section recovered consists dominantly of silts and clays. Although the core is discontinuous and the section is relatively uniform, the abundance and type of microflora have been used to identify five units, where unit boundaries have been placed halfway between cored intervals:

Unit 1 – This Quaternary unit is 20 m thick (sub-bottom depth of 0 to ~20 m) and contains diatom oozes interbedded with diatom-bearing silty clay and occasional very fine sand beds. Sand beds have sharp bases, and some tops are sharp while others grade into clayey silt.

Unit 2 – This Late Miocene to Pliocene unit is ~200 m thick (sub-bottom depth of ~20 to ~220 m) and consists mainly of silty clay, with some diatoms present. Silt beds and laminae are common and undisturbed by bioturbidation. Various types of stratification are found in the silts.

Unit 3 – This Late Miocene unit is 50 m thick (sub-bottom depth of ~220 to ~270 m) and contains diatom-rich nanno clay, diatom silty clay and diatom clayey silt. It is found in a single core, which is badly fractured.

Unit 4 – This ?Early to Late Miocene unit is ~160 m thick (sub-bottom depth of ~270 to ~430 m) and is similar to Unit 2. The unit is dominated by silty clay or clay, with minor diatoms. Silt beds and laminae are common, and numerous stratification types are preserved. At 360 m bsf and below, the sandy silt and silty clay–clay lithologies are in places lithified to porcellaneous chert.

Unit 5 – This ?Early Miocene and Oligocene unit is >528 m thick (sub-bottom depth of ~430 to >958 m) and consists of silty clay and clay, with beds and laminae of silt, silty clay and very fine sand. The unit contains trace quantities of nannofossils throughout and two foram assemblages. The whole unit has been 'semilithified', with sedimentary structures in the low part of the unit well preserved.

The units have a low microfossil content, with virtually no calcareous microfossils being present. Occasional Late(?) Oligocene to Early Miocene foraminifera assemblages are usually poorly preserved and contain only a few specimens (Kaneps, 1975). Nannofossils are rare and sporadic within the section, with the two species identified providing a Early Miocene and a mid-Oligocene age (Burns, 1975). However, these dated assemblages may be reworked. Radiolaria and diatoms are present in the Middle Miocene to Pleistocene sediments and are more abundant in post-Miocene sediments (Chen, 1975; McCollum, 1975). Silicoflagellates are present in post-Miocene sediments (Bukry, 1975).

Estimated means of sonic velocity and wet-bulk density for Site 269 increase from about 1.50 to 2.25 $km.s^{-1}$ and from about 1.30 to 1.95 g/cc, respectively. The associated acoustic impedance ranges from 2.0 to 4 x 10^5 g/cm^2 sec. However, all of the parameters are extremely variable within individual cores and sections of cores, with observed variations appearing to correlate with compositional and lithification variations. Very high velocities appear to correlate with chert nodules in some cores and there seems to be a stepped increase in velocities at about 400 m. This might represent an unconformity or a diagenetic change. ODP Site 1165 showed such a change associated with the Opal A/CT transformation at about 600 mbsf. A shallower depth might reflect higher heat flow at Site 269.

The calculation of two-way time versus depth from the core velocity measurements produced time-depths for unit boundaries that are similar to the calculations of Wannesson (1990) who used stacking velocities from an intersecting seismic line. The

core-based model (Table 9) gives slightly higher two-way times for the shallower horizons that the stacking velocities.

Unit boundary	Depth (m bsf)	Two-way time (sec below sea floor)
2/3	220	0.3029
3/4	270	0.3696
4/5	430	0.575
Total depth	958	1.11

Table 9: Calculated two-way time to major unit boundaries at DSDP Site 269. Units from Hayes, Frakes et al. (1975).

Dredges and cores

Core DF 79-38-PC from the George V Land margin (Plate 7) recovered a brecciated, carbonaceous siltstone that contains abundant Lower Cretaceous (?Aptian) palynomorphs. The core was located in the Mertz Trough, a deep inner-shelf basin, southeast of the Mertz Glacier (Domack et al., 1980). Domack (1987) examined pebble lithologies in the area and suggested that the Cretaceous sediments were part of a half-graben fill consisting of Mesozoic to Cainozoic sandstone, siltstone and basalt (Fig. 78).

Sato et al. (1984) reported a dredge site on the upper continental slope off Terre Adélie that recovered limestone fragments and an assemblage of sedimentary, metamorphic and igneous rocks. Most of the rock types are probably ice rafted to the site; however the limestones are not found elsewhere and so may be derived locally. They contain diatom assemblages indicating Miocene and Oligocene ages.

The presence of Mesozoic sediments beneath the inner shelf and Cainozoic sediments on the upper slope suggest a similar arrangement of sediments on the George V Land – Terre Adélie shelf to that on the Mac.Robertson Shelf described previously in this report. In these areas, older sediments are exposed on the inner shelf by late Cainozoic glacial erosion and canyon formation whereas younger sediments are preserved/deposited on the outer shelf and upper slope (e.g. Fig. 78).

The TH91 and TH95 surveys dredged rocks from three seamounts in deep water off Terre Adélie (Tanahashi et al., 1997; Yuasa et al., 1997; Table 10; Plate 7). The most seaward of these dredges (dredge D1201 on survey TH91, for which no post-survey report appears to be published) recovered *in-situ* peridotite that chemical analysis indicates is a fragment of fertile mantle emplaced at shallow crustal levels during rifting (Yuasa et al., 1997). Dredges D1601 and D1602, collected on survey TH95, were located in a slightly more landward setting and recovered granite, gneiss, slate, diorite, calcareous ooze, a manganese nodule and manganese crusts Table 10). Unfortunately, no further information appears to have been published on these latter two dredge hauls. However, their deep-water location well outboard of many

published locations of the continent–ocean boundary has important implications for the location of this boundary, as discussed later in this report.

Dredge	Latitude	Longitude	Lithologies and ages
D1201	62° 08” S	141° 22’ E	peridotite
D1601	61° 49’ 37” S 61° 49’ 13” S	140° 32’ 42” E 140° 34’ 42” E	granite, gneiss, diorite, calcareous ooze, manganese nodule
D1602	62° 18’ 55” S 62° 18’ 59” S	140° 56’ 24” E 140° 54’ 42” E	granite, gneiss, slate, calcareous ooze, manganese nodule and crust
DF-79-38	67° 44’ S	146° 51’E	non-marine siltstone with Cretaceous palynomorphs
TH82/D302	65° 31.6’ S 65° 31.4’ S	139° 32.1’ E 139° 31.4’ E	Oligocene and Miocene limestone

Table 10: Cores and dredges from offshore Terre Adélie and western George V Land containing basement rocks and Mesozoic and Cainozoic fossil material (Domack et al., 1980; Sato et al. 1984; Tanahsahi et al., 1997). Locations of the sampling sites are shown in Plate 7.

GEOPHYSICAL INTERPRETATION

Introduction

In common with other sectors of the margin of East Antarctica, there is little coverage of the continental shelf with good-quality reflection seismic data because of the prevalence of ice, even in the summer months. No Survey GA-227–229 lines extended inshore to the shelf edge. Several lines from the ATC82 survey (France) were recorded across the shelf almost to the coast of Terre Adélie in what must have been a relatively ice-free season. Inspection of these lines through the Antarctic Seismic Data Library System (SCAR, 1992) shows that the shelf is generally underlain by seaward-dipping sediments. The total thickness of these sediments is unknown as the seismic processing available at that time only achieved partial suppression of the multiples. However, the sediments are likely to be of Late Cretaceous and Cainozoic age and hence belong to the post-rift succession only. The inboard ends of some lines indicate that crystalline basement crops out at the seabed. In the same area, the L1-84-AN survey lines only extended inshore as far as the shelf edge.

Further west, the Japanese TH83 and TH94 surveys recorded two lines that extended part-way across the shelf to the northwest of Casey Station, and a single line on the shelf north of Porpoise Bay. However, these lines also reveal little of the geology underlying the shelf.

The tectonic elements map in this area (Plate 21; detailed map in Fig. 79) shows an inferred rift-bounding fault zone approximately underlying the shelf edge. This is interpreted on the basis that crystalline rocks crop out along the coast, whereas all the

available seismic data show that the continental slope is underlain by thick rift and post-rift sedimentary rocks. It is likely that the inferred location of this fault zone is considerably in error in many areas.

Although there is a broad degree of structural consistency along the length of this sector of the margin, there are some variations that allow the margin to be divided into several sectors, here named for the Antarctic coast that generally lies onshore from each sector (consistent with Colwell et al., in press) – *viz.* Knox sector; Sabrina sector; Banzare sector Adélie sector; and George V sector. Each of these sectors is described below with respect to key lines, which in some cases have been used for potential field modelling. Results of Survey GA-228 and GA-229 sonobuoys recorded in the region are given in Table 12 and Appendix 5.

Knox Sector

The Knox sector of the margin lies immediately to the east of the Bruce Rise and the Vincennes Fracture Zone from approximately 105° to 112°E. Its structure is shown in the interpreted seismic sections in Plate 15 (lines GA-228/17 to GA-228/18 and their extensions), in the integrated potential field model of line GA-228/18 (Fig. 80), and in the tectonics elements map (Plate 21).

Typical lines in the area clearly show the transition from an inboard, wide continent–ocean transition zone (COT), which is characterised by zones of highly-faulted continental crust interspersed with zones dominated by apparent magmatic material, to oceanic crust of the Australian–Antarctic Basin lying outboard of the COB. The COB is marked by a change in seismic character of the basement and a step up in basement level to the north (Fig. 81); basement continues to shallow to the north consistent with its decreasing age. The oceanic crust (*wwlo*; Table 11, Plate 15) has a fairly rugged and rough upper surface and a bland internal character when compared to the more heterogeneous and probably older (?Early Cretaceous) oceanic crust lying to the west off Bruce Rise/Queen Mary Land, and compared to the crust of the COT. The oldest magnetic anomaly picks in the area (A34y to A27o; Figs 26, 27, 79; Plate 21) lie inboard of the interpreted COB (i.e. within the COT) suggesting that they are related to linear magmatic bodies rather than to 'true' oceanic crust emplaced during seafloor spreading. The oldest magnetic anomaly lying to the north of the COB is A20o (Middle Eocene in age), which elsewhere along the Wilkes Land margin marks the transition from slow to fast spreading oceanic crust.

The COT in the Knox sector widens eastwards from about 250 km adjacent to the Vincennes Fracture Zone (~103°) to about 400 km at about 112°E. There are two major types of pre-breakup crust imaged in the seismic reflection data in this zone: (i) highly-faulted blocks of apparent pre-rift sedimentary rocks, which by correlation of the overlying unconformity with the conjugate southern Australian continental margin are of probable pre-Turonian age (equivalent to base *Tiger* unconformity of Totterdell et al., 2000); and (ii) highly-intruded sediments containing probable bodies of gabbro, peridotite and associated volcanics. The latter crustal type (beneath horizon COT in Fig. 81) is characterised by high-amplitude, discontinuous, generally dipping reflections, which in many cases may be sills, dykes or the top of volcanic piles. Sedimentary blocks within the COT vary in seismic character from strongly to weakly stratified. Preliminary potential-field modelling of one of the lines in this segment of the margin (GA228/18) includes the presence of an 'inner basement high' within the

COT. This 'high' is interpreted as being composed of highly intruded ?Jurassic sediments (bodies M1 & M2, Fig. 80).

The syn- and post-rift sediments along this part of the margin form a thick (up to 5 secs TWT, 7+ km), generally seaward-thinning blanket over the pre-rift sedimentary blocks and magmatic bodies of the COT. The axis of this massive sedimentary accumulation, here termed the *Sabrina Basin* (Plate 21), is located near the southern (inboard) end of the seismic lines where the crustal thinning is most rapid. The axis of the basin lies approximately 100 km to the north of the location of the margin rift-bounding fault system and extends along the margin for a distance of over 1000 km. The Sabrina Basin is the counterpart of the Bight Basin which extends for a similar distance along the conjugate southern Australian margin.

Preliminary potential field modelling has been undertaken of line GA228/18 in the Knox sector (see Appendix 7 for detailed notes on the model and specifics of the methodology used). The model (Fig. 80) shows a broad thinning of the crust corresponding to the maximum thickness (~9.5 km) of syn- and post-rift sediments of the largely post-rift Sabrina Basin (bodies A–F). The maximum thinning occurs immediately inboard of an 'inner basement high' (IBH) which is modelled as two strongly magnetic bodies of reverse polarity (bodies M1 and M2 in Fig. 80) thought to be highly-intruded ?Jurassic sediments. These bodies are overlain by horizon COT in the seismic interpretation shown in Plate 15. Inboard of the IBH the pre-rift rocks are interpreted as ?Jurassic–Early Cretaceous sediments (J) or lower crustal metasediments (L).

Outboard of the IBH, between body M2 and the COB (Fig. 80), rift-related volcanic flows and interflow sediments (body G) are interpreted to overlie highly faulted/structured blocks of ?Jurassic-Lower Cretaceous sediments (body K). These in turn overlie two dense, magnetic blocks (bodies N1 and N2) that are interpreted from their geophysical properties and setting to be composed of altered peridotites exhumed during movement along deep-penetrating listric faults that partly bound the overlying sedimentary basin. Oceanic crust consists of typical Layer 2A basalts (body O) overlying a sheeted dyke layer (body P) and the peridotite layer (body Q). As with other parts of the Wilkes Land margin, Layer 2A of the oceanic crust appears to be broken into a series of rotated fault blocks by listric faults which in some cases act as master faults offsetting both the sheeted dyke layer and the underlying peridotite layer. The faulting within the oceanic crust provides evidence of post-breakup mechanical extension.

In common with all other parts of the continental margin of the Australian Antarctic Territory, two factors here make the identification of the geometry and structure of the entire continental margin rift system impossible. Firstly, imaging of the margin rift bounding fault system is prevented by ice cover, and secondly the very thick cover of syn- and post-rift sediments shed off Antarctica makes imaging of basement structures difficult, particularly in the inner part of the COT. Consequently, in any complete margin reconstruction a heavy reliance should be placed on correlation and analogy with the relatively sediment-starved conjugate margin of southern Australia. A major study is currently being undertaken by Geoscience Australia of the conjugate margin to the Knox sector, the westernmost part of the Bight Basin. This will assist future margin reconstructions.

Sabrina–Banzare Sectors

The Sabrina–Banzare sectors of the margin extends from approximately 112°E to 132°E. The interpretation of this margin segment is shown typically by lines GA-228/23 and GA-228/24 (Plates 16 & 17), and by the integrated potential field models of these lines (Figs. 82 and 83) and line GA-228/21–229/10 (Fig. 84; Appendix 7). Because of ice cover, none of the lines cross the inferred margin rift bounding fault system to the south. The lines typically illustrate a clear oceanward transition from highly-extended continental crust at the landward end of the line, through a COT comprising a mixture of sedimentary and igneous components, to "normal" unequivocal oceanic crust lying outboard of the COB. This transition is much more obvious than in the Knox sector. Although based on an integration of all lines from the margin segment, the description below (largely following Colwell et al., in press) focuses in detail on line GA-228/24 (Plate 17, Fig. 83).

The landward (southern) end of the lines in this margin sector are characterised by a rapid thinning of the crystalline continental crust (the seismically transparent section below horizon *tran* (see Plates 16 and 17 ; bodies I1 & I2 in Fig. 83) from about 10 km to <4 km over a distance of about 80 km; the Moho (top of body J) shallows from about 18 km to about 12 km over the same distance (Fig. 83). This thinning is accompanied by extensive faulting of the overlying pre- and syn-rift section, and erosion and onlap of the post-rift section, particularly at the *eoc* horizon (Fig. 85). The unconformity at the top of the rift section (top of major structuring; horizon *tur*, equivalent to horizon *K1* of Eittreim & Smith, 1987) is postulated to be of Turonian age on the basis of seismic character correlation with a similar, dated unconformity on the conjugate Australian continental margin in the Great Australian Bight (*base Tiger* unconformity of Totterdell et al., 2000); this is similar to the Knox sector.

Much of the crustal thinning appears to be due to ductile deformation and thinning of the transparent lower crustal layer. The outboard edge of the margin rift basin is marked by a basement ridge (bodies K1 & K2 in Fig. 83) which the potential field modelling indicates is composed of material with physical properties consistent with those of altered/serpentinised peridotite (normally magnetised, magnetic susceptibility (k) 0.02 SI, densities 2.80 & 2.87 x 10^3 kg.m^{-3} , Appendix 7). This ridge is similar in form and interpreted composition to a basement ridge located in an equivalent structural position at the inboard edge of the COT on the conjugate Great Australian Bight margin (Sayers et al., 2001; Fig. 86). The upper parts of these bodies on both margins are marked by mantling caps of noisy, discontinuous, high-amplitude reflections interpreted as basaltic volcanics (RHS of Fig. 85). Seismic reflections in the inner parts of the ridges beneath the caps show little coherence, although some deep-penetrating planar faults can be detected offsetting reflectors. Both ridges are probably very complex bodies, likely comprising magma chambers, sills and dykes that are the product of mantle up-welling and partial melting focussed at the point of maximum change/necking of crustal thickness. These rocks are also likely to have been affected by infusing seawater, which would result in them being variably serpentinised. Inboard of the ridges on both margins, altered mantle peridotites (body J in Figs 82 & 83) are interpreted as underlying the now-brittle continental crust.

The broad COT zone in the Sabrina–Banzare sectors is dominated by a broad sedimentary basin (up to 50 km wide) that commonly contains 2+ s TWT of deeply-

faulted and highly-rotated syn-rift rocks of probable Cretaceous age (see for example Figs 87 & 88; body G in Fig. 83). These sediments have a similar seismic character (well-developed stratification with some high-amplitude events that probably represent sills, dykes and volcanics) and structuring to the pre-rift section lying inboard of the peridotite ridge (compare Fig. 85 with Figs 87 & 88). The higher velocity and density, but lower magnetisation of the outer set of fault blocks (Appendix 7) probably reflects greater degrees of metamorphism / metasomatism during rifting. Faulting of both the sedimentary section and the peridotite ridge largely terminates by Turonian time. The potential field model for line GA-228/24 shows that this depocentre is underlain by three blocks (M1 to M3 in Fig. 83); similar blocks occur outboard of the peridotite ridge on line GA-228/23 (L1 to L5 on Fig. 82). These have 'noisy' seismic character with few coherent reflections (see seismic sections in Plates 16 & 17), and an upper surface often bounded by a single, strong continuous high amplitude event which may be a detachment fault (subsequently re-faulted) similar to those imaged by Reston et al. (2001) and Perez-Gussinye & Reston (2001) in North Atlantic basins. The modelled properties of the blocks underlying the strong reflector (3.03×10^3 kg m^{-3}; 0.03 SI; 3.10×10^3 kg m^{-3}; 0.01 SI; 3.00×10^3 kg m^{-3}; 0.02 SI) are consistent with abandoned blocks of serpentinised continental lithospheric mantle. This scenario is similar to that modelled by Whitmarsh et al. (2001) on the analogous Iberian non-volcanic COT zone, and mapped by Muentener & Herrmann (2001) in exhumed COT successions in the Swiss Alps.

The potential field model of line GA-228/24 (Fig. 83) indicates that there has been massive (>10 km) thinning of the lower and middle crust beneath the tilted blocks, with little or no indication of the lower crustal petrophysical properties interpreted in the inboard section of the line beneath the continental slope.

The outer edge of the COT is marked by a basement high (~SP 4000 on line GA-228/24, Plate 17; body O in Fig. 83), which is interpreted as comprising mixed intrusions and flows at the locus of breakup. In the seismic reflection data, this body is characterised by variable-amplitude, discontinuous reflectors with faint, low-continuity reflectors at depth, particularly at its inboard edge. A thin, non-magnetic, landward-dipping wedge of relatively-continuous reflectors on the landward flank of the outer basement high (body N in Fig. 83) may be a stranded fragment of lower continental crust.

Immediately outboard of the outer basement high lies the COB and unequivocal oceanic crust. In the reflection seismic data, the COB is characterised by a change from the diverse but sediment-dominated seismic character of the COT to the low-reflectivity seismic character of the oceanic regime (line GA-228/24, Plate 17). Two types of oceanic basement are recognised (*wlo1* and *wlo2*; examples in Figs 89 & 90) separated by an oceanwards step-up in basement level at ~SP 5500 on line GA-228/24 (Plate 17). The basement level change of approximately 0.4 s TWT (~600 m) correlates closely with interpreted magnetic chron 24o (Early Eocene) and Tikku and Cande's (1999) change in spreading rate from an ultra-slow 1.5 $mm.a^{-1}$ to a slow 6.5 $mm.^{-1}$. Both *wlo1* and w*lo2* are characterised by a rugged upper surface, interpreted to be partly the result of mechanical extension in a low magma-input environment.

Potential field modelling indicates a typical three-layer structure for oceanic crust in this sector of the margin: Layer 2A (body P in Fig. 83) consists of normally and

reversely magnetised blocks of basalt; Layer 2B (body Q) comprises sheeted dykes; and Layer 3 (body R) is interpreted as gabbro/peridotite. All three layers appear to be cut by faults, which in some cases may also offset Moho and sole out in the upper mantle. These faults may have assisted the alteration and serpentinisation of much of the crust, producing relatively low densities, particularly in parts of the peridotite layer (altered peridotite layer densities of 2.75×10^3 kg.m^{-3} vs unaltered densities of ca. 3.30×10^3 kg.m^{-3}). Deep faulting and fracturing of brittle upper crust during early rifting has been interpreted as the mechanism for serpentinisation on other rifted margins, for example west Iberia (Perez-Gussinyé & Reston, 2001) and Ireland (Reston et al., 2001). Ingress of water along faults through brittle crust leads to serpentinisation of the uppermost mantle (Hopkinson et al., 2004). High-density bodies (bodies S in Fig. 83; density $2.8–2.9 \times 10^3$ kg.m^{-3}) correlate with bands of higher-amplitude seismic reflectors SP 4700-5300, ~9 s, line GA-228/24, Plate 17) and may be fossil magma chambers.

The post-rift section on the line (i.e. the section above horizons *tur*, *cot*, *wlo1* and *wlo2* in line GA-228/24, Plate 17; bodies A–E in Fig. 83) consists of a series of initially downlapping and later onlapping sedimentary packages of Late Cretaceous and Cainozoic age. A prominent margin-wide unconformity is dated as probable base Middle Eocene, based on seismic comparison with a similar unconformity in the Bight Basin (the base *Dugong* horizon of Totterdell et al., 2000). Sedimentary packages above this unconformity lap onto the surface. None of these successions is magnetised. None of the shallow sedimentary packages have been dated, due to a lack of core samples other than from a few metres below the seafloor. The total post-rift sedimentary package on this line attains a maximum thickness of ~4 km in the central part of the COT zone (Fig. 83). As noted by O'Brien & Stanley (2003), the seismic character of the Cainozoic section suggests that it is dominated by turbidite fan deposits with a large slump deposit located at about SP 2000 in the uppermost part of the section (line GA-228/24, Plate 17).

Adélie Sector

The Adélie sector extends from approximately 132° to 142°E. It is conjugate to the eastern end of the Great Australian Bight, and is located southwest of the major fracture zones which separate the Otway Basin margin of Australia from Antarctica (Miller et al., 2002). In part, the strike-slip movement on these fracture zones has produced structural complexities that are not seen on the segments of margin to the west where extension was entirely normal to the margin.

The structural style and geology of this sector is shown by the interpreted seismic lines in Plates 17 and 18, and by the corresponding potential field models of three of the lines, viz. lines GA-228/28, GA-228/29 and GA-229/06 (Figs 91–93; Appendix 7). West of about 135°E, the overall margin architecture is similar to that of the Sabrina sector, except that the major structures, such as the peridotite ridge, are progressively offset oceanwards to the east (Plate 21), and additional depocentres lie inboard of the COB and the peridotite ridge. The broad COT is dominated by a largely transparent lower crustal layer (below horizon *tran* in Plates 17 and 18; body K in Fig. 91) which is overlain by either highly-faulted blocks of pre- and syn-rift sediments or a section dominated by volcanic flows or other igneous material. A prominent basement ridge typically lies in the outer part of the COT and is interpreted

on line GA-228/28 on the basis of potential field modelling to be composed of serpentinised, unroofed mantle peridotites, and associated intrusions and extrusive products, from decompression melting (Fig. 91, bodies M1–M4). Elsewhere the outer basement ridge is largely non-magnetic and may be a stranded piece of lower continental crust (line GA-228/29, Appendix 7). The oceanic crust along this margin segment is typically rugged, possibly reflecting mechanical extension and faulting of the crust.

East of about 135°E, the most noticeable features of this sector are the presence of pinch-and-swell structures (boudins) in the lower crust and associated major deformation of the thick Cretaceous (?and Jurassic) mid-crustal rocks (Figs 94–96; Plate 18). The deformation is largely confined to a crustal block, referred to by Colwell et al. (in press) as the 'Adélie Rift Block' (ARB, SP 2200-5800 in line GA-229/06, Plate 18; Figs 94–96). The landward flank of this block is formed by a major landward-dipping, deep-penetrating fault system with an associated sediment trough, while oceanward it is flanked by igneous rocks of the continent–ocean transition zone. This block was referred to as the 'marginal high' by Tanahashi et al. (1987) who noted that it is composed of 'anticlinally folded continental and shallow-marine sequences'. They also noted that seafloor spreading probably started to the north of the high in the Middle Eocene (cf. Plate 21).

The pinch and swell structures of the lower crust and the major fault system at the inner edge of the ARB are the major controls on the distribution of the predominantly post-rift section above the unconformity *maas* (Colwell et al., in press). Correlation with similar structuring on the Australian Otway Basin margin (Moore et al., 2000) implies a Maastrichtian age for this unconformity. Up to ~5 km (3 s TWT) of post-rift sediment overlie the *maas* unconformity (SP 2100 line GA- 229/06, Plate 18).

Potential field modelling of line GA-229/06 (Fig. 93) indicates that the landward edge of the ARB is underlain by a dense, magnetised body interpreted as altered/serpentinised mantle (body K). This body separates blocks of magnetic, crystalline lower crust (bodies J1 and J2) that contain probable mafic intrusions (bodies M1–M2, L1–L3), and underlies thick, pre-rift to syn-rift, strongly-layered, faulted and folded sedimentary rocks (bodies H1, G1–G3, F1 & F3). At about SP 1500, the mid-crustal rocks are pierced by a body that is interpreted as a serpentinised gabbro/peridotite ridge (body I) analogous to the peridotite ridge interpreted elsewhere on this segment of the Antarctic margin and on the southern Australian continental margin (see Sayers et al., 2001). As is commonly the case (e.g. Fig. 83), this body is located at the point of maximum necking of the crust. Parts of bodies F, G & H adjacent to the basement ridge structure are strongly magnetised with reverse polarity, probably indicating the injection of significant volumes of mafic rocks into the sedimentary rocks above the ridge (Appendix 7). The inner flank of the ARB is marked by the thickening of the syn- to post-rift section against a major south-dipping fault at about SP 2200.

The crust of the ARB and the outboard COT zone is complex and distinctive. The basal layer (body N in Fig. 93) is interpreted from its density, geometry, non-magnetic properties and seismic character to be ductile crystalline crust that has formed a series of large-scale (4–5 km amplitude, 20–40 km wavelength) boudin structures at the base of the crust. Japanese surveys TH91 and TH95 recovered peridotite, granite, gneiss, slate and other rocks from deep water locations off Terre Adélie (Table 10;

Plate 7; Tanahashi et al., 1997), confirming an outboard location of the continent–ocean boundary along this segment of the margin. This position (Plate 21) lies well to the north of many previously published locations for the COB and confirms that the ARB clearly lies within the COT.

As in the Knox and Sabrina sectors, the COB in the Adélie sector is marked by a change in the seismic character from the structurally complex and diverse seismic character of the COT zone to the low-reflectivity seismic character of oceanic crust. The upper surface of oceanic crust (horizon *wlo2* in Plate 18) has a rugged topography, probably at least partly due to faulting. Potential field modelling again indicates a three-layer division of the oceanic crust: an upper layer of normally and reversely magnetised basalt (oceanic crust layer 2A; body P); a middle layer (layer 2B, body Q) comprising dolerite dyke swarms; and a lower layer of gabbro-peridotite (layer 3, body R). To date, none of the older (Late Cretaceous–Early Cainozoic) seafloor spreading magnetic anomalies identified in the Sabrina sector have been identified in the Adélie sector.

The Adélie sector is typically blanketed by 1–3 km of Cainozoic sediments, likely to be a mixture of turbidites and pelagic oozes. DSDP Site 269 located to the east of the line (Plate 7) recovered predominantly silts and clays from up to 958 m below the seafloor. The oldest material recovered was of Middle Oligocene or older age (Kaneps, 1975).

George V Sector

As previously noted, the acquisition of seismic data off George V Land (142–160°E) is limited by the severe ice conditions that characterise this area. Consequently the degree of understanding of this sector is less than in the sectors to the west.

The continental margin offshore George V Land lies in an oblique position with respect to the seafloor spreading direction within the Australian–Antarctic Basin. Consequently, many of the structures seen on the seismic data in the region are the product of oblique-slip or strike-slip movement and the oblique impact of transform faults (including the major George V/Spencer and Tasman Fracture Zones) on the margin (see Plates 8 and 21). The interpretation of the GA-227–229 survey seismic data in the region is shown in Plates 18 and 19; no potential field modelling has been undertaken of any of the lines. One major consequence of the oblique-slip/strike-slip setting of the margin segment is that the width of the margin rift basin decreases significantly from about 400 km off Terre Adélie to less than 50 km at 160°E (Plate 21). This narrowing is clearly shown in both the gravity and magnetic data (Plate 8), however few of the GA-227–229 seismic lines extend sufficiently far south to image much of the basin (Plate 7).

The composite seismic line GA-227/2904+227/4201+229/04 (Plate 18) is typical of the lines off the western part of George V Land. It shows a large amount of structuring of the outer part of the COT including folding of the pre-, syn- and post-rift sections, a rapid shallowing of the apparent reflection Moho and a rapid thinning of the overlying transparent lower crust, in response to deep biting faulting and compression. The structuring in the outer part of the COT is a lateral continuation of the Adélie Block. The COB is marked by a change from a faulted largely igneous body to the south within the COT (below horizon *cot*), to the relatively bland,

moderately rugged oceanic crust beneath horizon *gvo1*. The 1 s TWT deep slot beneath horizon *tur* at the COB marks the landward continuation of the George V–Spencer Fracture Zone.

Further to the east, line GA-228/31 also illustrates the pronounced change across the COB from highly structured sedimentary and igneous blocks within the COT to the much shallower and bland oceanic crust to the north (Plate 19). On this line the oceanic crust lies approximately 1 sec TWT above the average depth of the adjacent COT.

Two types of oceanic crust have been mapped on the seismic lines off George V Land: *gvo1* and *gvo2* (Plate 19). The main difference between the two types is the degree of faulting, with *gvo2* containing more faults, usually corresponding to major fracture zones (Figs. 97 and 98). Both crustal types have a moderately rugged upper surface (Table 11).

Consistent with other segments of the East Antarctic margin described in this report, offshore George V Land is characterised by a thick section of post-rift sediments which onlap/downlap components of the COT inboard of the COB or oceanic crust outboard of the COB.

Post-rift Sedimentary Section

The East Antarctic margin off Wilkes Land and Terre Adélie is characterised by an upper slope with canyons and closely spaced gullies. Dip sections in a number of places reveal steep foresets indicating progradation of the outer shelf (see Eittreim et al., 1995; De Santis et al., 2003). The region seaward of the steep upper slope is a zone of rough, gullied sea floor with erosion of sediments at the sea bed. Further seaward, broader channels are present, some with clearly-defined levee deposits. Reflection continuity varies from poor to good, with the uppermost levee deposits having the most continuous reflectors. Large sediment mounds are not present through most of the area. Combined with the channel levee deposits, this suggests turbidite deposition rather than contourite sedimentation (Escutia et al., 2000).

On a number of lines (GA-228/24 to GA-228/28, Plate 17), the deeper part of the post-rift section off Wilkes Land comprises several wedges of sediment that are thickest beneath the upper slope and that thin seawards beneath the lower slope. These wedges are characterised by low-amplitude reflectors with poor continuity. Several lines show reflectors within these wedges that downlap at the base (e.g. Fig. 85) and, higher in the section, indicate syn-deposition growth faulting (e.g. southern end of line GA-228/27, Plate 17). The upper surface of these wedges is interpreted to be Eocene in age by analogy with the southern margin of Australia. Younger sequences onlap this surface.

Post-rift facies of the Wilkes Land margin also include extensive debris flow deposits (e.g. SP 4000–6000, line GA-228/24, Plate 17). These deposits are characterised by reflection-free sequences within intervals of more reflective sediments. The most extensive deposit on line GA-228/24 extends for about 270 km from its landward edge. Near the landward edge, the sequence base is erosional with steep-sided channels. More distally, the base is concordant with underlying reflectors but it exhibits slight undulations, suggesting some minor erosion a considerable distance from the margin. The upper surface of the deposit also exhibits undulations and

shows small diffractions suggesting a rough, mounded surface. In several places there are high-frequency horizontal reflectors within the otherwise reflection-free unit suggesting that it a composite deposit, comprising multiple individual debris flows. Line GA-228/24 is a dip line, so the pinching and swelling of the deposit probably reflects multiple lobes of debris intersecting the line.

Between about 120°E and the eastern flank of Bruce Rise at about 100°E, the post-rift section increases in thickness to more than 8 km, and is characterised by large mounds. Sediment packages contain high-continuity, parallel reflectors (e.g. lines GA-228/18 and GA-228/19, Plate 15). Channels are present, but these are broad features, tens of kilometres across, that are filled with sequences of high-continuity, parallel reflectors, except in the uppermost part of the section where there are a few steed sided canyons a few kilometres across. Sediment waves are present in the more distal parts of the margin. The crests of the mounds are cut by modern canyons, suggesting the bulk of these deposits formed under a previous depositional regime.

The large depositional edifices, continuous reflectors and common sediment waves in this area resemble the 'mixed contourite-turbidite drift' deposits interpreted from the area seaward of Prydz Bay by Kuvaas & Leitchenkov (1992). They interpret these sediments as forming when large amounts of sediment are delivered to the continental margin and distributed by sediment gravity flows under the influence of strong along-slope currents.

DSDP Site 268 drilled sediments in this region, just to the east of Bruce Rise (Line 228/16, Plate 15, Hayes, Frakes et al., 1975). It penetrated 160 m of diatom ooze, silts and clays and beds of normally-graded fine sand of Pliocene to Quaternary age (Unit I, Hayes, Frakes et al., 1975). Piper & Brisco (1975) interpreted the sand beds as turbidites. Line GA-228/16 shows that Unit I overlies an erosion surface that forms a large channel (Fig. 58). This erosion surface is cut in sediments dominated by muds with thin silt laminae probably formed as contourites (Piper & Brisco, 1975). These sediments range in age from Early Miocene to Early Oligocene (Hayes, Frakes et al., 1975). This stratigraphy suggests a history of contourite deposition from the Oligocene to the Miocene followed by canyon incision and submarine channel and fan deposition through the Pliocene and Quaternary.

DISCUSSION

Plate 21 summarises the tectonic elements of the Antarctic continental margin from western Wilkes Land to George V Land based on an interpretation of all available data, while Figure 79 shows a more detailed interpretation of the Sabrina, Banzare and Adélie sectors. These maps are consistent with the interpretation of Tanahashi et al. (1987, 1997), but differ from Wannesson et al. (1985) and Eittreim & Smith (1987) in the location and identification of the continent–ocean boundary. As noted earlier in this report, the position of the rift bounding fault zone shown in the figure and plate is only an approximation because of a scarcity of data; the fault is inferred based on the outcrop of crystalline basement rocks along the coast, whereas all of the available seismic data show that the continental slope is underlain by a thick sedimentary basin. The main depocentre of this basin is named here the Sabrina Basin and extends along the margin from approximately 105–130°E. East of 130°E, the margin is complicated by the presence of the Adélie Rift Block (Plate 21) and east of ~140°E by major

oblique-slip or strike-slip movements associated with transform faults and fracture zones within the Australian–Antarctic Basin.

A broad (90–180 km wide) COT zone is interpreted in deep water along the Wilkes-Adélie continental margin from ~105–140°E; east of ~140°E the COT narrows dramatically (Plate 21). This zone consists of two major upper crustal types: (i) highly-extended continental crustal fragments that are commonly intruded and overprinted by volcanics, and (ii) magmatic bodies likely composed of mixtures of gabbro, peridotite (in many cases at least partly serpentinised) and associated volcanics. The COT lies between extended continental crust and the COB, which marks the inner edge of unequivocal oceanic crust (Colwell et al., in press). The COB is confidently located east of about 124°E, but becomes more difficult to define in the west where the distinction between oceanic crust and igneous components of the COT zone is blurred. The presence of the broad COT clearly illustrates that Antarctic continental crust extends into very deep water, analogous to the situation for the conjugate central Great Australian Bight margin (Sayers et al., 2001). Many of the features described for the Wilkes Land margin are also present on the conjugate Great Australian Bight margin. These include the presence of a major peridotite ridge in the inner part of the COT, the occurrence of highly-faulted well-stratified bodies of pre- and syn-rift sedimentary rocks beneath the deep-water (outer) parts of the COT, and a number of major unconformities within the sedimentary section which are correlated on the basis of similar characteristics.

The Sabrina sector is located approximately opposite the Australia–Antarctic Discordance, and it is possible that this regional-scale lithospheric anomaly has also impacted the structuring on the Antarctic margin. In this sector, the COT is more diffuse than to the east and the COB is difficult to define (Colwell et al, in press). Although Figure 79 and Plate 21 show the COB stepping out to the north, this conflicts with the interpreted seafloor spreading anomaly identifications of Tikku & Cande (1999) and B.J. Brown (pers. comm.; Figs 26 & 27). There are two obvious possibilities to explain this disagreement:

1. The seismic interpretation of the COB presented here is incorrect and it actually lies inboard of the position shown in Figure 79.
2. The lineated magnetic anomalies shown here as being in the COT were not the product of normal (albeit slow) seafloor spreading.

On the basis of the reflection seismic character and the potential field modelling undertaken in this sector, Colwell et al. (in press) believe that the second of these possibilities is the more likely. In further support of this, they note that Tikku & Cande (1999) found that their reconstructions were characterised by a ‘large’ (40-50 km) amount of continental overlap involving the South Tasman Rise, Tasmania and Victoria Land, Antarctica. One of their suggested reasons for this overlap was that the magnetic anomalies older than A31 may not be true isochrons and it was therefore possible that during the ‘long period of ultra-slow spreading there was considerable diffuse extension in the AAB which would have distorted the shape of the anomalies’. In Figure 79 and on Plate 21, a distinction is made graphically between magnetic anomalies lying within the COT (which are more likely to have been produced by magnetic igneous bodies oriented broadly parallel to the margin) and unequivocal seafloor spreading anomalies located on oceanic crust outboard of the COB.

By contrast, the COB and COT in the adjacent Banzare sector to the east are more clearly defined (see for example line GA-228/24, Plate 17 and Fig. 83). This sector has marked similarities and symmetry with the conjugate margin in the Great Australian Bight (GAB; Totterdell et al., 2000; Sayers et al., 2001; Colwell et al., in press; Fig. 86). In particular, the inner part of the continental margin is dominated by a thick, faulted Cretaceous–?Jurassic pre- and syn-rift section that is concentrated outboard of a major basement fault system and inboard of a prominent basement (?peridotite) ridge located within the inner part of COT. Also, on both margins:

1. The margin rift basin depocentre is underlain by largely-transparent lower crust which shows evidence of ductile deformation and thinning.
2. The COT is characterised by highly-extended continental crust, including faulted and rotated blocks of rift sediments immediately overlying altered lower crustal rocks, and possibly exhumed mantle (?serpentinised peridotites).
3. The COT zone includes a substantial magmatic component, parts of which are magnetic producing linear magnetic anomalies that may be confused with seafloor spreading anomalies.
4. The COB is clearly defined in both seismic and potential field data.
5. Oceanic crust has a typical three-layer structure: basalt underlain by sheeted dykes and gabbro/peridotite.

The inboard edge of the peridotite ridge on the Antarctic margin was identified as the COB by Eittreim & Smith (1987). However, as pointed out by Colwell et al. (in press), this identification was in error, mainly due to their data not extending sufficiently far into the ocean basin to image the outboard basin shown in Figures 87 and 88.

In the GAB on the Australian continental margin, magnetic anomalies, combined with the interpreted seismic data and potential-field modelling indicate that emplacement of oceanic crust commenced at about chron 33o time (i.e. at ~83 Ma, early Campanian; Sayers et al., 2001; Totterdell & Bradshaw, 2004), about 12 Ma later that interpreted by Tikku & Cande (1999). On the conjugate Antarctic margin, the relationship between the COB and the previously identified magnetic anomalies is less clear, although spreading is also believed to have commenced at about chron 33o time (Colwell et al., in press).

In the Adélie sector, the form of the margin is strongly influenced by its proximity to the major strike-slip fracture zones which separate the Otway Basin/west coast of Tasmania/South Tasman Rise margin of Australia from Antarctica; these fracture zones become more pronounced to the east (Plates 8 and 21). The Adélie Rift Block (ARB) in the outer COT (Fig. 79; Plate 21) coincides with a major northward salient of the COB and is interpreted by Colwell et al. (in press) as a continental fragment on the basis of its seismic character (see, for example, Figs 94–96; line GA-229/06, Plate 18), and the presence of continental rocks as dredged by the Japanese from its outer flank. As noted by Colwell et al. (in press), the ARB has the appearance of a marginal plateau that almost detached from the continent and has since subsided to abyssal depths. The location of the COB outboard of the ARB is in close agreement with that interpreted by Tanahashi et al. (1997).

To the east of Terre Adélie, the George V Land continental margin narrows to the east under the impact of transform faults on the margin. Structuring is largely due to oblique-slip or strike-slip faulting as opposed to the largely orthogonal rifting of the margin off Wilkes Land and Terre Adélie.

One of the major problems in dating the major tectonic/structuring events along the Antarctic margin from Wilkes Land to George V Land is the lack of any stratigraphic control on the syn-rift and early post-rift section. The very thick post-rift section of the continental slope requires deep drilling to sample many of the sequences of interest; this drilling has not taken place to date. Indeed, only one DSDP/ODP hole (DSDP 269) has been drilled on the margin and this bottomed in Tertiary sediments. However, strong similarities in seismic character and structure allow comparison of the deep-water sequences to sequences on the conjugate southern Australian margin where ages are relatively well constrained from industry and research seismic, and petroleum exploration drilling (e.g. Totterdell et al., 2000). On this basis Colwell et al. (in press) made a number of observations and correlations:

Firstly, the *tur* horizon, which marks the top of major faulting and other structuring along much of the Wilkes Land – George V Land margin (Plates 15–19, light green horizon, equivalent to horizon *K1* of Eittreim & Smith 1987), is correlated on the basis of structural style and seismic reflection character with the unconformity at the base of the Tiger sequence on the conjugate GAB continental margin. On the GAB margin this unconformity is dated as base Turonian age and therefore pre-dates the age of breakup (early chron 33 i.e. ~83 Ma) by about 7–10 million years. (Totterdell et al., 2000).

Secondly, strong character and structural similarities exist between the highly folded and faulted sedimentary section of the Adélie Rift Block (ARB) and the Late Cretaceous Sherbrook Group and the upper part of the Early Cretaceous Otway Supergroup of the Otway Basin of southeastern Australia (Moore et al., 2000; Krassay et al., 2004). This suggests that the yellow *mass* horizon, which marks the top of structuring on the ARB (line GA-229/06, Plate 18; Figs 94–96), is probably of Maastrichtian age as is the case for the top structuring event on the Australian margin.

Thirdly, the prominent dark green strong onlap *eoc* surface which occurs along almost all of the Wilkes Land–George V Land margin (Plates 15–19), is correlated with similar onlap surfaces in the Great Australian Bight (base Dugong sequence; Totterdell et al., 2000), in the Otway Basin (base Nirranda Group; Moore et al., 2000) and in the Sorell Basin on the west coast of Tasmania (unconformity U5; Hinz et al., 1986). Where dated on the Australian margin, these surfaces are of Middle Eocene age.

SUMMARY

1. The Antarctic continental margin between western Wilkes Land and George V Land (105–160°E) is the product of rifting between Australia and Antarctica, leading to the emplacement of the first unequivocal oceanic crust in the Late Cretaceous. Most of the rifting was largely orthogonal to the margin, however, east of ~140°E, margin development was strongly influenced by the largely strike-slip movement between Antarctica and the Otway Basin margin/South Tasman Rise of SE Australia.

2. Much of the Antarctic margin in this sector is underlain by a major rift basin, the Sabrina Basin. Beneath this basin, crystalline crust rapidly thins oceanwards through extensive faulting of the rift and pre-rift sedimentary section and by mainly ductile deformation of the crystalline crust. The total thickness of pre-rift, rift and post-rift sedimentary rocks in this basin is well over 7 km in places. The basin is generally in the order of 200 km wide but narrows significantly to the east of ~140°E in response to the west-to-east change from largely orthogonal to oblique rifting.

3. A 90–180 km-wide continent–ocean transition zone separates extended, clearly continental crust from unequivocal oceanic crust along most of the margin. The zone consists generally of a mixture of blocks of faulted continental sedimentary rocks and igneous bodies such as magma chambers, sills and dykes that are the product of mantle up-welling and partial melting. Many of these igneous bodies are magnetic and are orientated in rift segments parallel to the margin, producing lineated magnetic anomalies that could be mistaken for seafloor spreading lineations.

4. Potential field modelling of lines along the margin typically indicates major thinning of the lower and middle crust within the COT. This thinning is often accompanied by extensive faulting of the overlying pre- and syn-rift section, and erosion and onlap of the post-rift section.

5. The inner edge of the COT is commonly marked by a basement ridge, which the potential field modelling indicates is probably composed of altered/serpentinised peridotite. This ridge is similar in form and interpreted composition to a basement ridge located in a similar structural position at the inboard edge of the COT on the conjugate margin of the Great Australian Bight. Both ridges are probably the product of mantle up-welling and partial melting focused at the point of maximum necking of the crystalline crust.

6. The position of the continent–ocean boundary (i.e. the outer limit of the COT and the inboard edge of unequivocal ocean crust) is well constrained along parts of the margin but less well constrained in others. Generally, where well defined by potential field and seismic data, the COB lies in very deep water, and commonly outboard of earlier interpretations that were often based on inadequate seismic data or magnetic data only.

7. A major crustal block (Adélie Rift Block of Colwell et al., in press; ‘marginal high’ of Tanahashi et al., 1987), which lies inboard of the COB off Terre Adélie, is largely the product of pinch-and-swell structures (boudins) in the lower crust and the associated major deformation of the overlying thick Cretaceous (?and

Jurassic) mid-crustal rocks. This deformation is partly related to the oblique movement of Australia and Antarctica to the east of this area.

8. Overall, as noted by Colwell et al. (in press), there appears to be a high degree of symmetry in the rift structures observed between the deep-water parts of the conjugate central Great Australian Bight and Wilkes Land margins. However, the post-rift sections differ markedly due to different depositional processes. Most of the Antarctic continental margin is blanketed by a very thick layer of Cainozoic sediments.

Name	*Depth of basement top (s)*	*Basement surface*	*Internal reflections & character*	*Reflection Moho*	*Comments*
wwlo	7 – 8	Fairly rugged, rough	Variable, from non-reflective to moderately reflective, particularly above 9 s.	Not observed.	
wlo1	7.8 – 8.5	Fairly rugged, rough	Variable, from non-reflective to highly reflective, particularly above 9.5 s.	Not observed.	Inboard of *wlo2* on a few lines only. *wlo1*/*wlo2* boundary is not sharp.
wlo2	7.3 – 8.2	Moderately rugged and rough; very rugged to east	Mainly non-reflective; isolated areas of moderate continuity reflections.	Not observed.	
gvo1	5.8 – 7	Moderately rugged	Little or no reflectivity.	Not observed.	Basement down to 8 s at a fracture zone.
gvo2	6 – 7.5	Moderately rugged, faulted	Little or no reflectivity.	Not observed.	Only on one line; inboard of *gvo1*

Table 11: Seismic reflection characteristics of different types of crust from western Wilkes Land to George V Land. All time-depths are seconds two-way time (TWT). 'Rough' refers to short-wavelength, generally low-amplitude basement topography , whereas 'rugged' refers to longer-wavelength topography generally with high-amplitudes.

Sono #	*Line*	*WD*	*Vel*	*Depth*	*Vel*	*Depth*	*Vel*	*Depth*	*Comments*
228/SB15	228/24	4.41	5.2	6.6	6.7	9.3			*wlo2*
228/SB16	228/25	4.37	5.4	7.9	7.9	12.6			5.43 km.s^{-1} near top peridotite ridge.
228/SB17	228/26	3.53	6.9	8.4	7.8	16.4			Inboard of peridotite ridge. 7.8 km.s^{-1} near reflection Moho depth.
228/SB18	228/26	4.57	5.4	6.9	6.6	8.1			*wlo2*. 5.4 km.s^{-1} is at top basement.
228/SB20	228/27	4.62	(5.4)	7.4	6.7	10.0	8.2	12.2	*wlo2*. No reflection Moho.
228/SB21	228/28	4.25	5.4	6.4	6.5	9.9	8.2	14.8	Inboard of peridotite ridge. 8.2 km.s^{-1} near faulted Moho.
228/SB22	228/28	4.59	4.9	7.0	5.7	7.9			*wlo2*.
228/SB23	228/29	4.51	4.9	6.4	6.6	7.8	8.1	10.9	*wlo2*. No reflection Moho.
228/SB24	228/29	4.38	5.5	8.7					COT.
228/SB25	228/30	3.61	6.1	9.6					Inboard of COT. 6.1 km.s^{-1} is near top transparent crust.
228/SB26	228/30	3.94	5.5	5.9	7.1	8.9			*gvo1*.
228/SB28	228/31	3.88	4.9	5.9	6.0	8.5			Outboard COT.
228/SB30	228/31	3.77	5.8	5.9	6.3	9.9			Inboard COT.
229/SB02	229/01	3.54	5.4	5.8					*gvo1*.
229/SB03	229/02	3.41	5.4	~5.9	6.9	7.3	7.6	10.2	*gvo2*.
229/SB04	229/03	3.60	(5.0)	~5.0	6.3	5.9	8.0	9.0	*gvo1*. 8.0 km.s^{-1} too shallow for Moho, unless fracture zone crust.

Sono #	*Line*	*WD*	*Vel*	*Depth*	*Vel*	*Depth*	*Vel*	*Depth*	*Comments*
229/SB05	229/04	3.95	6.0	~7.9	? 8.8	11.3			Outer edge of continental crust; extreme relief on reflection Moho.
229/SB06	229/04	4.06	6.4	9.0					COT.
229/SB07	229/04	4.16	5.9	6.1	7.4	7.4	?8.9	13.7	*gvo1*. No reflection Moho to support extremely suspect velocity.
229/SB08	229/05	4.34	5.2	6.2	6.9	7.9			*gvo1*.
229/SB09	229/05	3.92	5.1	~7.2	5.9	8.2	7.4	10.0	Inboard of COT. 7.4 $km.s^{-1}$ is near top *tlcc*.
229/SB10	229/06	3.50	6.3	9.4					Inboard flank of Adélie Rift Block.
229/SB11	229/06	3.80	5.1	~6.6	5.4	10.1			Adélie Rift Block.
229/SB12	229/06	4.30	6.8	9.7					COT outboard of Adélie Rift Block. 6.8 $km.s^{-1}$ near top *tlcc*.
229/SB13	229/07	4.20	5.6	8.6	6.6	11.6			Outboard flank of Adélie Rift Block. 6.6 $km.s^{-1}$ near top *tlcc*.
229/SB15	229/07	3.97	5.1	~6.4	5.6	~11.9			Inboard flank of Adélie Rift Block. 5.6 $km.s^{-1}$ near top *tlcc*.
229/SB16	229/08	4.10	(5.0)	~8.2	6.3	10.9			COT.
229/SB17	229/08	4.25	(4.5)	~7.5	6.8	~9.6			*wlo1*.
229/SB18	229/09	4.45	(4.9)	~6.9	6.1	7.4			*wlo2*. 6.1 $km.s^{-1}$ is near top basement.
229/SB19	229/10	4.24	(4.5)	~7.4	6.6	9.0			Straddles *wlo1* / *wlo2* boundary.
229/SB22	229/12	3.90	5.5	7.2					

Sono #	*Line*	*WD*	*Vel*	*Depth*	*Vel*	*Depth*	*Vel*	*Depth*	*Comments*
229/SB25	229/13	4.24	5.2	~7.1	6.4	8.8			
229/SB26	229/14	4.19	4.9	6.0	5.9	7.5	7.1	8.5	
229/SB27	229/15	4.25	(5.0)	~6.0	6.3	6.9			
229/SB28	229/15	3.99	5.0	7.8					
229/SB29	229/16	4.44	5.2	~6.0	7.7	8.2			

Table 12: Sonobuoy locations and solutions for Surveys GA-228 and GA-229 in the Australia–Antarctica sector (western Wilkes Land to George V Land); only basement and deeper velocities are shown. Depths are km below sea level; velocities are $km.s^{-1}$. Velocities in parentheses are assumed. Depths preceded by a tilde ('~') are approximate, usually because of short-wavelength relief on an interface. '?' indicates highly questionable value.

TECTONIC HISTORY

The following tectonic history for the continental margin in the region of the Australian Antarctic Territory is speculative, reflecting both the manifest geological complexities and the lack of detailed data in many areas. However, it will attempt to synthesise the observations that are made in this report and similar studies of the conjugate southern Australian margin.

In this chapter, we will use the following abbreviations:

> GI–AA – spreading between Greater India and the combined Australia-Antarctic continent
>
> A–A – spreading between Australia and Antarctica

The locations of the principal geological and morphological features are shown in Figure 99 and Plate 21.

PERMIAN – TRIASSIC

Permian to Triassic terrigenous and glacigenic intracratonic rocks have been sampled from the Prince Charles Mountains (Mond, 1972), Prydz Bay (Cooper et al., 1991) and Horn Bluff in George V Land (Tingey, 1991). Rocks of similar age and composition are also known from the conjugate margins of India (e.g. Lisker & Fachmann, 2001; Ghosh, 2002) and Australia (e.g. Polda Basin; Stagg et al., 1992) and are extensively documented along the western margin of Australia and the North West Shelf. It is likely that rocks of this age are also widespread along the margin of East Antarctica where they are probably incorporated into the uppermost seismic basement and the tops of later Mesozoic rift blocks as, for example, beneath the Bruce Rise.

JURASSIC TO EARLY CRETACEOUS (RIFTING)

In the Late Jurassic, a major rift system, at least 6000 km in length, was initiated along the incipient plate boundary between Greater India and Antarctica–Australia with a future major triple junction developing in the vicinity of the Bruce Rise (BR) and Naturaliste Plateau (NP). A subsidiary branch of this rift system extended for at least 4000 km eastwards from the triple junction to south of Tasmania (Southern Rift System (SRS); Stagg et al., 1990).

Jurassic early rift-stage sediments are well-documented along the length of the Australian North West Shelf and into the southern Perth Basin (Vlamming Sub-basin). Similar-age sediments were deposited at least as far west as the margin of Enderby Land where Jurassic to Cretaceous palynomorphs have been recovered from an interpreted inner-shelf half graben (Truswell et al., 1999). Jurassic rift sediments have also been sampled at widely-separated localities along Australia's southern margin, including in the Bremer Basin (Blevin, 2005), Bight Basin (Sea Lion and Minke sequences; Totterdell et al., 2000) and Otway Basin (Casterton Formation; Krassay et al., 2004). It is highly likely that Jurassic sediments are also preserved along the East Antarctic margin from the Bruce Rise to George V Land, particularly beneath the landward flank of the rift, although such rocks have not yet been sampled.

Seafloor spreading commenced in the far north of the rift in the Argo Abyssal Plain prior to anomaly M26 time (~155 Ma). Spreading between Africa and East Antarctica (i.e. west of the Enderby Basin) started soon after, at about 148 Ma (Royer et al., 1992). It is possible that the small panel of very deep oceanic crust (*ebo3*; see earlier in this report) may have been a product of a contemporaneous spreading episode.

Minor Jurassic to Early Cretaceous depocentres developed on the high-standing proto-BR and NP, while a major N–S trending depocentre of this age was developed on the inboard flank of the NP (Mentelle Basin; Borissova, 2002) and an E–W trending depocentre, probably of the same age, was developed inboard of the Bruce Rise (shown by the depocentre axis in Fig. 62). The trends of these depocentres paralleled the incipient continental margin that was developing outboard of the plateaus, and the depocentres may have been connected at this time. These basins probably filled with largely clastic terrigenous sediments, with deposition continuing into the Early Cretaceous.

Sedimentation in the rift system continued through the Early Cretaceous, with non-marine sediments being deposited on the margin of Enderby Land (Truswell et al., 1999), in Prydz Bay (Cooper et al, 1991), and on the southern, western and northwestern Australian margins. While sediments of this age have not been sampled from the Antarctic margin east of the Bruce Rise, the seismic data indicate that they were deposited widely on the margin.

VALANGINIAN – HAUTERIVIAN (GI–AA BREAKUP)

Seafloor spreading commenced in the Gascoyne, Cuvier, Perth, Shackleton and Enderby Basins in the Valanginian or early Hauterivian. This event terminated the rift-stage sedimentation on the adjacent Australian and Antarctic margins and marked the onset of the post-rift, sag-phase sedimentation. In contrast to the generally sediment-starved Australian margin, the post-rift phase on the Antarctic margin saw the accumulation of an enormous quantity of sediment. While magnetic spreading anomalies as old as M14 have been identified in these basins (e.g. Cuvier Basin, Müller et al., 1998), it is likely that at least some of the oldest identifications are dubious as some anomalies are associated with highly-extended continental crust or volcanic margin crust (including areas of development of unequivocal seaward-dipping reflector sequences). Therefore, it is not possible to draw conclusions about the relative timing of opening in all these basins. It is notable that anomaly M9 has been identified independently on the highly-distinctive and reflective 'Enderby-Cuvier' type oceanic crust in the Enderby, Shackleton and Cuvier Basins, which gives us a high level of confidence in correlating the age of the crust in these basins.

Probably near the time of breakup, the SDRSs which are currently separated from the continental margin in the Shackleton Basin were emplaced on the Antarctic margin. We speculate that these SDRSs may have been emplaced as a precursor to the development of the Kerguelen Plume in the mid-Cretaceous.

Anomaly M9y has also been identified close inboard to the Bruce Rise (Brown, this report), indicating that some Early Cretaceous oceanic crust was emplaced between the NP and BR, although there was probably only a small amount of separation. Even if the exact dating of this anomaly is incorrect, the ENE–WSW trend of the magnetic

anomalies in this region suggests that the crust belongs to the GI–AA spreading episode, rather than to the later A–A spreading. The very narrow continent-ocean transition adjacent to Bruce Rise suggests that final breakup was highly asymmetric, with most of the COT crust remaining attached to the NP margin.

HAUTERIVIAN TO ?SANTONIAN (GI–AA SPREADING; A–A EXTENSION)

During this period, GI–AA spreading continued as GI drifted away to the northwest. This spreading continued until about 85 Ma (Santonian), at which time a significant plate reorganisation took place, resulting in a change of spreading direction and the rapid northwards drifting of India (Royer & Coffin, 1992). The minor spreading between the BR and the NP probably ceased fairly early in this spreading episode. At an undetermined time, the approximately N–S trending basement step in the Shackleton basin was formed, either at an oceanic transform or through a ridge jump. Also during this interval, the SDRSs emplaced on the Antarctic margin appear to have been detached from the margin by a ridge jump.

In the Barremian (117 Ma), major volcanic activity commenced in the region of the southern Kerguelen Plateau. This activity (the Kerguelen Plume) continued until the Albian, although its effects were probably limited to the western Shackleton Basin.

Contemporaneous with the GI–AA spreading, extension was continuing between Australia and Antarctica as a precursor to A–A breakup. The extension was probably on a similar NW–SE azimuth to that of the spreading to the west (Willcox & Stagg, 1990). Between 90 and 84 Ma, extension in the Diamantina Zone reached a critical point resulting in the exhumation of peridotites (Chatin et al., 1998). Similar peridotite exhumation probably took place in the Great Australian Bight (GAB; Sayers et al., 2001) and on the Wilkes Land margin (this report).

SANTONIAN-RECENT (A–A BREAKUP AND SPREADING)

The timing of final A–A breakup continues to be controversial, at least in the far east in the Otway Basin/Terre Adélie. In our view, given the extreme degree of crustal thinning between the continents, the extremely slow initial oceanic spreading rates, and the length (>2000 km) of this segment of the Southern Rift System, it is quite unreasonable to assume that the onset of seafloor spreading would have occurred synchronously (or in a regular, time-transgressive manner along the margin). In reality, we believe it is far more likely that breakup occurred at different times and locations along the rift, with the local timing of the event being dependent on many factors, including, for example, the composition and strength of the underlying crust, pre-existing structures, and local variations in magmatism and heat input. The best-constrained breakup age is probably in the central GAB where it is dated as Late Santonian–Campanian (~83 Ma; Sayers et al., 2001), on the basis of an integrated interpretation of all the available geophysical and geological data (Totterdell & Bradshaw, 2004). Breakup probably took place at a similar time between BR and NP, although there are few identifiable magnetic anomalies to fix this age. On the NP margin, breakup appears to have occurred south of the Diamantina Zone (Borissova et al., 2003a, b). It is unclear where the counterpart transitional crust (if any) is found on the Antarctic margin.

Initial seafloor spreading between Australia and Antarctica was at variable, extremely slow rates (Tikku & Cande, 1999), probably on a NW–SE azimuth. This spreading was largely amagmatic and accommodated by mechanical extension of the oceanic crust, as seen in the reflection seismic data and inferred in the potential field models from the margin of Wilkes Land.

Also during this period, extension continued between southeast Australia (Otway Basin – South Tasman Rise) and Antarctica (eastern Terre Adélie – George V Land) at the eastern end of the SRS, until breakup in about Paleocene time in this sector. Palmowski et al. (2004) interpret the almost complete removal of the lower continental crust and exhumation of continental mantle in deep water adjacent to the Otway Basin in an analogous manner to that which is interpreted to have occurred earlier in the GAB and south of the NP.

In the Middle Eocene (~43 Ma; anomaly 20), the Diamantina Zone and the Labuan Basin separated (Royer & Coffin, 1992), coincident with the onset of fast seafloor spreading in the Southeast Indian Ocean. Labuan-Diamantina breakup was preceded by uplift on the southern part of the NP, resulting in steep faults along the whole southern margin of the plateau (Borissova, 2002). It is likely that the BR was similarly affected.

The boundary with fast-spreading crust is reflected quite differently on the two margins. On the Australian margin, there is a gradational crustal boundary between the Diamantina Zone and the fast-spreading crust (see line 187-1 in plate 5 of Borissova, 2002). This boundary suggests continuous spreading on this margin. In contrast, the Antarctic margin is characterised by an abrupt basement step, across which basement shallow northwards by about 1 s. This indicates the juxtaposition of crust of very different ages, which further suggests that the onset of fast spreading was accompanied by a ridge jump towards the Antarctic margin.

ACKNOWLEDGEMENTS

The success of the Australian Antarctic and Southern Ocean Profiling Project is due to the exceptional efforts of a number of people since early 2000. Therefore, we would like to acknowledge the following people and organisations:

Project genesis in the 1990s: Phil Symonds and Doug Ramsay.

General project management: Richard Cooper, Jim McCrea and Uros Rokvic (Geoscience Australia); Peter Diddams and Simon Schiwy (Department of Finance & Administration); John Curran, Tom Gordon, Jane Lawson and other staff of Sinclair Knight Merz Pty Ltd.

Surveys: Fugro Geoteam AS (particularly David Nolan, John Carrey and the Masters and crews of the R/V *Geo Arctic* and M/V *Polar Duke*); Mark Alcock, Doug Ramsay, Peter Napier, Phil O'Brien, Steve Dutton, George Bernardel and Mike Sexton (Australian government representatives on the surveys); Frank Renton (Enquest Pty Ltd); Geoff Dannock and Ian Allison (Australian Antarctic Division).

Data processing: Fred Kroh; staff of Robertson Research (contract data processing).

Drafting of figures and plates: Silvio Mezzomo and Angie Jaensch.

Internal review and editing: Jennie Totterdell and Alix Post.

We also acknowledge Springer Science & Business Media B.V., publishers of *Marine Geophysical Researches*, for permission to reproduce part of the text and figures from Stagg et al. (in press), which comprise the major part of the interpretation of the Greater India–Antarctica section of this report.

REFERENCES

AGSO North West Shelf Study Group, 1994. Deep reflections on the North West Shelf: changing perceptions of basin formation. In P.G. & R.R. Purcell (eds), *The Sedimentary Basins of Western Australia: Proceedings of Petroleum Exploration Society of Australia Symposium*, Perth, 1994, 63–76.

Anderson, J.B., 1991. The Antarctic continental shelf: results from marine geological and geophysical investigations. In R.J. Tingey (ed.), *The Geology of Antarctica*, Clarendon Press, Oxford, 285–334.

Barron, J., Larsen, B. et al., 1989. *Proceedings of the Ocean Drilling Program Initial Report*, 119.

Beslier, M.-O., Le Bihan, T., Feraud, G., and Girardeau, J., 2001. Cretaceous ultra-slow spreading in the ocean-continent transition along the southwest Australian passive margin: constrains from $^{40}Ar/^{39}Ar$ dating. *Abstracts of the EUG XI meeting (8-12 April 2001)*.

Blevin, J.E. (ed.), 2005. Geological framework of the Bremer and Denmark Sub-basins, southwest Australia: R/V *Southern Surveyor* cruise SS3/04. Geoscience Australia Survey 265, Post-Survey Report. *Geoscience Australia Record*.

Borissova, I., 2002. Geological Framework of the Naturaliste Plateau. *Geoscience Australia Record* 2002/20.

Borissova, I, Colwell, J. & Stagg, H., 2003a – Asymmetric break-up defines margin architecture of Bruce Rise, Antarctica, and Naturaliste Plateau, southwest Australia. In A. Heap (ed.), *Abstracts Sixth Australian Marine Geoscience Conference*, Kioloa, 7-9 July 2003, 15.

Borissova, I, Colwell, J.B. & Stagg, H.M.J., 2003b. The conjugate margins of Bruce Rise, Antarctica, and Naturaliste Plateau, southwest Australia. In B. Goleby, B. Drummond, S. Bannister & S. Henrys (comp.), *The 10th International Symposium on Deep Seismic Profiling of the Continents and their Margins, Programme and Abstracts*, Institution of Geological and Nuclear Sciences information series 52, 44.

Borissova, I., Moore, A., Sayers, J., Parums, R., Coffin, M.F. & Symonds, P.A., 2002. Geological framework of the Kerguelen Plateau and adjacent ocean basins. *Geoscience Australia Record* 2002/05.

Brancolini, G., Busetti, M., Marchetti, A., De Santis, L., Zanolla, C., Cooper, A.K., Cochrane, G.R., Zayatz, I., Belyaev, V., Knyazev, M., Vinnikovskaya, O., Davey, F.J. & Hinz, K., 1995. Descriptive text for the seismic stratigraphic atlas of the Ross Sea, Antarctica. In A.K. Cooper, P.F. Barker & G. Brancolini (eds) *Geology and seismic stratigraphy of the Antarctic margin*, Antarctic Research Series, 68, A271–A286.

Brancolini, G. & Harris, P.T., 2000. Post-cruise report AGSO Survey 217: Joint Italian/Australian marine geoscience expedition aboard the R.V. Tangaroa to the George Vth Land region during February-March 2000. *Australian Geological Survey Organisation Record* 2000/38.

Brown, B.J., Ishihara, T. & Müller, R.D., 2003. Breakup and seafloor spreading between Antarctica, greater India and Australia. In D.K. Fütterer (ed.) *Abstracts 9th*

International Symposium on Antarctic Earth Sciences, Potsdam 8-12 September 2003, 40.

Bukry, D., 1975. Coccolith and silicoflagellate stratigraphy near Antarctica, Deep Sea Drilling Project, Leg 28. In D.E Hayes, L.A. Frakes et al., *Initial Reports of the Deep Sea Drilling Project*, Washington, D.C., U.S. Government Printing Office, 28, 709–724.

Burns, D.A., 1975. Nannofossil biostratigraphy for Antarctic sediments, Leg 28, Deep Sea Drilling Project. In D.E Hayes, L.A. Frakes et al., *Initial Reports of the Deep Sea Drilling Project*, Washington, D.C., U.S. Government Printing Office, 28, 589–598.

Cande S.C. & Kent D.V., 1995. Revised calibration of the geomagnetic polarity timescale for the Late Cretaceous and Cenozoic. *Journal of Geophysical Research*, 100, 6993–6995.

Cande, S.C. & Mutter, J.C., 1982. A revised identification of the oldest sea-floor spreading anomalies between Australia and Antarctica. *Earth & Planetary Science Letters*, 58, 151–160.

Charvis P. & Operto S., 1999. Structure of the Cretaceous Kerguelen volcanic province (southern Indian Ocean) from wide-angle seismic data. *Journal of Geodynamics*, 28, 51–71.

Chatin, F., Robert, U., Montigny, R. & Whitechurch, H., 1998. La Zone Diamantine (ocean Indien oriental), temoin de la separation entre l'Australia et l'Antarctique: arguments petrologique et geochimique. *C. R. Acad. Sci. Paris*, 326, 839–845.

Chen, G., Hill, K.C., Hoffman, N. & O'Brien, G.W., 2002. Geodynamic evolution of the Vulcan Sub-basin, Timor Sea, northwest Australia: a pre-compression New Guinea analogue? *Australian Journal of Earth Sciences*, 49, 719–736.

Chen, Pei-Hsin, 1975. Antarctic radiolaria. In D.E Hayes, L.A. Frakes et al., *Initial Reports of the Deep Sea Drilling Project*, Washington, D.C., U.S. Government Printing Office, 28, 437–514.

Childs, J.R. & Stagg, H.M.J., 1987. The deep crustal structure of the Wilkes Land continental margin. In S.L. Eittreim & M.A. Hampton (eds), *The Antarctic continental margin: geology and geophysics of offshore Wilkes Land*, Earth Science Series, Circum-Pacific Council for Energy & Resources, 5A, 99–115.

Coffin, M.F., Frey, F.A., Wallace, P.J. et al., 2000. *Proceedings of the Ocean Drilling Program, Initial Reports*, 183, Ocean Drilling Program, Texas A&M University, College Station, TX .

Coggon J.H., 1976. The magnetic and gravity anomalies of polyhedra. *Geoexploration*, 14, 93–105.

Coleman, P.J., Michael, P.J. & Mutter, J.C., 1982. The origin of the Naturaliste Plateau, SE Indian Ocean; implications from dredged basalts. *Journal Geological Society Australia*, 29, 457–468.

Colwell, J.B., Stagg, H.M.J., Direen, N.G., Bernardel, G. & Borissova, I., in press. The structure of the continental margin off Wilkes Land and Terre Adélie, East Antarctica. In D.K. Futterer (ed.) *Ninth International Symposium on Antarctic Earth*

Sciences (ISAES IX), Terra Nostra, Alfred Wegener Institute for Polar & Marine Research, Potsdam.

Cooper, A.K. & O'Brien, P.E., 2004. Leg 188 synthesis: transitions in the glacial history of the Prydz Bay region, East Antarctica, from ODP drilling. In A.K. Cooper, P.E. O'Brien & C. Richter (eds), *Proceedings of the Ocean Drilling Program, Scientific Results 188*,
http://www-odp.tamu.edu/publications/188_SR/synth/synth.htm

Cooper, A., Stagg, H. & Geist, E., 1991. Seismic stratigraphy and structure of Prydz Bay, Antarctica: implications from leg 119 drilling. In J. Barron, B. Larsen et al., *Proceedings of the Ocean Drilling Program Scientific Results 119*, College Station, TX (Ocean Drilling Program), 5–25.

Davey, F.J., 1985. The Antarctic margin and its possible hydrocarbon potential. In E.S. Husebye, G.L. Johnson & Y. Kristoffersen (eds) *Geophysics of the Polar Regions*, Tectonophysics, 114, 443–470.

Davies, T.A., Luyendyk, B.P. et al., 1974. *Initial Reports of the Deep Sea Drilling Project*, *26*: Washington, D.C., U.S. Government Printing Office.

De Santis, L., Brancolini, G. & Donda, F., 2003. Seismo-stratigraphic analysis of the Wilkes Land continental margin (East Antarctica): influence of glacially driven processes on the Cenozoic deposition. In P.T. Harris, G. Brancolini, N. Bindoff & L. De Santis (eds) *Recent investigations of the Mertz Polynya and George Vth Land continental margin, East Antarctica*, Deep Sea Research II, 50, 1563–1594.

Direen, N.G., 2004. *Potential field modelling of Australia's continental margins: Naturaliste-Diamantina Zone. Continental Evolution Research Group, School of Earth & Environmental Sciences, University of Adelaide*, March 2004 (unpub.).

Direen N.G. & Leaman D.E., 1997. Geophysical modelling of structure and tectonostratigraphic history of the Longford Basin, northern Tasmania. *Exploration Geophysics*, 28, 29–33.

Domack, E.W., 1987. Preliminary stratigraphy for a portion of the Wilkes Land continental shelf, Antarctica: evidence from till provenance. In S.L. Eittreim & M.A. Hampton (eds), *The Antarctic continental margin: geology and geophysics of offshore Wilkes Land*, Circum-Pacific Council for Energy and Mineral Resources Earth Sciences Series, Volume 5A, 195–204.

Domack, E.W., Fairchild, W.W. & Anderson, J.B., 1980. Lower Cretaceous sediment from the East Antarctic continental shelf. *Nature*, 287, 625–626.

Eittreim, S.L. & Smith, G.L., 1987. Seismic sequences and their distribution on the Wilkes Land margin. In S.L. Eittreim & M.A. Hampton (eds), *The Antarctic continental margin: geology and geophysics of offshore Wilkes Land*, Earth Science Series, Circum-Pacific Council for Energy & Resources, 5A, 15–43.

Escutia, C., Eittreim, S.L., Cooper, A.K. & Nelson, C.H. 2000. Morphology and acoustic character of the Antarctic Wilkes Land turbidite systems: ice-sheets-sourced versus river–sourced fans. *Journal of Sedimentary Research*, 70 (1), 84-93.

Exon, N., Kennett, J, Malone, M. and the Leg 189 Shipboard Scientific Party, 2002. Drilling reveals climatic consequences of Tasmanian Gateway opening. *EOS*, Transactions of American Geophysical Union 83(23), 253, 258–259.

Faugère, J.C., Stow, D.A.V., Imbert, P. & Viana, A., 1999. Seismic features diagnostic of contourite drifts. *Marine Geology*, 162, 1–38.

Fedorov, L.V., Ravich, M.G. & Hofmann, J., 1982. Geologic comparison of southeastern Peninsular India and Sri Lanka with a part of East Antarctica (Enderby Land, Mac.Robertson Land, and Princess Elizabeth Land). In: C. Craddock (ed.), *Antarctic Geoscience*, University of Wisconsin Press, Madison, Wisconsin, 73–78.

Ford, A.B., 1975. Volcanic rocks of Naturaliste Plateau, Eastern Indian Ocean, Site 264, DSDP Leg 28. In D.E. Hayes, L.A. Frakes et al., *Initial Reports of the Deep Sea Drilling Project*, 28, 821–833.

Gaina, C., Müller, R.D. Brown, B. & Ishihara, T., 2003. Microcontinent formation around Australia. In R.R. Hillis & R.D. Müller (eds) *Evolution and Dynamics of the Australian Plate*, Geological Society of Australia Special Publication 22 and Geological Society of America Special Paper 372, 399-410.

Gaina C., Müller R. D., Royer J-Y., Stock J., Hardbeck J. & Symonds P., 1998. The tectonic history of the Tasman Sea: a puzzle with 13 pieces. *Journal of Geophysical Research*, 103, 12413–12433.

Gandyukhin, V., Gouseva, Yu, Kudryavtsev, G., Ivanov, S. & Leitchenkov, G., 2002. Crustal structure, seismic stratigraphy and tectonic history of the Cosmonaut Sea sedimentary basin (Antarctica, southern Indian Ocean). *Exploration and Protection of Mineral Resources*, 9, 27–31.

Ghosh, S.C., 2002. The Raniganj coal basin: an example of an Indian Gondwana rift. *Sedimentary Geology*, 147, 155–176.

Gladczenko T.P. & Coffin M.F., 2001. Kerguelen Plateau crustal structure and basin formation from seismic and gravity data. *Journal of Geophysical Research*, 106, 16583–16601.

Golynsky, A.V., Alyavdin, S.V., Masolov, V.N., Tscherinov, A.S. & Volnukhin, V.S., 2002. The composite magnetic anomaly map of the East Antarctic. *Tectonophysics*, 347, 109–120.

Golynsky, A.V., Masolov, V.N., Nogi, Y., Shibuya, K., Tarlowsky, C. & Wellman, P., 1996. Magnetic anomalies of Precambrian terranes of the East Antarctic shield coastal region (20°E-50°E). *Proceedings NIPR Symposium on Antarctic Geoscience*, 9, 24–39.

Gradstein F.M., Agterberg F.P., Ogg J.G., Hardenbol J., Van Veen P., Thierny J. & Huong Z. 1994. A Mesozoic timescale. *Journal of Geophysical Research*, 99, 24051–24074.

Guseva, Yu., Gandyukhin, V., Leitchenkov, G., Kudryavtsev, G., Kuznetsova, L., Ivanov, S. & Kazankov, A., 2004. Crustal structure and tectonic evolution of the East Antarctic margin between 30° E and 100° E (conjugate with India margin). In W.B.F. Ryan & A. Malinverno (eds) *The Mediterranean Tethys and the development*

of new concepts of top-down tectonics, Abstracts 32nd International Geological Congress.

Handwerger, D., Cooper, A.K., Williams, T., Barr, S.R. & Jarrard, R.D., 2001. Synthetic seismograms linking ODP sites 1165 and 1166 to seismic profiles, continental rise and shelf of Prydz Bay, Antarctica. In Florindo, F. and Cooper, A.K. (eds), *The geological record of the Antarctic Ice Sheet from drilling, coring and seismic studies*, Extended abstracts from the International ANTOSTRAT Symposium, Quaderni di Geofisicca, 16, 85–88.

Harris, P.T., O'Brien, P.E., Quilty, P.G., Taylor, F., Domack, E., DeSantis, L. & Raker, B., 1997. Vincennes Bay, Prydz Bay and Mac.Robertson Shelf, AGSO Cruise 186, post cruise report. *Australian Geological Survey Organisation Record* 1997/51.

Harrowfield, M., Holdgate, G.R., Wilson, C.J.L. & McLoughlin, S., in press. Tectonic significance of the Lambert graben, East Antarctica: reconstructing the Gondwanan rift. *Geology*.

Hayes, D.E., Frakes, L.A. et al., 1975. *Initial Reports of the Deep Sea Drilling Project, 28*: Washington, D.C., U.S. Government Printing Office.

Heezen, B.C. & Tharp, M., 1973. USNS Eltanin 55, *Antarctic Journal of the US*, 8, 137–141.

Hinz, K., Willcox, J.B., Whiticar, M., Kudrass, H.-R., Exon, N.F. & Feary, D.A., 1986. The west Tasmanian margin: an underrated petroleum province? In R.C. Glenie (ed.) *Second south-eastern Australia oil exploration symposium*, Petroleum Exploration Society of Australia, Melbourne, 1986, 395–410.

Hopkinson, L., Beard, J.S. & Boulter, C.A., 2004. The hydrothermal plumbing of a serpentinite-hosted detachment: evidence from the West Iberia non-volcanic rifted continental margin. *Marine Geology*, 204, 301–315.

Houtz, R.E., Hayes, D.E. & Markl, R.G., 1977. Kerguelen Plateau bathymetry, sediment distribution and crustal structure. *Marine Geology*, 25, 95–130.

Ishihara, T., Tanahashi, M., Sato, M. & Okuda, Y., 1996. Preliminary report of geophysical and geological surveys of the west Wilkes Land margin. *Proceedings of the NIPR Symposium on Antarctic Geoscience*, 9, 91–108.

Jones, M.T., Tabor, A.R. & Weatherall, P., 1997. Supporting volume to the GEBCO digital atlas.

Jongsma, D. & Petkovic, P., 1977. The structure of the Naturaliste Plateau and trough. *APEA Journal*, 17 (1), 3-12.

Joshima, M., Ishihara, T., Nakajinma, T., Sugiyama, K., Tsuchida, K., Kato, A., Murakami, F. & Brown, B., 2001. Preliminary results of the TH99 geological and geophysical survey in the Cooperation Sea and Prydz Bay area. *Polar Geosciences*, 14, 244–262.

Kaneps, A.G., 1975. Cenozoic planktonic foraminifera from Antarctic deep-sea sediments, Leg 28, DSDP. In D.E. Hayes, L.A. Frakes et al., *Initial Reports of the Deep Sea Drilling Project*, 28, 573–584.

Kennett, J.P., 1982. Marine geology. *Prentice Hall*, 813 pp.

König M. & Talwani M., 1977. A geophysical study of the southern continental margin of Australia: Great Australian Bight and western sections. *Geology Society of America Bulletin*, 88, 1000–1014.

Krassay, A.A., Cathro, D.L. and Ryan, D.J., 2004. A regional tectonostratigraphic framework for the Otway Basin. In Boult, P.J., Johns, D.R. & Lang, S.C. (eds), *Eastern Australasian Basins Symposium II*, Petroleum Exploration Society of Australia, Special Publication, 97–116.

Kudryavtsev**,** G.A., Kuznetsova**,** L.A., Alyavdin**,** S.V. & Ivanov**,** S.V., 2003. Geophysical Investigation on the Princess Elizabeth Margin – new data from 2003 season. In D.K. Fütterer (ed.) *Abstracts 9th International Symposium on Antarctic Earth Sciences*, Potsdam 8-12 September 2003, 190.

Kurinin, R.G. & Grikurov, G.E., 1982. Crustal structure of part of East Antarctica from geophysical data. In: C. Craddock (ed.), *Antarctic Geoscience*, University of Wisconsin Press, Madison, Wisconsin, 895–902.

Kuvaas, B. & Leitchenkov, G., 1992. Glaciomarine turbidite and current controlled deposits in Prydz Bay, Antarctica. *Marine Geology*, 108, 365–381.

Larson, R.L., Mutter, J.C., Diebold, J.B., Carpenter, G.B. & Symonds, P., 1979. Cuvier Basin: a product of ocean crust formation by Early Cretaceous rifting off Western Australia. *Earth & Planetary Science Letters*, 45, 105–114.

Leaman D.E., 1994. Criteria for evaluation of potential field interpretations. *First Break*, 12 (4), 181–191.

Lee, T. J., 1980. Rapid computation of magnetic anomalies with demagnetisation included, for arbitrarily shaped magnetic bodies. *Geophysical Journal of the Royal Astronomical Society*, 60, 67–75.

Leitchenkov, G., O'Brien, P.E., Ishihara, T. & Gandyukhin, V.V., 1999. The rift structure of Prydz Bay - Cooperation sea and history of pre-breakup crustal extension between India and Antarctica. *Abstracts 8th International Symposium on Antarctic Earth Sciences*, New Zealand, 188.

Leitchenkov, G., Shelestov, F., Gandjuhin, V. & Butsenko, V., 1990. Outline of structure and evolution of the Cooperation Sea sedimentary basin. In A.K. Cooper and P.N. Webb (eds) *International Workshop on Antarctic Offshore Seismic Stratigraphy (ANTOSTRAT): Overview and Extended Abstracts*, U.S. Geological Survey Open-file Report 90-309, 202–211.

Lisker, F. & Fachmann, S., 2001. Phanerozoic history of the Mahanadi region, India. *Journal of Geophysical Research*, 106 (B10), 22027–22050.

Ludwig W. J., Nafe J. E. & Drake C. L., 1971. Seismic refraction. In A.E. Maxwell (Ed.) *New concepts of sea floor evolution, Part 1: Regional observations*, Willey-Interscience, 53–84.

Mahoney, J., Jones, W., Frey, F.A., Salters, V., Pyle, D. & Davies, H., 1995. Geochemical characteristics of lavas from Broken Ridge, the Naturaliste Plateau and Southernmost Kerguelen Plateau: Early volcanism of the Kerguelen hotspot. *Chem. Geol.*, 120, 315–345.

Marks, K.M. & Tikku, A.A., 2001. Cretaceous reconstructions of East Antarctica, Africa, and Madagascar. *Earth and Planetary Science Letters* 186, 479–495.

Mawson, D., 1942. Geographical narrative and cartography. Australasian Antarctic Expedition 1911-14. *Scientific Reports Series A*, 1, 1–350.

McAdoo, D. & Laxon, S., 1997. Antarctic tectonics: constraints from an ERS-1 satellite marine gravity field. *Science*, 276, 556–560.

McCollum, D.W., 1975. Cenozoic planktonic foraminifera from Antarctic deep-sea sediments, Leg 28, DSDP. In D.E. Hayes, L.A. Frakes et al., *Initial Reports of the Deep Sea Drilling Project*, 28, 573–584.

Mihut, D. & Müller, R.D., 1998. Revised sea-floor spreading history of the Argo Abyssal Plain. In P.G. & R.R. Purcell (eds) *The Sedimentary Basins of Western Australia 2*, Proceedings of Petroleum Exploration Society of Australia Symposium, Perth, 1998, 73–80.

Miller, J.McL., Norvick, M.S. & Wilson, C.J.L., 2002. Basement controls on rifting and the associated formation of ocean transform faults – Cretaceous continental extension of the southern margin of Australia. *Tectonophysics*, 359, 131–155.

Mizukoshi, T., Sunouchi, H., Saki, T., & Tanahashi, M., 1986. Preliminary report of the geological and geophysical surveys of Amery Ice Shelf, East Antarctica. *Memoirs of the National Institute of Polar Research*, Japan, Special Issue, 43, 48–62.

Mond, A., 1972. The Permian sediments of the Beaver Lake area, Prince Charles Mountains. In R.J. Adie (ed.), *Antarctic Geology and Geophysics*, Universitetsforlaget, Oslo, 585–589.

Montigny, R., Karpoff, A.-M. & Hofmann, C., 1993. Résultats d'un dragage par 55°18'S – 83°04'E dans le Bassin de Labuan (campagne MD 67, océan Indien meridional): implications géodynamiques. *Géosciences Marines, Soc., Géol. France*, 83.

Moore, A.M.G., Stagg, H.M.J. & Norvick, M.S., 2000. Deep-water Otway basin: a new assessment of the tectonics and hydrocarbon prospectivity. *APPEA Journal*, 40 (1), 66–84.

Morris, E., Detrick, R.S., Minshull, T.A., Mutter, J.C., White, R.S., Su, W., & Buhl, P., 1993. Variations in seismic structure of Mesozoic aged crust in the western North Atlantic. *Journal of Geophysical Research*, 98, 13879–13904.

Muentener, O. & Herrmann, J., 2001. The role of lower crust and continental upper mantle during formation of non-volcanic passive margins; evidence from the Alps. In R.C.L. Wilson, R.B. Whitmarsh & N. Froitzheim (eds), *Non-volcanic rifting of continental margins: a comparison of evidence from land and sea*, Geological Society London Special Publication, 187, 267–288.

Müller, R.D., Roest, W.R., Royer, J-Y., Gahagan, L.M. & Sclater, J.G., 1997. Digital isochrons of the world's ocean floor. *Journal of Geophysical Research*, 102, 3211–3214.

Mutter, J.C. & Cande, S.C., 1983. The early opening between Broken Ridge and Kerguelen Plateau. *Earth and Planetary Science Letters*, 65, 369–376.

Mutter, J.C., Hegarty, K.A., Cande, S.C. & Weissel, J.K., 1985. Breakup between Australia and Antarctica: a brief review in the light of new data. In E.S. Husebye, G.L. Johnson & Y. Kristoffersen (eds) *Geophysics of the Polar Regions*, Tectonophysics, 114, 255–279.

Mutter, J.C. & Karson, J.A., 1992. Structural processes at slow-spreading ridges. *Science*, 257, 627–634.

Murakami, F., Ishihara, T., Oda, H., Fujimoto, M., Oda, H., Sugiyama, K. & Joshima, M., 2000. Preliminary report of the geological and geophysical survey results in the Princess Elizabeth Trough and its vicinity by R/V *Hakurei Maru*. *Polar Geoscience*, National Institute of Polar Research, 13, 165-186.

Nakao, S., 1990. Japanese expedition data in the Prydz Bay and its vicinity. In A.K. Cooper & P.N. Webb (convenors) *International Workshop on Antarctic Offshore Seismic Stratigraphy (ANTOSTRAT): Overview and Extended Abstracts*, U.S. Geological Survey Open-file Report 90-309, 228–232.

O'Brien, P.E., Cooper, A.K. Florindo, F., Handwerger, D., Lavelle, M., Passchier, S., Pospichal, J.J., Quilty, P.G., Richter, C., Theissen, K.M. & Whitehead, J.M., 2004. Prydz Channel Fan and the history of extreme ice advances in Prydz Bay. In A.K. Cooper, P.E. O'Brien and C. Richter (eds) *Proceedings of the Ocean Drilling Program Scientific Results 188*, http://www-odp.tamu.edu/publications/188_SR/016/016.htm

O'Brien, P.E., Cooper, A.K., Richter, C. et al., 2001. Initial Reports, Prydz Bay-Cooperation Sea, Antarctica: glacial history and paleoceanography. *Proceedings of the Ocean Drilling Program, Initial Reports*, 188 (CD-ROM), Texas A & M University, College Station Texas.

O'Brien, P.E., Franklin, D. & O'Loughlin, M., 1993. Post cruise report, Prydz Bay and Mac. Robertson Shelf, Antarctica, January-March, 1993. *Australian Geological Survey Organisation Record* 1993/78.

O'Brien, P.E., Harris, P.T., Quilty, P.G. Taylor, F. & Wells, P., 1995. Post-cruise report, Antarctic CRC marine geoscience, Prydz Bay, Mac.Robertson Shelf and Kerguelen Plateau. *Australian Geological Survey Record* 1995/29.

O'Brien, P.E. & Leitchenkov, G., 1997. Deglaciation of Prydz Bay, East Antarctica based on echo sounder and topographic features. In P.F. Barker & A.K. Cooper (eds) *Geology and seismic stratigraphy of the Antarctic Margin, 2*, American Geophysical Union, Antarctic Research Series, 71, 109–126.

O'Brien, P.E., Neumann, N. & Butler, P., 2002. Drill hole and seabed sampling information from the Australian Antarctic and Southern Ocean Profiling Project (AASOPP) study area. *Geoscience Australia Record* 2002/04.

Palmowski, D., Hill, K.C. & Hoffman, N., 2004. Structural-stratigraphic styles and evolution of the offshore Otway Basin – a structural seismic analysis. In P.J. Boult, D.R. Johns & S.C. Lang (eds), *Eastern Australasian Basins Symposium II*, Petroleum Exploration Society of Australia, Special Publication, 75–96.

Passchier, S., O'Brien, P.E., Damuth, J.E., Janusczak, N., Handwerger, D.A., & Whitehead, J.M., 2003. Pliocene-Pleistocene glaciomarine sedimentation in eastern Prydz Bay and development of the Prydz trough-mouth fan, ODP Sites 1166 and 1167, East Antarctica. *Marine Geology*, 199, 279–305.

Perez-Gussinyé, M. & Reston, T.J., 2001. Rheological evolution during extension at nonvolcanic rifted margins: onset of serpentinization and development of detachments leading to continental breakup. *Journal of Geophysical Research*, 106 (B3), 3961–3975.

Petkovic, P., 1975. Origin of the Naturaliste Plateau. *Nature*, 253, 30–33.

Piper, D.J.W. & Brisco, C.D., 1975. Deep-water continental margin sedimentation, DSDP, Leg 28, Antarctica. In D.E. Hayes, L.A. Frakes et al., *Initial Reports of the Deep Sea Drilling Project*, 28, 727–755.

Powell, C.McA., Roots, S.R. & Veevers, J.J., 1988. Pre-breakup continental extension in East Gondwanaland and the early opening of the eastern Indian Ocean. *Tectonophysics*, 155, 261–283.

Quilty, P.G., Truswell, E.M., O'Brien, P.E. & Taylor, F., 1999. Paleocene-Eocene biostratigraphy and palaeoenvironment of East Antarctica: new data from the Mac.Robertson Shelf and western parts of Prydz Bay. *AGSO Journal of Australian Geology & Geophysics*, 17, 133–143.

Rebesco, M., Larter, R.D., Barker, P.F., Camerlenghi, A. & Vanneste, L.E., 1997. The history of sedimentation on the continental rise west of the Antarctic Peninsula. In P.F. Barker & A.K. Cooper (eds), *Geology and Seismic Stratigraphy of the Antarctic Margin (Pt. 2)*, American Geophysical Union, Antarctic Research Series, 71, 29–50.

Reston, T.J., 1993. Evidence for extensional shear zones in the mantle, offshore Britain, and their implications for the extension of the continental lithosphere. *Tectonics*, 12 (2**)**, 492–506.

Reston, T.J., Pennell, J., Stubenrauch, A, Walker, I. & Perez-Gussinyé, M., 2001. Detachment faulting, mantle serpentinzation, and serpentinite-mud volcanism beneath the Porcupine Basin, southwest Ireland. *Geology*, 29, 587–590.

Rotstein, Y., Munschy, M. & Bernard, A., 2001. The Kerguelen Province revisited: additional constraints on the early development of the Southeast Indian Ocean. *Marine Geophysical Researches*, **22**, 81–100.

Royer, J.-Y. & Beslier, M.-O., 1998. *Rapport de campagne MD110/MARGAU, 1998*, Universite de Bretagne Occidentale, IUEM.

Royer, J.-Y. & Coffin, M.F., 1992. Jurassic to Eocene plate tectonic reconstructions in the Kerguelen Plateau region. In J.S.W. Wise, A.P. Julson, R. Schlich & E. Thomas (eds) *Proceedings of the Ocean Drilling Program, scientific results*, 120, Texas A&M University, College Station, TX, 917–930.

Royer, J.Y. & Rollet, N., 1997. Plate-tectonic setting of the Tasmanian region. *Australian Journal of Earth Sciences*, 44, 543–560.

Royer, J.-Y., Sclater, J.G., Sandwell, D.T., Cande, S.C., Schlich, R., Munschy, M., Dyment, J., Fisher, R.L., Müller, R.D., Coffin, M.F., Patriat, P. & Bergh, H.W., 1992. Indian Ocean plate reconstructions since the Late Jurassic. In R.A. Duncan, D.K. Rea, R.B. Kidd, U. von Rad & J.K. Weissel (eds) *The Indian Ocean: a synthesis of results from the Ocean Drilling Program*, Geophysical Monograph, American Geophysical Union, 471–475.

Sandwell, D.T. & Smith, W.H.F., 1997. Marine gravity anomaly from Geosat and ERS-1 satellite altimetry. *Journal of Geophysical Research*, 102, 10039–10054.

Sato, S., Asakura, N., Saki, T., Oikawa, N. & Kaneda, Y., 1984. Preliminary results of geological and geophysical surveys in the Ross Sea and in the Dumont d'Durville Sea, off Antarctica. *Memoirs of the National Institute for Polar Research*, Special Issue, 33, 66–92.

Sayers, J., Borissova, I., Ramsay, D. & Symonds, P.A., 2002. Geological framework of the Wallaby Plateau and adjacent areas. *Geoscience Australia Record* 2002/21.

Sayers, J., Symonds, P.A., Direen, N.G. & Bernardel, G., 2001. Nature of the continent-ocean transition on the non-volcanic rifted margin of the central Great Australian Bight. In R.C.L. Wilson, R.B. Whitmarsh & N. Froitzheim (eds), *Non-volcanic rifting of continental margins: a comparison of evidence from land and sea*. Geological Society, London, Special Publication, 187, 51–76.

SCAR (Scientific Committee on Antarctic Research), 1992. A SCAR seismic data library system for cooperative research: summary report of the International Workshop on Antarctic Seismic Data, Oslo, Norway, 11-15 April 1991. *SCAR Report*, 9, 1–15.

Schlich, R., Wise, S.W. et al., 1989. *Proceedings of the Ocean Drilling Program Initial Report*, 120.

Seismic Image Software Ltd, 1995. SIGMA-1.0 Seismic Interpretation and Geological Modelling Application. *Geological Survey of Canada* (unpub.).

Smith, W.H.F., Sandwell, D.T. & Small, C., 1997. Predicted bathymetry and GTOPO30 for the world, *Ftp topex.ucsd.edu/pub/global_topo_2min*.

Stagg, H.M.J., 1985. The structure and origin of Prydz Bay and the Mac.Robertson Shelf, East Antarctica. In E.S. Husebye, G.L. Johnson & Y. Kristoffersen (eds) *Geophysics of the Polar Regions*, Tectonophysics, 114, 315–40.

Stagg, H.M.J., Cockshell, C.D., Willcox, J.B., Hill, A., Needham, D.J.L., Thomas, B., O'Brien, G.W. & Hough, P., 1990. Basins of the Great Australian Bight region: geology and petroleum potential. *Bureau of Mineral Resources, Australia, Continental Margins Program Folio* 5.

Stagg, H.M.J., Colwell, J.B., Direen, N.G., O'Brien, P.E., Bernardel, G., Borissova, I., Brown, B.J. & Ishihara, T., in press. Geology of the continental margin of Enderby and Mac. Robertson Lands, East Antarctica: insights from a new dataset. In W. Jokat (Ed.) *East-west Antarctic tectonics and Gondwana break-up 60W to 60E*, Marine Geophysical Researches.

Stagg, H.M.J. & Symonds, P.A., 1995. The Argo Abyssal Plain: a proposal to drill reflecting interfaces within oceanic crust. *AGSO Record* 1995/12.

Stagg, H.M.J., Willcox, J.B. & Needham, D.J.L., 1992. The Polda Basin – a seismic interpretation of a Proterozoic–Mesozoic rift in the Great Australian Bight. *BMR Journal of Australian Geology & Geophysics*, 13, 1–13.

Steed, R.H.N, 1980. Geophysical investigation of Wilkes Land, Antarctica. *PhD Thesis*, Univ of Cambridge (unpub.).

Steed, R.H.N., 1983. Structural interpretations of Wilkes Land, Antarctica. In R.L. Oliver, P.R. James & J.B. Jago (eds), *Antarctic Earth Science*, Australian Academy of Science, Canberra, 567–72.

Steed, R.H.N. & Drewry, D.J., 1982. Radio echo sounding investigations of Wilkes Land, Antarctica. In C. Craddock (Ed.), *Antarctic Geoscience*, University Wisconsin Press, Madison, 969–76.

Storey, M., Kent, R.W., Saunders, A.D., Salters, V.J., Hergt, J., Whitechurch, H., Sevigny J.H., Thirlwall, M.F., Leat, P., Ghose, N.C. & Gifford, M., 1992. Lower Cretaceous volcanic rocks on continental margins and their relationship to the Kerguelen Plateau. In J.S.W. Wise, A.P. Julson, R. Schlich & E. Thomas (eds) *Proceedings of the Ocean Drilling Program, scientific results*, 120, Texas A&M University, College Station, 33–53.

Takin M. & Talwani M., 1966. Rapid computation of the gravitational attraction of topography on a spherical earth. *Geophysical Prospecting*, 14, 119-142.

Talwani, M., Mutter, J., Houtz, R. & Koenig, M., 1979. The crustal structure and evolution of the area underlying the magnetic quiet zone on the margin south of Australia. *AAPG Memoir* 29, 151–175.

Tanahashi, M., Ishihara, T., Yuasa, M., Murakami, F. & Nishimura, A., 1997. Preliminary report of the TH95 geological and geophysical survey results in the Ross Sea and the Dumont d'Urville Sea. *Proceedings of the NIPR Symposium on Antarctic Geosciences*, 10, 36–58.

Tanahashi, M., Saki, T., Oikawa, N. & Sato, S., 1987. An interpretation of the multichannel seismic reflection profiles across the continental margin of the Dumont d'Urville Sea, off Wilkes Land, East Antarctica. In S.L. Eittreim & M.A. Hampton (eds) *The Antarctic continental margin: geology and geophysics of offshore Wilkes Land*, Earth Science Series, Circum-Pacific Council for Energy & Resources, 5A, 1-13.

Tikku, A.A. & Cande, S.C., 1999. The oldest magnetic anomalies in the Australian-Antarctic Basin: are they isochrons? *Journal of Geophysical Research*, 101 (B1), 661–677.

Tikku, A.A. & Cande, S.C., 2000. On the fit of Broken Ridge and Kerguelen Plateau. *Earth & Planetary Science Letters*, 180, 117–132.

Tingey, R.J., 1991. The geology of Antarctica. *Oxford University Press*, 680 pp.

Totterdell, J.M., Blevin, J.E., Struckmeyer, H.I.M., Bradshaw, B.E., Colwell, J.B. & Kennard, J.M., 2000. A new sequence framework for the Great Australian Bight: starting with a clean slate. *APPEA Journal*, 40, 95–117.

Totterdell, J.M. & Bradshaw, B.E., 2004. The structural framework and tectonic evolution of the Bight Basin. *In* P.J. Boult, D.R. Johns & S.C. Lang (eds), *Eastern Australasian Basins Symposium II*, Petroleum Exploration Society of Australia, Special Publication, 41–61.

Truswell, E.M., Dettmann, M.E. & O'Brien, P.E., 1999. Mesozoic palynofloras from the Mac. Robertson shelf, East Antarctica: geological and phytogeographic implications. *Antarctic Science*, 11, 237–252.

Tsumuraya, Y., Tanahashi, M., Saki, T., Machihara, T. & Asakura N., 1985. Preliminary report of the marine geophysical and geological surveys off Wilkes Land, Antarctica, in 1983-1984. *Memoirs National Institute Polar Research Special Issue* 37, 48–62.

Turner, B.R., 1991. Depositional environment and petrography of preglacial continental sediments from Hole 740A, Prydz Bay, Antarctica. In J. Barron, B. Larsen et al., *Proceedings of the Ocean Drilling Program Scientific Results 119*, College Station, TX (Ocean Drilling Program), 45–56.

UNCLOS, 1983. The Law of the Sea: United Nations Convention on the Law of the Sea with index and final act of the Third United Nations Conference on the Law of the Sea. *St Martins Press*, New York.

Veevers, J.J., 1986. Breakup of Australia and Antarctica estimated as mid-Cretaceous (95 +/- 5 Ma) from magnetic and seismic data at the continental margin. *Earth & Planetary Science Letters*, 77, 91–99.

Veevers, J.J., 1988. Seafloor magnetic lineation off the Otway/West Tasmania Basins: ridge jumps and the subsidence history of the southeast Australian margins. *Australian Journal of Earth Sciences*, 35(4), 451–462.

Veevers, J.J., 2000. *Billion-year Earth History of Australia and Neighbours in Gondwanaland*. GEMOC Press, Sydney, 388 pp.

Veevers, J.J., Stagg, H.M.J., Willcox, J.B. & Davies, H.L., 1990. Pattern of slow seafloor spreading (<4 mm/year) from breakup (96 Ma) to A20 (44.5 Ma) off the southern margin of Australia. *Bureau of Mineral Resources Journal of Australian Geology & Geophysics*, 11, 499–507.

Wannesson, J., 1990. Geology and petroleum potential of the Adelie Coast, East Antarctica. In B. St John (ed.), *Antarctica as an exploration frontier – hydrocarbon potential, geology and hazard,*. AAPG Studies in Geology, 31, 77–88.

Wannesson, J., Pelras, M., Petitperrin, B., Perret, M., & Segoufin, J., 1985. A geophysical transect of the Adelie Margin, East Antarctica. *Marine and Petroleum Geology*, **2**, 192–201.

Wellman, P. & Tingey, R.J., 1976. Gravity evidence for a major crustal fracture in eastern Antarctica. *Bureau of Mineral Resources Journal of Australian Geology & Geophysics*, 1, 105–108.

White, R.S., Detrick, R.S., Mutter, J.C., Buhl, P., Minshull, T.A. & Morris, E., 1990. New seismic images of oceanic crustal structure. *Geology*, 18, 462–465.

White, R.S., McKenzie, D. & O'Nions, R.K., 1992. Oceanic crustal thickness from seismic measurements and rare earth element inversions. *Journal of Geophysical Research*, 97 (B13), 19683–19715.

Whitmarsh, R.B., Manatschal, G. & Minshull, T.A., 2001. Evolution of magma-poor continental margins from rifting to seafloor spreading. *Nature*, 413, 150–154.

Willcox, J.B. & Stagg, H.M.J., 1990. Australia's southern margin: a product of oblique extension. *Tectonophysics*, 173, 269–81.

Yuasa, M., Niida, K., Ishihara, T., Kisimoto, K. & Murakami, F., 1997. Peridotite dredged from a seamount off Wilkes Land, the Antarctic: emplacement of fertile

mantle fragment at early rifting stage between Australia and Antarctica during the final breakup of Gondwanaland. In C.A. Ricci (ed.) *The Antarctic region: geological evolution and processes*, Terra Antarctica, Siena, 725–730.

APPENDIX 1: GLOSSARY OF ACRONYMS & ABBREVIATIONS

AAB	Australian–Antarctic Basin
AASOPP	Australian Antarctic & Southern Ocean Profiling Project
AAT	Australian Antarctic Territory
AGSO	Australian Geological Survey Organisation (now Geoscience Australia)
AUSLIG	Australian Surveying and Land Information Group
BMR	Bureau of Mineral Resources, Geology & Geophysics (now Geoscience Australia)
BSR	basement simulating reflector
CLCS	(United Nations) Commission on the Limits of the Continental Shelf
COB	continent–ocean boundary
COT	continent–ocean transition
DSDP	Deep Sea Drilling Project
EEZ	Exclusive Economic Zone
EOL	end of line
GA	Geoscience Australia
GAB	Great Australian Bight
GEBCO	General Bathymetric Chart of the Oceans
JNOC	Japan National Oil Corporation
Ma	million years ago
ODP	Ocean Drilling Program
SDRS	seaward-dipping reflector sequence
SOL	start of line
SP	shot point
TWT	two-way time
UNCLOS	United Nations Convention on the Law of the Sea
USGS	United States Geological Survey

APPENDIX 2: KEY GEOLOGICAL SAMPLE STATIONS IN THE REGION OF THE AUSTRALIAN ANTARCTIC TERRITORY

Sample	Latitude	Longitude	Age and fossils
AGSO 149/GC03	67° 29.9'S	64° 59.8'E	Valanginian-Aptian palynomorphs
AGSO 149/GC05	67°24.21'S	65o55.82'E	Tithonian-Valanginian palynomorphs
AGSO 149/GC06	67°17'S	66°01.3'E	Callovian-Bajocian palynomorphs
AGSO 149/GC39	67°09.4'S	65°45.1'E	Toarcian-Bajocian palynomorphs
AGSO 149/GC40	67°09.4'S	65°45.1'E	Toarcian-Bajocian palynomorphs
AGSO 901/SL2 (KROCK) (epibenthic sled)	66°53.95'S	63°09.3'E	Eocene palynomorphs
AGSO 149/GC07	66°50.7'S	64°55.2'E	Late Miocene
AGSO 149/GC09	67°05.2'S	65°19.3'E	Paleocene, E-M Eocene palyn. Eocene foraminifera
AGSO 149/GC10	67°05.1'S	65°27.9'E	Paleocene-Eocene foraminifers, palynomorphs
AGSO 149/GC13	67°05.3'S	65°59.0'E	Paleocene-M. Eocene palyn.
AGSO 149/GC21	66°33.1'S	72°17.6'E	Miocene? Foram. Cretaceous-Paleocene palyn.
AGSO 149/GC45	67°00'S	63°05.0'E	M-L Eocene palyn, L. Paleocene foram.
AGSO 149/GC46	66°54.3'S	63°06.0'E	Eocene foram, M. Eocene palyn., *Inoceramous* prisms
AGSO 149/GC47	66°49.0'S	63°14.0'E	M. Eocene palyn., *Inoceramous* prisms
AGSO 186/GC33	66°44.9'S	63°18.2'E	M-L. Eocene foram., *Inoceramous* prisms

Cores and dredges containing Mesozoic and Cainozoic fossil material (Truswell et al., 1999, Quilty et al., 1999).

Site	*Latitude*	*Longitude*	*Water depth*	*Description*
D1502	-63.4523 -63.4470	102.6933 102.6833	2446 – 2495	Semi-consolidated siltstone, granite, schist
D1503	-63.6961 -63.6911	102.7233 102.6950	2744 – 2834	Semi-consolidated siltstone, granite, schist
D1504	-63.7911 -63.8017	103.0083 103.0433	2896 – 2668	Semi-consolidated mudstone, granite, schist, quartzose sandstone

Summary of dredge samples recovered from Bruce Rise on survey TH-94 (from Ishihara et al., 1996).

Dredge	**Latitude**	**Longitude**	**Lithologies and ages**
D1201	62^{o} 08” S	141^{o} 22’ E	peridotite
D1601	61^{o} 49’ 37” S 61^{o} 49’ 13” S	140^{o} 32’ 42” E 140^{o} 34’ 42” E	granite, gneiss, diorite, calcareous ooze, manganese nodule
D1602	62^{o} 18’ 55” S 62^{o} 18’ 59” S	140^{o} 56’ 24” E 140^{o} 54’ 42” E	granite, gneiss, slate, calcareous ooze, manganese nodule & crust
DF-79-38	67^{o} 44’ S	146^{o}51’E	non-marine siltstone with Cretaceous palynomorphs
TH82/D302	65^{o} 31.6’ S 65^{o} 31.4’ S	139^{o} 32.1’ E 139^{0} 31.4’ E	Oligocene & Miocene limestone

Cores and dredges from offshore Terre Adélie and western George V Land containing basement rocks and Mesozoic and Cainozoic fossil material (Domack et al., 1980, Sato et al. 1984; Tanahsahi et al., 1997).

APPENDIX 3: SEISMIC SURVEYS IN THE REGION OF THE AUSTRALIAN ANTARCTIC TERRITORY

Survey / area	**Survey GA-33; Prydz Bay**
Institution	Geoscience Australia
Reference	Stagg (1985)
Vessel	*Nella Dan*
Year	1982
km of seismic data	5000
Streamer length (m)	300 m
Seismic channels	5 or 6
Sample rate / rec. length (ms)	2, 6000
Group length/interval (m)	50
Shot interval (m)	25 / 50 m
Recording fold	3 / 6
Cable depth (m)	6
Source type / power or volume	1 x 8.2 litre airgun
Nominal vessel speed (kn)	5.5
Primary navigation	Transit Satellite navigation
Primary echo-sounder	3.5 KHz
Secondary echo-sounder	none
Magnetic data	yes
Gravity data	no

Survey / area	**ATC82; Terre Adélie**
Institution	Institut Français du Pétrole
Reference	Wannesson et al. (1985)
Vessel	*Explora*
Year	1982
km of seismic data	3190
Streamer length (m)	2400 m
Seismic channels	48
Sample rate / rec. length (ms)	4, 8000
Group length/interval (m)	50
Shot interval (m)	50
Recording fold	24
Cable depth (m)	15
Source type / power or volume	airgun array, 35.54 litres
Nominal vessel speed (kn)	5
Primary navigation	Transit satellite
Primary echo-sounder	
Secondary echo-sounder	
Magnetic data	yes
Gravity data	yes

Survey / area	**L1-84-AN; Wilkes Land and Terre Adélie**
Institution	United States Geological Survey
Reference	Eittreim & Smith (1987)
Vessel	*S.P. Lee*
Year	1984
km of seismic data	1800
Streamer length (m)	2400
Seismic channels	24
Sample rate / rec. length (ms)	2, 10000
Group length/interval (m)	100
Shot interval (m)	50
Recording fold	24
Cable depth (m)	12.5
Source type / power or volume	airgun array, 21.49 litres
Nominal vessel speed (kn)	5
Primary navigation	Transit satellite
Primary echo-sounder	12 KHz
Secondary echo-sounder	3.5 KHz
Magnetic data	yes
Gravity data	yes

Survey / area	**TH82; Terre Adélie**
Institution	Japan National Oil Corporation
Reference	Sato et al. (1984)
Vessel	*Hakurei Maru*
Year	1982-83
km of seismic data	820
Streamer length (m)	600
Seismic channels	24
Sample rate / rec. length (ms)	4, 5000
Group length/interval (m)	25
Shot interval (m)	50
Recording fold	6
Cable depth (m)	
Source type / power or volume	1 x 9.2 litre airgun
Nominal vessel speed (kn)	4
Primary navigation	Transit satellite
Primary echo-sounder	12 KHz
Secondary echo-sounder	3.5 KHz
Magnetic data	yes
Gravity data	yes

Survey / area	**TH83; Wilkes Land**
Institution	Japan National Oil Corporation
Reference	Tsumuraya et al. (1985)
Vessel	*Hakurei Maru*
Year	1983-84
km of seismic data	3700
Streamer length (m)	600
Seismic channels	24
Sample rate / rec. length (ms)	4, 5000
Group length/interval (m)	25
Shot interval (m)	50
Recording fold	6
Cable depth (m)	
Source type / power or volume	1 x 9 litre or 1 x 7.4 litre airgun
Nominal vessel speed (kn)	4
Primary navigation	Transit satellite
Primary echo-sounder	12 KHz
Secondary echo-sounder	3.5 KHz
Magnetic data	yes
Gravity data	yes

Survey / area	**TH84; Prydz Bay**
Institution	Japan National Oil Corporation
Reference	Mizukoshi et al. (1986)
Vessel	*Hakurei Maru*
Year	1984-85
km of seismic data	2350
Streamer length (m)	600
Seismic channels	24
Sample rate / rec. length (ms)	4, 5000
Group length/interval (m)	25
Shot interval (m)	50
Recording fold	6
Cable depth (m)	
Source type / power or volume	2 x 6.6 litre water gun
Nominal vessel speed (kn)	4
Primary navigation	Transit satellite
Primary echo-sounder	12 KHz
Secondary echo-sounder	3.5 KHz
Magnetic data	yes
Gravity data	yes

Survey / area	**TH89; Enderby Basin & Prydz Bay**
Institution	Japan National Oil Corporation
Reference	Nakao (1990)
Vessel	*Hakurei Maru*
Year	1989-90
km of seismic data	1836
Streamer length (m)	600
Seismic channels	24
Sample rate / rec. length (ms)	4, 5000
Group length/interval (m)	25
Shot interval (m)	50
Recording fold	6
Cable depth (m)	15
Source type / power or volume	water guns; 13.1 litres
Nominal vessel speed (kn)	
Primary navigation	
Primary echo-sounder	
Secondary echo-sounder	
Magnetic data	yes
Gravity data	yes

Survey / area	**TH94; West Wilkes Land**
Institution	Japan National Oil Corporation
Reference	Ishihara et al. (1996)
Vessel	*Hakurei Maru*
Year	1994-95
km of seismic data	2377 (multichannel); 1867 km (single channel)
Streamer length (m)	1200
Seismic channels	48
Sample rate / rec. length (ms)	4, 6000
Group length/interval (m)	25
Shot interval (m)	50
Recording fold	12
Cable depth (m)	15
Source type / power or volume	4 x SSI GI-guns, 13.8 litres
Nominal vessel speed (kn)	
Primary navigation	
Primary echo-sounder	
Secondary echo-sounder	
Magnetic data	yes
Gravity data	yes

Survey / area	**TH95; Ross Sea & Terre Adélie**
Institution	Japan National Oil Corporation
Reference	Tanahashi et al. (1997)
Vessel	*Hakurei Maru*
Year	1995-96
km of seismic data	1978
Streamer length (m)	2100
Seismic channels	168
Sample rate / rec. length (ms)	4, 12000
Group length/interval (m)	12.5
Shot interval (m)	50
Recording fold	21
Cable depth (m)	
Source type / power or volume	4 x SSI GI-guns, 13.8 litres
Nominal vessel speed (kn)	4.4
Primary navigation	
Primary echo-sounder	12 KHz
Secondary echo-sounder	
Magnetic data	yes
Gravity data	yes

Survey / area	**TH98; Princess Elizabeth Trough**
Institution	Japan National Oil Corporation
Reference	Murakami et al. (2000)
Vessel	*Hakurei Maru*
Year	1998-99
km of seismic data	2490
Streamer length (m)	3000
Seismic channels	240
Sample rate / rec. length (ms)	
Group length/interval (m)	12.5
Shot interval (m)	50
Recording fold	30
Cable depth (m)	not known
Source type / power or volume	SSI G-guns; 65.6 litres
Nominal vessel speed (kn)	4.4 kn
Primary navigation	
Primary echo-sounder	
Secondary echo-sounder	
Magnetic data	yes
Gravity data	yes

Survey / area	**Prydz Bay**
Institution	Soviet Antarctic Expedition
Reference	Leitchenkov et al. (1990)
Vessel	*Capitan Gotsky*
Year	1985-86
km of seismic data	930
Streamer length (m)	2 300
Seismic channels	24
Sample rate / rec. length (ms)	2/9000
Group length/interval (m)	100
Shot interval (m)	50
Recording fold	24
Cable depth (m)	10
Source type / power or volume	P1-B/7.5 litres
Nominal vessel speed (kn)	4.6-5.0 kn
Primary navigation	MX-4400
Primary echo-sounder	12 kHz
Secondary echo-sounder	
Magnetic data	yes (930 km)
Gravity data	yes (930 km)
Sonobuoys	2

Survey / area	**Prydz Bay / Eastern Cooperation Sea**
Institution	Soviet Antarctic Expedition
Reference	Leitchenkov et al. (1999)
Vessel	*Capitan Markov*
Year	1986-87
km of seismic data	3 700
Streamer length (m)	2 300
Seismic channels	24
Sample rate / rec. length (ms)	2/9000
Group length/interval (m)	100
Shot interval (m)	50
Recording fold	24
Cable depth (m)	10
Source type / power or volume	P1-B/7.5 litres
Nominal vessel speed (kn)	4.6-5.0 kn
Primary navigation	MX-4400
Primary echo-sounder	12 kHz
Secondary echo-sounder	
Magnetic data	yes (3700 km)
Gravity data	yes (3700 km)
Sonobuoys	11

Survey / area	**Prydz Bay / Eastern Cooperation Sea**
Institution	Soviet Antarctic Expedition
Reference	Leitchenkov et al. (1999)
Vessel	*Capitan Mishevsky*
Year	1987-88
km of seismic data	3 700
Streamer length (m)	2 300
Seismic channels	24
Sample rate / rec. length (ms)	2/9000
Group length/interval (m)	100
Shot interval (m)	50
Recording fold	24
Cable depth (m)	10
Source type / power or volume	P1-B/7.5 litres
Nominal vessel speed (kn)	4.6-5.0 kn
Primary navigation	MX-4400
Primary echo-sounder	12 kHz
Secondary echo-sounder	
Magnetic data	yes (3700 km)
Gravity data	yes (4250 km)
Sonobuoys	7

Survey / area	**Prydz Bay / Eastern Cooperation Sea**
Institution	Soviet Antarctic Expedition
Reference	Leitchenkov et al. (1999)
Vessel	*Navarin*
Year	1990-91
km of seismic data	700
Streamer length (m)	2 300
Seismic channels	12/24
Sample rate / rec. length (ms)	2/9000
Group length/interval (m)	100
Shot interval (m)	50
Recording fold	24
Cable depth (m)	10
Source type / power or volume	P1-B/7.5 litres
Nominal vessel speed (kn)	4.6-5.0 kn
Primary navigation	MX-4400
Primary echo-sounder	12 kHz
Secondary echo-sounder	
Magnetic data	yes (1000 km)
Gravity data	yes (1000 km)
Sonobuoys	6

Survey / area	**Prydz Bay / Eastern Cooperation Sea**
Institution	Russian Antarctic Expedition
Reference	Leitchenkov et al. (1999)
Vessel	*Akademik Alexander Karpinsky*
Year	1993-94
km of seismic data	2 500
Streamer length (m)	2 350
Seismic channels	48
Sample rate / rec. length (ms)	4 / 7000
Group length/interval (m)	50
Shot interval (m)	50
Recording fold	12/24
Cable depth (m)	15
Source type / power or volume	6P-20/40 litres
Nominal vessel speed (kn)	40 litres
Primary navigation	"Svisix"
Primary echo-sounder	12 kHz
Secondary echo-sounder	
Magnetic data	yes (2500 km)
Gravity data	yes (2500 km)
Sonobuoys	5

Survey / area	**Prydz Bay / Eastern Cooperation Sea**
Institution	Russian Antarctic Expedition
Reference	Leitchenkov et al. (1999)
Vessel	*Akademik Alexander Karpinsky*
Year	1994-95
km of seismic data	3 400
Streamer length (m)	2 350
Seismic channels	48
Sample rate / rec. length (ms)	4 / 7000
Group length/interval (m)	50
Shot interval (m)	50
Recording fold	12/24
Cable depth (m)	15
Source type / power or volume	6P-20
Nominal vessel speed (kn)	40 litres
Primary navigation	"Svisix"
Primary echo-sounder	12 kHz
Secondary echo-sounder	
Magnetic data	yes (3400 km)
Gravity data	yes (3400 km)
Sonobuoys	6

Survey / area	**Western Cosmonaut Sea**
Institution	Russian Antarctic Expedition
Reference	Gandyukhin et al. (2002)
Vessel	*Akademik Alexander Karpinsky*
Year	1999-2000
km of seismic data	3 400
Streamer length (m)	2 350
Seismic channels	48
Sample rate / rec. length (ms)	4 / 7000
Group length/interval (m)	50
Shot interval (m)	50
Recording fold	12/24
Cable depth (m)	15
Source type / power or volume	6P-20 / 40 litres
Nominal vessel speed (kn)	4.6-5.0
Primary navigation	"Svisix"
Primary echo-sounder	12 kHz
Secondary echo-sounder	
Magnetic data	yes (3400 km)
Gravity data	yes (3400 km)
Sonobuoys	12

Survey / area	**Eastern Cosmonaut Sea**
Institution	Russian Antarctic Expedition
Reference	Gandyukhin et al. (2002)
Vessel	*Akademik Alexander Karpinsky*
Year	2000-01
km of seismic data	4 400
Streamer length (m)	2 350
Seismic channels	48
Sample rate / rec. length (ms)	4 / 7000
Group length/interval (m)	50
Shot interval (m)	50
Recording fold	12/24
Cable depth (m)	15
Source type / power or volume	6P-20 /40 litres
Nominal vessel speed (kn)	4.6-5.0
Primary navigation	"Svisix"
Primary echo-sounder	12 kHz
Secondary echo-sounder	
Magnetic data	yes (3400 km)
Gravity data	yes (3400 km)
Sonobuoys	10

Survey / area	**Western Cooperation Sea**
Institution	Russian Antarctic Expedition
Reference	Gandyukhin et al. (2002)
Vessel	*Akademik Alexander Karpinsky*
Year	2001-02
km of seismic data	4 400
Streamer length (m)	2 350
Seismic channels	48
Sample rate / rec. length (ms)	4 / 7000
Group length/interval (m)	50
Shot interval (m)	50
Recording fold	12/24
Cable depth (m)	15
Source type / power or volume	6P-20/40 litres
Nominal vessel speed (kn)	4.6-5.0
Primary navigation	
Primary echo-sounder	12 kHz
Secondary echo-sounder	
Magnetic data	yes (3400 km)
Gravity data	yes (3400 km)
Sonobuoys	10

Survey / area	**Elizabeth Trough / Davis Sea**
Institution	Russian Antarctic Expedition
Reference	Kudryavtsev et al. (2003)
Vessel	*Akademik Alexander Karpinsky*
Year	2002-03
km of seismic data	4 200
Streamer length (m)	3 000
Seismic channels	240
Sample rate / rec. length (ms)	2 / 11000-13000
Group length/interval (m)	12.5
Shot interval (m)	50
Recording fold	30
Cable depth (m)	10
Source type / power or volume	6P-20/40 litres
Nominal vessel speed (kn)	4.6-5.0
Primary navigation	GP-80
Primary echo-sounder	12 kHz
Secondary echo-sounder	
Magnetic data	yes (3400 km)
Gravity data	yes (3400 km)
Sonobuoys	10

Survey / area	**Davis Sea / Mawson Sea**
Institution	Russian Antarctic Expedition
Reference	Guseva et al. (2004)
Vessel	*Akademik Alexander Karpinsky*
Year	2003-04
km of seismic data	4 000
Streamer length (m)	4 387.5
Seismic channels	352
Sample rate / rec. length (ms)	2 / 11000
Group length/interval (m)	12.5
Shot interval (m)	50
Recording fold	44
Cable depth (m)	10
Source type / power or volume	Sleeve Gun IIB Input/Output inc. / 16.5 litres
Nominal vessel speed (kn)	4.6-5.0
Primary navigation	GP-80
Primary echo-sounder	12 kHz
Secondary echo-sounder	
Magnetic data	yes (4 000 km)
Gravity data	yes (4 000 km)
Sonobuoys	10

APPENDIX 4: SONOBUOY SOLUTIONS (EXCLUDING SURVEYS 228 & 229)

Station	*Latitude*	*Longitude*	*WD*	V_1	T_1	V_2	T_2	V_3	T_3	V_4	T_4	V_5	T_5	V_6
14E42	-57.516667	170.503333	5.35	1.8	0.37	5.49	1.42	6.67						
15E42	-57.016081	170.676667	5.4	1.8	0.23	5.38	1.23	6.85						
16E42	-57.54	170.008333	5.22	1.94	0.5	5.4	1.53	6.62						
9E43	-51.633333	178.453333	4.91	2.41	0.95	5.82	1.82	6.61						
10E43	-51.2	177.548333	4.83	1.64	1.34	5.41								
11E43	-50.851667	176.908333	4.5	2.34	1.02	5.6	1.04	6.57	0.63	7.17				
31E53	-47.968333	147.806667	1.56	1.66	0.35	5.34	1.36	6.61						
32E53	-47.98	148.038333	1.61	1.6	0.31	2.56	0.82	3.28	0.78	4.85	1.11	5.8	1.42	6.86
33E53	-47.991667	148.753333	1.62	2.21	0.84	5.69								
34E53	-47.918333	148.546667	1.45	1.8	0.27	4.7	0.57	5.48						
27E53	-51.163333	147.953333	4.2	1.8	0.53	5.12								
28E53	-51.151667	147.676667	4.24	1.69	0.5	3.13	0.65	4.43	1.04					
29E53	-51.383333	147.828333	4.03	1.95	0.62	5.0	2.26	5.95						
30E53	-49.078333	148.346667	4.14	2.67	1.05	5.5	1.94	6.23						
1E53	-43.116667	160.053333	5.0	1.86	0.67	5.15	2.11	7.1						
2E53	-43.16	159.835	4.94	2.6	1.09	4.65	1.5	7.05						

Station	*Latitude*	*Longitude*	*WD*	V_1	T_1	V_2	T_2	V_3	T_3	V_4	T_4	V_5	T_5	V_6
4E53	-43.326667	159.251667	4.93	1.84	0.37	1.99	0.46	4.9						
6E53	-44.041667	154.438333	4.87	1.75	0.63	5.19	2.04	7.37						
8E53	-43.735	154.071667	4.71	1.73	0.52	2.2	0.4	5.5						
9E53	-43.186667	155.225	4.47	2.05	1.04	4.8	2.15	6.2						
L184AN-1	-63.328333	130.423333	4.12	2.02	0.57	2.94	0.97	3.8	2.43	6.31				
L184AN-2	-63.733333	130.396667	3.73	2.05	1.5	3.79	2.39	5.28	0.88	6.57	9.14	8.55		
L184AN-3	-64.063333	131.416666	2.86	1.8	0.64	2.06	0.45	2.97	0.64	3.57	2.37	5.75		
L184AN-4	-63.596667	131.73	3.85	1.8	0.54	2.34	1.19	3.33	1.8	4.01	3.15	7.68		
L184AN-5	-63.153333	132.411667	4.23	1.8	0.36	2.51	0.55	3.13	2.96	5.09	1.53	7.93		
L184AN-6	-63.246667	133.31	4.17	1.8	0.24	2.18	1.43	3.29	1.72	6.0				
L184AN-7	-63.625	133.343333	3.67	1.8	0.27	2.17	0.85	2.74	1.02	3.74	2.45	6.49		
L184AN-9	-64.025	134.903333	3.26	1.83	1.32	3	0.83	3.46	1.55	6.42				
L184AN-10	-63.678333	134.94	3.9	1.8	0.46	2.26	0.79	2.9	0.4	3.44	0.98	5.79		
L184AN-11	-63.428333	134.873333	4.07	1.8	0.4	2.31	0.78	2.66	0.79	3.4	1.97	5.02		
L184AN-12	-63.111667	134.921666	4.11	1.8	0.24	2.27	1.68	3.82	2.12	5.22	0.89	6.87		
L184AN-13	-63.423333	135.391667	3.93	1.88	0.74	2.58	1.16	3.65	2.81	6.87				
L184AN-14	-63.66	135.83	3.63	1.8	0.56	2.45	0.72	3.05						
L184AN-15	-63.92	136.15	3.37	1.8	0.56	2.37	0.8	2.9	1.14	3.79	2.57	6.12	7.16	8.22

Station	*Latitude*	*Longitude*	*WD*	V_1	T_1	V_2	T_2	V_3	T_3	V_4	T_4	V_5	T_5	V_6
L184AN-16	-64.346667	136.858333	2.38	1.8	1.18	3.24								
L184AN-17	-64.14	138.01	3.39	1.8	0.61	2.34	0.83	2.93	0.3	3.55	3.79	7.87		
L184AN-18	-64.371667	138.421666	3.33	1.83	0.48	2.48	0.9	2.65	0.62	3.56	3.91	6.09	5.13	7.54
L184AN-19	-64.733333	138.763333	2.75	1.8	0.81	2.47	0.71	2.69	0.86	3.84	4.54	6.07		
L184AN-20	-65.258333	140.741667	2.1	1.8	0.92	2.35	0.73	3.12	1.17	3.83	4.44	5.69		
L184AN-21	-64.673333	141.486667	3.29	1.8	0.3	2.2	0.79	3.68	4.53	5.63				
L184AN-23	-64.72	142.415	3.08	1.8	0.62	2.18	0.6	3.52	1.47	4.06	2.97	5.29		
L184AN-24	-64.733333	142.896667	3.21	1.8	0.23	2.23	0.86	3.83	1.39	4.4	3.57	6.51		
L184AN-25	-64.78	143.681667	3.34	1.78	0.32	2.25	0.71	3.84	5.6	7.71				
L184AN-26	-64.82	144.446666	3.11	1.8	0.2	2.27	1.09	3.97	3.46	4.61				
L184AN-27	-64.873333	145.155	3.37	1.8	0.66	2.94	0.21	3.34	3.68	5.0				
L184AN-28	-64.983333	146.02	3.16	1.8	0.54	2.47	0.72	4.16	5.26	6.39				
L184AN-31	-65.488333	145.808333	2.79	1.8	0.63	2.4	0.65	3.64	1.68	4.09				
L184AN-32	-65.971667	145.526667	0.46	2.5	0.88	3.43	0.7	3.69						
L184AN-33	-66.273333	145.406667	0.19	1.8	0.39	2.71	1.49	3.62	1.07	4.36				
TH82-SB1	-64.0368	139.727		1.7	1.3	3.0	1.1	4.0	3.0	5.0				
TH82-SB2	-65.745	139.54		1.6	0.15	2.2	0.75	3.0	0.4	3.9	1.9	4.7		
TH82-SB3	-64.1	138.94		1.7	0.7	2.3	0.9	2.9	0.95	3.5	0.15	5.8		

Station	*Latitude*	*Longitude*	*WD*	V_1	T_1	V_2	T_2	V_3	T_3	V_4	T_4	V_5	T_5	V_6
TH84-SB1	-64.497222	75.73625	3.45	1.75	0.3	2.0	0.35	2.3	0.44	2.65	0.4	3.0	0.8	3.4
TH84-SB2	-64.493639	71.524972	3.35	1.85	0.3	1.95	0.65	2.65	0.25	2.85	0.35	4.0	2.7	4.3
TH84-SB3	-63.185139	75.011917	3.8	2.0	0.4	2.25	0.3	2.5	0.5	2.7	0.3	2.85	0.7	3.5
TH84-SB5	-64.493139	79.011833	3.65	1.8	0.25	2.1	0.85	3.0	1.55	3.3	0.7	4.3	0.6	
TH84-SB6	-65.821583	74.861444	3.0	2.15	1.1	2.95	0.7	3.15	0.6	3.55	0.4	4.1	1.4	5.15
TH84-SB7	-67.403778	72.946778	0.6	1.7	0.15	2.4	0.5	2.85	0.75	3.85	1.65	4.15	0.8	
TH84-SB8	-66.913639	70.881056	0.45	1.7	0.15	2.1	0.1	1.9	2.2					
TH84-SB9	-65.74425	70.927722	0.8	1.6	0.5	1.8	0.55	2.5	0.15	3.85				
TH84-SB10	-62.777833	79.507583	3.5	2.7	0.7	3.85								
TH94-OBS2	-63.24	116.0	3.3	2.15	1.42	2.46	1.28	3.76	1.47	4.1	0.93	4.41	0.35	4.72
(cont.)					1.35	5.15	1.7	5.62						
TH94-OBS3	-62.57	116.0	3.74	1.58	0.98	2.31	0.28	2.59	1.34	3.33	0.99	3.82	1.02	4.18
(cont.)					1.21	4.75	3.64	6.13						
TH94-OBS4 (N-S)	-63.45	102.0	1.24	1.76	0.88	2.28	0.59	2.84	0.15	3.05	2.63	5.15	0.77	6.8
TH94-OBS4 (E-W)	-63.45	102.0	1.24	1.55	0.37	1.85	0.59	2.35	0.29	2.98	0.59	3.18	0.8	3.53
(cont.)					1.32	4.24								

Station	*Latitude*	*Longitude*	*WD*	V_1	T_1	V_2	T_2	V_3	T_3	V_4	T_4	V_5	T_5	V_6
TH94-OBS5	-63.62	102.0	1.36	1.78	0.43	2.0	0.66	2.57	0.55	2.81	0.41	3.75	0.66	4.37
(cont.)					0.8	5.85								
TH98-OBS1	-65.495	85.961	2.1	1.5	0.35	2.34	3.83	4.54						
TH98-OBS3	-64.827	85.994	3.46	1.63	0.54	2.55	1.94	4.64	1.93	5.65				
R2E37	-65.083333	143.783333	2.87	2.5	1.72	3.75	0.89	4.36						
R3E37	-65.366666	142.783333	2.7	2.5	2.08									
R5E37	-62.716667	126.9	4.23	1.82	0.7	1.95	0.41	3.37	1.69	4.2	1.27			
R6E37	-61.65	126.716667	4.43	1.82	0.4	2.14	0.83	2.46	0.41	4.18	1.15			
R7E37	-60.633333	126.316667	4.54	1.64	0.36	2.05	0.39	3.41	1.08					
R8E37	-59.166667	125.883333	4.62	1.87	0.68	1.9	0.36	2.5	0.37					
R2E41	-62.7	132.016667	4.45	2.19	0.64									
R7E44	-58.016667	128.833333	4.71	2.5	1.76	3.24								
R8E44	-58.016667	126.35	4.69	1.64	0.65	2.5	0.37	5.51	2	6.85				
R9E44	-59.033333	122.383333	4.65	2.37	1.17	5.4								
R2E45	-60.733333	113.85	4.44	2.19	0.56	2.84	0.37							
R2E50	-60.766667	107.2	4.39	2.86	0.92									
R3E50	-63.016667	132.1	4.19	1.86	0.78	2.99	1.12	3.47	0.89					
R4E50	-64.35	144.016667	3.54	1.96	1.13	3.06	0.51	2.85	0.51					

Station	*Latitude*	*Longitude*	*WD*	V_1	T_1	V_2	T_2	V_3	T_3	V_4	T_4	V_5	T_5	V_6
R5E50	-63.916667	144.65	3.8	1.64	0.41	1.89	0.44	2.79	0.95	3.46	0.99			
R13E53	-61.416667	140.066667	4.37	1.74	0.36	2.51	0.43	3.56	0.8	5.68				
R14E53	-61.633333	140.016667	4.32	1.49	0.4	2.74	1.14	3.02	2.22	6.59				
R17E53	-62.033333	139.9	4.24	1.5	0.46	3.25	1.48	4.87						
R20E53	-62.066667	138.266667	4.0	1.86	0.73	1.98	0.48	3.65	3.55	6.22				
R21E53	-61.9	138.066667	4.15	1.67	0.37	2.85	0.66	3.45	1.46					
R23E53	-61.45	137.716667	4.57	1.94	1.08	3.45	1.44	3.85	0.82					
R24E53	-61.3	137.633333	4.38	1.95	0.65	3.26	1.72							
R25E53	-61.9	141.05	4.23	1.65	0.41	3.06	0.62	4.0	0.95					
R26E53	-61.816667	141.383333	4.29	1.7	0.52	2.35	0.74							

APPENDIX 5: SONOBUOY SOLUTIONS, SURVEYS 228 & 229

Columns are as follows:

VEL ($km.s^{-1}$)	Layer velocity in $km.s^{-1}$
BASE (km)	Depth of base of layer in km
THICK (km)	Thickness of layer in km
THICK (TWT)	Thickness of layer in seconds of two-way time
BASE (TWT)	Depth of base of layer in seconds of two-way time

Velocities in parentheses are assumed.
Depths preceded by a tilde are approximate; this is usually because the velocity boundary has significant relief.

228/SB02 Line 228/06 Start SP 1770
Lat/long = –65.391389 65.253056

VEL ($km.s^{-1}$)	***BASE (km)***	***THICK (km)***	***THICK (TWT)***	***Base (TWT)***
1.50	2.74	2.74	3.65	3.65
1.78	3.48	0.74	0.83	4.49
2.37	3.78	0.30	0.25	4.74
2.76	4.12	0.35	0.25	4.99
3.55	4.42	0.30	0.17	5.15
4.24	9.65	5.23	2.47	7.62
6.12	9.65			7.62

228/SB05 Line 228/08 Start SP 6660
Lat/long = –62.197778 70.549722

VEL ($km.s^{-1}$)	***BASE (km)***	***THICK (km)***	***THICK (TWT)***	***Base (TWT)***
1.50	4.12	4.12	5.49	5.49
1.86-2.45	4.46	0.34	0.37	5.86
2.55	5.74	1.27	1.00	6.86
3.14	6.23	0.49	0.31	7.17
5.39	8.29	2.06	0.76	7.94
6.76	8.29			7.94

228/SB08 Line 228/12 Start SP 6610
Lat/long = –60.702500 93.933056

VEL (km.s^{-1})	***BASE (km)***	***THICK (km)***	***THICK (TWT)***	***Base (TWT)***
1.50	4.36	4.36	5.81	5.81
1.92	5.17	0.81	0.84	6.65
1.97	5.47	0.30	0.30	6.95
2.57	5.84	0.38	0.29	7.25
3.65	6.83	0.99	0.54	7.79
(3.95)	6.83			7.79

228/SB11 Line 228/24 Start SP 930
Lat/long = –63.950000 128.281944

VEL (km.s^{-1})	***BASE (km)***	***THICK (km)***	***THICK (TWT)***	***Base (TWT)***
1.50	3.79	3.79	5.05	5.05
1.73	4.38	0.59	0.69	5.74
2.37	4.88	0.49	0.42	6.16
2.57	6.21	1.33	1.04	7.19
3.36	6.21			7.19

228/SB15 Line 228/24 Start SP 5760
Lat/long = –61.830000 127.600000

VEL (km.s^{-1})	***BASE (km)***	***THICK (km)***	***THICK (TWT)***	***Base (TWT)***
1.50	4.41	4.41	5.88	5.88
1.69	4.71	0.30	0.35	6.23
1.99	5.11	0.40	0.40	6.63
2.43	6.10	0.99	0.82	7.45
3.43	6.60	0.50	0.29	7.74
5.17	9.28	2.68	1.04	8.78
6.66	9.28			8.78

228/SB16 Line 228/25 Start SP 4480
Lat/long = –62.921111 129.340000

VEL (km.s^{-1})	***BASE (km)***	***THICK (km)***	***THICK (TWT)***	***Base (TWT)***
1.50	4.37	4.37	5.83	5.83
1.78	4.86	0.49	0.56	6.38
1.83	5.11	0.25	0.27	6.65
2.37	5.46	0.35	0.29	6.94
2.96	6.05	0.59	0.40	7.34
4.05	7.92	1.88	0.93	8.27
5.43	12.56	4.64	1.71	9.98
7.89	12.56			9.98

228/SB17 Line 228/26 Start SP 190
Lat/long = –63.875000 131.847500

VEL (km.s^{-1})	***BASE (km)***	***THICK (km)***	***THICK (TWT)***	***Base (TWT)***
1.50	3.53	3.53	4.71	4.71
1.76-1.86	4.02	0.49	0.56	5.26
2.16-3.82	5.10	1.08	1.00	6.26
4.12-6.47	8.43	3.33	1.62	7.88
6.86	16.37	7.94	2.31	10.20
7.84	16.37			10.20

228/SB18 Line 228/26 Start SP 5350
Lat/long = –61.630556 130.966111

VEL (km.s^{-1})	***BASE (km)***	***THICK (km)***	***THICK (TWT)***	***Base (TWT)***
1.50	4.57	4.57	6.09	6.09
1.72	4.93	0.36	0.42	6.52
2.21	5.32	0.39	0.36	6.87
2.35	5.91	0.59	0.50	7.37
3.33	6.89	0.98	0.59	7.96
5.39	8.12	1.23	0.45	8.41
6.57	8.12			8.41

228/SB20 Line 228/27 Start SP 830
Lat/long = –60.818056 132.650278

VEL (km.s^{-1})	***BASE (km)***	***THICK (km)***	***THICK (TWT)***	***Base (TWT)***
1.50	4.62	4.62	6.16	6.16
1.85	5.01	0.39	0.42	6.58
2.24	5.20	0.19	0.17	6.75
3.12	6.42	1.22	0.78	7.54
3.90	7.35	0.93	0.48	8.01
(5.36)	9.98	2.63	0.98	8.99
6.72	12.22	2.24	0.67	9.66
8.18	12.22			9.66

228/SB21 Line 228/28 Start SP 2930
Lat/long = –62.867222 134.333333

VEL (km.s^{-1})	***BASE (km)***	***THICK (km)***	***THICK (TWT)***	***Base (TWT)***
1.50	4.25	4.25	5.67	5.67
1.78	4.74	0.49	0.56	6.22
2.02	4.94	0.20	0.20	6.42
2.42-2.96	5.30	0.36	0.29	6.71
3.16-3.65	6.42	1.13	0.71	7.42
5.43	9.88	3.45	1.27	8.70
6.51	14.81	4.93	1.52	10.21
8.19	14.81			10.21

228/SB22 Line 228/28 Start SP 7700
Lat/long = –60.727222 134.333333

VEL (km.s^{-1})	***BASE (km)***	***THICK (km)***	***THICK (km)(TWT)***	***Base (TWT)***
1.50	4.59	4.59	6.12	6.12
1.78	4.92	0.33	0.37	6.49
2.07	5.21	0.30	0.29	6.77
2.76	5.71	0.49	0.36	7.13
2.96	6.10	0.39	0.27	7.40
3.75	6.99	0.89	0.47	7.87
4.93	7.88	0.89	0.36	8.23
5.72	7.88			8.23

228/SB23 Line 228/29 Start SP 1740
Lat/long = –60.906111 136.000000

VEL (km.s^{-1})	***BASE (km)***	***Tick.***	***THICK (TWT)***	***Base (TWT)***
1.50	4.51	4.51	6.01	6.01
1.76	5.05	0.54	0.61	6.62
2.16	5.74	0.69	0.64	7.26
3.53	6.42	0.69	0.39	7.65
4.90	7.79	1.37	0.56	8.21
6.57	10.93	3.14	0.96	9.16
8.14	10.93			9.16

228/SB24 Line 228/29 Start SP 3720
Lat/long = –61.793056 136.000000

VEL (km.s^{-1})	***BASE (km)***	***THICK (km)***	***THICK (TWT)***	***Base (TWT)***
1.50	4.38	4.38	5.84	5.84
1.83	4.77	0.39	0.43	6.27
2.27	5.42	0.64	0.57	6.84
2.96	6.06	0.64	0.43	7.27
3.95	7.54	1.48	0.75	8.02
4.44	8.72	1.18	0.53	8.55
5.53	8.72			8.55

228/SB25 Line 228/30 Start SP 280
Lat/long = –64.481111 145.450000

VEL (km.s^{-1})	***BASE (km)***	***THICK (km)***	***THICK (TWT)***	***Base (TWT)***
1.50	3.61	3.61	4.81	4.81
1.91	4.25	0.64	0.67	5.48
2.35	4.98	0.74	0.63	6.11
3.04	5.77	0.78	0.52	6.62
3.73	7.34	1.57	0.84	7.46
4.41	9.59	2.25	1.02	8.49
6.08	9.59			8.49

228/SB26 Line 228/30 Start SP 2950
Lat/long = –63.283056 145.450278

VEL (km.s^{-1})	***BASE (km)***	***THICK (km)***	***THICK (TWT)***	***Base (TWT)***
1.50	3.94	3.94	5.25	5.25
1.92	4.56	0.62	0.65	5.90
2.66	4.96	0.39	0.30	6.20
3.40	5.94	0.99	0.58	6.78
5.53	8.90	2.96	1.07	7.85
7.11	8.90			7.85

228/SB28 Line 228/31 Start SP 1590
Lat/long = –63.496389 147.310000

VEL (km.s^{-1})	***BASE (km)***	***THICK (km)***	***THICK (TWT)***	***Base (TWT)***
1.50	3.88	3.88	5.17	5.17
1.81	4.27	0.39	0.43	5.61
1.96	4.57	0.29	0.30	5.91
2.16	4.76	0.20	0.18	6.09
2.84	5.11	0.34	0.24	6.33
3.63	5.94	0.83	0.46	6.79
4.90	8.49	2.55	1.04	7.83
5.98	8.49			7.83

228/SB30 Line 228/31 Start SP 2980
Lat/long = –64.108889 147.099722

VEL (km.s^{-1})	***BASE (km)***	***THICK (km)***	***THICK (TWT)***	***Base (TWT)***
1.50	3.77	3.77	5.03	5.03
1.85	4.16	0.39	0.42	5.45
2.14-3.41	4.65	0.49	0.45	5.90
3.90-4.09	5.91	1.27	0.65	6.55
5.84	9.91	3.99	1.37	7.92
6.33	9.91			7.92

229/SB02 Line 229/01 Start SP 320
Lat/long = –64.700000 152.350000

VEL (km.s^{-1})	***BASE (km)***	***THICK (km)***	***THICK (TWT)***	***Base (TWT)***
1.50	3.54	3.54	4.72	4.72
2.13	4.12	0.58	0.55	5.27
2.32	~4.47	0.35	0.30	~5.57
2.42	~4.66	0.19	0.16	~5.73
3.44	~5.82	1.16	0.68	~6.40
5.42	~5.82			~6.40

229/SB03 Line 229/02 Start SP 1440
Lat/long = –64.642800 151.890800

VEL (km.s^{-1})	***BASE (km)***	***THICK (km)***	***THICK (TWT)***	***Base (TWT)***
1.50	3.41	3.41	4.55	4.55
1.78	3.84	0.43	0.49	5.04
2.07	4.20	0.36	0.34	5.38
2.27	4.48	0.28	0.24	5.62
3.36	5.34	0.87	0.52	6.14
3.95	~5.87	0.52	0.27	~6.40
5.43	7.31	1.44	0.53	6.94
6.91	10.21	2.90	0.84	7.78
7.60	10.21			7.78

229/SB04 Line 229/03 Start SP 770
Lat/long = –64.050000 150.800000

VEL (km.s^{-1})	***BASE (km)***	***THICK (km)***	***THICK (TWT)***	***Base (TWT)***
1.50	3.60	3.60	4.80	4.80
1.79	3.94	0.34	0.38	5.18
1.84	4.23	0.29	0.31	5.49
2.19	4.29	0.06	0.05	5.55
2.78	~4.96	0.68	0.49	~6.03
(4.97)	5.90	0.94	0.38	6.41
6.26	8.96	3.06	0.98	7.39
7.95	8.96			7.39

229/SB05 Line 229/04 Start SP 450
Lat/long = –63.708200 143.769500

VEL (km.s^{-1})	***BASE (km)***	***THICK (km)***	***THICK (TWT)***	***Base (TWT)***
1.50	3.95	3.95	5.27	5.27
1.75	4.40	0.45	0.51	5.78
1.85	4.55	0.16	0.17	5.95
2.34	4.97	0.42	0.36	6.30
2.53	5.61	0.63	0.50	6.80
2.92	~6.68	1.07	0.73	~7.54
3.31	~7.89	1.22	0.74	~8.27
6.04	11.30	3.41	1.13	9.40
8.77	11.30			9.40

229/SB06 Line 229/04 Start SP 1260
Lat/long = –63.333300 143.383300

VEL (km.s^{-1})	***BASE (km)***	***THICK (km)***	***THICK (TWT)***	***Base (TWT)***
1.50	4.06	4.06	5.41	5.41
1.75	4.43	0.37	0.42	5.84
1.85	4.52	0.09	0.09	5.93
2.24	5.11	0.59	0.53	6.46
3.17	6.05	0.94	0.59	7.05
3.27	~6.92	0.88	0.54	~7.59
4.38	8.97	2.05	0.93	8.52
6.43	8.97			8.52

229/SB07 Line 229/04 Start SP 2610
Lat/long = –62.733300 143.533300

VEL (km.s^{-1})	***BASE (km)***	***THICK (km)***	***THICK (TWT)***	***Base (TWT)***
1.50	4.16	4.16	5.55	5.55
1.79	4.49	0.33	0.37	5.91
1.84	4.74	0.25	0.27	6.18
2.19	5.09	0.36	0.33	6.51
3.18	5.49	0.40	0.25	6.76
3.97	6.09	0.60	0.30	7.06
5.86	7.38	1.29	0.44	7.50
7.35	13.68	6.30	1.71	9.22
8.94	13.68			9.22

229/SB08 Line 229/05 Start SP 330
Lat/long = –61.866700 142.000000

VEL (km.s^{-1})	***BASE (km)***	***THICK (km)***	***THICK (TWT)***	***Base (TWT)***
1.50	4.34	4.34	5.79	5.79
1.76	4.79	0.45	0.51	6.30
1.96	5.04	0.25	0.25	6.55
2.45	5.15	0.12	0.10	6.64
2.79	~5.77	0.62	0.44	~7.09
3.19	6.22	0.45	0.28	7.37
5.20	~7.93	1.71	0.66	~8.03
6.86	~7.93			~8.03

229/SB09 Line 229/05 Start SP 3110
Lat/long = –63.116700 142.000000

VEL (km.s^{-1})	***BASE (km)***	***THICK (km)***	***THICK (TWT)***	***Base (TWT)***
1.50	3.92	3.92	5.23	5.23
1.78	4.56	0.64	0.72	5.95
1.88	4.81	0.25	0.26	6.21
2.32	~6.17	1.36	1.17	~7.39
3.36	~7.16	0.99	0.59	~7.97
5.13	8.24	1.09	0.42	8.40
5.92	~10.02	1.78	0.60	~9.00
7.40	~10.02			~9.00

229/SB10 Line 229/06 Start SP 1260
Lat/long = –63.883300 137.466700

VEL (km.s^{-1})	***BASE (km)***	***THICK (km)***	***THICK (TWT)***	***Base (TWT)***
1.50	3.50	3.50	4.67	4.67
1.85	3.80	0.30	0.32	4.99
2.00	4.57	0.77	0.77	5.76
2.70	5.60	1.03	0.76	6.52
3.50	6.50	0.90	0.51	7.04
4.00	9.40	2.90	1.45	8.49
6.30	9.40			8.49

229/SB11 Line 229/06 Start SP 3330
Lat/long = –62.983300 138.500000

VEL (km.s^{-1})	***BASE (km)***	***THICK (km)***	***THICK (TWT)***	***Base (TWT)***
1.50	3.80	3.80	5.07	5.07
1.76	4.06	0.26	0.30	5.37
1.96	4.44	0.37	0.38	5.75
2.11	4.64	0.21	0.20	5.94
2.47	5.07	0.43	0.35	6.29
2.89	5.92	0.84	0.58	6.87
3.77-4.12	~6.55	0.63	0.33	~7.21
5.10	10.07	3.53	1.53	8.74
5.39	10.07			8.74

229/SB12 Line 229/06 Start SP 5680
Lat/long = –61.966700 139.050000

VEL (km.s^{-1})	***BASE (km)***	***THICK (km)***	***THICK (TWT)***	***Base (TWT)***
1.50	4.30	4.30	5.73	5.73
1.85	4.79	0.49	0.53	6.26
2.06	5.08	0.29	0.28	6.54
2.48	5.61	0.54	0.43	6.97
3.31	6.15	0.54	0.32	7.30
3.60	8.49	2.34	1.30	8.59
4.09	9.66	1.17	0.57	9.17
6.82	9.66			9.17

229/SB13 Line 229/07 Start SP 4370
Lat/long = –62.216700 137.416700

VEL (km.s^{-1})	***BASE (km)***	***THICK (km)***	***THICK (TWT)***	***Base (TWT)***
1.50	4.20	4.20	5.60	5.60
1.86	4.59	0.39	0.42	6.02
2.01	4.98	0.39	0.39	6.41
2.30	5.77	0.78	0.68	7.09
3.28	5.99	0.23	0.14	7.23
3.58	7.83	1.83	1.02	8.25
4.07	8.61	0.78	0.39	8.64
5.59	11.55	2.94	1.05	9.69
6.57	11.55			9.69

229/SB15 Line 229/07 Start SP 6250
Lat/long = –62.966700 136.833300

VEL (km.s-1)	***BASE (km)***	***THICK (km)***	***THICK (TWT)***	***Base (TWT)***
1.50	3.97	3.97	5.29	5.29
1.88	4.42	0.45	0.48	5.78
2.09	4.89	0.46	0.44	6.22
2.71-3.95	~6.37	1.48	1.09	~7.31
5.13	~11.89	5.53	2.43	~9.75
5.63	~11.89			~9.75

229/SB16 Line 229/08 Start SP 390
Lat/long = –62.983300 124.066700

VEL ($km.s^{-1}$)	***BASE (km)***	***THICK (km)***	***THICK (TWT)***	***Base (TWT)***
1.50	4.10	4.10	5.47	5.47
1.78	4.58	0.48	0.54	6.00
2.04	4.72	0.14	0.14	6.14
2.28	5.37	0.66	0.57	6.71
2.78	5.54	0.17	0.12	6.83
3.33	~6.52	0.98	0.59	~7.43
3.63	~7.03	0.51	0.28	~7.71
4.37	~8.17	1.14	0.52	~8.23
(4.97)	10.92	2.75	1.11	9.34
6.26	10.92			9.34

229/SB17 Line 229/08 Start SP 3220
Lat/long = –61.950000 122.550000

VEL ($km.s^{-1}$)	***BASE (km)***	***THICK (km)***	***THICK (TWT)***	***Base (TWT)***
1.50	4.25	4.25	5.67	5.67
1.79	4.65	0.40	0.44	6.11
2.04	4.90	0.25	0.24	6.36
2.48	5.29	0.40	0.32	6.68
2.58	5.99	0.70	0.54	7.21
2.98	6.49	0.50	0.33	7.55
4.07	~7.48	0.99	0.49	~8.03
(4.47)	~9.56	2.09	0.93	~8.97
6.75	~9.56			~8.97

229/SB18 Line 229/09 Start SP 580
Lat/long = –60.900000 124.233300

VEL (km.s^{-1})	***BASE (km)***	***THICK (km)***	***THICK (TWT)***	***Base (TWT)***
1.50	4.45	4.45	5.93	5.93
1.68	4.87	0.42	0.51	6.44
2.37	5.09	0.22	0.18	6.62
2.47	5.49	0.39	0.32	6.94
2.66	5.95	0.46	0.35	7.29
3.38	~6.92	0.97	0.57	~7.86
(4.93)	7.35	0.43	0.18	8.04
6.12	7.35			8.04

229/SB19 Line 229/10 Start SP 560
Lat/long = –61.666700 120.866700

VEL (km.s-1)	***BASE (km)***	***THICK (km)***	***THICK (TWT)***	***Base (TWT)***
1.50	4.24	4.24	5.65	5.65
1.69	4.62	0.38	0.45	6.10
2.04	5.03	0.42	0.41	6.51
2.48	5.59	0.56	0.45	6.96
2.83	6.17	0.58	0.41	7.37
3.73	~7.38	1.21	0.65	~8.02
(4.47)	8.97	1.59	0.71	8.73
6.56	8.97			8.73

229/SB21 Line 229/11 Start SP 3860
Lat/long = –62.283300 118.633300

VEL (km.s^{-1})	***BASE (km)***	***THICK (km)***	***THICK (TWT)***	***Base (TWT)***
1.50	4.27	4.27	5.69	5.69
1.66	4.53	0.26	0.32	6.01
1.82	5.00	0.47	0.51	6.52
2.92	6.39	1.39	0.95	7.48

229/SB22 Line 229/12 Start SP 620
Lat/long = –62.716700 117.183300

VEL (km.s^{-1})	***BASE (km)***	***THICK (km)***	***THICK (TWT)***	***Base (TWT)***
1.50	3.90	3.90	5.20	5.20
1.70	4.24	0.34	0.40	5.60
1.90	4.58	0.34	0.36	5.96
2.45	5.20	0.62	0.51	6.46
3.15	5.48	0.28	0.18	6.64
3.90	6.82	1.34	0.69	7.33
4.60	7.15	0.33	0.14	7.47
5.50	7.15			7.47

229/SB23 Line 229/12 Start SP 2410
Lat/long = –62.066700 116.200000

VEL (km.s^{-1})	***BASE (km)***	***THICK (km)***	***THICK (TWT)***	***Base (TWT)***
1.50	4.30	4.30	5.73	5.73
1.67	4.79	0.49	0.59	6.32
1.96	5.04	0.25	0.25	6.57
2.55	5.36	0.32	0.25	6.83
3.28	6.05	0.69	0.42	7.24
3.63	6.31	0.26	0.15	7.39
3.82	7.07	0.76	0.40	7.79
4.02	~7.80	0.73	0.36	~8.15

229/SB25 Line 229/13 Start SP 3180
Lat/long = –61.433300 112.450000

VEL (km.s^{-1})	***BASE (km)***	***THICK (km)***	***THICK (TWT)***	***Base (TWT)***
1.50	4.24	4.24	5.65	5.65
1.90	4.60	0.36	0.38	6.03
1.95-2.10	4.85	0.25	0.26	6.29
2.30	5.06	0.21	0.19	6.48
2.60	5.78	0.72	0.55	7.03
3.78	~7.07	1.29	0.68	~7.72
5.20	8.76	1.69	0.65	8.37
6.40	8.76			8.37

229/SB26 Line 229/14 Start SP 150
Lat/long = –61.433300 110.766700

VEL (km.s^{-1})	***BASE (km)***	***THICK (km)***	***THICK (TWT)***	***Base (TWT)***
1.50	4.19	4.19	5.59	5.59
1.68-1.88	4.38	0.19	0.21	5.80
1.88	4.58	0.21	0.22	6.02
2.37	5.32	0.74	0.63	6.64
2.42	~5.58	0.26	0.21	~6.85
(3.16)	5.96	0.38	0.24	7.09
4.93	7.53	1.57	0.64	7.73
5.92	8.50	0.98	0.33	8.06
7.11	8.50			8.06

229/SB27 Line 229/15 Start SP 820
Lat/long = –61.216700 109.083300

VEL (km.s^{-1})	***BASE (km)***	***THICK (km)***	***THICK (TWT)***	***Base (TWT)***
1.50	4.25	4.25	5.67	5.67
1.90	4.72	0.47	0.49	6.16
2.00	~5.08	0.36	0.36	~6.52
2.55	~5.43	0.35	0.27	~6.80
3.00	~5.97	0.54	0.36	~7.16
(5.00)	6.86	0.89	0.36	7.51
6.30	6.86			7.51

229/SB28 Line 229/15 Start SP 4270
Lat/long = –62.500000 108.050000

VEL (km.s^{-1})	***BASE (km)***	***THICK (km)***	***THICK (TWT)***	***Base (TWT)***
1.50	3.99	3.99	5.32	5.32
1.81-1.96	4.70	0.71	0.75	6.07
2.45	5.06	0.36	0.33	6.40
2.75	5.41	0.35	0.26	6.66
3.43	~6.94	1.53	0.89	~7.55
(3.92)	7.75	0.81	0.42	7.96
5.00	7.75			7.96

229/SB29 Line 229/16 Start SP 360
Lat/long = –61.250000 107.400000

VEL (km.s^{-1})	***BASE (km)***	***THICK (km)***	***THICK (TWT)***	***Base (TWT)***
1.50	4.44	4.44	5.92	5.92
1.88	4.82	0.38	0.40	6.32
1.97	5.01	0.20	0.20	6.52
2.17	5.19	0.18	0.16	6.68
3.36	~5.98	0.79	0.47	~7.15
5.23	8.20	2.22	0.85	8.00
7.65	8.20			8.00

229/SB30 Line 229/17 Start SP 750
Lat/long = –61.283300 105.716700

VEL (km.s^{-1})	***BASE (km)***	***THICK (km)***	***THICK (TWT)***	***Base (TWT)***
1.50	4.41	4.41	5.88	5.88
1.88	4.96	0.55	0.58	6.46
1.99	~5.55	0.60	0.60	~7.06
4.57	~5.55			~7.06

229/SB31 Line 229/17 Start SP 2430
Lat/long = –61.933300 105.283300

VEL (km.s^{-1})	***BASE (km)***	***THICK (km)***	***THICK (TWT)***	***Base (TWT)***
1.50	4.36	4.36	5.81	5.81
1.79	4.74	0.38	0.42	6.24
1.95	~5.00	0.26	0.27	~6.50
2.43	~5.55	0.56	0.46	~6.96
3.43	~6.19	0.64	0.37	~7.33
6.26	~8.96	2.77	0.89	~8.21
7.95	~8.96			~8.21

229/SB32 Line 229/18 Start SP 210
Lat/long = -61.283300 104.016700

VEL (km.s^{-1})	***BASE (km)***	***THICK (km)***	***THICK (TWT)***	***Base (TWT)***
1.50	4.42	4.42	5.89	5.89
1.80	~4.82	0.40	0.44	~6.34
3.40	~5.33	0.51	0.30	~6.64
(5.00)	7.45	2.12	0.85	7.49
6.80	9.46	2.01	0.59	8.08
7.10	9.46			8.08

229/SB33 Line 229/19 Start SP 500
Lat/long = –60.876000 102.378600

VEL (km.s^{-1})	***BASE (km)***	***THICK (km)***	***THICK (TWT)***	***Base (TWT)***
1.50	4.45	4.45	5.93	5.93
1.72	4.71	0.26	0.31	6.24
1.77	5.00	0.28	0.32	6.56
2.13	5.19	0.19	0.18	6.74
2.84	5.77	0.58	0.41	7.15
3.45	6.36	0.59	0.34	7.49
4.86	8.50	2.15	0.88	8.37
5.88	11.19	2.69	0.91	9.29
8.51	11.19			9.29

229/SB34 Line 229/19 Start SP 1680
Lat/long = –61.399000 102.341000

VEL (km.s^{-1})	***BASE (km)***	***THICK (km)***	***THICK (TWT)***	***Base (TWT)***
1.50	4.55	4.55	6.07	6.07
1.63	4.84	0.29	0.35	6.42
1.68	~4.97	0.14	0.16	~6.58
2.27	~5.49	0.51	0.45	~7.04
4.24	~6.67	1.18	0.56	~7.59
4.93	7.26	0.59	0.24	7.83
6.22	12.69	5.43	1.75	9.58
7.99	12.69			9.58

229/SB35 Line 229/19 Start SP 3040
Lat/long = –62.003000 102.248000

VEL (km.s^{-1})	***BASE (km)***	***THICK (km)***	***THICK (TWT)***	***Base (TWT)***
1.50	4.48	4.48	5.97	5.97
1.88	4.96	0.48	0.52	6.49
1.97	~5.13	0.17	0.17	~6.66
2.30	~5.78	0.65	0.57	~7.23
3.45	~6.57	0.79	0.46	~7.68
5.92	~6.57			~7.68

229/SB36 Line 229/19 Start SP 4350
Lat/long = –62.584000 102.023000

VEL (km.s-1)	*BASE (km)*	*THICK (km)*	*THICK (TWT)*	*Base (TWT)*
1.50	4.46	4.46	5.95	5.95
1.79	4.80	0.34	0.38	6.32
1.89	5.14	0.34	0.36	6.68
2.28	5.59	0.46	0.40	7.08
2.33	6.34	0.75	0.64	7.72

229/SB37 Line 229/20 Start SP 600
Lat/long = –61.916700 97.850000

VEL ($km.s^{-1}$)	*BASE (km)*	*THICK (km)*	*THICK (TWT)*	*Base (TWT)*
1.50	4.10	4.10	5.47	5.47
1.73	4.36	0.26	0.29	5.76
1.89	4.49	0.13	0.14	5.90
2.04	4.78	0.30	0.29	6.19
2.65	5.78	1.00	0.75	6.95
2.86	6.67	0.89	0.62	7.57
3.37	~7.26	0.59	0.35	~7.92
(5.10)	8.49	1.22	0.48	8.40
7.14	8.49			8.40

229/SB38 Line 229/20 Start SP 4030
Lat/long = –60.583300 98.983300

VEL ($km.s^{-1}$)	*BASE (km)*	*THICK (km)*	*THICK (TWT)*	*Base (TWT)*
1.50	4.53	4.53	6.04	6.04
1.69	5.20	0.67	0.79	6.83
2.78	~5.49	0.30	0.21	~7.04
3.16	~5.89	0.40	0.25	~7.29
3.38	~6.49	0.60	0.35	~7.65
(4.97)	~7.78	1.29	0.52	~8.17
(6.66)	12.94	5.17	1.55	9.72
8.15	12.94			9.72

229/SB39 Line 229/21 Start SP 390
Lat/long = –60.133300 95.600000

VEL (km.s^{-1})	***BASE (km)***	***THICK (km)***	***THICK (TWT)***	***Base (TWT)***
1.50	4.60	4.60	6.13	6.13
1.95	5.34	0.74	0.76	6.89
2.19	5.71	0.37	0.34	7.23
2.63	6.06	0.35	0.27	7.50
3.70	~6.84	0.78	0.42	~7.92
4.87	~8.59	1.75	0.72	~8.64
6.33	~8.59			~8.64

229/SB40 Line 229/21 Start SP 2890
Lat/long = –61.250000 95.616700

VEL (km.s^{-1})	***BASE (km)***	***THICK (km)***	***THICK (TWT)***	***Base (TWT)***
1.50	4.24	4.24	5.65	5.65
1.78	4.79	0.55	0.62	6.28
1.92	4.94	0.15	0.15	6.43
2.32	5.48	0.54	0.47	6.90
3.11	5.84	0.36	0.23	7.13
3.26	6.73	0.89	0.55	7.67
4.24	~8.15	1.42	0.67	~8.34
4.64	~9.23	1.09	0.47	~8.81
6.61	~9.23			~8.81

229/SB41 Line 229/21 Start SP 4750
Lat/long = –62.066700 95.800000

VEL (km.s^{-1})	***BASE (km)***	***THICK (km)***	***THICK (TWT)***	***Base (TWT)***
1.50	3.93	3.93	5.24	5.24
1.90	4.36	0.43	0.45	5.69
2.00	4.60	0.24	0.24	5.93
2.50	5.05	0.45	0.36	6.29
2.90	6.50	1.45	1.00	7.29
3.10	~6.95	0.45	0.29	~7.58
6.50	~6.95			~7.58

229/SB42 Line 229/21 Start SP 6230
Lat/long = –62.650000 96.350000

VEL (km.s^{-1})	***BASE (km)***	***THICK (km)***	***THICK (TWT)***	***Base (TWT)***
1.50	3.70	3.70	4.93	4.93
1.90	4.00	0.30	0.32	5.25
2.00	4.40	0.40	0.40	5.65
2.35	4.70	0.30	0.26	5.90
3.00	~5.50	0.80	0.53	~6.44
(5.00)	6.80	1.30	0.52	6.96
6.40	6.80			6.96

229/SB43 Line 229/22 Start SP 240
Lat/long = –62.450000 93.900000

VEL (km.s^{-1})	***BASE (km)***	***THICK (km)***	***THICK (TWT)***	***Base (TWT)***
1.50	3.88	3.88	5.17	5.17
1.74	4.22	0.34	0.39	5.56
2.09	4.66	0.45	0.43	5.99
2.38	5.29	0.63	0.53	6.52
2.88	5.42	0.13	0.09	6.61
3.23	6.83	1.41	0.87	7.48
3.92	8.37	1.54	0.78	8.26
5.66	8.37			8.26

229/SB44 Line 229/22 Start SP 2700
Lat/long = –61.566700 92.483300

VEL (km.s^{-1})	***BASE (km)***	***THICK (km)***	***THICK (TWT)***	***Base (TWT)***
1.50	4.25	4.25	5.67	5.67
1.69	4.47	0.22	0.26	5.93
1.89	5.14	0.68	0.72	6.64
2.43	5.41	0.27	0.22	6.86
2.85	6.37	0.95	0.67	7.53
3.40	7.26	0.89	0.53	8.06
4.97	8.70	1.44	0.58	8.64
6.75	13.44	4.74	1.40	10.04
8.54	13.44			10.04

229/SB45 Line 229/22 Start SP 4850
Lat/long = –60.783300 91.316700

VEL (km.s^{-1})	***BASE (km)***	***THICK (km)***	***THICK (TWT)***	***Base (TWT)***
1.50	4.52	4.52	6.03	6.03
1.76	4.89	0.37	0.42	6.45
1.91	5.42	0.53	0.55	7.00
2.70	~6.27	0.84	0.63	~7.63
3.14	~6.76	0.49	0.31	~7.94
5.49	8.62	1.86	0.68	8.62
7.06	13.85	5.24	1.48	10.10
7.65	13.85			10.10

229/SB46 Line 229/23 Start SP 390
Lat/long = –60.366700 92.800000

VEL (km.s^{-1})	***BASE (km)***	***THICK (km)***	***THICK (TWT)***	***Base (TWT)***
1.50	4.37	4.37	5.83	5.83
1.73	4.65	0.28	0.32	6.15
1.83	5.04	0.39	0.43	6.58
2.49	5.98	0.94	0.75	7.33
3.36	6.16	0.18	0.11	7.44
3.60	~7.21	1.06	0.59	~8.03
(4.93)	8.84	1.63	0.66	(8.69)
(6.71)	~13.38	4.54	1.35	~10.04
7.89	~13.38			~10.04

229/SB47 Line 229/23 Start SP 1850
Lat/long = –61.016700 92.850000

VEL (km.s^{-1})	***BASE (km)***	***THICK (km)***	***THICK (TWT)***	***Base (TWT)***
1.50	4.40	4.40	5.87	5.87
1.73	4.69	0.29	0.34	6.21
1.96	5.08	0.38	0.39	6.60
2.35	5.57	0.49	0.42	7.01
2.55	6.28	0.72	0.56	7.58
3.63	~8.17	1.89	1.04	~8.62
3.87	8.94	0.76	0.39	9.01
6.67	13.52	4.58	1.37	10.39
8.33	13.52			10.39

229/SB48 Line 229/24 Start SP 2660
Lat/long = –61.483300 90.516700

VEL (km.s^{-1})	*BASE (km)*	*THICK (km)*	*THICK (TWT)*	*Base (TWT)*
1.50	4.20	4.20	5.60	5.60
1.73	4.92	0.72	0.83	6.43
2.66	~6.71	1.79	1.34	~7.78
5.53	~6.80	0.09	0.03	~7.81
6.51	10.17	3.38	1.04	8.84
8.39	10.17			8.84

229/SB49 Line 229/25 Start SP 1040
Lat/long = –62.166700 89.883300

VEL (km.s^{-1})	*BASE (km)*	*THICK (km)*	*THICK (TWT)*	*Base (TWT)*
1.50	4.04	4.04	5.39	5.39
1.97	4.79	0.75	0.76	6.15
2.47	5.22	0.43	0.35	6.50
2.76	6.53	1.30	0.94	7.44
3.16	~6.76	0.24	0.15	~7.59
6.51	10.81	4.05	1.24	8.83
7.60	10.81			8.83

229/SB50 Line 229/27 Start SP 570
Lat/long = –64.083300 79.650000

VEL (km.s^{-1})	*BASE (km)*	*THICK (km)*	*THICK (TWT)*	*Base (TWT)*
1.50	3.70	3.70	4.93	4.93
1.89	4.22	0.52	0.55	5.48
2.09	4.75	0.54	0.51	5.99
2.38	4.99	0.24	0.20	6.19
2.93	5.45	0.46	0.31	6.51
3.28	~6.08	0.64	0.39	~6.89
5.17	9.36	3.28	1.27	8.16
6.16	9.36			8.16

229/SB52 Line 229/28 Start SP 620
Lat/long = –63.550000 77.066700

VEL (km.s^{-1})	***BASE (km)***	***THICK (km)***	***THICK (TWT)***	***Base (TWT)***
1.50	3.83	3.83	5.11	5.11
1.85-2.09	4.26	0.43	0.46	5.57
2.24	4.84	0.58	0.54	6.11
2.53	5.12	0.27	0.22	6.32
3.02	6.24	1.12	0.74	7.07
3.31	6.72	0.49	0.29	7.36
5.36	8.67	1.95	0.73	8.09
6.82	13.54	4.87	1.43	9.52
8.28	13.54			9.52

229/SB53 Line 229/28 Start SP 2630
Lat/long = –64.450000 77.066700

VEL (km.s^{-1})	***BASE (km)***	***THICK (km)***	***THICK (TWT)***	***Base (TWT)***
1.50	3.66	3.66	4.88	4.88
1.95	4.12	0.46	0.47	5.35
2.14	4.65	0.54	0.50	5.85
2.44	5.16	0.51	0.42	6.27
2.92-3.41	6.04	0.88	0.60	6.87
3.31	7.11	1.07	0.64	7.50
3.60	8.18	1.07	0.59	8.10
6.14	12.17	3.99	1.30	9.40
7.40	12.17			9.40

229/SB54 Line 229/28 Start SP 3940
Lat/long = –65.033300 77.133300

VEL (km.s^{-1})	***BASE (km)***	***THICK (km)***	***THICK (TWT)***	***Base (TWT)***
1.50	3.60	3.60	4.80	4.80
1.75	3.84	0.24	0.28	5.08
1.85	4.18	0.34	0.37	5.45
2.03	4.53	0.34	0.34	5.78
2.82	6.04	1.51	1.07	6.85
3.56	6.88	0.85	0.48	7.33
4.43	~7.98	1.10	0.50	~7.83
(4.68)	9.78	1.79	0.77	8.59
5.11	9.78			8.59

229/SB55 Line 229/28 Start SP 5190
Lat/long = –65.583300 77.233300

VEL (km.s^{-1})	***BASE (km)***	***THICK (km)***	***THICK (TWT)***	***Base (TWT)***
1.50	3.20	3.20	4.27	4.27
1.86	3.82	0.62	0.66	4.93
1.96	4.47	0.66	0.67	5.60
2.75	4.77	0.29	0.21	5.81
3.04	5.90	1.13	0.74	6.56
4.02	~7.81	1.91	0.95	~7.51
(4.90)	9.67	1.86	0.76	8.27
5.74	9.67			8.27

229/SB56 Line 229/29 Start SP 170
Lat/long = –65.550000 75.650000

VEL (km.s^{-1})	***BASE (km)***	***THICK (km)***	***THICK (TWT)***	***Base (TWT)***
1.50	3.35	3.35	4.47	4.47
1.85-2.05	3.75	0.40	0.41	4.88
2.34	4.66	0.92	0.78	5.66
3.07	5.41	0.74	0.48	6.14
3.12	6.81	1.40	0.90	7.04
4.58	~8.56	1.75	0.77	~7.81
(5.06)	12.36	3.80	1.50	9.31
5.99	12.36			9.31

229/SB57 Line 229/29 Start SP 3210
Lat/long = –64.183300 75.650000

VEL (km.s^{-1})	***BASE (km)***	***THICK (km)***	***THICK (TWT)***	***Base (TWT)***
1.50	3.80	3.80	5.07	5.07
1.95	4.17	0.37	0.38	5.45
2.05	4.77	0.60	0.59	6.04
2.11	4.93	0.16	0.15	6.18
2.87	5.11	0.19	0.13	6.31
3.26	6.99	1.87	1.15	7.46
4.24	6.99			7.46

229/SB58 Line 229/30 Start SP 400
Lat/long = –62.400000 72.150000

VEL (km.s^{-1})	***BASE (km)***	***THICK (km)***	***THICK (TWT)***	***Base (TWT)***
1.50	4.12	4.12	5.49	5.49
1.76	4.39	0.27	0.31	5.80
2.01	4.82	0.42	0.42	6.22
2.60	5.57	0.75	0.58	6.81
2.75	5.87	0.29	0.21	7.02
3.33	6.23	0.36	0.22	7.24
3.92	6.59	0.36	0.19	7.42
(4.90)	7.92	1.33	0.54	7.97
6.27	7.92			7.97

229/SB59 Line 229/30 Start SP 2080
Lat/long = –63.166700 72.150000

VEL (km.s^{-1})	***BASE (km)***	***THICK (km)***	***THICK (TWT)***	***Base (TWT)***
1.50	4.05	4.05	5.40	5.40
1.95	4.93	0.88	0.90	6.30
2.73	5.71	0.78	0.57	6.87
3.21	6.78	1.07	0.67	7.54
3.70	7.58	0.80	0.43	7.97
(4.87)	8.02	0.45	0.18	8.15
6.53	14.23	6.20	1.90	10.06
8.38	14.23			10.06

229/SB60 Line 229/30 Start SP 4370
Lat/long = –64.183300 72.150000

VEL (km.s^{-1})	***BASE (km)***	***THICK (km)***	***THICK (TWT)***	***Base (TWT)***
1.50	3.60	3.60	4.80	4.80
1.88	4.49	0.89	0.95	5.75
2.57	4.98	0.49	0.38	6.13
3.06	5.18	0.20	0.13	6.26
3.65	5.48	0.30	0.16	6.42
4.00	7.15	1.68	0.84	7.26
4.24	~8.04	0.89	0.42	~7.68
4.84	~10.21	2.17	0.90	~8.58
6.51	~10.21			~8.58

229/SB61 Line 229/30 Start SP 6130
Lat/long = –65.016700 72.150000

VEL (km.s^{-1})	***BASE (km)***	***THICK (km)***	***THICK (TWT)***	***Base (TWT)***
1.50	3.33	3.33	4.44	4.44
1.90	4.13	0.80	0.84	5.28
2.50	4.63	0.50	0.40	5.68
3.05	5.05	0.42	0.28	5.96
3.90	7.64	2.59	1.33	7.29
4.20	7.84	0.20	0.10	7.38
4.70	~10.20	2.36	1.00	~8.39
(5.00)	11.70	1.50	0.60	8.99
5.60	11.70			8.99

229/SB62 Line 229/31 Start SP 180
Lat/long = –65.833300 72.200000

VEL (km.s^{-1})	***BASE (km)***	***THICK (km)***	***THICK (TWT)***	***Base (TWT)***
1.50	2.70	2.70	3.60	3.60
1.76	3.04	0.34	0.39	3.99
1.96	3.48	0.44	0.45	4.44
2.35	4.05	0.57	0.48	4.92
3.04	4.46	0.41	0.27	5.19
3.82	5.21	0.75	0.39	5.58
4.41	8.03	2.82	1.28	6.86
5.10	8.03			6.86

229/SB63 Line 229/31 Start SP 3180
Lat/long = –64.833300 70.050000

VEL (km.s^{-1})	***BASE (km)***	***THICK (km)***	***THICK (TWT)***	***Base (TWT)***
1.50	3.25	3.25	4.33	4.33
1.88	3.67	0.42	0.45	4.79
2.02	4.03	0.36	0.35	5.14
2.37	4.56	0.53	0.45	5.59
3.26	5.32	0.76	0.47	6.05
4.44	8.11	2.78	1.25	7.31
4.98	~9.81	1.71	0.69	~7.99
(5.23)	11.37	1.56	0.60	8.59
6.12	11.37			8.59

229/SB64 Line 229/31 Start SP 5420
Lat/long = –64.033300 68.833300

VEL (km.s^{-1})	***BASE (km)***	***THICK (km)***	***THICK (TWT)***	***Base (TWT)***
1.50	3.48	3.48	4.64	4.64
1.79	3.97	0.49	0.54	5.18
1.99	4.73	0.76	0.77	5.95
3.68	5.04	0.31	0.17	6.12
4.12	7.05	2.01	0.97	7.10
4.47	~7.64	0.60	0.27	~7.36
(4.97)	8.81	1.17	0.47	7.83
5.96	9.78	0.96	0.32	8.16
6.85	14.65	4.87	1.42	9.58
8.54	14.65			9.58

229/SB65 Line 229/31 Start SP 8340
Lat/long = –62.716700 68.850000

VEL (km.s^{-1})	***BASE (km)***	***THICK (km)***	***THICK (TWT)***	***Base (TWT)***
1.50	4.25	4.25	5.67	5.67
1.76	4.76	0.51	0.58	6.24
1.93	4.99	0.23	0.23	6.48
2.40	5.36	0.37	0.31	6.79
2.77	5.55	0.20	0.14	6.93
3.43	6.36	0.80	0.47	7.40
3.63	7.11	0.75	0.42	7.81
(4.90)	8.54	1.43	0.58	8.40
6.57	13.61	5.07	1.54	9.94
8.43	13.61			9.94

229/SB67 Line 229/32 Start SP 390
Lat/long = –62.233300 65.450000

VEL (km.s^{-1})	***BASE (km)***	***THICK (km)***	***THICK (TWT)***	***Base (TWT)***
1.50	4.48	4.48	5.97	5.97
1.76	4.94	0.46	0.52	6.50
1.91	5.38	0.44	0.46	6.96
2.94	6.51	1.13	0.77	7.72
3.43	6.84	0.33	0.19	7.92
(4.90)	7.17	0.32	0.13	8.05
6.32	7.17			8.05

229/SB68 Line 229/32 Start SP 3420
Lat/long = –63.600000 65.450000

VEL (km.s^{-1})	***BASE (km)***	***THICK (km)***	***THICK (TWT)***	***Base (TWT)***
1.50	4.16	4.16	5.55	5.55
1.75	4.55	0.39	0.44	5.99
2.05	4.98	0.43	0.42	6.41
2.19	5.37	0.39	0.36	6.77
3.41	5.66	0.29	0.17	6.94
3.75	6.83	1.17	0.62	7.56
3.90	7.29	0.46	0.23	7.80
(4.87)	9.00	1.71	0.70	8.50
7.01	~15.11	6.11	1.74	~10.24
7.99	~15.11			~10.24

229/SB69 Line 229/32 Start SP 5650
Lat/long = –64.566700 65.300000

VEL (km.s^{-1})	***BASE (km)***	***THICK (km)***	***THICK (TWT)***	***Base (TWT)***
1.50	4.00	4.00	5.33	5.33
1.76	4.44	0.44	0.50	5.83
2.16	5.18	0.74	0.68	6.52
3.43	5.91	0.74	0.43	6.94
4.02	8.07	2.16	1.07	8.02
4.51	~9.20	1.13	0.50	~8.52
(5.20)	10.08	0.88	0.34	8.86
6.18	10.08			8.86

229/SB70 Line 229/33 Start SP 1090
Lat/long = –64.683300 63.866700

VEL (km.s^{-1})	***BASE (km)***	***THICK (km)***	***THICK (TWT)***	***Base (TWT)***
1.50	3.59	3.59	4.79	4.79
1.79	4.30	0.71	0.79	5.58
2.48	5.05	0.75	0.61	6.18
4.07	6.01	0.96	0.47	6.66
4.27	~8.44	2.42	1.13	~7.79
4.47	10.43	2.00	0.89	8.68
4.97	10.43			8.68

229/SB71 Line 229/33 Start SP 3210
Lat/long = –63.966700 62.683300

VEL (km.s^{-1})	***BASE (km)***	***THICK (km)***	***THICK (TWT)***	***Base (TWT)***
1.50	3.97	3.97	5.29	5.29
1.78	4.69	0.72	0.81	6.10
2.37	5.06	0.37	0.31	6.41
3.06	5.48	0.42	0.28	6.69
3.70	~6.76	1.28	0.69	~7.38
3.95	~7.95	1.18	0.60	~7.98
4.34	8.74	0.79	0.36	8.35
6.22	10.87	2.13	0.69	9.03
7.70	10.87			9.03

229/SB72 Line 229/33 Start SP 5440
Lat/long = –63.000000 62.033300

VEL (km.s^{-1})	***BASE (km)***	***THICK (km)***	***THICK (TWT)***	***Base (TWT)***
1.50	4.53	4.53	6.04	6.04
1.78	5.07	0.54	0.61	6.65
2.37	5.68	0.61	0.52	7.17
2.76	6.28	0.59	0.43	7.60
3.95	7.16	0.89	0.45	8.05
4.93	7.52	0.36	0.14	8.19
6.51	13.09	5.57	1.71	9.90
8.49	13.09			9.90

229/SB73 Line 229/34 Start SP 580
Lat/long = –63.583300 60.466700

VEL (km.s^{-1})	***BASE (km)***	***THICK (km)***	***THICK (TWT)***	***Base (TWT)***
1.50	4.43	4.43	5.91	5.91
1.80	5.00	0.57	0.63	6.54
2.50	5.53	0.53	0.42	6.96
3.00	~6.80	1.27	0.85	~7.81
(5.00)	7.85	1.05	0.42	8.23
6.40	7.85			8.23

229/SB74 Line 229/35 Start SP 1010
Lat/long = –66.633300 44.950000

VEL (km.s^{-1})	***BASE (km)***	***THICK (km)***	***THICK (TWT)***	***Base (TWT)***
1.50	2.27	2.27	3.03	3.03
1.78	2.95	0.68	0.77	3.79
1.86	3.15	0.20	0.21	4.01
2.63	~4.17	1.03	0.78	~4.79
2.96	~5.06	0.89	0.60	~5.39
4.29	~7.63	2.57	1.20	~6.58
(4.74)	11.18	3.55	1.50	8.08
5.53	11.18			8.08

229/SB76 Line 229/35 Start SP 5470
Lat/long = –64.866700 42.716700

VEL (km.s^{-1})	***BASE (km)***	***THICK (km)***	***THICK (TWT)***	***Base (TWT)***
1.50	4.59	4.59	6.12	6.12
1.96	5.09	0.50	0.51	6.63
2.06	5.48	0.39	0.38	7.01
2.35	5.84	0.36	0.31	7.32
3.14	~7.54	1.70	1.08	~8.40
4.41	~7.54			~8.40

229/SB77 Line 229/35 Start SP 8410
Lat/long = –63.650000 41.500000

VEL (km.s^{-1})	***BASE (km)***	***THICK (km)***	***THICK (TWT)***	***Base (TWT)***
1.50	4.80	4.80	6.40	6.40
1.89	5.20	0.40	0.42	6.82
1.99	5.47	0.27	0.27	7.09
2.28	~6.19	0.73	0.63	~7.73
(4.97)	6.39	0.20	0.08	7.81
6.16	6.39			7.81

229/SB79 Line 229/36 Start SP 3240
Lat/long = –64.500000 40.366700

VEL (km.s^{-1})	***BASE (km)***	***THICK (km)***	***THICK (TWT)***	***Base (TWT)***
1.50	4.78	4.78	6.37	6.37
1.91	5.07	0.29	0.31	6.68
1.93	5.61	0.54	0.56	7.24
2.40	5.86	0.25	0.20	7.44
2.78	~7.22	1.36	0.98	~8.42
(4.90)	~7.64	0.42	0.17	~8.59
6.67	~7.64			~8.59

229/SB80 Line 229/37 Start SP 380
Lat/long = –64.500000 45.583300

VEL (km.s^{-1})	***BASE (km)***	***THICK (km)***	***THICK (TWT)***	***Base (TWT)***
1.50	4.12	4.12	5.49	5.49
1.57-1.67	4.52	0.4	0.5	5.99
2.16	4.90	0.38	0.35	6.34
2.50	5.13	0.23	0.18	6.53
2.45	5.57	0.44	0.36	6.89
2.65	6.22	0.65	0.49	7.37
3.30	~7.53	1.31	0.80	~8.17
5.39	~7.69	0.16	0.06	~8.23
6.57	11.42	3.74	1.14	9.36
7.84	11.42			9.36

229/SB81 Line 229/37 Start SP 3870
Lat/long = –62.966700 44.983300

VEL (km.s^{-1})	***BASE (km)***	***THICK (km)***	***THICK (TWT)***	***Base (TWT)***
1.50	4.78	4.78	6.37	6.37
1.52	5.24	0.46	0.61	6.98
2.11-2.21	5.48	0.24	0.22	7.20
2.21	5.48			7.20
2.35	5.65	0.18	0.15	7.36
2.57	6.47	0.81	0.63	7.99
(4.90)	7.00	0.53	0.22	8.21
6.18	10.63	3.64	1.18	9.39
7.65	10.63			9.39

229/SB82 Line 229/38 Start SP 1220
Lat/long = –63.066700 43.183300

VEL (km.s^{-1})	*BASE (km)*	*THICK (km)*	*THICK (TWT)*	*Base (TWT)*
1.50	4.97	4.97	6.63	6.63
1.76	5.51	0.54	0.61	7.24
2.15	5.63	0.12	0.11	7.35
2.30	6.18	0.55	0.48	7.82
2.94	~6.72	0.54	0.37	~8.19
6.27	8.17	1.45	0.46	8.65
6.86	8.17			8.65

229/SB84 Line 229/38 Start SP 3580
Lat/long = –64.066700 43.733300

VEL (km.s^{-1})	*BASE (km)*	*THICK (km)*	*THICK (TWT)*	*Base (TWT)*
1.50	4.45	4.45	5.93	5.93
1.70	4.83	0.38	0.45	6.38
1.90	5.05	0.22	0.23	6.61
2.25	5.18	0.13	0.12	6.73
2.50	5.93	0.75	0.60	7.33
3.05	6.95	1.02	0.67	8.00
6.90	10.53	3.58	1.04	9.03
7.95	10.53			9.03

229/SB85 Line 229/39 Start SP 630
Lat/long = –64.300000 49.233300

VEL (km.s^{-1})	*BASE (km)*	*THICK (km)*	*THICK (TWT)*	*Base (TWT)*
1.50	~3.90	3.90	5.20	~5.20
2.00	~4.39	0.49	0.49	~5.69
1.85	4.97	0.58	0.63	6.32
2.05	5.26	0.29	0.29	6.61
2.74	6.14	0.88	0.64	7.25
2.78	6.87	0.73	0.53	7.77
4.48	~8.48	1.61	0.72	~8.49
(5.06)	9.12	0.64	0.25	8.74
6.33	12.34	3.21	1.02	9.76
7.60	12.34			9.76

229/SB86 Line 229/39 Start SP 4360
Lat/long = –62.683300 48.450000

VEL (km.s^{-1})	***BASE (km)***	***THICK (km)***	***THICK (TWT)***	***Base (TWT)***
1.50	5.10	5.10	6.80	6.80
1.84	5.39	0.29	0.32	7.12
2.25	5.78	0.39	0.34	7.46
2.61	6.50	0.73	0.56	8.01
2.98	8.03	1.53	1.03	9.04

229/SB88 Line 229/40 Start SP 1320
Lat/long = –62.633300 51.883300

VEL (km.s^{-1})	***BASE (km)***	***THICK (km)***	***THICK (TWT)***	***Base (TWT)***
1.50	5.07	5.07	6.76	6.76
2.00	5.54	0.47	0.47	7.23
2.02	5.87	0.33	0.32	7.55
2.30	6.57	0.70	0.61	8.16

229/SB89 Line 229/41 Start SP 1030
Lat/long = –63.216700 53.366700

VEL (km.s^{-1})	***BASE (km)***	***THICK (km)***	***THICK (TWT)***	***Base (TWT)***
1.50	4.94	4.94	6.59	6.59
1.78	5.32	0.38	0.43	7.02
1.97	5.71	0.38	0.39	7.41
2.32	6.56	0.85	0.73	8.14
3.21	~7.61	1.06	0.66	~8.80
6.32	10.33	2.71	0.86	9.66
7.70	10.33			9.66

229/SB90 Line 229/41 Start SP 2640
Lat/long = –62.783300 54.666700

VEL (km.s^{-1})	***BASE (km)***	***THICK (km)***	***THICK (TWT)***	***Base (TWT)***
1.50	5.13	5.13	6.84	6.84
1.95	5.59	0.46	0.47	7.31
2.05	6.07	0.49	0.48	7.79
2.60	6.89	0.82	0.63	8.42
3.41	7.12	0.22	0.13	8.55
5.65	9.50	2.39	0.84	9.39
7.60	9.50			9.39

APPENDIX 6: SEISMIC HORIZONS

The following table contains the horizon abbreviations used in the interpretation of the seismic reflection data. These horizon names are used in the interpretations shown in Plates 10-19.

Reflector	***Description***
aabo	Australian-Antarctic Basin oceanic
cont	continental basement
cot	continent-ocean transition
ebo1 to *ebo10*	Enderby Basin oceanic crust – types 1 to 10
ecot1	Enderby Basin continent-ocean transition – type 1
ecot2	Enderby Basin continent-ocean transition – type 2
eoc	Eocene
gvo1	George V Land oceanic – type 1
gvo2	George V Land oceanic – type 2
K	Cretaceous marker (age undefined)
maas	Maastrichtian
moho	Moho
peo1 to *peo9*	Princess Elizabeth Land oceanic – types 1 to 9
qmo1	Queen Mary Land oceanic – type 1
qmo2	Queen Mary Land oceanic – type 2
qmu1 to *qmu11*	Queen Mary Land undifferentiated basement – types 1 to 11
sdrs	seaward-dipping reflector sequence (SDRS)
tlam	laminated lower oceanic crust
tlcc	lower continental (reflective) crust
tlow	lower continental crust
tran	transparent continental crust
tur	Turonian
wlo1	Wilkes Land oceanic crust – type 1
wlo2	Wilkes Land oceanic crust – type 2
wwlo	west Wilkes Land oceanic crust

APPENDIX 7: NOTES ON POTENTIAL FIELD MODELS

N.G. Direen, University of Adelaide

INTRODUCTION

The interpretation process described in this appendix was designed to quantitatively validate preliminary time-based interpretations of structurally significant seismic sections against coincident potential field data, with the objective of elucidating the tectonic framework of the margin. This was done by integrating migrated depth-converted seismic reflection images and their interpretations, with density data derived from numeric conversion of seismic refraction and stacking velocities. The gravity and magnetic fields of these petrophysically-attributed geometric models were then concurrently forward-modelled in 3 dimensions, by giving the sections limited strike extents. Limited information on magnetic physical properties has been derived from analysis of dredge samples at analogue sites in the Southern Ocean; however, the magnetic properties remain the least constrained part of the validation process.

The crooked line acquisition geometry of the seismic reflection surveys has been accommodated by modelling the data in three dimensions, rather than by projecting onto a common datum. Models have been continued out of the plane of the section for distances up to 125 km in both directions, where regional strike allows. Because the geological information is limited out of the plane, this approach is equivalent to '2.5D' methods that calculate the potential field anomalies in 2D assuming 'infinite' strike lengths.

Modelling

Initial density estimates were derived by conversion of both seismic refraction velocities from sonobuoys acquired on the lines (see Appendix 5), and stacking velocities derived from the seismic processing sequence. These velocities were converted using the equation of Ludwig et al. (1971). This equation is in the form

$$\rho_{app} = -0.6997 + 2.23 \times V_p - 0.598 \times V_p^2 + 0.07036 \times V_p^3 - 0.0028311 \times V_p^4$$

where:

ρ_{app} is the apparent density;

v_p is the P-wave refraction or stacking velocity in km s^{-1} of the interval for which a density is required.

It must be noted that this method is designed only to produce a set of starting parameters for the initial forward model, as the densities may be later varied during modelling and inversion.

Methods

Two-way time seismic data were converted to depth using smoothed stacking velocities in DISCO-Focus. A range of megasequences was then interpreted from these data and images of the profiles exported from Geoquest. The data were imported into ModelVision Pro v4.0 as 8-bit per pixel bitmaps and stretched using the SOL and EOL geodetic coordinates, projected into SUTM rectangular Cartesian

coordinates. The base of the section was set at 20 km below sea level, with the top of section being 0 m (msl).

Gravity data were 1967 GRS Free Air Anomalies at msl in milligals. These data had been smoothed using a 3-minute RC filter on averaged one second data. The data have been meter, drift, tide and Eotvos corrected, and then further low-pass filtered to reduce high frequency signals / noise. The estimated final RMS noise envelope of the data is 5 –10 $\mu m.s^{-2}$.

Three-component total magnetic intensity data supplied were residual after removal of the IGRF (2001.3 / 2002.3 epochs). These data have been filtered and smoothed using a three point de-spiking and interpolation process, but have not been diurnally corrected. Thus, as well as remanent and induced magnetisations, the data will also include a time-variant component. High frequency sferics noise is apparent on some of the lines modelled.

General Modelling Assumptions

Background density contrast of model 2.67 x 10^3 $kg.m^{-3}$

Body responses are modelled in their correct x, y and z locations, not projected into a plane. The solutions are 3-D analytic for polyhedra, based on the algorithms of Coggon (1976) and Lee (1980).

Calculations do not account for sphericity of the earth over the distances of the baselines. Induced errors due to this assumption, based on comparison of similar 2.5 and spherical 3D models by Takin & Talwani (1966), are of the order of 30 $\mu m.s^{-2}$ and are not expected to exceed 50 $\mu m.s^{-2}$. Given the noise envelope of ~10 $\mu m.s^{-2}$, and the dynamic range of the data (typically ~550 $\mu m.s^{-2}$), this is not considered significant.

For each model, a brief description will be given of the characteristics of the gravity and magnetic fields, followed by a summary of each of the bodies in the model, including their interpreted lithologies. In all models, the density of seawater is assumed to be 1.03 x 10^3 $kg.m^{-3}$.

Referencing to Figures

Each figure is correlated with the text in the following ways:

Bodies: Bodies are referenced by letters. Where multiple bodies of the same rock type and origin are present in a model, each body is also given a number — e.g. bodies L1, L2 and L3 in Figure 93. Body parameters and interpreted rock types are described in detail in the text for each model.

Position referencing along lines: Between the gravity and magnetic profiles for each model, the X-axis is annotated with distance in kilometres from the southern (landward) end of the line. At the top of each model (below the magnetic profile), the X-axis is annotated with the seismic shot-point number. Each line starts at shot-point (SP) 100, and lines may be shot from north-to-south or south-to north. For brevity, and to avoid lengthy references to the 'southern end of line' or 'northern end of line', we will use 'SOL' (for start of line = SP 100) and 'EOL' (end of line) in the text.

228/28 – EASTERN WILKES LAND

Model RMS: 4.9

Gravity Field

Second-order regional field rises from –400 μm.s^{-2} over continental crust to a constant –100 μm.s^{-2} over ocean floor.

Mantle (ρ = 3.30 x 10^{3} kg.m^{-3}) down to 31 km sets DC level of regional field. Relief on Moho provides third-order control of regional gravity field

A gradient in the Moho of approximately 6.4 km vertical relief over 55 km distance (SOL to ~SP 1500) produces a coincident gravity anomaly of ~550 μm.s^{-2} (peak-to-trough). A Moho bulge / dome of 4.25 km maximum vertical relief under the thinned continental crust (SP 1500–4300) gives a trough-to-peak gravity anomaly of ~280 μm.s^{-2}.

Magnetic Field

Magnetic regional at 0 nT, along level of Magnetic Quiet Zone (MQZ), SP 2200–3500.

Magnetic field parameters (2001.3): B 60 000 nT; I –79.5°; D –12.3°. Body susceptibilities in SI units.

Model Details (Fig. 91)

Post-rift Section

Seawater ρ 1.03 x 10^{3} kg.m^{-3} / bathymetric gradient provides a ~500 μm.s^{-2} gradient from the southern end of the line to about SP 2000, but asymptotic to zero at the northern end of the line.

A (v_p 1800–2070 m.s^{-1}, ρ 1.92 x 10^{3} kg.m^{-3}) is a thinly laminated, flat-lying section, probably siliceous ooze that contributes a 140 μm.s^{-2} gradient from the SOL to ~SP 3000, and a base level of ~ –180 μm.s^{-2}.

B (v_p 2400-2750 m.s^{-1}, ρ 2.05 x 10^{3} kg.m^{-3}) is a well-laminated, flat-lying section, probably siliceous ooze, contributing a 95 μm.s^{-2} gradient from about SP 1700–3700, and thereafter a base level of ~ –90 μm.s^{-2}.

C (v_p 3000 m.s^{-1}, ρ 2.10 x 10^{3} kg.m^{-3}) is a well-laminated section, mantling underlying topography and onlapping underlying section landward. It probably comprises siliceous ooze or chalk. This section contributes a 40 μm.s^{-2} gradient from about SP 3300–8500.

D (v_p 2800 m.s^{-1}, ρ 2.30 x 10^{3} kg.m^{-3}) is a layered sequence with more diffuse seismic characteristics onlapping basement highs both to landward and seaward. The sequence shows large variations ain thickness and probably comprises muddy turbidites. A prograding wedge at the southern end of the line contributes a 200 μm.s^{-2} gradient from the SOL to ~SP 1600. A second thick sequence, onlapping a basement high, produces a peak-to-trough gravity anomaly of ~100 μm.s^{-2}. Towards the northern end of the line, this sequence produces a base

level of between 115 and 55 $\mu m.s^{-2}$ as it pinches and swells over relief in the underlying oceanic crust.

Syn-rift section

E (v_p 2600 $m.s^{-1}$, ρ 2.35 x 10^3 $kg.m^{-3}$) upper rift sediments form a downlapping wedge from the SOL, pinching out at ~SP 2600. This produces a 220 $\mu m.s^{-2}$ gradient at the southern edge of the model

F Lower rift section sediments (v_p 3300 $m.s^{-1}$, ρ 2.50 x 10^3 $kg.m^{-3}$) underlie the upper sequence at the southern end of the line, and wedge out at ~SP 1700. This section produces a ~90 $\mu m.s^{-2}$ gradient.

G The upper rift section contains stacked basaltic flows (purple, v_p 4000 $m.s^{-1}$; 2.85 x 10^3 $kg.m^{-3}$, 0.08 SI) that are manifest as high-amplitude, layered reflectors emanating from basement ridge in the COT, and flowing landward from the basement high from about SP 3300–3900. These produce coincident gravity and magnetic anomalies of 23 $\mu m.s^{-2}$ and 72 nT respectively. An outlier of these volcanics farther south (~SP 2900–3300) produces only a minor (~50 $\mu m.s^{-2}$) gravity and magnetic (2.8 nT) response. A third probable correlative of this sequence, seaward of the basement high (SP 4400–5400), has a lower density (2.70 x 10^3 $kg.m^{-3}$), probably indicating more volcaniclastic material, and/or alteration, within the flow package. The latter package also has a significant component of both normal remanent, and induced magnetisation (k = 0.02 SI, Q = 1.15, I = -74 D = 0), producing a 60 nT anomaly.

H The lower rift section contains stacked basaltic flows and sediments (purple, v_p 4000 $m.s^{-1,}$ 2.8 x 10^3 $kg.m^{-3}$) thinning landwards from the basement high and producing a ~100 $\mu m.s^{-2}$ anomaly superimposed on the gravity low due to mantle relief from SP 2000–4000.

Pre-rift sequences

I This section, from the SOL to ~SP 3700, has been split into several units, with contrasting reflection character. The northernmost unit, which appears to comprise a series of domino-faulted sedimentary blocks in a sinistral-simple shear system, and is pierced by the major basement high, has been ascribed a density of 2.67 x 10^3 $kg.m^{-3}$. This unit may represent well-lithified, cemented unmetamorphosed quartzose sandstones. Other blocks within this sequence have the following properties:

Body	Density x 10^3 kg.m^{-3}	k SI	Polarity	Q	D	I	G μm.s^{-2}	M nT
I1	2.70	0.05	R	1	79.5	12.3	13	-132
I2	2.75	0.09	N	1	–79.5	12.3	20	234
I3	2.60	0					-17	
I4	2.55	0.06	N	1	–79.5	12.3	-35	200
I5	2.65	0.03	R	1	79.5	12.3	-5	-70
I6	2.65	0.02	N	1	–79.5	12.3	-6	50
I7	2.60	0.065	R	1	79.5	12.3	-15	-120
I8	2.60	0.05	N	1	–79.5	12.3	-40	160
I9	2.67	0						

The highly magnetic signature of these blocks, coupled with their low density, makes them unusual. The reflection character of these blocks includes some layered and high-angle high-amplitude events, together with lower amplitude, coherent parallel reflections indicative of bedding, and a lot of noise. We interpret these features to be indicative of faulted blocks of ?Jurassic volcanic sequences (basaltic flows) and subvolcanic features (dolerite dykes and sills), interbedded with, and intruding sedimentary rocks. Volcanics and their hypabyssal feeders can provide both the alternating magnetic signature, due to positive and negative remanence (cf. Direen & Leaman, 1997), and a higher density contribution (2.90×10^3 kg.m^{-3} average). A ratio of between 10 and 40% dolerite to sandstone of average density 2.55 x 10^3 kg.m^{-3} would be sufficient to produce the observed apparent densities of these blocks. An analogue scenario for these types of lithologies forming basement to the Cretaceous rifting can be found in the 175 Ma Ferrar Group tholeiites and Permo-Triassic Victoria Group of George V and North Victoria Land farther to the east (Elliott, 1992), and the ~180 Ma dolerites intruding Parmeener Supergroup rocks in Tasmania (Direen & Leaman, 1997).

J The generally non-reflective pre-?Jurassic basement at the southern end of the section is modelled with a southerly thickening wedge of non-magnetic basement, density 2.89 x 10^3 kg.m^{-3}. This could either represent more non-reflective (meta-)sediments, or fractured and sheared granitic / gneissic basement similar to that exposed in the southern Gawler Craton in Australia (Direen, unpublished data).

K The wedge of moderate to non-reflective lower crust which infills the depression in the mantle has been modelled with a high density (2.91 x 10^3 kg.m^{-3}), non-magnetic body. These properties produce 300 μm.s^{-2} gravity and 0 nT magnetic responses. It is believed this piece of crust contributes substantially to the long-wavelength, slightly negative (–2 to –15 nT) anomaly known as the Magnetic Quiet Zone. The high density of this crust may be indicative of a high degree of igneous intrusion and underplating from the time of breakup, or during the Jurassic magmatic event inferred above. Alternatively, this crust may represent a

piece of metamorphic basement with high density components such as marbles (2.90–3.50 x 10^3 kg.m^{-3}), mafic gneisses (2.74–3.76 x 10^3 kg.m^{-3}) and amphibolites (2.80–3.00 x 10^3 kg.m^{-3}; all measurements, Direen unpublished data), such as are exposed in the southern Gawler craton. However, this latter proposal is considered less likely.

L 3.10, non-magnetised

Basement Ridge Complex

M Similar to the GAB margin (Sayers et al., 2001), line 228/28 exhibits coincident high-amplitude, long-wavelength gravity and magnetic anomalies spatially associated with an elevated zone of basement. This zone is characterised by the thinning of the overlying sedimentary package, and the thinning of the rift sequences and lower crust onto its landward margin. The reflection character of the basement high includes some coherent high-amplitude events (?lavas) and a lot of noise. The crest of the high forms a twin-peaked structure, which appears to be infilled by a wedge of noisy reflection character. Seaward of the high, the reflection section appears broken up by a seaward-dipping fault set, with significant throws (up to 1500 m) and heave (up to 200 m). The dominoes formed by these faults contain a mixture of steeply dipping high-amplitude events and incoherent character, which may indicate heavy intrusion by dykes and sills. The velocity of the top of the ridge is around 4000 m.s^{-1}, which is lower than the 5200–6200 m.s^{-1} deduced for the top of the GAB basement ridge by Sayers et al. (2001). The ridge is modelled by three pink bodies with the following properties:

Body	Density x 10^3 kg.m^3	k SI	Polarity
M1	2.67	0.05	N
M2	2.67	0.05	N
M3	2.67	0.03	N

These highly magnetic rocks probably represent serpentinised peridotite containing magnetite as the spinel phase. It is unlikely that they are unaltered peridotite (3.15 x 10^3 kg.m^{-3}) or pyroxenites (3.20 x 10^3 kg.m^{-3}), which are also generally non-magnetic, with chromite as the main spinel phase. Based on the relationships outlined in Miller & Christensen (1997) and Ludwig et al. (1971), these rocks are likely to be *c.* 65% serpentinised peridotite. This scenario is equivalent to that modelled by Sayers et al. (2001) for the conjugate GAB margin.

O The block of crust more seaward, and immediately adjacent to the identified oceanic crust, also shows many high amplitude events. This has been modelled with a dense (2.87 x 10^3 kg.m^{-3}), remanently magnetised (k = –0.04 SI, Q = 2; I = –74°; D = 0°) body, producing positive 44 μm.s^{-2} gravity and negative 160 nT magnetic responses.

P Incised into this block (O) are three small half graben, characterised by coherent, layered reflections. These have been modelled with non-magnetised wedges of

2.45 x 10^3 kg.m^{-3} and 2.55 x 10^3 kg.m^{-3}. These produce gravity anomalies of –25 and –10 μm.s^{-2} respectively.

N The section overlying the basement high has been modelled with similar properties (N1: 2.67 x 10^3 kg.m^{-3}, 0.065 SI [135 nT] and N2: 2.67 x 10^3 kg.m^{-3}, 0.01 SI [25 nT]), probably indicating a strong influence from basaltic volcanic activity (e.g. 35% dolerite, 2.90 x 10^3 kg.m^{-3}, intruding 65% quartzite, 2.55 x 10^3 kg.m^{-3}, will give an apparent bulk density of 2.67 x 10^3 kg.m^{-3}).

Oceanic crust

The oceanic crust in this section is unusual, in containing large topographic highs and/or depressions, filled with sediment. The highs appear to be draped by high-amplitude events, which may reflect lava build-ups. The character beneath the highs contains a mixture of high amplitude, shallow and steeply dipping events, and many incoherent noisy returns. Moho is not imaged under the ocean crust, and a simple layered structure is not apparent. This contrasts to 'normal' seafloor, where the crust is simply layered in the following sequences: Layer 1 sediments; Layer 2 (Q) basaltic pillow lavas, usually up to 500 m thick, with a mostly remanent magnetic response; Layer 3 (R), sheeted dolerite dykes, usually not ascribed any magnetic response; Layer 4 (S) peridotite and gabbroic layer, also usually not ascribed any magnetic response.

The 'traditional' approach to modelling 'normal' seafloor (e.g. Tikku & Cande, 1999) is to assume the top of layer 2 is flat, and that the magnetic response is generated from the juxtaposition of normal and remanently magnetised blocks. This produces a simple sinusoidal series of magnetic anomalies about a flat mean response. In contrast to this scenario, the magnetic anomalies on line 228/28 are highly complex, with at least 3 recognisable wavelength components. The longest of these is an order 1 regional gradient of 380 nT. Superimposed on this are a series of sinusoidal responses with peak-to-trough amplitudes of ~100 nT. High frequency responses (noise?) are further superimposed on these anomalies.

In order to determine whether a 'standard' approach, replicating a simple 4 layer crust would work, we applied several tests, to determine if the complexity of magnetic signal could be modelled with relatively simple, flat-lying layers with or without remanence dominant in the upper layer. These tests comprised:

Test 1: (no remanence; tests topographic response of upper basaltic layer) Layer 2 = 0.05 SI; Layer 3 (fills topographic highs) & 4 (flat) = 0 SI => poor fit

Test 2: (tests if regional gradient is due to differing remanence polarity in upper layer) Landward = 0.05 SI, Q = 2 Rev I =74, D =0; Seaward = 0.05 SI Q = 2 Norm I = –74°, D = 0°

Test 3: (tests if regional gradient is due to differing magnitude of remanence - Konigsberger Ratio - in upper layer, all normal) Landward Normal Q =1.25 k = 0.02 Seaward = Normal Q =2 k =0.05

These tests (Figs 100–102) show that it is unlikely that a simple layered solution will be sufficient to produce the complexity of the magnetic response, which includes both positive and negative shorter wavelength components superimposed on a longer wavelength trend that rises seaward.

In addition, the nature of the topography on the ocean crust needs to be more rigorously examined. The magnitude of the ocean floor topography is in the order of 2 km vertical relief by approximately 10 km spatial wavelength wide. There are at least two alternative explanations for these highs: 1) they are volcanic buildups formed during extrusion at the spreading ridge; or 2) they are the peaks of rotated hanging-wall fault-blocks in a fault set that dips seaward, due to late mechanical extension of the seafloor. Given the difficulties of modelling the responses with flat underlying layers as noted above, we have chosen the second of these options as the starting model, and modelled a series of fault dominoes in a sinistral shear-system. The faults separating the blocks are deep biting (down to 6-8 km below the regional level of ocean floor), and penetrate/offset both the pillow lava and dolerite sheeted dyke layers. Although apparently planar in the top part of the crust, at true scale, these faults appear to be shallowly dipping and listric, detaching within the peridotite layer, which also shows displacement due to the extension. These faults are typical of the slow-spreading, mechanically extended seafloor crust also found on the conjugate GAB margin (Sayers et al., 2001).

The ocean crust was modelled in three main segments, separated by shallow-dipping faults with large amounts (~4, ~8 and ~10 km) of heave. Because of the difficulty of ascertaining the true remanent vector within a rotated block, a vector has been chosen that is parallel to the present field, either reinforcing or opposing it. The estimated apparent vector from simple modelling studies is I = 74°, D = 0°. This procedure is adopted for all subsequent models.

Segment 1 (landward): three periods of mainly reverse polarity apparent remanence, two mainly normal polarity periods. Mostly lower density upper layers, indicating either alteration of primary mineralogy, or interbedded sediments, or both. Mostly low Q values.

Block	**Density x 10^3 kg.m^3**	**k SI**	**Pol**	**Q**	**Dip / Dip Az**
Q1	2.65	0.04	R	1	79 / 0
Q2	2.65	0.025	R	2	79 / 0
Q3	2.65	0.04	R	2.5	79 / 0
Q4	2.65	0.04	R	2.5	79 / 0
Q5	2.65	0.04	R	2.3	79 / 0
Q6	2.75	0.008	N	1	–79 / 0
Q7	2.92	0.05	R	2.5	79 / 0
Q8	2.85	0.05	R	2.5	79 / 0
Q9	2.65	0.03	R	2	79 / 0
Q10	2.55	0.05	R	1	79 / 0
Q11	2.55	0.01	N	1	–79 / 0
Q12	2.70	0.03	R	1.2	79 / 0

Some of the flows may post-date the faulting, as they appear to pond into the depressions created by rotation of the blocks on the listric faults. Therefore attempting to match apparently 'normal' and 'reversely' polarised blocks to given sea-floor spreading anomalies should only be attempted with extreme caution. The sheeted dyke layer to this segment (R) is modelled with an irregular faulted sheet, density 2.85 x 10^3 kg.m^{-3}.

This segment forms four half-graben that have normal reflectivity layered events probably sedimentary fill. The most landward also contains high amplitude events indicative of volcanics. The properties of these wedges of material are:

Block	**Density x 10^3 kg.m^3**	**k SI**	**Pol**	**Q**	**Dip / Dip Az**
1	2.60	0.05	R	2.1	79 / 0
2	2.45	0	-	-	-
3	2.45	0	-	-	-
4	2.42	0	-	-	-

Segment 2 (Intermediate): all apparently mainly normal remanence. Mostly typical basalt densities –i.e. unspilitised and no significant interflow sediments. Q values intermediate. Quite dense sheeted dyke layer (R).

Block	**Density x 10^3 kg.m^3**	**k SI**	**Pol**	**Q**	**Dip / Dip Az**
Q1	2.85	0.04	N	1	–79 / 0
Dykes	2.90	0.09	-	-	-
Q2	2.75	0.07	N	2	–79 / 0
Q3	2.75	0.08	N	2.5	–79 / 0
Q4	2.75	0.08	N	2.6	–79 / 0
Q5	2.65	0.08	N	2.5	–79 / 0

The 'Dykes' body models a small volume of high-amplitude events internal to the first fault domino in this segment. The sheeted dyke layer to this segment (R) is modelled with an irregular faulted sheet, density 2.92 x 10^3 kg.m^{-3}.

Segment 3 (Seaward): all apparently mainly normal remanence; lower densities, high susceptibilities and Q values. Low density dyke layer.

Block	Density x 10^3 kg.m^3	k SI	Pol	Q	Dip / Dip Az
Q1	2.65	0.06	N	3	–79 / 0
Q2	2.65	0.08	N	3	–79 / 0
Q3	2.65	0.06	N	2.5	–79 / 0

The sheeted dyke layer to this segment (R) is modelled with an irregular faulted sheet, density 2.70 x 10^3 kg.m^{-3}.

The peridotite beneath all three segments (S) is modelled with an irregularly faulted and extended (tectonically thinned) lower layer of density 2.90 x 10^3 kg.m^{-3}.

Key findings 228/28

- Moho has considerable relief in the COT.
- Lower crust is inhomogeneous in the COT, probably due to massive localised intrusion landward of the COT. However, pre-existing inhomogeneities (e.g. lower crustal metamorphic complexes) cannot be ruled out.
- The pre-rift crustal section (?Jurassic) probably contains large amounts of volcanics and intrusives. These may be equivalent to the Ferrar Group dolerites and basalts.
- The basement ridge complex in the COT is an amalgam of low and high density, but strongly magnetic bodies. As such, it may represent serpentinised, unroofed mantle peridotites, associated intrusions, and extrusive products from decompression melting, similar to those inferred in the conjugate GAB COT.
- The COT is obscured by positively magnetised landward-flowing basalts. These overlie hybridised, non-oceanic crust, but their magnetic signature contributes to the large positive anomaly previously labelled 34o.
- The oceanic crust in this section is clearly defined by areas of large topographic relief. This arises from mechanical extension and faulting of the brittle crust post-cooling, forming rotated fault dominoes. Some faults within this set have very large components of heave (up to 10 km) and throw (up to 4 km). Post-breakup basalts have flowed into some of the depressions created by this activity.
- The lower peridotite layer of the oceanic crust is strongly extended and tectonically thinned.
- Anomalies picked as seafloor spreading reversal patterns, are probably better explained by the offset and rotation of magnetised layers than by simple, layered remanent blocks. Episodes of dominantly positive and negative remanence are identifiable, but these should be analysed carefully to identify the true periods of magnetic reversal. A general caveat applies on any magnetic seafloor spreading anomalies identified in this sector.

228/29 – EASTERN WILKES LAND

Model RMS: 5.3

Gravity field

Second-order regional rises from c.-250 μm.s^{-2} landward to *ca*. –50 μm.s^{-2} on oceanic crust. Lowest values recorded in faulted zone landward of the inner basement ridge. Superimposed on the regional are three major long-wavelength (*ca.* 100km) broadly symmetric highs of 100, 250 and 150 μm.s^{-2}. The latter two correspond spatially to inner and outer basement ridges. Lowest gravity values are found in the faulted zone landward of the inner basement ridge.

The base level of the gravity field, and many of the second order features are due to the combination of bathymetric gradient (seabed descending from 3 km to 4.4 km depth oceanward over 360 km), and relief on the Moho, as illustrated above.

Magnetic Field

The magnetic field in this transect is centred on a relatively flat, negative (–60 nT) regional field. Superimposed on this are second order features of *ca*. 200 km wavelength, and third order anomalies of *ca*. 50 km wavelengths.

Magnetic field parameters (2001.3): B = 67 000 nT; I –89°; D –19.6°; body susceptibilities in SI units.

Model Details (Fig. 92)

Post-rift section

The post rift section (including seawater) provides a negative gradient gravity response, falling from –250 to –330 μm.s^{-2} along the line. Much of this is due to the changing depth of seawater. The onlap of this section onto the basement high at ~SP 5000–5500 gives rise to a relative positive anomaly. Two bodies in the lowest parts of the section have been given susceptibility, and produce high-frequency magnetic responses probably due to volcaniclastic material or lavas within the section.

A (v_p 1800 m.s^{-1}; ρ 1.76 x 10^3 kg.m^{-3}): well-laminated sequence, with evidence of erosion of the upper surface, and slumping/ canyoning; downlaps onto the underlying sequence landwards. Probable siliceous ooze.

B (v_p 2300 m.s^{-1}; ρ 2.00 x 10^3 kg.m^{-3}): seaward-thickening, well-laminated package similar to body A; downlaps onto the underlying sequence inboard, and conformable outboard. Probable siliceous ooze.

C v_p 3000 m.s^{-1}; ρ 2.30 x 10^3 kg.m^{-3}): well-laminated package only found seaward of the inner basement ridge (~SP 5000) which it onlaps. Probable siliceous ooze.

D (v_p 2500 m.s^{-1}; ρ 2.13 x 10^3 kg.m^{-3}): seismically noisy, roughly laminated wedge onlapping the inner basement ridge, but contains downlapping clinoforms that prograde landward form the high. Probable sandy turbidite fan facies.

E (v_p 2800 m.s^{-1}; ρ 2.23 x 10^3 kg.m^{-3}): seismically noisy wedge, restricted to southern end of line. Probable sandy facies.

F (v_p 3200 $m.s^{-1}$; ρ 2.35 x 10^3 $kg.m^{-3}$): well-laminated package forming gentle synclines infilling eroded topographic lows inboard of the inner basement ridge, and onlapped by sand wedge. Probable clay-filled / marly restricted basin.

G (v_p 3900 $m.s^{-1}$; ρ 2.23 x 10^3 $kg.m^{-3}$): wedge of well-laminated sediments, outboard of the inner basement ridge

Syn-rift section

A change of character from rifted sediments with minor volcanics landward, to rifted volcanics and minor sediment oceanward of the COB produces a 400 km wavelength step in gravity anomaly, from –30 to +300 $\mu m.s^{-2}$.

K Upper syn-rift sediments (v_p 3500–3700 $m.s^{-1}$; ρ 2.60–2.70 x 10^3 $kg.m^{-3}$) are a broadly laminated but seismically noisy section with some pinch-and-swell structuring. In places, the sequence is broken by arrays of steep, landward-dipping planar faults. The sequence is magnetically active, with dominantly reverse polarity. This response could be due to intrusion during rifting, or contained volcanic flows within the sedimentary pile.

Block	k SI	Q	Polarity (wrt I -89°, D -19.6°)
K1	0.04	1	R
K2	0.05	2.8	R
K3	0.02	1.5	R
K4	0.05	2.1	R
K5	0.04	1	R

I The lower syn-rift section sediments (v_p 5400 $m.s^{-1}$; ρ 2.58–2.77 x 10^3 $kg.m^{-3}$) are seismically noisy, with some coherent layered reflectors, generally lying below limit of clearly-defined planar faulting. This sequence is magnetically active, with reverse polarity: k SI 0.01, Q 1.

J The upper syn-rift section also contains stacked basaltic flows (ρ 2.55–2.80 x 10^3 $kg.m^{-3}$, 0.07 SI) in scattered pockets to extensive layers marked by sequences of thick, high-amplitude events bounding noisier, discontinuous reflectors that are interpreted as mixed lavas and volcaniclastics. These accumulations are often wedge-shaped, and infill half-graben between tilted domino faults. Lenses cover areas that are more extensive. These reflector packages also cap the crest of the broad basement high at ~SP 5000–5500. This sequence is magnetically active, producing high-frequency responses from the isolated accumulations and second-order anomalies from the stacked lenses.

Block	*ρ x 10^3 kg.m^{-3}*	*k SI*	*Q*	*Polarity* *(wrt I -89°, D -19.6°)*
J1 (extensive flows)	2.80	0.07	2.8	R
J2 (pocket)	2.55	0.04	1	N
J3 (pocket)	2.55	0.05	1	N
J4 (pocket)	2.55	0.08	2.5	R
J5 (pocket)	2.55	0.08	3	R
J6 (extensive flows)	2.75	0.04	2	R
J7 (extensive flows)	2.75	0.02	1	N
J8 (cap of dome)	2.60	0.01	1	N
J9 (cap of dome)	2.60	0.02	2	R
J10 (cap of dome)	2.60	0.02	2	R

H Upper syn-rift intrusions (v_p ?5400 m.s^{-1}; ρ 2.85 x 10^3 kg.m^{-3}): faulted blocks within the syn-rift package containing high-amplitude events, spatially coincident with magnetic anomalies, and are interpreted as mostly reversely magnetised basic sills and dykes intruding the syn-rift section.

Block	*k SI*	*Q*	*Polarity* *(wrt I -89°, D -19.6°)*
H1	0.03	1.5	R
H2	0.11	1	N
H3	0.3	1.5	R
H4	0.01	1.5	R

Pre-rift section

The pre-rift section contributes significantly to the overall regional field level, and longer wavelength components. There is a major 250 µm.s^{-2} level contribution, mostly from 31 km of mantle.

L The middle crust (v_p 6500 m.s^{-1}; ρ 2.90 x 10^3 kg.m^{-3}) is characterised by a noisy, incoherent seismic character with occasional high-amplitude, discontinuous events. The base of this section is marked by moderately continuous, high-amplitude reflections with considerable relief.

M The lower crust (v_p 8100 m.s^{-1}; ρ 3.10 x 10^3 kg.m^{-3}) has a noisy, incoherent seismic character with occasional high-amplitude, discontinuous events.

Considerable relief is modelled on Moho (mantle ρ 3.30 x 10^3 kg.m^{-3}) in order to produce long-wavelength second-order gravity highs. Two main topographic highs are apparent: Moho shallows from 20 to 12 km between the EOL and ~SP 7500, then rapidly descends to 17 km at ~SP 6700, before shallowing again from 17 km to

11.5 km depth at ~SP 4600. The strong relief, particularly at the landward end of the line, may reflect a failed rift. The landward mantle high also appears to have produced significant volcanism (1500 m of stacked volcanics) and intrusion in the syn-rift section, and a thinned zone filled by a deep, synclinal sequence. The outer shallowing of Moho, seaward of a thick, boudin-like crustal package, has produced massive intrusion and crustal modification of the outer COT, manifest as high-amplitude mid-crustal reflections and the extensive volcanics on the inner basement ridge.

Transitional crust in the COT

This zone, seaward of the inner basement ridge, contains a large variety of blocks often bound by steep, planar faults.

O1 'Hybrid crust 1' has two velocity estimates (4200 & 4400 $m.s^{-1}$), and contains continuous high-amplitude and noisy reflectors. It is similar in seismic character to the intruded upper syn-rift section, and is magnetically active. Its higher overall density probably indicates a greater volume of intrusives near the COB.

O2 'Hybrid crust 2' contains less continuous coherent reflectors and more high-amplitude reflectors than Hybrid crust 1. Its equivalent density and magnetic properties indicate that it is a mixed zone of syn-rift sediments and intrusions.

P There is a domain beneath these blocks between the 'ghosts' of two sets of discontinuous, high-amplitude events. This dense, non-magnetic block may either be a piece of middle crust or less intruded syn-rift sedimentary rock

Q The outer basement ridge (OBR) has a pinnacle that is characterised by noisy reflections. It is a magnetically active, low-density block which is probably a volcanic buildup in the COT.

R Outboard of the pinnacle, but still on the OBR, are three noisy but continuously reflective tilt blocks, with a mantle of laminated sediment. The two outer blocks are separated by a small graben block with high amplitudes that is probably of volcanic origin. These three blocks are interpreted as a stranded raft of syn-rift section, including minor volcanics, due to their low /null magnetisation.

The stranded raft overlies the OBR, which is a very dense, incoherent, noisy and non-magnetic block. This could be interpreted as a peridotite complex, similar to line 228/28 and the conjugate GAB lines (Sayers et al., 2001). The non-magnetic character of the OBR, indicates minimal serpentinite content and is unusual for a peridotite complex, but it could be related to the protective thin 'cap' of rafted sediments above it. The lack of magnetic volcanics (from decompression melting) expected in such a block is also unusual. Alternatively, and perhaps more likely, this block may be a piece of stranded crystalline basement, as it has the same density and magnetic characteristics as the thinned and necked lower crust modelled further inboard on this line. The block is bound by two listric faults dipping outwards; one of these faults forms the COB.

Block	*ρ x 10^3 kg.m^{-3}*	*k SI*	*Q*	*Polarity* *(wrt I -89°, D -19.6°)*
O1 Hybrid crust 1	2.85	0.035	2	R
O2 Hybrid crust 2	2.84	0.04	2	R
P Lower block	2.77	0		
Q Volcanic cap of OBR	2.55	0.02	2	R
R1 Tilt block	2.55	0.01	1	R
R2 Tilt block	2.55	0		
R3 Tilt block	2.55	0.008		
S Volcanic pocket	2.55	0.05	2	N
T Laminated seds	2.42	0.01		
U Lower crystalline crust	3.05	0		

Oceanic Crust

As with line 228/28, this section preserves a record of post-eruption mechanical extension, producing domino-style normal faults with block rotations and large amounts of heave. High-amplitude, coherent and continuous seismic packages at the tops of blocks (lavas) are rotated to high angles, and/or pond into the half-grabens opened by this process. Faults are apparently listric and deep biting, causing offset and rotation of the dyke and peridotite / gabbro layers. These faults may sole out into a thinned and extended layer at the top of the mantle.

Block	*ρ x 10^3 kg.m^{-3}*	*k SI*	*Q*	*Polarity* *(wrt I -89°, D -19.6°)*
W1	2.55	0.01	1	R
W2	2.55	0.03	1	N
W3	2.55	0.025	2	N
W4	2.55	0.02	1.2	N
W5	2.55	0.03	1.5	R
W6	2.60	0.02	1.5	N
W7	2.65	0.05	2.5	R
W8	2.55	0.04	2	R
W9	2.55	0.05	2.2	R
W10	2.60	0.03	1	N
W11	2.60	0.03	2	N
W12	2.55	0.025	1.6	N
W13	2.55	0.03	1.2	N
W14	2.55	0.04	1	N

V (ρ 2.23-2.5 x 10^3 kg.m^{-3})

X **(**ρ 2.83 x 10^3 kg.m^{-3}; non-magnetised**)** sheeted dyke layer.

Y (ρ 3.00 x 10^3 kg.m^{-3}; k = 0.01) oceanic peridotites.

Key findings 228/29:

- Moho has considerable relief in the COT, and if the COT is defined on the basis of rifting activity impacting on the brittle mantle lithosphere, the COT is wider than would be interpreted from seismic data alone
- The pre-rift crustal section (?Jurassic) probably contains large amounts of volcanics and intrusives. These may be equivalent to the Ferrar Group dolerites and basalts.
- The non-magnetic basement ridge complex in the COT at this location may be a stranded piece of lower continental crust (core complex?) with an overlying upper crustal 'cap'.
- The entire continental crust appears to form a set of thinned and necked sections with intervening mantle highs flowing into the spaces. This pattern is very similar to extensional mesoscale, boudinage but at a macroscopic, whole-of-crust scale.
- The COT is obscured by positively magnetised landward-flowing basalts, . These overlie hybridised, non-oceanic crust, but their magnetic signature contributes to the large positive anomaly previously mis-identified as 34o.

- The oceanic crust in this section is clearly defined by areas of large topographic relief. This arises from mechanical extension and faulting of the brittle crust post-cooling, forming rotated fault dominoes. Some faults within this set have very large components of heave (up to 10 km) and throw (up to 4 km). Post-breakup basalts have flowed into some of the depressions created by this activity.
- The lower peridotite layer of the oceanic crust is strongly extended and tectonically thinned.
- Anomalies that have previously been identified as seafloor spreading reversal patterns, are probably better explained by the offset and rotation of magnetised layers than by simple, layered remanent blocks. Episodes of dominantly positive and negative remanence are identifiable, but these should be analysed carefully to identify the true periods of magnetic reversal.

228/23 – CENTRAL WILKES LAND

Model RMS: 3.9

Gravity Field

Order 2 regional gradient increases from –300 μm.s^{-2} to –50 μm.s^{-2}

Major gravity low of c.-450 μm.s^{-2} overlies continental crust, corresponding to MQZ, rising to +50 μm.s^{-2} in COT. Generally flat at around –50 μm.s^{-2} thereafter, with minor negative excursions.

Magnetic Field
Generally flat regional field around 0 nT.

MQZ is major negative domain (–150 nT) which differs from lines farther east.

Two third order anomalies of *ca*.150 and 50 nT in COT.

Seafloor spreading anomalies vary between –50 and +200 nT.

Magnetic field parameters (2001.3): B = 60 000 nT; I –79.5°; D –12.3°. Body susceptibilities in SI units

Model Details (Fig. 82)

Post-rift section

The post rift section (including seawater) produces a negative gradient gravity response, falling from 500 to –500 μm.s^{-2} along the line, most of which is due to the changing water depth.

The change in water depth (ρ 1.03 x 10^3 kg.m^{-3}) gives –1900 to –2600 μm.s^{-2} decrease from the SOL to ~SP 2000 to a constant level up to SP 4000, then constant depth gives a constant response of 1900 μm.s^{-2} to the northern end of the line.

A (v_p 1700–2000 m.s^{-1}; ρ 1.92 x 10^3 kg.m^{-3}): well-laminated seismic package, with evidence of erosion of upper surface, and slumping/ canyoning; downlaps onto the underlying sequence to landward. Probable siliceous ooze.

B (v_p 2400–2450 m.s^{-1}; ρ 2.05 x 10^3 kg.m^{-3}): well-laminated seismic package; some diffuse character indicative of sandy input; onlaps underlying sequence landward. ?Mixed chalk / siliciclastics.

C (v_p 3400–3450 m.s^{-1}; ρ 2.10 x 10^3 kg.m^{-3}): deep basinal, well-laminated seismic package; onlaps the underlying sequence and wedges out landward. Probable siliceous ooze.

Syn-rift section

D (v_p 2600–3600 m.s^{-1}; ρ 2.10 x 10^3 kg.m^{-3} inboard, and 2.30 x 10^3 kg.m^{-3} near the COB). The inboard part of the sequence thins seaward and is well-laminated with diffuse internal character. At the most inboard part of the line, the sequence appears to be affected by planar faulting. It probably comprises muddy turbidite fan facies. The sequence thickens again into the COT zone, where it becomes a thick, well-laminated package that drapes the basement topography, and is structured into synclines. This part of the sequence is possibly stacked abyssal basin floor fans.

E (v_p *ca.* 4000 m.s^{-1}). Grabens and half grabens onlap the COT crust and oldest ocean floor. Laminated, often high-amplitude reflections, overlying deeper zones of diffuse or incoherent character. These basins frequently contribute high frequency magnetic responses, and are probably filled with basalt flows, volcaniclastic and siliciclastic materials. Properties (landward to seaward) are:

Density x 10^3 kg.m^{-3}	***k SI***
2.45	0.01
2.65	0.01
2.45	0.05
2.45	0.04
2.40	0.00
2.45	0.00
2.45	0.00
2.45	0.00
2.55	0.00
2.55	0.02 Q = 1.2 Reverse polarity

F 2.62 x 10^3 kg.m^{-3}, 0.02 SI): high-amplitude, noisy, laminated sequence, dipping landwards from COB.

G Domino-blocks, laminar and rough, high amplitude events (v_p 3400–3800 m.s^{-1}; 2.45 x 10^3 kg.m^{-3}; 0.05 SI; Q 1.6 R; (I = 79°; D = 0°). Probable ?Jurassic siliciclastic sedimentary rocks intruded and capped by basaltic sills/volcanics.

Pre-rift section

H Upper crust (v_p 5000 m.s^{-1}; 2.53 x 10^3 kg.m^{-3}; 0.045 SI, Q = 2, reverse polarity): noisy / coherent, but discontinuously reflective. Probable Jurassic or older rocks intruded by dolerite sills.

I Middle crust (v_p 6500 m.s^{-1}; 2.70–2.75 x 10^3 kg.m^{-3}): largely transparent, with occasional high-amplitude events; no magnetisation. Probable continental lower crustal metasediments.

J Lower crust (v_p 5000 m.s^{-1}; 2.75 x 10^3 kg.m^{-3}): strongly reflective and laminated with high-amplitude reflectors. Continental lower crustal metasediments.

Mantle (3.30 x 10^3 kg.m^{-3}): shallows from a depth of ~16.5 km at the southern end of the profile, to ~11 km at ~SP 2300.

Transitional crust in the COT

K Inner hybrid crust (v_p 5000 m.s^{-1}; 2.82 x 10^3 kg.m^{-3}; 0.008 SI): noisy reflection character, usually with high-amplitude events, probably representing sills or dykes, intruding crystalline lower crust or pre-rift ?Jurassic section; high density weakly to strongly magnetic.

L Structurally high, high relief blocks in inner COT (v_p 5100 m.s^{-1}): some high-amplitude events, possibly representing intrusions; highly magnetic; variable low to high density; cut by deep-biting faults with overlying incised half-graben. Possible serpentinised peridotite complexes, with 25–65% serpentinisation indicated by densities. L1 is interpreted to be highly serpentinised, while L2–L5 are gabbros or peridotites that are partially serpentinised.

Block	***Density x 10^3 kg.m^{-3}***	***Susceptibility SI***
L1	2.67	0.055
L2	2.82	0.08
L3	2.80	0.05
L4	2.92	0.04
L5	2.90	0.03

M Outer hybrid crust (salmon pink): topographically subdued fault blocks, containing many high-amplitude reflectors, and overlain by more extensive half-graben, immediately adjacent landward to the COB. These lower density, moderately magnetic blocks may represent a stranded raft of the pre-?Jurassic sequence heavily intruded by mafic dykes and sills. Alternatively, their low density might indicate a higher degree of hydrothermal, magnetite-destructive alteration of mafic rocks adjacent to the COB. Blocks have the following properties: M1 — 2.67 x 10^3 kg.m^{-3}, 0.01 SI; M2 — 2.57 x 10^3 kg.m^{-3}, 0.02 SI.

Oceanic Crust

Oceanic crust appears to be divided into three domains, separated by seaward dipping faults with large amounts of heave.

Domain 1 (SP 4300-5800): Mildly faulted blocks with small amounts of rotation and heave / throw; overlying half-graben; mixture of normal and reverse polarised blocks; standard density.

Density 10^3 kg.m^{-3}	***SI***	***Q***	***Polarity***
2.62	0.02	0	N
2.60	0.04	1.5	N
2.65	0.04	1.7	R
2.65	0.02	1.5	N
2.65	0.04	1.8	R
2.65	0.03	1.6	R

Domain 2 (SP 5800-7100): Strongly faulted, large blocks with large amounts of heave, and thickened overlying section. Dominantly normal polarity magnetisation,

and denser blocks. Underlain by a zone of structured mantle, and boudinaged Layer 4 (peridotite)

Density 10^3 ***kg.m***$^{-3}$	***SI***	***Q***	***Polarity***
2.65	0.018	1.4	N
2.7	0.04	1.7	N
2.7	0.02	1.5	R

Domain 3 (SP 7100 to end of line): Weakly faulted tabular blocks, lower density than the other two domains. Dominantly apparent normal polarity magnetisation.

Density 10^3 ***kg.m***$^{-3}$	***SI***	***Q***	***Polarity***
2.55	0.045	2	N
2.55	0.008	1	N

O & P All three domains are underlain by Layer 3 (dolerite dyke swarms) with density 2.70 x 10^3 kg.m^{-3}, and Layer 4 (peridotite) with density 2.90 x 10^3 kg.m^{-3}.

Key findings 228/23:

- More subdued Moho topography on this line compared to lines 228/28 & 228/29.
- Lower crustal section appears to be less thinned than line 228/28.
- No evidence for a dense underplated section.
- Evidence for probable serpentinised mantle intrusions in the basement ridge complex.
- More widespread evidence for intrusion and crust hybridisation on both sides of the COT basement complex.
- Evidence, as in line 228/28, for segmentation of the ocean crust by mechanical extension. Deep cutting faults separate blocks of differing physical character, and boudinage the peridotite layer. Mantle topography appears to have developed in response to this. Termination of fault displacements in the peridotite layer suggests serpentinisation of this layer to accommodate shear.
- Some evidence for break-up basalts flowing back landward over the COB onto hybrid continental crust.

228/24 – CENTRAL WILKES LAND

Model RMS: 4.0

Gravity Field

Second-order regional gradient increasing from –400 μm.s^{-2} to –100 μm.s^{-2} representing a general base level shift of –50 μm.s^{-2} compared to 228/23.

Major gravity low of *ca* –500 μm.s^{-2} over continental crust, correlating with MQZ, rising to –100 μm.s^{-2} in COT.

Generally flat at around –100 μm.s^{-2}, thereafter, major –200 μm.s^{-2} negative anomaly from SP 4700–6500 over oceanic crust.

Magnetic Field

Generally flat regional field around –10 nT.

MQZ is a major negative domain (–100 to –200 nT), which differs from lines farther east.

Two third order anomalies of *ca* 20 and 100 nT in COT.

Seafloor spreading anomalies vary between –100 and +80 nT.

Major asymmetric negative anomaly of –260 nT peak amplitude from SP 4800–5700.

Magnetic field parameters (2001.3): B = 66 550 nT; I –87.2°; D –75.9°. Body susceptibilities in SI units.

Model Details (Fig. 83)

Post-rift section

The post-rift section (including seawater) provides a negative gradient gravity response, falling from 740 to –460 μm.s^{-2} along the line. Much of this is due to the changing depth of seawater.

Seawater (ρ 1.03 x 10^{3} kg.m^{-3}): change in depth gives –200 to –290 μm.s^{-2} decrease from SOL to ~SP 2000, to a constant level out to ~SP 4000, then constant depth gives a constant response of –300 μm.s^{-2} to the EOL.

A (v_p 1800 m.s^{-1}; ρ 1.76 x 10^{3} kg.m^{-3}): well-laminated seismic package, with evidence of erosion of upper surface, and slumping/ canyoning. Probably siliceous ooze.

B (v_p 2400–2430 m.s^{-1}; ρ 2.36 x 10^{3} kg.m^{-3}): well-laminated seismic package; onlaps underlying surface and wedges out landward. Probable siliceous ooze.

C (v_p 3400–3430 m.s^{-1}; ρ 2.10 x 10^{3} kg.m^{-3}): well-laminated seismic package, with some diffuse seismic character; onlaps underlying package and wedges out landward. Probable ?mixed chalk / siliciclastic or ooze with some sandy input.

Syn-rift section

These low-density blocks contribute substantially to the major positive gravity gradient across the COT from *ca* –400 μm.s^{-2} to –10 μm.s^{-2} where they wedge out.

The blocks form an inner and outer set, divided by an inner basement high (IBH; SP 1800–2600) and bounded by an outer basement high (OBH; SP 4000) to seaward.

E (v_p 2500–2570 $m.s^{-1}$; ρ 2.14 x 10^3 $kg.m^{-3}$ landward of IBH; v_p 3700 $m.s^{-1}$ 2.30 x 10^3 $kg.m^{-3}$ in COB area): landward, a well-laminated package with internal diffuse character that wedges and thins seaward. Probable muddy turbidite fan facies. Package thickens into main COT zone, outboard of IBH, becoming a well-laminated package draping basement topography, and structured into synclines. This part probably stacked abyssal basin floor fans.

D A thin package of rougher, high amplitude reflectors overlies the turbidite package (v_p ?3700 $m.s^{-1}$; ρ 2.65 x 10^3 $kg.m^{-3}$; k 0.05 SI Q = 2). This package, originates at the OBH and thickens landward, and is strongly magnetic with normal polarity. It is interpreted as stacked volcanic flows and interflow sediments from the time of breakup.

F A package of well-laminated, domino fault blocks thickening into the IBH (v_p 3360–3400 $m.s^{-1}$; ρ 2.30 x 10^3 $kg.m^{-3}$; 0.03R) is interpreted as ?Jurassic to ?Lower Cretaceous syn-rift sedimentary rocks intruded by sills. The sills, as on other lines, are inferred from high-amplitude reflectors, and a dominant reverse polarity magnetic signature

G A pair of half graben situated between the IBH and OBH comprise a 4.5 km thick basin (v_p 4000 $m.s^{-1}$; ρ 2.75 x 10^3 $kg.m^{-3}$). The fill is characterised by well-laminated and some discontinuous reflectors, indicative of siliciclastic fill. These sediments are structured into hanging-wall synclines on major seaward dipping listric faults. The basin also contains a high volume of discontinuous, rough, high-amplitude reflections especially lower in the section. These are probably indicative of intrusions during late rifting, although they have negligible magnetic response.

Pre-rift section

This section contributes extensively to the base level of the gravity response seaward of the IBH. Relief on the mantle is the overall control on the gravity response, especially the 1000 $\mu m.s^{-2}$ gradient to landward to achieve the base level. This section also contributes the majority of the magnetic anomalies.

H A seaward-thinning wedge of discontinuous, often high-amplitude reflectors (v_p 5000 $m.s^{-1}$; ρ 2.53 x 10^3 $kg.m^{-3}$; k 0.04 SI; Q = 2.5 reverse polarity), underlies the domino faulted ?Jurassic package. This lower package is also cut by planar faults, and is interpreted as an older Jurassic section, highly intruded by sills, especially approaching the IBH, where the volume of high-amplitude reflections increases.

I1 Unit H is underlain by a wedge of noisy, seismically transparent crust that appears to thicken landward (v_p 5800 $m.s^{-1}$; ρ 2.73 x 10^3 $kg.m^{-3}$). This quite dense crust has no discernible magnetic response, and is interpreted as crystalline middle crust, probably of granitic or gneissic composition.

I2 Beneath the transparent layer is a block obscured by residual seismic noise. This package, initially interpreted as top mantle, is probably laminated, non-magnetic lower crust, with a density of 2.75 x 10^3 $kg.m^{-3}$.

J Partially serpentinised upper mantle peridotite, with a density of 3.05×10^3 kg.m^{-3}.

Thirty kilometres of the upper mantle (v_p 8200 m.s^{-1}; ρ 3.30×10^3 kg.m^{-3}), has been included in the model. The landward portion is bounded on its upper surface by a packet of very high amplitude reflectors that appear to ramp upward into the IBH. The large density difference across the Moho explains the high-amplitude seismic signature at the boundary of the packages, which requires at least a large local density variation to produce a high acoustic impedance contrast.

Transitional crust in the COT

K The inner basement high (IBH) is composed of two magnetic bodies with normal polarity (v_p 5000 m.s^{-1}; ρ 2.80 (K1) & 2.87 (K2) x 10^3 kg.m^{-3}; k 0.02 SI). The upper parts of these bodies are characterised by mantling caps of noisy, discontinuous high-amplitude reflections interpreted as basaltic volcanics. The inner parts are uniformly noisy and low-amplitude, although some deep-biting planar faults can be detected offsetting reflectors. The high densities and magnetic character of these bodies are attributed to massive gabbro / peridotite intrusions.

L The outer edge of the IBH is marked by a thick magnetised wedge of noisy, continuous high-amplitude reflections (v_p 5000 m.s^{-1}; ρ 2.90 x 10^3 kg.m^{-3}, k 0.035 SI). These are interpreted as stacked volcanic flows and sills, related to the IBH magmatic complex.

M The half-graben between the IBH and OBH are underlain by a series of noisy, seismically transparent blocks, the upper surfaces of which are often marked by a single, strong continuous high amplitude event. Three dense, magnetic blocks are used to model this zone (deep green), with the following properties:

Block	Density $\times 10^3$ kg.m^{-3}	k SI (normal polarity)
M1	3.03	0.03
M2	3.10	0.01
M3	3.00	0.02

These blocks are interpreted as altered peridotites, probably exposed during movement on the deep penetrating listric faults that bound the overlying deep basin. This interpretation, if correct, is an extremely interesting result, as it means a sedimentary basin lies directly on top of the upper mantle which has been mechanically exposed between a magmatic complex (IBH) and the COB, without proceeding to full breakup and oceanic spreading.

N A thin, non-magnetic, landward-dipping wedge of more continuous reflectors lying on the landward side of the outer basement high (OBH; ρ 2.85 x 10^3 kg.m^{-3}), and beneath the deep basin, is interpreted as a stranded and intruded fragment of lower crust in the COT.

O The OBH at the COB is capped by a packet of mixed amplitude, discontinuous reflectors. The modelled body (ρ 2.65 x 10^3 kg.m^{-3}; k 0.01 SI, normal polarity) is interpreted as mixed intrusions and flows at the locus of break-up.

Ocean Crust

Q Layer 1 comprises half-graben with seaward-dipping planar faults cut into the underlying basement. Reflector packages are characterised by high-amplitude and continuity, occasionally noisy. Probably mixed ooze / volcaniclastic fill. Densities: 2.47 x 10^3 kg.m^{-3}; 2.40 x 10^3 kg.m^{-3}; 2.40 x 10^3 kg.m^{-3}; 2.40 x 10^3 kg.m^{-3}; and 2.55 x 10^3 kg.m^{-3}.

The basement of Layer 2 is broken up into a series of seaward-dipping rotated fault blocks by an array of generally planar faults. Several of these appear to act as listric master structures that broadly divide the crust into five domains with differing elevations. These faults also dissect the sheeted dyke and gabbro/peridotite layers, and in some cases, apparently offset the Moho.

Domain 1 (SP 4200-4100): all normal polarity crust with mixed / minor remanent components.

Density x10^3 kg.m^{-3}	**k SI**	**Q**
2.55	0.02	1
2.55	0.05	2.5
2.55	0.03	1.2
2.55	0.03	2

Sheeted dykes (R; ρ 2.70 x 10^3 kg.m^{-3}) and peridotite layer (S; ρ 3.05 x 10^3 kg.m^{-3}) underlying this domain are non- or negligibly magnetic.

Domain 2 (SP 5100-5600): all reversely-magnetised blocks, with high remanent and induced components, dipping landward into a major listric structure.

Density x10^3 kg.m^{-3}	**SI**	**Q**
2.80	0.08	2.5
2.55	0.06	2.5
2.55	0.04	2

Sheeted dykes (R; ρ 2.70 x 10^3 kg.m^{-3}, k 0.05 SI, Q = 2) and peridotite layer (S; ρ 2.75 x 10^3 kg.m^{-3}, k 0.01 SI, Q =1) underlying this domain are magnetic and remanent. The low density of the peridotite layer is indicative of serpentinisation of around 50%. This is consistent with development of a large volume of continuous high amplitude reflectors in this block. It is possible that ingress of seawater into the bounding fault structure may be the cause of these effects.

Domain 3 (SP 5600-6250): all normal polarity blocks with mixed remanence. Topographically high block, isostatically supported by depressed Moho, producing a coincident gravity low.

Density x10^3 kg.m^{-3}	**SI**	**Q**
2.55	0.03	1.4
2.55	0.03	1.2
2.55	0.03	2

Sheeted dykes (R; ρ 2.70 x 10^3 kg.m^{-3}, k 0.06 SI, Q = 2.2) and peridotite layer (S; ρ 2.75 x 10^3 kg.m^{-3}, k 0.01 SI, Q = 1) underlying this domain are magnetic and remanent, and are also interpreted as altered and serpentinised.

Domain 4 (SP 6250-6800): mixed polarity blocks, with low susceptibilities and mixed remanence. Topographically low block, supported by a Moho high.

Density x10^3 kg.m^{-3}	**SI**	**Q**	**Polarity**
2.55	0.01	1	N
2.55	0.02	1.5	R
2.55	0.035	2	N

Sheeted dykes (R; ρ 2.70 x 10^3 kg.m^{-3}, k 0.02 SI, Q = 1) and peridotite layer (S; ρ 2.75 x 10^3 kg.m^{-3}, k 0.01 SI, Q =1) underlying this domain are also magnetic and remanent. An irregular mid-crustal zone of discontinuous, high-amplitude reflectors (bodies S, ρ 2.80 x 10^3 kg.m^{-3}) is interpreted as a fossil magma chamber.

Domain 5 (SP 6800 to end of line): mixed polarity blocks, with low susceptibilities and mixed remanence. Topographically higher block.

Density x10^3 kg.m^{-3}	**SI**	**Q**	**Polarity**
2.55	0.03	1.5	R
2.55	0.03	1.2	N
2.55	0.02	1	N

Sheeted dykes (R; ρ 2.70 x 10^3 kg.m^{-3}, k 0.02 SI, Q = 1) and peridotite layer (S; ρ 2.75 x 10^3 kg.m^{-3}, k 0.01 SI, Q =1) underlying this domain are again magnetic and remanent.

Key findings 228/24:

- Strongly necked lower crustal section
- Major intrusive activity in the inner part of the COT, adjacent to necked and thinned lower continental crust.

- Extreme thinning of lower crust in the COT has exposed dense lower crustal rocks, and possibly continental mantle peridotites. Continued rifting of this section has resulted in a thick depocentre of ?Jurassic age resting directly on lower crustal material.
- Direct imaging of high-amplitude, high density bodies consistent with fossil magma chambers.
- All three layers of oceanic basement have been extended, forming rotated fault blocks. Faults are listric, penetrating the upper mantle, and may sole into an intra-mantle decollement.
- Intra-oceanic crust alteration and serpentinisation has taken place on a large scale (hundreds of km^3).

228/18 - WESTERN WILKES LAND

Model RMS: 3.1

Gravity Field

Second-order regional gradient decreasing from 400 μm.s^{-2} to –100 μm.s^{-2} and then returning to 200 μm.s^{-2} ; very different regional field shape compared to lines further east.

Major gravity low of *c.* –100 μm.s^{-2} over faulted COT. Two positive excursions of +150 μm.s^{-2} either side of major low.

Magnetic Field

Similar field response to lines to east: generally flat regional field around 0 nT, but rising gradually from –150 nT. This effect explained by edge anomaly due to the broad magnetic sheet of oceanic crust.

MQZ is major negative domain (–100 to –200 nT) associated with continental crust.

Two third order anomalies of *ca* 100 and 120 nT in COT.

Seafloor spreading anomalies vary between +100 and +300 nT ptp.

Major asymmetric negative anomaly of 260 nT peak amplitude from ~SP 4800–2600.

Magnetic field parameters (2001.3): B = 64 100 nT; I –82.3°; D –86.2°; body susceptibilities in SI units.

Model Details (Fig. 80)

Post-rift section

Interpretation of modelling results from this line is tentative. This line lies well to the west of other modelled sections, and within a different structural regime with differing geophysical expression. Initial results thus require further testing against other transects within the same environment before being considered in any way conclusive, according to the criteria for evaluating potential field models established by Leaman (1994).

The post-rift section (including seawater) provides a negative gradient gravity response, falling from –2300 μm.s^{-2} to a minimum of –3600 μm.s^{-2} at ~SP 4000, before returning to a 3400 μm.s^{-2} base level for the remainder of the line. Much of this variation is due to the changing depth of seawater, and the thicker than average, low-density sediment pile.

Seawater (ρ 1.03 x 10^{3} kg.m^{-3}); change in depth gives –1000 to –2760 μm.s^{-2} decrease from the EOL to ~SP 2000.

A (v_p 1800 m.s^{-1}; ρ 1.76 x 10^{3} kg.m^{-3}). Well-laminated and 'sculptured' seismic package, with evidence of erosion of upper surface, slumping/ canyoning, and macroscopic climbing ripples. Onlapped at ~SP 3500 by a younger, more diffuse package with less continuous laminations. Probably siliceous ooze grading into ?sandy contourite.

B (v_p 2450 $m.s^{-1}$; ρ 2.11 x 10^3 $kg.m^{-3}$). Roughly-laminated seismic package with evidence of slumping/ canyoning, and macroscopic climbing ripples. Probably mixed siliceous ooze and sandy contourite.

C (v_p 3400 $m.s^{-1}$; ρ 2.36 x 10^3 $kg.m^{-3}$). Roughly-laminated seismic package, thinning over an outer basement high (OBH; SP 2600–2800). Onlaps underlying package and wedges out landward, thickens seaward becoming more diffuse in character. Probably siliceous ooze with some sandy input.

D (v_p 3500 $m.s^{-1}$; ρ 2.37 x 10^3 $kg.m^{-3}$). Roughly-laminated, discontinuous thick reflective wedge thinning onto OBH. Probably sandy turbidites.

E (v_p 3600 $m.s^{-1}$; ρ 2.39 x 10^3 $kg.m^{-3}$). Roughly-laminated, more continuous reflections wedge onlapping inner edge of OBH. Probably muddy turbidites.

Syn-rift section

These blocks vary from being sediment-dominated landward to volcanic or volcaniclastic-dominated seaward, with the seaward limits of the two packages delimited by the inner basement high (IBH; SP 5300–6200) and OBH, respectively. The more landward package (F) creates a gravity low of *ca* –360 $\mu m.s^{-2}$ to –50 $\mu m.s^{-2}$ where it wedges out on the IBH. The outer package creates a broad high of 70 $\mu m.s^{-2}$ peak amplitude, and *ca* 250 km wavelength.

F (v_p 3700 $m.s^{-1}$; ρ 2.40 x 10^3 $kg.m^{-3}$). A coarsely-laminated package with internal diffuse character wedging and thinning seaward. Probably marginal marine facies.

G A series of irregular packages of rougher, high-amplitude discontinuous reflections lies between the IBH and OBH, and beneath the interpreted shallow marine package (v_p 4500 $m.s^{-1}$; ρ 2.55-2.77 x 10^3 $kg.m^{-3}$). These packages are strongly magnetic with variable polarity, and are interpreted as stacked volcanic flows, interflow sediments and hypabyssal intrusives from the time of rifting

.

Density x10^3 $kg.m^{-3}$	**SI**	**Q**	**Polarity**
2.55	0.04	3	R
2.55	0.06	3	R
2.87	0.013	0	N
2.77	0.05	3	R
2.55	0.06	3	R
2.77	0.04	2	N
2.65	0.02	3	R

H A thin reflective basin occupies a topographic low immediately seaward of the OBH. This has been ascribed a density of 2.55 x 10^3 $kg.m^{-3}$, and may comprise volcaniclastic material.

Pre-rift section

This section contributes large positive anomalies to the gravity field, with relief on the mantle being the major control. This section also produces the majority of the magnetic anomalies.

J The upper part of the pre-rift section is highly structured package with variable thickness, and characterised by high-amplitude reflections at its base and top, but is generally seismically transparent (v_p 4500 $m.s^{-1}$; ρ 2.53 x 10^3 $kg.m^{-3}$. k 0.05 SI Q = 2, reverse polarity). This package is modelled as terminating on the IBH, and is interpreted to be equivalent to the ?Jurassic-Lower Cretaceous section modelled on lines farther east.

K A similar package outboard of the IBH (v_p 4500 $m.s^{-1}$; ρ 2.50 x 10^3 $kg.m^{-3}$; k 0.04 SI Q = 1.5, reverse polarity) wedges out on the OBH.

L The sedimentary packages J and K are underlain by reflective lower crust with many variable-geometry high- and low-amplitude reflectors, that thins seaward (v_p ?6000 $m.s^{-1}$; ρ 2.75 x 10^3 $kg.m^{-3}$; k 0.05 SI Q = 2.5 reverse polarity. This lower unit may be metasedimentary material of the crystalline lower crust.

Thirty kilometres of the upper mantle (v_p ?8000 $m.s^{-1}$; ρ 3.30 x 10^3 $kg.m^{-3}$) has been included in the model. The interpreted Moho depths vary from 17 km inboard to 14.7 km on a structural high beneath oceanic crust.

Transitional crust in the COT

M The IBH is modelled with two strongly magnetic bodies with reverse polarity (v_p 5000 $m.s^{-1}$; ρ 2.67 x 10^3 $kg.m^{-3}$; k 0.04 [M1] & 0.02 [M2] SI, Q = 2 & 2.5). The absence of mantling caps of noisy, discontinuous high-amplitude, and the presence of internal dipping, high amplitude reflections terminating on planar structures suggests that these blocks are highly intruded ?Jurassic sediments, rather than massive gabbro / peridotite intrusions and associated volcanics, as observed elsewhere on this margin.

N The wedge of intruded sedimentary rocks between the IBH and OBH is underlain by a series of noisy, 'transparent' blocks, the upper surfaces of which are often bounded by a single, strong continuous high amplitude event. Two dense, magnetic blocks are used to model this zone, with the following properties:

Block	$\rho \times 10^3$ $kg.m^{-3}$	k SI (normal polarity)
N1	3.00	0.01
N2	2.90	0.01

These blocks are interpreted as altered peridotites, exhumed during movement on the deep biting listric faults that bound the overlying deep basin. This interpretation is comparable to that for line 228/24 to the east, and may indicate that this unusual situation may be widespread along the margin. The high relief on both the upper and lower surfaces of this basement and the presence of offset reflectors at depths down to 16 km, suggests deep-biting faults at great depths under this section, further supporting an extensional process in exposing this crust.

Oceanic Crust

O Layer 2 of oceanic crust is broken into a series of seaward-dipping, rotated fault blocks by an array of interpreted listric faults. Several of these faults appear to act as master structures, but the crust appears only to be broadly divided into two contrasting domains. These faults also dissect the sheeted dyke layer, gabbro/peridotite layer, and in some cases, apparently offset the Moho.

Domain 1 (SP 2700-900): all reverse polarity crust with strong remanent components; V_p 5100 $m.s^{-1}$.

Density x10^3 kg.m^{-3}	***k SI***	***Q***
2.55	0.04	3
2.55	0.04	2.5
2.55	0.07	3.5
2.55	0.04	3
2.55	0.07	3
2.55	0.07	2.5

Sheeted dykes (P; v_p 6700 $m.s^{-1}$; ρ 2.75 x 10^3 $kg.m^{-3}$) underlying this domain are non- or negligibly magnetic. Gabbro / peridotite layer (Q; ρ 2.75 x 10^3 $kg.m^{-3}$) under this domain is highly altered (?50% serpentinised) but only weakly magnetic (0.01 SI).

Domain 2 (SP 900 to SOL): all normally magnetised blocks, with high remanent and induced components.

Density x10^3 kg.m^{-3}	**SI**	**Q**
2.55	0.04	2
2.55	0.05	2.5
2.55	0.05	3

Sheeted dykes (P) and peridotite layer (Q) underlying this domain have the same properties as Domain 1.

Key findings 228/18:

- Generally different structural style to lines further east.
- More volcanic flows in COT and adjacent continental rift section.
- Pre- to syn-rift section in COT overlies a highly extended zone, and possibly directly overlies altered mantle peridotites, and intruded by mafic rocks, but without onset of seafloor spreading, as to east.

- Lower oceanic crust / peridotite layer and upper mantle extended by deep-biting faults, as to east.
- Evidence of post-seafloor spreading mechanical extension, as to east.

228/21-229/10 - WESTERN WILKES LAND

Model RMS: 5.9

Gravity Field

First-order regional gradient increasing from –300 μm.s^{-2} to –100 μm.s^{-2} seaward.

Major gravity high of *ca* 200 μm.s^{-2} over faulted COT. Two positive excursions of +250 μm.s^{-2} and +80μm.s^{-2} on highly-attenuated continental crust (HACC) approaching COT.

Magnetic Field

Quite flat regional field, approximately –200 nT.

Generally 'saw-tooth' magnetic field response, over both COT and oceanic crust.

MQZ is major negative domain (–100 to –200 nT) over continental crust.

Two third order anomalies of *ca* 100 and 120 nT in COT.

Seafloor spreading anomalies vary between +100 and +400 nT ptp.

Magnetic field parameters (2001.3): B = 55130 nT; I = –72.5°; D = –78°; body susceptibilities in SI units

Model Details (Fig. 84)

A Ooze (v_p = 1800 m.s^{-1}; ρ = 1.76 x 10^3 kg.m^{-3}). Well-laminated and 'sculptured' seismic package, with evidence of erosion of upper surface, slumping/ canyoning, and macroscopic channelling/filling. Thinning seaward.

B Ooze (v_p = 2000 m.s^{-1}; ρ = 1.89 x 10^3 kg.m^{-3}). Roughly-laminated seismic package, thinning seaward, and becoming more laminar. Probably siliceous ooze with some terrigenous sandy input.

C Ooze (v_p = 2400 m.s^{-1} inboard to 2000 m.s^{-1} seaward; ρ = 2.09 x 10^3 kg.m^{-3}). Roughly-laminated seismic package, thinning seaward, and becoming more laminar. Probably siliceous ooze with some terrigenous sandy input.

D Turbidites (v_p = 2700 m.s^{-1}; ρ = 2.20 x 10^3 kg.m^{-3}). Roughly-laminated, discontinuous thick reflective wedge thinning landward. Probably sandy turbidites.

E Turbidites (v_p = 3000-3400 m.s^{-1}; ρ = 2.36 x 10^3 kg.m^{-3}). Roughly-laminated, more continuous reflections wedge thinning and onlapping underlying sequences landward. Probably muddy turbidites.

F Marginal marine sandstones / coal / chalk / mud (v_p = 3600 m.s^{-1}; ρ = 2.40 x 10^3 kg.m^{-3}). Wedge shaped package onlapping underlying sequence landward, and continuing to deposit on oceanic crust seaward. Laminated, slightly noisy, generally high amplitude seismic sequence with many continuous reflections seaward.

G Marginal marine limestone, sandstone, conglomerate, chalk, claystone, coal (v_p = 4000 m.s^{-1}; ρ = 2.43 x 10^3 kg.m^{-3}). Laminated, slightly noisy, generally low amplitude seismic sequence with occasional high amplitude continuous reflections (coal seams?), thinning seaward to COB.

H Terrigeneous rift fill (v_p = 4300 m.s^{-1}; ρ = 2.50 x 10^3 kg.m^{-3}). Very thin package with two high amplitude continuous reflectors. Wedges out laterally landward, thickens into COT ponding against a volcanic build-up. ?Volcaniclastic deposits (eg ignimbrites). Seaward of the volcanic buildup, continuous, high-amplitude reflectors with some diffuse character, wedging out against a palaeo-high in the outer COT. Possible lacustrine and fan-delta deposits.

I Rift volcanics /intrusions (ρ = 2.60 x 10^3 kg.m^{-3}, k = 0.07 SI reversed); Volcanic pile (v_p = 4800 m.s^{-1}; ρ = 2.75 x 10^3 kg.m^{-3}, k = 0.04 SI normal). High-amplitude, discontinuous reflectors in rifted continental crust.

J1 ?Jurassic-Cretaceous. (v_p = 4500 m.s^{-1}; ρ = 2.50 x 10^3 kg.m^{-3}, non-magnetic). Diffuse, low-amplitude reflectors, with occasional higher amplitude continuous bands, cut by seaward-dipping faults.

J2 Intruded ?Jurassic-Cretaceous (ρ = 2.90 x 10^3 kg.m^{-3}, k = 0.03 SI reversed). Strongly laminated fault blocks with high-amplitude reflectors, interpreted as sills in layered sedimentary packages.

J3 Basement peridotite / gabbro ridge (v_p = 5000 m.s^{-1}; ρ = 2.8 x 10^3 kg.m^{-3}, k = 0.04 SI normal). Noisy, diffuse seismic reflection character, with high-amplitude, irregular upper surface, interpreted as basaltic volcanics overlying seismically homogeneous igneous intrusive rocks.

J4 Intruded ?Jurassic-Cretaceous (ρ = 2.60 x 10^3 kg.m^{-3}, k = 0.03 SI reversed). Diffuse, low-amplitude reflectors, with occasional higher amplitude continuous bands, overlain by noisy, high-amplitude, irregular upper reflector, interpreted as basaltic volcanics.

J5 ?Jurassic-Cretaceous (ρ = 2.45 x 10^3 kg.m^{-3}, k = 0 SI normal) rifted sediments

J6 Basement peridotite / gabbro ridge (v_p = 5000 m.s^{-1}; ρ = 2.8 x 10^3 kg.m^{-3}, k = 0.04 SI normal). Noisy, diffuse seismic reflection character, with occasional internal high-amplitude, steeply dipping reflections (dykes?). High-amplitude, irregular upper surface, interpreted as basaltic volcanics overlying intrusive rocks.

K Pre-rift basement (v_p = 6200 m.s^{-1}; ρ = 2.72 x 10^3 kg.m^{-3}; K1 — k = 0.022 SI Q = 2, normal; K2 — k = 0.02 SI, Q = 1, normal). Possible equivalents to Coompana block of onshore South Australia. Noisy, diffuse reflection character, mostly processing artefacts and noise.

L Oceanic crust basalts (v_p = 5000 m.s^{-1}; ρ = 2.55 x 10^3 kg.m^{-3}, k variable). Rugose basement with pinnacle type topography. Noisy, discontinuous, high-amplitude reflection character, sometimes coherently layered suggesting stacked lava flows, often with steep dips. Layered sediments onlap blocks and are rotated, suggesting post-deposition fault movement.

Block	Mag susc. (x 10^{-5} SI)	Polarity	Konigsberger Ratio
A32o?	0.03	R	1.5
A32y?	0.04	N	2
A31o?	0.04	R	1.5
A31y?	0.04	N	2
A30o?	0.05	R	2
A30y?	0.01	N	1
A29o?	0.08	R	4
A29y?	0.01	N	1

N Dolerite dyke swarms (v_p = ?5500 m.s^{-1}; ρ = 2.70 x 10^3 kg.m^{-3}). Noisy seismic character, sometimes with steeply-dipping high-amplitude reflectors that may be dykes.

O Peridotites (v_p = 6500 m.s^{-1}; ρ = 3.00 x 10^3 kg.m^{-3}). Noisy seismic character, sometimes with steeply-dipping, high-amplitude reflectors that may be serpentinised faults as observed in Enderby Land (this report).

Q Altered mantle (v_p = 6500 m.s^{-1}; ρ = 3.10 x 10^3 kg.m^{-3})

Mantle (v_p = ?8000 m.s^{-1}; ρ = 3.30 x 10^3 kg.m^{-3})

Key Findings 228/21-229/10:

- Tapered continental crust similar to line 199/07 on GAB margin.
- Split basement gabbro /peridotite ridge (J3, J6) — an effect of late mechanical separation, or of ridge jumping?
- Altered mantle peridotites (Q) underlie the COT as on other lines

229/06 – TERRE ADÉLIE

Model RMS: 6.9

Gravity Field

Second-order regional, minimum at –400 μm.s^{-1}. Two positive 'shoulder' anomalies of +150 μm.s^{-1} superimposed on this.

Minimum over maximum thickness of sedimentary section.

Magnetic Field

Second-order regional rising from –200 nT over continental crust to ~0 nT over oceanic crust.

Seafloor spreading anomalies vary between +100 and +250 nT ptp.

Spurious anomaly due to drop-out at around SP 7900.

Continental anomalies over sediment ridge up to 200 nT ptp.

Magnetic field parameters (2002.3): B = 66090 nT; I = –88.5°; D = 17; body susceptibilities in SI units.

Model Details (Fig. 93)

A Oozes (v_p = 1900–2100 m.s^{-1} increasing offshore; ρ = A1: 1.89 x 10^3 kg.m^{-3}; A2: 1.82 x 10^3 kg.m^{-3} ; A3: 1.82 x 10^3 kg.m^{-3}; A4: 1.89 x 10^3 kg.m^{-3}). Well-laminated and 'sculptured' seismic package, with evidence of erosion of upper surface, slumping and canyoning, and macro-scale climbing ripples. Thins onto basement high (body F5), then thickens in outer troughs (A2, A3).

B Oozes (v_p = 2300–2200 m.s^{-}1; ρ = B1: 2.04 x 10^3 kg.m^{-3} ; B2: 2.10 x 10^3 kg.m^{-3} ; B3: 2.20 x 10^3 kg.m^{-3} B4: 1.99 x 10^3 kg.m^{-3}; B5: 1.99 x 10^3 kg.m^{-3}; B6: 1.80 x 10^3 kg.m^{-3}; B7: 1.80 x 10^3 kg.m^{-3}). Well-laminated and 'sculptured' seismic package, with more diffuse character inboard. Probably siliceous ooze with some terrigenous sandy input.

C Turbidites? (v_p = 2600 m.s^{-1}; ρ = 2.16 x 10^3 kg.m^{-3}). Roughly-laminated, discontinuous, thick reflective wedge, thinning and downlapping landward, and thinning and onlapping onto basement high (body F5). Thickest extent is in fault-controlled trough near E2. Probably sandy turbidites.

D ?Contourites (v_p = 2500–2800 m.s^{-1}; ρ = 2.05 x 10^3 kg.m^{-3}). Very finely laminated continuous reflectors transgressing basement high (body F5), and cut by normal faults. Thickest extent in fault trough near body E2.

E ?Marginal Marine (chalk, coal, sands etc) (v_p: E1 = 3200 m.s^{-1}; E2 = 3800 m.s^{-1}; E3 = 3600 m.s^{-1}; E4 = 3600 m.s^{-1}; ρ = E1: 2.32 x 10^3 kg.m^{-3}; E2: 2.41 x 10^3 kg.m^{-3}; E3: 2.10 x 10^3 kg.m^{-3}; E4: 2.25 x 10^3 kg.m^{-3}). Inboard, this sequence comprises a seaward thinning, laminated, slightly noisy, generally high-amplitude seismic sequence with many continuous reflections. In the trough E2, the character becomes noisy and diffuse, with some suggestion of steep dips (possible conglomerate?) On the basement high, this unit is cut by many faults which obscure the character, but it appears to be a finely laminated sequence with some high-amplitude events.

F ?Terrigenous rift fill. Laminated, slightly noisy, generally low-amplitude seismic sequence with occasional high-amplitude continuous reflections (coal seams?), cut by many normal faults. Magnetic properties indicate significant volcanic input either as lavas or intrusives within the sequence.

F1: (v_p = 3900 m.s^{-1}; ρ = 2.42 x 10^3 kg.m^{-3}, k = 0.05 SI reversed polarity);

F2: This body is probably a gabbro/peridotite ridge piercing F, as it has substantially different seismic character (noisy, diffuse, with occasional internal high-amplitude, steeply-dipping reflections = dykes?) and properties (v_p = 5700 m.s^{-1}; ρ = 2.680 x 10^3 kg.m^{-3}, k = 0.03 SI reversed polarity);

F3: (v_p = 4000 m.s^{-1}; ρ = 2.43 x 10^3 kg.m^{-3}, k = 0.05 SI reversed polarity);

F4: (v_p = 4000 m.s^{-1}; ρ = 2.43 x 10^3 kg.m^{-3}, k = 0.02 SI reversed polarity);

F5: (v_p = 3500 m.s^{-1}; ρ = 2.38 x 10^3 kg.m^{-3}, k = 0). The non-magnetic character and low velocity indicates that this sequence has no igneous characteristics, and may be part of the sequence E above it.

F6: (v_p = 3600 m.s^{-1}; ρ = 2.09 x 10^3 kg.m^{-3}). Again, the non-magnetic character and low velocity indicates that this sequence has no igneous characteristics, and may be part of C, D, or E);

F7: (v_p = 3600 m.s^{-1}; ρ = 2.30 x 10^3 kg.m^{-3}). Again, the non-magnetic character and low velocity indicates that this sequence has no igneous characteristics, and may be part of E.

G Pre-rift ?Jurassic-Cretaceous: strongly laminated tilt blocks with high-amplitude reflectors – sills in layered sedimentary packages.

G1: (v_p = 4500 m.s^{-1}; ρ = 2.48 x 10^3 kg.m^{-3}, k = 0.06 SI reversed polarity);

G2: (v_p = 5000 m.s^{-1}; ρ = 2.53 x 10^3 kg.m^{-3}, k = 0.04 SI reversed polarity);

G3: (v_p = 5100 m.s^{-1}; ρ = 2.48 x 10^3 kg.m^{-3}, k = 0.06 SI reversed polarity);

G4: (v_p = 5100 m.s^{-1}; ρ = 2.48 x 10^3 kg.m^{-3}, k = 0.03 SI reversed polarity);

G5: (v_p = 5100 m.s^{-1}; ρ = 2.48 x 10^3 kg.m^{-3}, k = 0).

H Pre-rift middle crust. Diffuse, low-amplitude reflectors, with occasional higher amplitude continuous bands, cut by tilt-block faulting inboard, and with pinch-and-swell structuring beneath basement high.

H1: (v_p = 5000 m.s^{-1}; ρ = 2.55 x 10^3 kg.m^{-3});

H2: (v_p = 5000 m.s^{-1}; ρ = 2.60 x 10^3 kg.m^{-3});

H3: ρ(= 2.60 x 10^3 kg.m^{-3}),

I Gabbro/peridotite ridge piercing H: (v_p = 5700 m.s^{-1}; ρ = 2.68, k = 0.035 SI, reversed polarity, Q = 2). Capped by altered ?mafic volcanics (ρ = 2.5 x 10^3 kg.m^{-3}, k = 0.05 SI reversed polarity)

J Lower crystalline crust. Noisy, diffuse reflection character, mostly processing artefacts and noise.

J1: (v_p = ?5800 m.s^{-1}; ρ = 2.95 x 10^3 kg.m^{-3}, k = 0.04 SI reversed polarity);

J2: (v_p = 5800 m.s^{-1}; ρ = 2.85 x 10^3 kg.m^{-3}, k = 0).

K Altered /serpentinised mantle. Very high-amplitude continuous reflectors deep in the crust. (ρ = 3.26 x 10^3 kg.m^{-3}, k = 0.03 SI reversed polarity).

L Mafic intrusions in basement, type 1 (L to R): No real reflection character – if anything, diffuse to transparent zones within more layered sequences.

L1: (ρ = 2.85 x 10^3 kg.m^{-3}, k = 0.04 SI reversed polarity);

L2: (ρ = 2.85 x 10^3 kg.m^{-3}, k = 0.04 SI reversed polarity);

L3: (ρ = 2.85 x 10^3 kg.m^{-3}, k = 0.05 SI reversed polarity).

M Mafic intrusions in basement, type 2 (L to R): No real reflection character – if anything, diffuse to transparent zones within more layered sequences.

M1: (ρ = 2.85 x 10^3 kg.m^{-3}, k = 0.02 SI normal polarity);

M2: (ρ = 2.85 x 10^3 kg.m^{-3}, k = 0.01 SI normal polarity).

N Lower ductile crystalline crust: Intense, thick, very high-amplitude reflection character in lower crust, often with very steep dips, overall pinch-and-swell configuration, varying from <1 km to ~6 km in thickness (v_p = 6600 m.s^{-1}; ρ = 2.87 x 10^3 kg.m^{-3}).

O ?Serpentinite (ρ = 2.67 x 10^3 kg.m^{-3}, k = 0.07 SI).

P Oceanic crust: (v_p = 5000 m.s^{-1}; ρ = 2.50 x 10^3 kg.m^{-3}). Rugose basement with pinnacle type topography. Noisy, discontinuous, high-amplitude reflectors, sometimes coherently layered suggesting stacked lava flows, often with steep dips. Layered sediments onlap blocks and are rotated, indicating post-deposition fault movement.

Block	**Mag susc (x 10^{-5} SI)**	Polarity	**Konigsberger Ratio**
1	0.055	R	2
2	0.03	R	2
3	0.065	R	3
4	0.025	N	2
5	0.03	R	2

Q Dolerite dyke swarms. Noisy seismic character, sometimes with steeply-dipping high-amplitude events which may be dykes (v_p = ?5500 m.s^{-1}; ρ = 2.60 x 10^3 kg.m^{-3}).

R Gabbro-peridotite. Diffuse seismic character, sometimes with steeply-dipping high-amplitude events which may be dykes (v_p = 6700 m.s^{-1}; ρ = 2.70 x 10^3 kg.m^{-3}).

S Volcaniclastic and lava flows of breakup sequence. Distinctive thinly-laminated, high-amplitude sequence with more diffuse base, thinning from topographic

highs (volcanoes?) and ponding into topographic lows at COB (v_p = 3500 m.s^{-1}; ρ = 2.30 x 10^3 kg.m^{-3},

Mantle. Strong high amplitude reflector, probably Moho, interpreted at base of thickened lower ductile crust (6600 m.s^{-1} unit) near COB (v_p = 8200 m.s^{-1}; ρ = 3.30 x 10^3 kg.m^{-3}).

Key Findings 229/06:

- Structurally complex, probably affected by proximity to strike-slip King George V Fracture Zone to the east.
- Basement peridotite /gabbro ridge present in this line (body I).
- Altered, magnetic mantle also present beneath peridotite ridge as in other lines (body K)
- Lower section beneath body G looks very ductile, with major pinch-and-swell structures, and detached blocks (?boudins) in the COT.

228/06 – MAC. ROBERTSON LAND

Gravity Field

Base level of field approximately at 100 $\mu m.s^{-2}$

Order 2 regional field ~200 $\mu m.s^{-2}$ in south, falling to ~100 $\mu m.s^{-2}$ at ~SP 6300, rising to ~ 200 $\mu m.s^{-2}$ at EOL.

Major anomalies, S to N: ~380 $\mu m.s^{-2}$, symmetric, from SP 500–4200; 120 $\mu m.s^{-2}$ asymmetric, 'north verging', SP 4200–6200; 170 $\mu m.s^{-2}$ asymmetric, 'south verging', SP 7000 to EOL.

Magnetic Field

Series of ~100 km spatial wavelength 'continental' anomalies with superimposed high frequency noise from SOL to ~SP 3000; 70 nT ptp.

Series of ~40 km spatial wavelength anomalies with superimposed high-frequency noise from SP 3000–5300; maximum 50 nT ptp.

Pronounced high-amplitude, variable-wavelength seafloor spreading anomalies from SP 5300 to EOL. Half-wavelengths ~25 to ~50 km; 450 nT to 100 nT ptp. Much high-frequency, superimposed noise (average 20 nT ptp); possibly instrumental noise or sferics.

Main field parameters: B = 57 000 nT; I = –68.1°; D = –66.5°. Units in SI.

Model Details (Fig. 103)

Post-rift section

Major negative contribution from this low density section: 1.03–2.40 x 10^3 $kg.m^{-3}$, producing an overall negative free air anomaly of –3000 to –3300 $\mu m.s^{-2}$.

Major gradient due to effect of changing water depth: –600 $\mu m.s^{-2}$ from SOL to ~SP 1100, then a further 1200 $\mu m.s^{-2}$ from SP 1100–6000.

No magnetic signature.

A (v_p 1800 $m.s^{-1}$, ρ 1.89 x 10^3 $kg.m^{-3}$). Sculptured, laminated sedimentary wedge with multiple slump characters, thinning over COT. Probably siliceous ooze

B (v_p 2500 $m.s^{-1}$, ρ 2.05 x 10^3 $kg.m^{-3}$). Laminated sedimentary wedge with multiple slump features, generally consistent thickness across entire section. Probably siliceous ooze and/or glacial drift

C (v_p 2800–3100 $m.s^{-1}$, ρ 2.11 x 10^3 $kg.m^{-3}$). Thick laminated sedimentary wedge, probably siliceous ooze and/or glacial drift

D (v_p 3500 $m.s^{-1}$, ρ 2.23 x 10^3 $kg.m^{-3}$). Layered sequences with 'rough' seismic reflection character, uniform thickness across section. Probably siliciclastic distal turbidite fan sediments.

E (v_p 3500 $m.s^{-1}$, ρ 2.23 x 10^3 $kg.m^{-3}$). Layered sequence with 'rough' seismic reflection character, thins across COB. Probably siliciclastic distal turbidite fan sediments.

F (v_p 4300 m.s^{-1}, ρ 2.40 x 10^3 kg.m^{-3}). Prograding sediment wedge with prominent clinoforms, pinching out onto faulted COT. Probably siliciclastic turbidites

G Sediment wedge: (ρ 2.36 x 10^3 kg.m^{-3}). Well-layered sequence, with some evidence of graben development at southern end, infilling valleys cut into poorly reflective continental basement. Probably terrigenous clastics — gravels, sands conglomerates etc.

Syn-rift section

H–L Fault dominoes of well-layered crust with internal high-amplitude events. Fault sets in the COT dip predominantly seaward (v_p 5000–5500 m.s^{-1}, ρ 2.70 x 10^3 kg.m^{-3}). This layer may represent pre- to syn-rift supracrustal sedimentary rocks intruded by basaltic sills and dykes during initial rifting. A ratio of 60:40 quartzose sediments of density 2.55 x 10^3 kg.m^{-3} intruded by dolerite of density 2.90 x 10^3 kg.m^{-3} could produce this apparent density. In this scenario, the age of this section would probably be Jurassic. Alternatively, this body could represent layered metapelites overlying the older granulite basement, as seen cropping out onshore. Magnetic anomalies of up to 100 nT associated with this body are modelled with bodies of ρ 2.80 x 10^3 kg.m^{-3}, k 0.06 SI; and ρ 2.70 x 10^3 kg.m^{-3}, k 0.07 SI.

Body	ρ x 10^3 kg.m^{-3}	k SI	Q	Polarity
H	2.80	0.03	2	R
I	2.80	0.06	0	N
J	2.80	0.03	2	R
K	2.70	0.04	1.5	R
L	2.78	0.03	2	R

The most seaward of these flows appears to flow back landward from the COB.

Pre-rift section

Major positive contribution from generally higher than crustal average density section: 2.65–3.30 x 10^3 kg.m^{-3}.

Largest effect is due to inferred mantle Moho surface: 2800 μm.s^{-2} rising to 3300 μm.s^{-2} from SOL to ~SP 2500, then buffered between 3170 μm.s^{-2} and 3320 μm.s^{-2} thereafter.

Q Continental lower crust (v_p 6100 m.s^{-1}, ρ 2.80 x 10^3 kg.m^{-3}, k 0-0.03 SI). This dense, 5–6 km thick, areally extensive section is interpreted to comprise continental metamorphic crystalline basement. Likely correlatives include the exposed Napier Complex granulites of onshore Enderby Land, in particular the Mawson Charnockite (Plag-opx-gt ± mt, kfs rock), and charnockites of the Indian Eastern Ghats Province. Data from the Eastern Ghats of India suggest that the charnockites have average densities of 2.78 x 10^3 kg.m^{-3}. Gladczenko & Coffin (2001) also describe a lower crustal layer under the Kerguelen Plateau to the north, comprising a plagioclase rich metamorphic rock, of density 2.80 x 10^3 kg.m^{-3}, and velocities of 6700–7000 m.s^{-1}.

Oceanic Crust

R Seaward-dipping reflector sequences (SDRS; ρ 2.65 x 10^3 kg.m^{-3}) probably comprising spilitised basaltic flows, pillow lavas, and interflow sediments. Comprises eleven blocks with magnetic reversals.

S (ρ 2.70 x 10^3 kg.m^{-3}) comprising sheeted dolerite dykes with negligible magnetic signature, which probably indicates lack of post-intrusive alteration.

T (ρ 2.75 x 10^3 kg.m^{-3}, 0.02 SI) comprising a probable gabbro-peridotite layer. Seismic data show evidence of a set of strong reflectors dipping ~30° S. These are interpreted here as shear zones in a dextral shear system, faulting the peridotite layer into a set of rotated dominoes. If this is the case, hydrothermal fluids either from above or below may have been mobilised through this part of the section, altering reactive olivine to serpentine and magnetite.

U (ρ 2.85 x 10^3 kg.m^{-3}, k 0.02 SI). This layer is modelled beneath the Moho interpreted in the seismic data, and may consist of possibly sheared & altered layer, or alternatively a basaltic /gabbroic underplate. The former is considered more likely if the reflectors in the overlying layer are in fact fluid-permeable shear-zones allowing ingress of alteration fluids into the deeper crust. However, the latter option cannot be ruled out, as this profile lies in the margin sector that was adjacent to areas of crust impacted by the Kerguelen plume, which formed a LIP (Borissova et al., 2002; Charvis & Operto, 1999). Gladczenko & Coffin (2001) report evidence from the Kerguelen Plateau of extensive areas of high lower crustal density (3.10 x 10^3 kg.m^{-3}) and high velocity (7200-7500 m.s^{-1})

The unaltered oceanic mantle has been ascribed a standard density of 3.30 x 10^3 kg.m^{-3}. Moho has significant relief (up to 1 km), caused by what appear to be low angle (~10°) seaward-dipping detachments. These give rise to substantial amplitude (100 μm.s^{-2}) asymmetric gravity anomalies.

Revisions to 228/06

In light of the modelling of lines 229/30, 229/31 and 229/35 in the Enderby Basin, the model for 228/06 was revised to make it more consistent with the geological parameters of the models along strike (Fig. 104).

RMS = 5.4

The main changes were as follows:

- Removal of the dense ‘underplate’ between the Moho and the gabbro peridotite layer under the oceanic crust.
- Addition of a body with a density of 2.90 x 10^3 kg.m^{-3}, probably gabbro / gabbronorite, which may represent a fossil magma chamber. The size and geometry of this feature may indicate a fossil spreading centre.
- To keep the model in isostatic balance, the level of the Moho under the ocean crust was raised from ~18 km to ~16 km.

A second revision of the model was produced that more accurately incorporated new picks of seafloor spreading magnetic anomalies (Brown, unpublished data; Fig. 54).

RMS =10.1

The properties of the revised oceanic basaltic layer are as follows:

Anomaly ID	ρ x 10^3 kg.m^{-3}	k SI	Q	Polarity
M10N	2.53	0.1	2.5	N
M10o	2.53	0.001	0.1	R
M10y	2.53	0.08	3	N
M9o	2.53	0.002	1	R
M9y	2.55	0.02	2	N
M8o	2.53	0.08	6	R
M8y	2.53	0.04	2	N
M7o	2.53	0.04	3	R
M7y	2.53	0.07	2	N
M6o	2.53	0.02	4	R
M6y	2.53	0.04	2	N
M5	2.53	0.001	0.1	R
M4	2.53	0.12	3	N

With the exception of the block used for the M5 reversal, most of the other blocks fit quite well. M10N is the first anomaly in the Hauterivian, matching well the break-up age for India and Australia/Antarctica established in the Perth Basin and along the WA margin (e.g. Borissova et al., 2002).

Key findings 228/06:

- The pre-rift section is likely to be partially covered by early rift to syn-rift basaltic flows, and intruded by mafic magmatic rocks
- Proterozoic Mawson Charnockite equivalents probably extend through most of the lower crust to the COB.
- The COB is a steep landward-dipping contact.
- Oceanic crust looks like normal spreading, with little evidence of mechanical extension in Layer 2 (*cf.* Wilkes Land).
- Anomalies from M10N (Hauterivian) to M4 (Hauterivian-Barremian) have been modelled, matching established break-up and seafloor spreading ages in other parts of the rifted India-Australia/Antarctica margin system.
- Oceanic Layer 3 (peridotite) is faulted and thinned.
- A fossil gabbroic body exists at the top of the mantle, which may be an extinct spreading centre / magma chamber system.

228/01 – ENDERBY LAND

Gravity Field

Base level of field approximately at 8 $\mu m.s^{-2}$

Essentially flat regional field; minor, higher frequency (20 km ptp) lows due to canyons in the seabed.

Major anomalies: ~250 $\mu m.s^{-2}$ SP 9000–11000; broad major 350 $\mu m.s^{-2}$ peak SP 3000–9000; +230 $\mu m.s^{-2}$ peak over a topographic (?volcanic) buildup at SP 500–1000.

Magnetic Field

Base level of field –75nT; inadequate removal of IGRF?

Main field parameters: B = 42570 nT; I = -63.5^{o}; D = -52.5^{o}. Units in SI.

Model Details (Fig. 53)

Post-rift section

Major negative contribution from this low-density section: 1.03–2.34 x 10^3 $kg.m^{-3}$, producing an overall negative free air anomaly of –280 to –380 $\mu m.s^{-2}$.

Gradient due to effect of bathymetry / changing water depth: –1000 $\mu m.s^{-2}$ over almost the entire line. Higher frequency effects due to channelling and buildups.

No magnetic signature.

A (v_p 1800 $m.s^{-1}$, ρ 1.76 x 10^3 $kg.m^{-3}$). Sculptured, laminated sedimentary wedge with multiple slump characters. Eroded /channelled through in places. Probably siliceous ooze

B (v_p 2200 $m.s^{-1}$, ρ 1.99 x 10^3 $kg.m^{-3}$). Laminated sedimentary wedge with multiple slump features, generally consistent thickness across entire section. Eroded /channelled through in places. Probably siliceous ooze and/or glacial drift

C (v_p 2500 $m.s^{-1}$, ρ 2.13 x 10^3 $kg.m^{-3}$). Layered sequence with 'rough' seismic reflection character, thinning seaward across section. Probably siliciclastic distal turbidite fan sediments.

D (v_p 3300 $m.s^{-1}$, ρ 2.34 x 10^3 $kg.m^{-3}$). Layered wedge with alternating high amplitude laminations and 'rough' seismic reflection character, thinning radically along section. Probably mixed siliciclastic distal turbidite fan sediments.

Syn-rift section

General landward negative gradient of –3200 $\mu m.s^{-2}$.

E (v_p 4000 $m.s^{-1}$, ρ 2.45 x 10^3 $kg.m^{-3}$). Prograding sediment wedge with low-frequency laminations. Possible marine / marginal marine rift fill, overlying rough, (faulted) basement surface.

Pre-rift section

Major positive contribution from generally higher than crustal average density section: 2.65–3.30 x 10^3 kg.m^{-3}.

Largest effect is due to inferred mantle Moho surface: 2600 μm.s^{-2} rising to 3750 μm.s-2 from EOL to SP 6000, then around 3700 μm.s^{-2} thereafter. Regional (Vening-Meinesz-type) isostatic compensation of seafloor topography depresses Moho response to ~3450 μm.s^{-2} from ~SP 1600 to SOL.

F (v_p ?6100 m.s^{-1}, ρ 2.77 x 10^3 kg.m^{-3}, k – 0.02–0.08 SI). This dense, ~2 km thick, faulted section is believed to represent continental metamorphic crystalline basement. Likely correlatives include the exposed Napier Complex granulites as described for line 228/06.

G (ρ 2.85 x 10^3 kg.m^{-3}, k – 0.01 SI). This dense, ~5.5-2 km thick section is necked and thinned, and is also interpreted to represent continental metamorphic crystalline basement. No equivalent crust to this section, in either density or structure, is found in line 228/06 to the east. This crust may be equivalent to the Archaean layered gt-qz-fsp gneisses and metasediments of the Napier Complex described by Tingey (1991). Rocks of this age and type that are exposed in the Gawler Craton of South Australia have densities in the range 2.75–2.98 x 10^3 kg.m^{-3}. The observation of a thinner charnockitic layer and thicker lower crustal layer is consistent with Tingey's (1991) observation that deeper levels of the Napier Complex are exposed onshore and in Casey Bay to the southwest.

H (H1: 2.65 x 10^3 kg.m^{-3}, 0.04 SI; H2: 2.75 x 10^3 kg.m^{-3}, 0.05 SI). These more magnetic domains sit within a structurally high, seismically transparent part of the lower crust adjacent landward of the COB. They are interpreted as domains of intrusion or hybridisation of the charnockitic crust. Alternatively, they may represent heterogeneous or altered domains of the charnockite near the locus of breakup.

Oceanic Crust

Ocean crust on this line, in contrast to Line 228/06, and the Wilkes Land lines, has a noticeable landward dip, and an absence of faulting. It is possible that this geometry represents the response of rigid crust bowed down under the load of overlapping and onlapping siliciclastic sediments. The difference with line 228/06 can be seen in the elevation of the upper surface of layer 2, which varies from ~9.5 km at the COB to 7.5 km over 220 km, a landwards dip of ~0.5°.

I (v_p 5200-5400 m.s^{-1}, ρ 2.50–2.65 x 10^3 kg.m^{-3}) probably representing spilitised basaltic flows, pillow lavas, and interflow sediments. Ten blocks with magnetic reversals are modelled:

Block	ρ	k SI	Polarity	Q	D	I
1	2.55	0.07	N	1.6	–63.5	–52.5
2	2.65	0.008	N	1	–63.5	–52.5
3	2.65	0.03	N	1	–63.5	–52.5
4	2.55	0.06	R	2	63.5	–52.5
5	2.60	0.04	R	2	63.5	–52.5
6	2.55	0.07	R	3	63.5	–52.5
7	2.50	0.06	N	2	–63.5	–52.5
8	2.58	0.04	R	1.8	63.5	–52.5
9	2.55	0.08	N	3	–63.5	–52.5
10	2.55	0.04	R	1.5	63.5	–52.5

A zone of misfit between blocks 3 (N) and 4 (R) is very difficult to model, due to the oblique intersection of the seismic transect with a broad NNE-trending linear feature around SP 6000. This feature, corresponding to the transition between two blocks of apparently opposite magnetic polarity may reflect an oceanic fracture zone. This interpretation is also supported by the presence of a very steep-walled basin faulted into the oceanic basement at this position. This zone also corresponds to a zone of elevated mantle topography and possibly a sheared peridotite layer (see below).

J (v_p 6400 m.s^{-1}, ρ 2.70 x 10^3 kg.m^{-3}) represents sheeted dolerite dykes; negligible magnetic signature, probably indicating lack of post-intrusive alteration.

K (ρ 3.00 x 10^3 kg.m^{-3}, 0.01 SI) probable gabbro-peridotite layer. This layer displays significant basal topography, reflecting possible limited through-going shears (280-320 km) and isostatic compensation of seafloor topography (530-580 km).

The unaltered oceanic mantle has been assigned a standard density of 3.30 x 10^3 kg.m^{-3} (no velocity information is available for this layer). The Moho surface has significant relief (up to 1 km) near the COB, in the ?sheared zone from SP 5000–6500, and from SP 100–1000, where there is major seafloor topography.

Revisions to 228/01:

In the light of the new magnetic picks of the seafloor spreading anomalies (B.J. Brown, unpublished data), the model for 228/01 was revised to more closely match the new seafloor spreading interpretation. Figure 53 incorporates these revisions.

RMS = 7.7

The properties of the revised oceanic basaltic layer are as follows:

Anomaly ID	*ρ x 10^3 kg.m^{-3}*	*k SI*	*Q*	*Polarity*
M10o	2.55	0.04	2	R
M10y	2.55	0.03	2	N
M9o	2.55	0.001	1	R
M9y	2.55	0.055	3	N
M8o	2.55	0.001	1	R
M8y	2.55	0.05	2	N
M7o	2.55	0.01	1	R
M7y-6y composite	2.65	0.05	1.6	N
M5	2.68	0.04	2	R
M4	2.65	0.02	1	N
M3	2.75	0.06	4	R
M2	2.55	0.001	1	N
M1	2.55	0.001	1	N
M2 mirror	2.55	0.001	1	N
M3 mirror	2.55	0.09	3	R
M4 mirror	2.50	0.06	2	N
M5 mirror	2.55	0.001	1	R
M6o-M9 composite mirror	2.58	0.04	1.8	N
M10y-M10N mirror	2.55	0.08	3	R

Key findings 228/01:

- Similar thickness of post-rift sedimentary section to line 228/06;
- Thinner section of potential orthogneissic (charnockite) Napier Complex basement.
- Presence of a thinned lower crustal wedge, probably comprising Archaean Napier complex paragneisses.
- Limited amount of intrusion around the COB.
- COB magnetic anomaly less pronounced than on 228/06 (225 nT vs 460 nT)
- Initiation of seafloor spreading during M10 time (Hauterivian).
- Apparent evidence for a fossil spreading centre, marked by mirroring of seafloor spreading anomalies about M1 (121 Ma; Barremian-Aptian).
- Apparent loading of the rigid oceanic crust producing downwarping to landward.

- Relatively low relief Moho. Exceptions include adjacent to the COB, in the oblique zone of shearing (SP 5000–6500), and under a major topographic high (SOL to SP 1000).
- Evidence for regional Vening-Meinesz-type rigid downwarping isostatic responses to support loading of the ocean floor by major volcanic buildups.

229/30 – OFFSHORE PRYDZ BAY

RMS: 6.8

Gravity Field

Base level of field approximately at 50 $\mu m.s^{-2}$

Second-order regional field ~70 $\mu m.s^{-2}$ in south, falling to ~45 $\mu m.s^{-2}$ at SP 6000, rising to ~140 $\mu m.s^{-2}$ at northern end of line.

Major anomalies, S to N: ~–70 $\mu m.s^{-2}$ asymmetric, from SP 7200–5600 in COT; 130 $\mu m.s^{-2}$ ptp symmetric, from SP 5600–3100; 125 $\mu m.s^{-2}$ ptp asymmetric, 'north verging', SP 3100–1200.

Magnetic Field

Base level of field ~0 nT

Series of ~80 km spatial wavelength 'continental' anomalies with superimposed high-frequency noise from EOL to SP 4700; 75 nT ptp.

Pronounced high-amplitude, variable-wavelength seafloor spreading anomalies from SP 4400 to SOL; half-wavelengths ~25 to ~40 km, 40 nT to 200 nT ptp. Much high-frequency superimposed noise (average 20 nT ptp): possibly instrumental noise or sferics, including possible storm activity (e.g. around SP 3500).

Main field parameters: B = 51 400 nT; I = –69.7°; D = –68.5°. Units in SI.

Model Details (Fig. 55)

A (v_p 1900 $m.s^{-1}$, ρ 1.82 x 10^3 $kg.m^{-3}$). Sculptured, laminated sedimentary wedge with multiple slump characters, thinning over COT. Probable siliceous ooze.

B (v_p 2600 $m.s^{-1}$, ρ 2.16 x 10^3 $kg.m^{-3}$). Laminated sedimentary wedge with multiple slump characters, thinning onto oceanic crust. Probable siliceous ooze and/or glacial drift

C (v_p 3100 $m.s^{-1}$, ρ 2.30 x 10^3 $kg.m^{-3}$). Layered sequences with some 'rough' seismic reflection character, uniform thickness across section, but tending to wedge out landward. Probable siliciclastic turbidite fan sediments.

D (v_p 3800 $m.s^{-1}$, ρ 2.41 x 10^3 $kg.m^{-3}$). Layered sequence with 'rough' seismic reflection character, thins across COB and to seaward. Probable siliciclastic distal turbidite fan sediments.

E (v_p 4200 $m.s^{-1}$, ρ 2.45 x 10^3 $kg.m^{-3}$). Prograding, laminated sediment wedge with some diffuse seismic character, pinching out onto faulted COT. Probably siliciclastic marginal marine sediments

F (v_p 4400 $m.s^{-1}$, ρ 2.47 x 10^3 $kg.m^{-3}$). Prograding, well-laminated sediment wedge, with high amplitude responses, pinching out onto faulted COT. Probable siliciclastic marginal marine sediments, chalks, coal, marls etc.

G (v_p 4700 $m.s^{-1}$, ρ 2.45 & 2.49 x 10^3 $kg.m^{-3}$). Layered sequence, with some evidence for graben development at southern end, infilling valleys cut into poorly reflective continental basement. Probably terrigenous clastics –gravels, sands

conglomerates etc. k = 0.04 SI reversed, indicating some ?mafic volcanic detritus or lavas.

H (v_p 5600 m.s^{-1}, ρ = 2.90×10^3 kg.m^{-3}; k = 0.008 SI normal polarity). Metamorphic basement with noisy, diffuse seismic character. Onshore there is an exposed gneissic basement of mixed marbles, calc-silicates, mafic orthoamphibolites, and garnet bearing gneisses (Tingey, 1991, pp 31–36) that would produce a response consistent with these properties.

I Mafic intrusions, rift volcanics or magnetic amphibolites within metamorphic basement (v_p 5000 m.s^{-1}, ρ = 2.90×10^3 kg.m^{-3}); I1: k = 0.05 SI reversed; I:2 k = 0.05 SI reversed; I3: k = 0.07 SI reversed; I4: k = 0.05 SI reversed; I5: k = 0.04 SI reversed; I6: k = 0.04 SI reversed.

J Ocean crust (v_p = 4900 m.s^{-1}; ρ = 2.45-2.80 x 10^3 kg.m^{-3}). Rugose basement with pinnacle type topography. Noisy, discontinuous, high amplitude reflection character, sometimes coherently layered suggesting stacked lava flows, often with steep dips.

Anomaly ID	ρ x 10^3 kg.m^{-3}	k SI	Q	Polarity
M10No	2.65	0.03	1.4	R
M10Ny	2.75	0.02	1.5	N
M10y	2.80	0.045	2	N
M9o	2.65	0.03	2	R
M9yb	2.45	0.055	2	N
M9ya	2.45	0.03	1	N
M8o	2.45	0.04	1.3	R
M8y	2.55	0.006	1	N
M7o	2.65	0.06	2	R
M7y	2.68	0.006	1	N
M6o	2.55	0.03	2	R
M6y	2.55	0.055	2	N
M5	2.55	0.005	1	R
M4	2.48	0.06	2	N
M3	2.55	0.03	1.2	R

K Dolerite dyke swarms ρ = 2.85 x 10^3 kg.m^{-3}. k = 0 SI.

L Faulted peridotites: ρ L1 = 2.96 x 10^3 kg.m^{-3}; L2 = ρ 2.95 x 10^3 kg.m^{-3}; L3 = ρ 2.75 x 10^3 kg.m^{-3} k = 0.05 SI; Q= 1.5 normal polarity; L4 = ρ 2.80 x 10^3 kg.m^{-3}. Variation possibly due to degree of alteration/serpentinisation of peridotites related to faulting and ingress of hydrothermal fluids.

Mantle (v_p 8400 $m.s^{-1}$, $\rho = 3.40 \times 10^3$ $kg.m^{-3}$). The mantle under this section has a higher velocity (and thus density) then 'normal' (i.e. compared to other sections e.g. Wilkes Land). The Moho under oceanic crust appears in places as a broken, high amplitude reflector with up to 2 km of relief, indicative of tectonic complexity.

Key Findings 229/30:

- Thicker section of post-rift sedimentary section compared to line 228/06 to the east, possibly due to the proximity of the Lambert Graben / Prydz Bay depocentre on this line.
- Equivalent orthogneissic (charnockite) Napier Complex basement as on 228/06.
- Presence of a thinned lower crustal wedge, probably Archaean Napier complex paragneisses.
- Limited intrusion at COB.
- COB magnetic anomaly is a magnetic low, due to remanently magnetised intrusions in the basement adjacent to the COB.
- Initiation of seafloor spreading during M10 (Hauterivian).
- No evidence mirroring of seafloor spreading anomalies about M1 (121 Ma; Barremian-Aptian) on this line (*cf* line 228/06).
- Apparent loading of the rigid oceanic crust producing downwarping to landward.
- Oceanic crust is split into fault-bounded segments with differing seismic reflection characteristics, domino faulted lower crust, velocity and density profiles.
- Relatively low relief Moho. Exceptions occur at the COB, and under relatively low density segments of ocean floor.
- Moho velocity is high, and mantle has a higher density than 228/06. This may be related to igneous underplating during formation of the Lambert Graben in the Palaeozoic.

229/31 – OFFSHORE PRYDZ BAY

RMS = 11.6

Gravity Field

Base level of field approximately at 50 – 180 μm.s^{-2}

Order 2 regional field ~50 μm.s^{-2} in south, rising to ~220 μm.s^{-2}, falling to ~180 μm.s^{-2} at northern end of line.

Major anomalies, S to N: ~–100 μm.s^{-2} asymmetric, from SP 500–3300 over continental crust; ~200 μm.s^{-2} ptp asymmetric, twin peak, SP 3300–6000; –160 μm.s^{-2} ptp symmetric, SP 6500–9000.

Magnetic Field

Base level of field ~0 nT

Series of ~60 km spatial wavelength, 'continental' anomalies with superimposed high frequency noise from SP 100–5500; 75 nT ptp.

Pronounced high-amplitude, variable-wavelength seafloor anomalies from SP ~5500 to the EOL. Half-wavelengths ~15 to ~30 km, 20 nT to 100 nT ptp. Much high-frequency superimposed noise (average 20 nT ptp): possibly instrumental noise or sferics, including possible storm activity e.g. SP 7300–8000.

Main field parameters: B = 50 450 nT; I = –68.9°; D = –68.0°; SI units.

Model Details (Fig. 56)

This line has a ~50° course change at around SP 4900. This causes some irresolvable 3-dimensional effects in the model, from around SP 4200–6200, due to the interference of the 3-D bodies in the models having non-parallel strikes, and long strike lengths (300 km).

A (v_p 1900 m.s^{-1}, ρ 1.82 x 10^3 kg.m^{-3}). Sculptured, laminated sedimentary wedge with multiple slump and climbing ripple characters, thinning onto oceanic crust. Probable siliceous ooze.

B (v_p 2350 m.s^{-1}, ρ 2.16 x 10^3 kg.m^{-3}). Laminated sedimentary wedge with slump and climbing ripple characters, thinning onto oceanic crust. Occasional diffuse character, especially in lower part. Probable siliceous ooze and/or glacial drift.

C (v_p 3400–3000 m.s^{-1}, ρ 2.30 x 10^3 kg.m^{-3}). Well-layered sequences with some 'rough' seismic reflection character, uniform thickness across section, but tending to wedge out seaward. Probable siliciclastic distal turbidite fan sediments.

D (v_p 4400–3700 m.s^{-1}, ρ 2.41 x 10^3 kg.m^{-3}). Layered sequence with 'rough' seismic reflection character, thins across COB and to seaward. Probable siliciclastic distal turbidite fan sediments.

E (v_p 4700 m.s^{-1}, ρ 2.45 x 10^3 kg.m^{-3}). Prograding, roughly laminated sediment wedge with diffuse seismic character, wedging out onto faulted oceanic crust, and becoming more laminated on oceanic crust. Probable siliciclastic marginal marine sediments.

F (v_p 5000 m.s^{-1}, ρ 2.47 x 10^3 kg.m^{-3}). Prograding, well-laminated sediment wedge, with high amplitude responses, pinching out onto faulted COT / ocean crust. Probable siliciclastic marginal marine sediments, chalks, coal, marls etc.

G (v_p 5100 m.s^{-1}, ρ 2.49 & 2.80 x 10^3 kg.m^{-3}). Layered sequence, with some evidence for half-graben development at southern end, infilling valleys cut into poorly reflective continental basement. Probable terrigenous clastics –gravels, sands conglomerates etc. High k = 0.06 SI normal, Q =2, probably indicating some ?mafic volcanic detritus or lavas.

H Mafic intrusions, rift volcanics, or magnetic amphibolites within metamorphic basement (v_p 5200 m.s^{-1}, $\rho = 2.90 \times 10^3$ kg.m^{-3}); H1: k = 0.04 SI reversed, Q = 4; H2: $\rho = 2.87 \times 10^3$ kg.m^{-3} k = 0.05 SI reversed Q = 3; H3: k = 0.02 SI reversed Q = 4; H4: k = 0.05 SI reversed Q = 4; H5: k = 0.06 SI reversed Q = 4; H6: k = 0.03 SI reversed Q = 3; H7: k = 0.02 SI reversed Q = 4.

I Metamorphic basement with noisy, diffuse seismic character ($\rho = 2.90 \times 10^3$ kg.m^{-3}; I1: k = 0.02 SI normal polarity Q = 1; I2: k = 0.015 SI normal polarity Q = 1; I3: k = 0.01 SI normal polarity Q = 1; I4: k = 0.007 SI, normal polarity Q = 1). Again, an exposed onshore gneissic basement of mixed marbles, calc-silicates, mafic orthoamphibolites, and garnet-bearing gneisses (Tingey, 1991, pp 31-36) would produce a response consistent with these properties.

J Ocean crust (v_p = 5000 m.s^{-1}). Rugose basement with subdued topography, and apparently shallowing oceanwards. Noisy, discontinuous, high-amplitude reflection character, sometimes coherently layered, suggesting stacked lava flows, often with steep oceanward dips. Several 'panels' of ocean crust from SP 7950–8650 appear to be very planar with twin, continuous top reflectors.

Anomaly ID	ρ x 10^3 kg.m^{-3}	k SI	Q	Polarity
M10Ny	2.45	0.045	1.3	N
M10o	2.50	0.001	1	R
M10y	2.53	0.03	1.2	N
M9o	2.50	0.06	2	R
M9y-M7o composite	2.45	0.05	2	N
M7y	2.68	0.006	1	N
M6o	2.55	0.038	2	R
M6y	2.55	0.02	2	N
M5	2.55	0.02	1.2	R
M4o	2.55	0.03	2	N
M4y	2.65	0.01	1	N
M3	2.55	0.03	2	R

K Dolerite dyke swarms ($\rho = 2.75 \times 10^3$ kg.m^{-3}. k = 0 SI).

L Faulted peridotites: (ρ L1 = 2.94 x 10^3 kg.m^{-3} k = 0 SI; L2 = ρ 2.80×10^3 kg.m^{-3}; k = 0 SI). Variation possibly due to degree of alteration of peridotites related to faulting and ingress of hydrothermal fluids.

Mantle (v_p 8400 m.s^{-1}, ρ = 3.40×10^3 kg.m^{-3}). The mantle under this section, as in line 229/30, has a higher P wave velocity (and thus density) then 'normal' (i.e. compared to other sections e.g. Wilkes Land margin). The Moho under oceanic crust appears in places as a semi-continuous, high-amplitude reflector with up to 6.5 km of relief, indicative of tectonic complexity.

Key Findings 229/31:

- Thicker section of post-rift sedimentary section compared to line 228/06, and similar to that on 229/30, probably due to proximity to Lambert Graben / Prydz Bay depocentres.
- Equivalent orthogneissic (charnockite) Napier Complex basement as on lines 228/06 and 229/30.
- Presence of a thinned lower crustal wedge, probably Archaean Napier complex paragneisses.
- Limited intrusion at COB.
- COB magnetic anomaly is positive, due to the magnetic edge effect of strong normally magnetised ocean crust abutting weakly magnetised continental crust.
- Initiation of seafloor spreading during M10 (Hauterivian).
- No evidence of mirroring of seafloor spreading anomalies about M1 (121 Ma; Barremian-Aptian) on this line.
- Apparent loading of the rigid oceanic crust producing downwarping to landward.
- Oceanic crust is split into fault-bounded segments with differing seismic reflection characteristics, velocity and density profiles.
- The inner oceanic crustal segment appears not to contain the distinctive domino-faulting of the gabbro/peridotite layer of the outer panel. This may reflect changes in spreading rate with time.
- Relatively low-relief Moho. Exceptions to this are at the COB, and under relatively low density segments of ocean floor.
- As with line 229/30, the Moho velocity is high, and mantle has a higher density than 228/06. This may be related to igneous underplating during formation of the Lambert Graben in the Palaeozoic.

229/35 – WESTERN ENDERBY LAND

RMS: 5.6

Gravity Field

Base level of field approximately at 200 $\mu m.s^{-2}$

Order 2 regional field ~0 $\mu m.s^{-2}$ in south, rising to ~250 $\mu m.s^{-2}$ at SP 5000, falling to ~200 $\mu m.s^{-2}$ at the northern end of the line.

Three major highs of up to 200 $\mu m.s^{-2}$ ptp, from SP 500–3600 over continental crust; major negative excursion of ~ –420 $\mu m.s^{-2}$ ptp, SOL to SP 500; long-wavelength highs and lows of up to 90 $\mu m.s^{-2}$ ptp characterise the oceanic crust.

Magnetic Field

Base level of field ~ 0 nT

Series of ~120 km spatial wavelength 'continental' anomalies with superimposed high frequency noise from SOL to SP 3600; 600 and 200 nT ptp.

Pronounced high-amplitude, variable-wavelength seafloor spreading anomalies from SP 3600 to EOL; half-wavelengths ~30 to ~60 km, 30 nT to 260 nT ptp. Much high-frequency superimposed noise (average 20 nT ptp): possibly instrumental noise or sferics.

Main field parameters: B = 41 800 nT; I = –63.0°; D = –49.9°; SI units.

Model Details (Fig. 52)

A (v_p 1900 $m.s^{-1}$, ρ 1.89 x 10^3 $kg.m^{-3}$). Sculptured, laminated sedimentary wedge with multiple slump and climbing ripple characters, thickest at COB. Probable siliceous ooze.

B (v_p 1900 $m.s^{-1}$, ρ 2.09 x 10^3 $kg.m^{-3}$). Laminated sedimentary wedge with diffuse character, thinning onto oceanic crust. Probable siliceous ooze and/or glacial drift.

C (v_p 2800 $m.s^{-1}$, ρ 2.23 x 10^3 $kg.m^{-3}$). Well-layered sequences with some 'rough' seismic reflection character, thickened at COB section, but tending to wedge out seaward. Probable siliciclastic distal turbidite fan sediments.

D (v_p 2400 $m.s^{-1}$, ρ 2.30 x 10^3 $kg.m^{-3}$). More layered, high-amplitude sequence than C, with diffuse seismic reflection character. Offshore equivalents are half-graben fill on oceanic crust with strongly laminated character. Probable siliciclastic distal turbidite fan sediments.

E (E1: v_p 3600 $m.s^{-1}$, ρ 2.45 x 10^3 $kg.m^{-3}$; E2: v_p 3100 $m.s^{-1}$, ρ 2.30 x 10^3 $kg.m^{-3}$). Prograding, roughly laminated sediment wedge with diffuse seismic character, wedging out onto faulted oceanic crust, and becoming more laminated on oceanic crust. Probable siliciclastic marginal marine sediments.

F (F1: v_p 4500 $m.s^{-1}$, ρ 2.77 x 10^3 $kg.m^{-3}$; F2: v_p 5000 $m.s^{-1}$, ρ 2.77 x 10^3 $kg.m^{-3}$). Tilted fault blocks with some internal stratiform character marked by faint high-amplitude parallel reflectors, cut by normal faults; often diffuse. Adjacent to COB, G2 shows half-graben development on seaward dipping normal faults.

G (v_p 5500 m.s^{-1}, ρ 2.80 x 10^3 kg.m^{-3}; G1 k = 0.03 SI normal Q = 1; G2 k = 0.02 SI normal Q = 1.2). Noisy basement sequence, with some evidence for large, steeply dipping, reflective structures from SP 350-850. Probable metamorphic basement.

H Metamorphic basement with noisy, diffuse seismic character (grey, ρ = 2.80 x 10^3 kg.m^{-3}; k = 0.02 SI reverse polarity Q = 2. Possibly a Palaeozoic or Proterozoic infrabasin, as exposed on the conjugate east Indian margin e.g. Cuddapah Basin which has a reported density of up to 2.81 (Geol. Surv. India, unpublished data).

I Ocean crust (v_p = 5000 m.s^{-1}). Rugose basement with subdued topography, and apparently shallowing to N. Noisy, discontinuous, high-amplitude reflection character, sometimes coherently layered suggesting stacked lava flows, often with steep oceanward dips. Several 'panels' of ocean crust from SP 7950–8650 appear to be very planar with twinned, continuous reflectors.

Anomaly ID	ρ x 10^3 kg.m^{-3}	k SI	Q	Polarity
M10o	2.55	0.03	1.6	R
M10y	2.55	0.03	1	N
M9o	2.55	0.03	1.6	R
M9y-M6y composite	2.55	0.02	1	N
M5	2.55	0.005	0.5	R
M4	2.55	0.04	1.8	N
M3	2.55	0.03	2	R
M2	2.55	0.02	2	N
M1o	2.55	0.02	1.4	R
M2 mirror	2.55	0.02	1.6	N
M3 mirror	2.55	0.03	2	R
M4 mirror	2.55	0.05	2	N
M5 mirror	2.55	0.005	0.5	R
M6y mirror	2.55	0.04	2	**N**

J Dolerite dyke swarms (v_p = 6700 m.s^{-1}, ρ = 2.75 x 10^3 kg.m^{-3}. k = 0 SI).

K Oceanic peridotites (ρ = 2.85 x 10^3 kg.m^{-3}, k = 0 SI).

Mantle (v_p 7800 m.s^{-1}, ρ = 3.30 x 10^3 kg.m^{-3}).

Key Findings 229/35:

- Thinner post-rift sedimentary section than lines 229/30 and 31, to the east.
- Basement rocks are unlike those modelled to the east on lines 228/01 & 228/06. The basement rocks on this line may be Archaean or Proterozoic shield rocks,

possibly gneisses and schists, similar to those exposed in the Eastern Ghats or Dharwar Craton of conjugate India.

- The denser basement appear to be rifted by a Palaeo- or Proterozoic infrabasin, similar to those exposed on the conjugate east Indian coast (eg Cuddapah Basin).
- The COB is not marked by a positive magnetic anomaly, but by a magnetic low. This is due to an edge effect of non-magnetic supracrustal rocks in contact with lower magnetisation, negative polarity seafloor crust.
- Initiation of seafloor spreading was during M10 (Hauterivian), consistent with sectors in the Enderby Basin to the east.
- Some evidence for mirroring of seafloor spreading anomalies about M1 (121 Ma; Barremian-Aptian) on this line, suggesting a spreading ridge jump in this sector.
- Apparent loading of the rigid oceanic crust producing downwarping to landward.

228/12-229/22-229/23 – SHACKLETON BASIN

RMS = 5.6

Gravity Field

Base level of field approximately at –170 μm.s^{-2}

Second-order regional field ~30 μm.s^{-2} in south, falling to ~–170 μm.s^{-2} at SP 1400/line 229/22, rising to ~ –10 μm.s^{-2} in north (SOL/line 229/23).

Highs and lows of up to 60 μm.s^{-2} ptp and 160 km half-wavelength superimposed on regional trend

Magnetic Field

Base level of field ~40 nT

Pronounced high-amplitude, variable-wavelength seafloor spreading anomalies along entire line. Half-wavelengths ~30 to ~60 km, 60 nT to 600 nT ptp. Occasional high-frequency superimposed noise (~20 nT ptp): possibly instrumental noise or sferics (eg SP 1600–2000/line 229/23).

Main field parameters: B = 66550 nT; I = –87.2°; D = –75.9°; SI units.

Model Details (Fig. 66)

A (v_p 1800 m.s^{-1}, ρ 1.76 x 10^3 kg.m^{-3}). Sculptured, laminated sedimentary wedge with multiple slump and climbing ripple characters. Probable siliceous ooze.

B (v_p 2200 m.s^{-1}, ρ 1.99 x 10^3 kg.m^{-3}). Laminated sedimentary wedge offshore with diffuse character inshore. Probable siliceous ooze and/or glacial drift.

C (v_p 2500-2800 m.s^{-1}, ρ 2.13 x 10^3 kg.m^{-3}). Well-layered sequences offshore with some 'rough' /diffuse seismic reflection character, onshore, and tending to thicken out seaward. Probable siliciclastic distal turbidite fan sediments.

D (v_p 3400 m.s^{-1}, ρ 2.25 x 10^3 kg.m^{-3}). Thicker, more layered, high-amplitude sequence than C. Tends to thin both landward and oceanward, onlapping underlying sequences. Probable siliciclastic turbidite fan lobe sediments.

E (v_p 3900 m.s^{-1}, ρ 2.47 x 10^3 kg.m^{-3}). Roughly laminated sediment wedge with diffuse seismic character, wedging out onto faulted oceanic crust. Passively infills graben developed on ocean floor. Probable siliciclastic marine sediments.

F Ocean crust (v_p = 5000 m.s^{-1}). Rugose basement with subdued topography, and apparently shallowing to N. The crust becomes more broken up by normal faulting from SP 2550, increasing in intensity seaward from SP 1550 on line 229/23, with major canyon development (4 km depth). Noisy, discontinuous, high amplitude reflection character, sometimes coherently layered suggesting stacked lava flows, often with steep dips seaward. At least 4 main 'panels' of ocean crust are identifiable based on reflection characteristics: SP 0–3100, 228/12; SP 0–1450 229/22; SP 1450, 229/22 to SP 2550, 229/23; and SP 2550 to SOL, 229/23.

Block_ID	ρ x 10^3 kg.m^{-3}	k SI	Q	Polarity
1	2.53	0.03	2	R
2	2.53	0.03	1.9	N
3	2.53	0.02	2	R
4	2.53	0.03	1.5	N
5	2.53	0.02	1.5	R
6	2.53	0.032	2	N
7	2.53	0.022	2	R
8	2.53	0.03	2	N
9	2.53	0.01	1	R
10	2.53	0.06	2.5	N
11	2.53	0.02	2	R
12	2.53	0.02	2	N
13	2.53	0.04	2.5	R
14	2.53	0.04	2	N
15	2.53	0.02	2	R
16	2.53	0.04	2	N
17R	2.53	0.09	3.4	R
17N	2.53	0.05	2.5	N
18N	2.53	0.043	1.4	N
18a	2.50	0.02	1.5	N
19	2.50	0.06	2.2	N
20	2.53	0.01	2	R
21	2.53	0.07	2.5	R
22	2.53	0.08	2.8	N
23	2.53	0.06	2.5	R
24	2.53	0.07	3	N
24A	2.53	0.05	2.2	R
25	2.53	0.04	3	N
26	2.53	0.05	2.2	N
27	2.53	0.04	2	N

G Dolerite dyke swarms. G1: v_p = 5600 m.s^{-1}, $\rho = 2.70\times10^3$ kg.m^{-3}, k = 0.01 SI; G2: v_p = 6700 m.s^{-1}, $\rho = 2.70\times10^3$ kg.m^{-3}, k = 0.01 SI; G3: v_p = 6700 m.s^{-1}, $\rho = 2.75\times10^3$ kg.m^{-3}, k = 0.01 SI.

H Oceanic peridotites (v_p 7900 m.s^{-1}): H1: $\rho = 2.85 \times 10^3$ kg.m^{-3}, k = 0 SI; H2: 3.11×10^3 kg.m^{-3}, k = 0 SI; H3: 2.85×10^3 kg.m^{-3}, k = 0 SI; H4: 3.05×10^3 kg.m^{-3}, k = 0 SI.

Mantle (v_p 8400 m.s^{-1}, $\rho = 3.30\times10^3$ kg.m^{-3}). Moho is a strong, continuous high-amplitude reflector under oceanic panels H3 and H4

Key Findings 228/12-229/22- 229/23:

- This sector, northwest of the Bruce Rise, is comprised entirely of oceanic crust
- The oceanic crust is divided into fault-bound segments with differing seismic reflection characteristics, and varying deeper crustal properties (within dolerite dykes and gabbro/peridotite layers).
- This line has not been checked for consistency with global seafloor spreading reversal models.

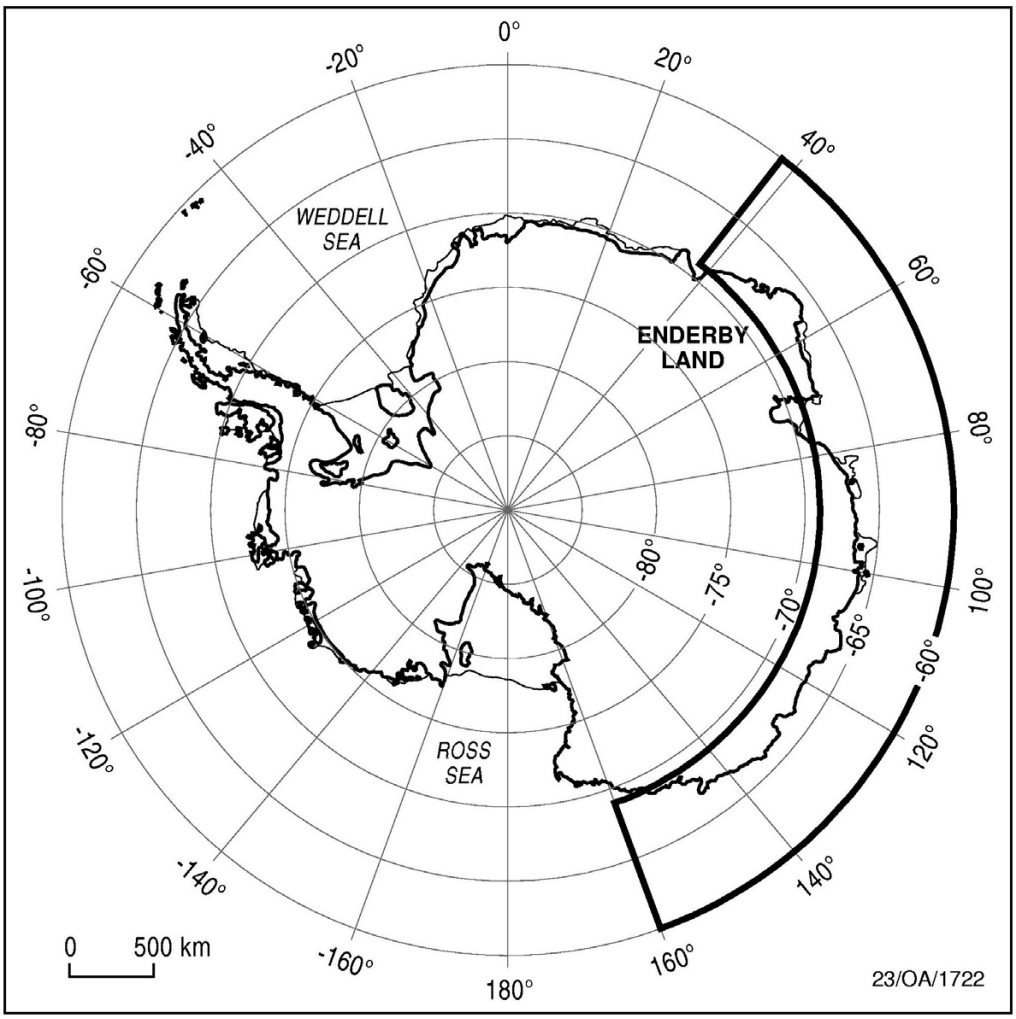

Figure 1: Polar stereographic projection of Antarctica. Box shows approximate area covered by the Australian Antarctic and Southern Ocean Profiling Project.

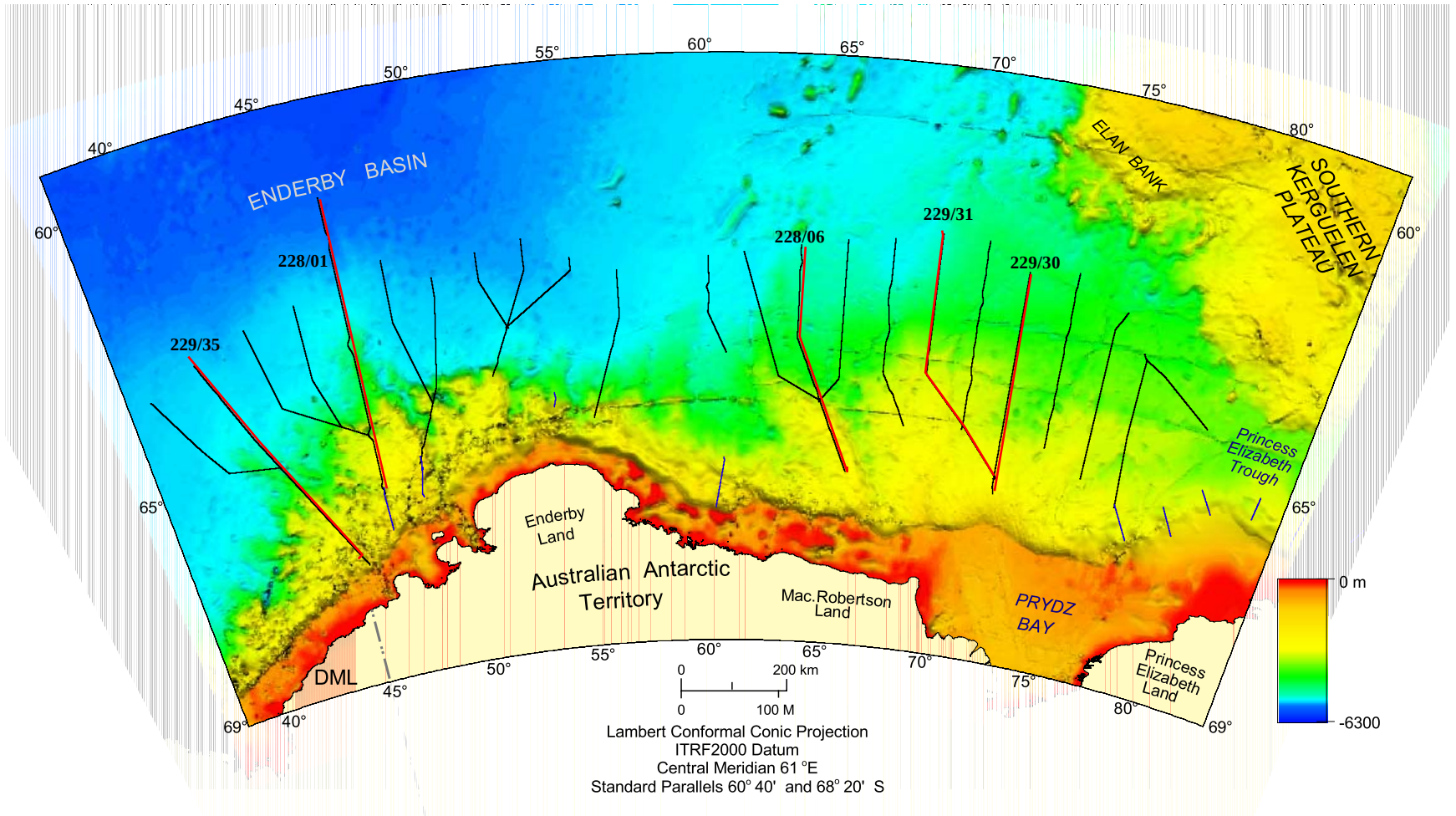

Figure 2: Bathymetry image of the western sector of the region of the Australian Antarctic Territory, showing the locations of the Survey GA-227, GA-228 and GA-229 seismic lines. Tracks highlighted in red are locations of potential field models and line numbers.

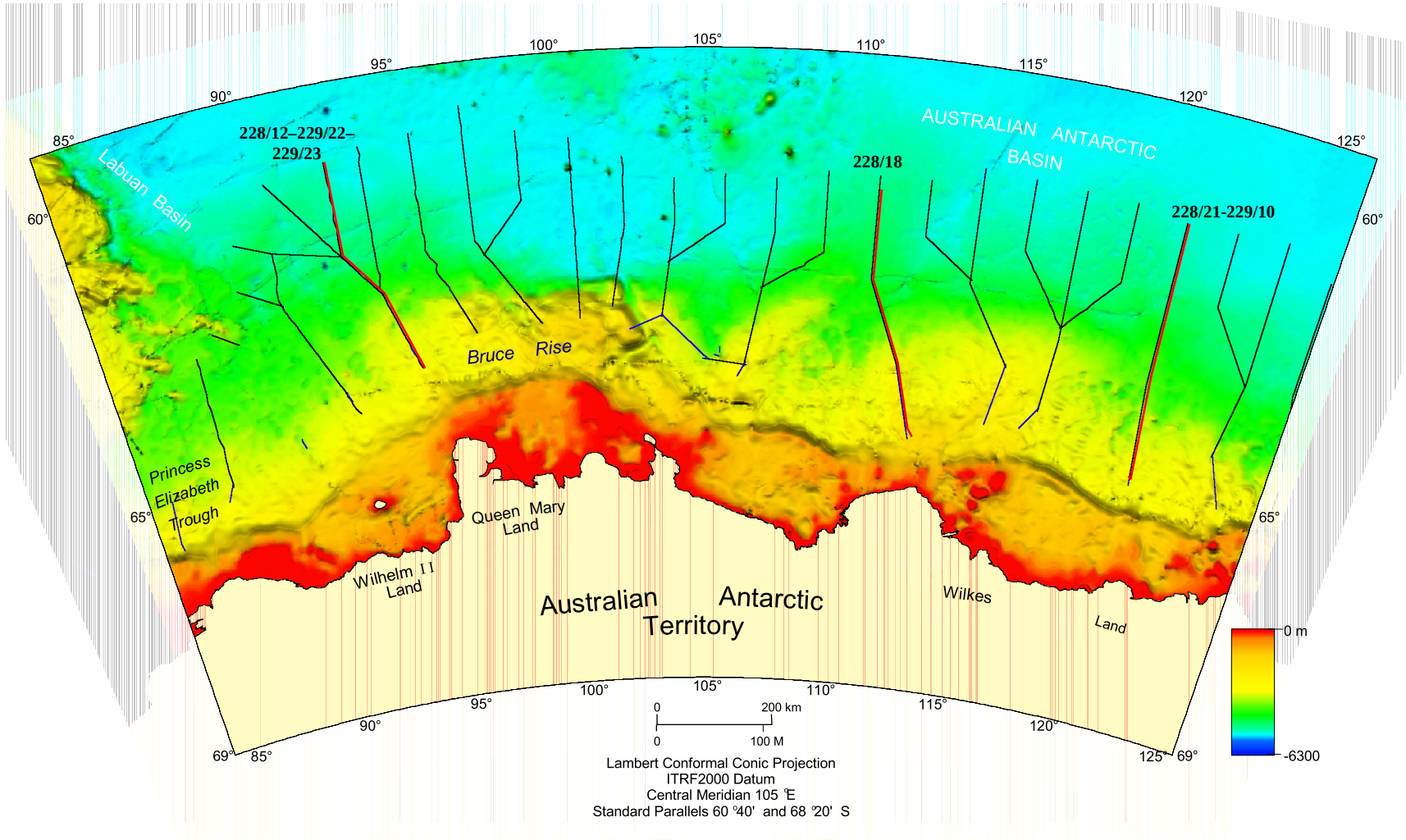

Figure 3: Bathymetric image of the central sector of the region of the Australian Antarctic Territory, showing the locations of the Survey GA-227, GA-228 and GA-229 seismic lines. Tracks highlighted in red are locations of potential field models and line numbers.

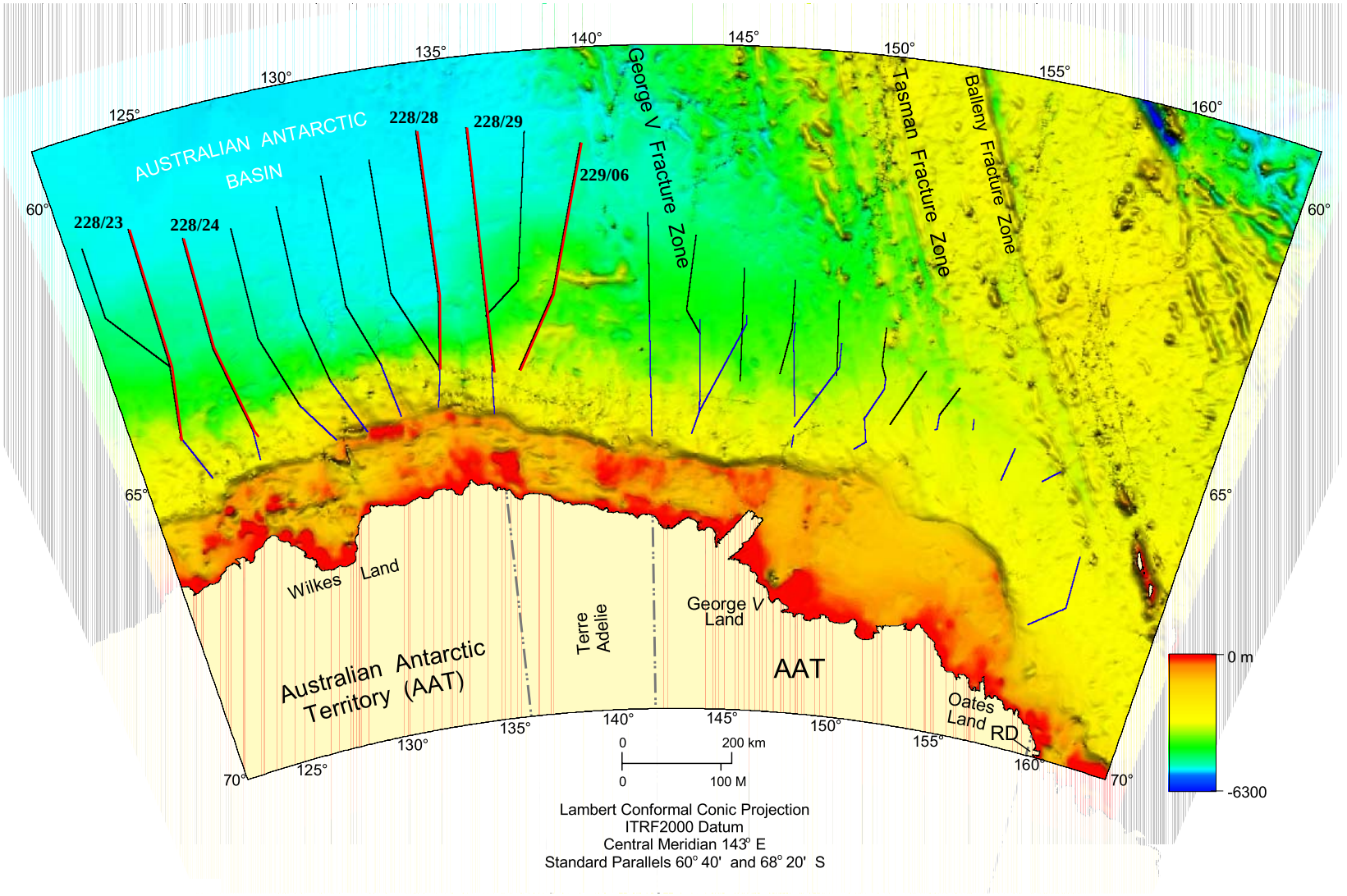

Figure 4: Bathymetry image of the eastern sector of the region of the Australian Antarctic Territory, showing the locations of the Survey GA-227, GA-228 and GA-229 seismic lines. Tracks highlighted in red are locations of potential field models and line numbers.

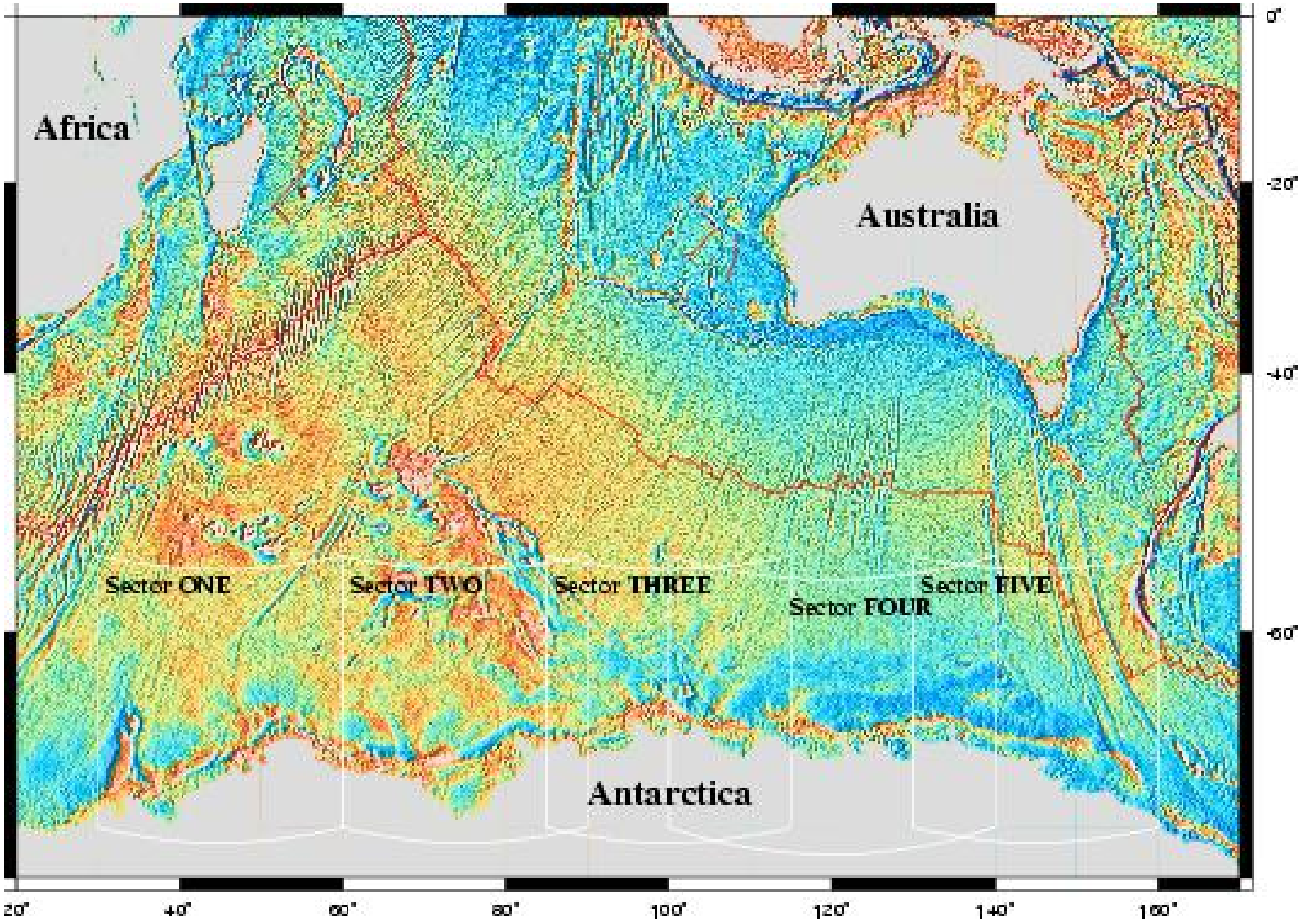

Figure 5: Marine gravity anomaly derived from satellite altimetry (Sandwell & Smith, 1997), 20°E to 170°°E.

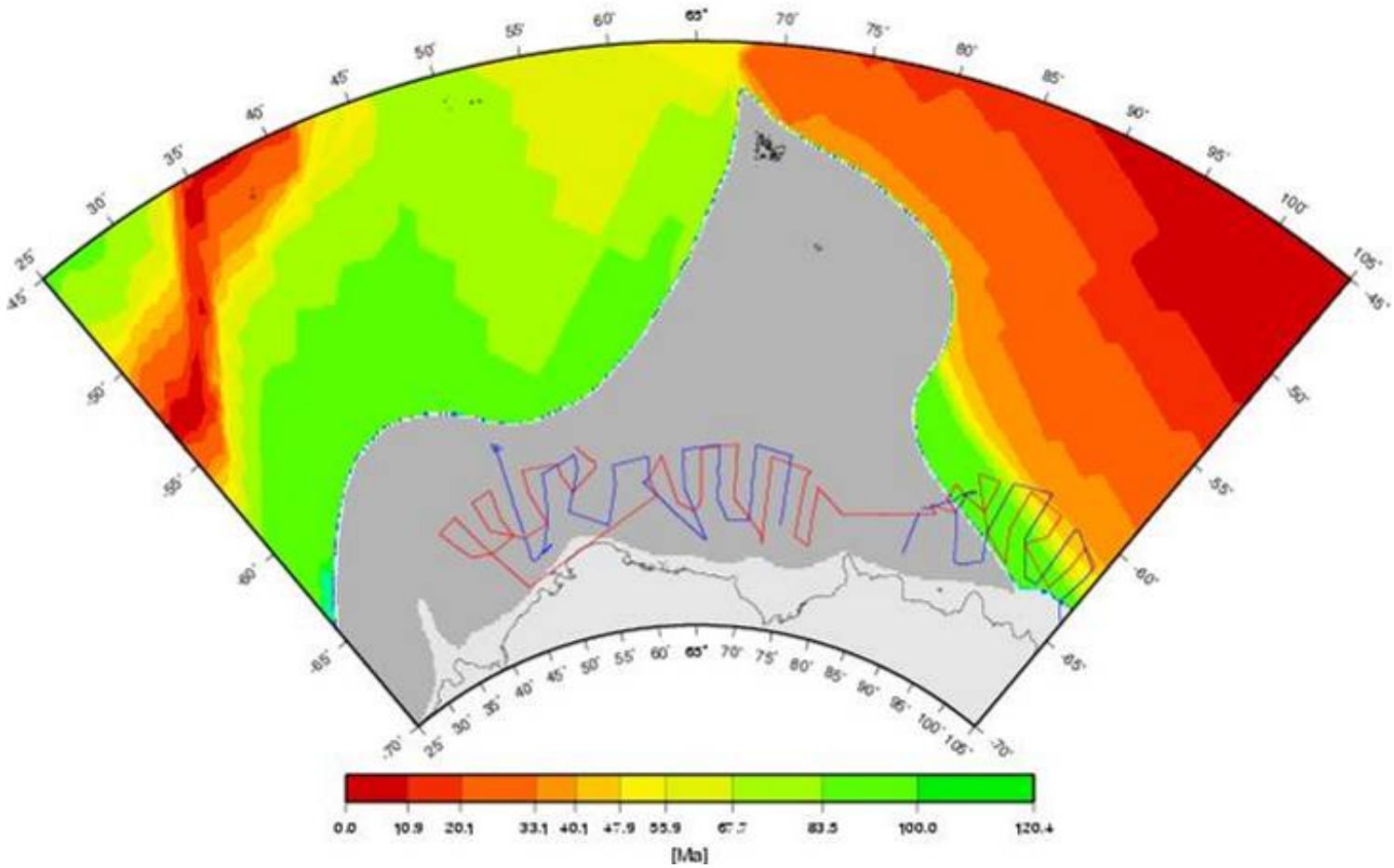

Figure 6: Digital age grid of the ocean floor (Müller et al., 1997) for the area from 25–105°E. Trackline coverage of survey 228 (blue) and 229 (red).

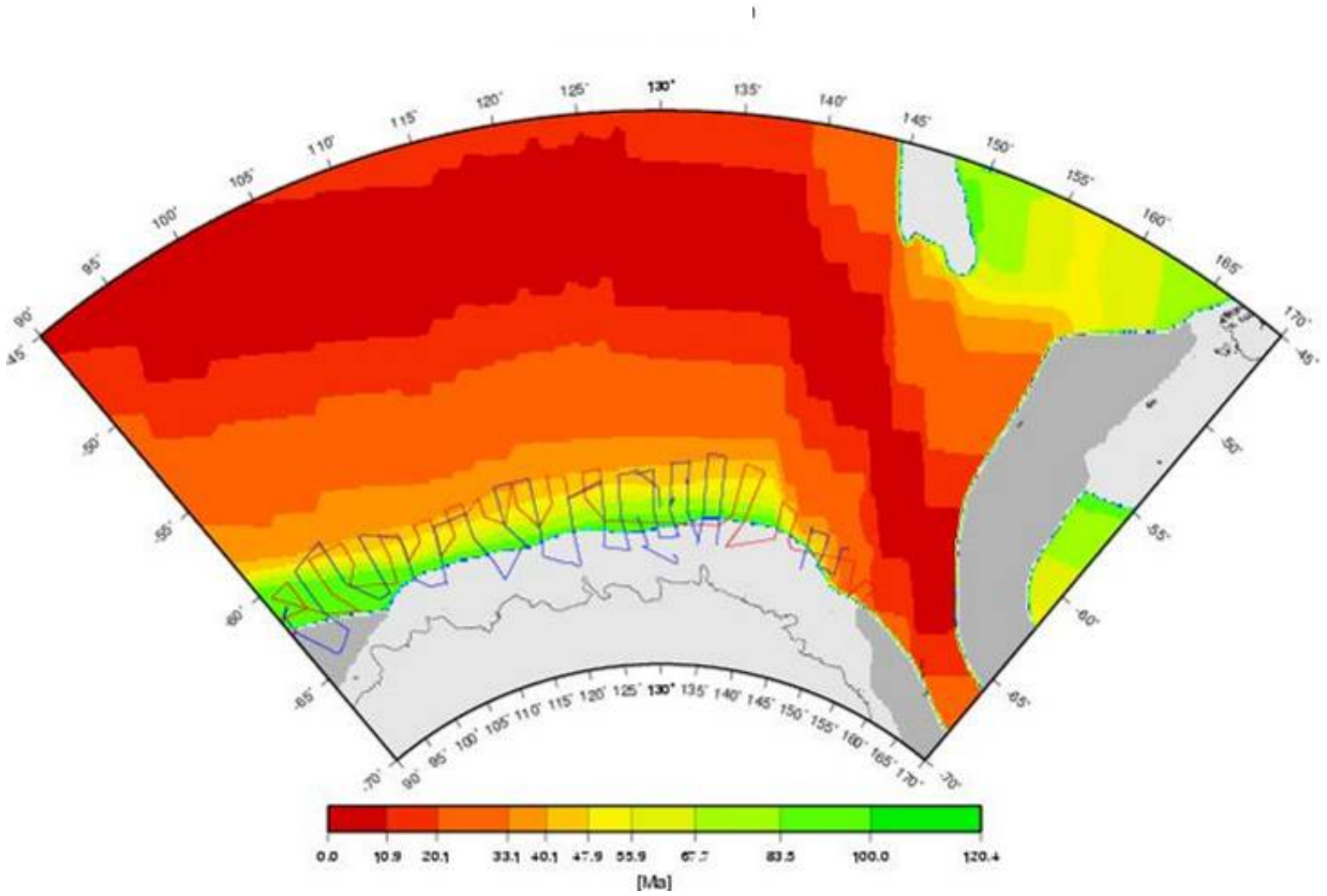

Figure 7: Digital age grid of the ocean floor (Müller et al. 1997) for the area from 90–170°E. Trackline coverage of survey 228 (blue) and 229 (red).

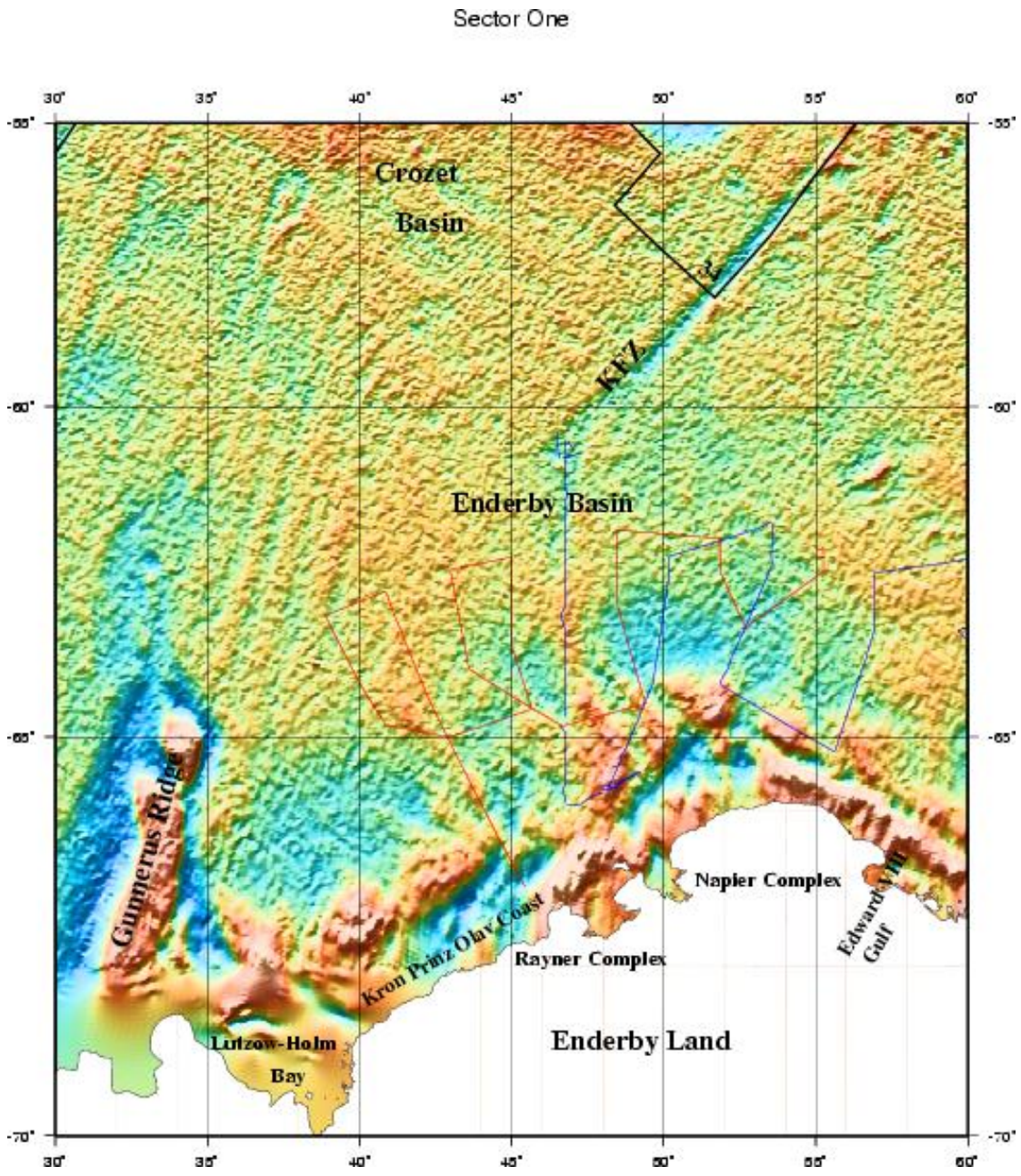

Figure 8: Marine gravity field (from McAdoo & Laxon 1997) in the western Enderby Basin (Sector 1) with illumination azimuth from NNW (330°). Trackline coverage of survey 228 (blue) and 229 (red).

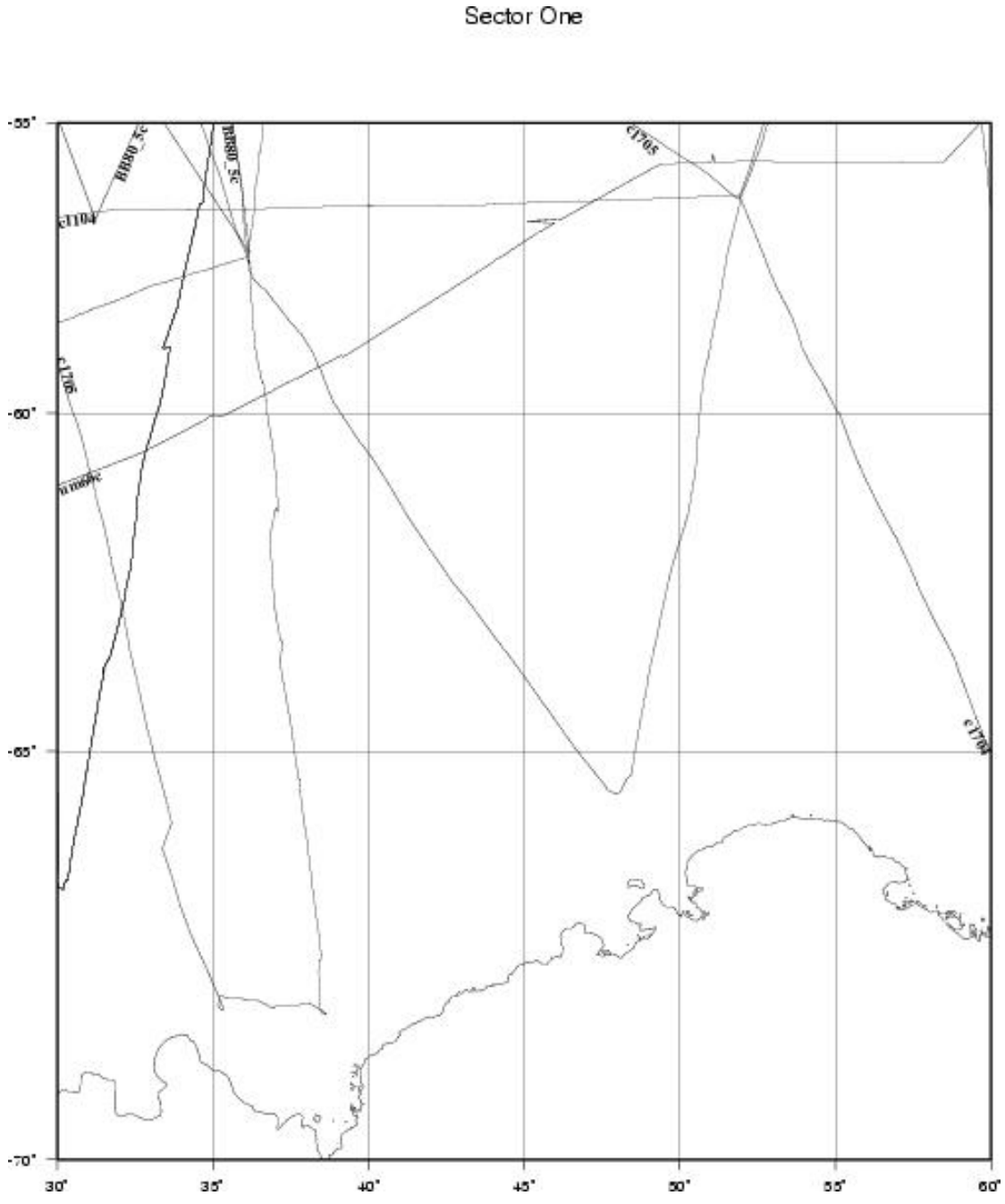

Figure 9: Shiptrack survey coverage of open-file magnetic anomaly data from the NGDC database (Sector 1).

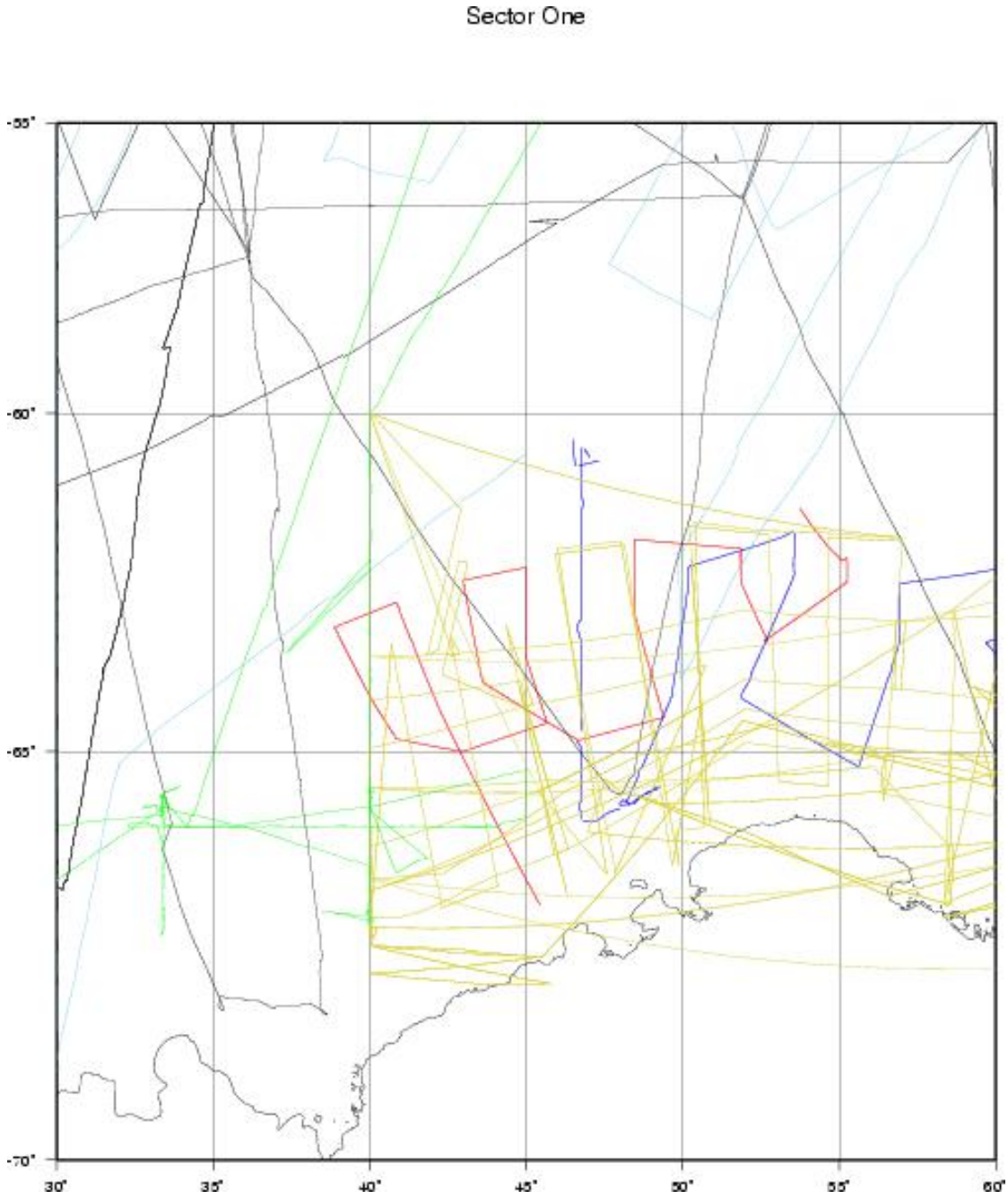

Figure 10: Shiptrack survey coverage (Sector 1) of magnetic anomaly data from the NGDC database (black) and other surveys: Japan (green), France (light blue), Russia (olive), GA-228 (blue), and GA-229 (red).

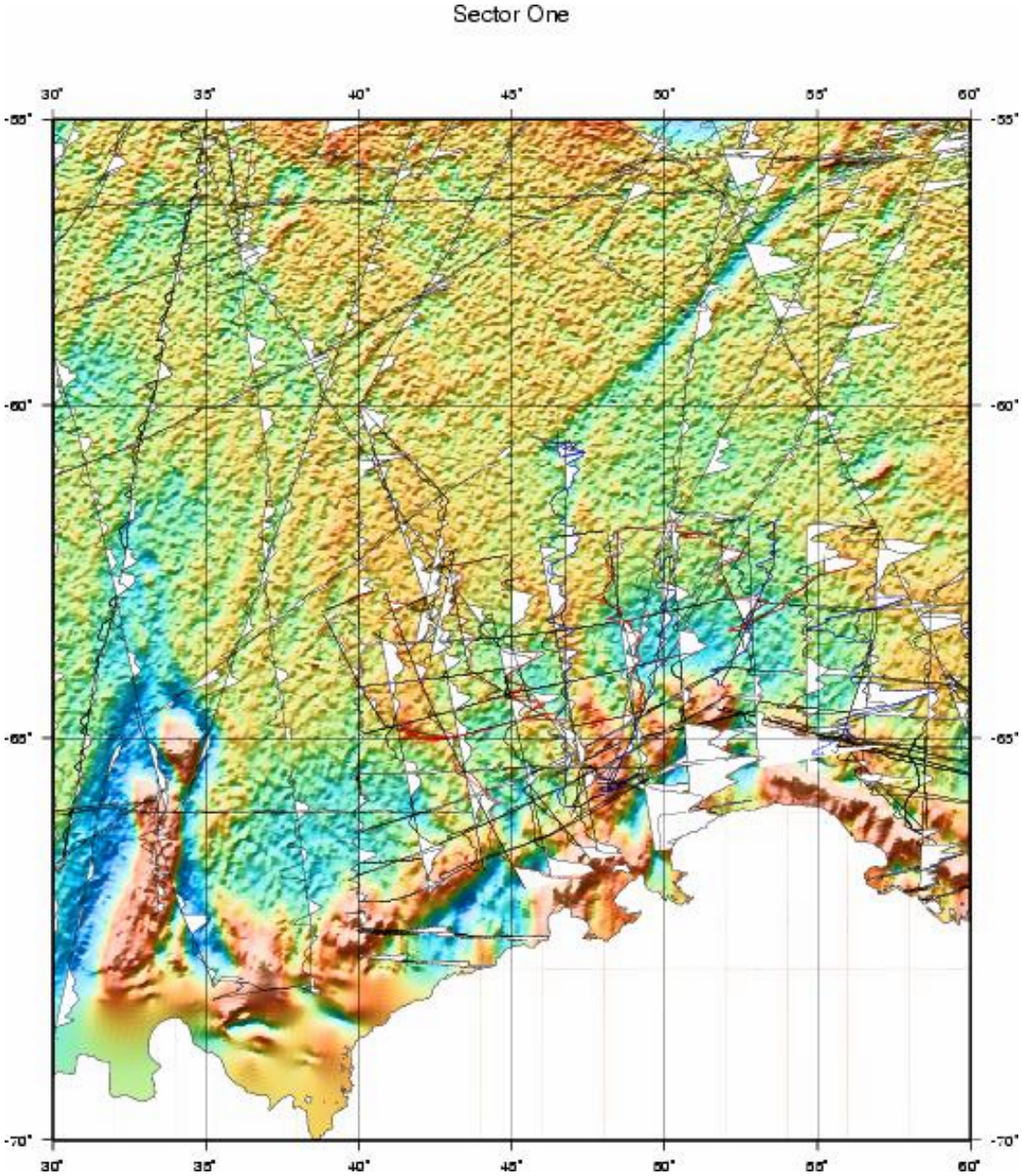

Figure 11: Filtered and trended magnetic anomaly profiles (Sector 1) with positive amplitude filled white, superimposed over satellite gravity. Also shown are tracklines from survey GA-228 (blue) and GA-229 (red).

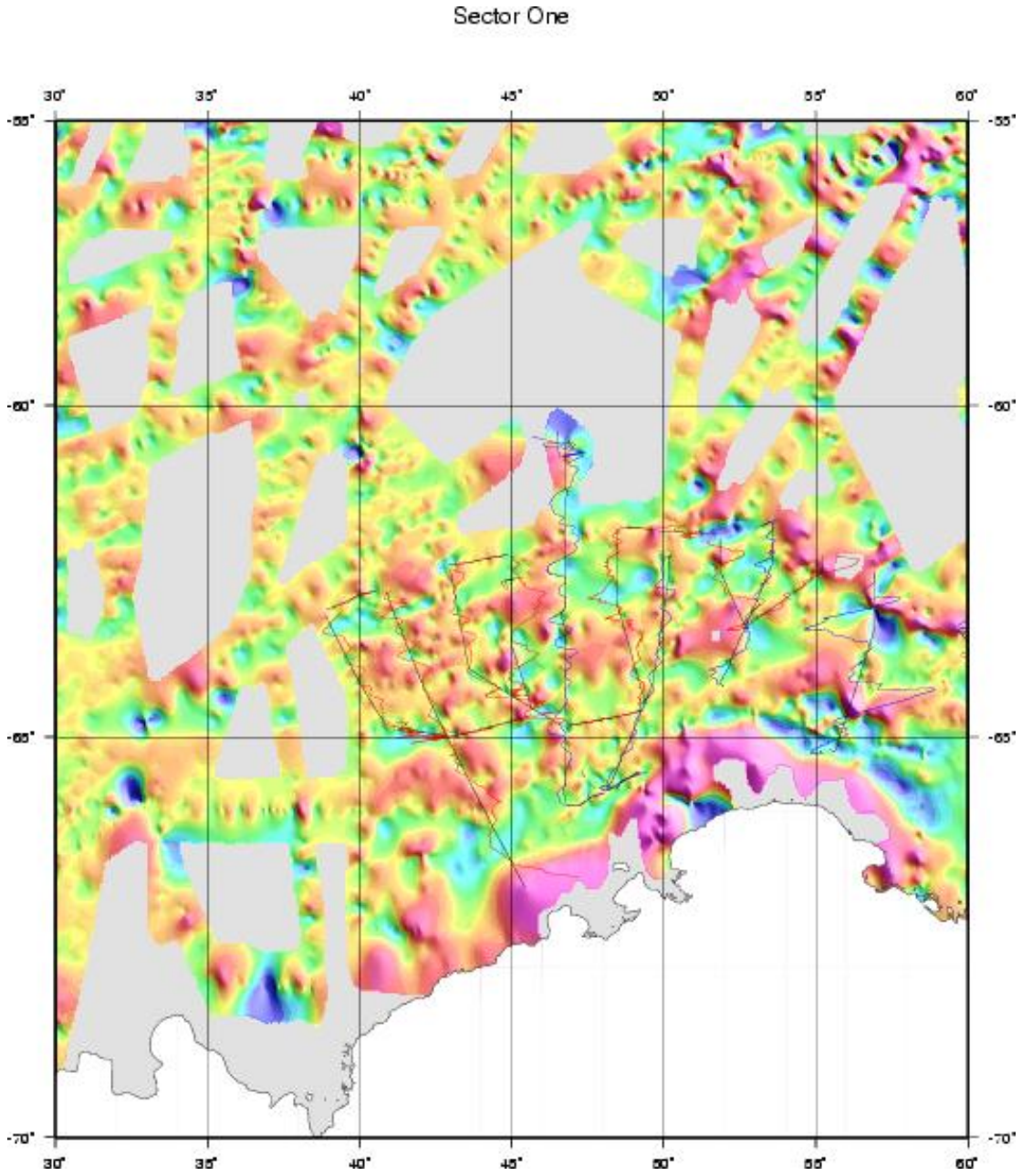

Figure 12: Colour-shaded, gridded magnetic anomaly data for Sector 1. Grey areas denote insufficient data coverage for interpolation. Superimposed are filtered and trended magnetic anomaly profiles from surveys GA-228 (blue) and GA-229 (red).

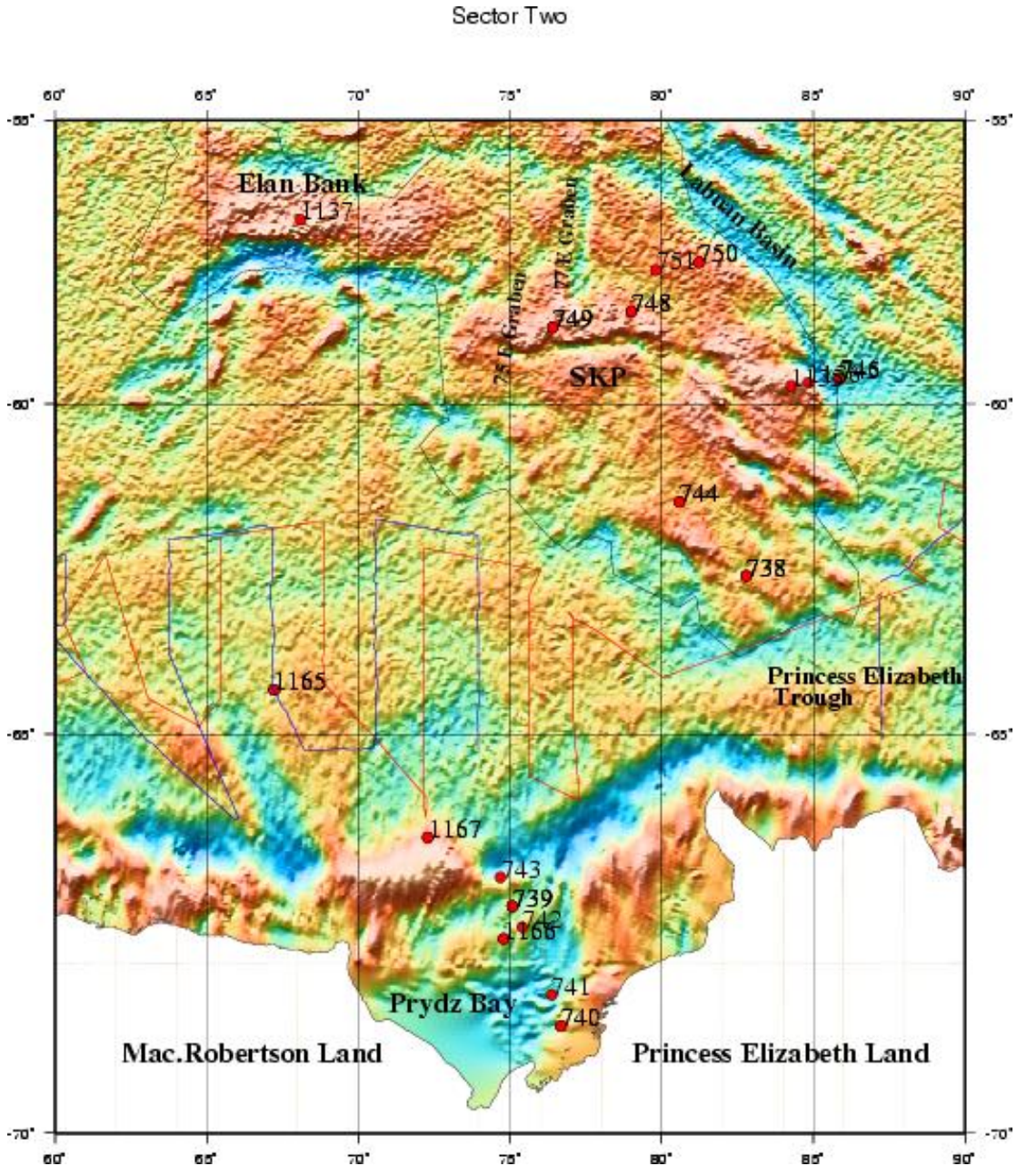

Figure 13: Marine gravity field (from McAdoo & Laxon 1997) in the eastern Enderby Basin (Sector 2) with illumination azimuth from NNW (330°). Trackline coverage of surveys GA-228 (blue) and GA-229 (red). Red numbered circles indicate DSDP/ODP sites in this region. Black line: shows estimated outline of Elan Bank and Kerguelen Plateau. SKP: Southern Kerguelen Plateau.

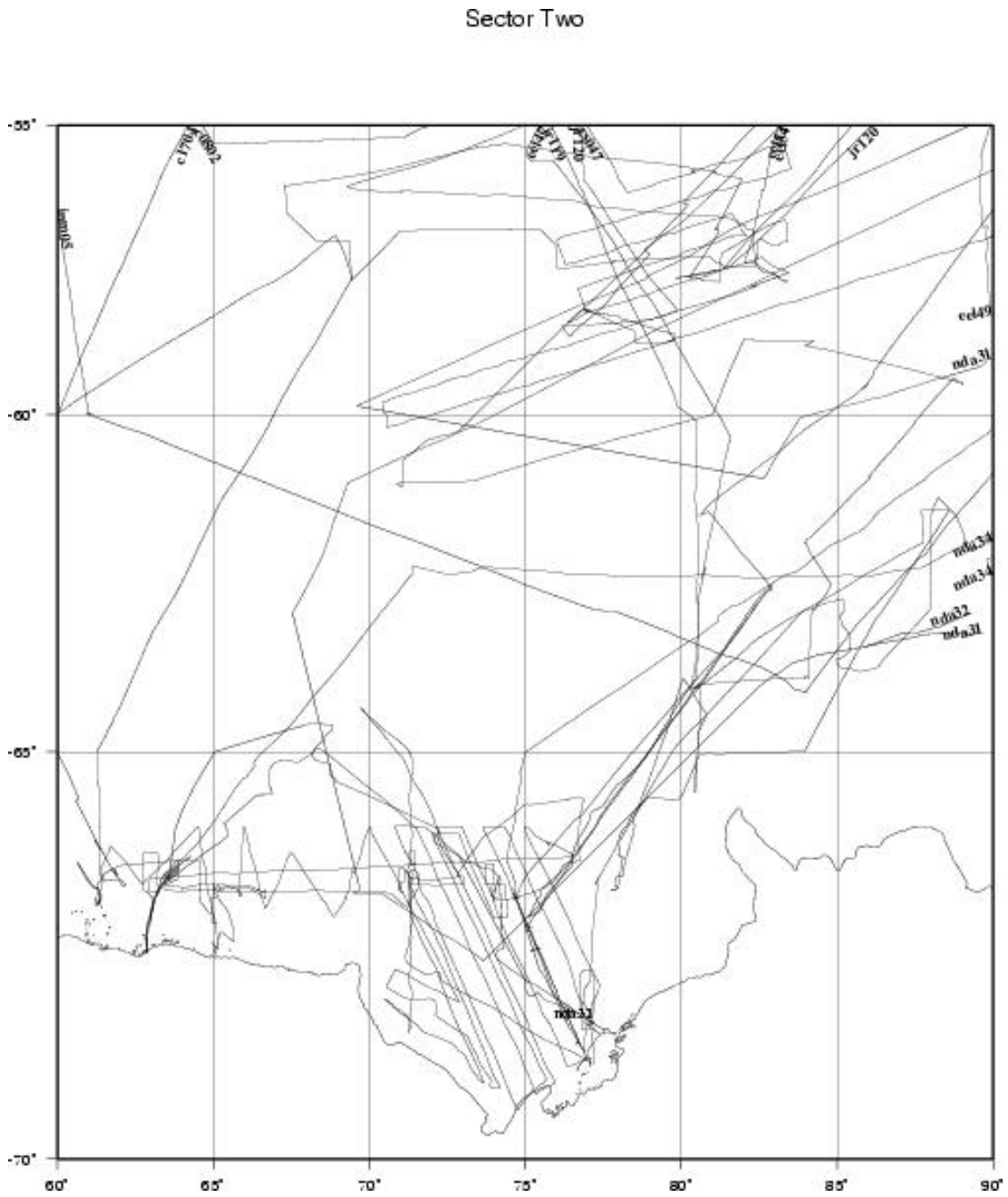

Figure 14: Shiptrack survey coverage of open-file magnetic anomaly data from the NGDC database (Sector 2).

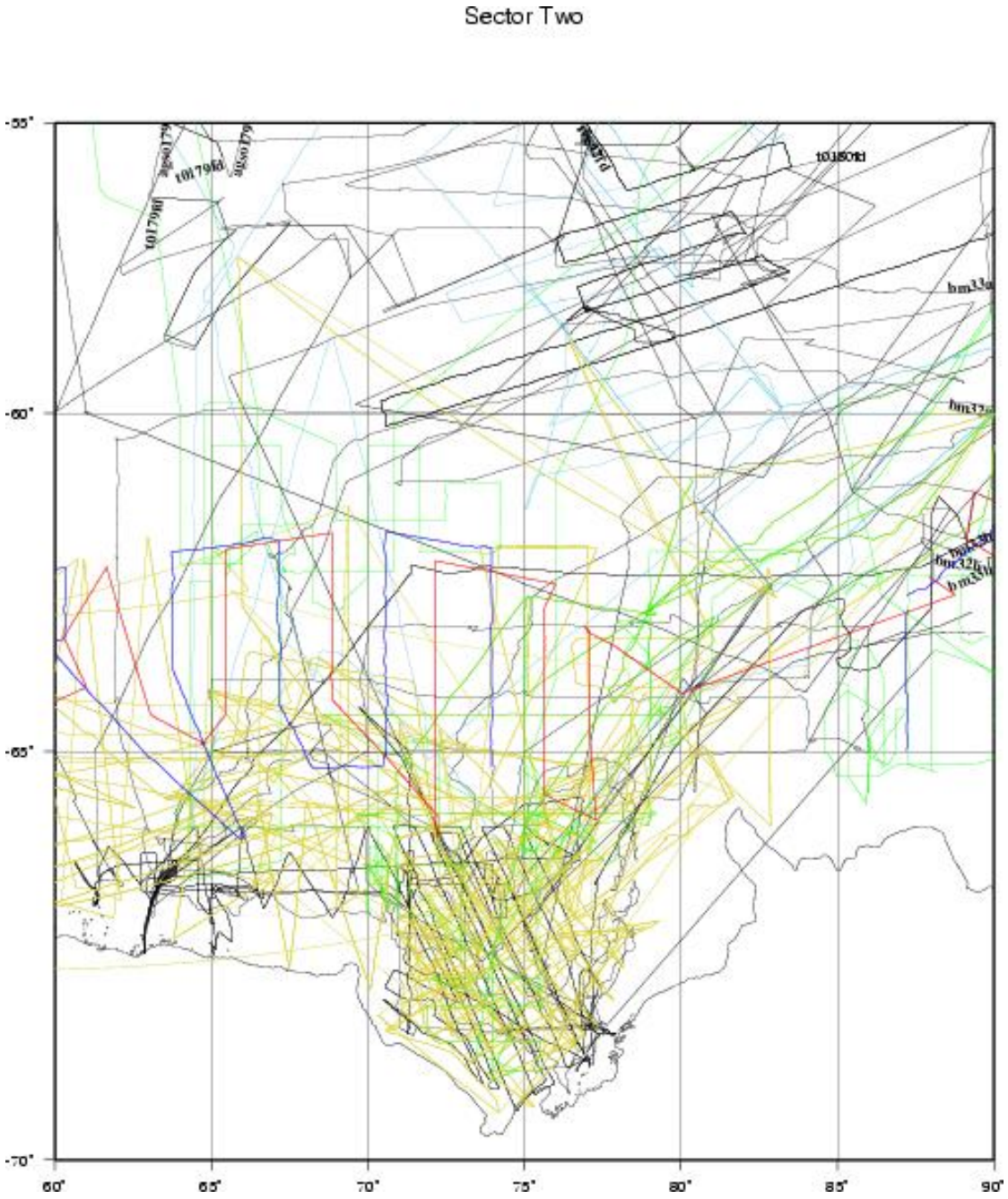

Figure 15: Shiptrack survey coverage of magnetic anomaly data (Sector 2) from the NGDC database (black) and other surveys: Japan (green), France (light blue), Russia (olive), GA-228 (blue), and GA-229 (red).

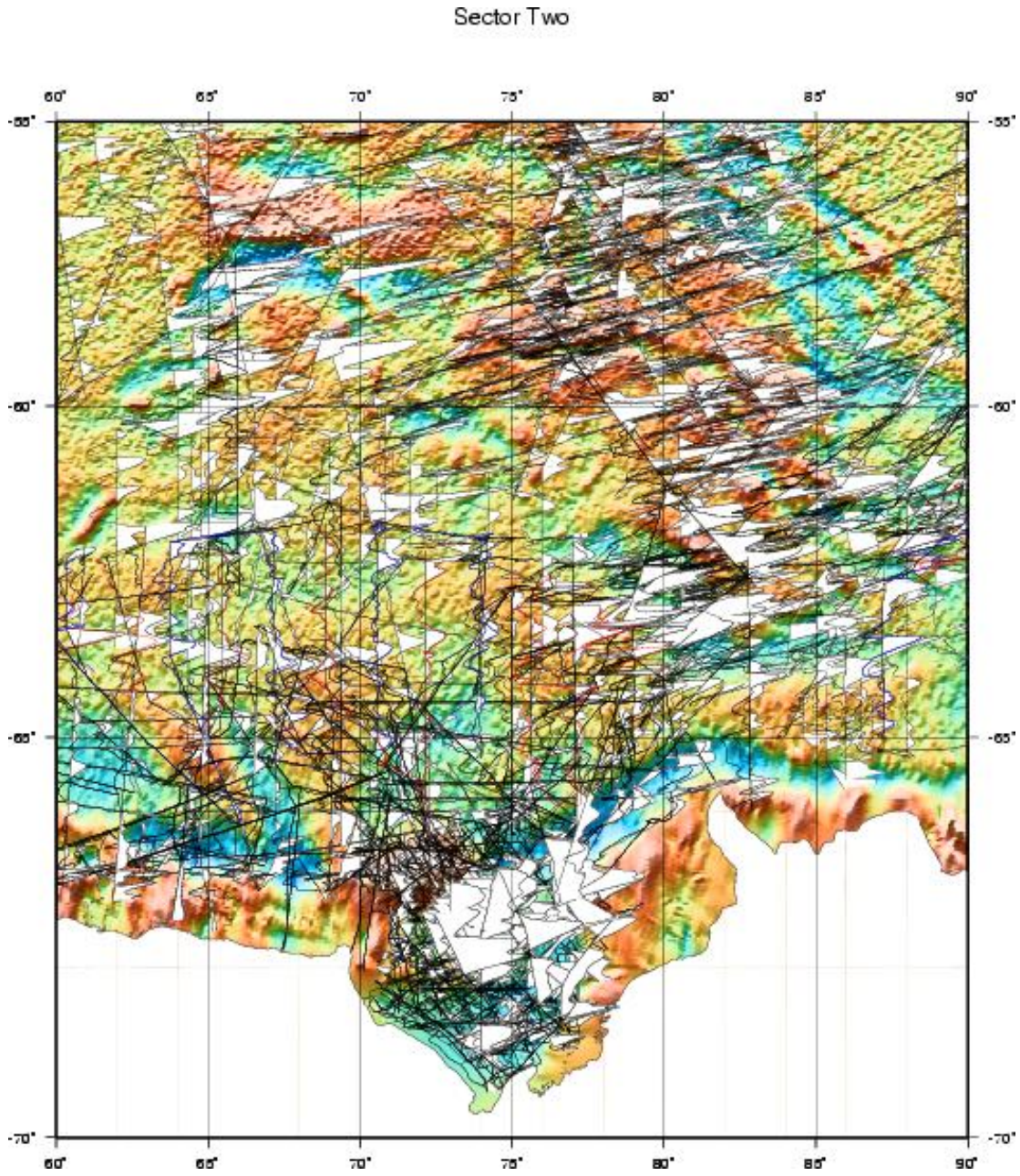

Figure 16: Filtered and trended magnetic anomaly profiles (Sector 2) with positive amplitude filled white, superimposed over satellite gravity. Also shown are tracklines from survey GA-228 (blue) and GA-229 (red).

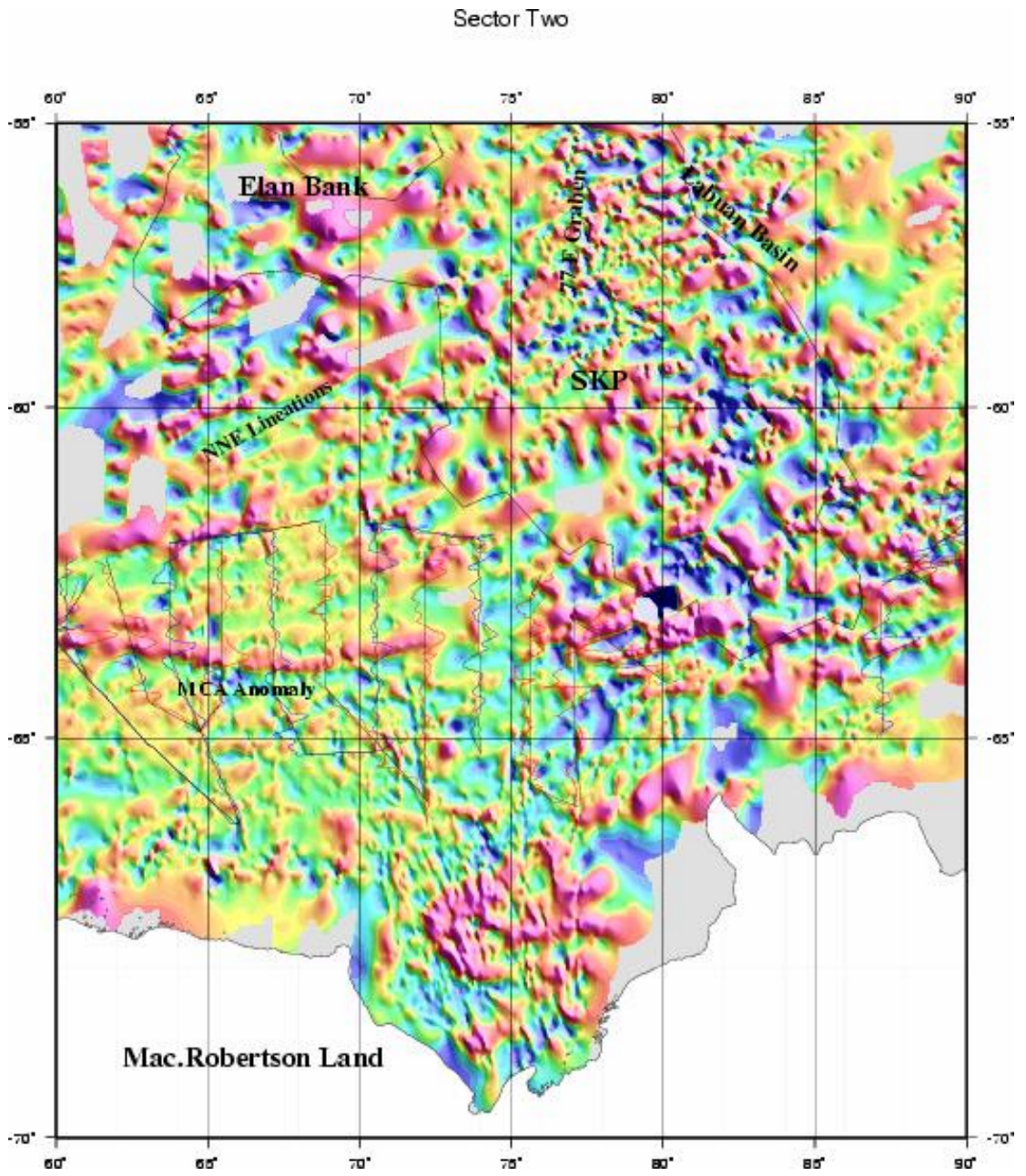

Figure 17: Colour-shaded, gridded magnetic anomaly data for Sector 2. Grey areas denote insufficient data coverage for interpolation. Superimposed are filtered and trended magnetic anomaly profiles from surveys GA-228 (blue) and GA-229 (red).

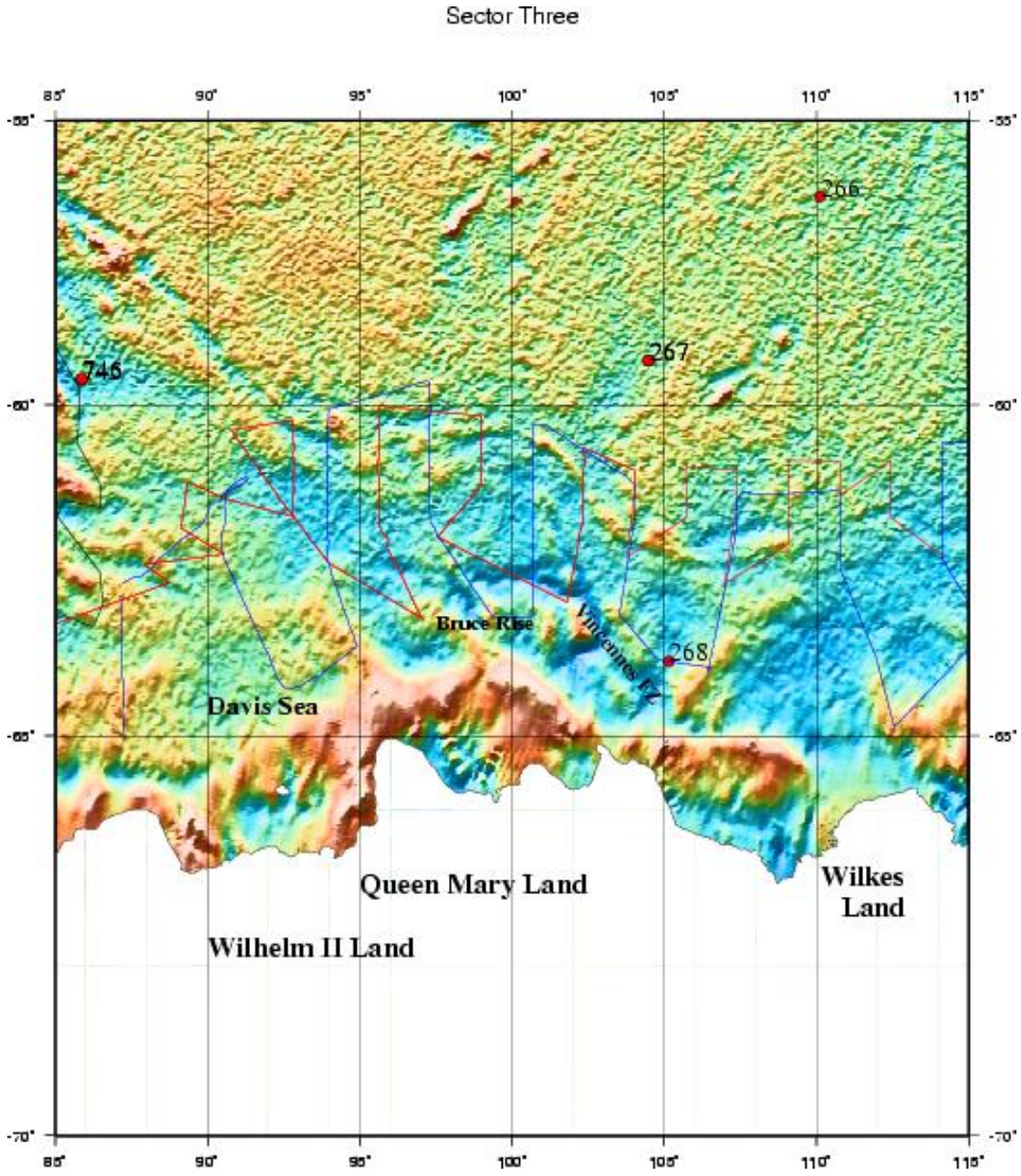

Figure 18: Marine gravity field (from McAdoo & Laxon 1997) in the Bruce Rise region (Sector 3) with illumination azimuth from NNW (330°). Trackline coverage of surveys GA-228 (blue) and GA-229 (red). Red numbered circles indicate DSDP/ODP sites in this region.

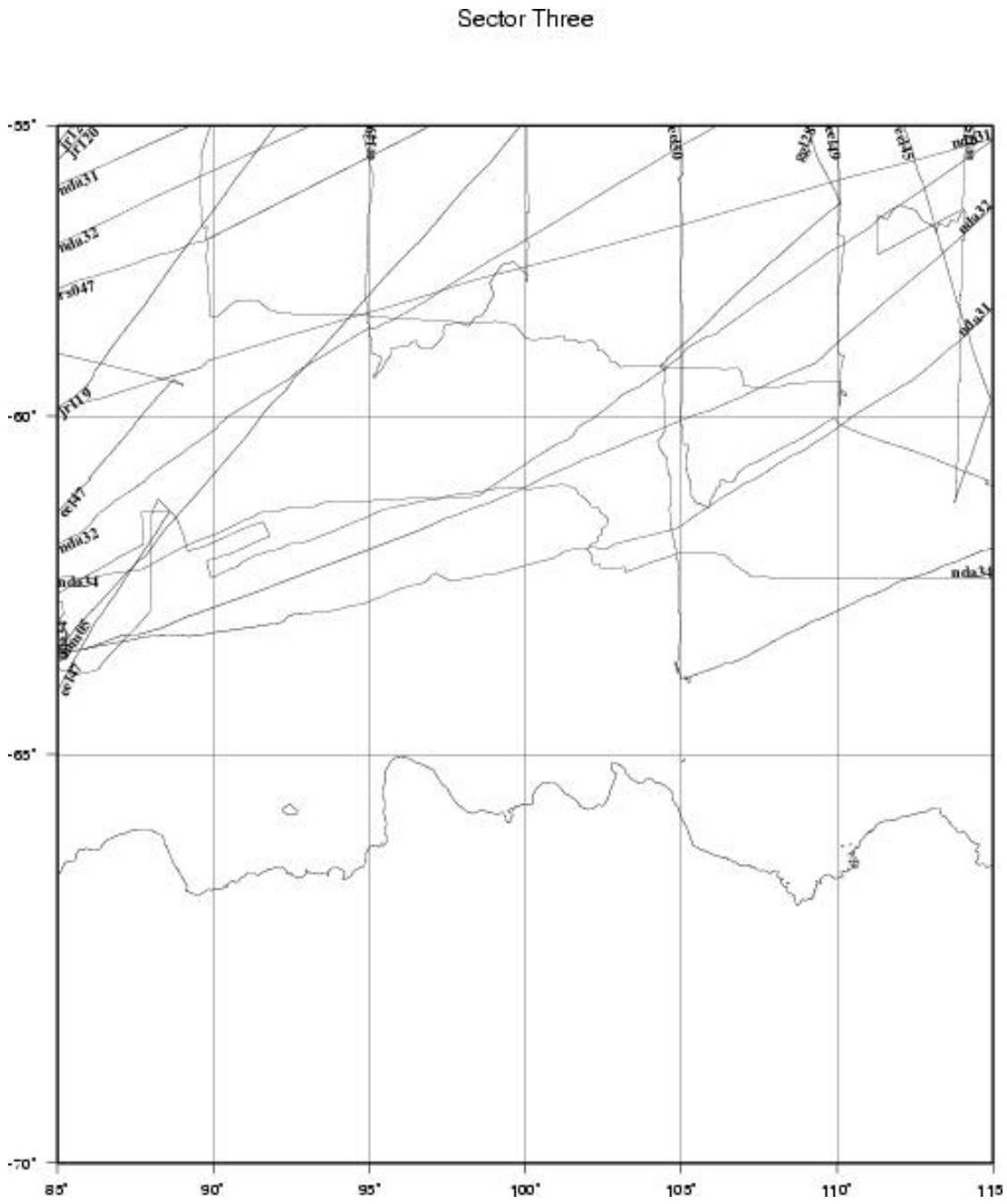

Figure 19: Shiptrack survey coverage of open-file magnetic anomaly data from the NGDC database (Sector 3).

Sector Three

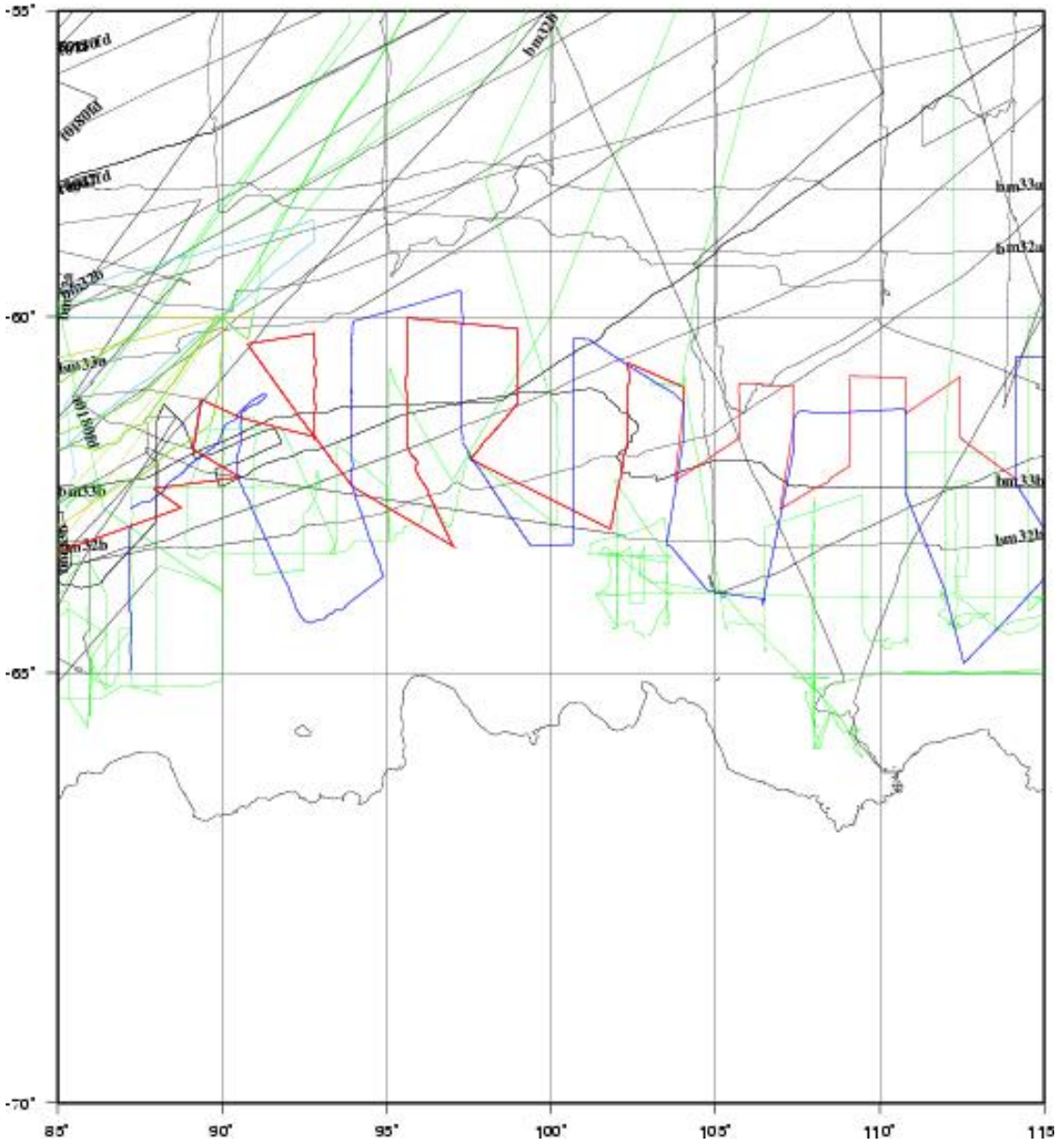

Figure 20: Shiptrack survey coverage of magnetic anomaly data (Sector 3) from the NGDC database (black) and other surveys: Japan (green), France (light blue), Russia (olive), GA-228 (blue), and GA-229 (red).

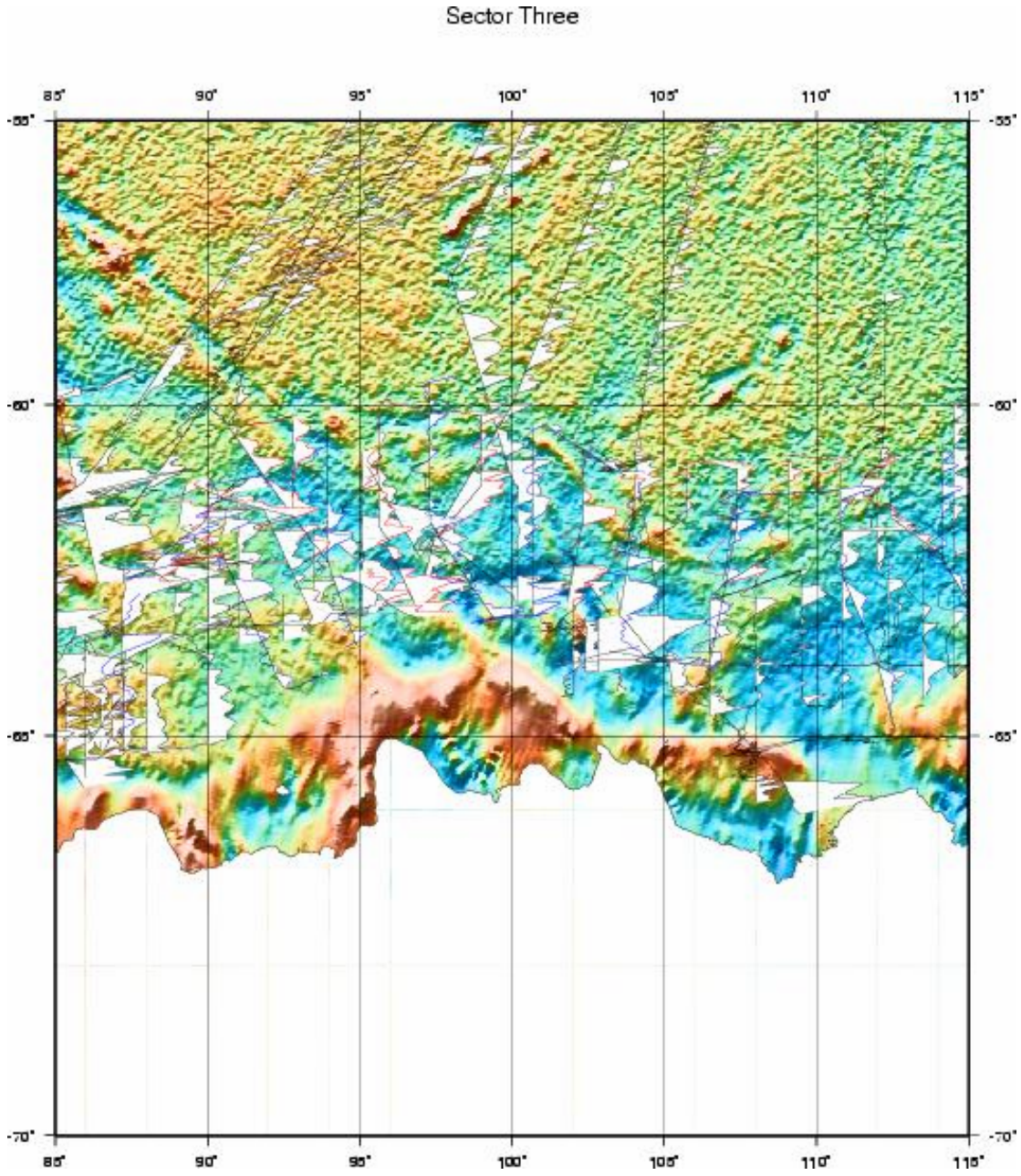

Figure 21: Filtered and trended magnetic anomaly profiles (Sector 3) with positive amplitude filled white, superimposed over satellite gravity. Also shown are tracklines from surveys GA-228 (blue) and GA-229 (red).

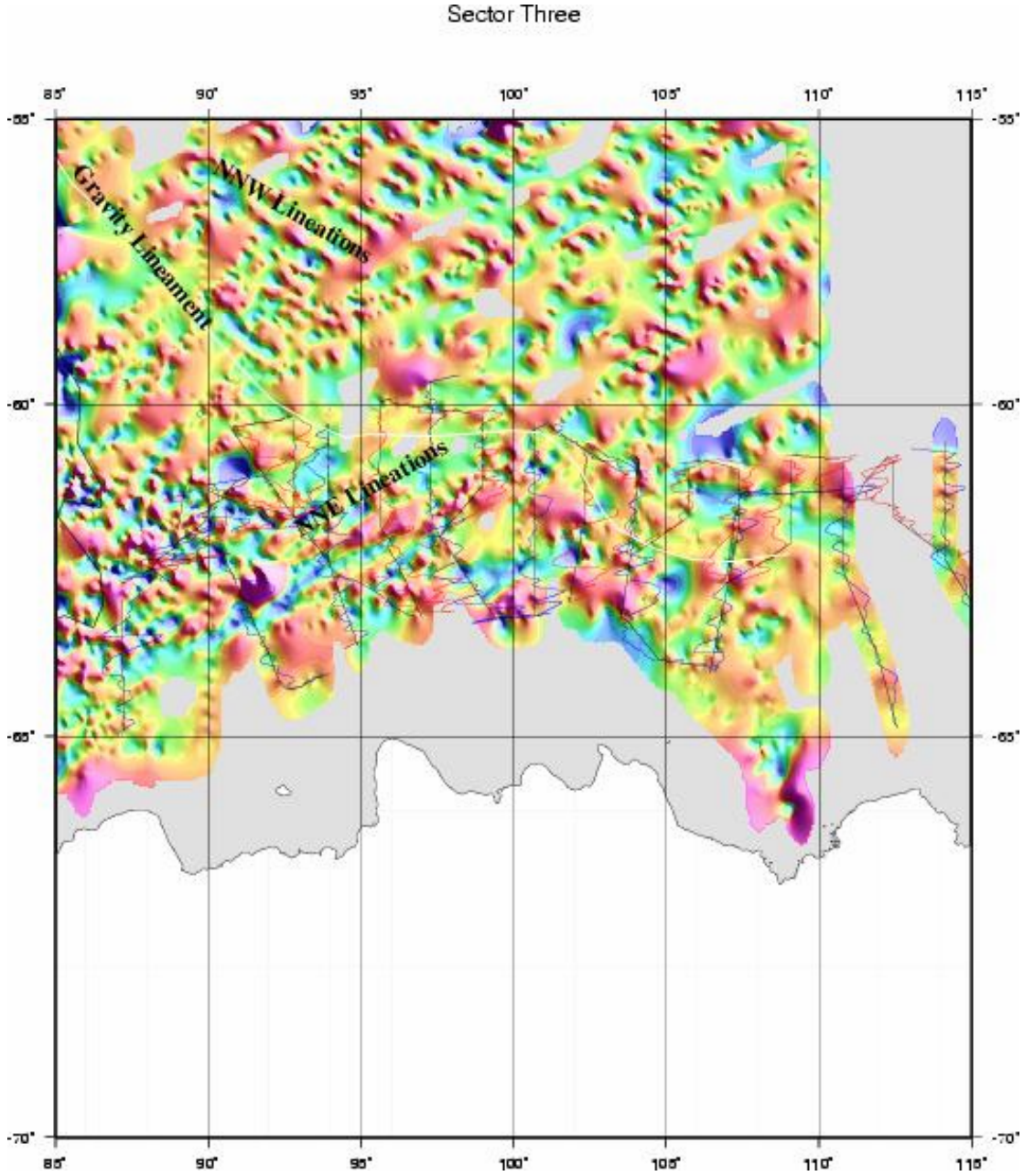

Figure 22: Colour-shaded, gridded magnetic anomaly data for Sector 3. Grey areas denote insufficient data coverage for interpolation. Superimposed are filtered and trended magnetic anomaly profiles from surveys GA-228 (blue) and GA-229 (red).

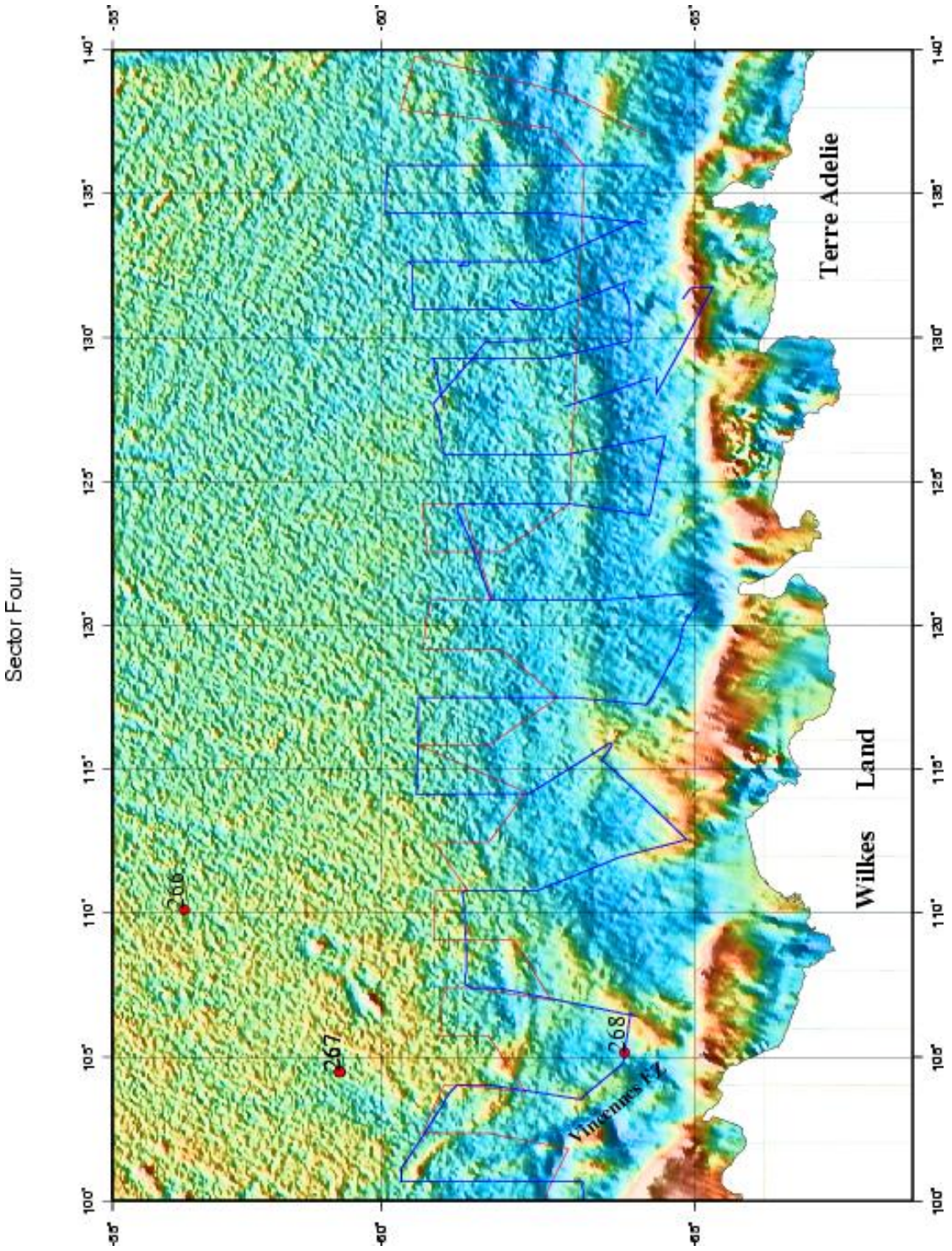

Figure 23: Marine gravity field (from McAdoo & Laxon 1997) off Wilkes Land (Sector 4) with illumination azimuth from the north). Trackline coverage of surveys GA-228 (blue) and GA-229 (red). Red numbered circles indicate DSDP/ODP sites in this region.

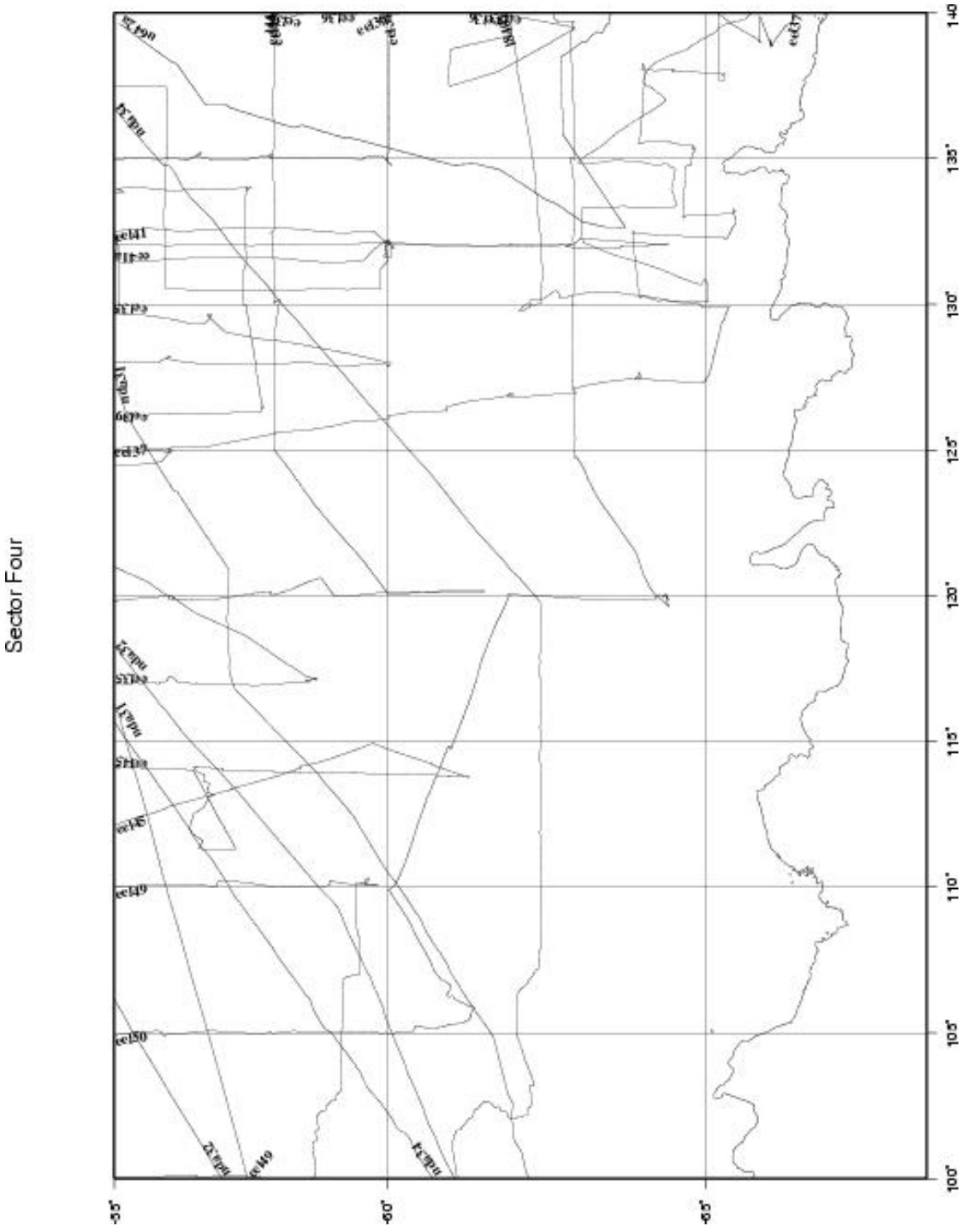

Figure 24: Shiptrack survey coverage of open-file magnetic anomaly data from the NGDC database (Sector 4).

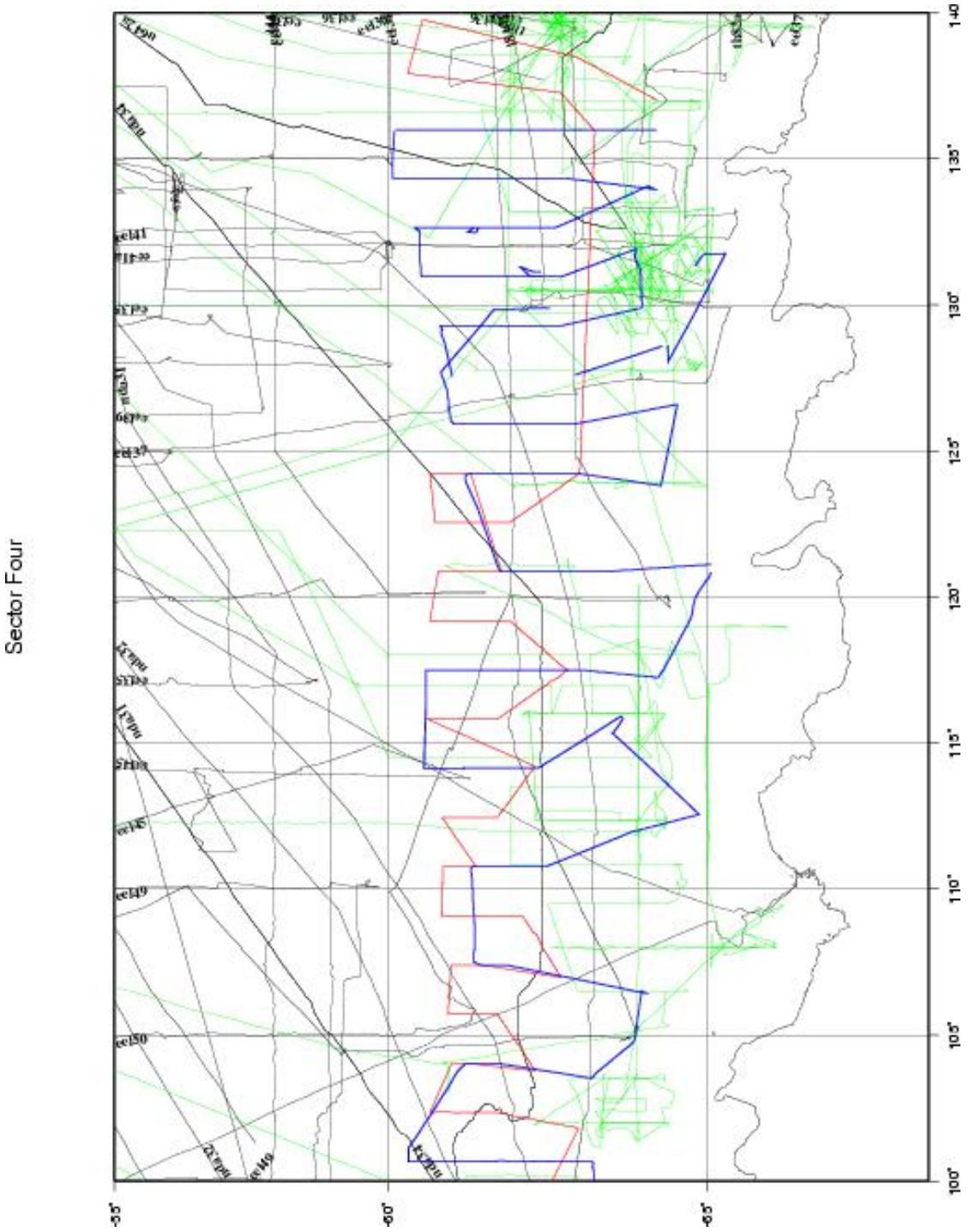

Figure 25: Shiptrack survey coverage of magnetic anomaly data (Sector 4) from the NGDC database (black) and other surveys: Japan (green), GA-228 (blue), and GA-229 (red).

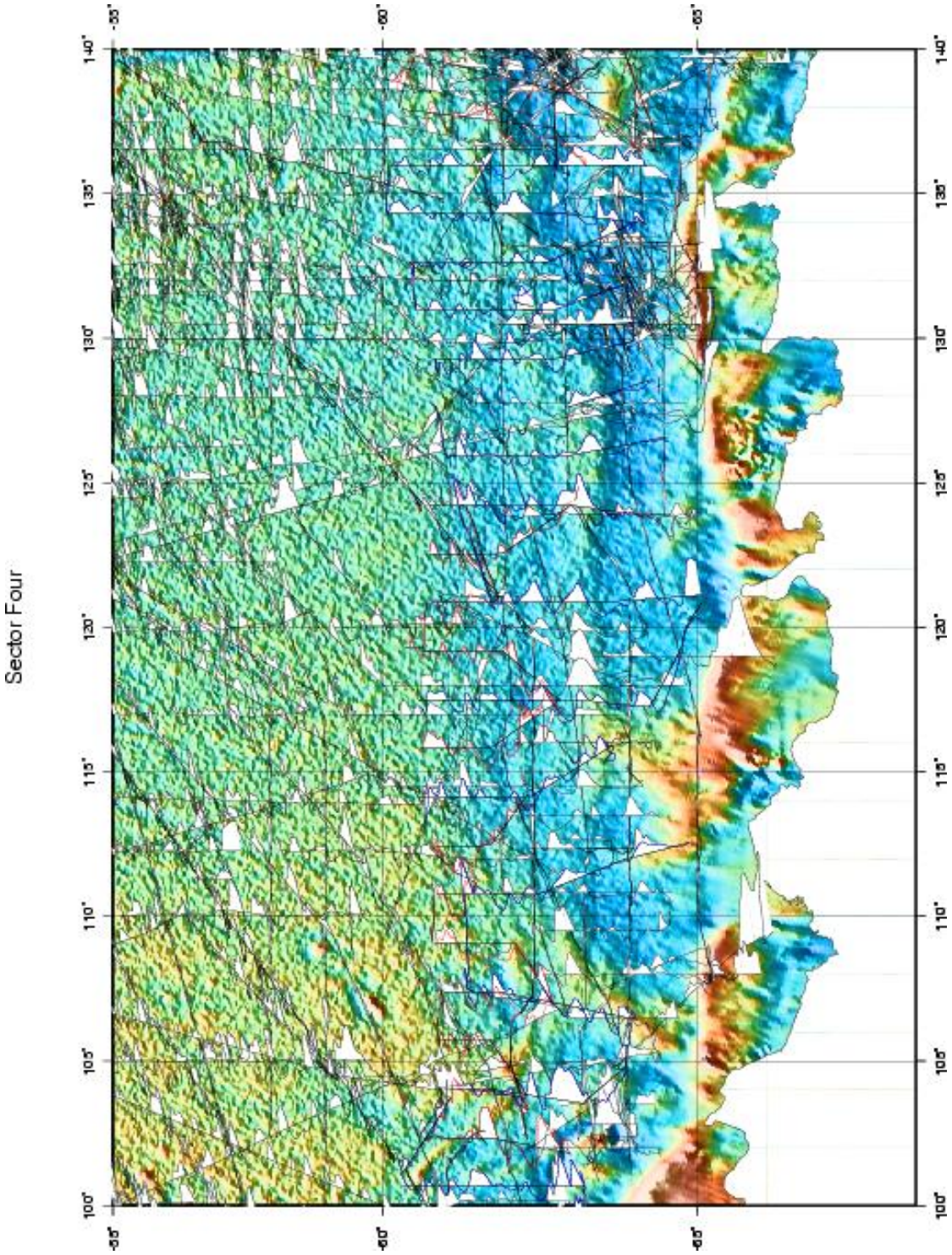

Figure 26: Filtered and trended magnetic anomaly profiles (Sector 4) with positive amplitude filled white, superimposed over satellite gravity. Also shown are tracklines from surveys GA-228 (blue) and GA-229 (red).

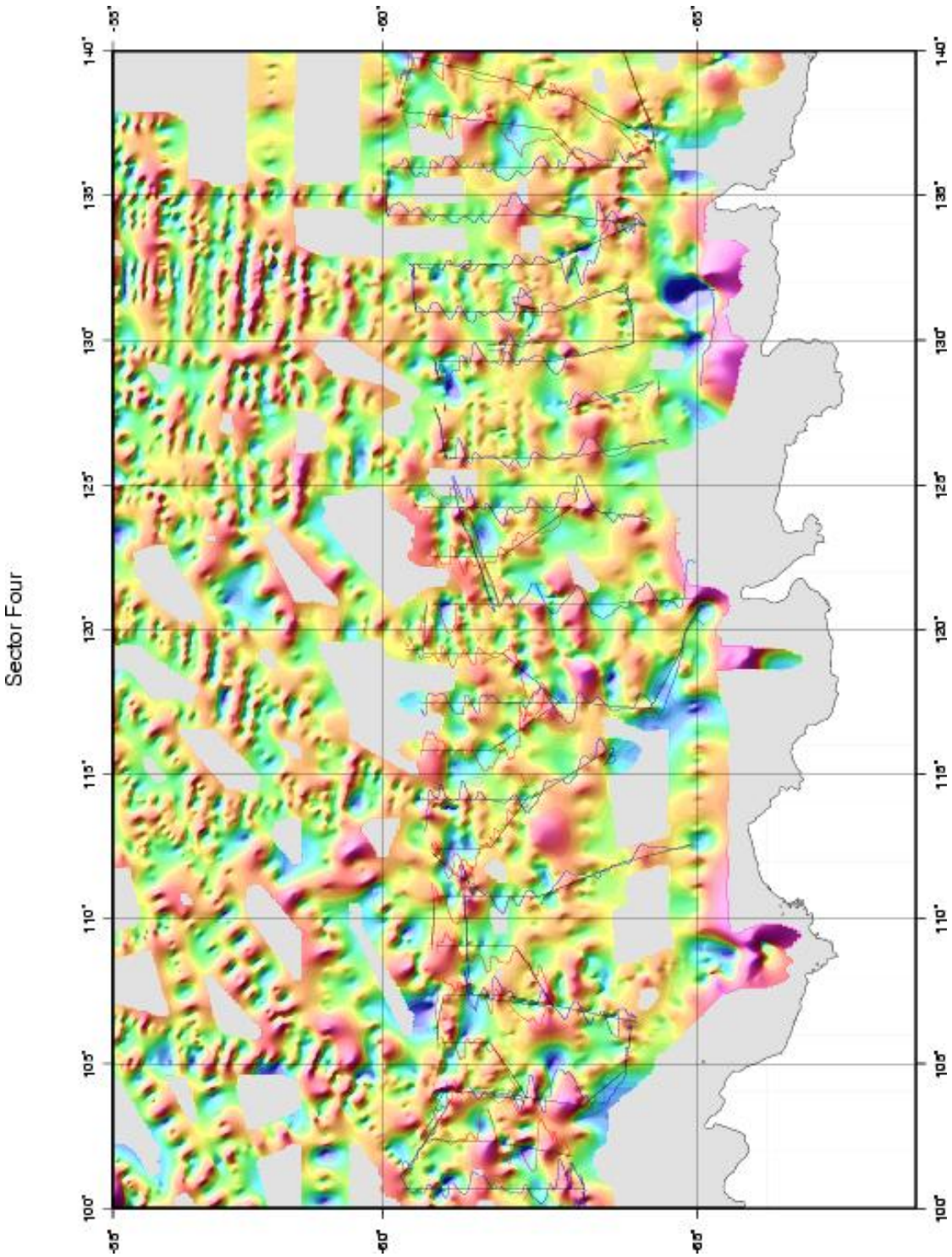

Figure 27: Colour-shaded, gridded magnetic anomaly data for Sector 4. Grey areas denote insufficient data coverage for interpolation. Superimposed are filtered and trended magnetic anomaly profiles from surveys GA-228 (blue) and GA-229 (red).

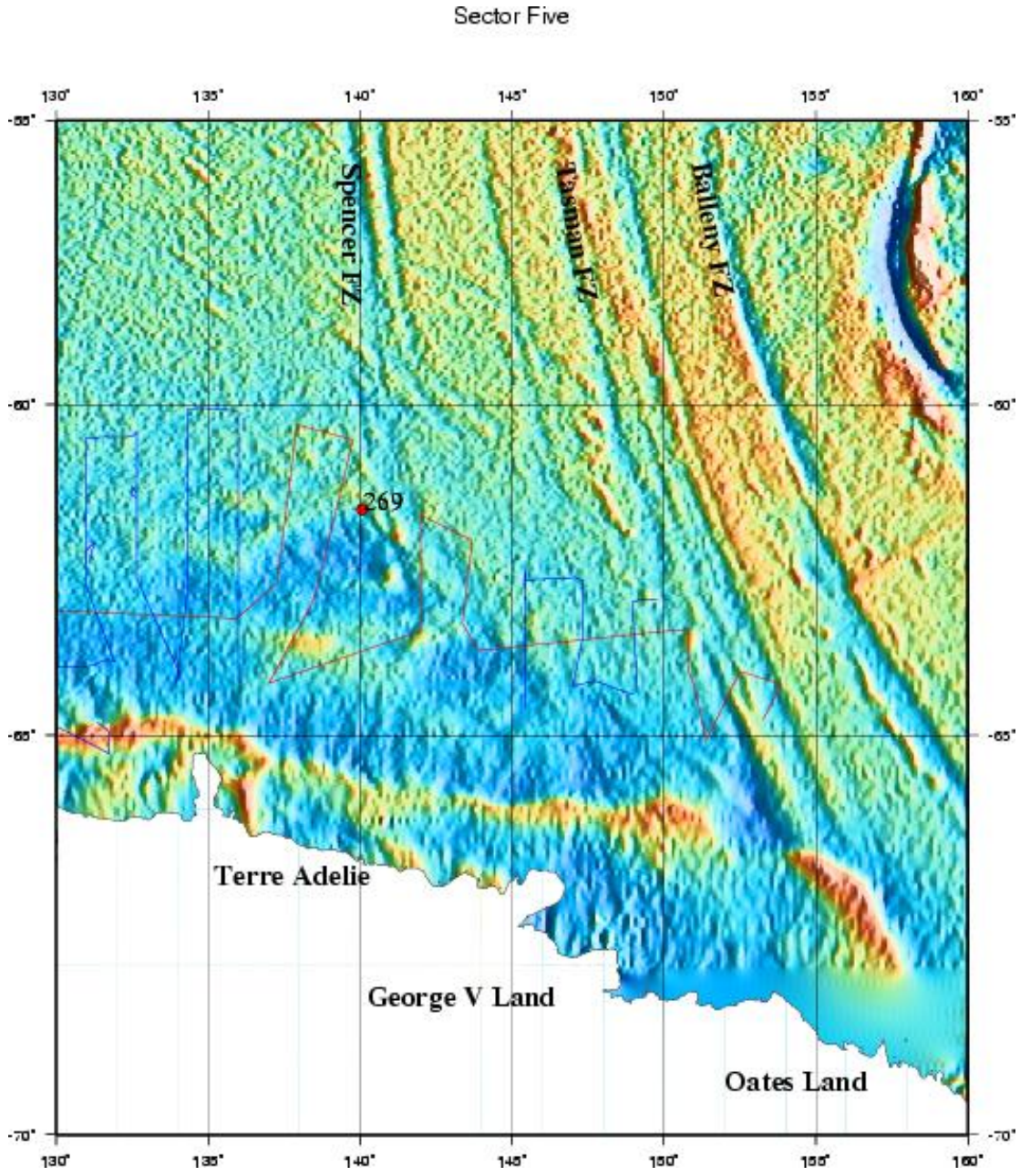

Figure 28: Marine gravity field (from McAdoo & Laxon 1997) off Terre Adélie, George V Land, and Oates Land (Sector 5) with illumination azimuth from the north. Trackline coverage of surveys GA-228 (blue) and GA-229 (red).

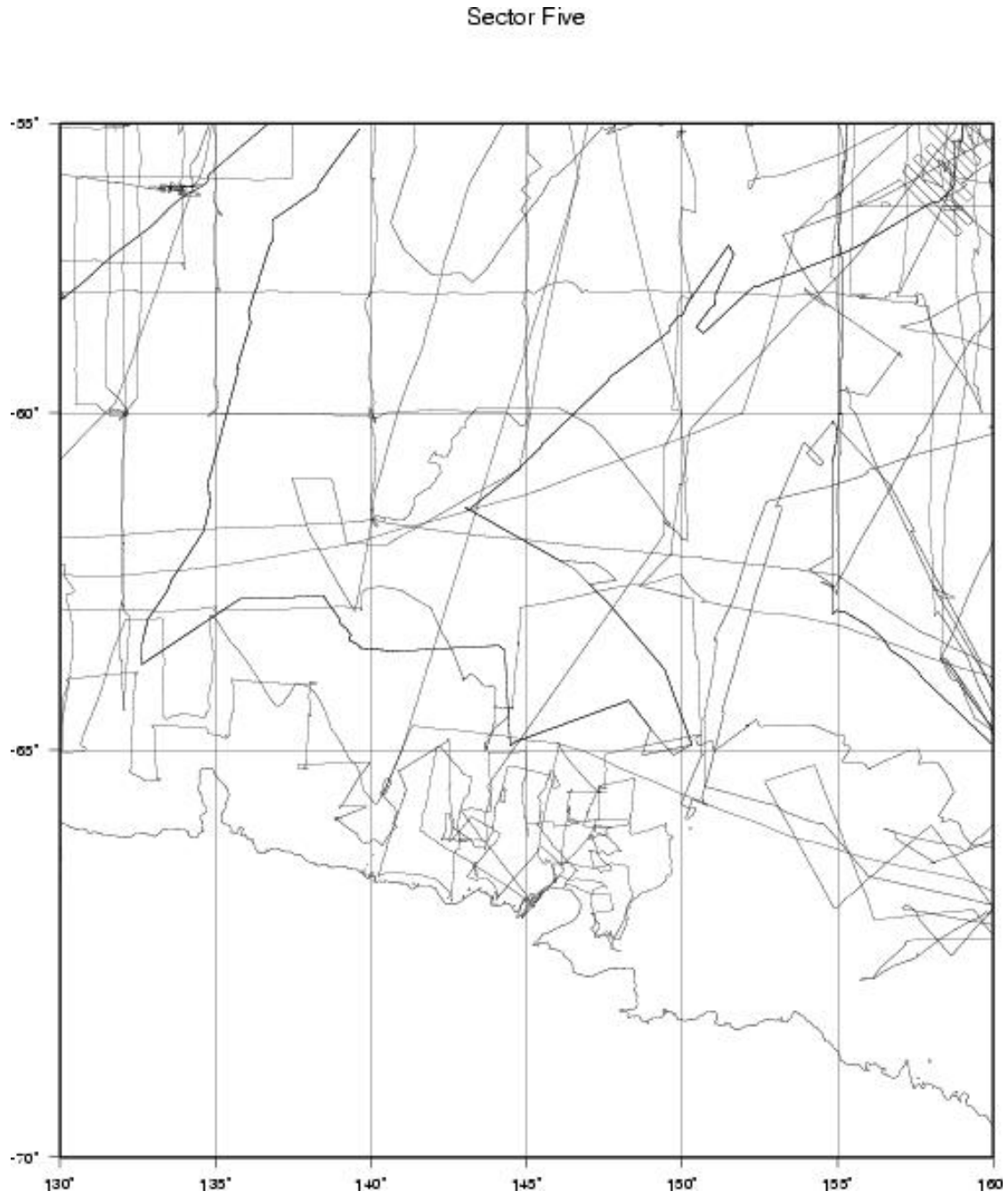

Figure 29: Shiptrack survey coverage of open-file magnetic anomaly data from the NGDC database (Sector 5).

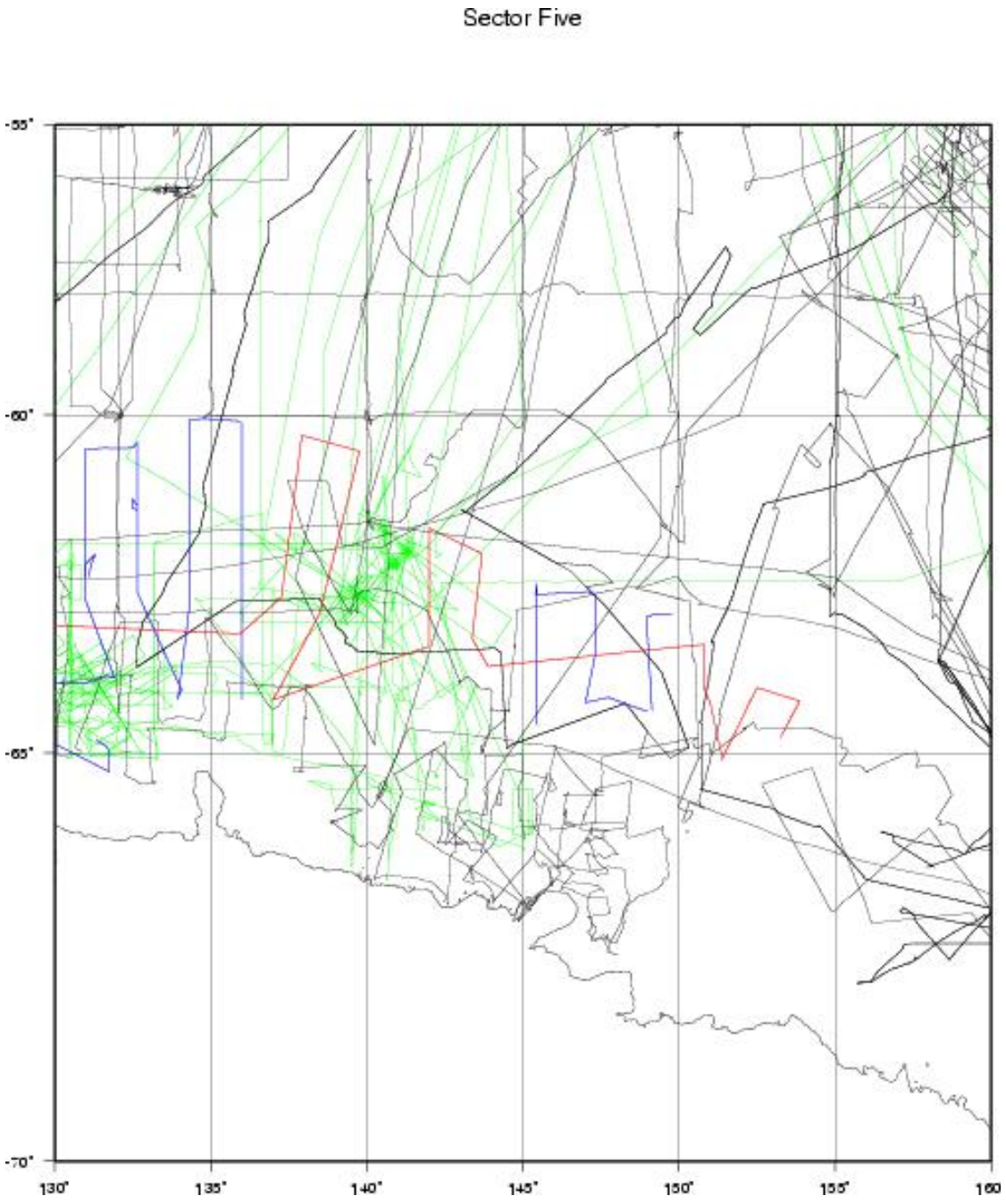

Figure 30: Shiptrack survey coverage of magnetic anomaly data (Sector 5) from the NGDC database (black) and other surveys: Japan (green), GA-228 (blue), and GA-229 (red).

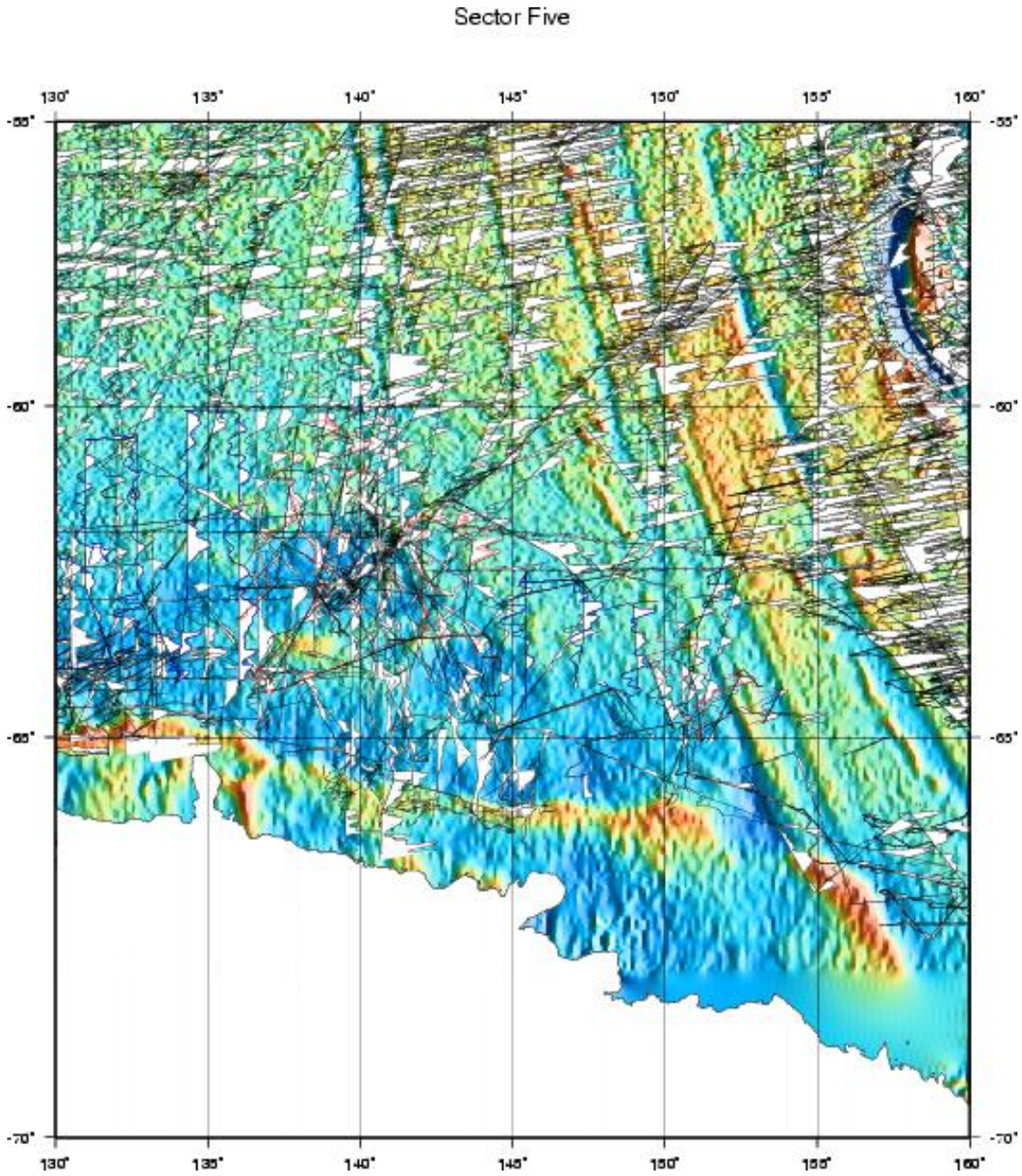

Figure 31: Filtered and trended magnetic anomaly profiles (Sector 5) with positive amplitude filled white, superimposed over satellite gravity. Also shown are tracklines from surveys GA-228 (blue) and GA-229 (red).

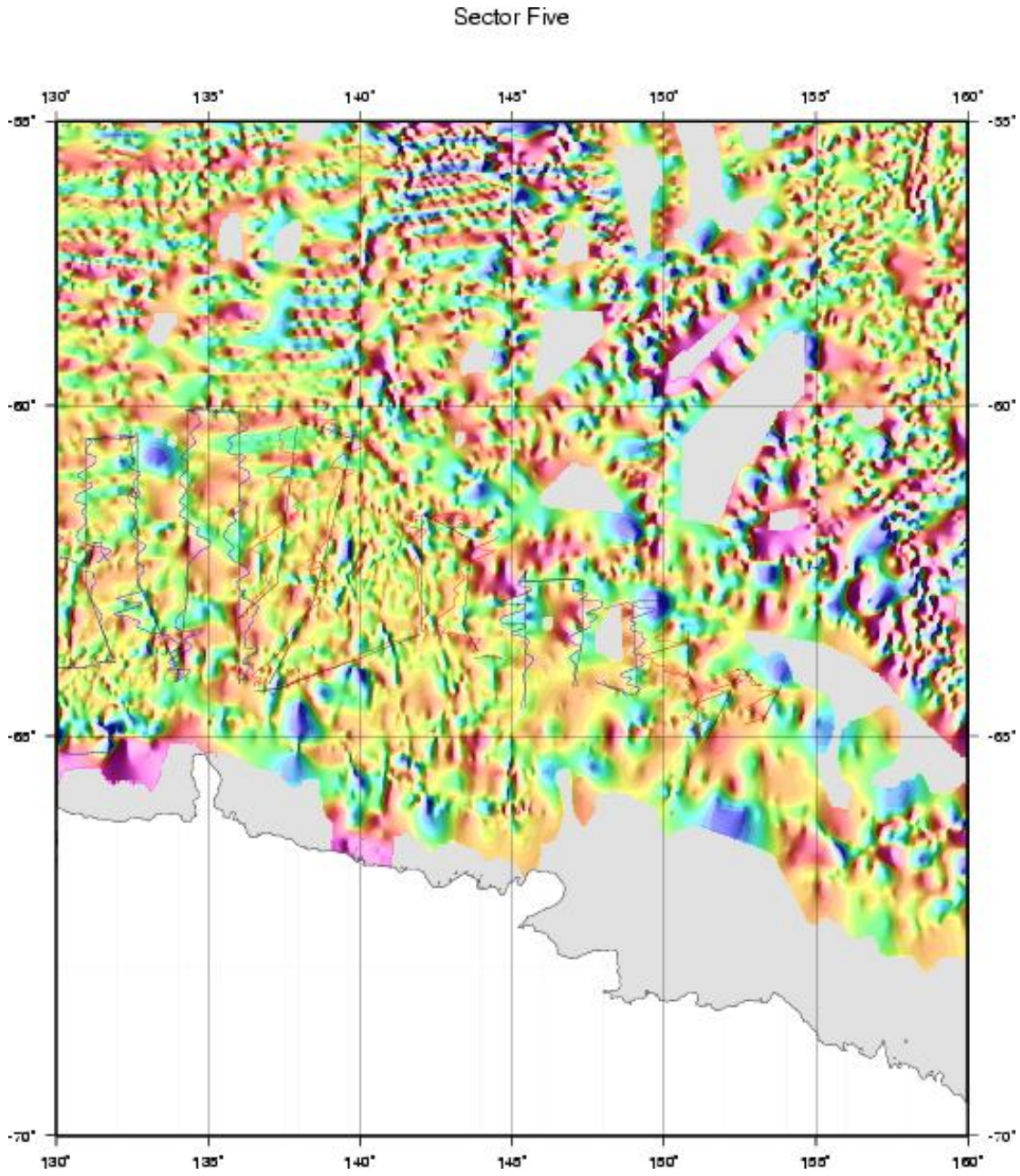

Figure 32: Colour-shaded, gridded magnetic anomaly data for Sector 5. Grey areas denote insufficient data coverage for interpolation. Superimposed are filtered and trended magnetic anomaly profiles from surveys GA-228 (blue) and GA-229 (red).

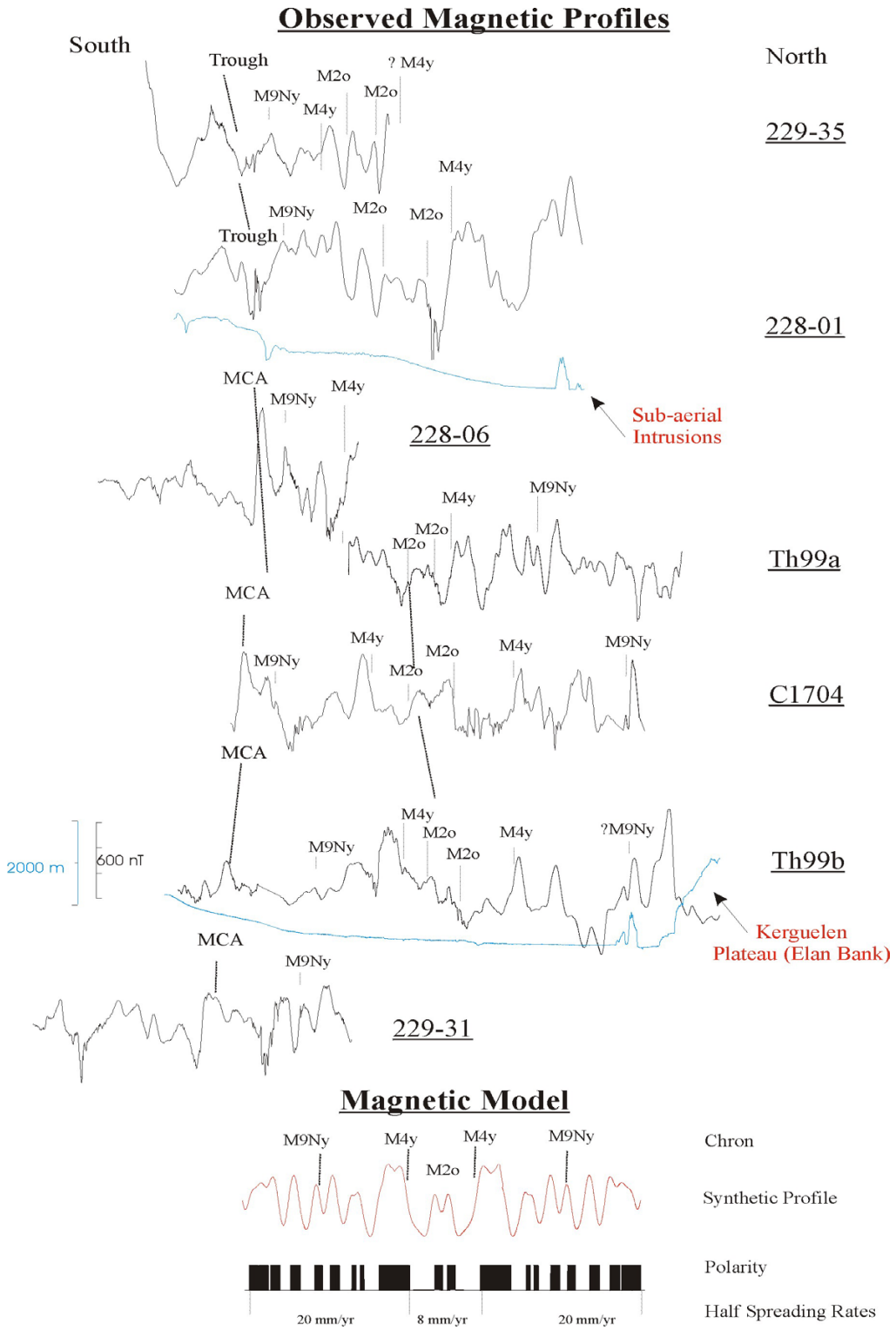

Figure 33: Selected magnetic anomaly profiles and synthetic model for the magnetic sequence identified in the GI–A segment of the region of the AAT.

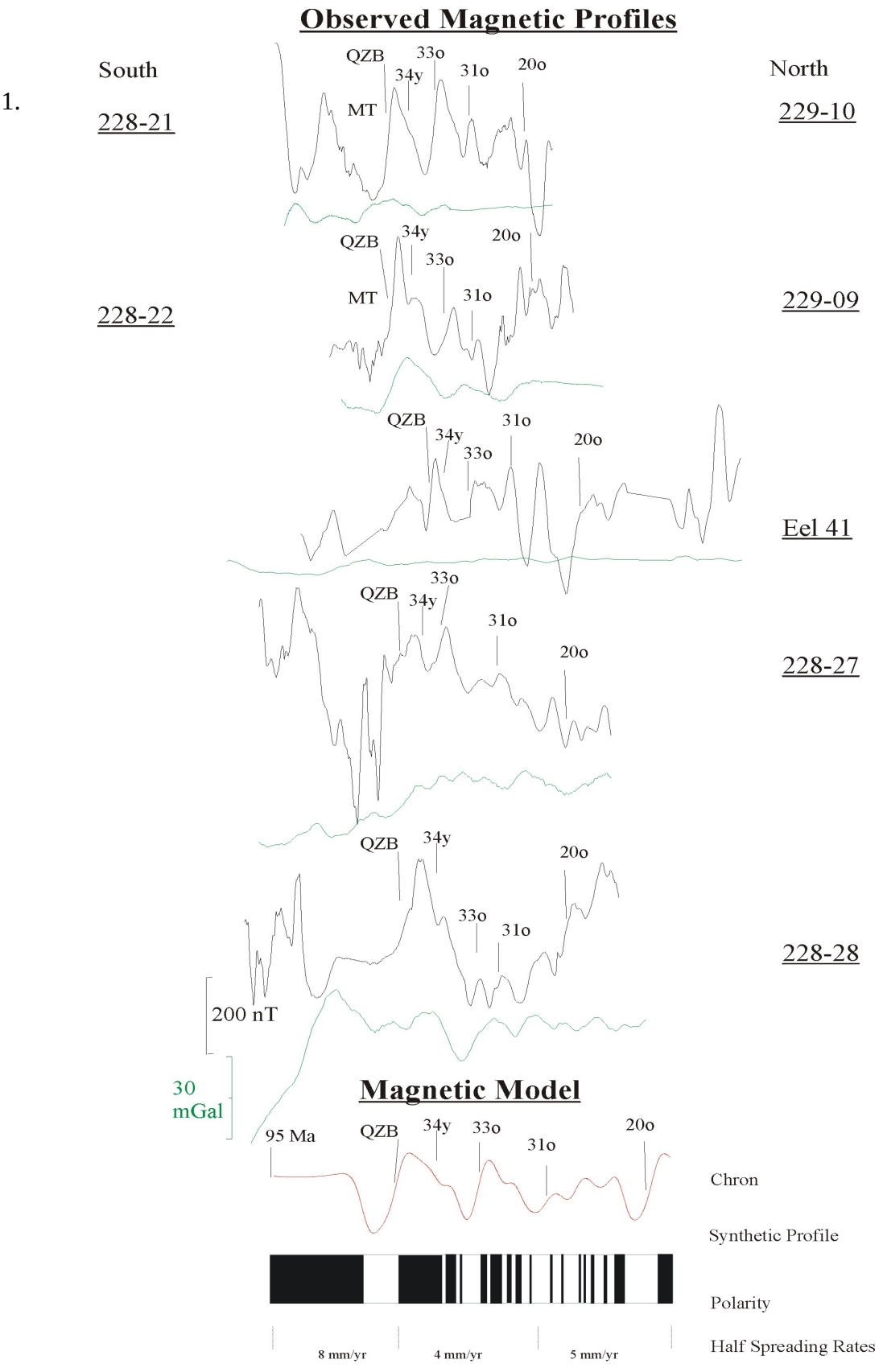

Figure 34: Selected magnetic anomaly profiles and synthetic model for the magnetic sequence identified in the A–A segment of the region of the AAT.

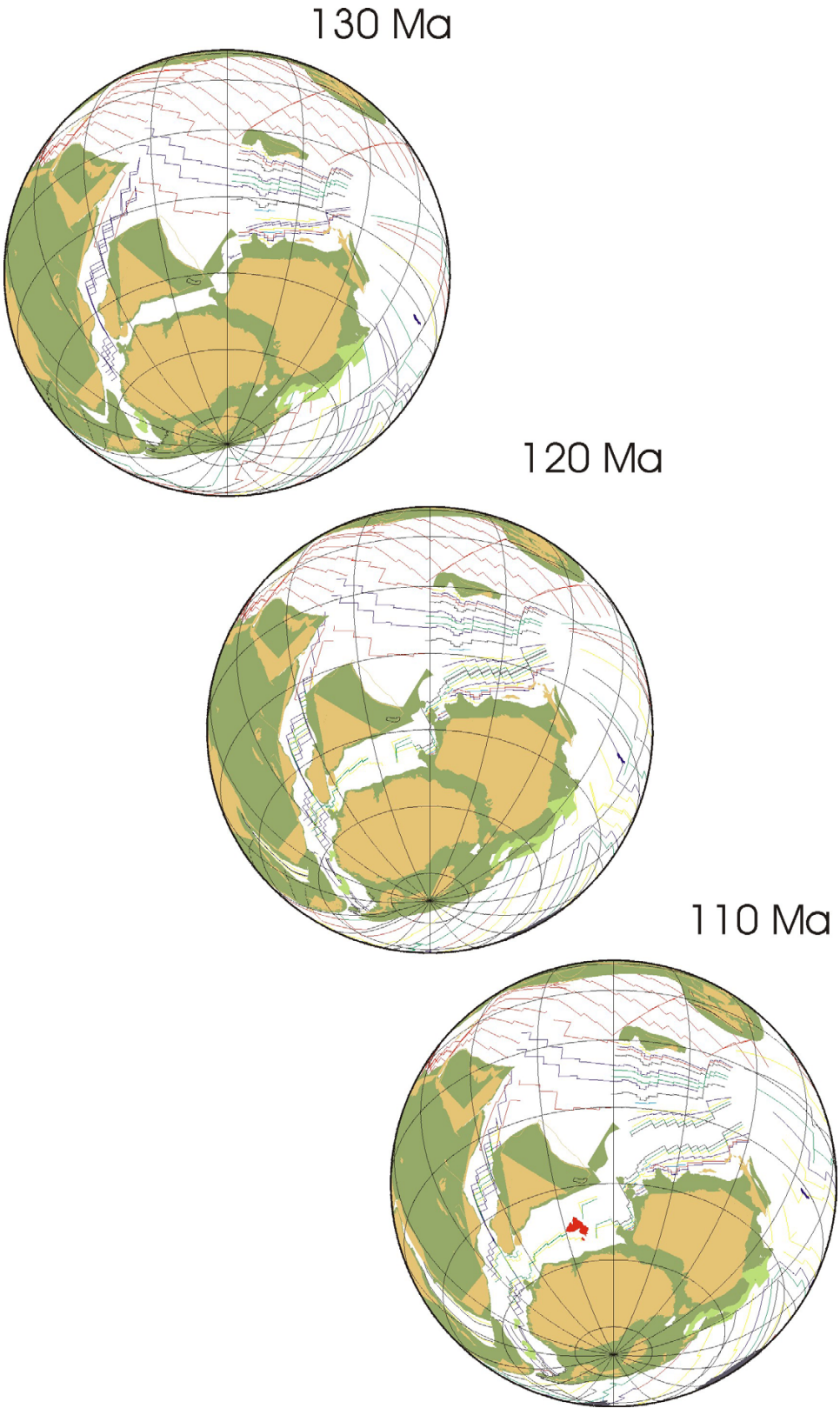

Figure 35: Plate reconstruction model for the Indian and Southern Ocean using new data from the Enderby Basin. Time intervals 130 Ma, 120 Ma and 110 Ma show the early breakup between Greater India and Antarctica, and the growth of the Kerguelen Plume (red).

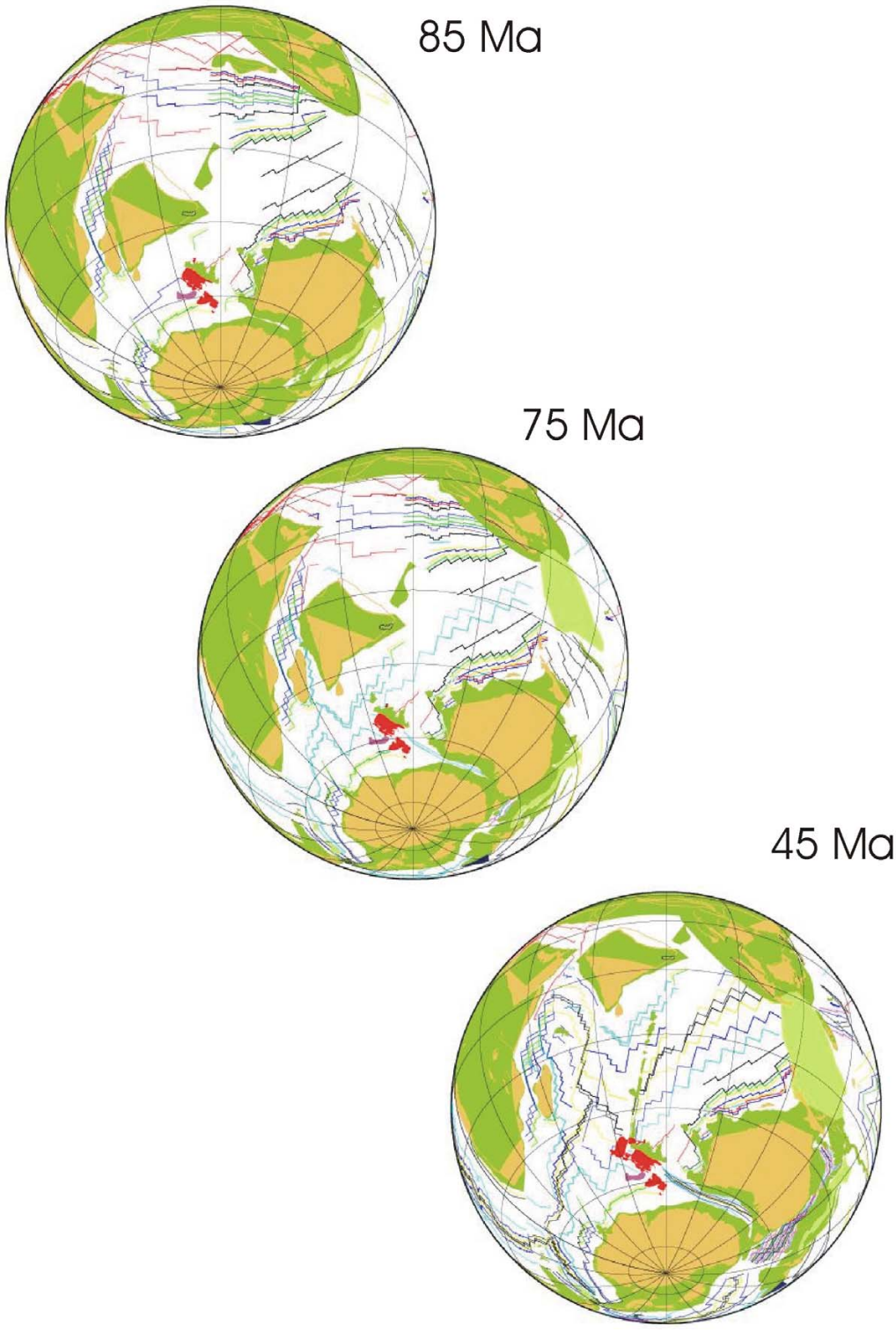

Figure 36: Plate reconstruction model for the Indian and Southern Ocean using new data from the Enderby Basin. Time intervals 85 Ma, 75 Ma, and 45 Ma show the long period of slow seafloor spreading during the separation between the Australian and Antarctic plates.

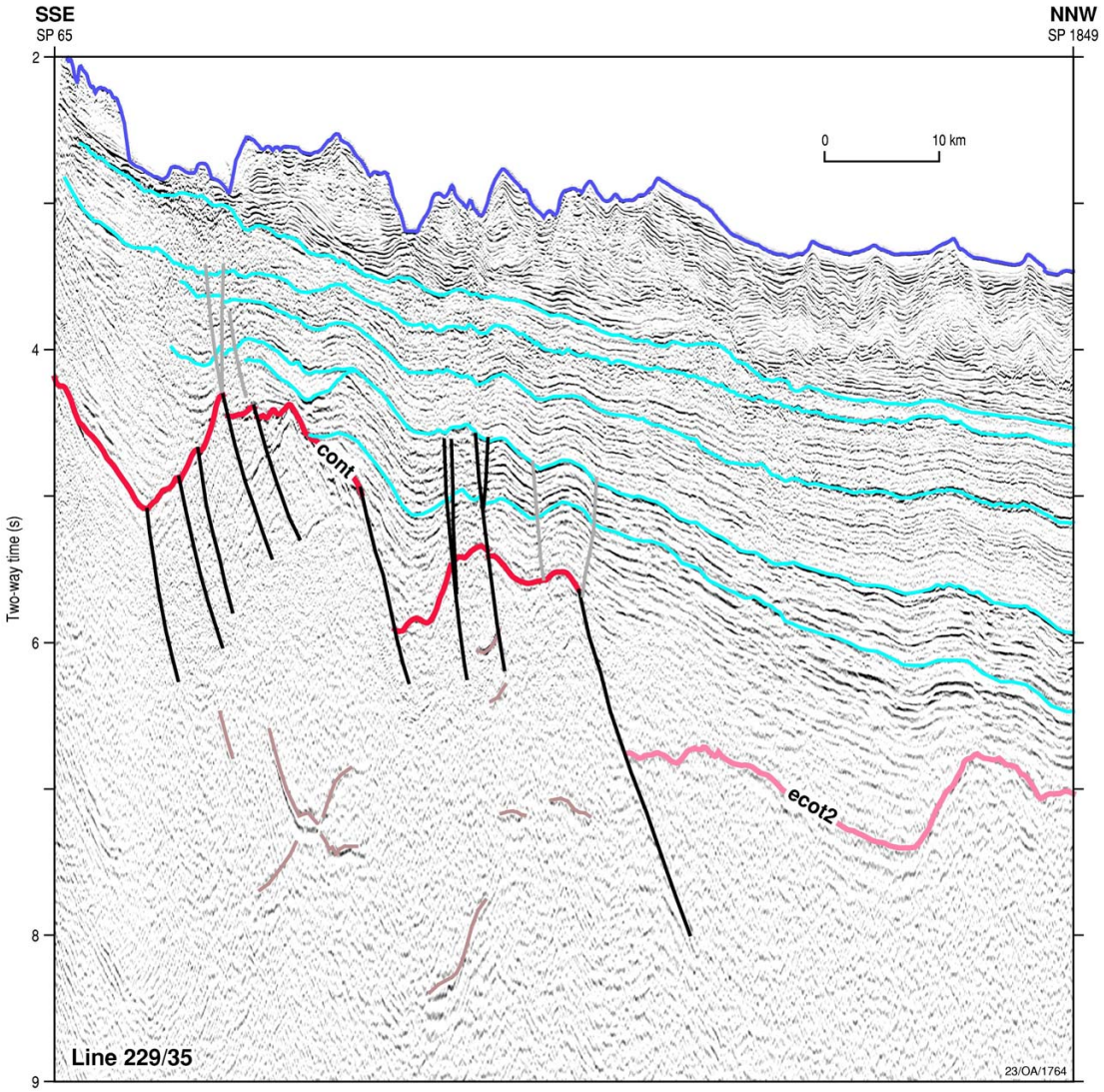

Figure 37: Detailed seismic section line GA-229/35, offshore western Enderby Land, showing continental basement (*cont*) down-faulted beneath the upper continental slope and transitional crustal type *ecot2*. Full line shown in Plate 10.

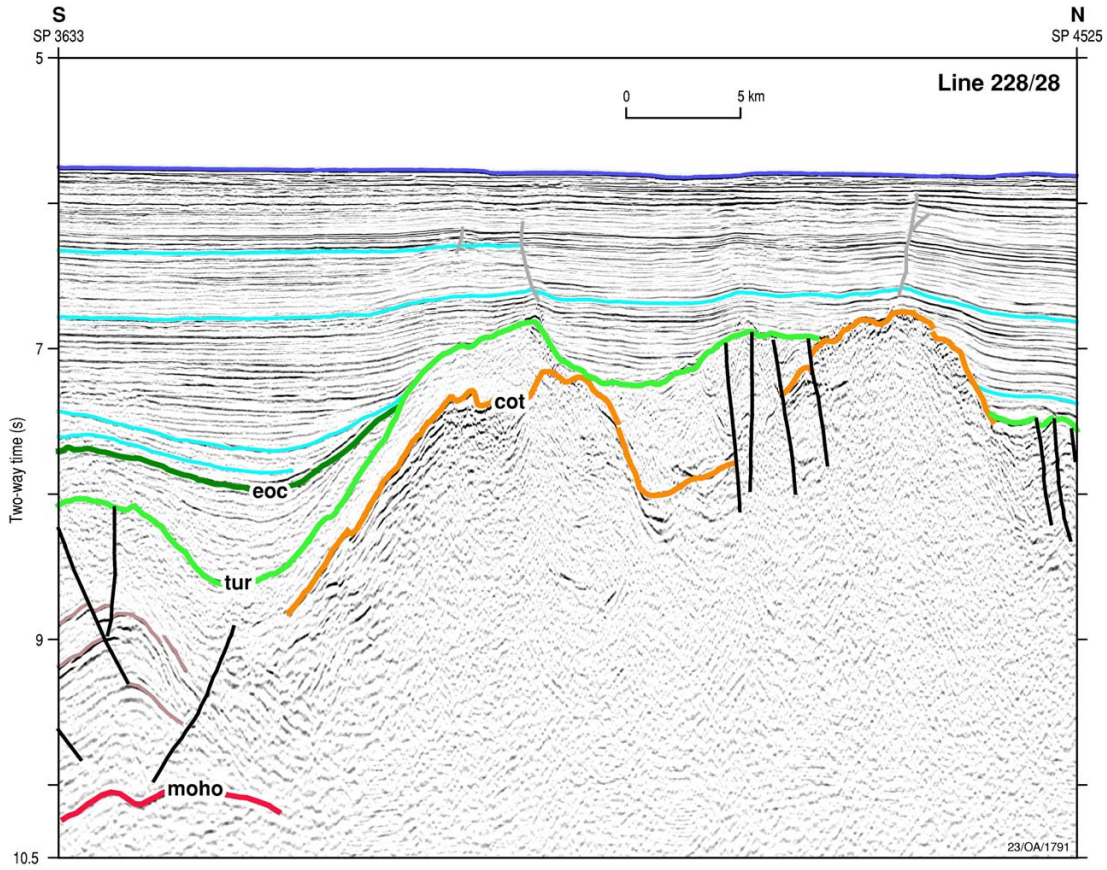

Figure 38: Detailed seismic section line GA-228/28, offshore eastern Wilkes Land, showing the interpreted peridotite ridge (below horizon *cot*). The crust immediately adjacent landward (south) has undergone extreme thinning. *tur* – Turonian; *eoc* – Eocene. Full line shown in Plate 17.

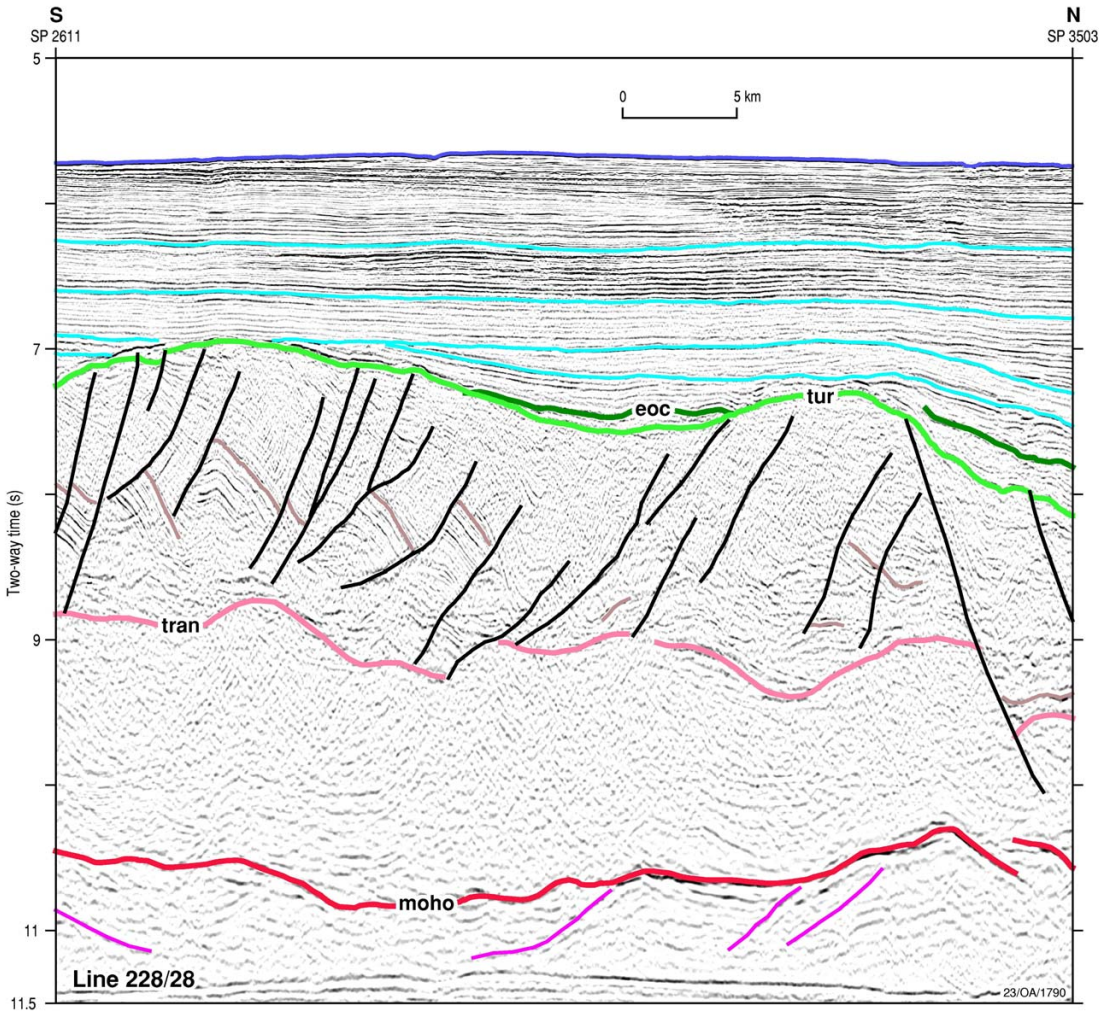

Figure 39: Detailed seismic section line GA-228/28, offshore eastern Wilkes Land, showing reflection Moho, transparent crystalline crust, highly faulted and rotated mid-Cretaceous and older section overlying a detachment surface at about 9 s TWT. *tur* – Turonian; *eoc* – Eocene. Full line shown in Plate 17.

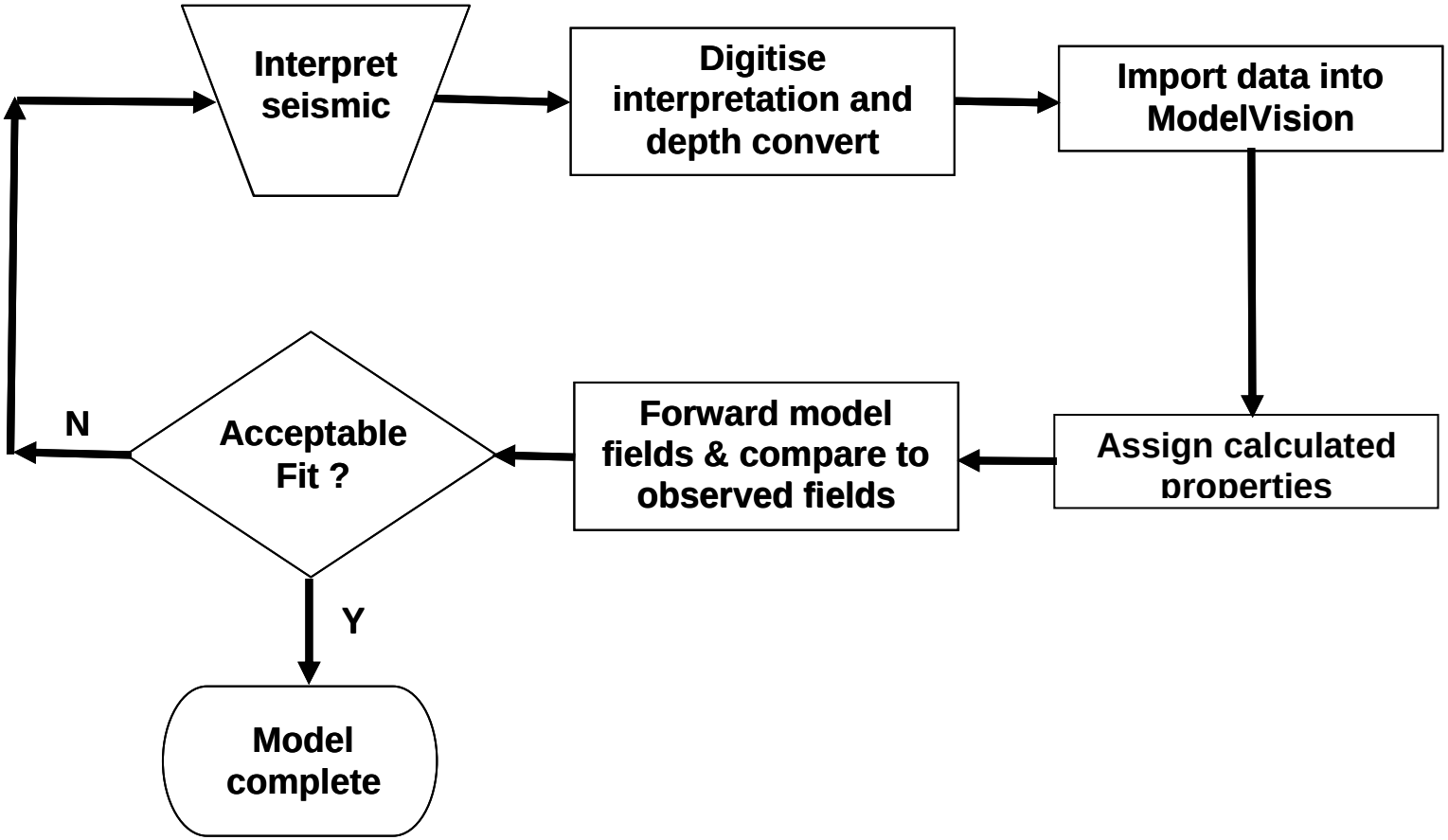

Figure 40: Processing flow for potential field modelling integrated with interpretation of deep-seismic data.

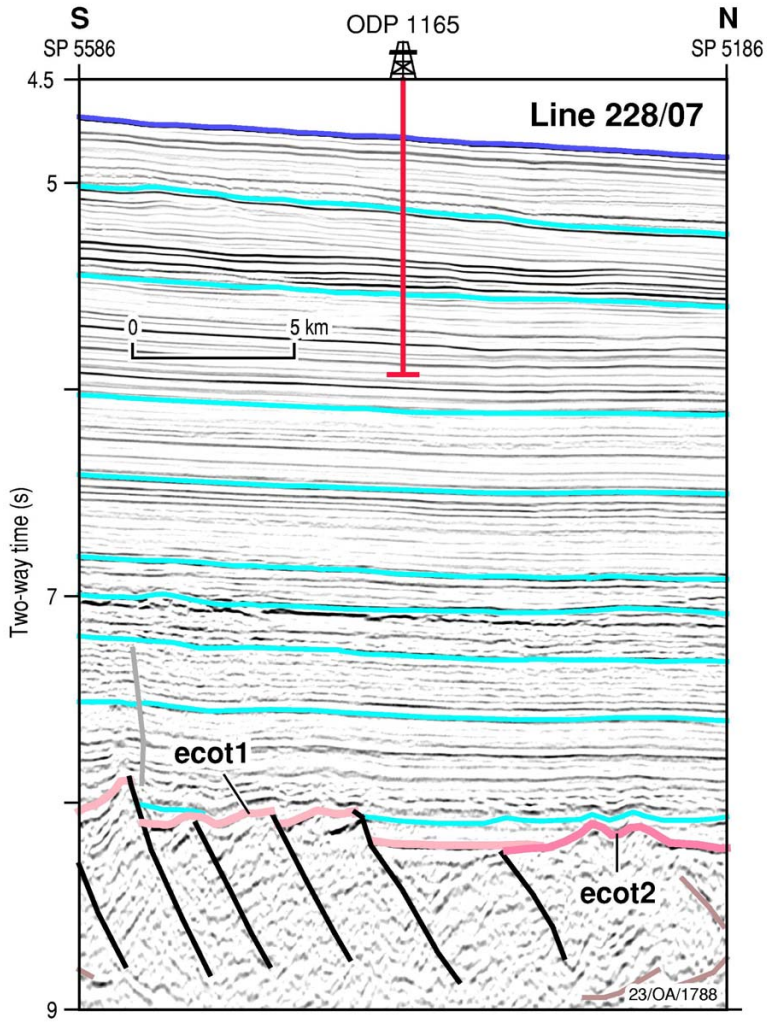

Figure 41: Detailed seismic section line GA-228/07, offshore Mac. Robertson Land, showing the location and penetration of ODP Site 1165, and transitional crustal types *ecot1* and *ecot2*. Full line shown in Plate 12.

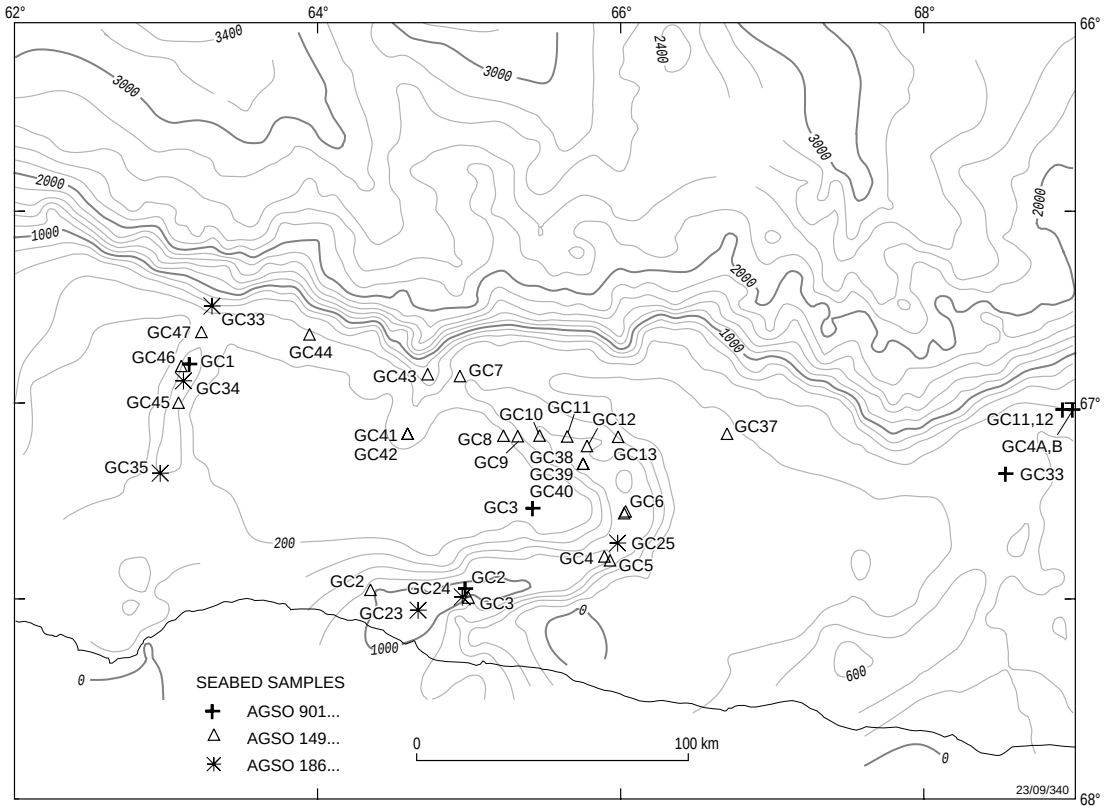

Figure 42: Sample locations on the Mac. Robertson Shelf (after O'Brien et al., 2002).

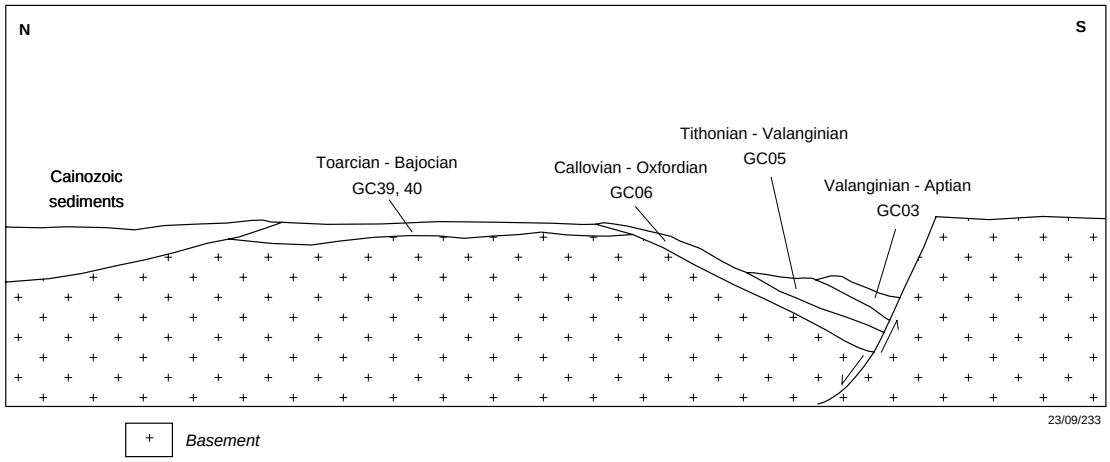

Figure 43: Inferred stratigraphic relationships on the Mac.Robertson Shelf (after Truswell et al., 1999). Antarctic continent is on the right.

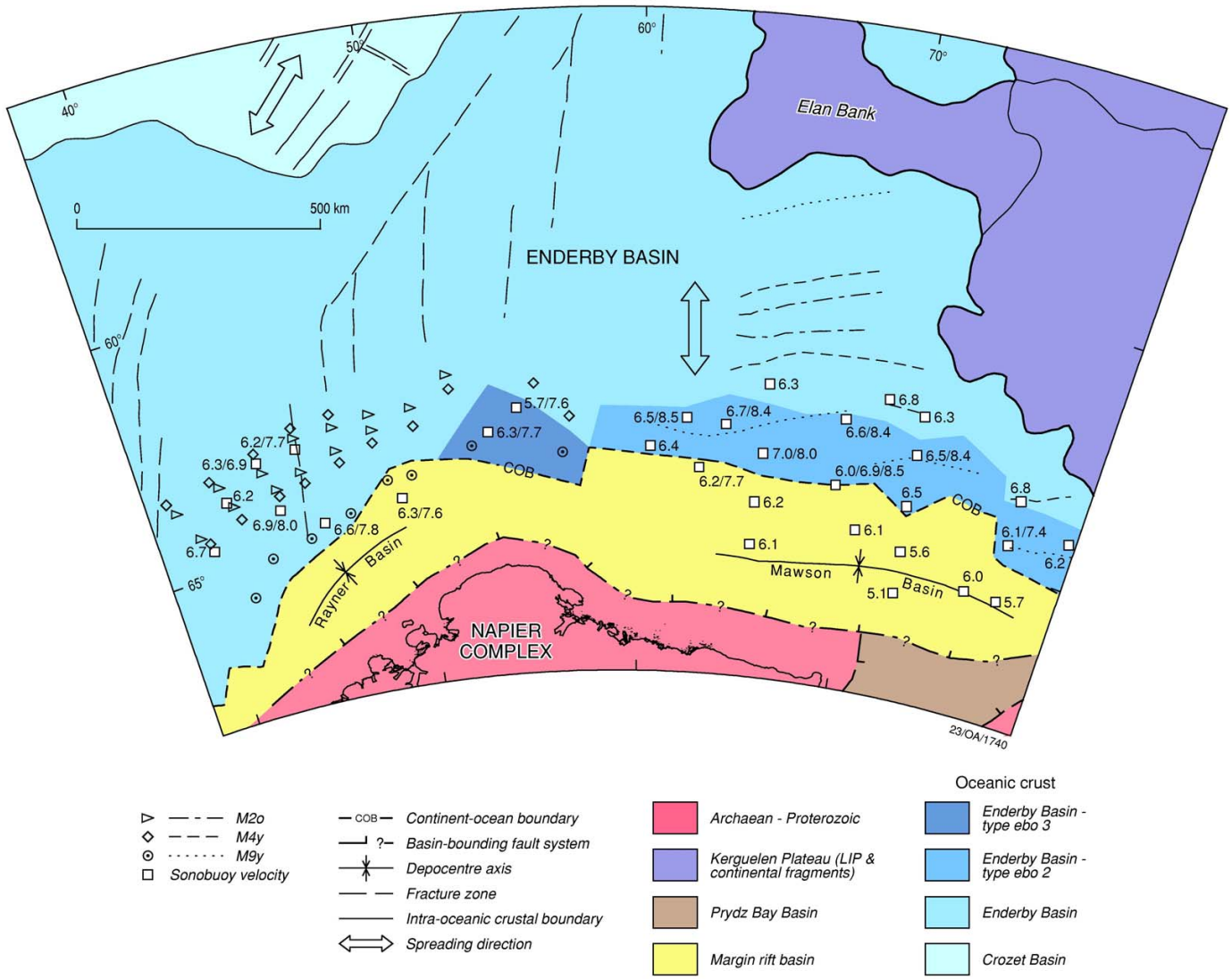

Figure 44: Tectonic elements of the East Antarctic margin from western Enderby Land to Prydz Bay (after Stagg et al., in press).

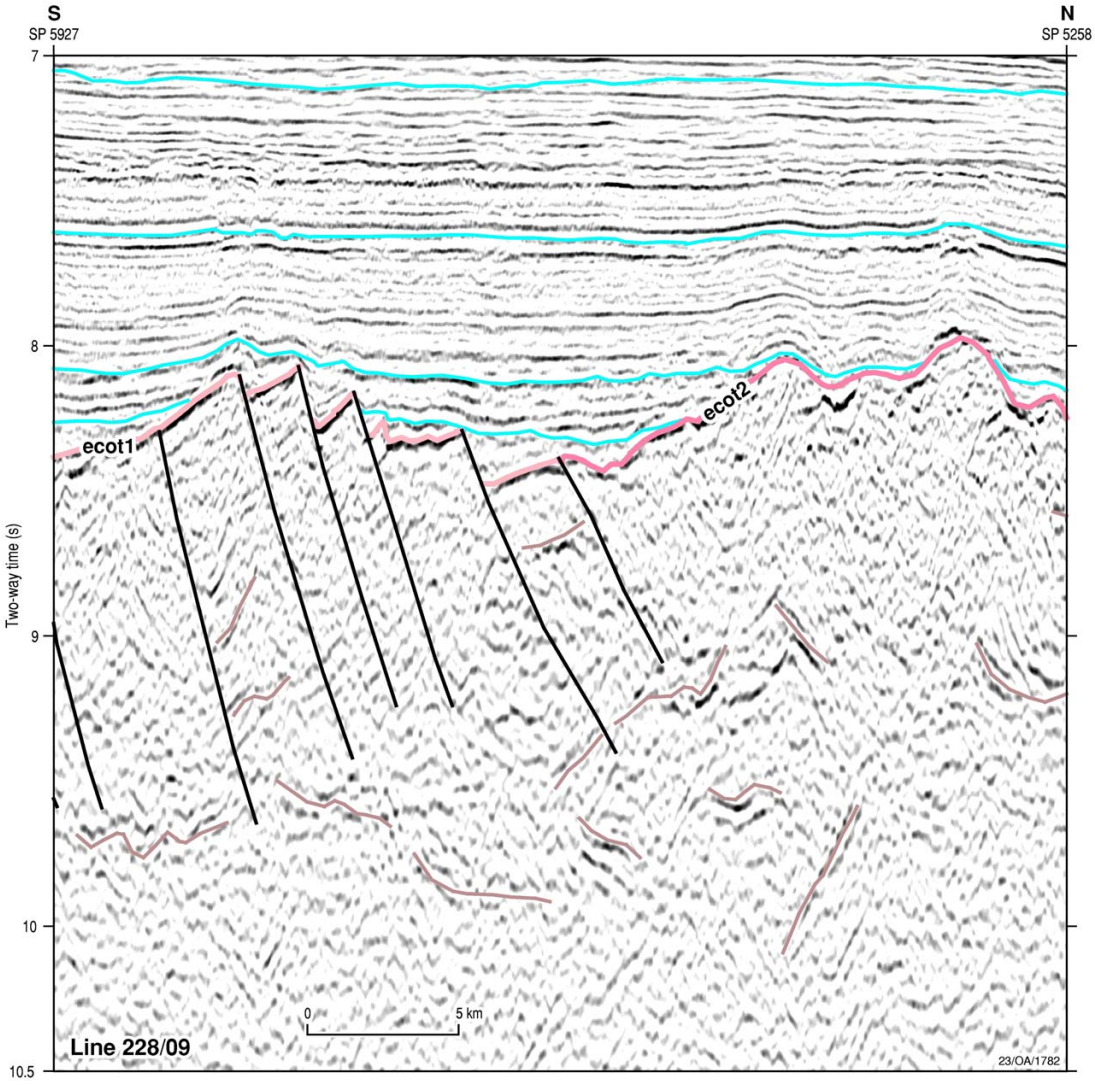

Figure 45: Detailed seismic section line GA-228/09, offshore from Prydz Bay, showing characteristics of the transitional crustal types *ecot1* and *ecot2*. Full line shown in Plate 12.

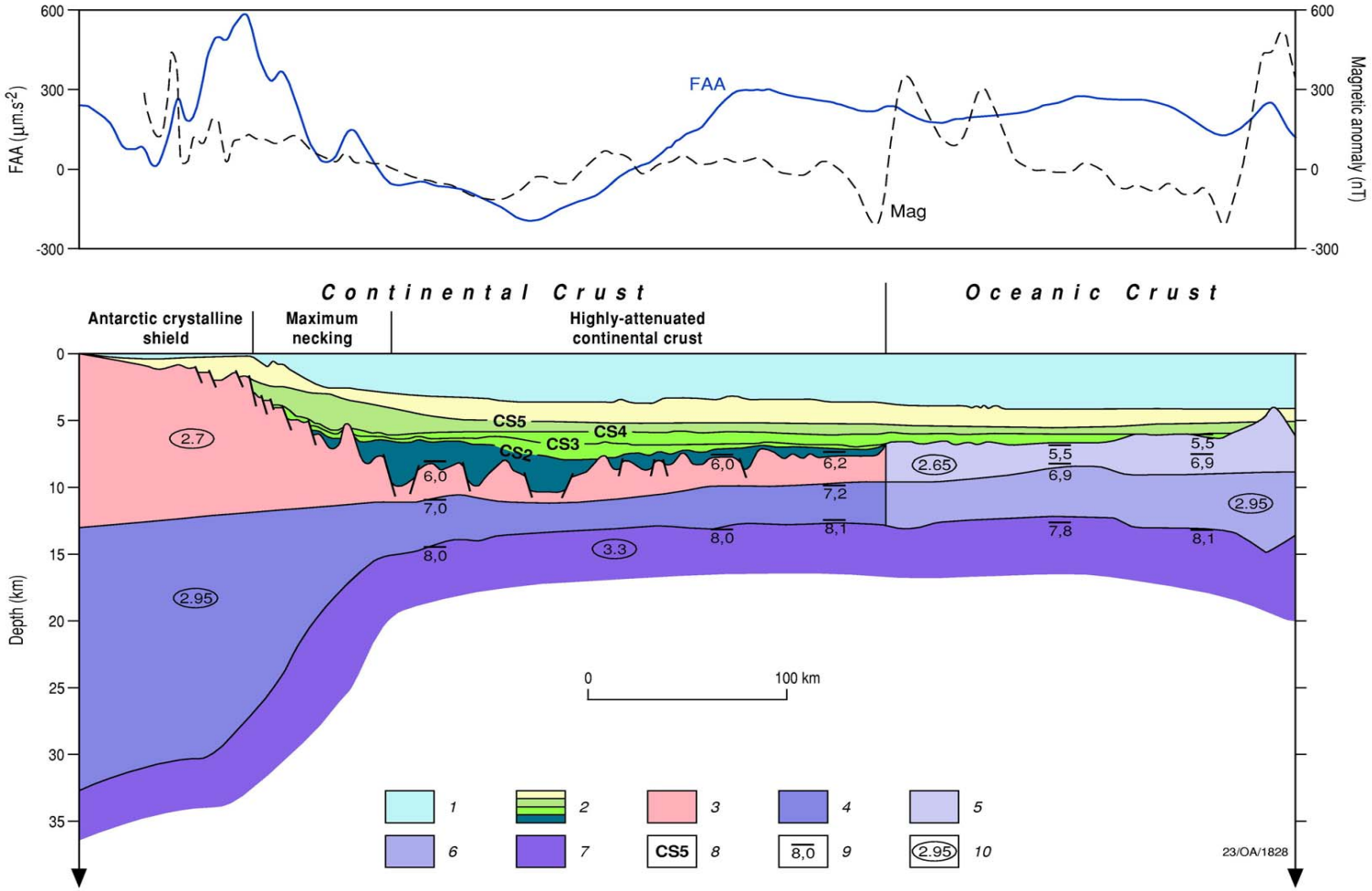

Figure 46: Potential field model from the margin off Mac. Robertson Land (modified from Gandyukhin et al., 2002). Legend: 1 – water layer; 2 – sedimentary layers; 3 – upper crust; 4 – lower crust; 5 – oceanic layer 2; 6 – oceanic layer 3; 7 – upper mantle; 8 – major unconformities; 9 – refracting crustal boundaries and values of boundary velocities; 10 – densities ($kg.m^{-3}$).

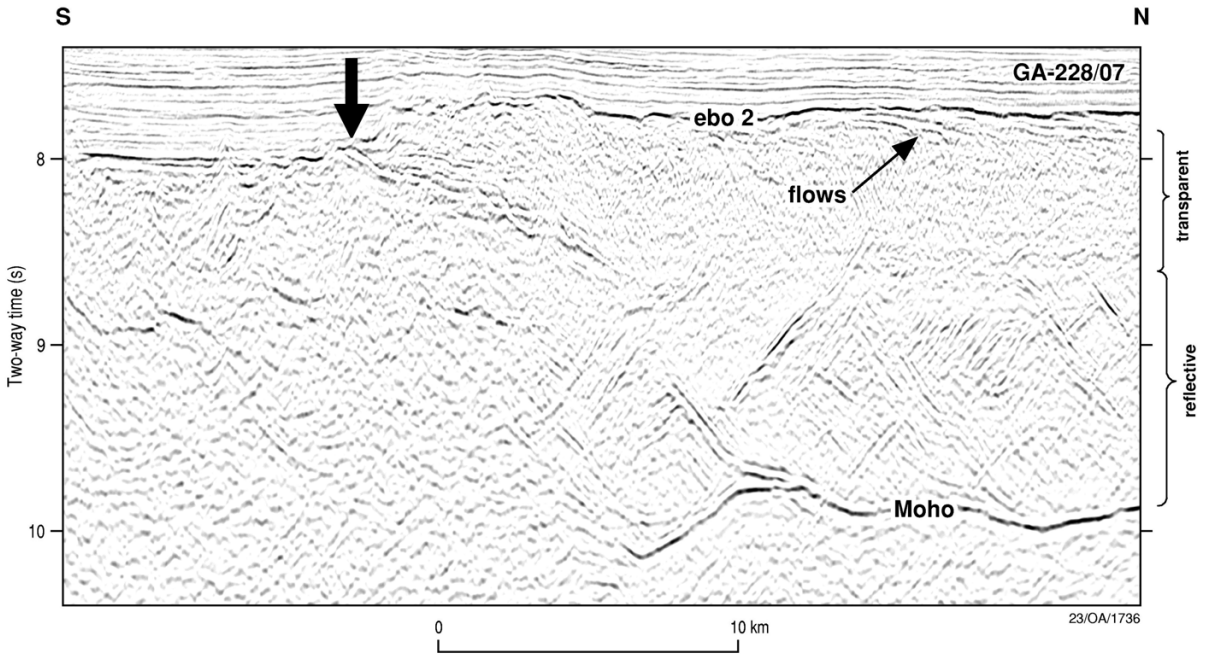

Figure 47: Seismic detail from line GA-228/07 showing the interpreted continent–ocean boundary zone east of 58°E (continental/transitional crust to the south). In particular, note the step up from continental/transitional crust on the left to oceanic crust on the right, and the abrupt southwards termination of reflection Moho beneath the inboard edge of oceanic crust at ~10 s TWT. Note also the horizontal partitioning of the oceanic crust into a thin upper layer of short, seaward-dipping flows; semitransparent upper-middle crust; lower, highly-reflective crust; and high-amplitude, continuous reflection Moho. Full line shown in Plate 12. After Stagg et al. (in press).

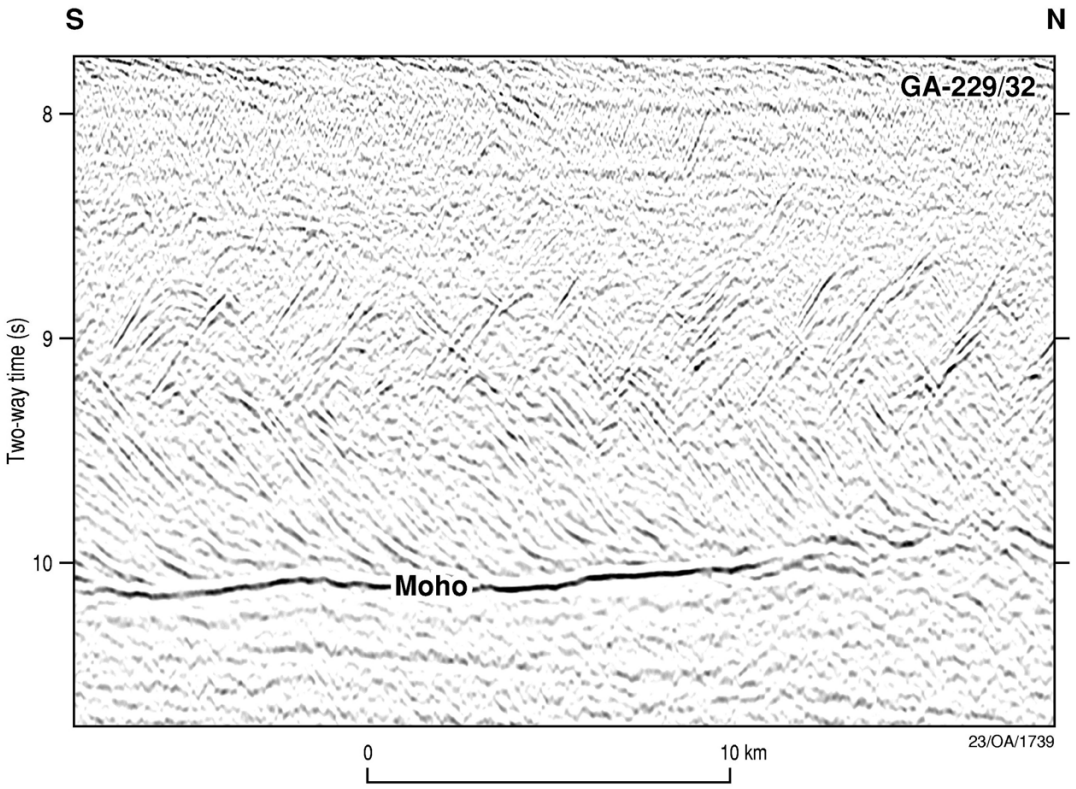

Figure 48: Seismic detail line GA-229/32 showing highly reflective lower oceanic crust (below ~8.8 s TWT) underlain by highly continuous reflection Moho at 10 s TWT. The deepest reflections in the crust sole out on to the Moho reflection. Full line shown in Plate 12. After Stagg et al. (in press).

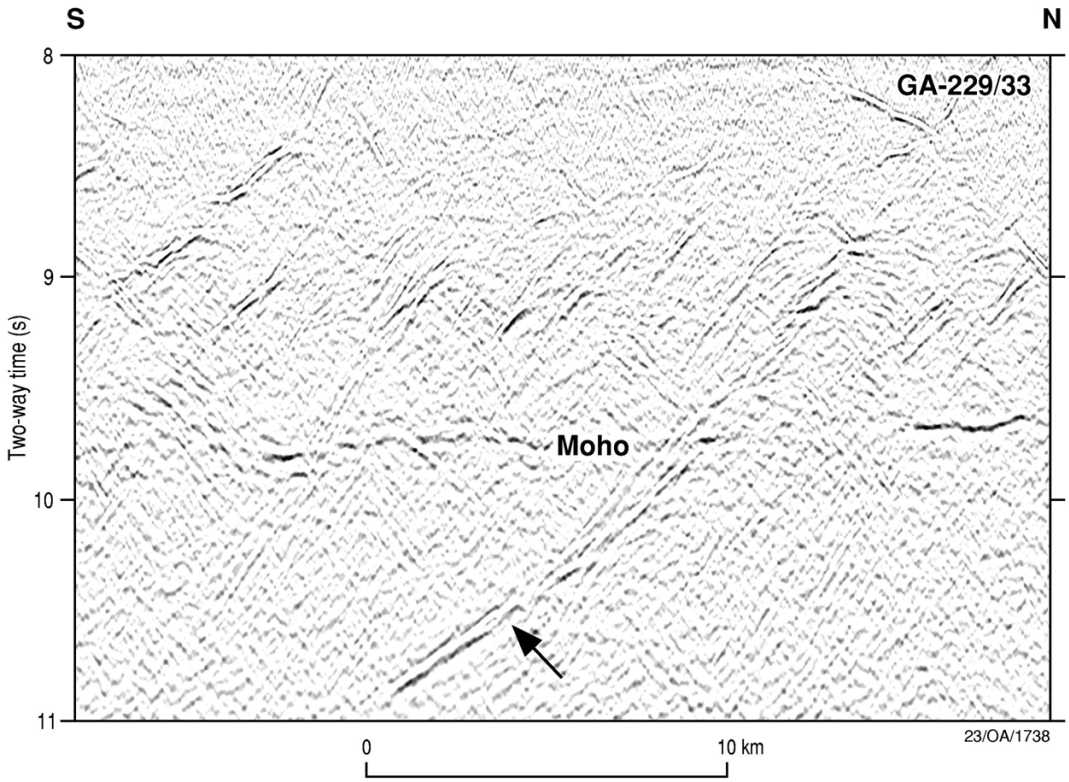

Figure 49: Seismic detail line GA-229/33 showing reflective lower oceanic crust underlain by a discontinuous reflection Moho at about 9.8 s TWT. The south-dipping reflector in the upper mantle (arrow) may be related to dipping reflectors in the overlying crust. Full line shown in Plate 11. After Stagg et al. (in press).

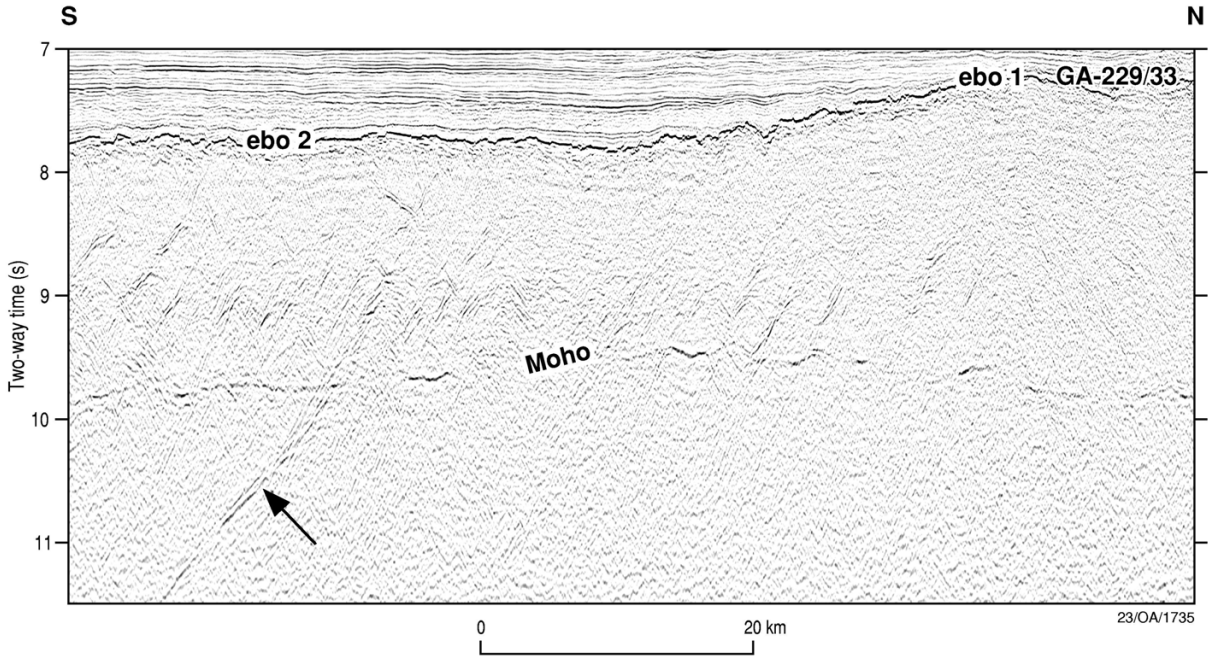

Figure 50: Seismic detail from line GA-229/33 showing oceanic basement types *ebo 1* and *ebo 2*. *ebo 2* is at a depth of approximately 7.8 s TWT; the crust below ~8.5 s TWT is highly reflective and reflection Moho is strong and continuous. *ebo 1* is considerably shallower (~7.3 s TWT; the underlying crust is much less reflective and reflection Moho is weaker and less continuous. Note also the south-dipping upper mantle reflections (arrow) at the left-hand end of the profile. Full line shown in Plate 11. After Stagg et al. (in press).

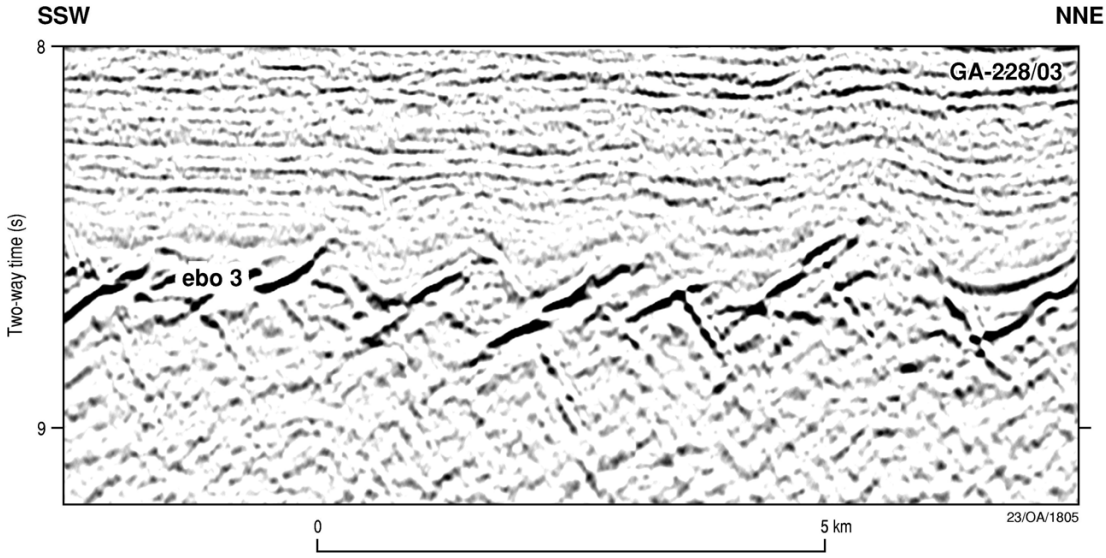

Figure 51: Seismic detail from line GA-228/03 showing the basement type *ebo 3*. The depth of 8.5-8.7 s TWT for this basement type is significantly deeper than other basement types in the Enderby Basin, and is comparable to the depth of the Jurassic oceanic crust beneath the Argo Abyssal Plain off northwest Australia. Note also the characteristic form of the basement surface, with short, landward-dipping ?volcanic flows with sharp scarps at their oceanward terminations. Full line shown in Plate 11. After Stagg et al. (in press).

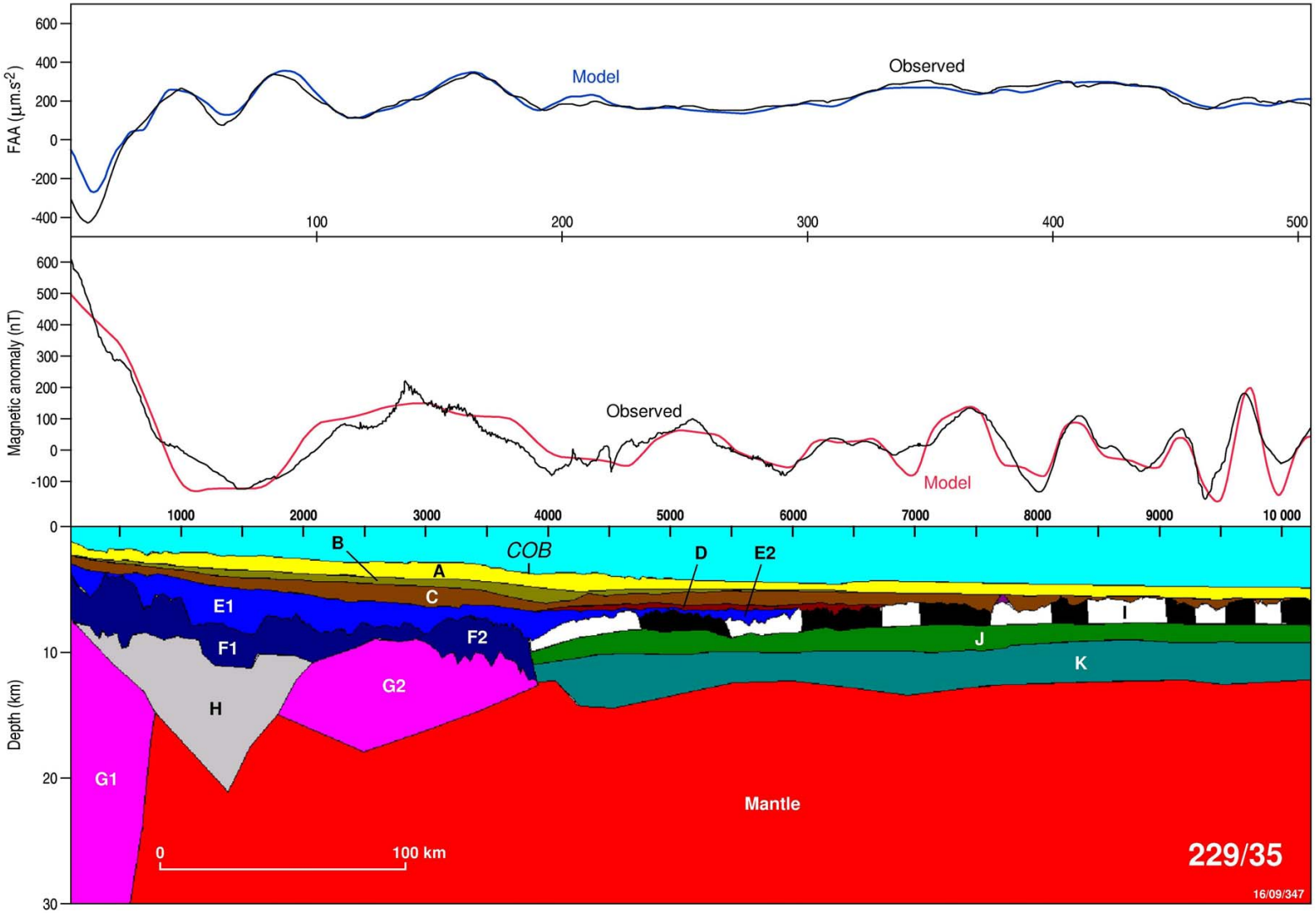

Figure 52: Potential field model for line GA-229/35, offshore western Enderby Land; south on the left. Model bodies are identified in full in Appendix 7. 'COB' shows interpreted continent–ocean boundary. After Stagg et al. (in press).

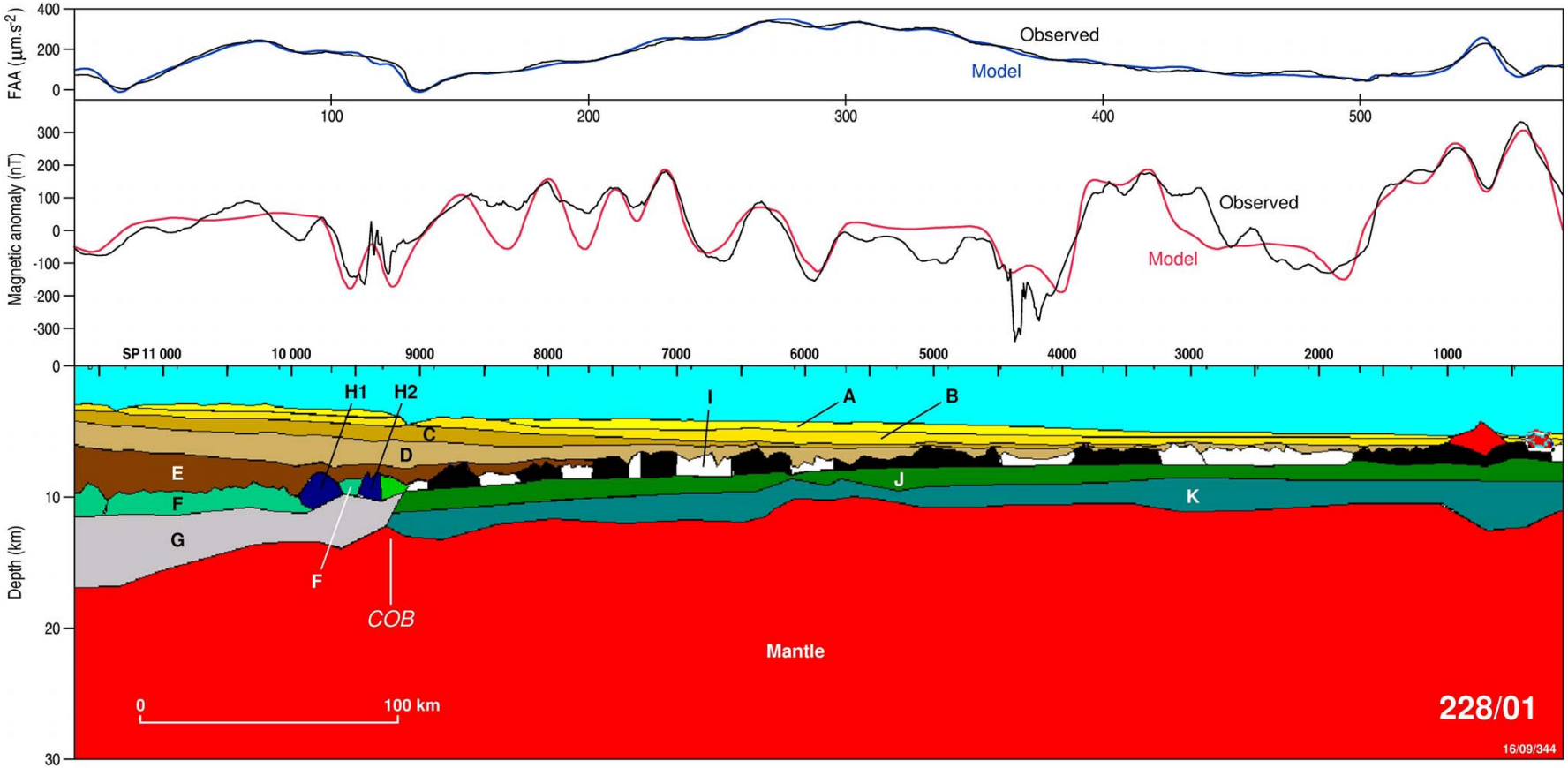

Figure 53: Potential field model for line GA-228/01, Enderby Land; south on the left. Model bodies are identified in full in Appendix 7. COB is the location of the interpreted continent–ocean boundary.

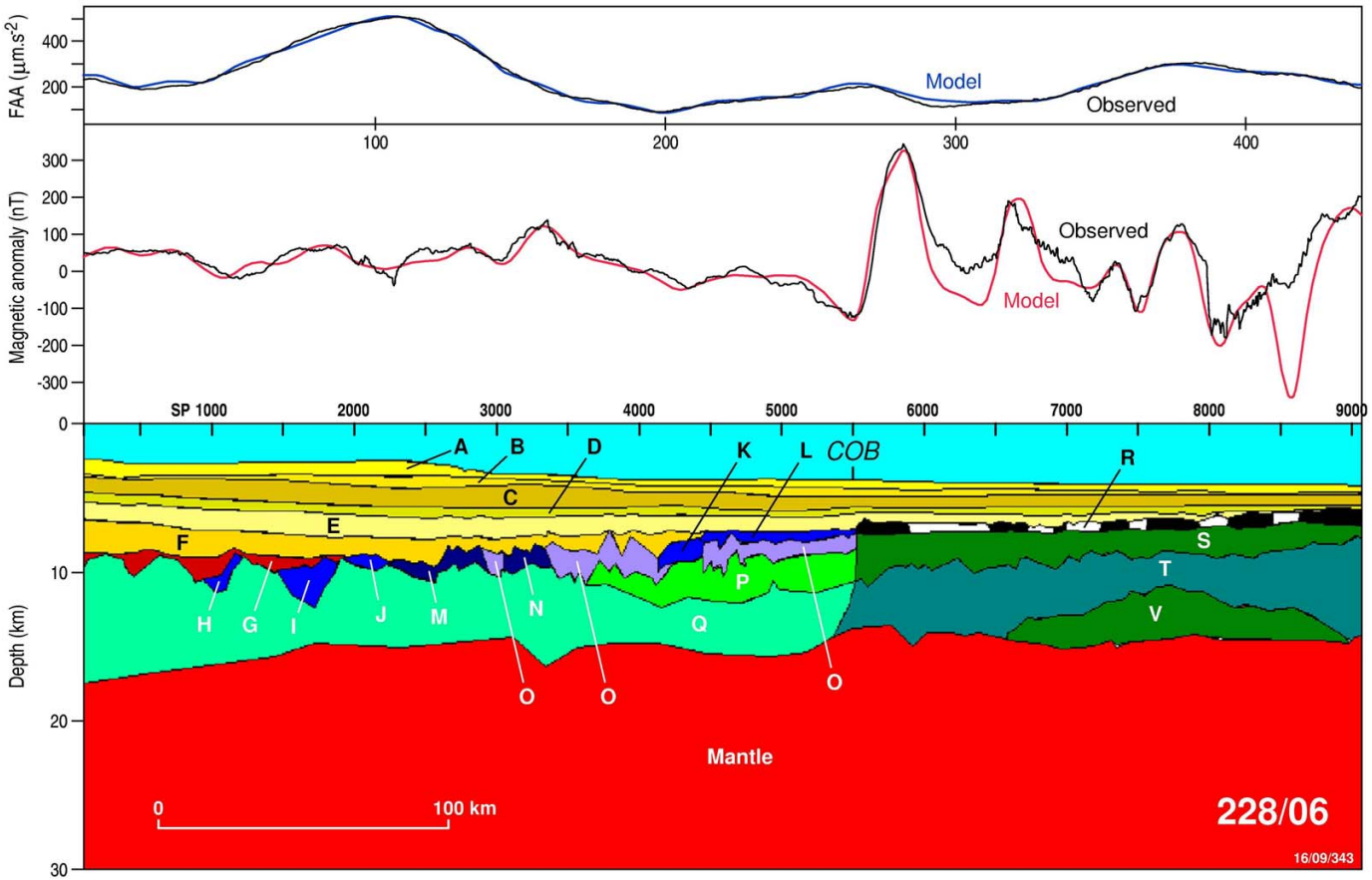

Figure 54: Potential field model for line GA-228/06, Mac. Robertson Land; revision to incorporate interpreted seafloor spreading magnetic anomaly reversals. South on the left. Model bodies are identified in full in Appendix 7. COB is the location of the interpreted continent–ocean boundary.

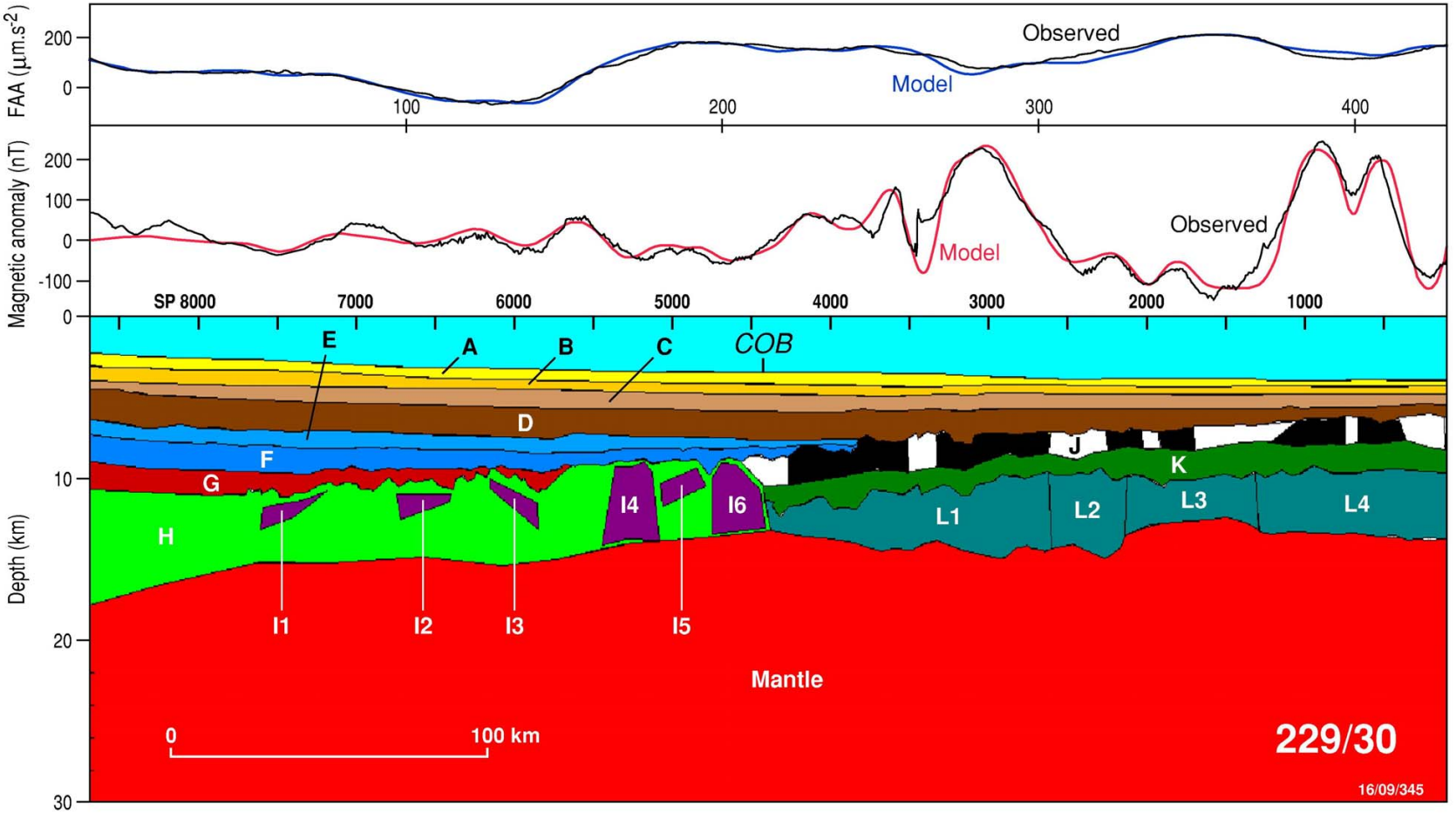

Figure 55: Potential field model for line GA-229/30, offshore Prydz Bay. South on the left. Model bodies are identified in full in Appendix 7. 'COB' shows interpreted continent–ocean boundary. After Stagg et al. (in press).

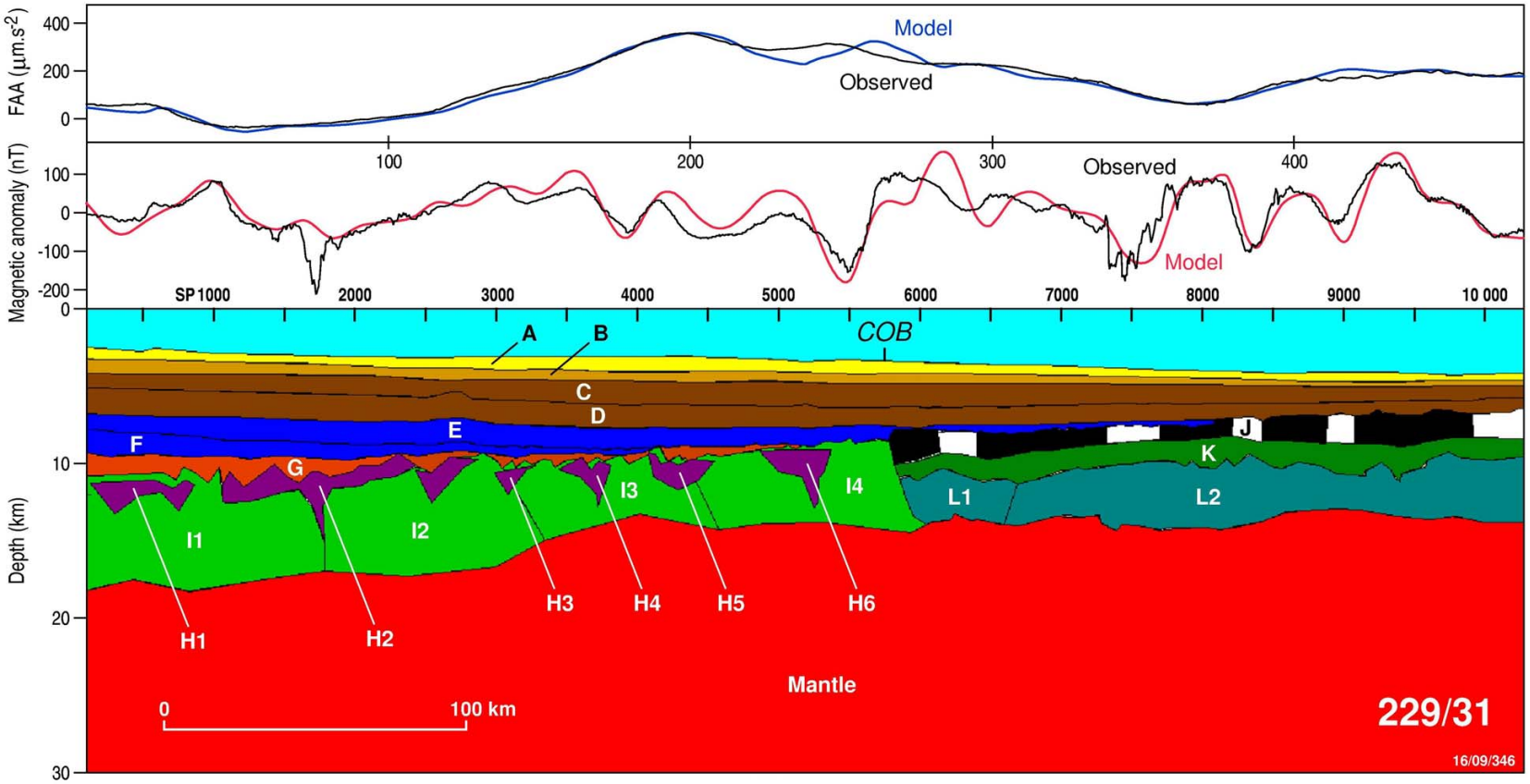

Figure 56: Potential field model for line GA-229/31, offshore from Prydz Bay. South on the left. Model bodies are identified in full in Appendix 7. COB is the location of the interpreted continent–ocean boundary.

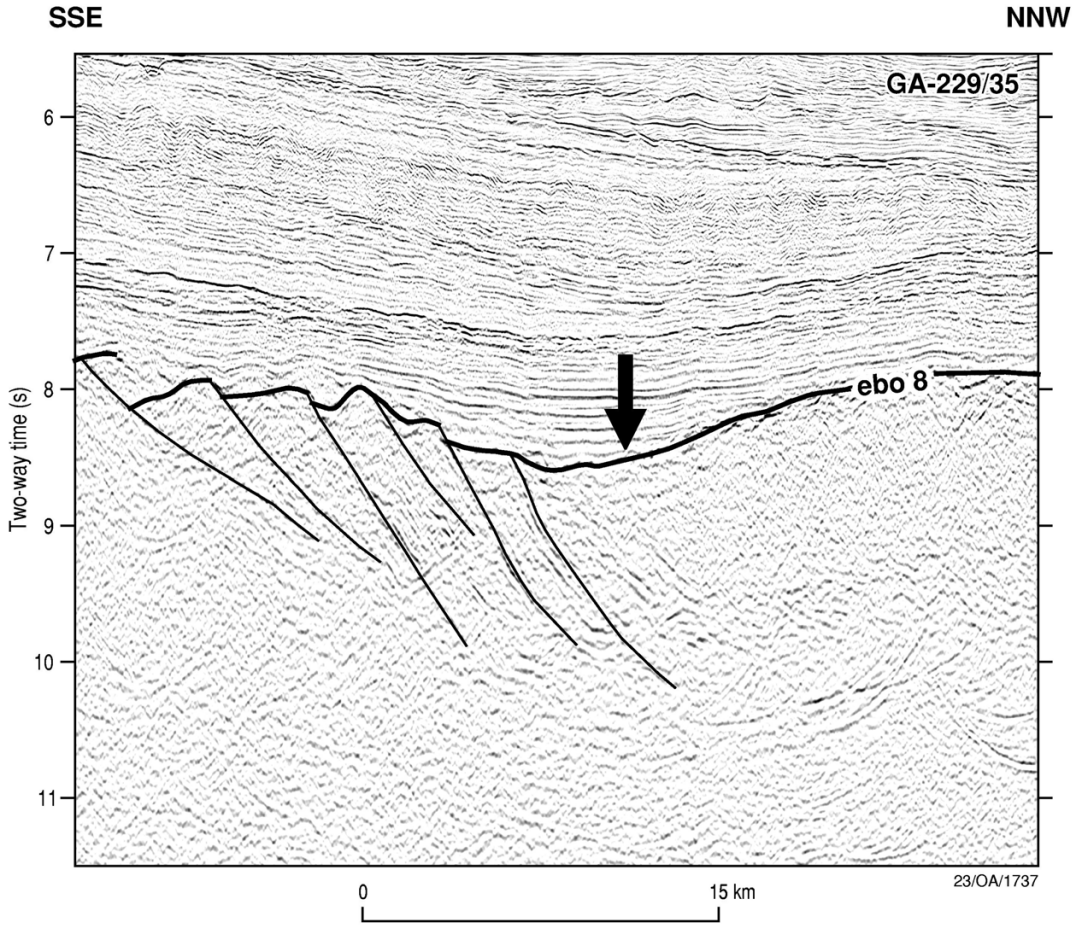

Figure 57: Seismic detail line from line GA-229/35 showing an example of the interpreted continent-ocean boundary west of 58°E. Full line shown in Plate 10. After Stagg et al. (in press).

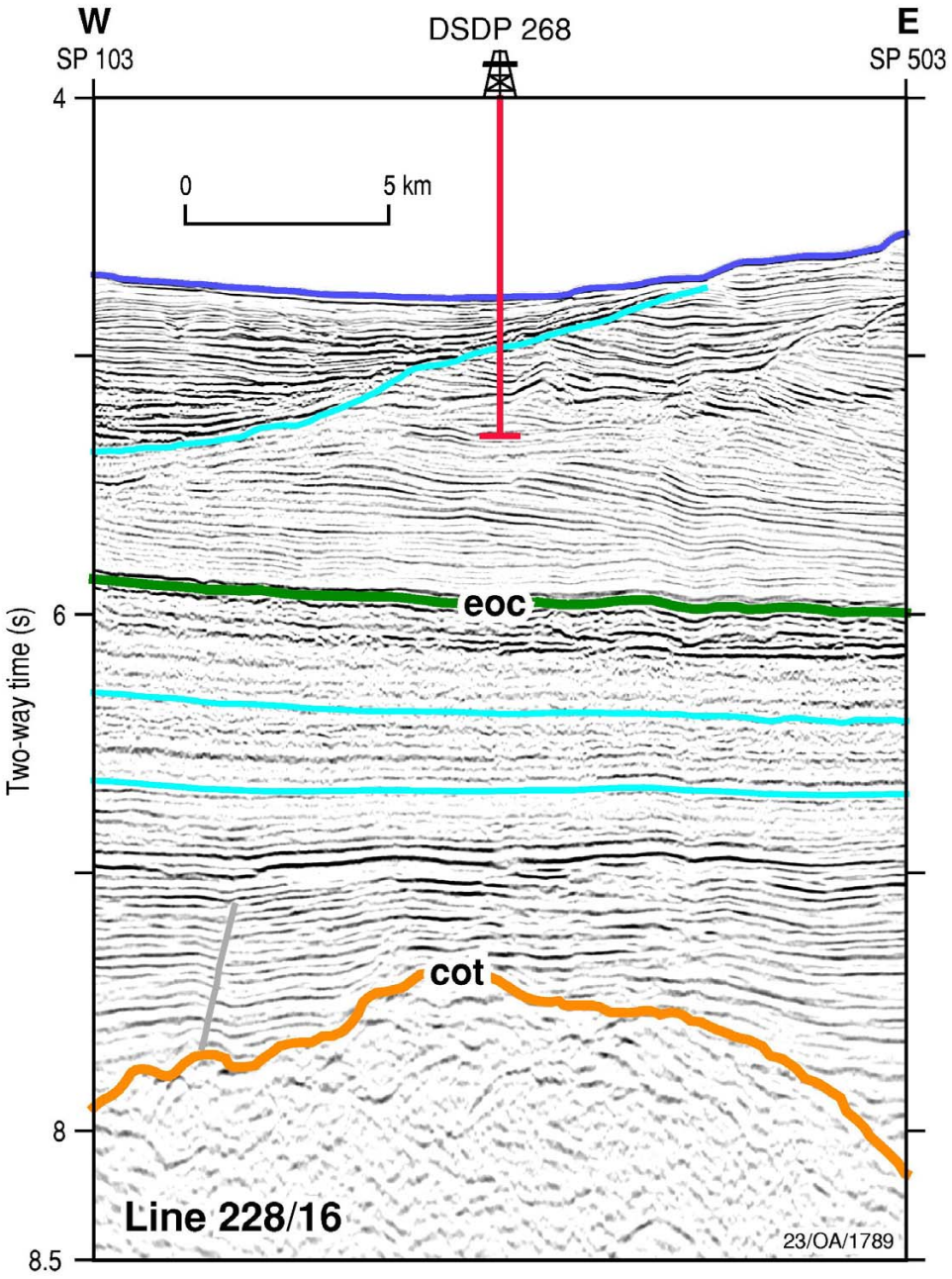

Figure 58: Detailed seismic section line GA-228/16, offshore western Wilkes Land, showing the location and penetration of DSDP Site 268 and the regional Eocene unconformity (*eoc*). The prominent unconformity penetrated by Site 268 is probably of Early Miocene age. Full line shown in Plate 15.

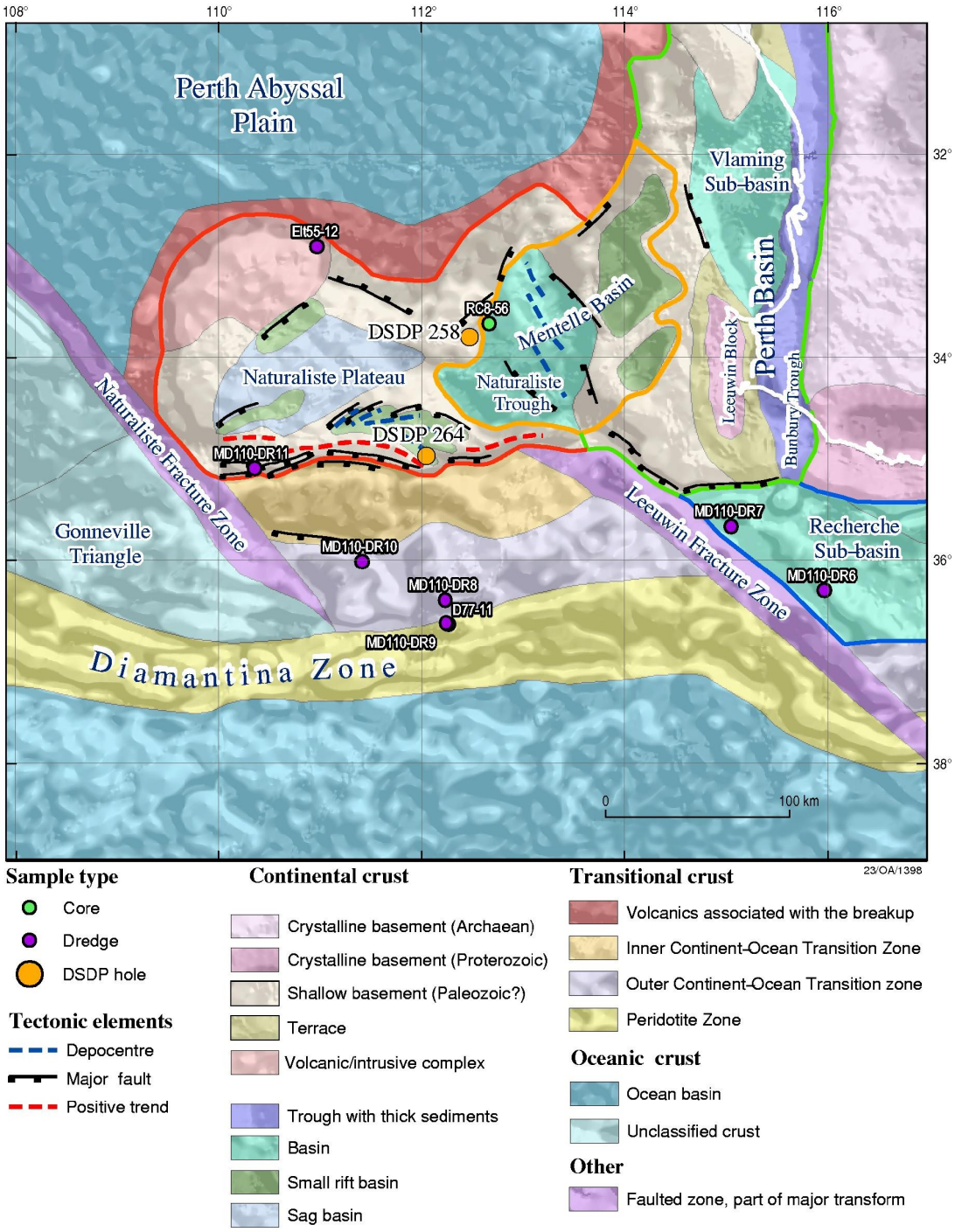

Figure 59: Tectonic provinces and structural elements of the Naturaliste Plateau region (after Borissova, 2002).

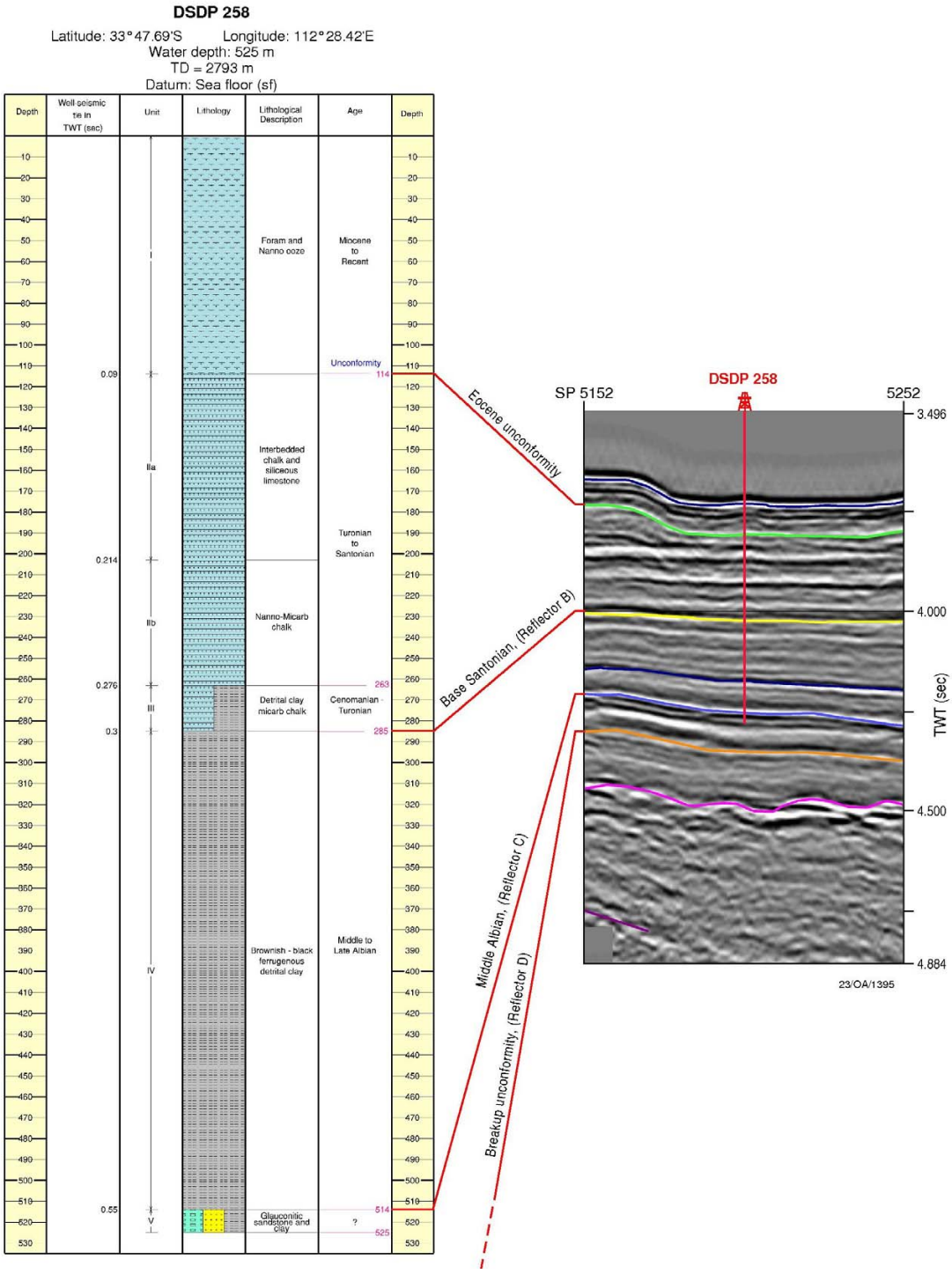

Figure 60: Lithostratigraphic column at DSDP Site 258 (after Davies, Luyendyk et al., 1974), showing sequence picks and correlation with a seismic profile. Equivalent Jongsma & Petkovic (1977) horizon names are shown in parentheses. Figure is after Borissova (2002).

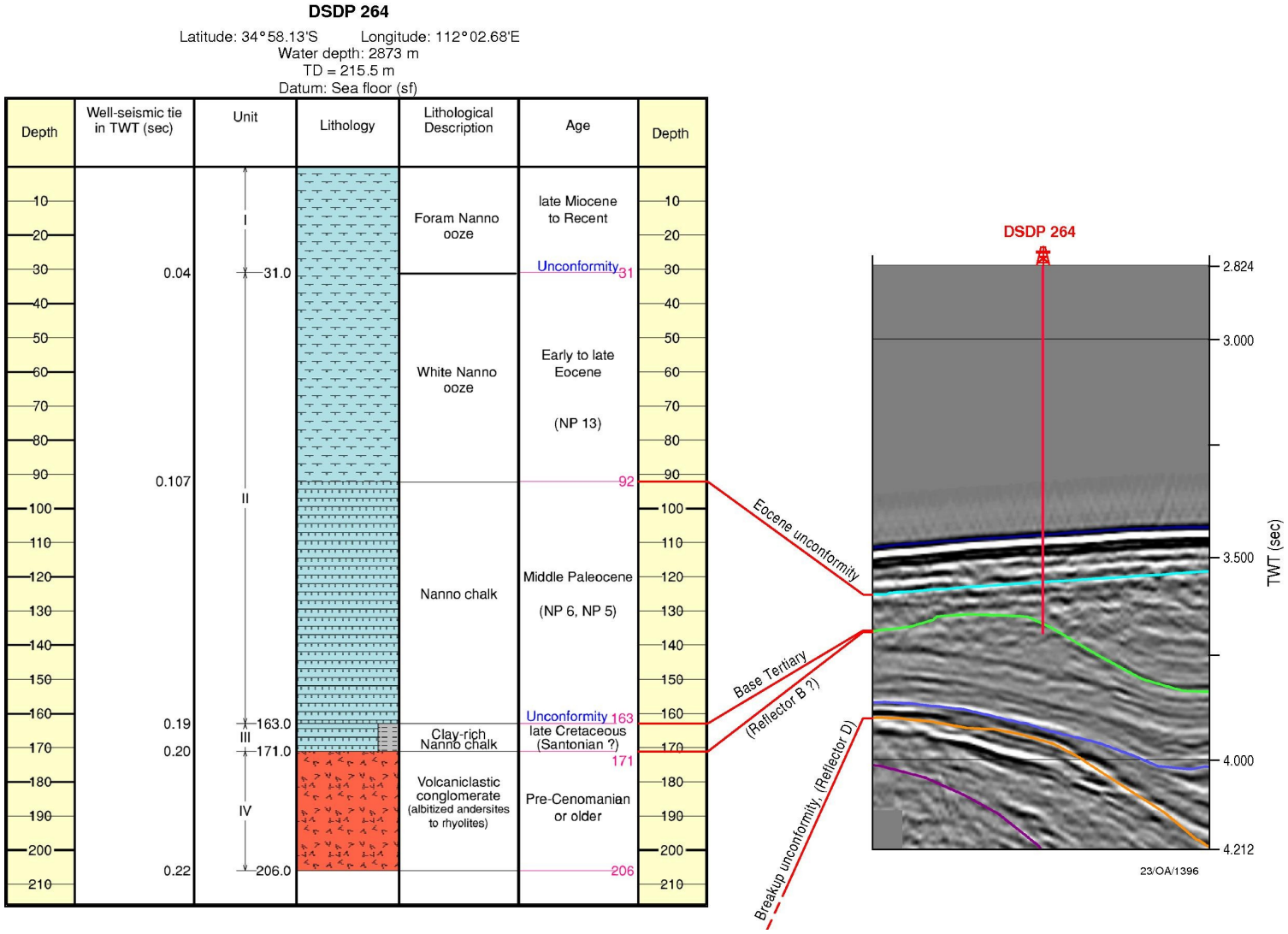

Figure 61: Lithostratigraphic column at DSDP Site 264 (after Hayes, Frakes et al., 1975), showing sequence picks and correlation with a seismic profile. Equivalent Jongsma & Petkovic (1977) horizon names are shown in parentheses. Figure is after Borissova (2002).

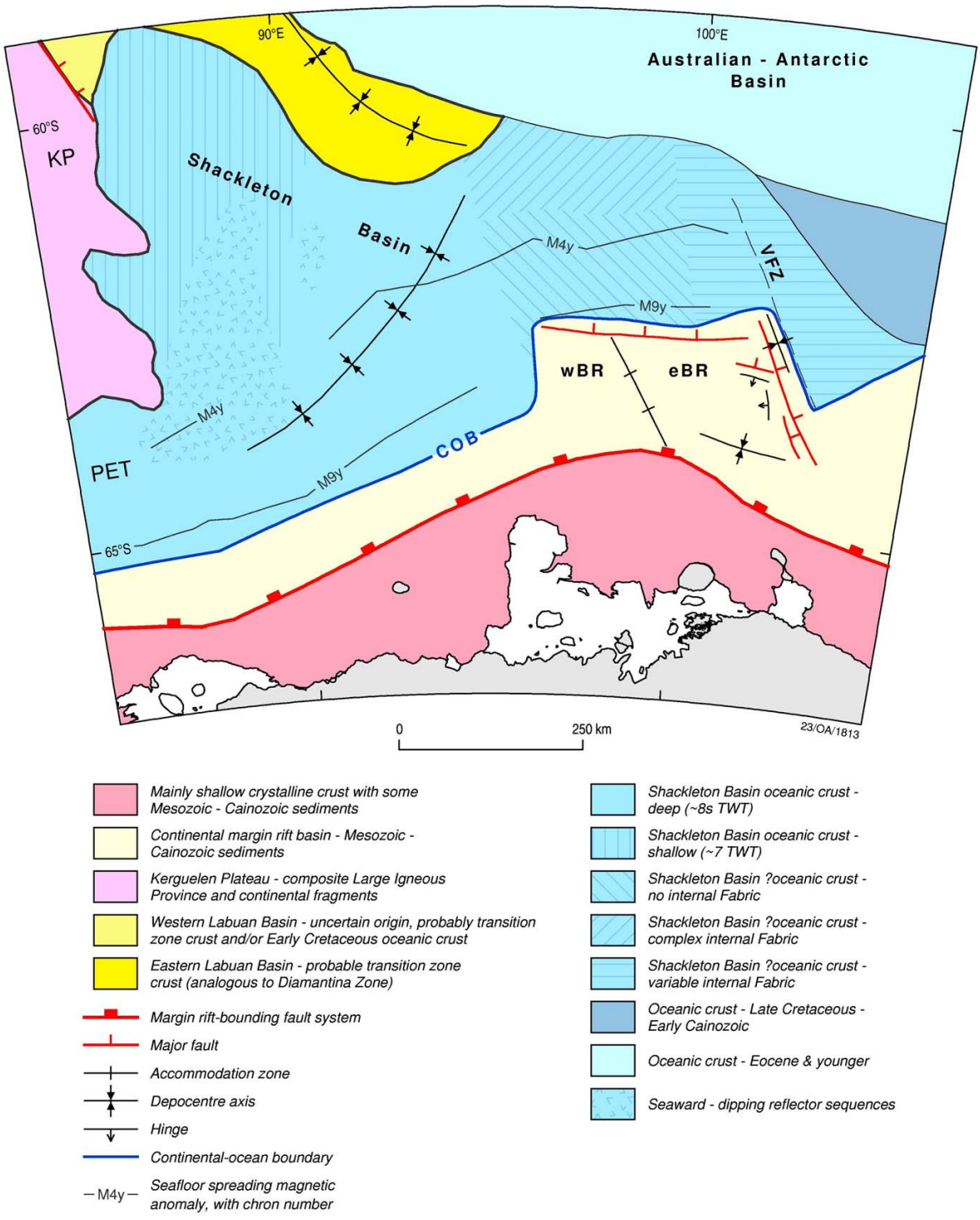

Figure 62: Tectonic elements of the Bruce Rise and adjacent ocean basins. eBR – east Bruce Rise; wBR – west Bruce Rise; VFZ – Vincennes Fracture Zone; PET – Princess Elizabeth Trough; KP – Kerguelen Plateau; COB – continent-ocean boundary.

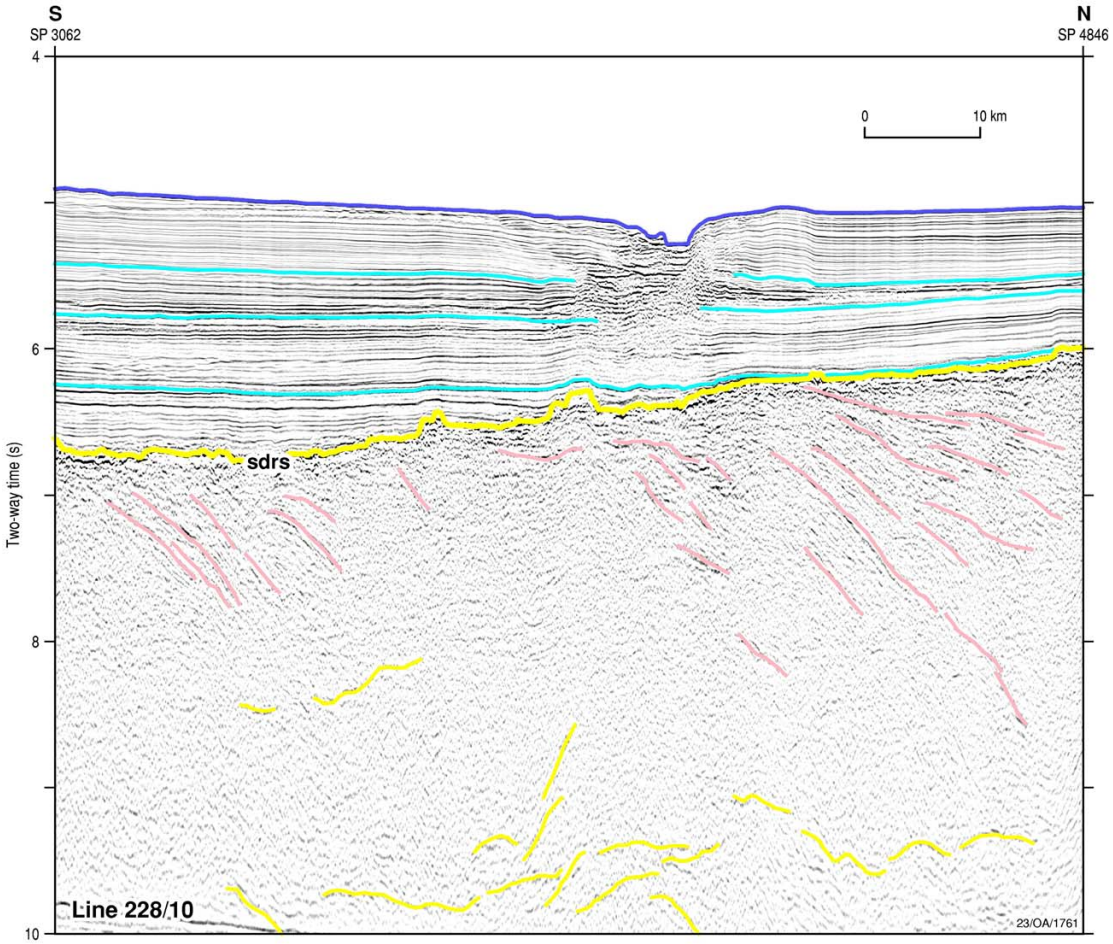

Figure 63: Detailed seismic section line GA-228/10, eastern end of the Princess Elizabeth Trough and southeast of Kerguelen Plateau, showing seaward-dipping reflector sequences (*sdrs*). Full line shown in Plate 13.

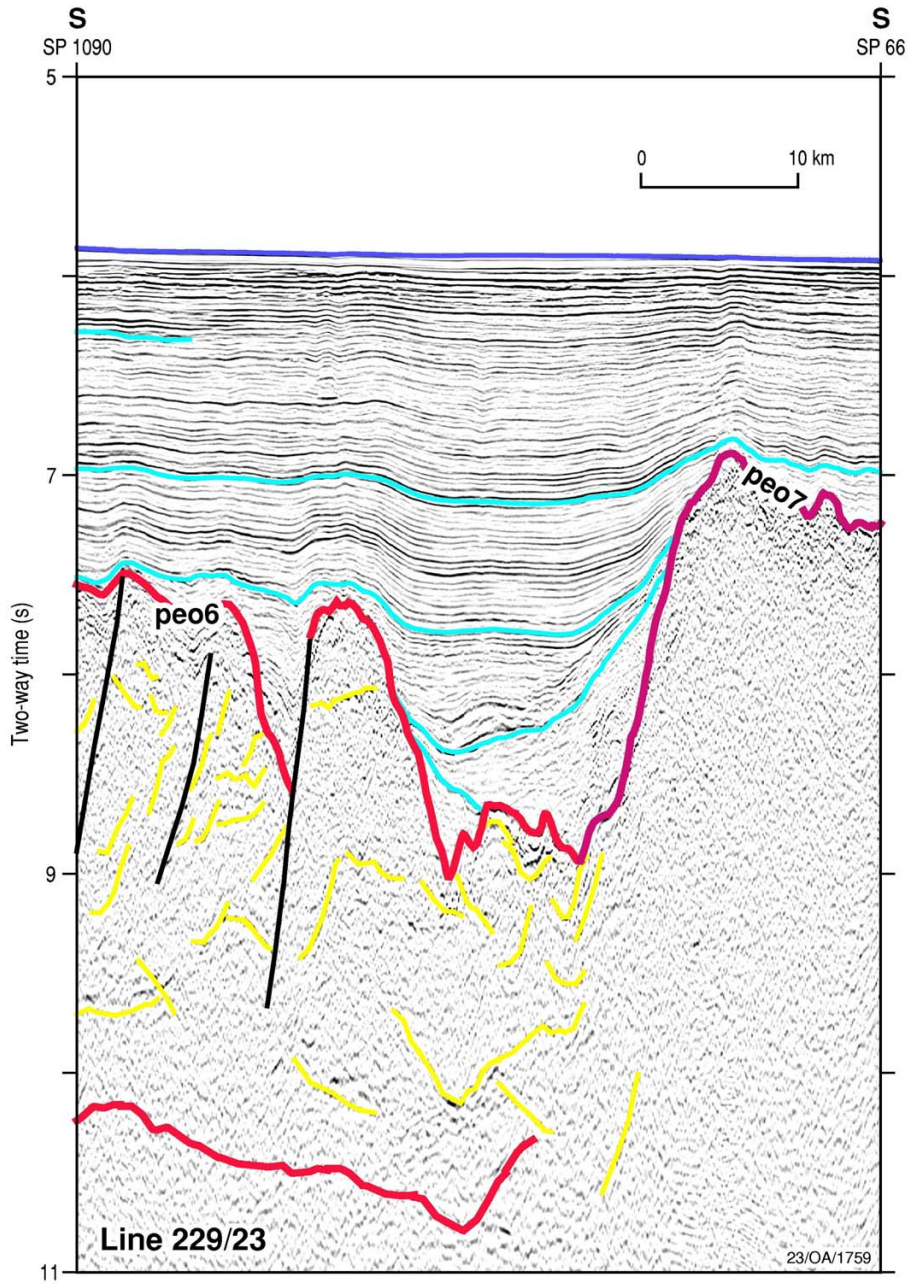

Figure 64: Detailed seismic section line GA-229/23, northwest of Bruce Rise, showing the deep trough that marks the boundary between ?oceanic crustal types *peo6* and *peo7*. Full line shown in Plate 13.

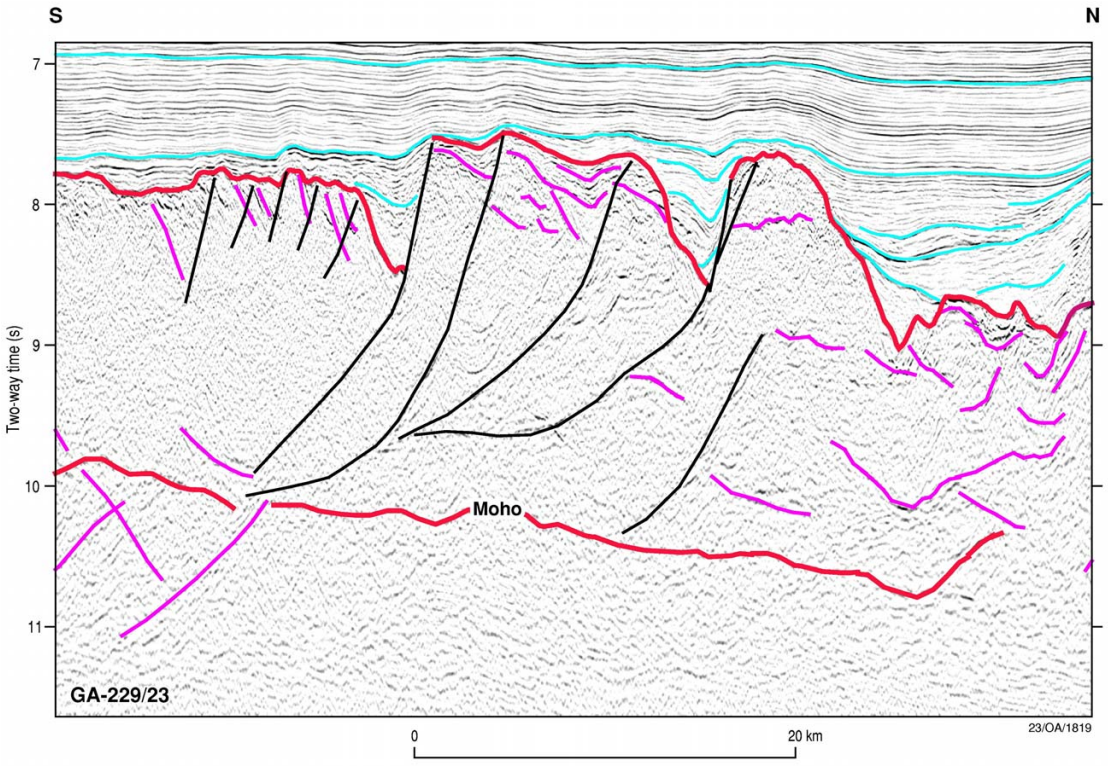

Figure 65: Detailed seismic section line GA-229/23, northwest of Bruce Rise, showing the complex faulting and structural fabric of the *peo6* crust immediately south of the deep trough shown in the previous figure. Full line shown in Plate 13.

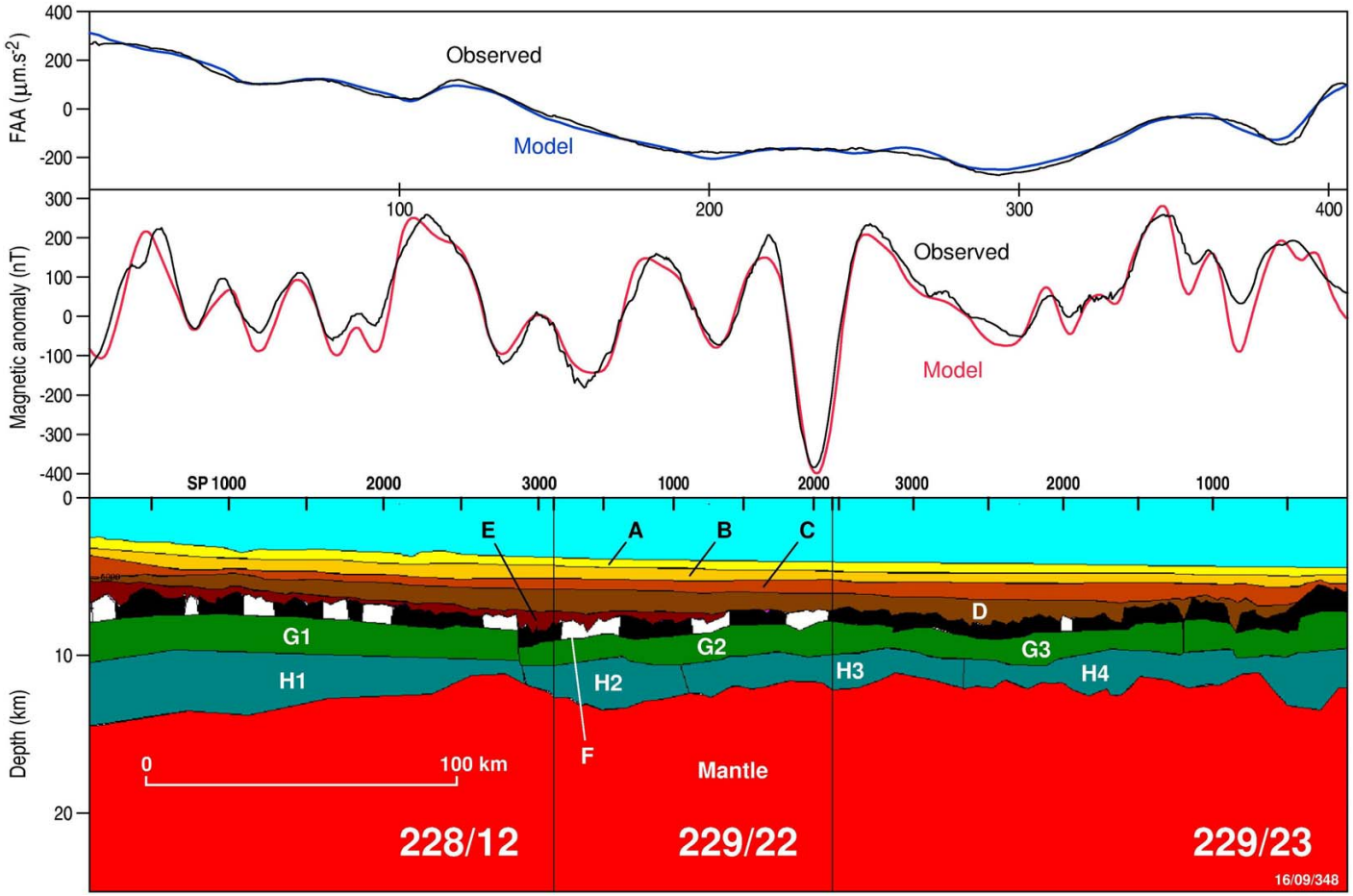

Figure 66: Potential field model for composite line GA-228/12 + GA-229/22 + GA-229/23, offshore Queen Mary Land. South on the left. Model bodies are identified in full in Appendix 7.

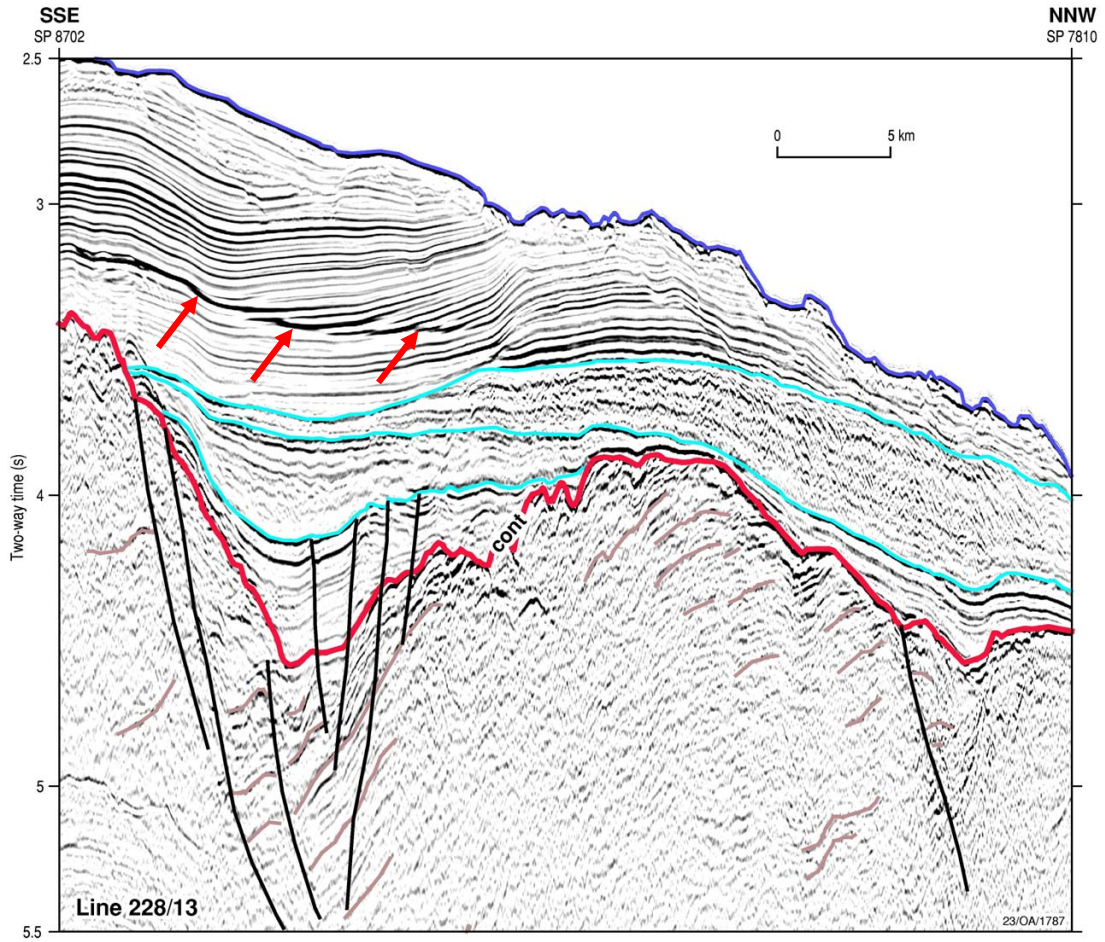

Figure 67: Detailed seismic section line GA-228/13, on Bruce Rise, showing faulted continental basement and the typical Bruce Rise sedimentary section. The basal blue erosional unconformity above the graben on the left of the section is probably of Valanginian age. Red arrows point to a bottom-simulating reflector (BSR). Full line shown in Plate 14.

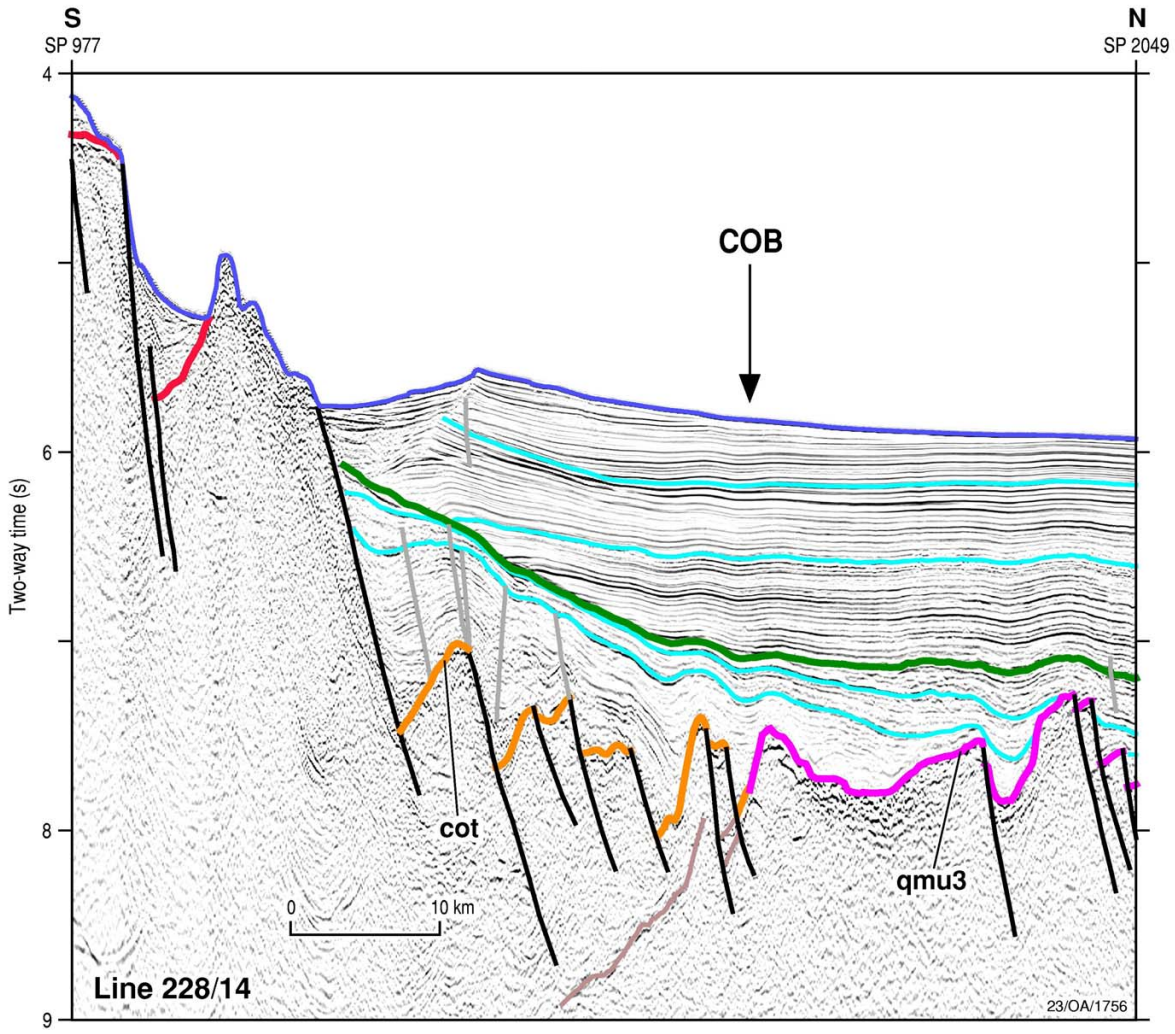

Figure 68: Detailed seismic section line GA-228/14, northern flank of Bruce Rise, showing the large-offset basement faults that characterise this margin of Bruce Rise and the narrow COT zone. COB is interpreted continent–ocean boundary. The crustal type *qmu3* is probably oceanic; however, there is the possibility that it is of continental origin. Full line shown in Plate 14

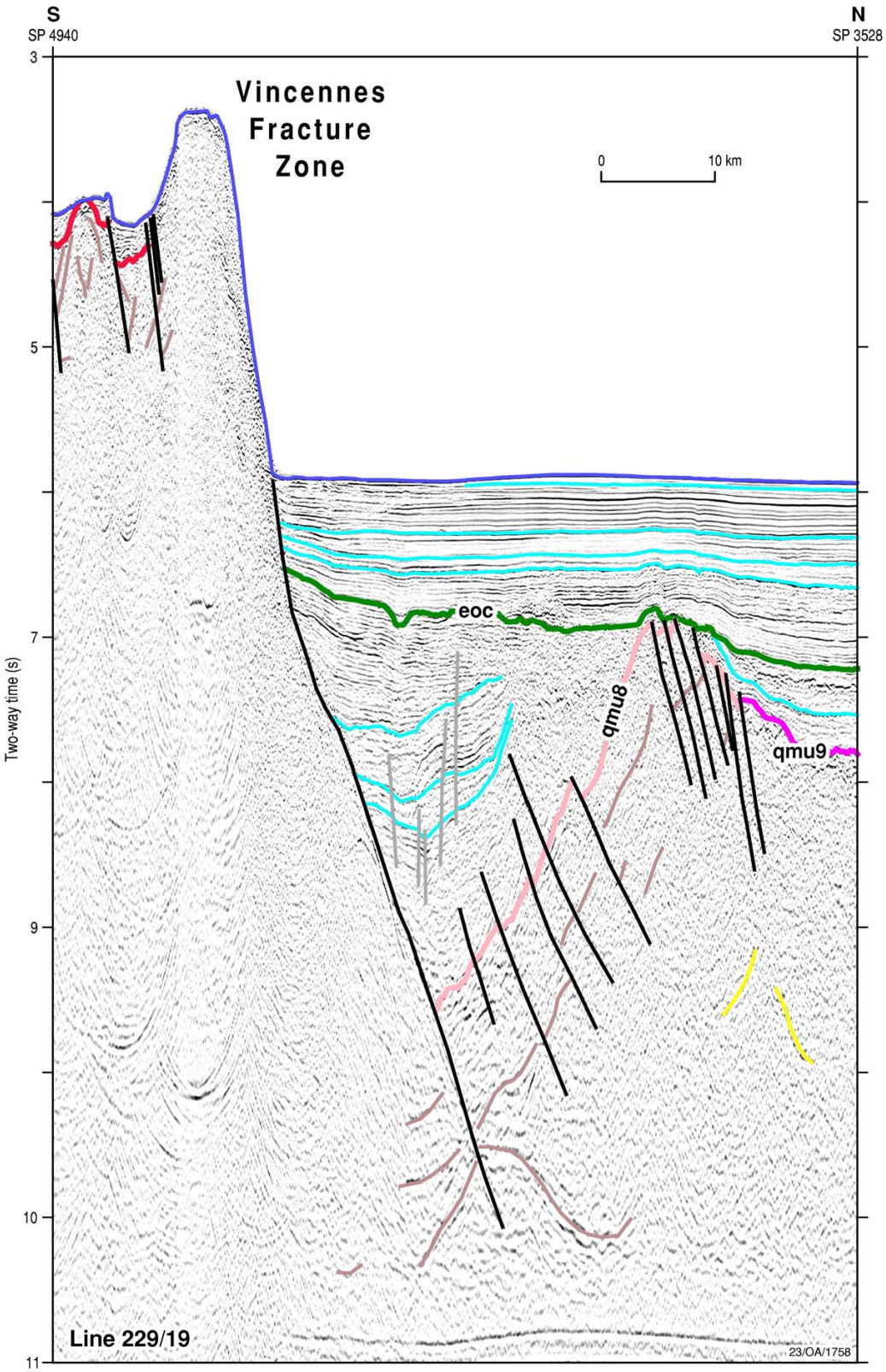

Figure 69: Detailed seismic section line GA-229/19, eastern flank of Bruce Rise, showing the steep Vincennes Fracture Zone. The deeply-subsided crustal type *qmu8* is probably continental or transitional. Full line shown in Plate 14.

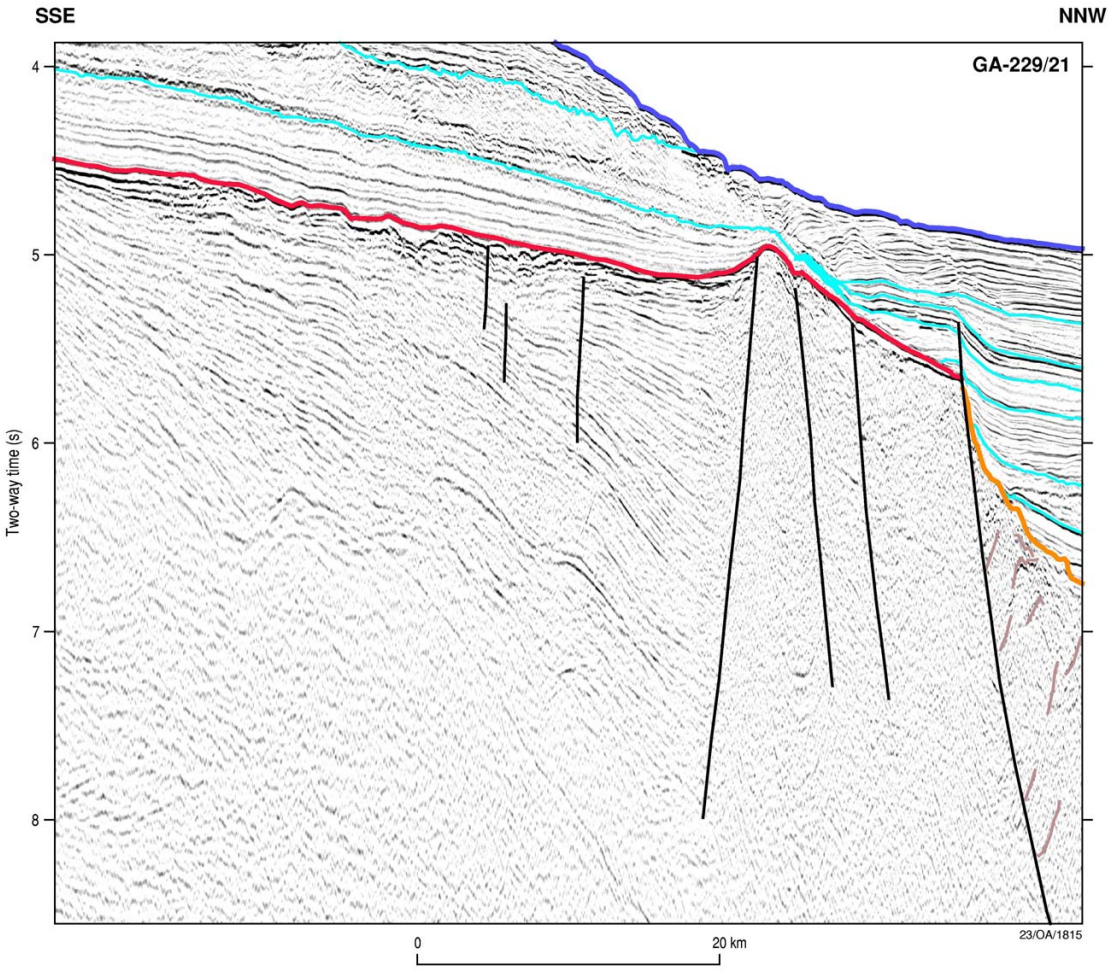

Figure 70: Detailed seismic section line GA-229/21, northwest flank of Bruce Rise, showing the typical form of the western half of Bruce Rise. Full line shown in Plate 14.

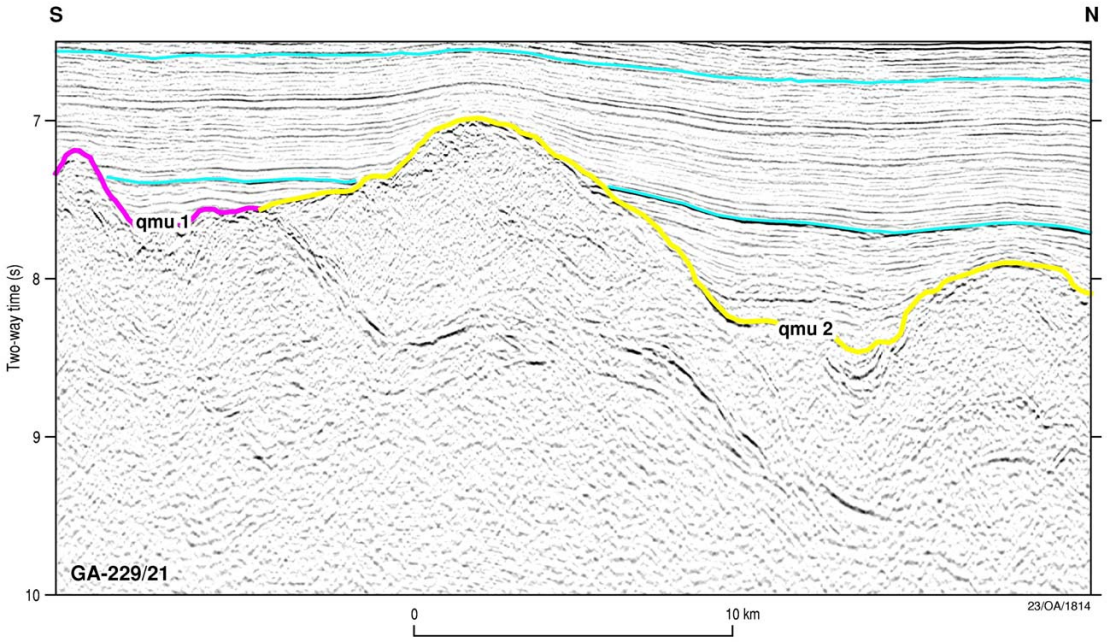

Figure 71: Detailed seismic section line GA-229/21, north of Bruce Rise, showing the complex boundary between the undifferentiated crustal types *qmu1* and *qmu2*. Full line shown in Plate 14.

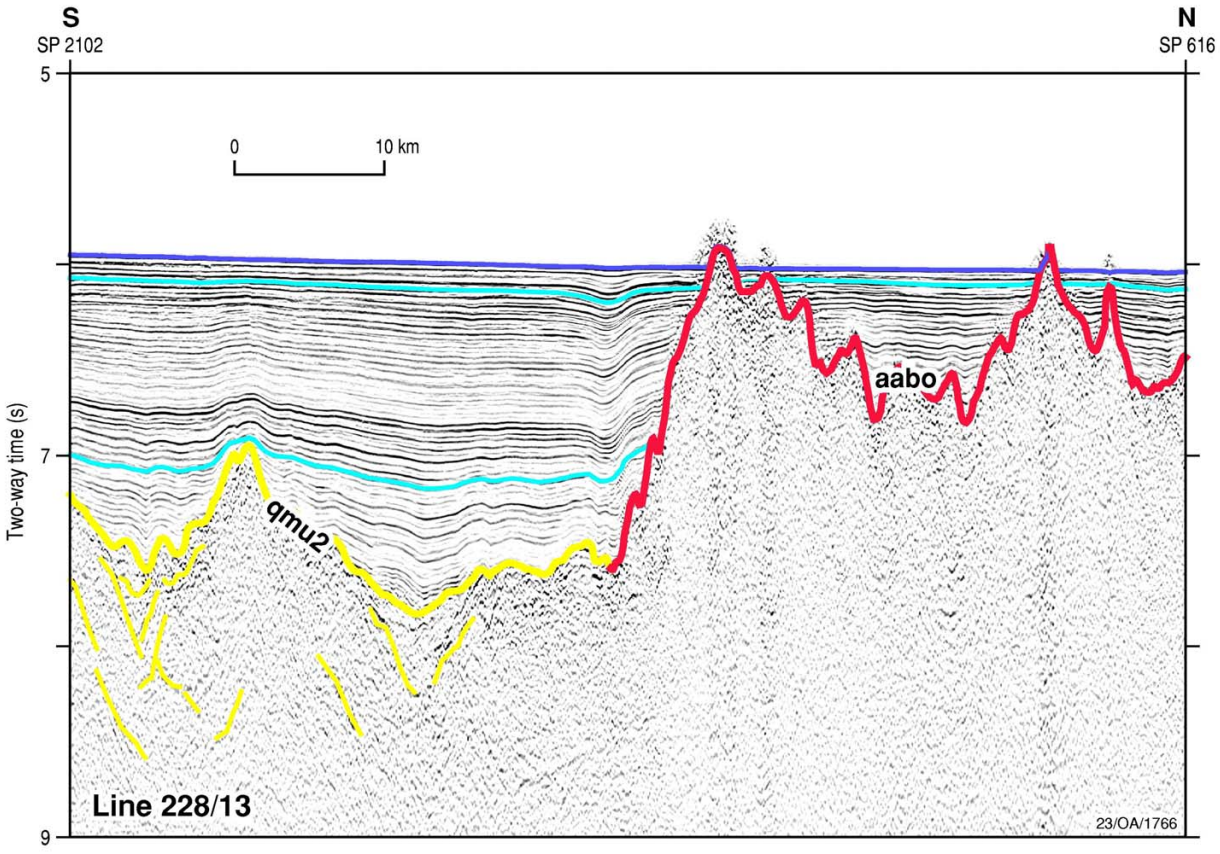

Figure 72: Detailed seismic section line GA-228/13, north of Bruce Rise showing the boundary between the undifferentiated crustal type *qmu2* and the fast-spreading Eocene crust of the Australian–Antarctic Basin (*aabo*). Full line shown in Plate 14.

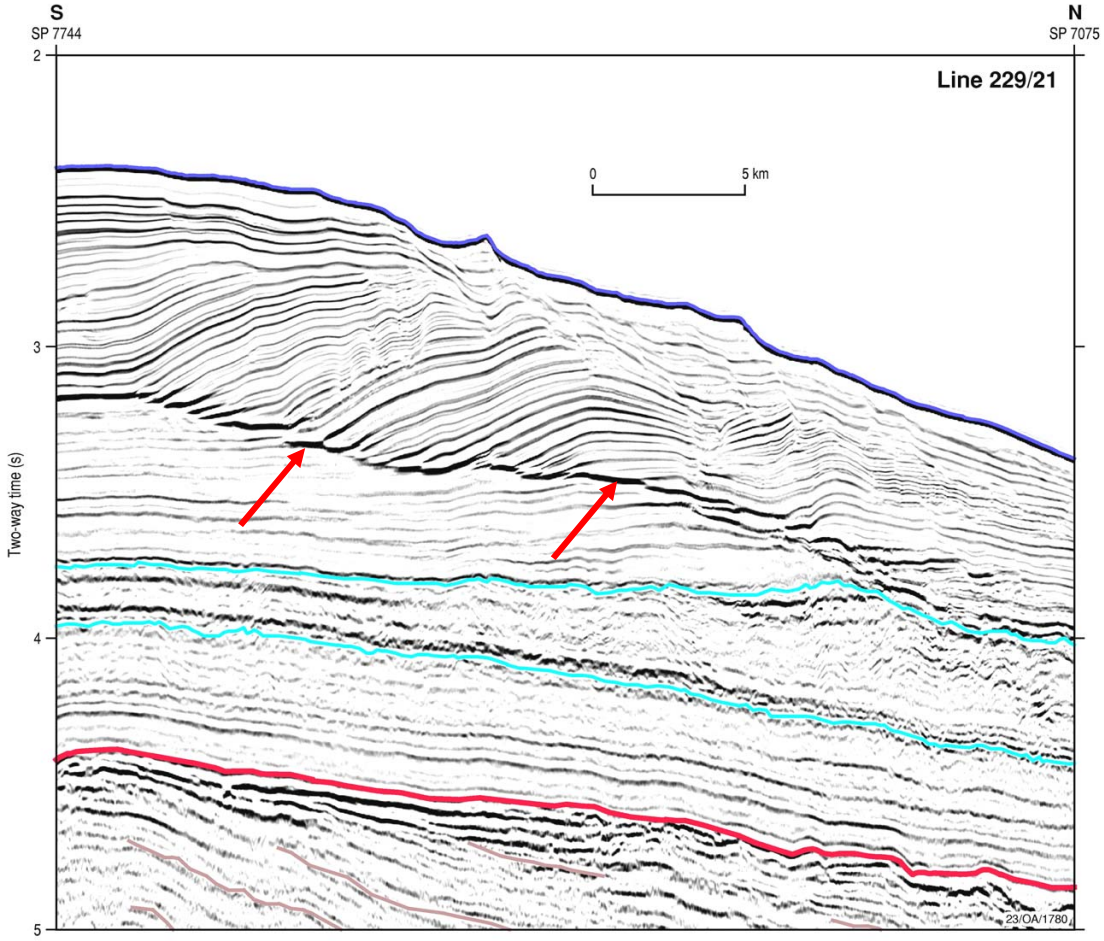

Figure 73: Detailed seismic section line GA-229/21, northwest flank of Bruce Rise, showing the showing the thicker post-rift sedimentary section on the western half of Bruce Rise and a strong bottom-simulating reflector (BSR; shown by red arrows). Full line shown in Plate 14.

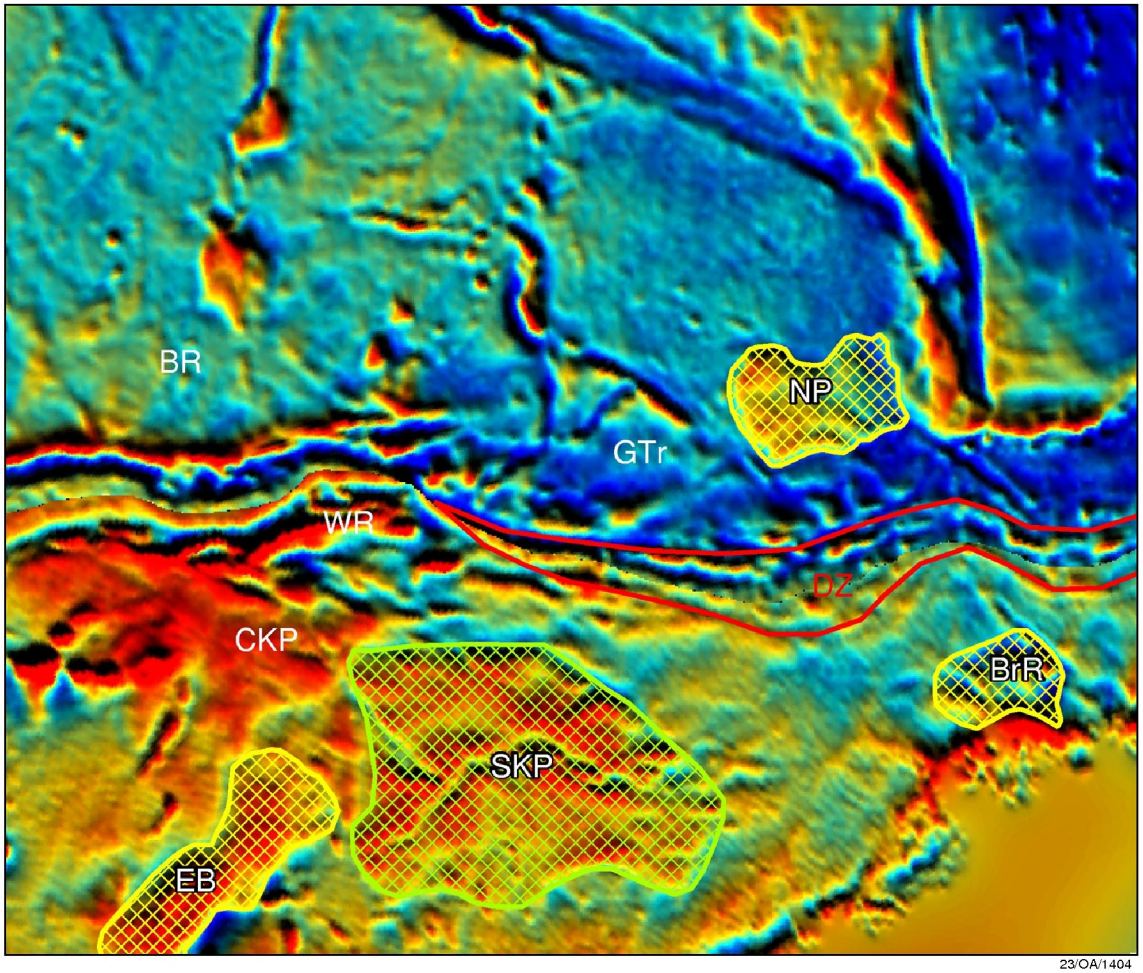

Figure 74: Satellite gravity pre-Early Eocene reconstruction of the Naturaliste Plateau – Bruce Rise region (after Borissova, 2002). Continental blocks are shown by yellow hachuring and possible continental blocks are shown by hachuring. Diamantina Zone is outlined by the thick red line. NP – Naturaliste Plateau; BrR – Bruce Rise; DZ – Diamantina Zone; GTr – Gonneville Triangle; BR – Broken Ridge; WR – Williams Ridge; CKP – central Kerguelen Plateau; SKP – southern Kerguelen Plateau; EB – Elan Bank.

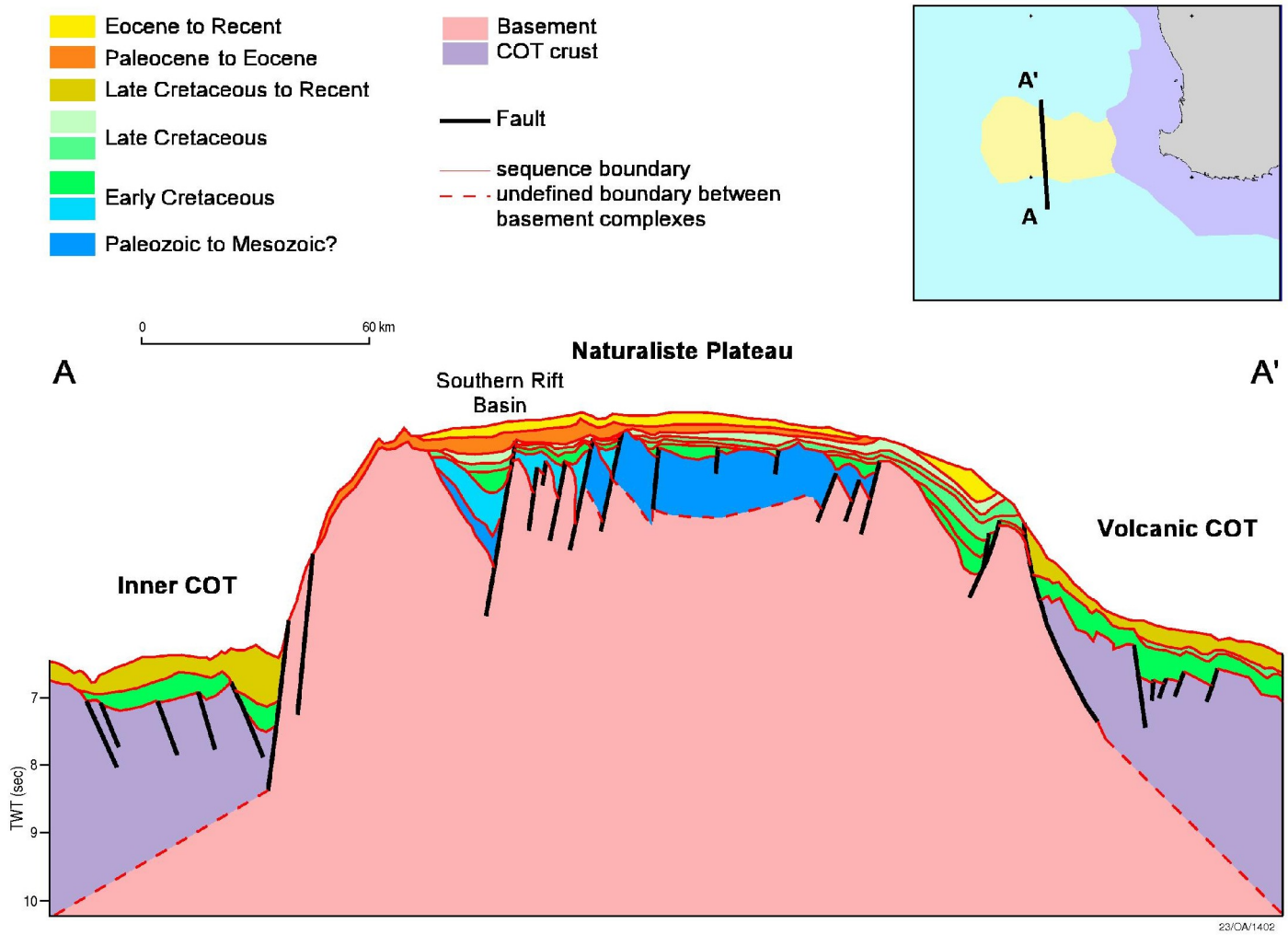

Figure 75: N–S cross-section through the Naturaliste Plateau based on interpreted seismic line N322 (after Borissova, 2002).

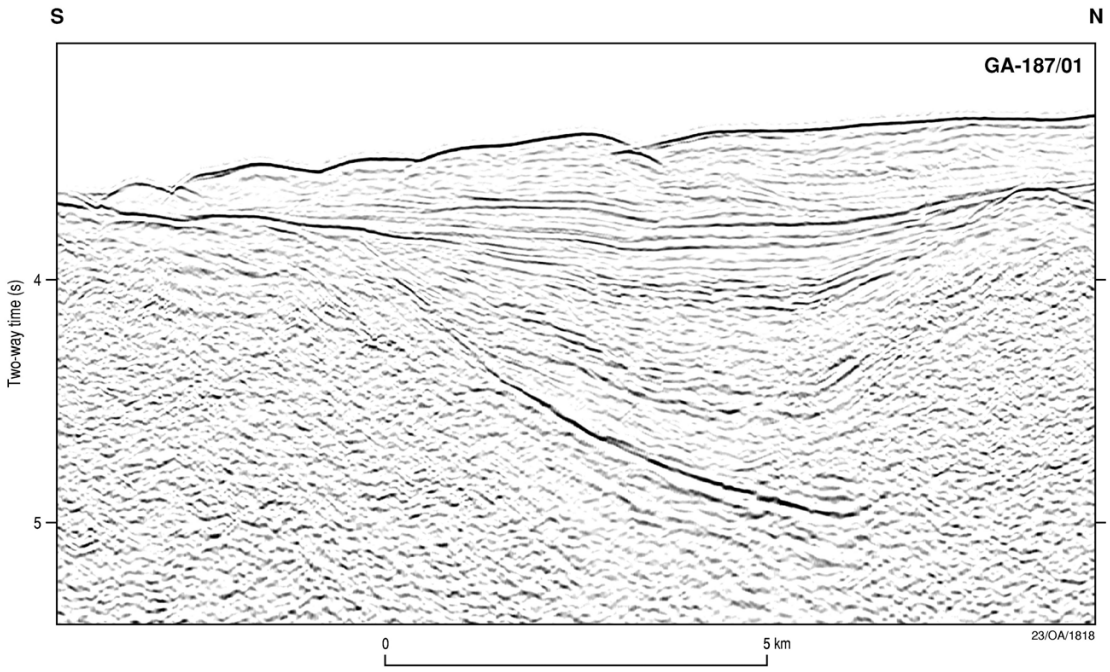

Figure 76: Detailed seismic section from line GA-187/01 on the southern flank of the Naturaliste Plateau, showing a typical ?Late Jurassic – Early Cretaceous half graben, analogous to those on the Bruce Rise.

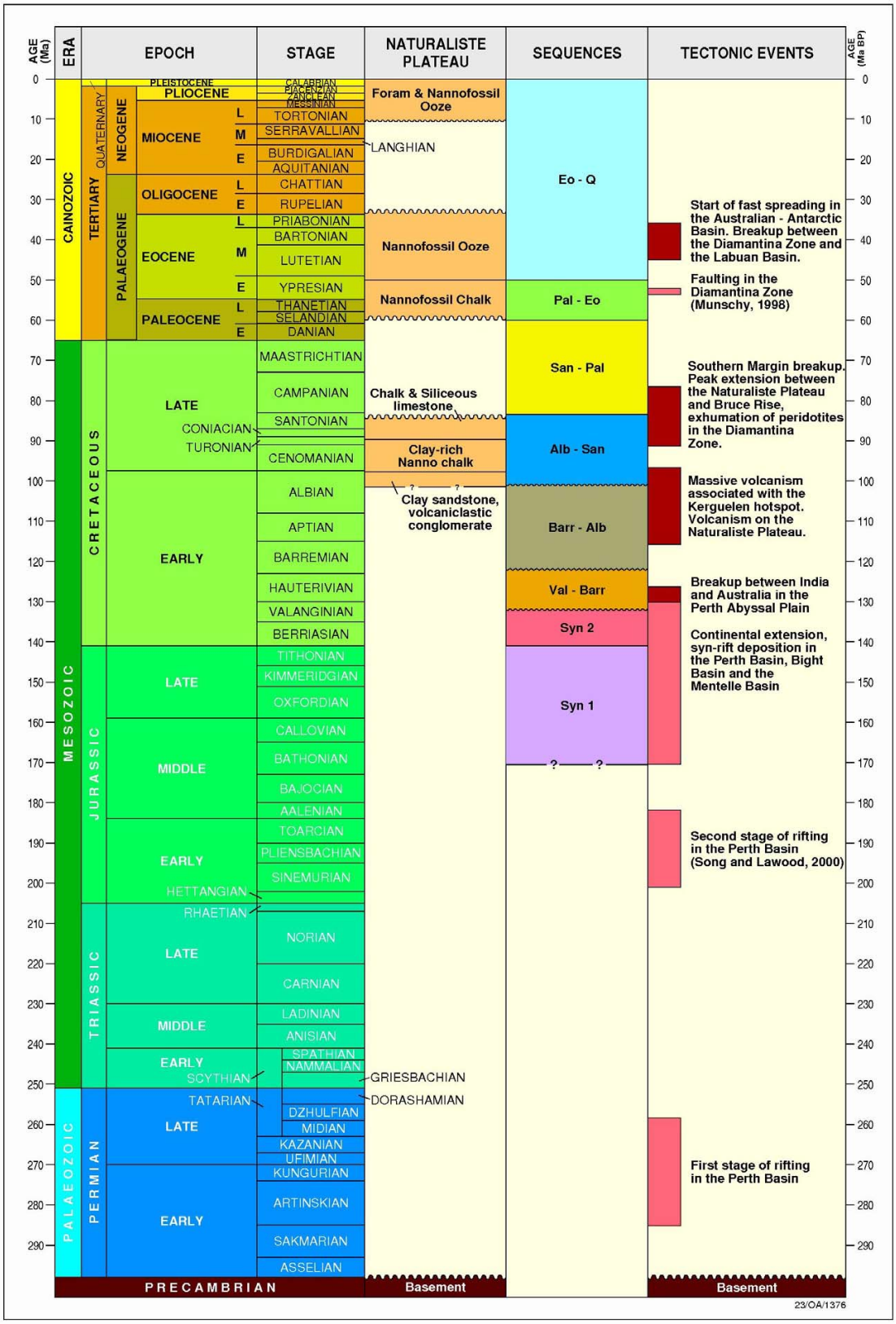

Figure 77: Correlation between seismic sequences, drilled stratigraphy and regional tectonic events in the Naturaliste Plateau area (after Borissova, 2002).

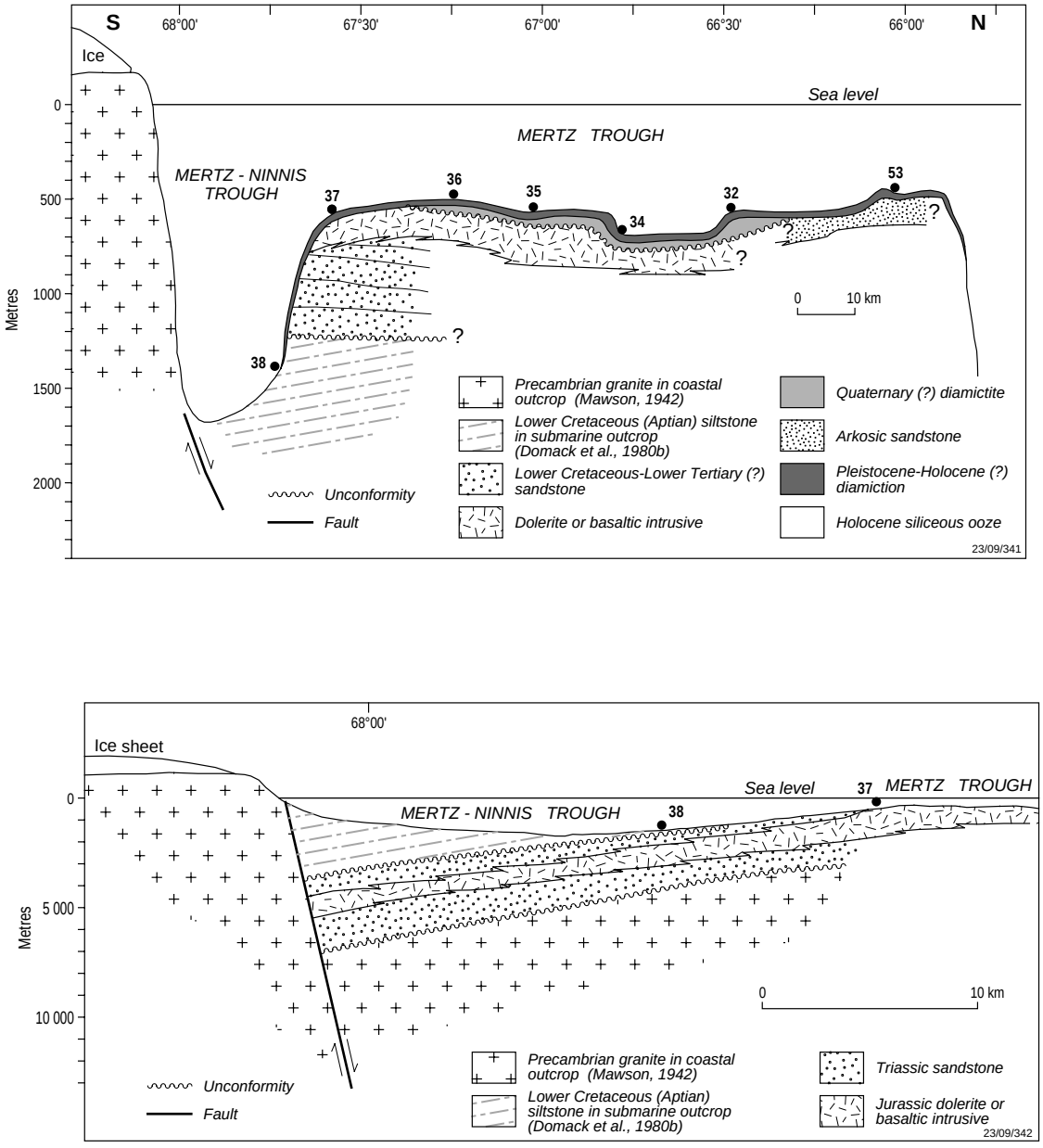

Figure 78: (top) Stratigraphic model for the Mertz Trough, George V Shelf (modified after Domack, 1987. Stratigraphic units are: A – Precambrian basement; B – Lower Cretaceous siltstone; C – Lower Cretaceous to Lower Tertiary (?) sandstone; D – dolerite; E – Quaternary (?) diamictite; F – arkosic sandstone; G – Pleistocene to Holocene (?) diamicton; H – Holocene siliceous ooze. Core locations shown as dots. (bottom) Alternative stratigraphic model for the Mertz Trough (modified after Domack, 1987). Letters as above. Bathymetric profile shown without vertical exaggeration.

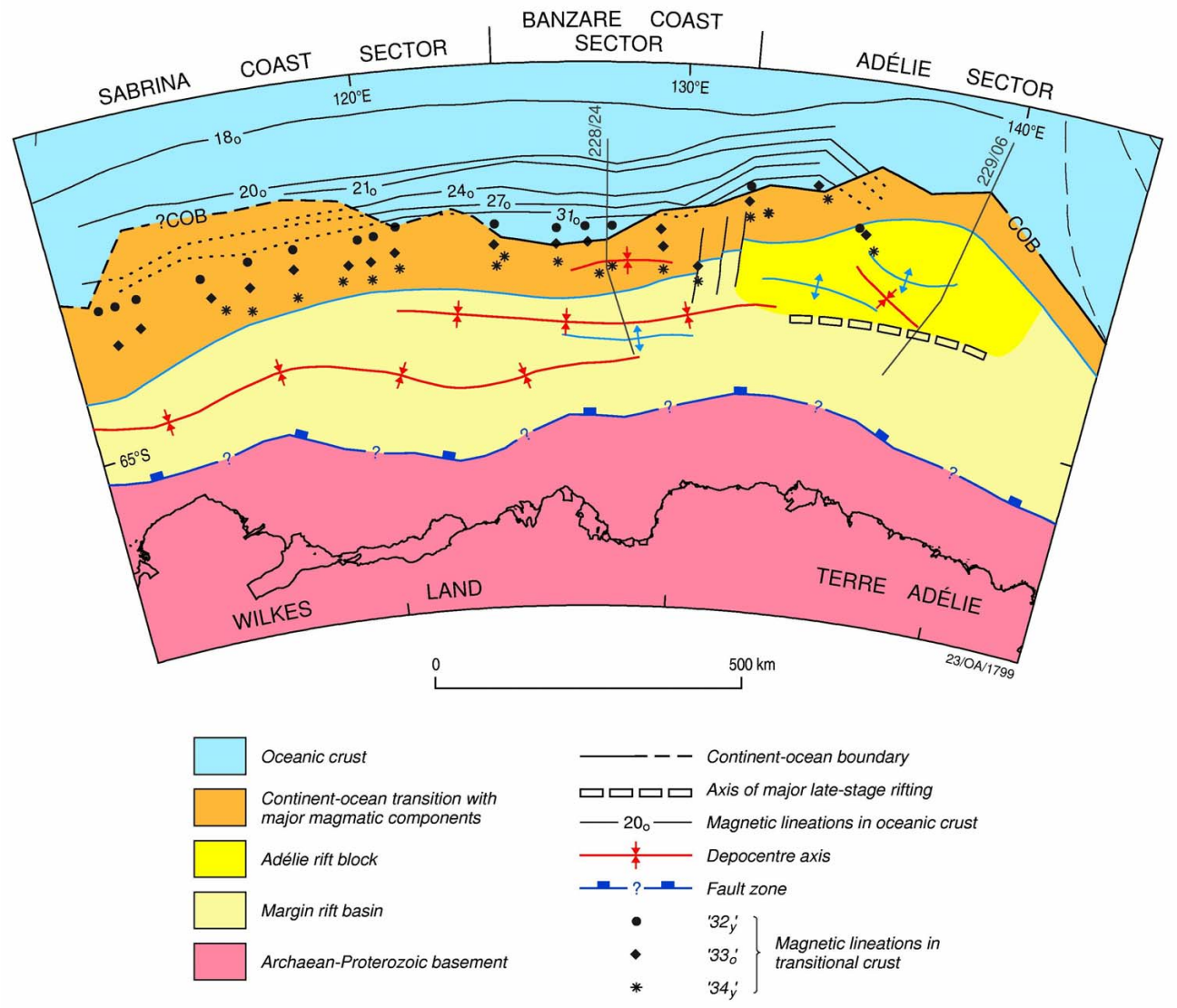

Figure 79: Tectonic elements of offshore Wilkes Land and Terre Adélie (after Colwell et al., in press).

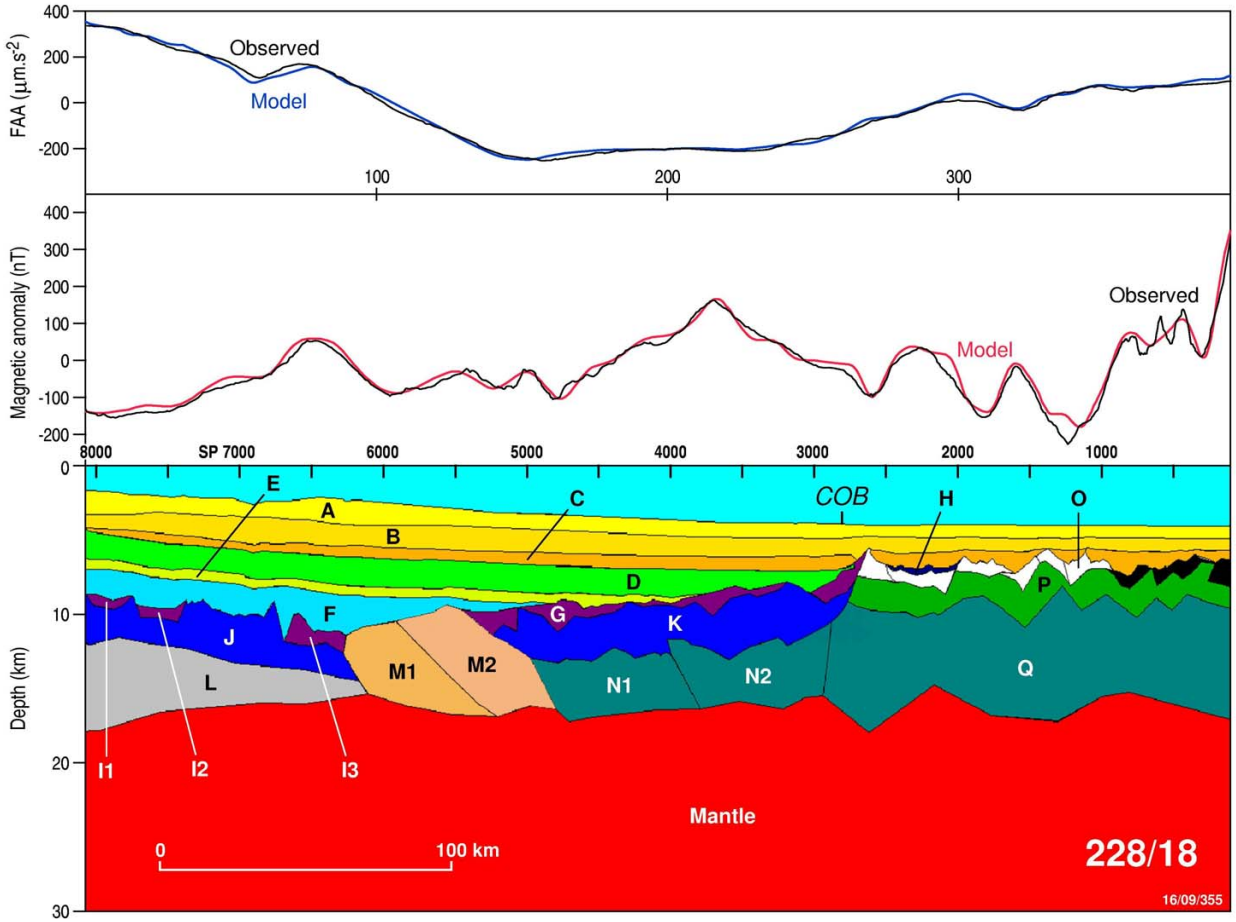

Figure 80: Potential field model for line GA-228/18, western Wilkes Land. COB is the location of the interpreted continent–ocean boundary. South on the left. Model bodies are identified in full in Appendix 7.

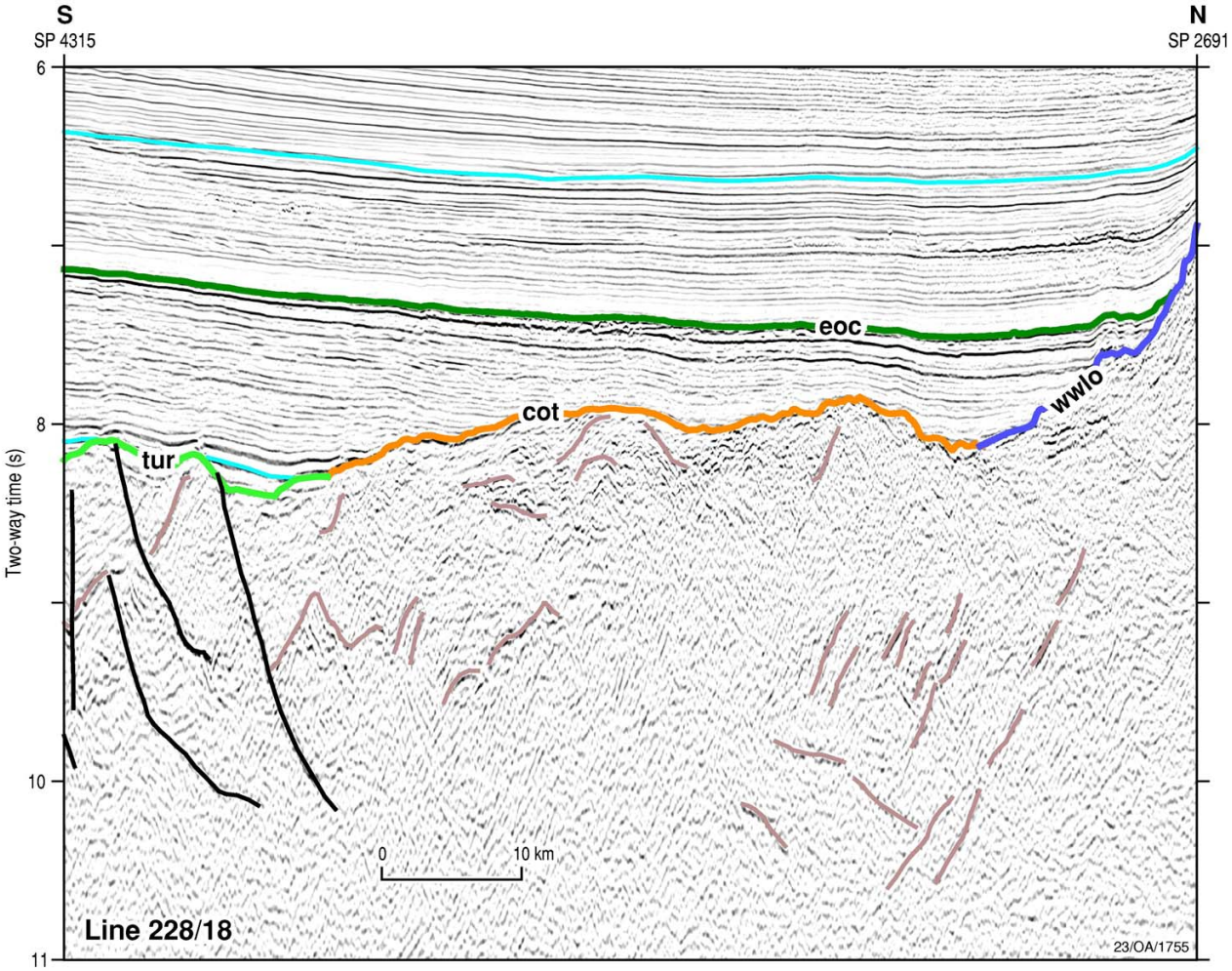

Figure 81: Detailed view of part of seismic line GA-228/18 showing the northward transition from rocks of the COT (overlain by horizons *tur* and *cot*) to oceanic crust of the Australian–Antarctic Basin (*wwlo*) on the right. The COB is marked by a change in seismic character and an approximately 1 s TWT step up in average basement level to the north. Full line is shown in Plate 15.

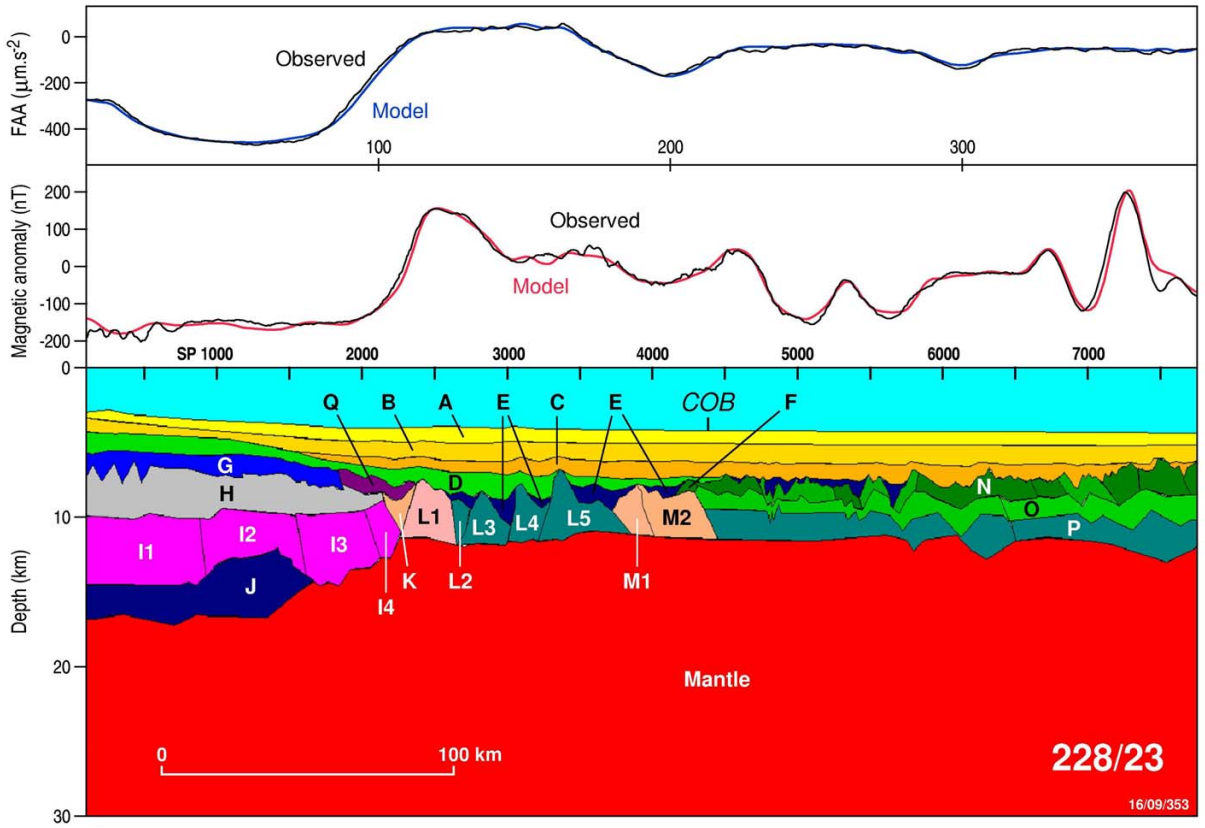

Figure 82: Potential field model for line GA-228/23, central Wilkes Land. COB is the location of the interpreted continent–ocean boundary. South on the left. Model bodies are identified in full in Appendix 7.

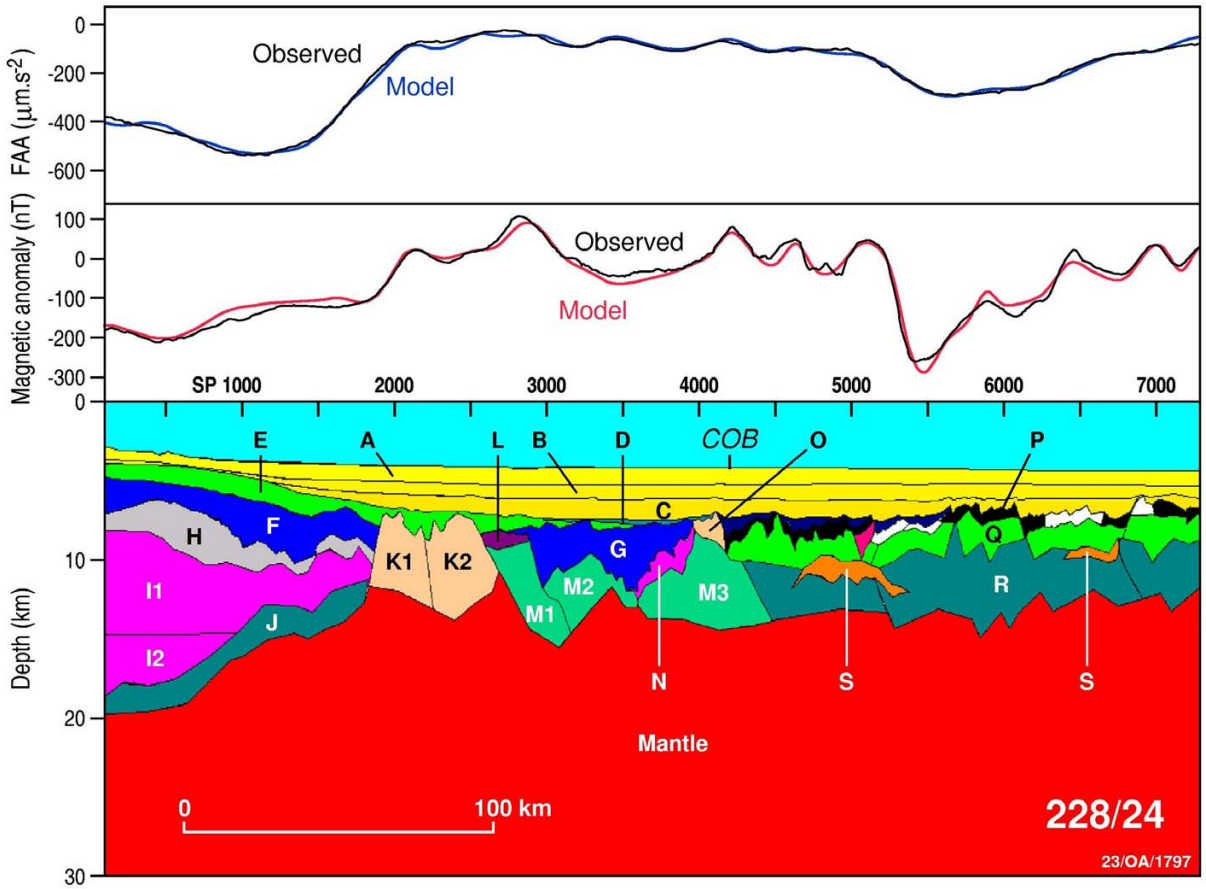

Figure 83: Potential field model for line GA-228/24, central Wilkes Land (after Colwell et al., in press). COB is the location of the interpreted continent–ocean boundary. South on the left. Model bodies are identified in full in Appendix 7.

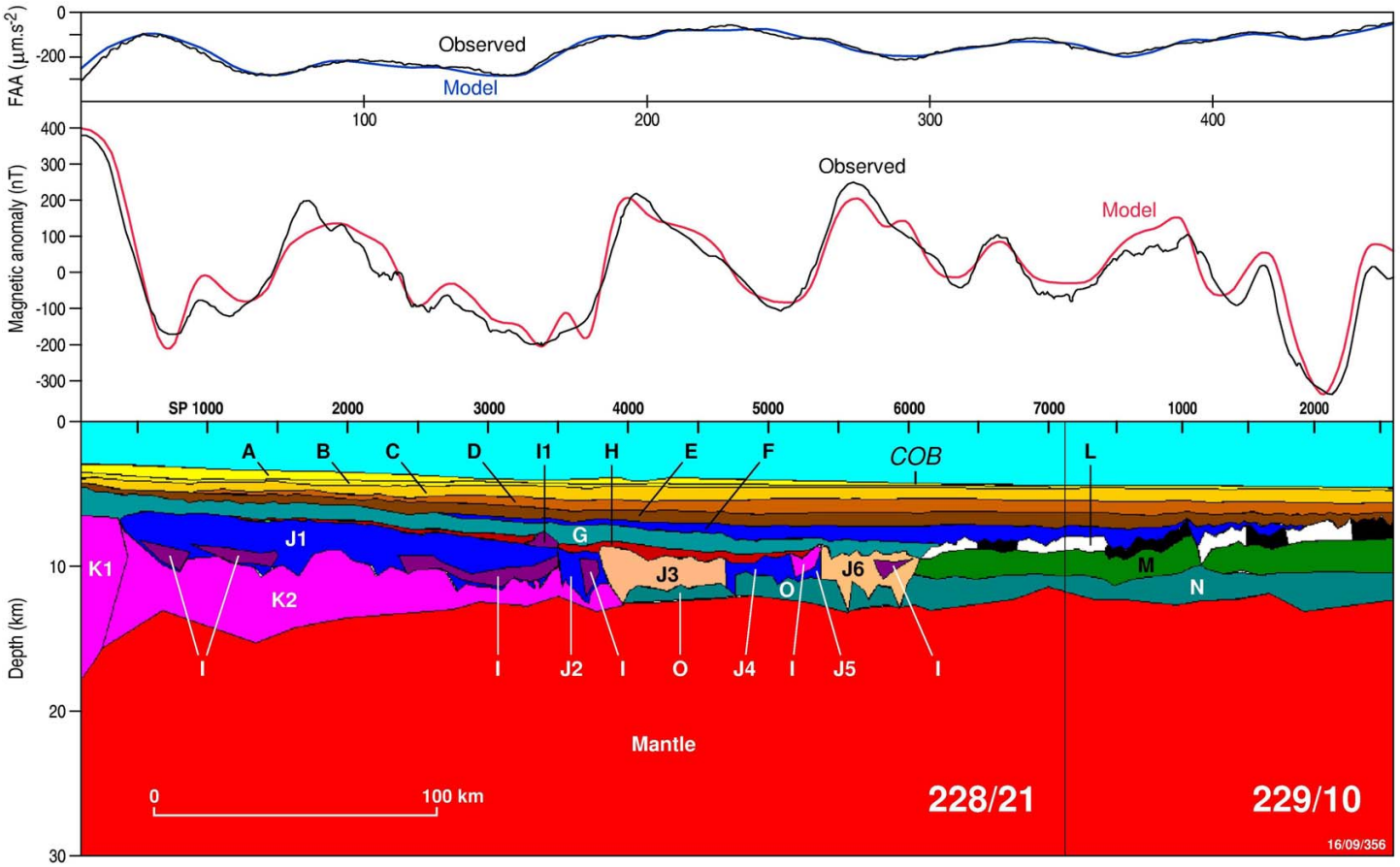

Figure 84: Potential field model for line GA-228/21 + GA-229/10, central Wilkes Land. COB is the location of the interpreted continent–ocean boundary. South on the left. Model bodies are identified in full in Appendix 7.

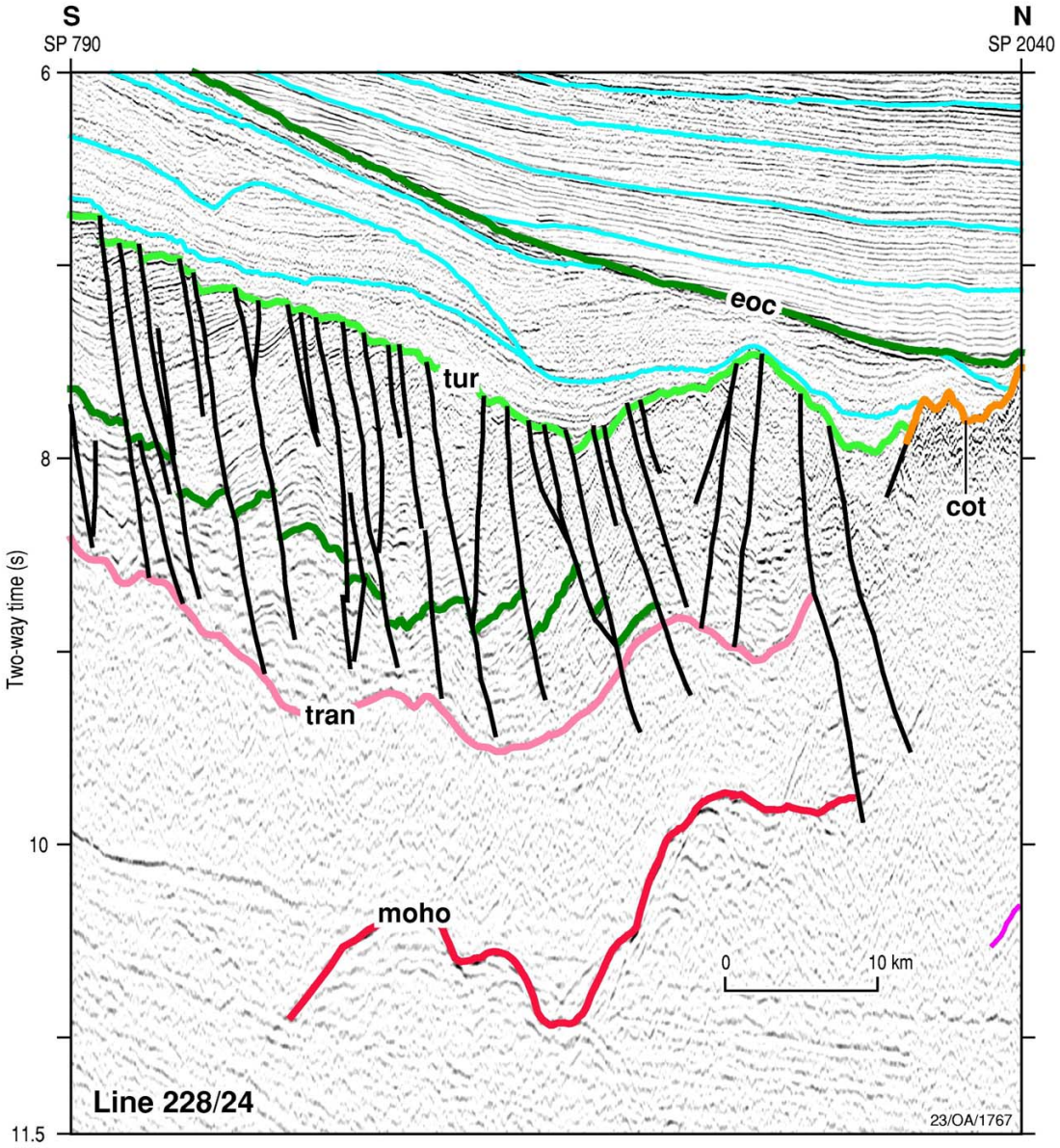

Figure 85: Detailed seismic section line GA-228/24, offshore Wilkes Land, inboard of the interpreted peridotite ridge, showing reflection Moho, transparent crystalline crust, thick faulted mid-Cretaceous and older section and post-rift section. *tran* – top transparent crystalline crust; *cot* – top transitional crust; *tur* – Turonian; *eoc* – Eocene. Full line shown in Plate 17.

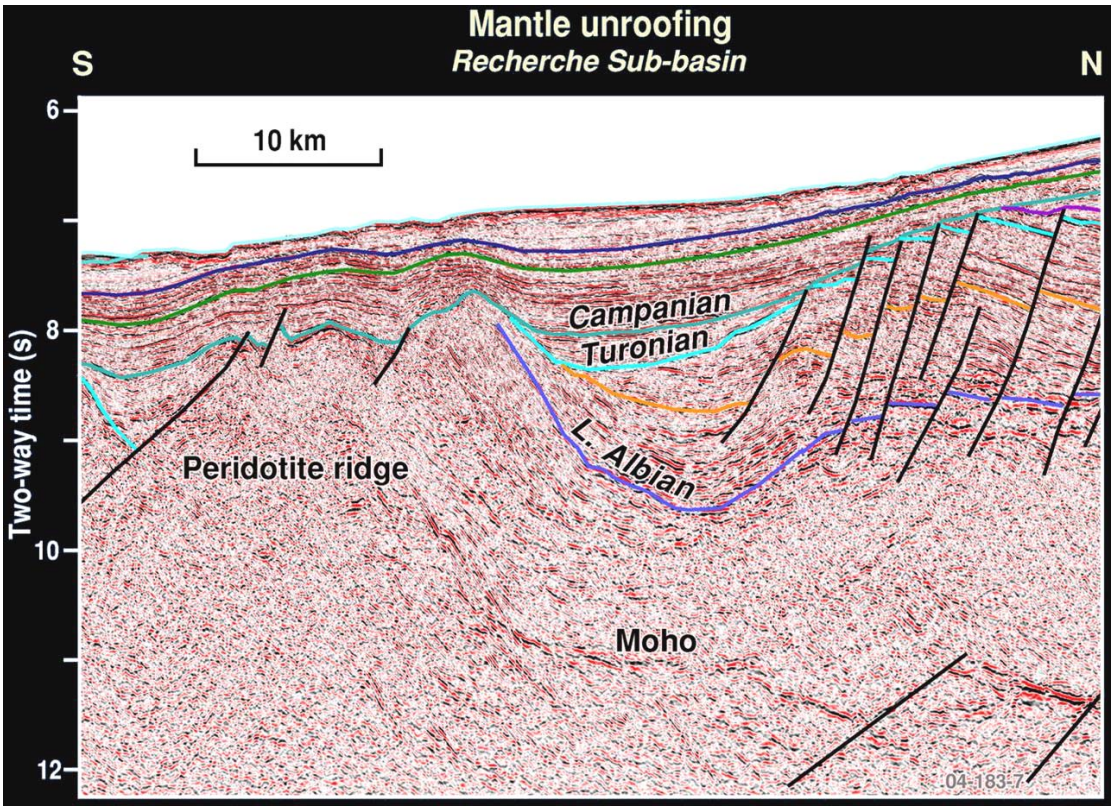

Figure 86: Seismic profile from the deep-water Great Australian Bight, southern Australian margin, conjugate to Wilkes Land. As with the Wilkes Land margin, this profile shows the interpreted peridotite ridge, faulted Moho, transparent lower crust and thick, faulted Cretaceous sedimentary section.

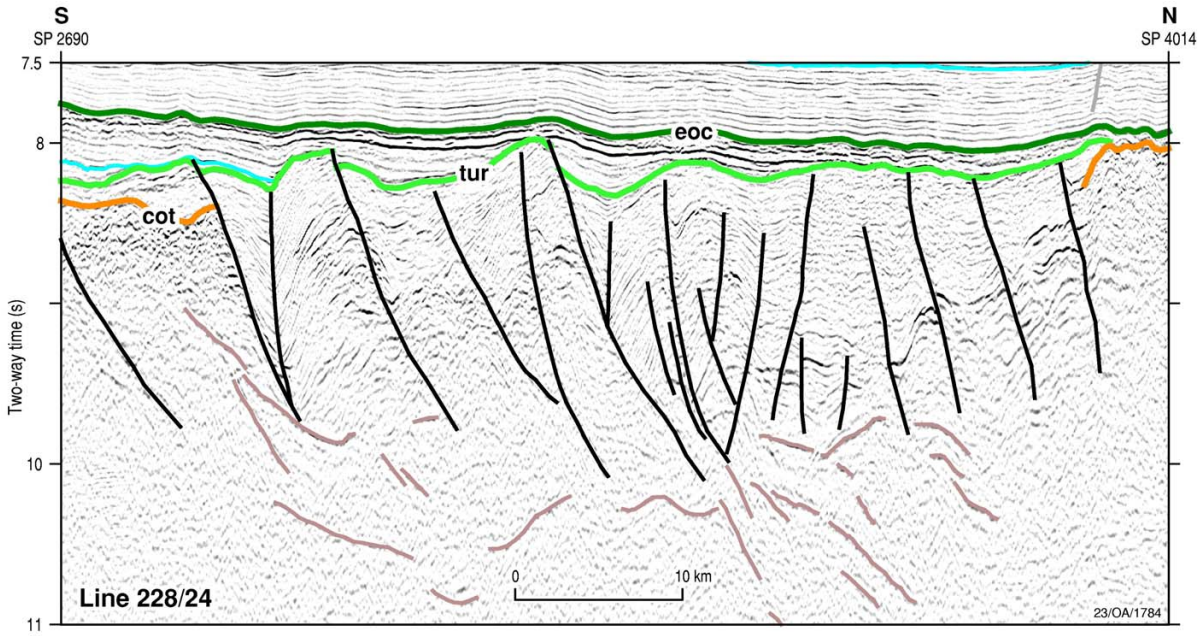

Figure 87: Detailed seismic section line GA-228/24, offshore Wilkes Land, outboard of the interpreted peridotite ridge. This section is interpreted to be a basin containing highly faulted and rotated sedimentary rocks of pre-Turonian age overlying either very thin crystalline continental crust or altered mantle. Full line shown in Plate 17.

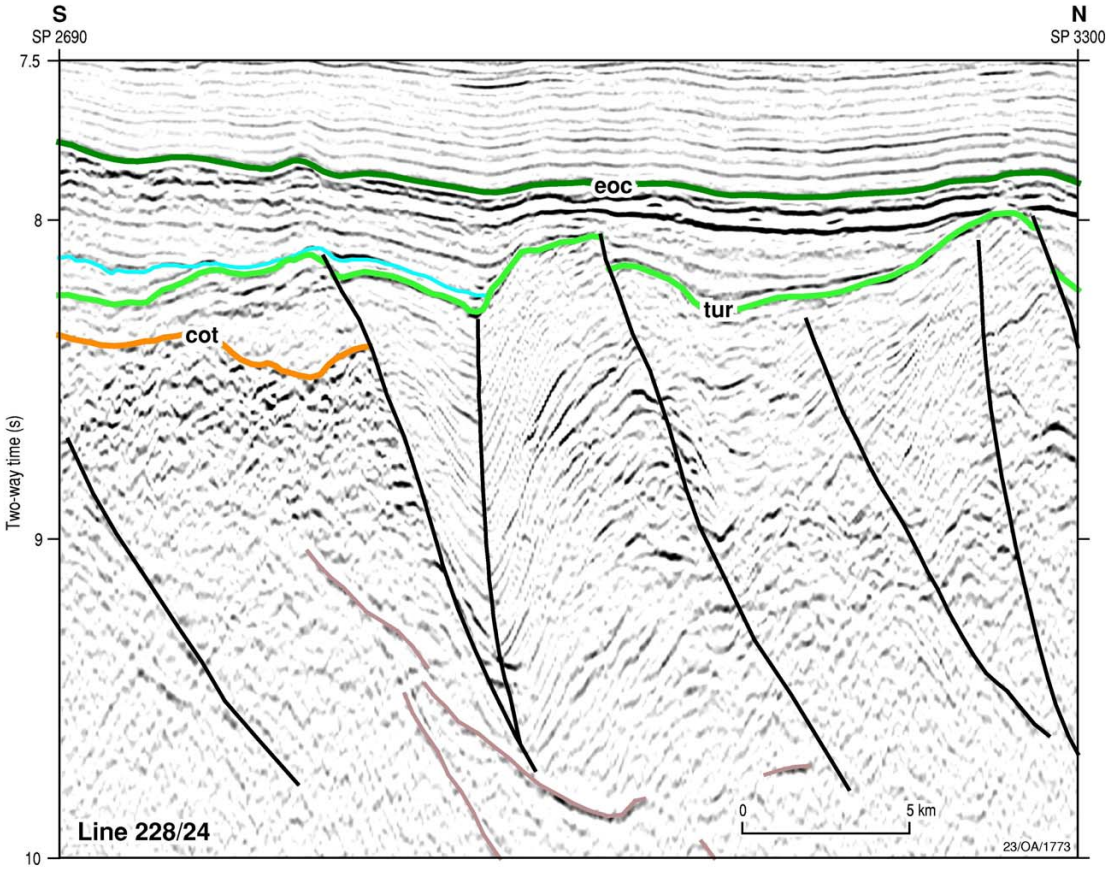

Figure 88: Detailed seismic section, line GA-228/24, offshore Wilkes Land, immediately outboard of the interpreted peridotite ridge. This an enlargement of the left-hand end of the section shown in Figure 87. Full line shown in Plate 17.

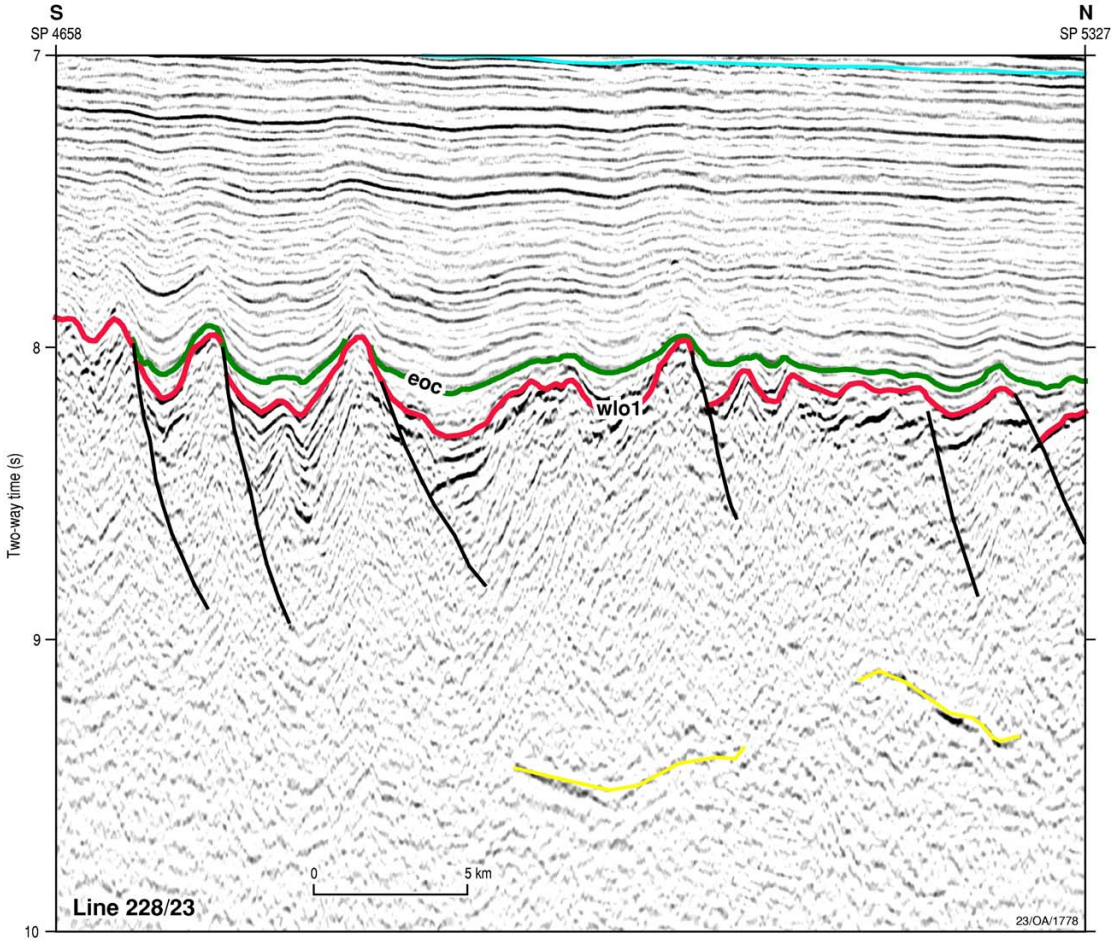

Figure 89: Detailed seismic section, line GA-228/23, central Wilkes Land, showing the characteristic appearance of oceanic crustal type *wlo1*. Full line shown in Plate 16.

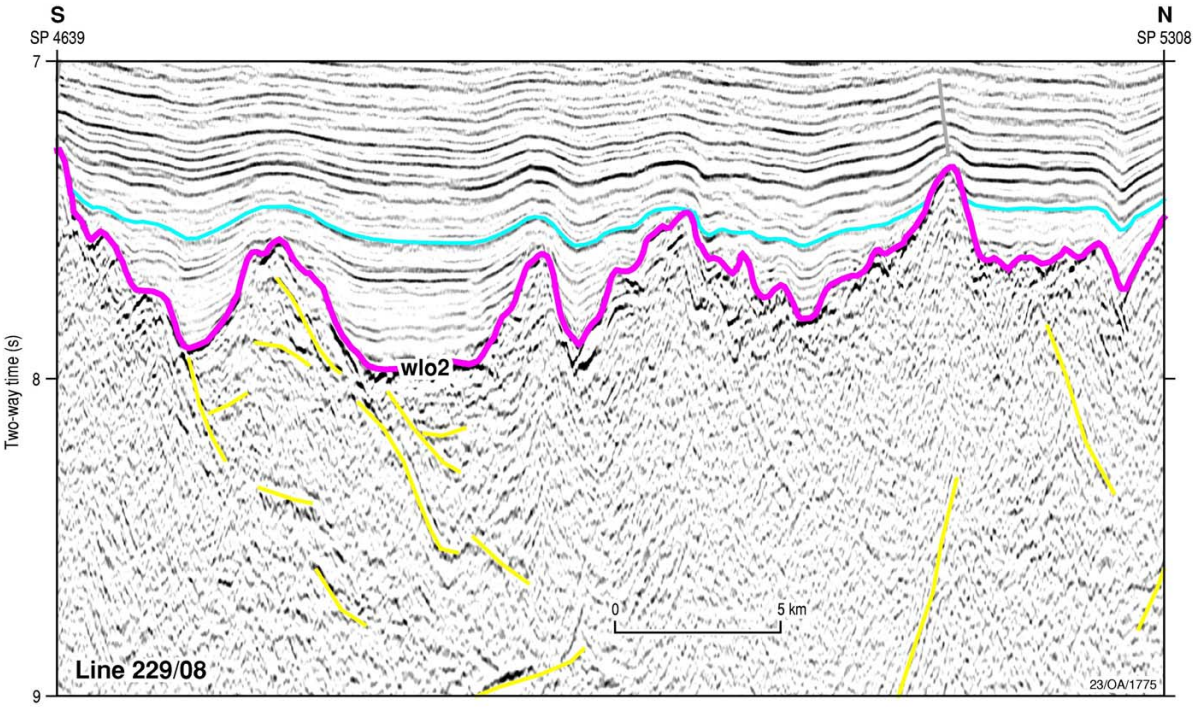

Figure 90: Detailed seismic section, line GA-229/08, central Wilkes Land, showing the characteristic appearance of oceanic crustal type *wlo2*. Full line shown in Plate 16.

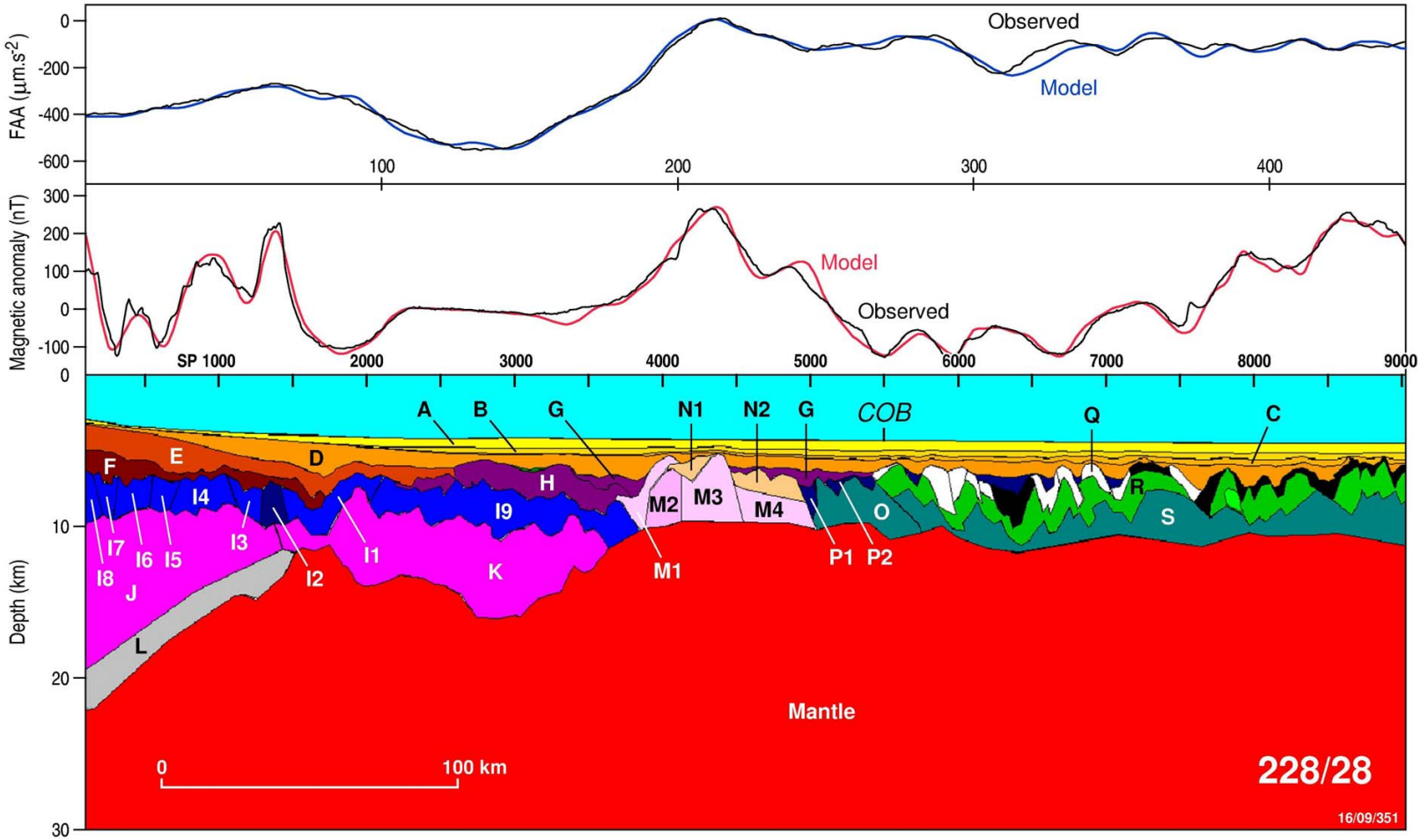

Figure 91: Potential field model for line GA-228/28, eastern Wilkes Land. COB is the location of the interpreted continent–ocean boundary. South on the left. Model bodies are identified in full in Appendix 7.

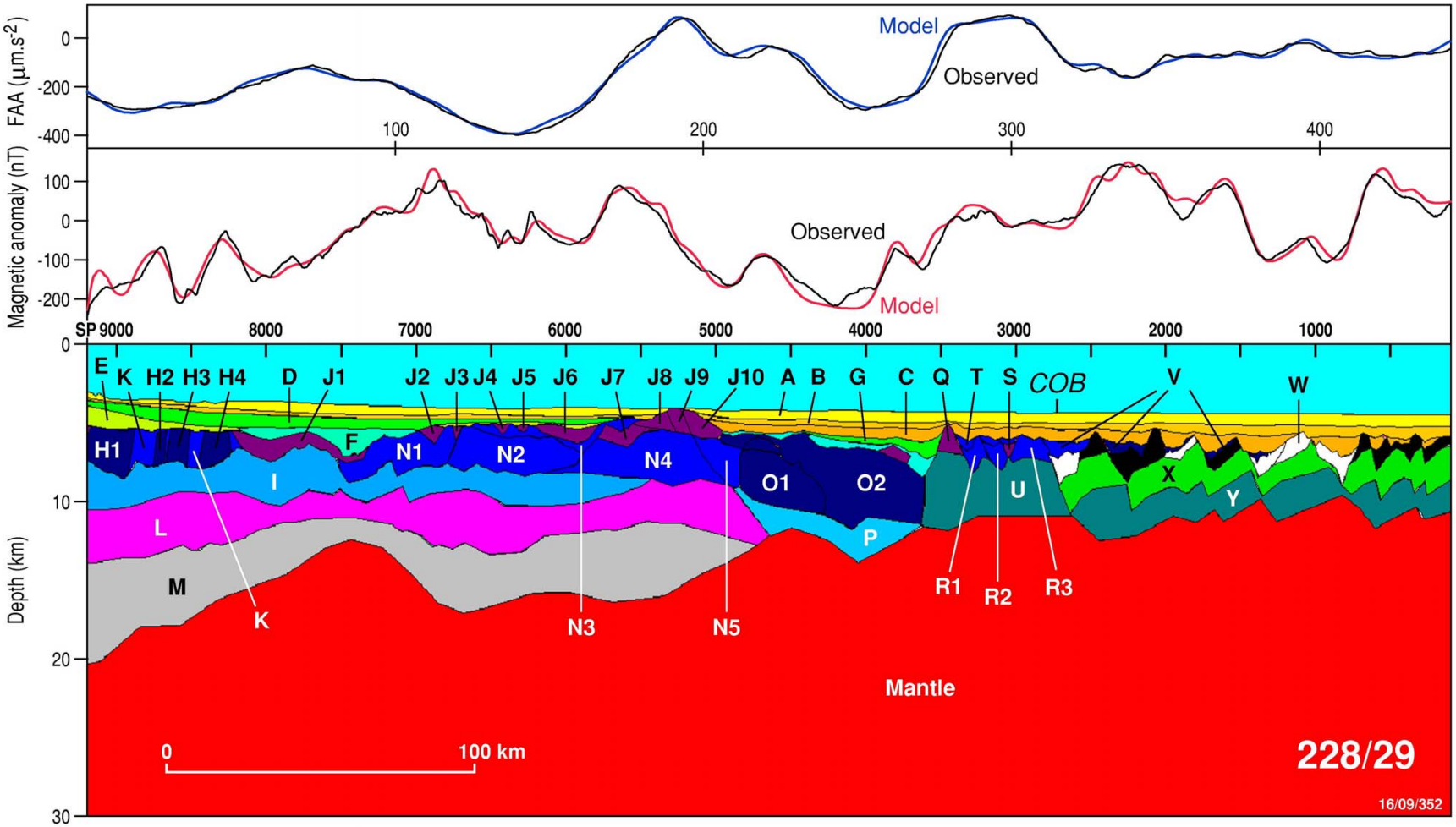

Figure 92: Potential field model for line GA-228/29, eastern Wilkes Land. COB is the location of the interpreted continent–ocean boundary. South on the left. Model bodies are identified in full in Appendix 7.

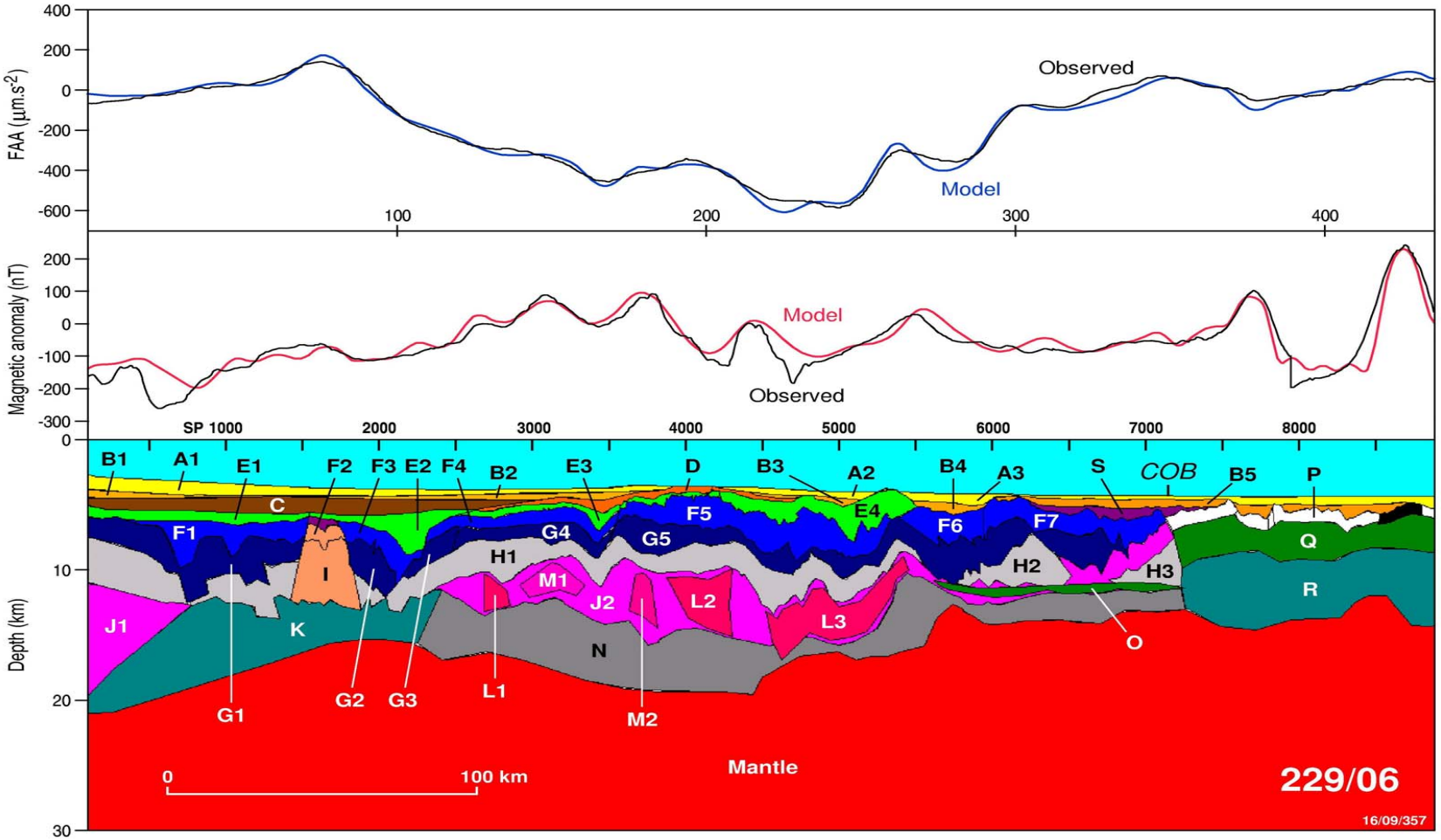

Figure 93: Potential field model for line GA-229/06, offshore Terre Adélie (after Colwell et al., in press). COB is the location of the interpreted continent–ocean boundary. The Adélie Rift Block extends from SP 2200–5500. South on the left. Model bodies are identified in full in Appendix 7.

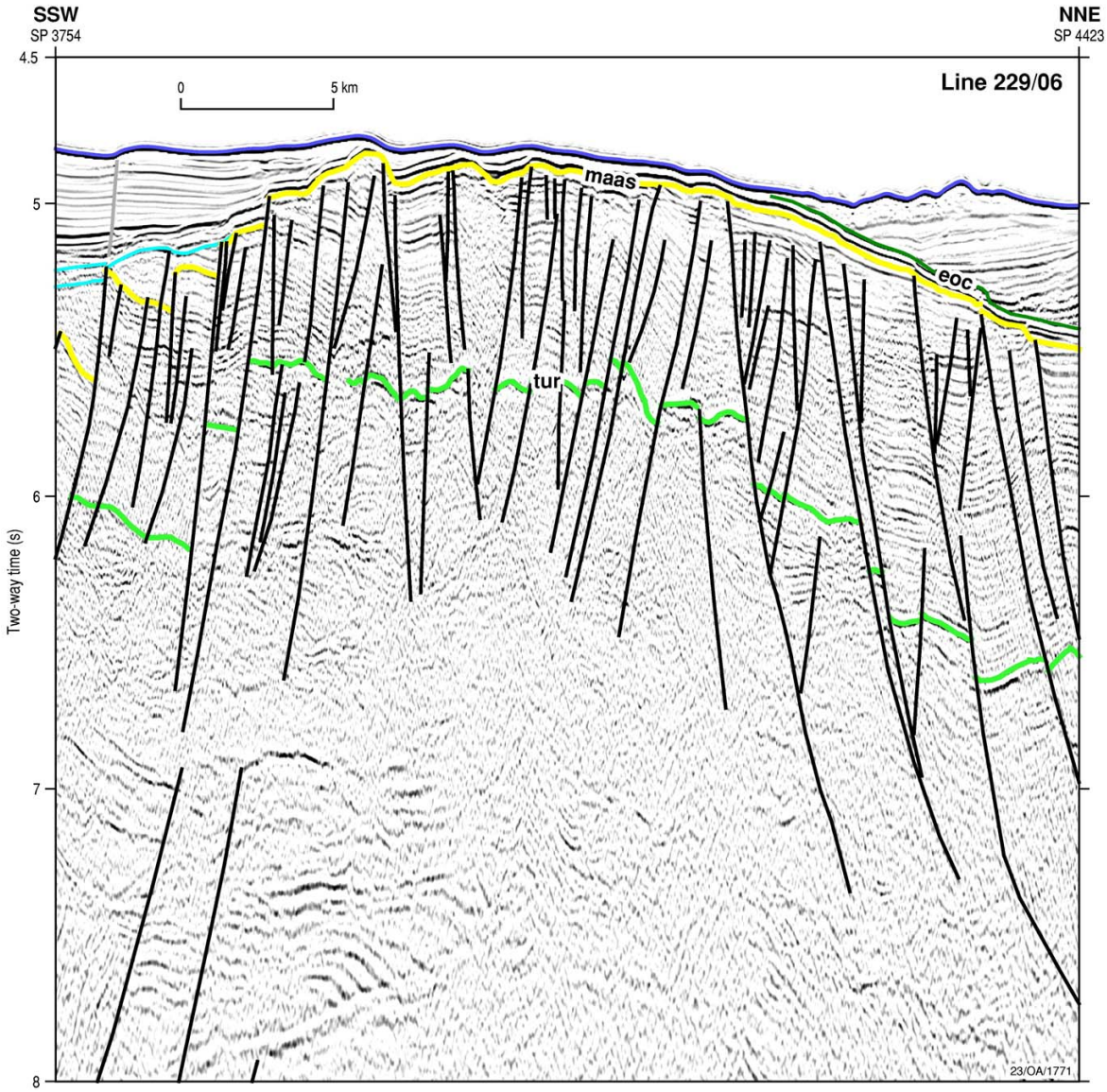

Figure 94: Detailed seismic section, line GA-229/06, offshore Terre Adélie, showing the thick sedimentary section near the crest of the Adélie Rift Block. *tur* – Turonian; *maas* – Maastrichtian; *eoc* – Eocene. Full line shown in Plate 18.

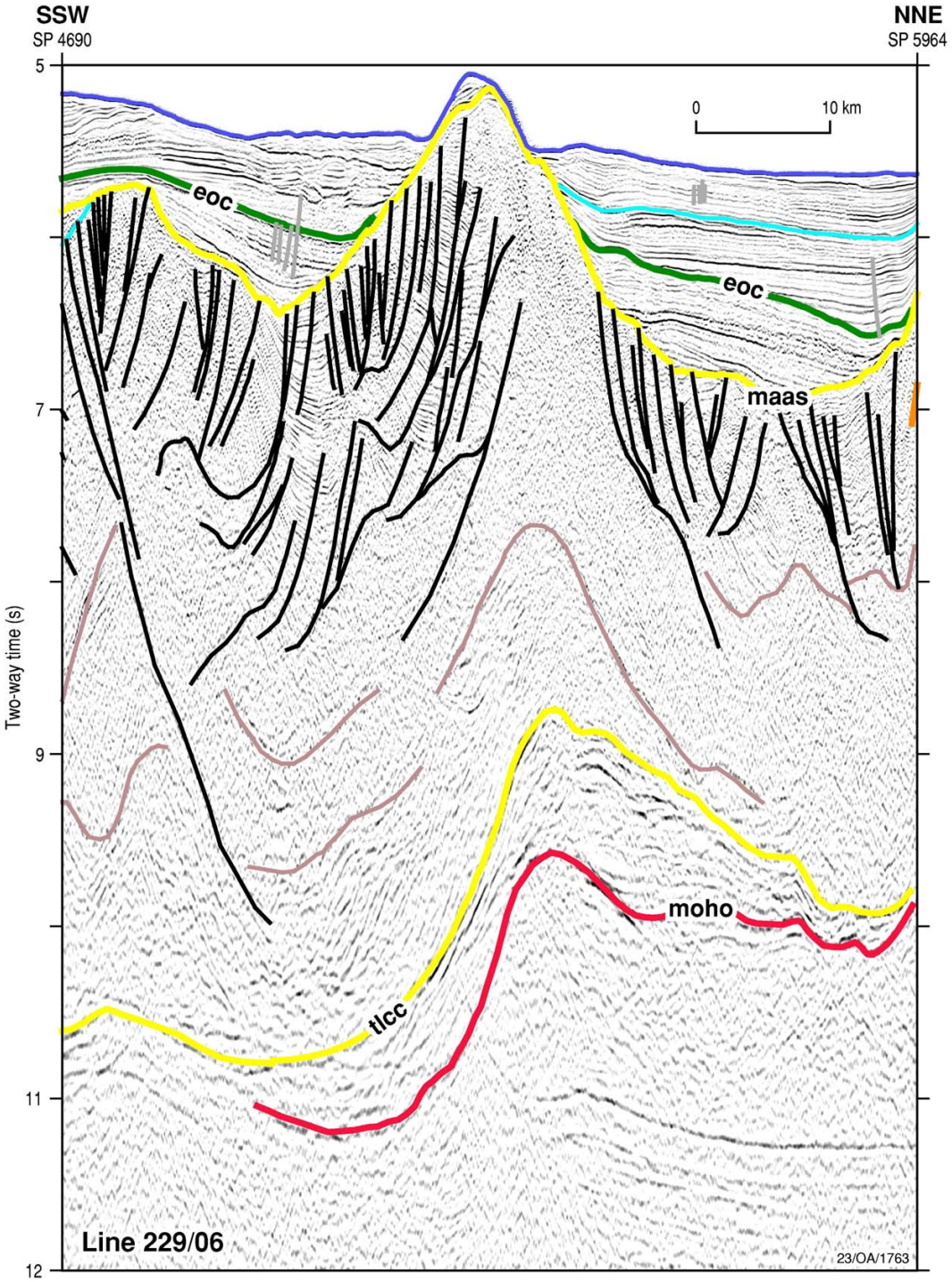

Figure 95: Detailed seismic section, line GA-229/06, offshore Terre Adélie, showing the thick, folded and faulted sedimentary section outboard of the crest of the Adélie Rift Block. Note the pinch-and-swell structures in the lower crust that have strongly influenced the structuring of the overlying sedimentary section. *maas* – Maastrichtian; *eoc* – Eocene. Full line shown in Plate 18.

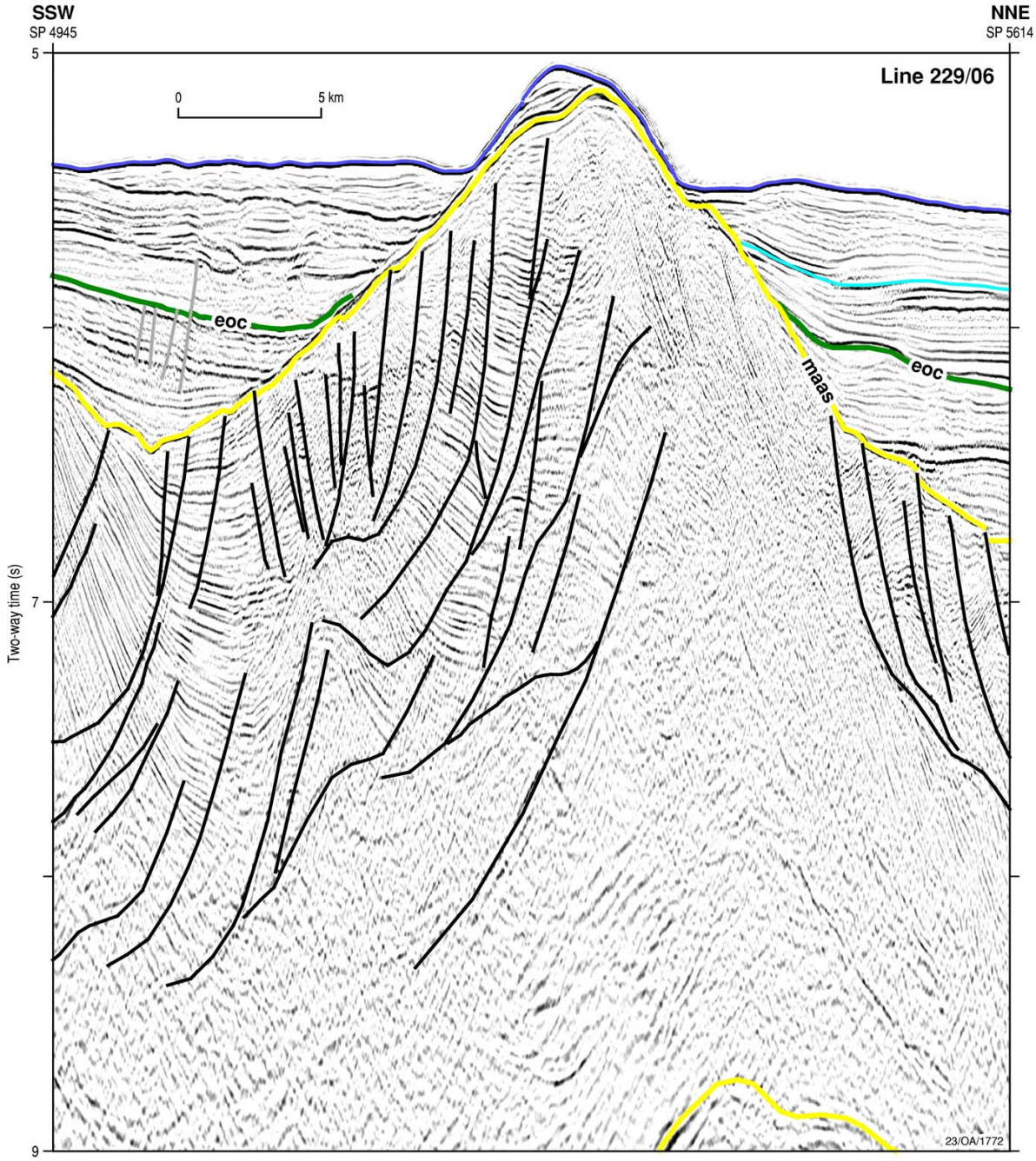

Figure 96: Detailed seismic section, line GA-229/06, offshore Terre Adélie, showing the thick, folded and faulted sedimentary section outboard of the crest of the Adélie Rift Block. *maas* – Maastrichtian; *eoc* – Eocene. Full line shown in Plate 18.

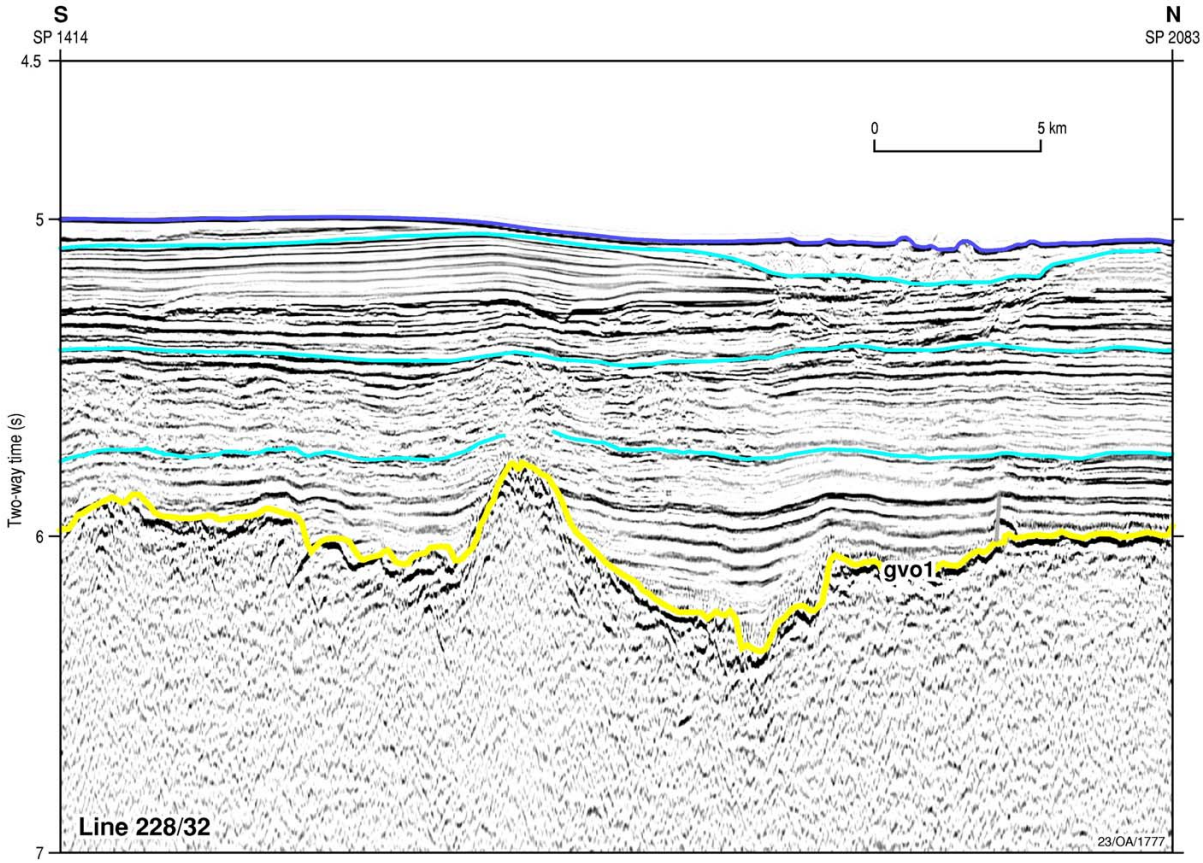

Figure 97: Detailed seismic section, line GA-228/32, off George V Land, showing the nature of oceanic crust *gvo1*.

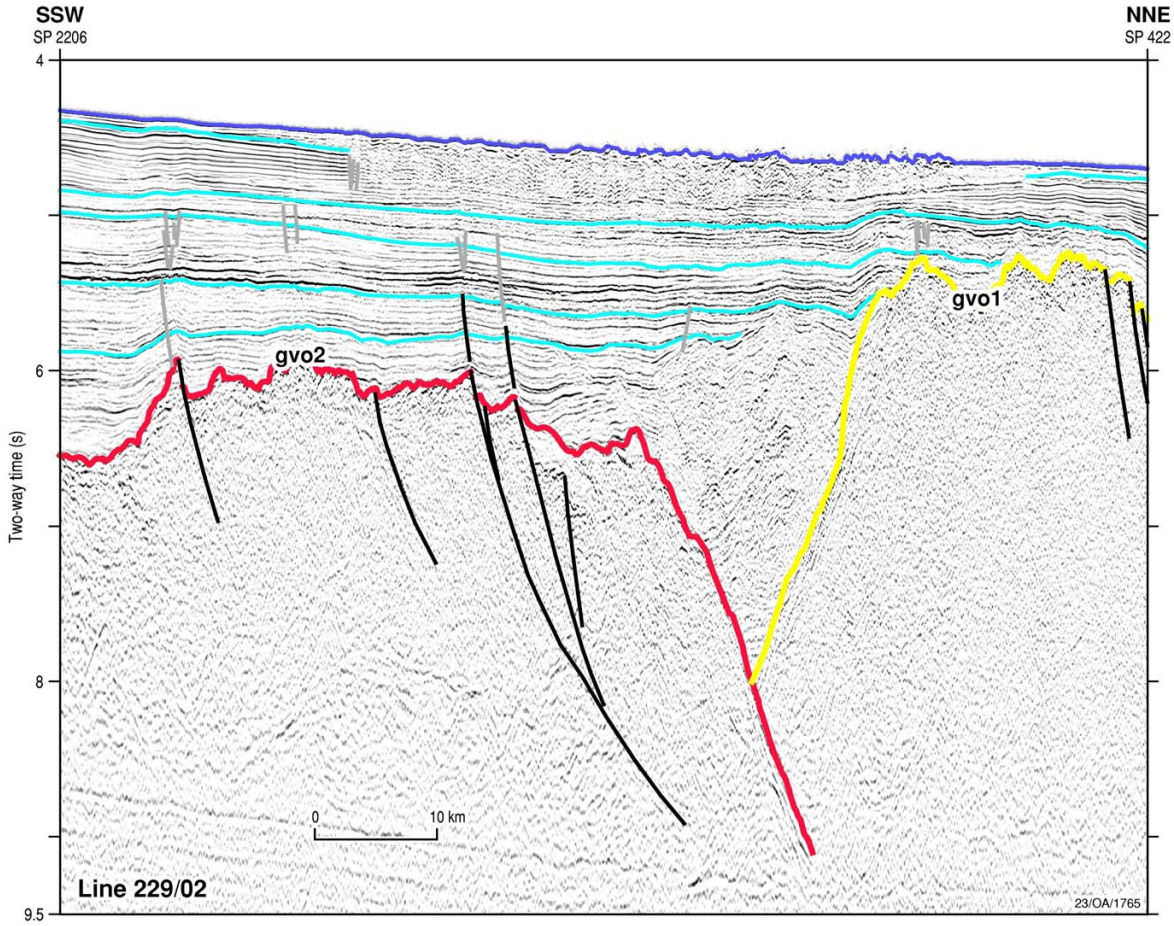

Figure 98: Detailed seismic section, line GA-229/02, off George V Land, showing the more-highly-faulted nature of oceanic crust type *gvo2* in comparison to type *gvo1*. The deep slot between the two crustal types corresponds to the western part of the Tasman Fracture Zone (Plate 21).

1. Enderby Basin
2. Prydz Bay
3. Princess Elizabeth Trough
4. Kerguelen Plateau
5. Labuan Basin
6. Shackleton Basin
7. Bruce Rise
8. Wilkes Land margin
9. Terre Adélie margin
10. South Tasman Rise
11. Otway basin
12. Great Australian Bight (Bight Basin)
13. Australian–Antarctic Basin
14. Diamantina Zone
15. Naturaliste Plateau
16. Perth basin
17. Cuvier Basin
18. Gascoyne Abyssal Plain
19. Argo Abyssal Plain
20. Broken Ridge

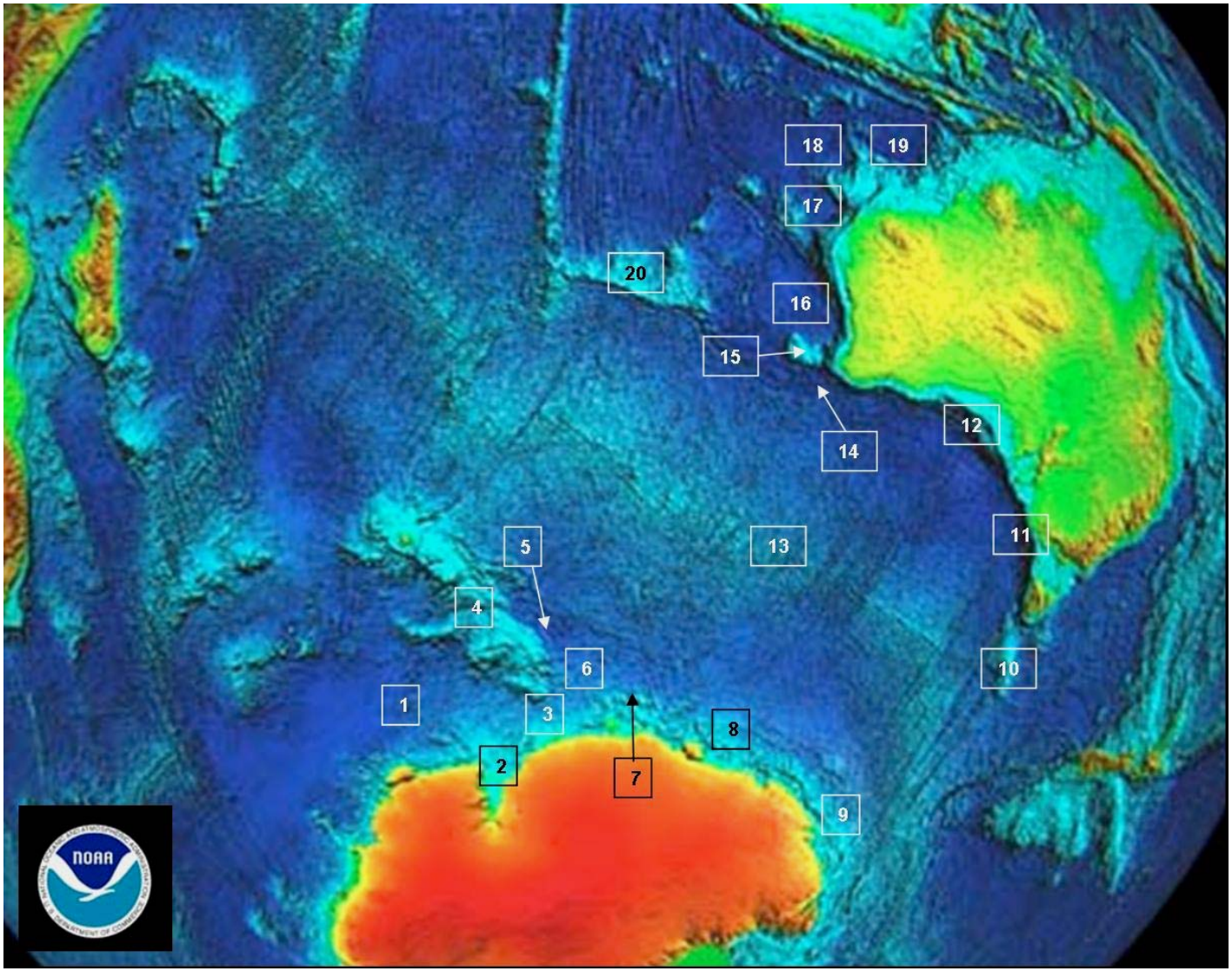

Figure 99: NOAA image of the morphology of the Indian and Southern Oceans and adjacent continents.

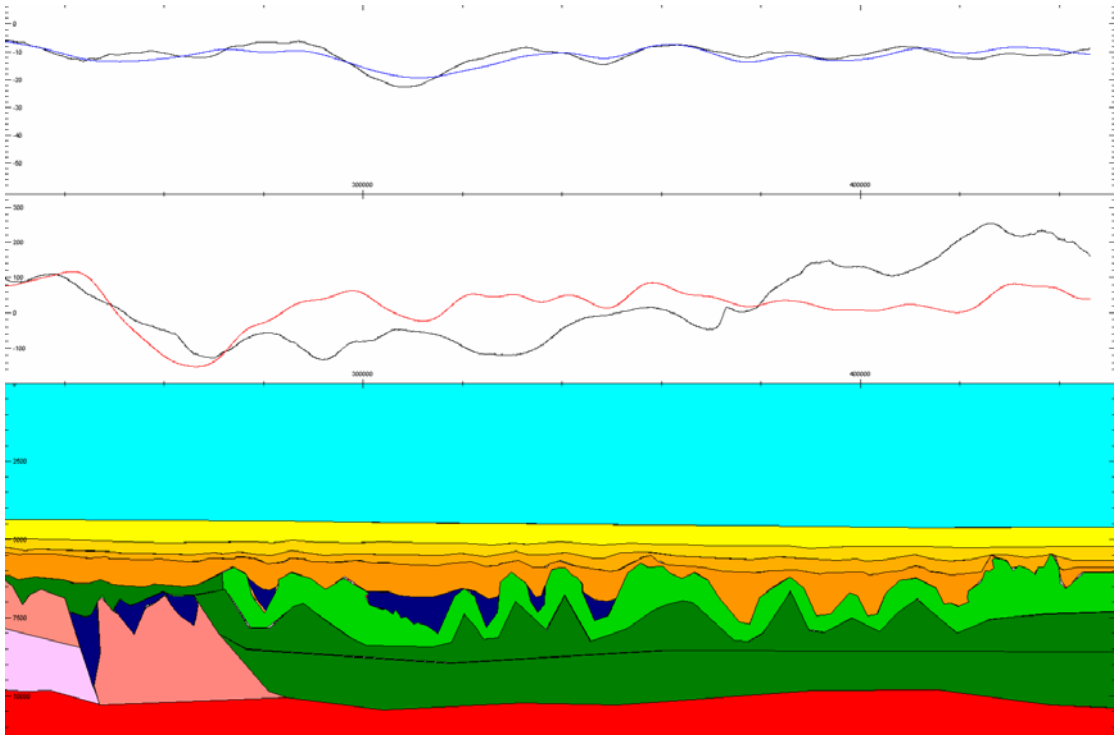

Figure 100: Potential field model for part of line GA-228/28, eastern Wilkes Land. South on the left Test 1: (no remanence; tests topographic response of upper basaltic layer) Layer 2 = 0.05 SI; Layer 3 (fills topographic highs) & 4 (flat) =0 SI. This test produced a poor fit of the model and observed data.

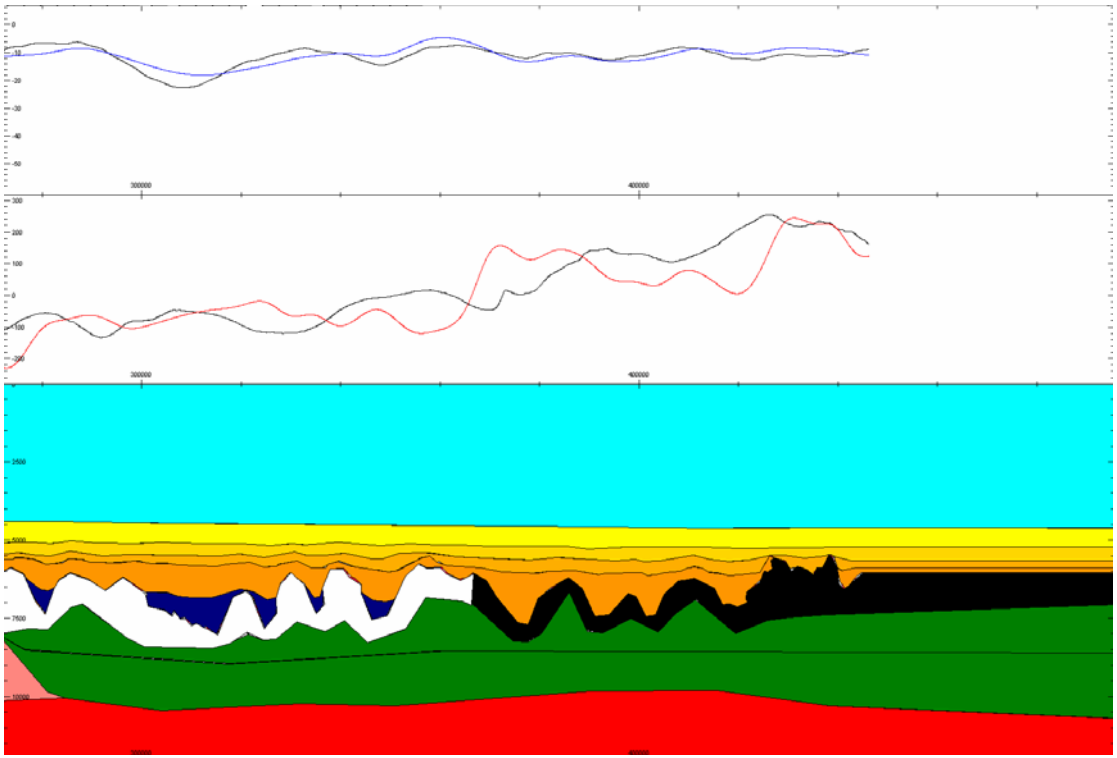

Figure 101: Potential field model for part of line GA-228/28, eastern Wilkes Land. South on the left. Test 2: (tests if regional gradient is due to differing remanence polarity in upper layer). Landward = 0.05 SI, Q = 2 Rev I =74, D =0; Seaward = 0.05 SI Q = 2 Norm I =-74, D =0.

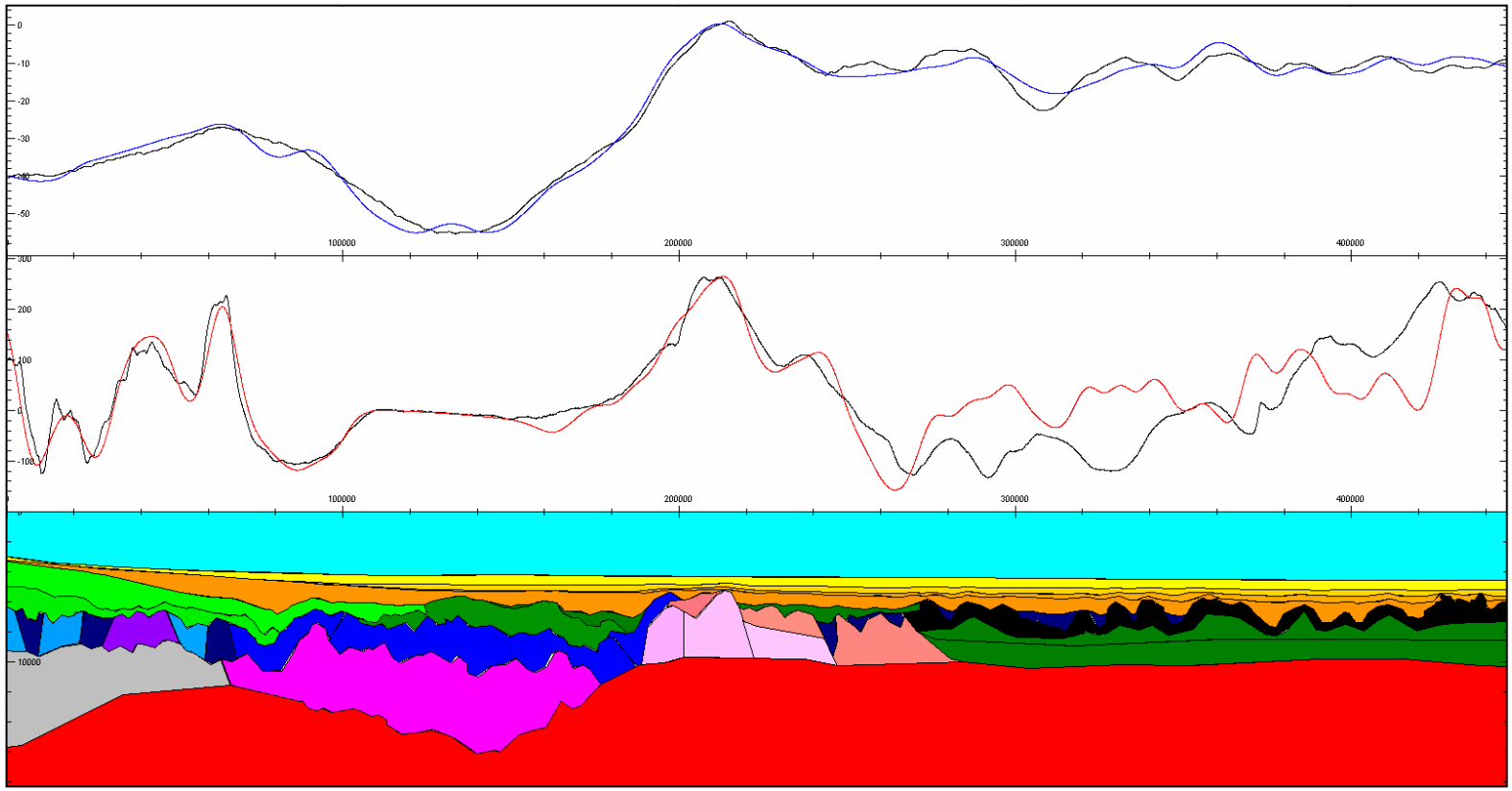

Figure 102: Potential field model for line GA-228/28, eastern Wilkes Land. South on the left. Test 3: (tests if regional gradient is due to differing magnitude of remanence -Konigsberger Ratio- in upper layer, all normal). Landward Normal Q =1.25 k = 0.02 Seaward = Normal Q =2 k =0.05.

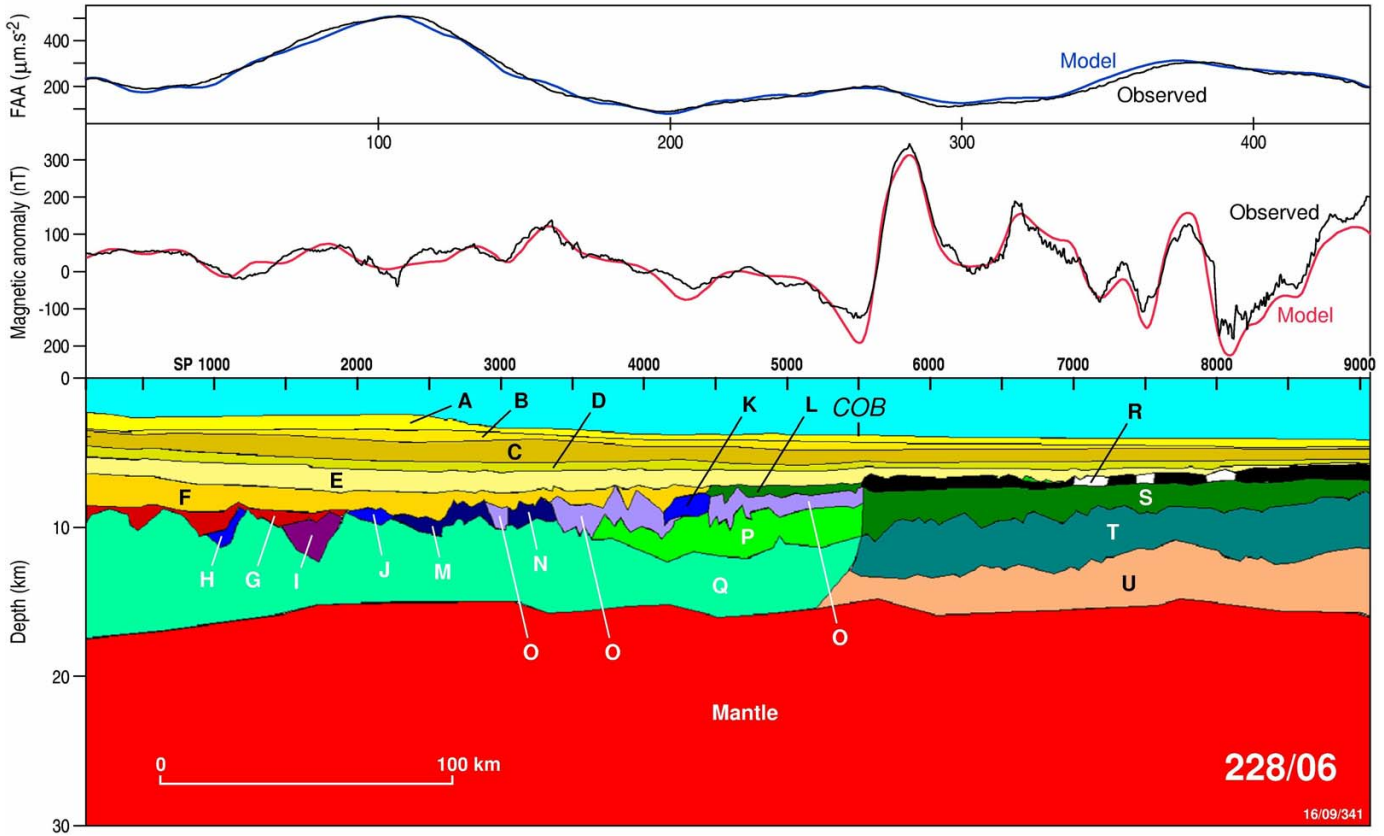

Figure 103: Potential field model for line GA-228/06, Mac. Robertson Land; original model. South on the left. COB is the location of the interpreted continent–ocean boundary.

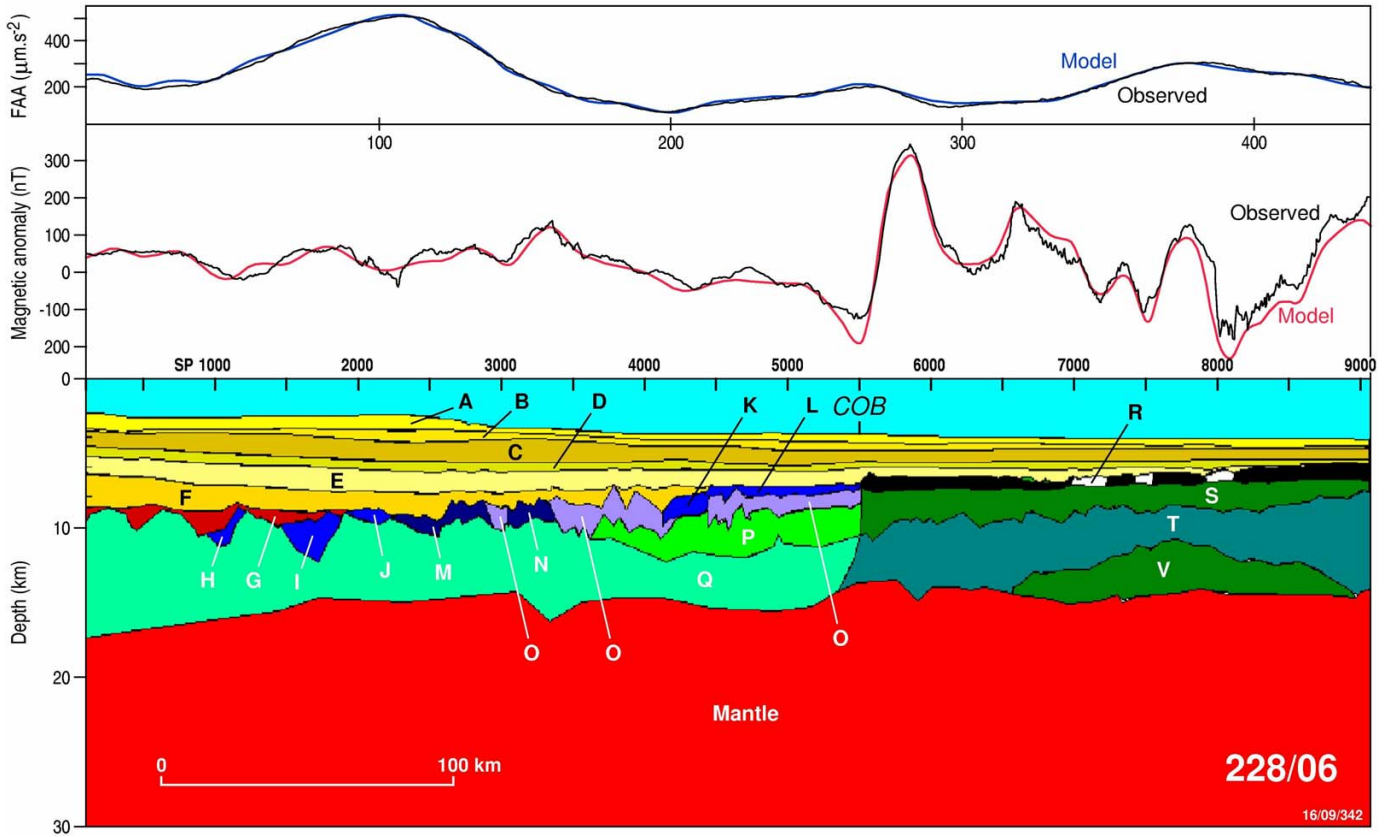

Figure 104: Potential field model for line GA-228/06, Mac. Robertson Land; revision to structure of oceanic crust. South on the left. COB is the location of the interpreted continent–ocean boundary.

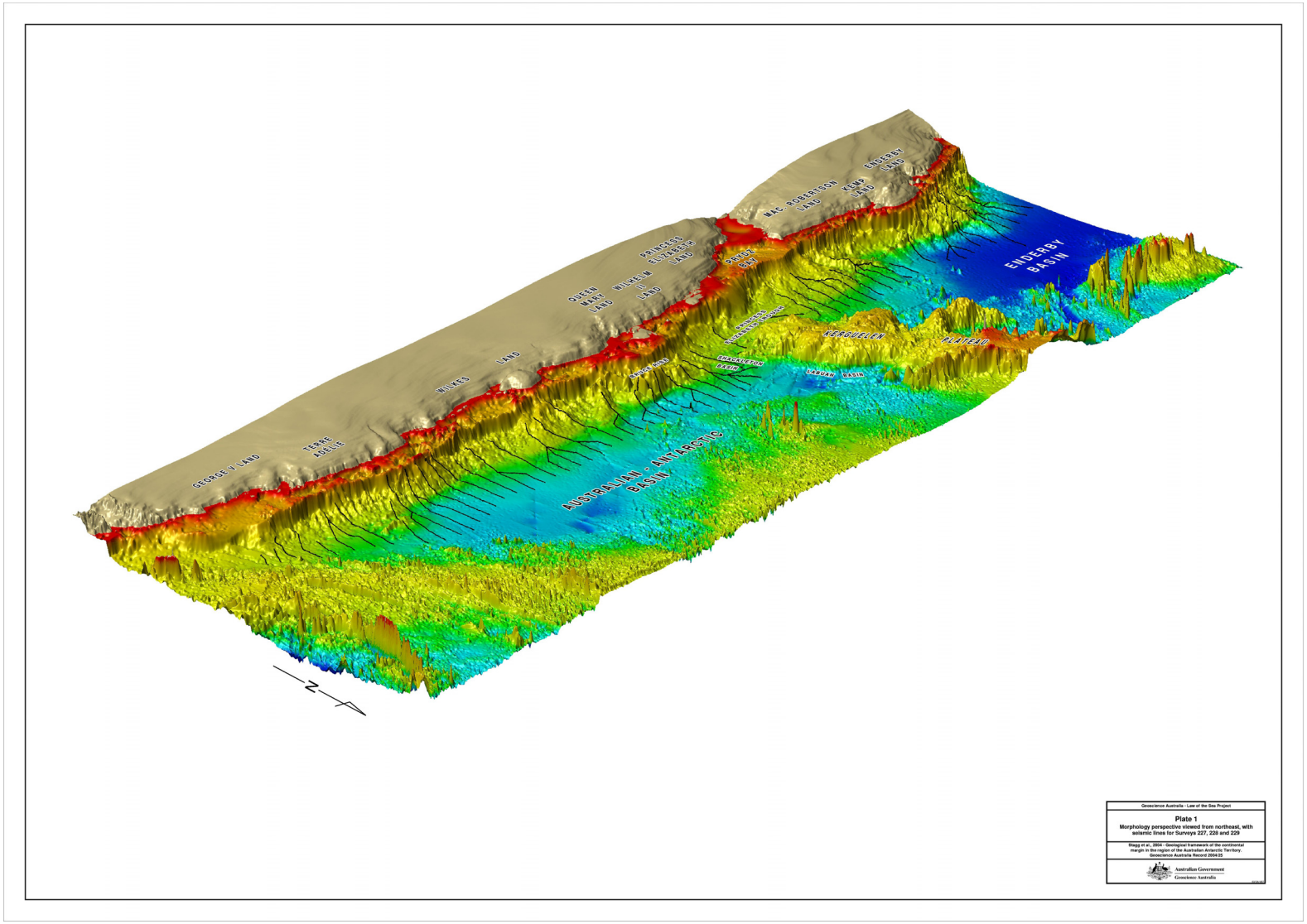

Plate 1: Morphology perspective viewed from northeast, with seismic lines for surveys 227, 228 and 229.

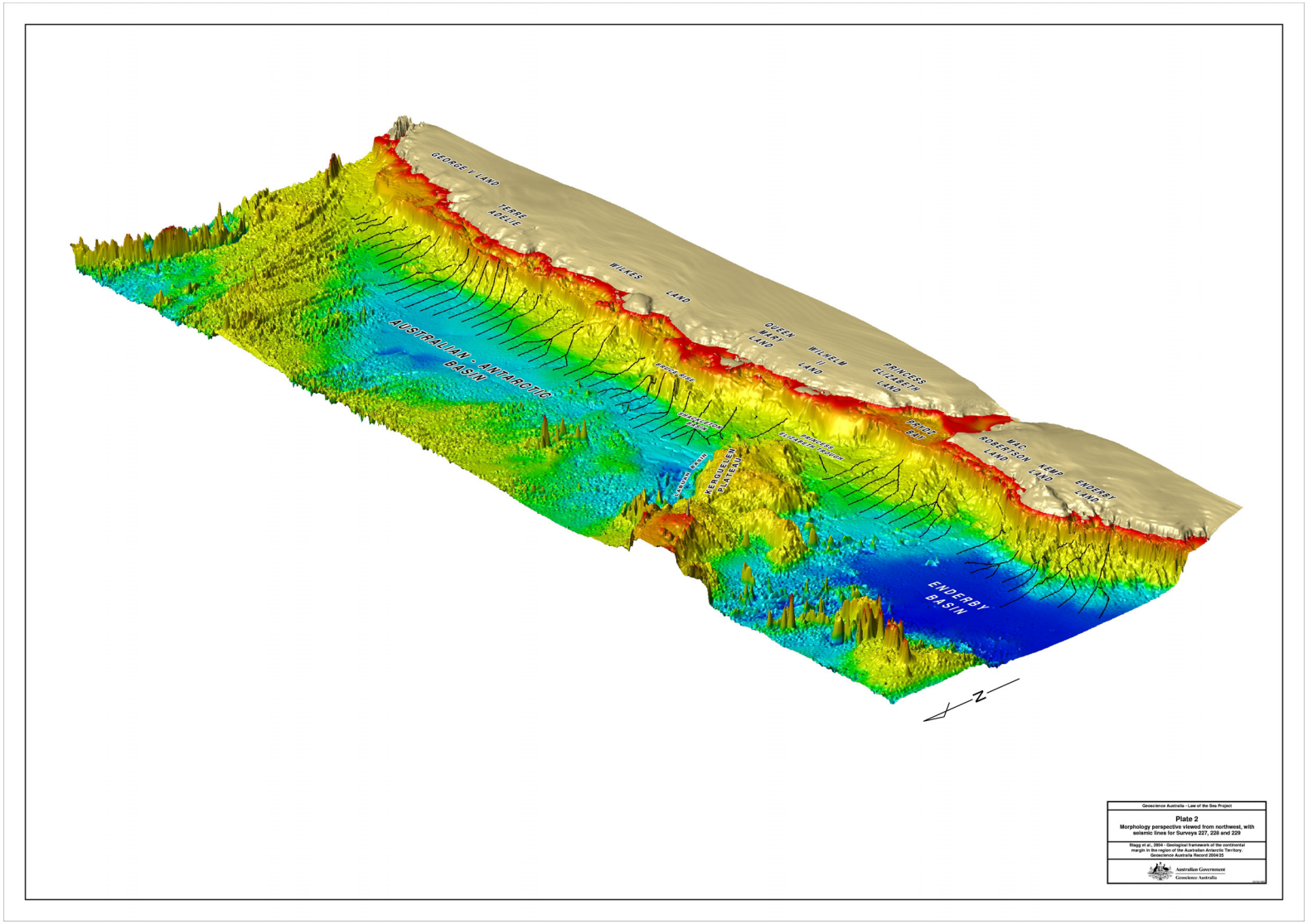

Plate 2: Morphology perspective viewed from northwest, with seismic lines for surveys 227, 228 and 229.

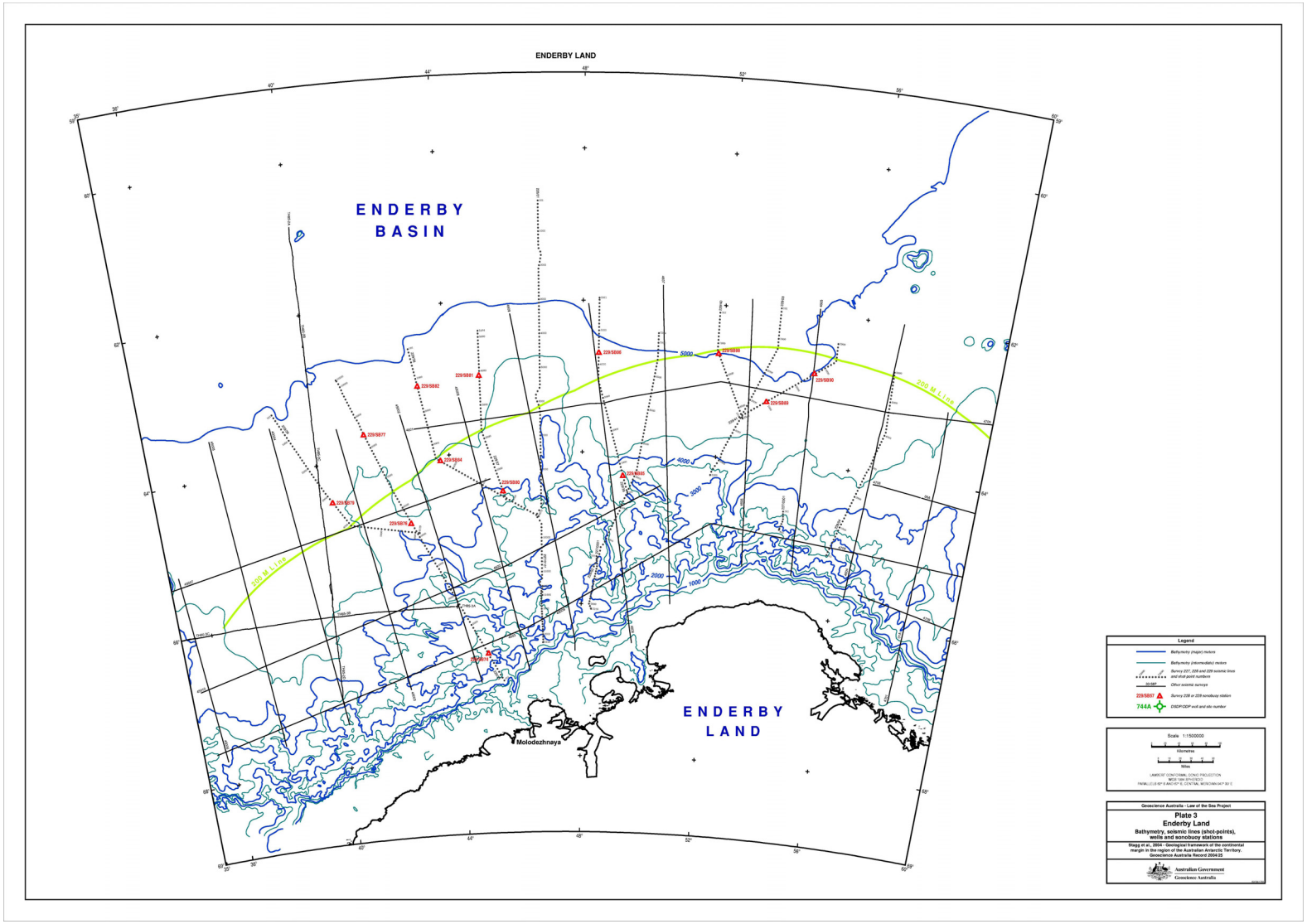

Plate 3: Enderby Land – bathymetry, seismic lines (shot-points), wells and sonobuoy stations.

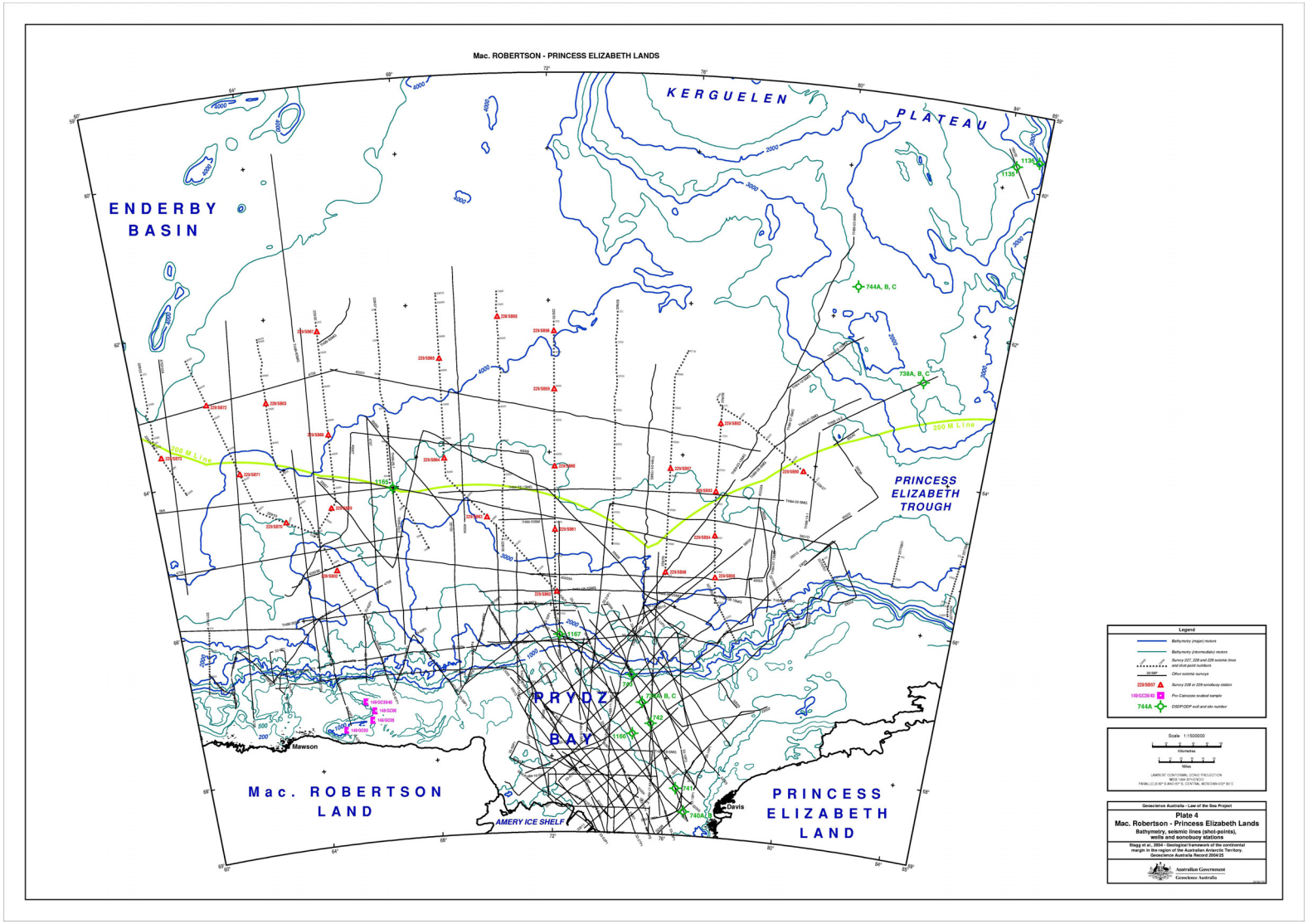

Plate 4: Mac. Robertson – Princess Elizabeth Lands – bathymetry, seismic lines (shot-points), wells and sonobuoy stations.

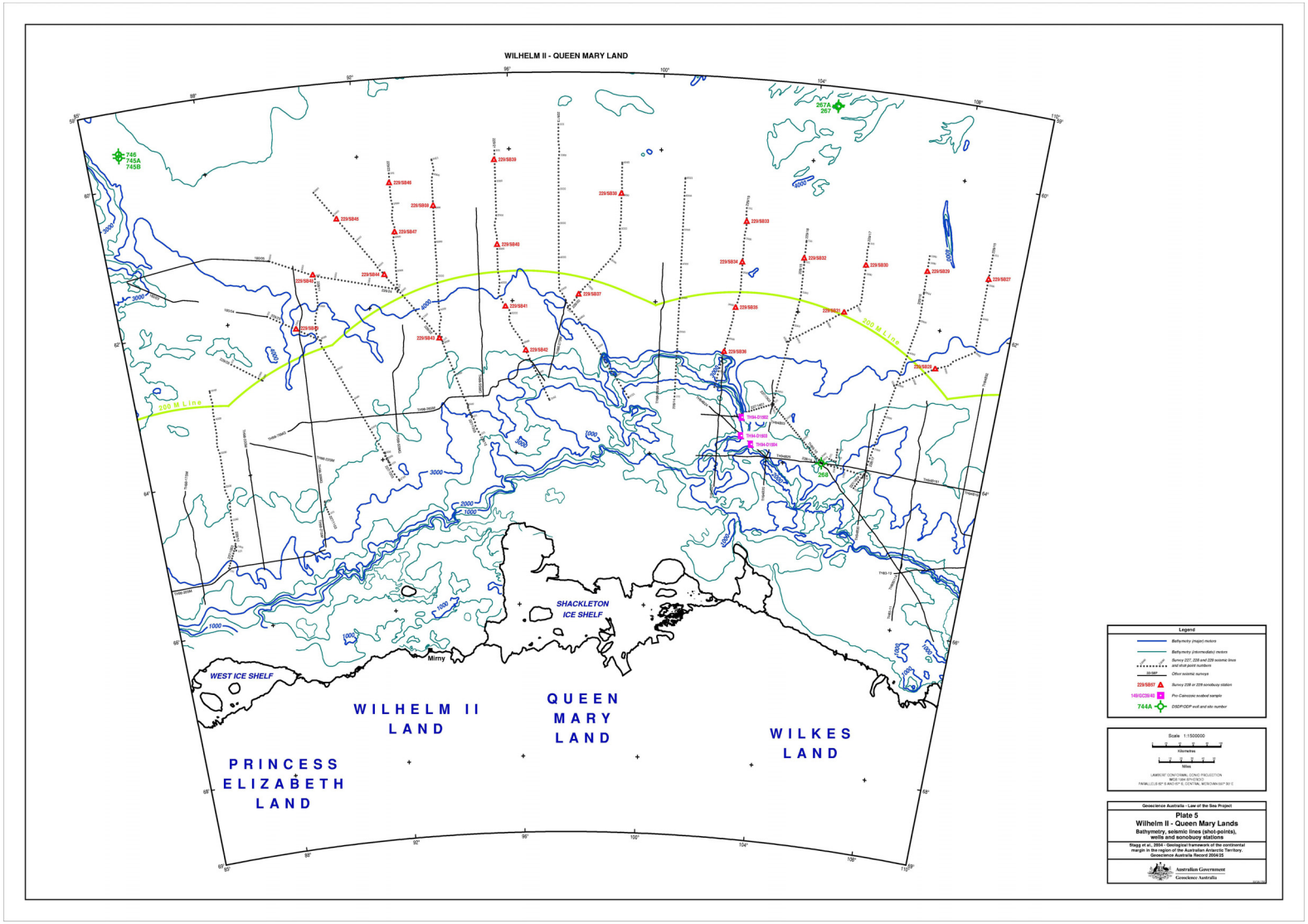

Plate 5: Wilhelm II – Queen Mary Lands – bathymetry, seismic lines (shot-points), wells and sonobuoy stations.

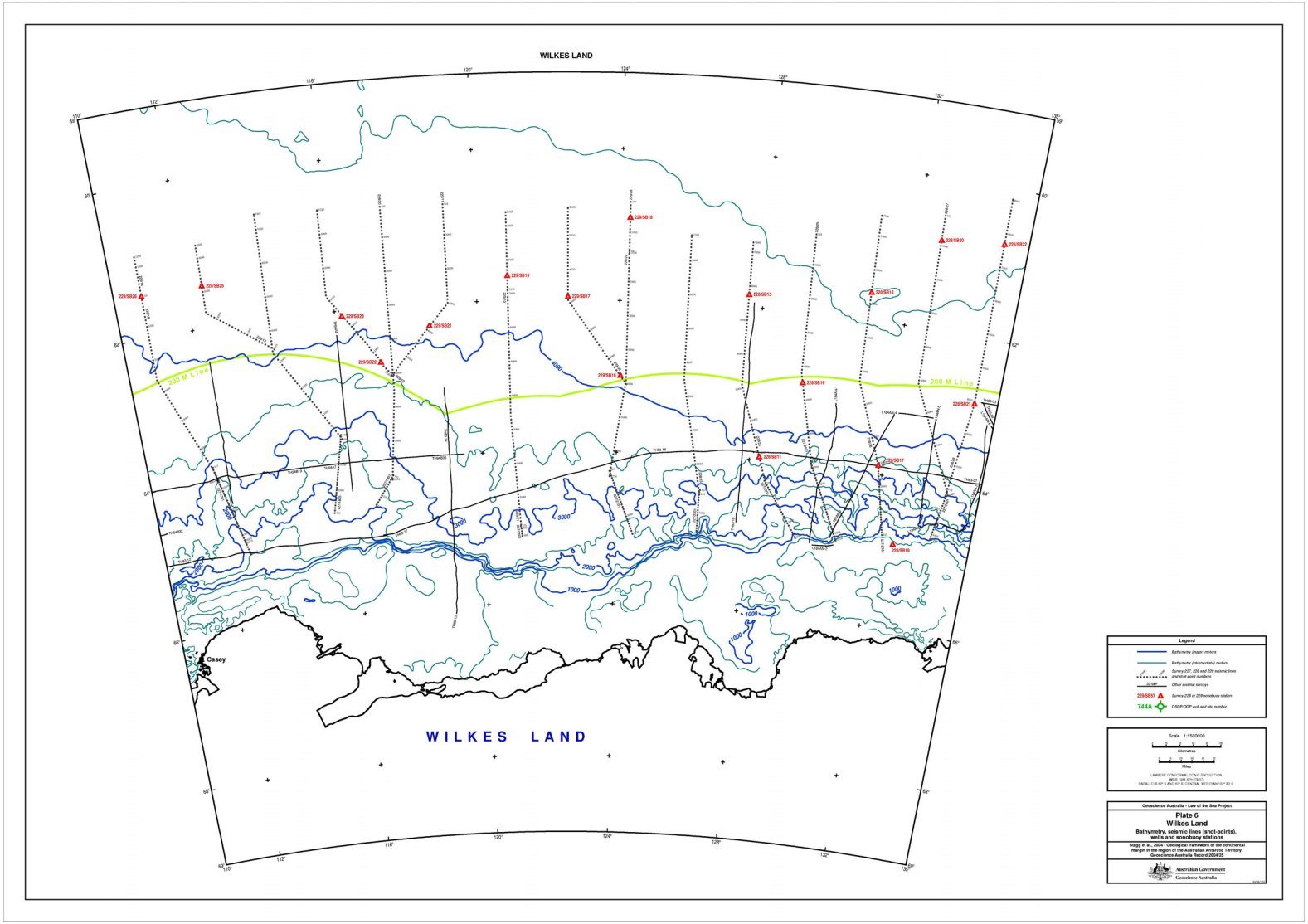

Plate 6: Wilkes Land – bathymetry, seismic lines (shot-points), wells and sonobuoy stations.

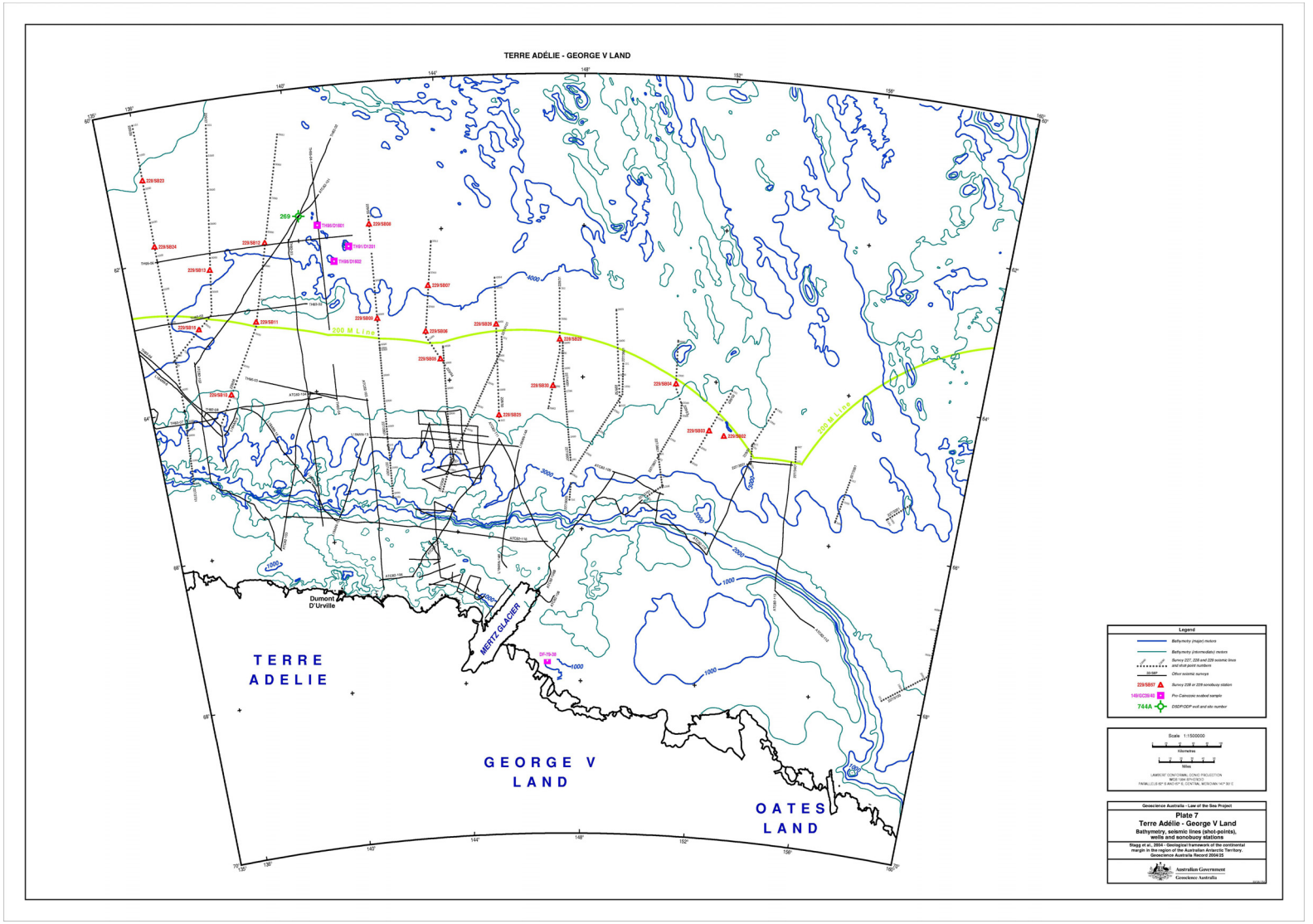

Plate 7: Terre Adélie – George V Land – bathymetry, seismic lines (shot-points), wells and sonobuoy stations.

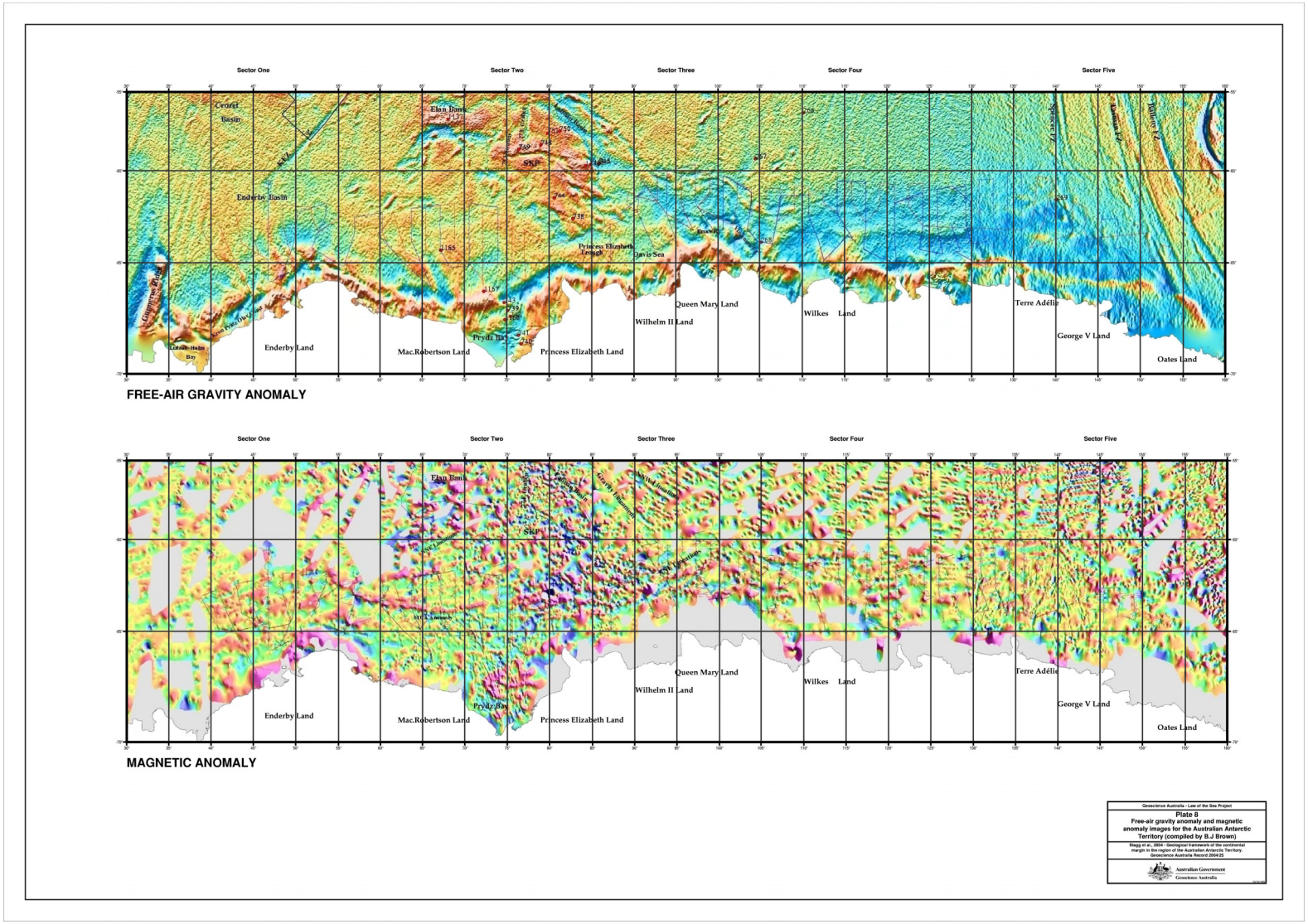

Plate 8: Free-air gravity anomaly and magnetic anomaly images for the Australian Antarctic Territory (compiled by B.J. Brown).

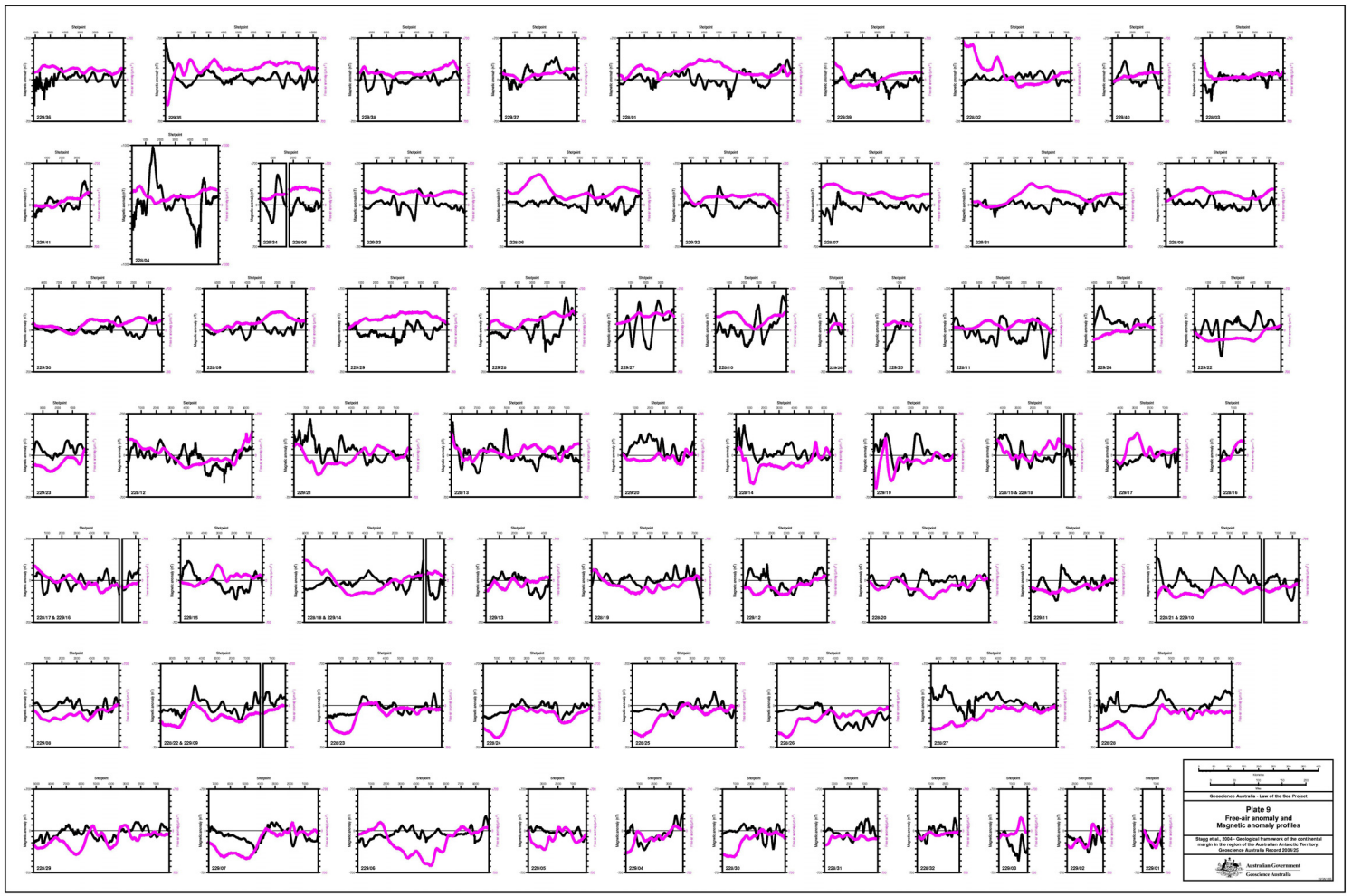

Plate 9: Free-air anomaly and magnetic anomaly profiles.

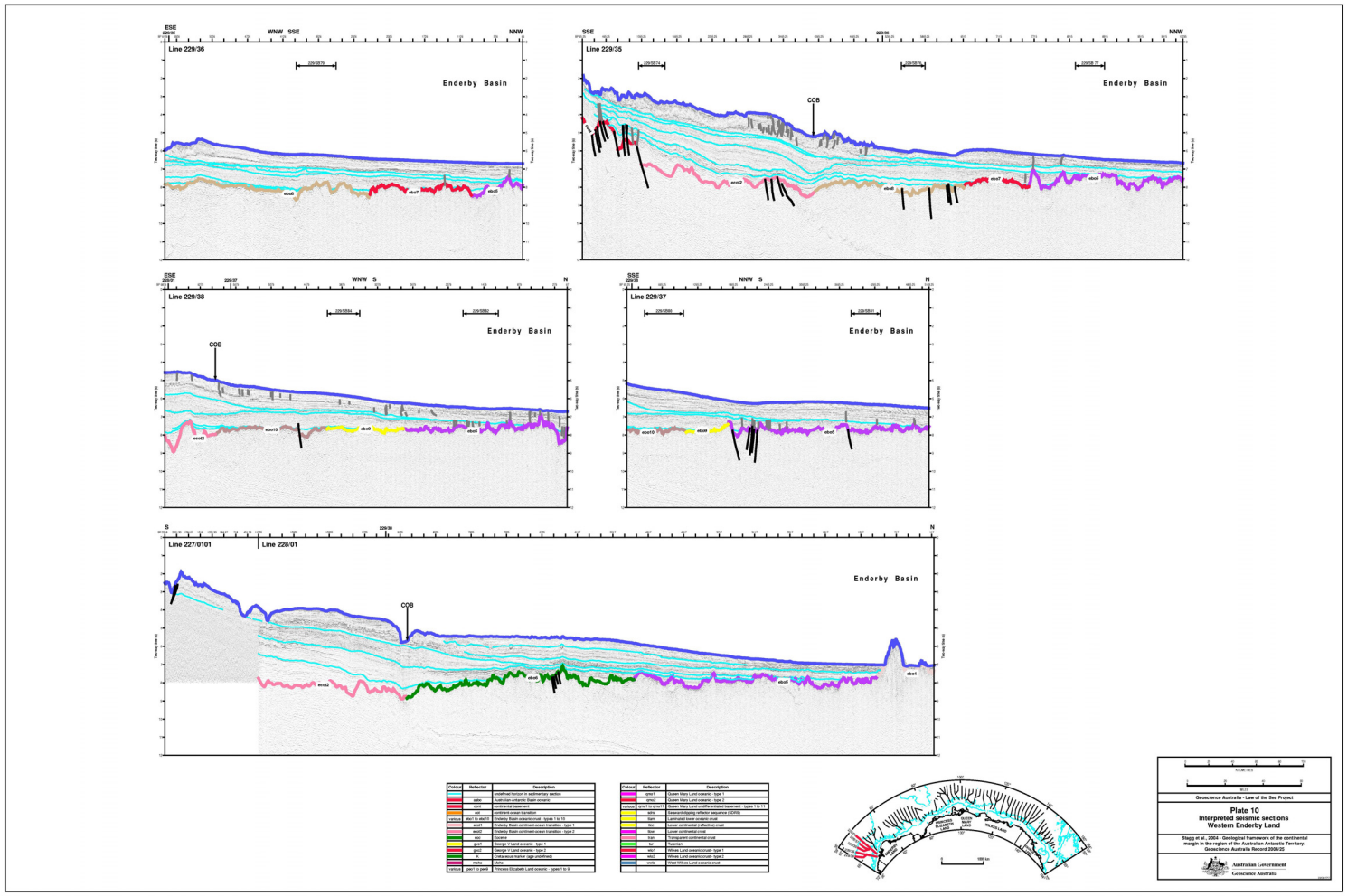

Plate 10: Interpreted seismic sections – western Enderby Land.

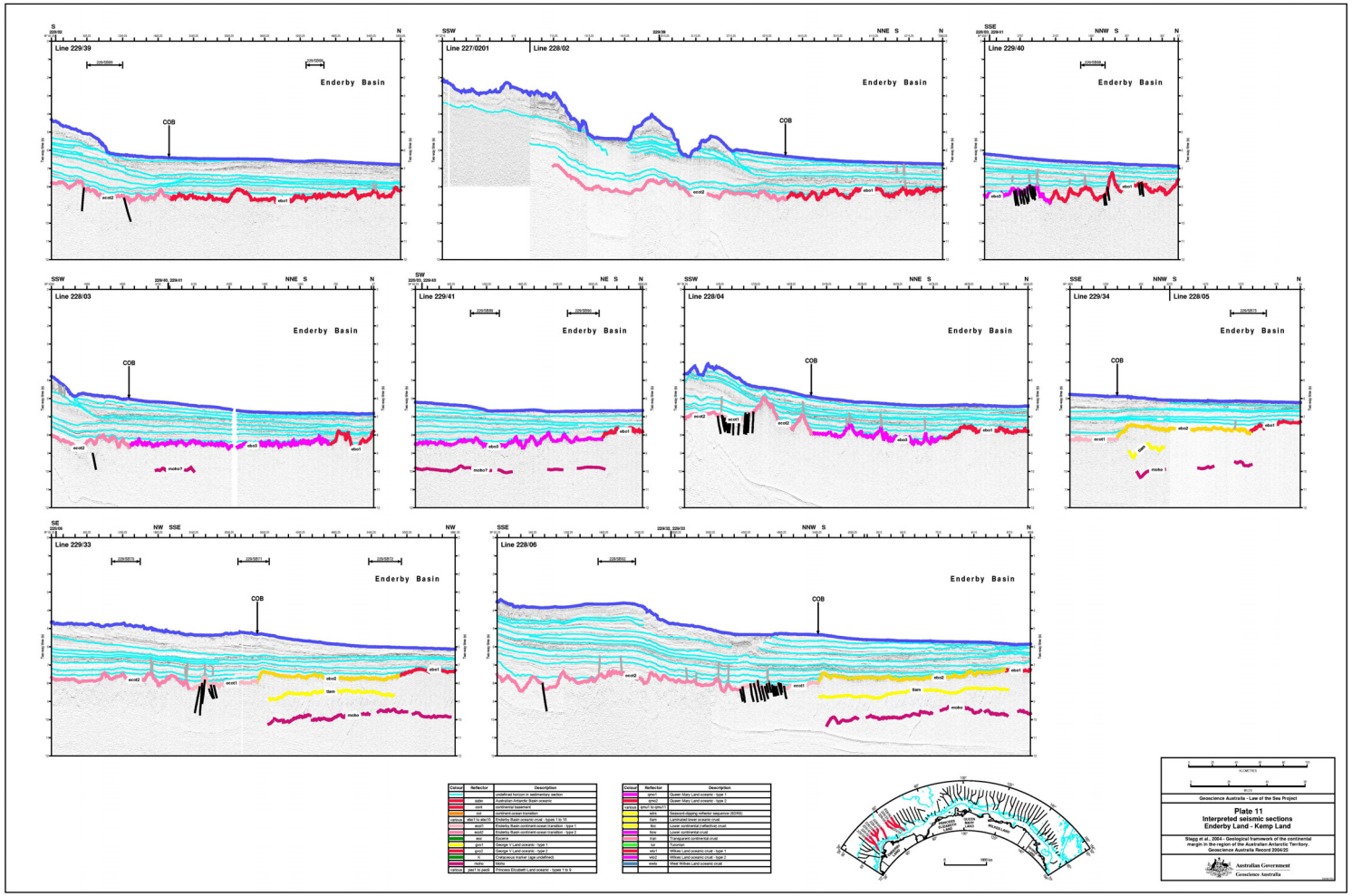

Plate 11: Interpreted seismic sections –Enderby Land – Kemp Land.

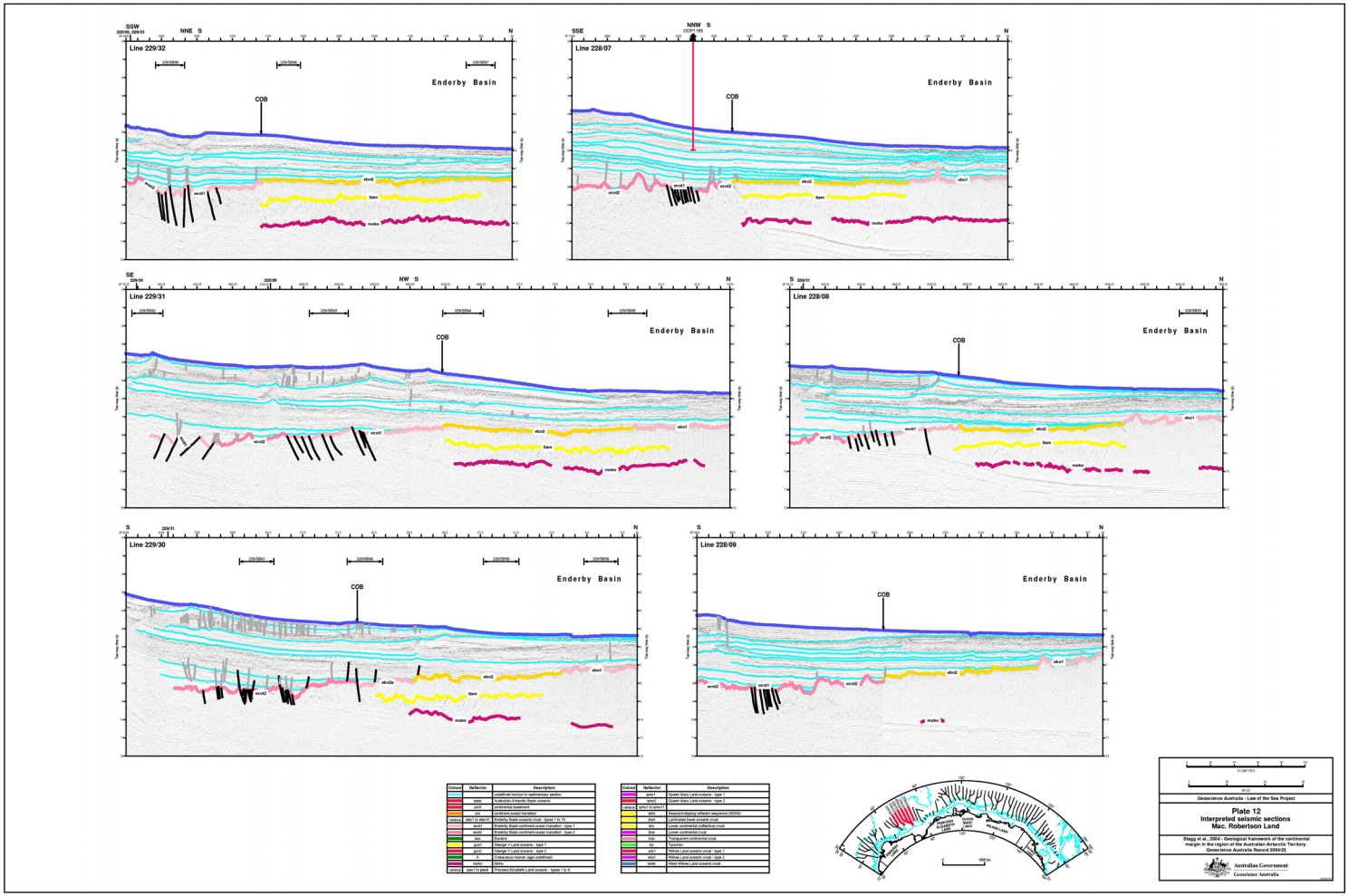

Plate 12: Interpreted seismic sections – Mac. Robertson Land.

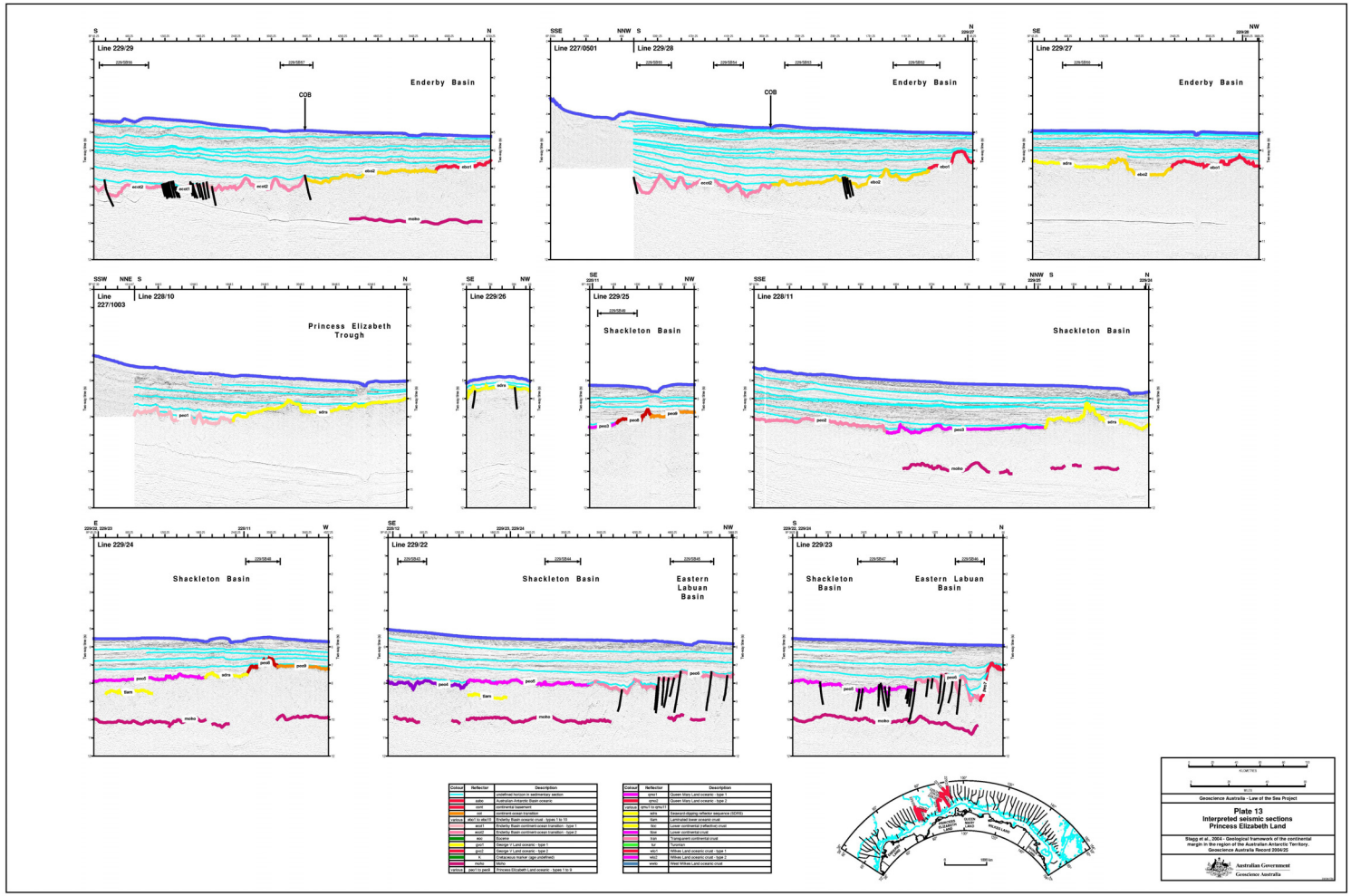

Plate 13: Interpreted seismic sections – Princess Elizabeth Land.

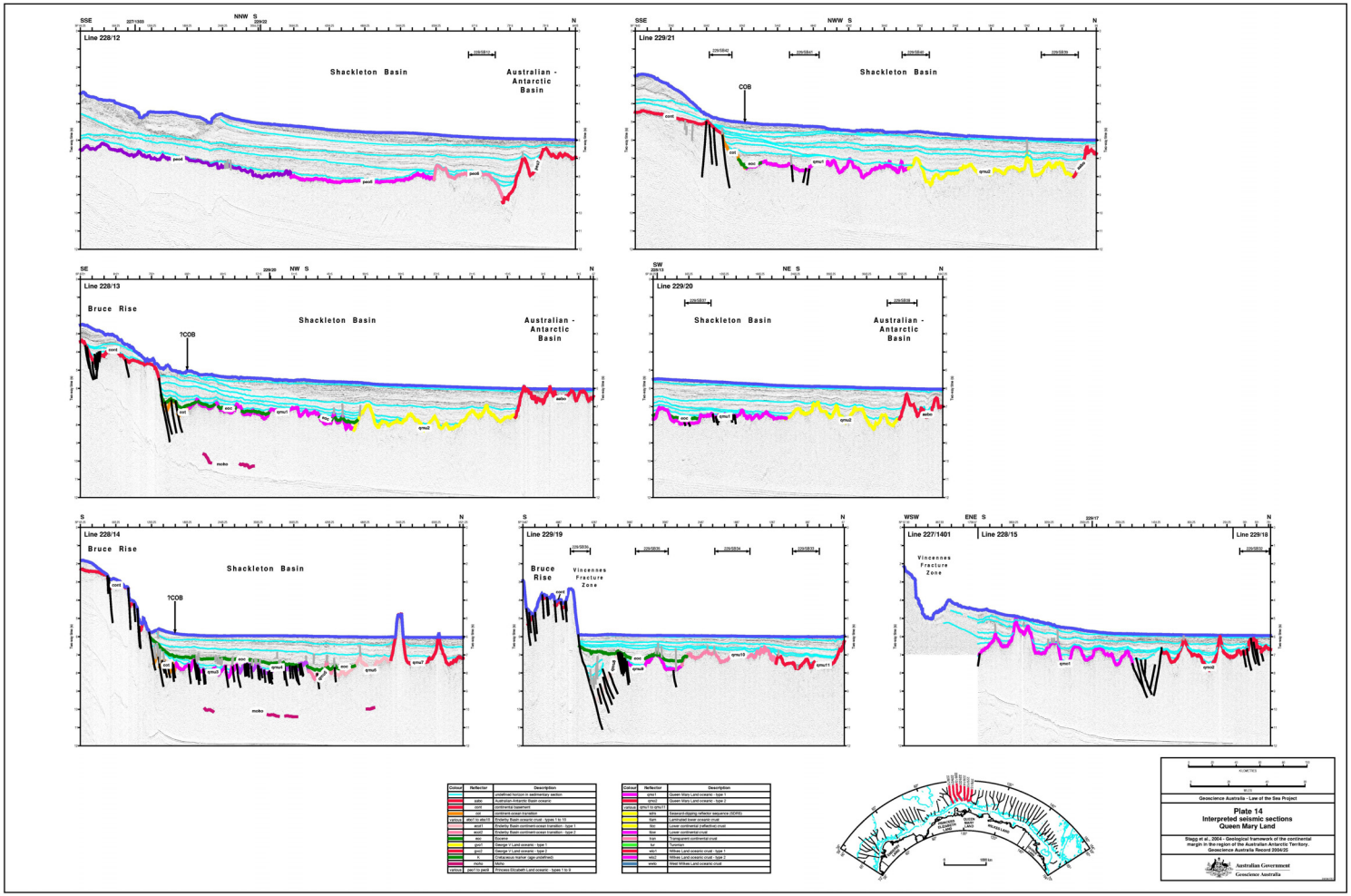

Plate 14: Interpreted seismic sections – Queen Mary Land.

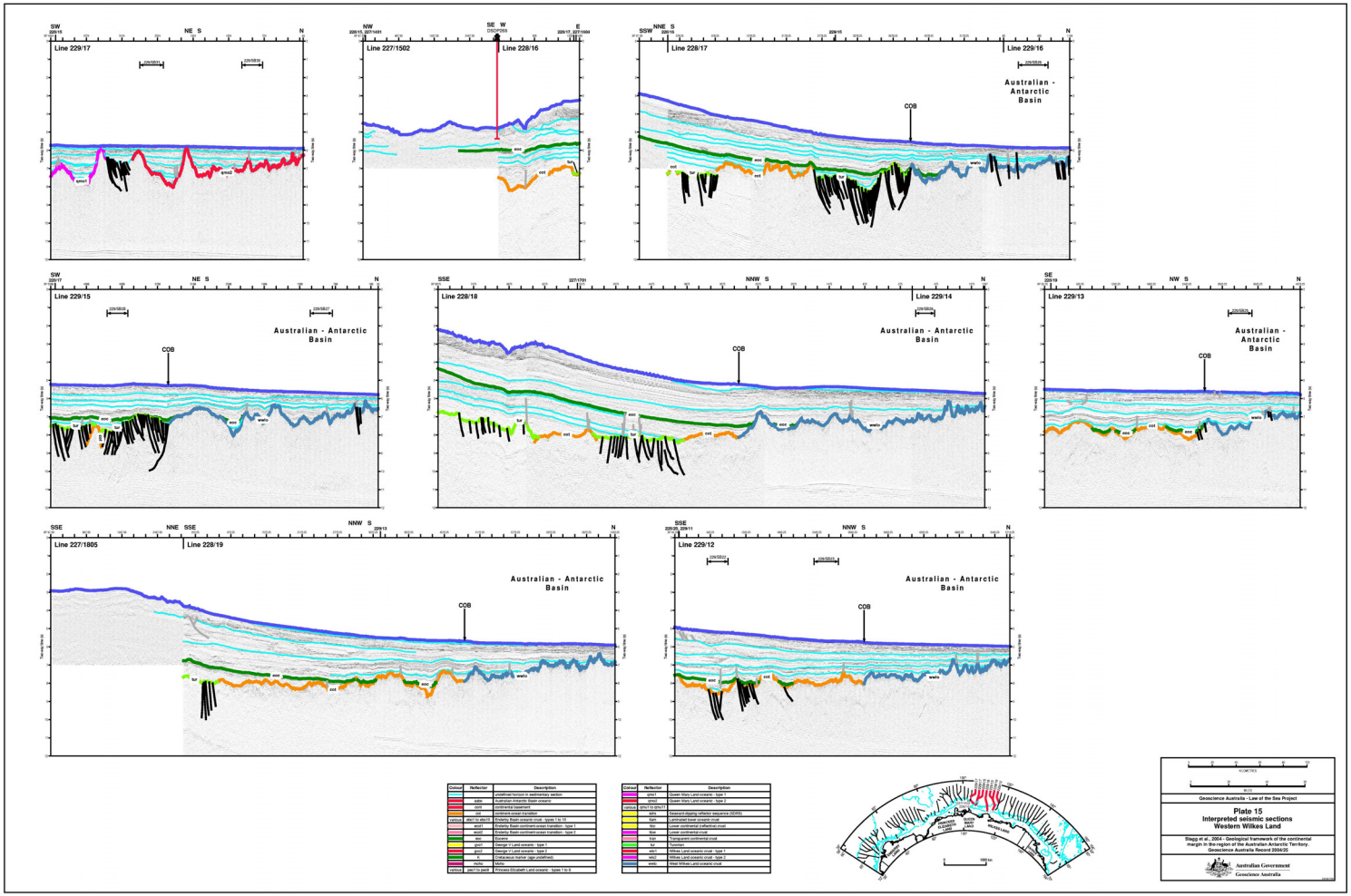

Plate 15: Interpreted seismic sections – western Wilkes Land.

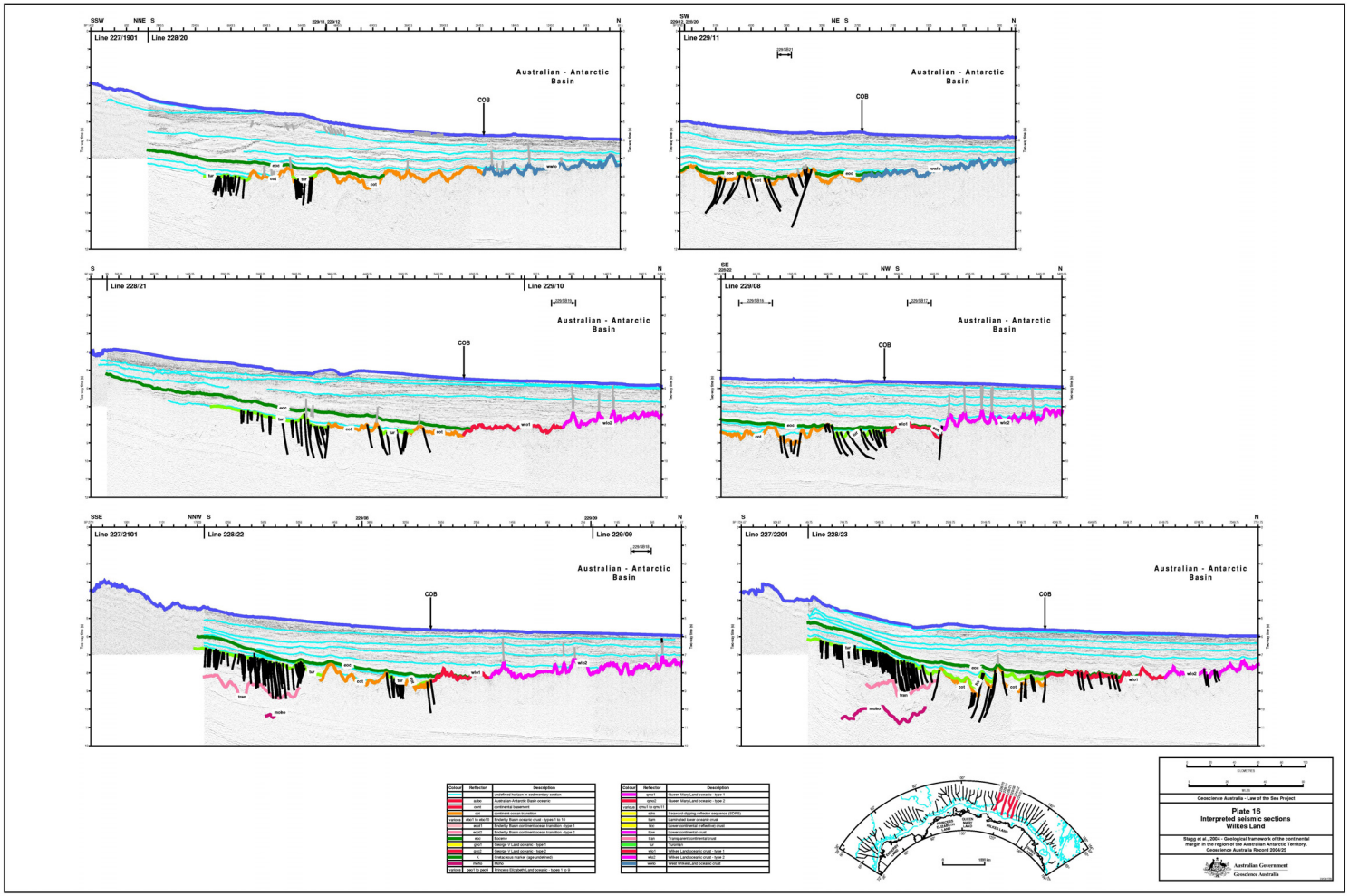

Plate 16: Interpreted seismic sections – Wilkes Land.

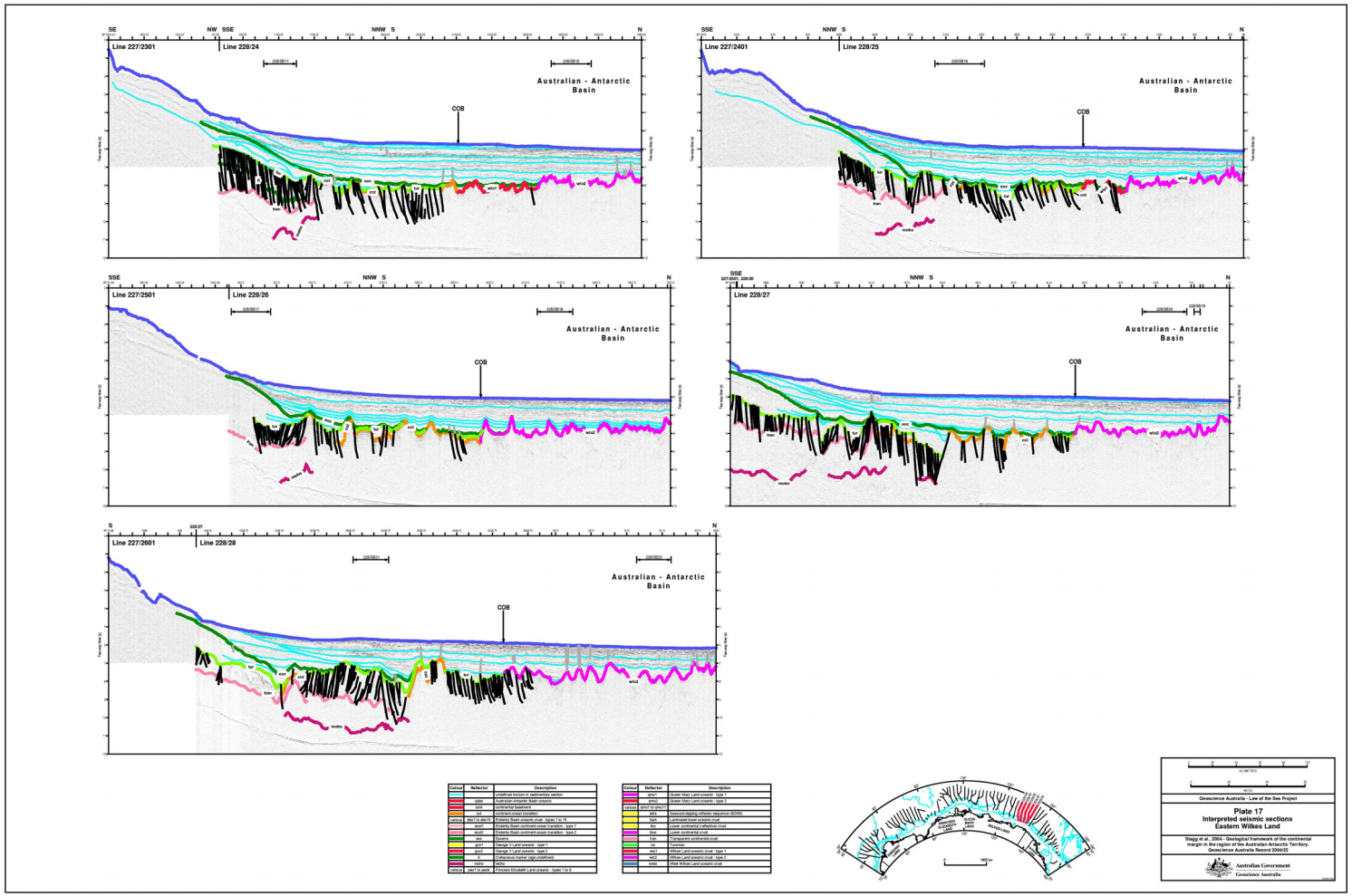

Plate 17: Interpreted seismic sections – eastern Wilkes Land.

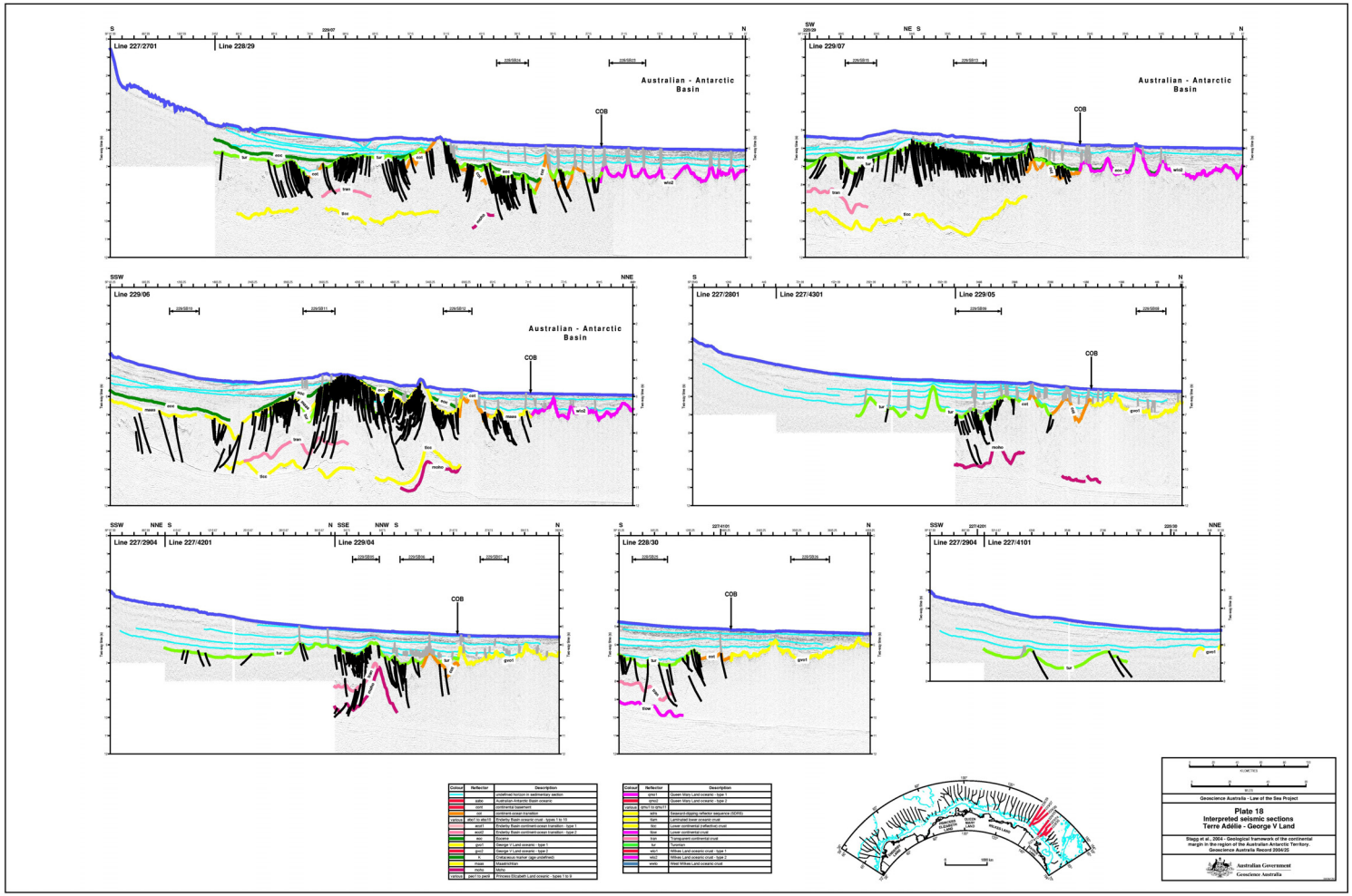

Plate 18: Interpreted seismic sections – Terre Adélie – George V Land.

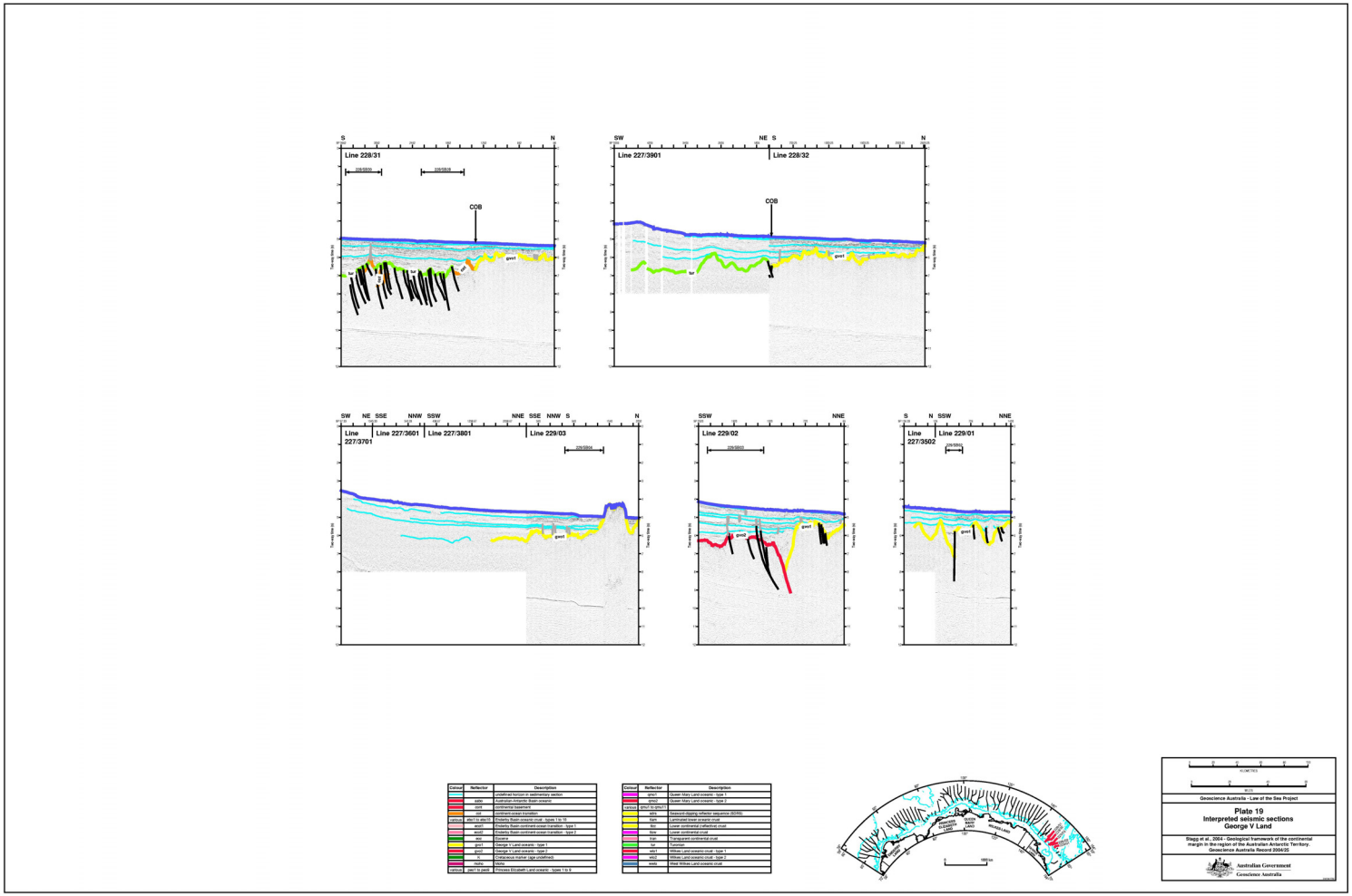

Plate 19: Interpreted seismic sections – George V Land.

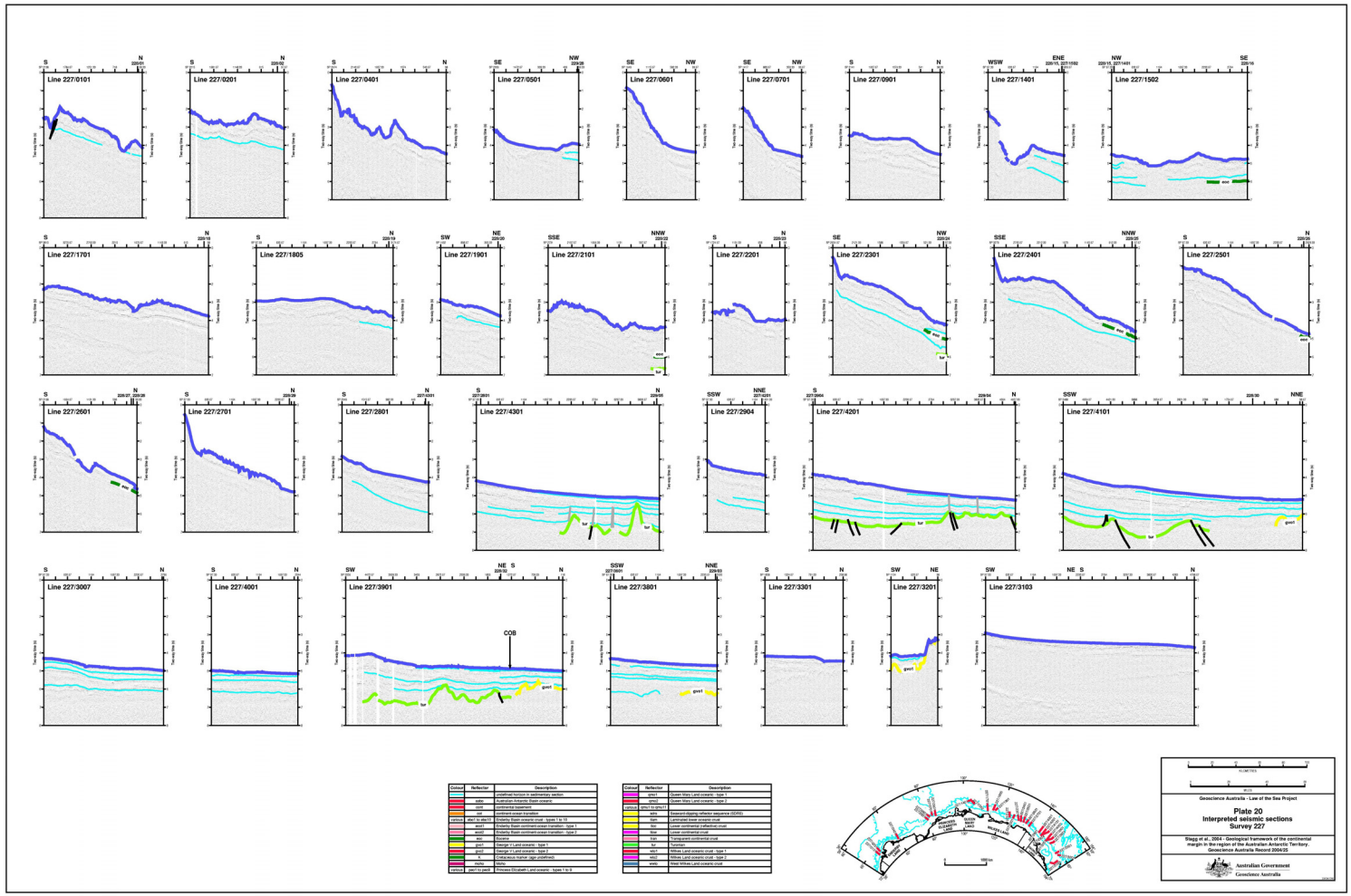

Plate 20: Interpreted seismic sections – Survey 227.

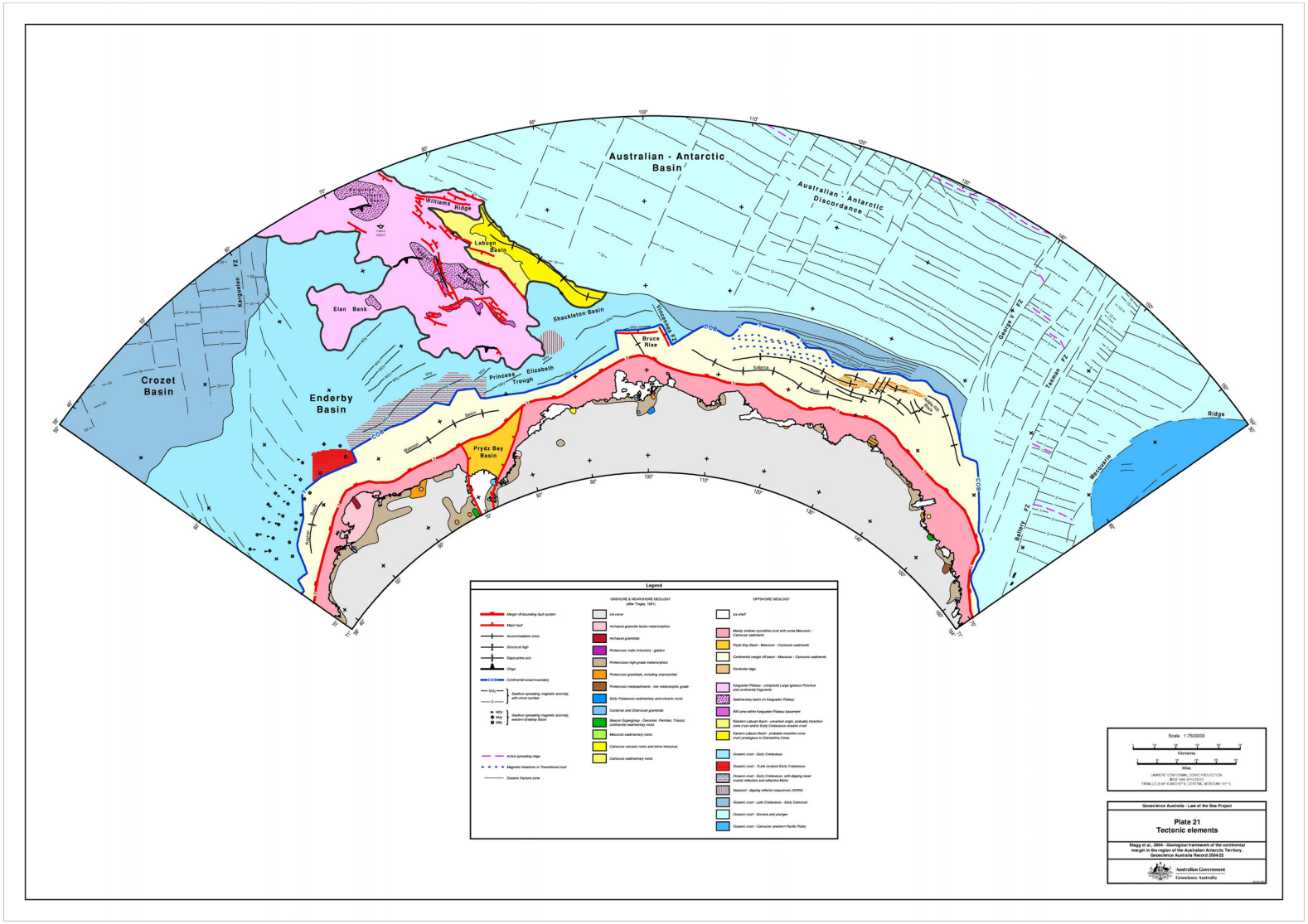

Plate 21: Tectonic elements.

Instructions for the DVD

GEOLOGICAL FRAMEWORK OF THE CONTINENTAL MARGIN IN THE REGION OF THE AUSTRALIAN ANTARCTIC TERRITORY

This **DVD contains the above-titled report as Record2004_25.pdf**
View this .pdf document using Adobe Acrobat Reader (click Adobe.txt for information on readers)

Click on: Record2004_25.pdf to launch the document.

Directories on this DVD:

Plot_files
with sub-directories containing postscript (.ps) and joint photographics experts group (.jpg) plot files of the plates used in this Record. These are all suitable for plotting to large format plotters.
